UNCLASSIFIED

AD NUMBER
ADB126979
NEW LIMITATION CHANGE
TO Approved for public release, distribution unlimited
FROM Distribution authorized to U.S. Gov't. agencies and their contractors; Administrative/Operational Use; 16 JUN 1988. Other requests shall be referred to Commander, Naval Oceanography Command, Bay St. Louis, MS 39529.
AUTHORITY
COMNAVMENTOCCOM ltr, 31 Jan 2007

THIS PAGE IS UNCLASSIFIED

DTIC FILE COPY

(2)

Naval Environmental Prediction Research Facility
Monterey, CA 93943-5006

Contractor Report CR 88-11 June 1988

FORECASTERS HANDBOOK FOR JAPAN AND ADJACENT SEA AREAS

AD-B126 979

88 10 3 008

UNCLASSIFIED

SECURITY CLASSIFICATION OF THIS PAGE

AD-B126977

REPORT DOCUMENTATION PAGE

1a REPORT SECURITY CLASSIFICATION UNCLASSIFIED	1b RESTRICTIVE MARKINGS
2a SECURITY CLASSIFICATION AUTHORITY	3 DISTRIBUTION/AVAILABILITY OF REPORT Distribution authorized to U.S. Government agencies and their contractors; administrative or operational use; 16 June 1988. Other requests for this document shall be referred to Commander, Naval Oceanography Command.
2b DECLASSIFICATION / DOWNGRADING SCHEDULE	
4 PERFORMING ORGANIZATION REPORT NUMBER(S)	5 MONITORING ORGANIZATION REPORT NUMBER(S) CR 88-11
6a NAME OF PERFORMING ORGANIZATION Science Applications International Corporation 6b OFFICE SYMBOL (If applicable)	7a NAME OF MONITORING ORGANIZATION Naval Environmental Prediction Research Facility
6c ADDRESS (City, State, and ZIP Code) 205 Montecito Ave., Monterey, CA 93940	7b ADDRESS (City, State, and ZIP Code) Monterey, CA 93943-5006
8a NAME OF FUNDING/SPONSORING ORGANIZATION Commander, Naval Oceanography Command 8b OFFICE SYMBOL (If applicable)	9 PROCUREMENT INSTRUMENT IDENTIFICATION NUMBER N00228-84-C-3183
8c ADDRESS (City, State, and ZIP Code) Bay St. Louis, MS 39529	10 SOURCE OF FUNDING NUMBERS PROGRAM ELEMENT NO: OM&N-1 PROJECT NO: TASK NO: WORK UNIT ACCESSION NO: DN656794

11 TITLE (Include Security Classification)

Forecasters Handbook for Japan and Adjacent Sea Areas (U)

12 PERSONAL AUTHOR(S)

Englebretson, Ronald E. and Gilmore, Richard D.

13a TYPE OF REPORT	13b TIME COVERED	14 DATE OF REPORT (Year, Month, Day)	15 PAGE COUNT
Final	FROM 9/15/84 TO 1/31/87	1988, June	659

16 SUPPLEMENTARY NOTATION

17 COSATI CODES			18 SUBJECT TERMS (Continue on reverse if necessary and identify by block number)	
FIELD	GROUP	SUB-GROUP		
04	02		Sea of Japan	Philippine Sea
			East China Sea	Sea of Okhotsk
			Yellow Sea	Western North Pacific Ocean

19 ABSTRACT (Continue on reverse if necessary and identify by block number)

Weather conditions for the Sea of Japan, East China Sea, Yellow Sea, Sea of Okhotsk, Philippine Sea and western North Pacific Ocean (W of 160 deg E) are examined. Each of these regions is addressed separately with information directed toward operational forecasters. A general overview chapter provides seasonal climatology charts for the entire area. In most cases, satellite imagery examples are included in discussions of particular weather conditions. These examples provide references for various seasonal atmospheric and oceanic synoptic scale features. Also included are numerous forecast rules that have direct application to naval operational planning. Appendices provide information on local geographic terminology, tropical cyclones, and superstructure icing.

20 DISTRIBUTION/AVAILABILITY OF ABSTRACT ☐ UNCLASSIFIED/UNLIMITED ☒ SAME AS RPT ☐ DTIC USERS	21 ABSTRACT SECURITY CLASSIFICATION UNCLASSIFIED
22a NAME OF RESPONSIBLE INDIVIDUAL Dennis C. Perryman, contract monitor	22b TELEPHONE (Include Area Code) (408) 647-4709 22c OFFICE SYMBOL OM&N-1

DD FORM 1473, 84 MAR — 83 APR edition may be used until exhausted. All other editions are obsolete.

SECURITY CLASSIFICATION OF THIS PAGE

UNCLASSIFIED

TABLE OF CONTENTS

FOREWORD

The Japan and Adjacent Seas handbook is one of a series of regional forecaster handbooks produced by the Naval Environmental Prediction Research Facility (NEPRF). This publication has been developed in response to Commander, Naval Oceanography Command requirement PACMET 84-10, validated by the Chief of Naval Operations (OP-096).

The primary objective of this publication is to provide fleet forecasters and other decision makers with a single, comprehensive reference on environmental conditions for the Far East. Included are several satellite pictures, which provide reference images for various seasonal phenomena, and specific examples of satellite imagery interpretation.

This handbook should be regarded as a flexible document, capable of being updated and revised as applicable. Fleet users are urged to submit comments and suggested changes which can be incorporated into the handbook to increase its usefulness.

W. L. SHUTT
Commander, U.S. Navy

PREFACE

This handbook examines environmental conditions for the Sea of Japan, East China Sea, Yellow Sea, Sea of Okhotsk, Philippine Sea and western North Pacific (west of 160 deq East) and is orqanized by reqion for easy access.

A qeneral overview chapter follows the introductory chapter. The overview includes seasonal climatoloqy charts for the entire Far East area. In the reqional chapters, references are made to these charts to assist the reader in differentiatinq seasons and sub-areas.

Chapters 3 through 8 are dedicated to the six sub-areas of interest. Each of these chapters follows a similar format in that information is presented by seasons. Generous use of actual satellite pictures (similar to those used in the NEPRF NTAG series of publications) is made to give the forecaster guidelines to follow in predictinq specific conditions based on these data.

The final chapter contains forecast aids and rules of thumb for the sub-areas. In most cases, these aids have direct applications to naval operations. Most of the rules and aids were obtained from forecaster handbooks produced locally by both the U.S. Air Force and the U.S. Navy at various airfields and bases in the Far East reqion.

The appendices include a qlossary (Appendix A) of applicable terms used by the various countries in the reqion. Appendix B presents statistics and climatoloqy on typhoons in the reqion while Appendix C contains information on superstructure icinq.

RECORD OF CHANGES

CHANGE NUMBER	DATE OF CHANGE	DATE ENTERED	PAGE NUMBER	ENTERED BY

1.0 GENERAL INTRODUCTION

1.1 Objective

The Objectives of this Handbook are to:

a. Provide operational forecasters with a single reference text of information on the Sea of Japan, East China Sea, Yellow Sea, Sea of Okhotsk, Philippine Sea, and western North Pacific west of 160°E.

b. Organize the material for easy access to a general overview chapter with seasonal climatological charts and successive chapters on regional environmental conditions within the area of each of the above named marginal seas or oceanic areas.

c. Employ satellite imagery and graphics to illustrate discussions of operationally important phenomena, to provide reference images for various seasonal atmospheric and oceanic synoptic scale features, and present specific examples of imagery interpretation and deduction of environmental conditions.

d. List FORECAST RULES/AIDS which may have direct application to naval operational planning, tactics, and daily operations.

e. Identify pertinent and more detailed sources of information in the Reference Section.

f. Attach supplemental data/information from various sources as Appendices.

1.2 Approach

The following approach was used in development of this Handbook:

a. An operationally-oriented outline was stratified by: (1) A Large Scale Overview, (2) Regional Area Conditions, and (3) Seasonal Sections on Environmental Conditions.

b. Pertinent reference material from the technical libraries at the Naval Environmental Prediction Research Facility (NEPRF) and the Naval Postgraduate School (NPS) Monterey was collected and reviewed.

c. Operational reports of significant environmental events/conditions were reviewed.

d. Naval Oceanographic Command personnel who have had recent WESTPAC experience were interviewed.

e. Satellite imagery from the area was reviewed for specific illustrations of key phenomena.

f. FORECAST RULES/AIDS which have been developed by area forecasters were collected, screened, and selected for use in forecasting both local airfield and large area conditions.

g. The general reference information, satellite imagery, and forecast rules/aids were merged to provide a comprehensive reference text.

1.3 Organization and Contents

The Handbook is organized to provide large area general information, regional information, and specific location/condition information. Because of the extensive latitudinal range of the regions addressed, plus the unique monsoonal influences a simple four season year was not always appropriate. However, the four seasonal approach was generally retained with modification where necessary for regional variations.

Because of the varied countries and languages inclusive in the area covered an appendix of geographic terms was included. Information on such varied subjects as tropical cyclones and superstructure icing are included. The general text and appendix material is taken from the various references provided. The satellite imagery interpretation is based on references from the NEPRF NTAG series, Air Force interpretation manuals, various journal articles that made use of satellite imagery, and the Authors interpretation.

2.0 LARGE SCALE OVERVIEW

2.1 Physical Characteristics

The physical makeup of eastern Asia and adjacent ocean areas exerts a significant influence on the weather of the region. Many meteorological conditions described herein are the result of airmass trajectory coupled with modifications imposed by the land and water areas over which the airmass travels. Steep sea surface temperature gradients may cause markedly different weather conditions in some adjacent water areas with similar flow patterns. A careful study of the topography of eastern Asia and the bathymetry of adjacent water areas is essential to successful forecasting.

Appendix A contains a glossary which lists the non-English words for geography, topography, and bathymetry features most commonly encountered in the western North Pacific Ocean and marginal seas.

2.1.1 Geography

Figure 2-1 shows the geography of the land masses which border the water areas addressed in this handbook. The figure has been expanded westward to include central and western China, which contain the highest land elevations in the world and exert a significant influence on the large scale weather patterns which occur.

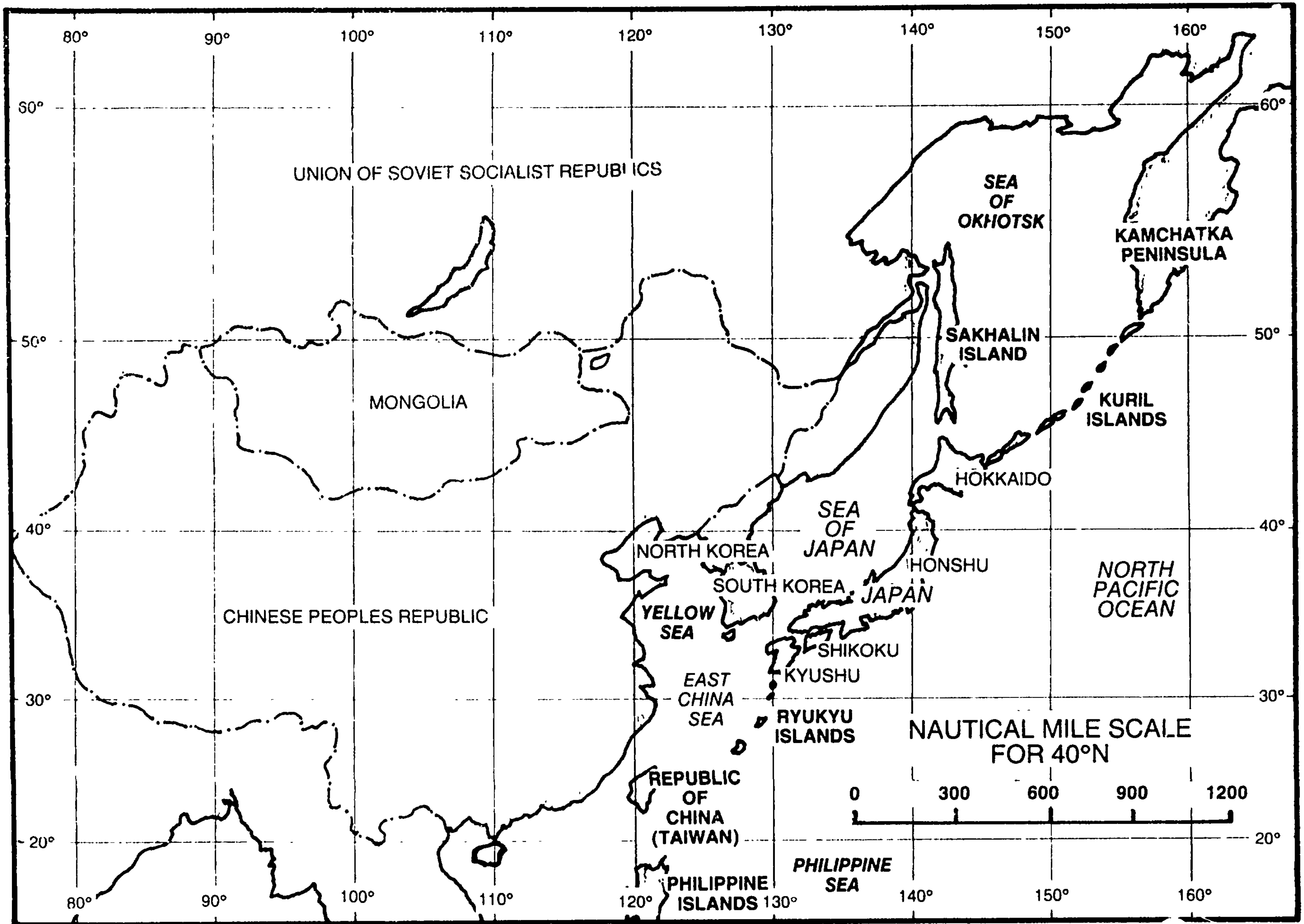

Figure 2-1. Geography of Eastern Asia.

2.1.2 Topography

Figure 2-2 depicts some of the major topographic features of the Asian continent. Asia contains some of the most rugged terrain in the world, with elevations ranging from the 29,028 ft (8,848 m) of Mt. Everest to the -154 ft (-47 m) of the Turpan Depression. The topography of eastern Asia can be classified by three major physical features: (1) the volcanic area, (2) the eastern ridge line of the continent, and (3) the mountains of Central China and Mongolia, an area commonly referred to as the Tibetan Plateau.

The volcanic area is composed of a mountainous chain, formed by the Kamchatka Peninsula and three island chains, the Kuril, Japan, and the Ryukyu Islands. Japan is the most significant of the three island chains because it poses the greatest barrier to air flow. The Japanese Alps average near 7874 ft (2,400 m) in elevation and cause frequent strong dynamic troughs which form in their lee to the southeast and east of the country.

The eastern ridge line of the Asian continent is composed of mountains averaging some 3,281 to 4,921 ft (1,000 to 1,500 m) in elevation with some peaks exceeding 8,202 ft (2,500 m). Included in the ridge line are the Sikhote Alin range which is most prominent along the northwest coast of the Sea of Japan but continues southward into the Korean peninsula, the Dzugdzhur and Kolyma ranges along the west and north coasts of the Sea of Okhotsk, and other less significant coastal mountains in eastern China which seldom reach more than 2,953 ft (900 m) in elevation.

The Tibetan Plateau in central and western China has elevations commonly ranging from 9,843 to 19,685 ft (3,000 to 6,000 meters) with many peaks exceeding the 6,000 m level. The plateau is irregular in shape and is comprised of several mountain ranges, the most prominent of which is the Himalayas. Also included are the Kunlun Mountains, Tian Shan, Qilian Shan, and Altun Shan. Immediately north of the Tibetan Plateau lie the extensive wastelands of the Taklimakan Desert and the Dzungarian Basin. The eastern extension of the wastelands forms the famous Gobi Desert, where strong winds are frequent and the annual rainfall averages just four inches (FWC/JTWC, Guam, 1978).

The remainder of eastern Asia is a complex mixture of mountain ranges and extensive plains and valleys. The more prominent mountain ranges include the 2,953 to 5,906 ft (900 to 1,800 m) Greater Khingan Range just east of the Gobi Desert, and the Koryak Range which lies along the eastern coast of Siberia north of the Kamchatka Peninsula. Elevations in these ranges are predominantly in the 2,953 to 6,562 ft (900 to 2,000 m) range with some peaks exceeding 7,874 ft (2,400 m). An extension of the Koryak Range runs the length of the Kamchatka Peninsula and has elevations frequently exceeding 9,843 ft (3,000 m), with one peak reaching 15,584 ft (4,750 m).

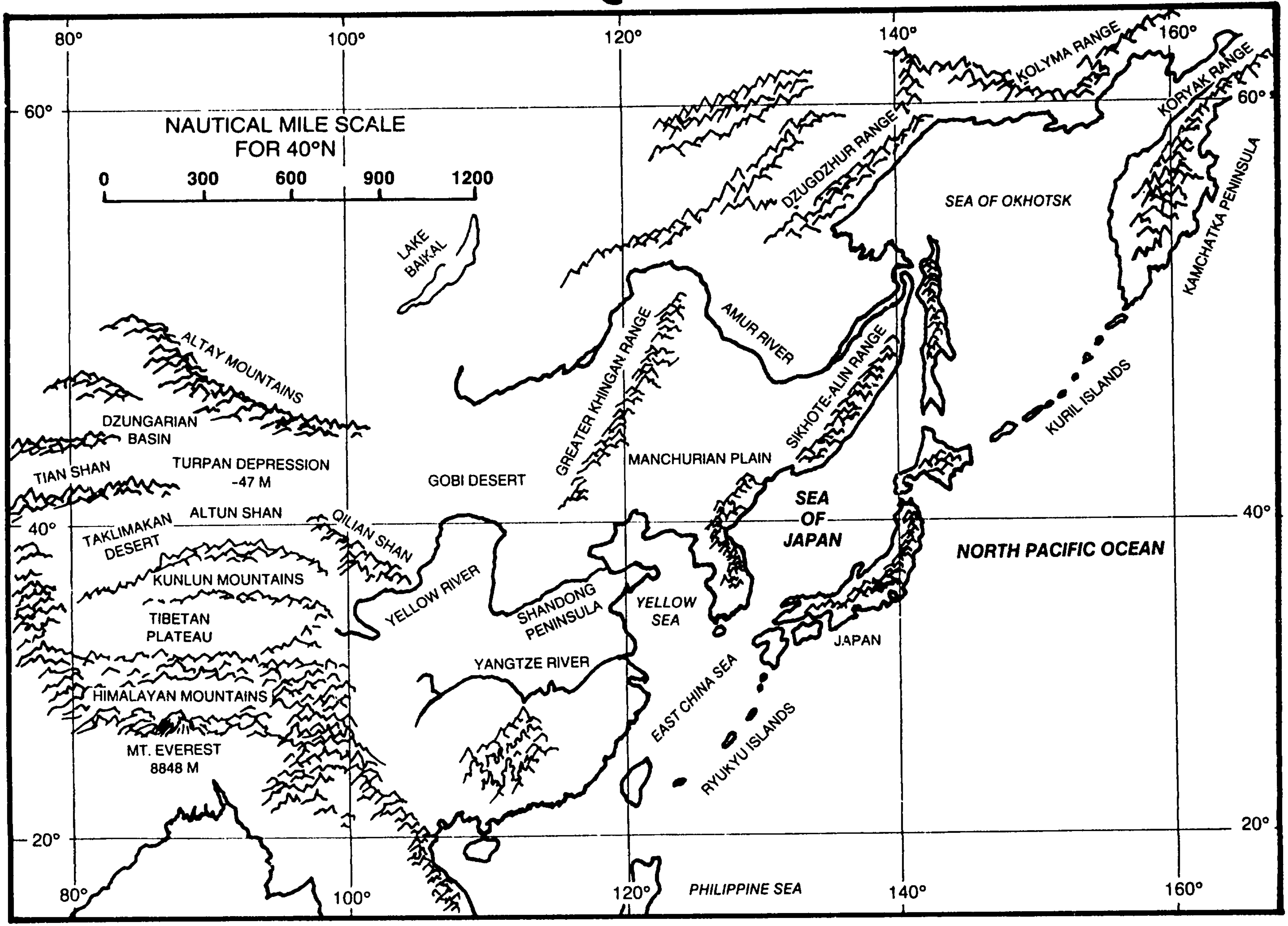

Figure 2-2. Major topographical features of eastern Asia.

2.1.3 Oceanographic Features

This handbook addresses oceanic regions that include both marginal seas and deep ocean areas of the western North Pacific Ocean. Significant differences in physical properties exist between the marginal seas and deep ocean regimes that impact temperature and salinity structures and bottom characteristics and, therefore, sound speed profiles critical to acoustic propagation. Critical physical properties of interest are:

(1) bathymetry and bottom topography features

(2) ocean fronts and current structures

(3) temperature and salinity change due to precipitation, river inflow, and fluctuations in evaporation due to variations in atmospheric circulations

A large-scale overview of each of these critical properties for the region addressed in this handbook follows. Detailed discussions addressing interrelated facets of these and other properties will be provided in the individual sea and oceanic area sections.

2.1.3.1 Bathymetry and Bottom Topography

The bottom features of the western North Pacific and adjacent seas range from deep ocean trenches, troughs, ridges, and basins to regions of extensive continental shelf (Figure 2-3).

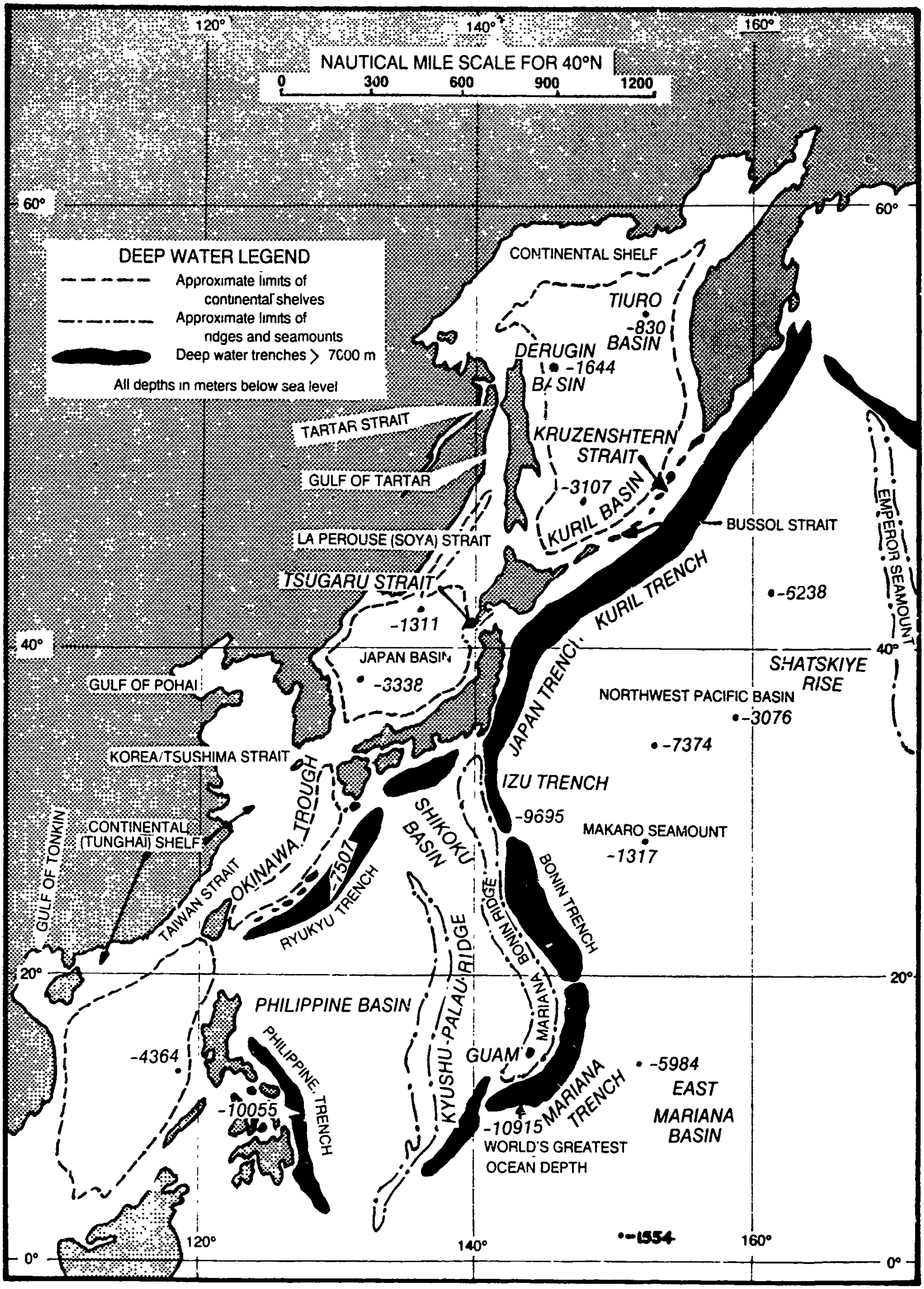

Figure 2-3. Major bathymetric features of the Sea of Japan, Yellow Sea, East China Sea, Sea of Okhotsk, Philippine Sea and western North Pacific Ocean.

The Philippine Sea is an abyssal zone (depths generally greater than 2,000 m). The bottom topography is complicated by deep trenches (greatest depth over 6,000 m), belts of seamounts, deep basins, and a number of island arcs. The sea is separated on the east from the Pacific Basin proper by a number of oceanic island arcs and on the west from the marginal seas by the continental arcs of Japan, the Ryukyu Islands, and the Philippines (Figure 2-3). The abyssal deep basin is separated into east and west basins by the Kyushu-Palau Ridge. The bottom sediments are pelagic red clays and oozes with volcanic material along the island arcs.

The East China Sea has two contrasting bathymetric zones, a broad continental shelf and the Okinawa Trough. The shelf, known as the Tunghai Shelf, is part of one of the largest in the world extending from the Yellow Sea south through the Taiwan straits to the South China Sea and the Gulf of Tonkin. The shelf width is about 150 n mi at the southern boundary of the East China Sea (near the northern end of Taiwan) and broadens northward to about 400 n mi near the northern boundary (near 33°N). The majority of the shelf has depths less than 100 m with the shelfbreak near 150 to 170 m. The shelf bottom consists of terrigenous sediment primarily from the Yangtze (Changjiang) River (Figure 2-2) with 400 million tons of sediment deposited annually (as compared to 500 million by the Mississippi River).

The Okinawa Trough extends from Taiwan to Kyushu (the southernmost island of Japan) along the inner side of the Ryukyu Islands arc. A large area of the trough has depths of 1,000 m with a maximum of over 2,700 m. The trough bottom is composed of a mixture of terrigenous muds and pelagic oozes.

The Yellow Sea and Gulf of Pohai form a broad semi-enclosed sea with maximum depths of 60-80 m in the central and southeastern parts (Fairbridge, 1966). The entire sea floor is part of the continental shelf and is comprised of terrigenous sediments brought down from the eastern watershed region of China via such rivers as the Yellow, Liao, White, and Yangtze (Changjiang). The westward flowing rivers of Korea, Yalu, Han, and Kum also carry large flowing rivers of Korea, Yalu, Han, and Kum, also carry large amounts of sediment into the Yellow Sea. Broad tidal mudflats are typical coastal features of the Yellow Sea.

The Sea of Japan contains both continental shelf and deep basin regions. The shelf is very narrow except in the extreme southern and northern narrows. The majority of sea depths exceed 1,000 m with a large area of the basins greater than 3,000 m. The Japan Sea Basin is separated from the Pacific floor by the Japanese Island Arc on the southeast side and bounded by the continental shelf elsewhere. The Sea of Japan is connected on the south and north to marginal seas by the Tsushima (Korea) Strait, and La Perouse (Soya) and Tartar straits respectively. Only the Tsushima (Korea) Strait has a sill depth greater than 100 m. The Tsugaru Strait located between Honshu and Hokkaido on the northeastern side of the Sea of Japan connects it with the main Pacific Ocean.

The Sea of Okhotsk has three main categories of bottom topography: (a) continental and island shelves, (b) the bottom of the central part of the sea, and (c) the bottom of the southern deep-water basin. The shelf area occupies more than 40% of the entire sea area and is composed primarily of sands or silts. The widths, outer margin depths, and slopes toward the basins vary widely (see section on the Sea of Okhotsk for details). The central floor area has several systems of elevations and troughs. Depths over the systems range from 200 m to near 1,750 m. The Kuril Basin runs along the inner side of the Kuril Islands and has a greatest depth of over 3,000 m. The basin is surrounded on all sides by steep slopes (15-20°). The sediments range from pebbly gravel and sand in the nearshore and over open sea summits and slopes, through bands of silts and clays to ooze over the majority of the central part and abyssal plain of the Kuril Basin. In contrast to the Sea of Japan, which is nearly landlocked, the Sea of Okhotsk has free exchange of water with the Pacific. Bussol (Boussole) Strait accounts for over 40 percent of the cross sectional opening of the straits and has a sill depth of over 2,300 m. Kruzenshtern Strait accounts for about 25 percent more of the total opening and has a sill depth over 1,900 m.

2.1.3.2 Currents

An overview of the major currents is provided here. Additional details on these currents as well as on local currents are presented in the regional sections.

The Kuroshio Current is the dominant ocean current of the western North Pacific and resembles the Gulf Stream of the western Atlantic. The Kuroshio begins east of northern Luzon, the northernmost of the Philippine Islands, (Strommel and Yoshida, 1972) and flows close to the east coast of Taiwan and then into the East China Sea (Figure 2-4 and see Figures S-3-7, page 3-36 and S-3-8, page 3-52). In the East China Sea the Kuroshio follows the Okinawa Trough between the continental shelf and the Ryukyu Ridge. The current splits in two parts southwest of Kyushu. The major part flows east

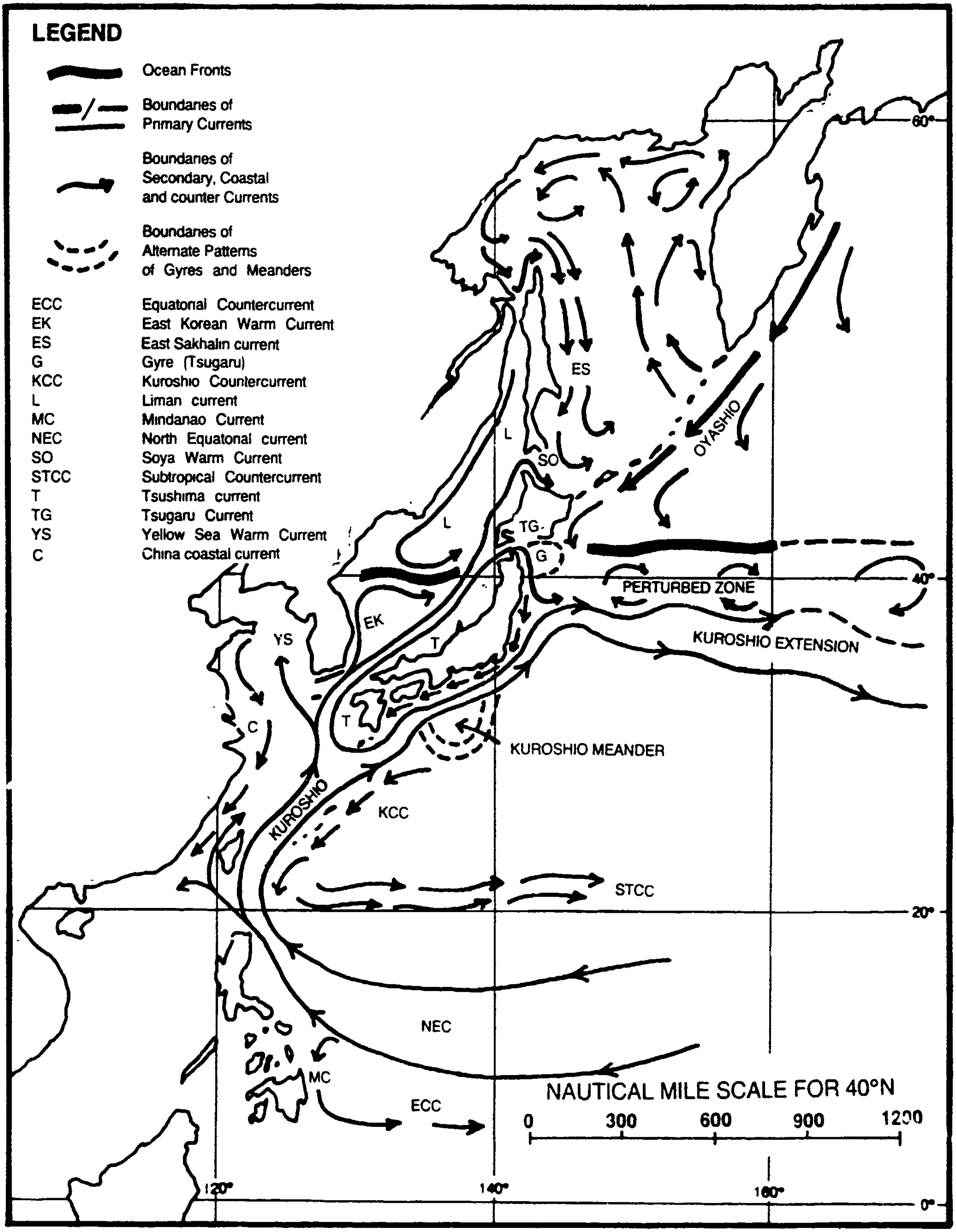

Figure 2-4. Schematic Distribution of currents, ocean fronts, gyres, meanders and perturbed areas.

to south of Shikoku and then northeastward along southern Japan. The minor branch flows north as the Tsushima Current west of Kyushu through the Tsushima (Korea) Strait into the Sea of Japan. The Kuroshio Current south of Japan either flows northeastward close to the continental slope, or makes a large meander to near 31°N south of Honshu. Once formed, this large meander tends to persist for several years. The Kuroshio leaves the Japan coast near 36°N and flows generally east but with a meandering path. This portion of the current flowing eastward from Japan is called the Kuroshio Extension (See Figure S-8-2, page 8-23). The Kuroshio retains its form of a relatively narrow concentrated current until about 160°E where it transforms into the weak, broad North Pacific Current.

The Tsushima Current is a major feature of the Sea of Japan (See Figure S-3-3, page 3-15). It has been defined by Sverdrup et al. (1942) as the warm current that branches off on the left-hand side of the Kuroshio and enters the Sea of Japan through the Tsushima Strait. The Tsushima Current splits just south of the Strait with one branch following the western coast of Japan to the north and a second weaker branch entering the central Yellow Sea. The Tsushima carries water of high temperature and high salinity northward. The major portion of the Tsushima Current transport (about 75 percent) flows out of the Sea of Japan through the Tsugaru Strait as the warm Tsugaru Current (See Figure S-3-4, page 3-22). The remainder continues northward along the west side of Hokkaido and then splits. One branch turns eastward through the Soya (La Perouse) Strait and returns southward as the warm Soya Current along the northeast coast of Hokkaido. The other branch continues northward as a warm current off western Sakhalin Island. The cold

Liman Current has a southerly set in the western portion of the Sea of Japan (See Figure S-3-3, page 3-15).

The Oyashio Current is a cold current that originates in the Bering Sea and flows southwest along the Kamchatka Peninsula, the Kuril Islands, and Hokkaido, meeting the Kuroshio off the northeastern coast of Honshu near 37-40°N (See Figure S-8-2, page 8-23). This region, where arctic waters meet warm waters, is called the Perturbed Area. Numerous eddies and thermohaline fronts are irregularly distributed in the Perturbed Area causing complicated hydrographic conditions (Strommel and Yoshida, 1972). The major features of this area have been theoretically described as four parallel rows of stationary vortices or eddies that rotate in alternate directions (Barkley, 1968). A review of Japanese Hydrographic Division quarterly isotherm analyses for 1955-64, by Barkley (Marr, 1970) provides empirical support for the theoretical configuration. The Perturbed Area extends from near the Japanese coast eastward to beyond 160°E and north-south from about 37°N to near 50°N. The area has a north-south dimension of 200-300 n mi in the near-shore region and increases eastward. There is also a normal north-south seasonal displacement.

2.1.3.3 Temperature and Salinity

The seasonal variations in near-surface temperature and salinity differ throughout the region. For a given location the near-surface temperature values are affected by two principal heating processes. First is the seasonal variation in solar heating, with the typical oceanic lag resulting in a maximum in August and minimum in February/March. Second, the advection process due to shifting ocean currents can modify the seasonal cycle at a given point. The extreme minimum and maximum temperatures discussed in the text for each sea refer to the value for which 1% of all reported are lower or higher. Near the surface, salinity values reflect the effects of additional fresh water due to precipitation or run-off (reduces salinity) and evaporation processes (increases salinity). The shifting ocean currents also play a role in changing salinity values at a given location, reflecting the values of their source regions. Local variations in precipitation, evaporation, and currents result in salinity minimums in late summer and fall (following the rain and tropical cyclone season) and maximums in late winter and spring as a result of high evaporation rates.

2.2 Typical Atmospheric Features

The water areas discussed in this handbook span more than 50 degrees of latitude, from the southern reaches of the Philippine Sea to the northern limit of the Sea of Okhotsk. The weather over these diverse areas ranges from tropical to sub-arctic, making it difficult, if not impossible, to address in general terms a "typical" atmospheric feature that would apply to or impact all of the areas discussed herein. Consequently, this section addresses only large scale events that normally occur in the course of the seasons, without regard for their effects, or lack thereof, on a particular area.

2.2.1 Seasonal Variations

In the mid-latitudes, one would normally expect to find four reasonably distinct seasons: the traditional spring (mid-March to mid-June), summer (mid-June to mid-September), autumn (mid-September to mid-December), and winter (mid- December to mid-March). Not all of the areas discussed in this handbook are in the mid-latitudes however, and even those that are do not all have the standard seasons.

Because this section is intended only as an overview of the whole of eastern Asia, it will address the four traditional seasons, and leave the discussions of regional differences to those sections that apply to each specific region. The selection of individual months that best represent each season was made after considering several factors, the most significant of which was to best describe the majority of the covered areas. Ultimately, the months of February, May, August, and November were chosen. They fall within the traditional quarterly seasons and also fit reasonably well into the more detailed seasonal breakdown of southern Japan and adjacent areas.

Although the start and end of the seasons usually occur in the middle of calendar months, most available climatology reference documents have data grouped and summarized by whole months. Consequently, unless otherwise indicated, it has been nece ary to treat each season as a four-month period when describi the conditions that prevail at its start or end. For example, to present the conditions that exist at the start and end of winter in the East China Sea, the whole months of December and March are considered.

2.2.1.1 Monsoons

A significant portion of eastern Asian weather is controlled by the Asiatic monsoon. The term "monsoon" originated with the Arabic "mausim", a season, and was originally applied to the wind regimes of the Arabian Sea where winds blow for six months from the northeast (winter monsoon) and six months from the southwest (summer monsoon). Monsoon and monsoonal areas have been defined in many ways, but most have a central theme -- seasonality -- surface winds which blow persistently from one general direction during one season and just as persistently from a markedly different direction during another season (FWC/JTWC, 1978).

In winter, the Siberian high, a large, shallow high pressure cell, dominates the eastern USSR. The cold, snow covered surface absorbs little solar radiation because of a high albedo, and subsequent cooling and light surface winds allow a massive pool of shallow but intensely cold air to develop. Surface pressures of 1050 mb are not uncommon, and pressures of 1082 mb were analyzed on surface pressure charts over Siberia during 1974 and 1975 (FWC/JTWC, 1978). The high pressure cell creates the winter monsoon, also called the Northeast Monsoon, resulting in a strong north or northeasterly airflow predominating over eastern Asia and adjacent waters.

Conversely, in summer, the warming landmass causes a large thermal low to form over Asia, creating the summer monsoon, also known as the Southwest Monsoon. It transports warm, moist air northward along the coastal area of eastern Asia. The summer monsoon of the western North Pacific is relatively weak compared to the summer monsoon of India. Gale force winds seldom occur, and then only when they are associated with strong inflow near a large tropical cyclone or with channeling (Venturi effect) through restricted waters such as the Taiwan Strait between mainland China and Taiwan (Figure 2-3). The summer monsoon of Asia is less intense than that of India and Asia Minor due to:

(1) less intense heating at higher latitudes and periodic invasions of cool air from the north

(2) a wider range of sea surface temperatures

(3) clouds associated with the periodic formation of an extratropical or tropical cyclone reduces the incoming solar radiation that reaches the surface and eliminates the heat low

(4) the more northerly position of the Polar Front (FWC/JTWC, 1978).

In the mid-latitude coastal areas the local meteorological conditions are controlled by the seasonal advance and retreat of the Polar Front, the boundary between continental polar and maritime tropical airmasses. The autumn transition from the summer to winter monsoon occurs rapidly. It involves a shift from light and variable southerly winds to stronger, steadier northerly winds as the mean position of the Polar Front migrates rapidly from near 40°N southward to 20-25°N (Figure 2-5).

The winter monsoon season dissipates as the Siberian high weakens during the spring, resulting in a northward migration of the Polar Front to its summer position and the establishment of the summer monsoon over the coastal waters of eastern Asia (Huh, 1982). This spring transition usually results in many vacillations between

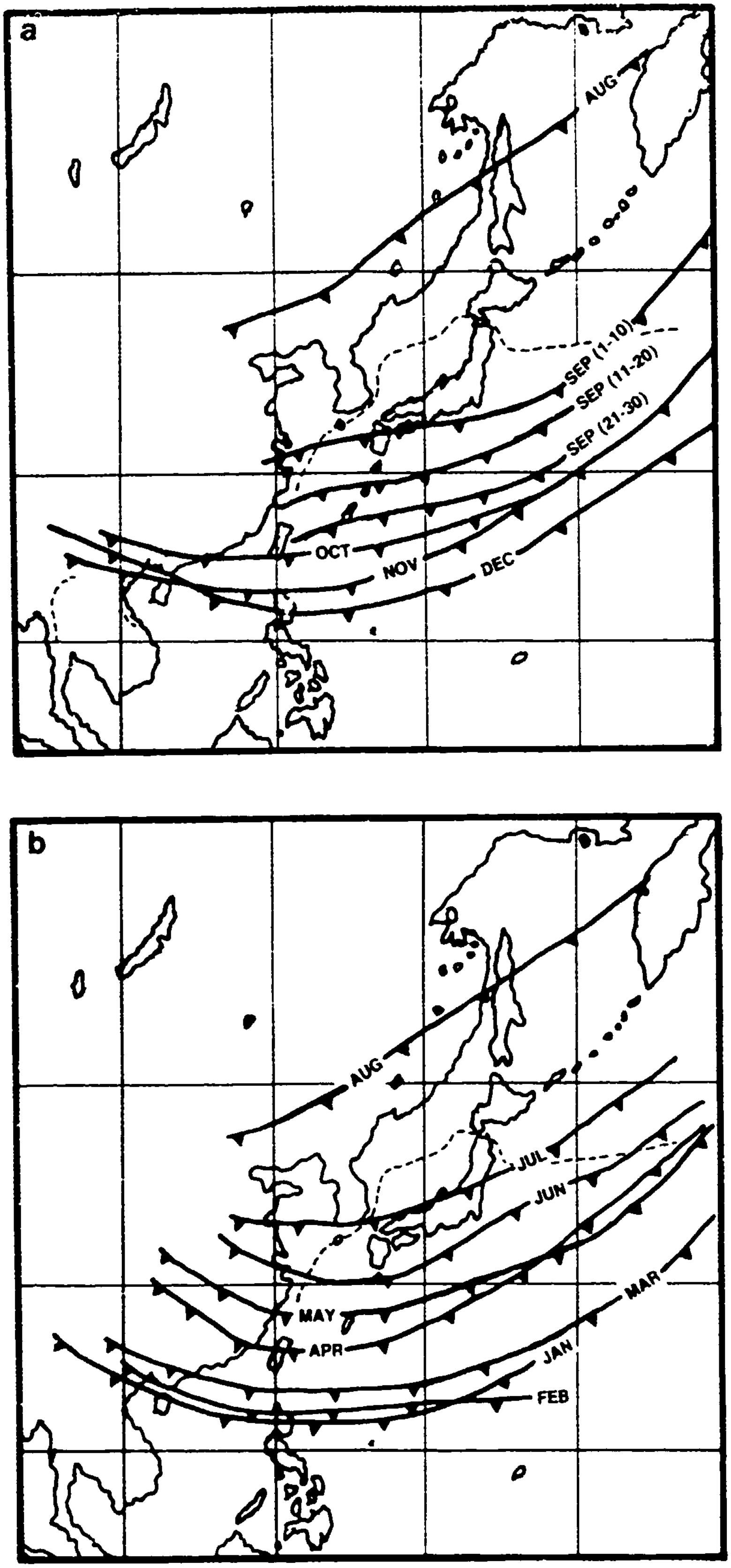

Figure 2-5. Seasonal migration of the primary polar front/polar trough system
(a) Summer to mid-winter seaward advance. (b) Spring to summer landward retreat
(Adapted from Huh (1982), with U.S. Air Force (1970) as original data source)

northeast and southwest flow in the mid-latitudes before the thermal low becomes firmly established over central Asia.

The transitions from one monsoon regime to the other occur during the traditional late spring, summer and early autumn months and, in some areas, cause such pronounced changes in the climate that the transition periods are treated as separate seasons. For example, the southern half of Japan experiences six distinct seasons plus a typhoon season that overlaps three of the other seasons. These seven seasons, as outlined by NOCD, Atsugi, (1980) and NOCF, Yokosuka, (1981) are:

(1) Winter - - - - - - - - - - December to mid-March

(2) Spring - - - - - - - - - - mid-March to mid-June

(3) Bai-U (wet season)
also called Mei-Yu
Plum Rain in China - - - mid-June to mid-July

(4) Summer - - - - - - - - - - mid-July to mid-September

(5) Typhoon - - - - - - - - - July, August, September

(6) Autumn Bai-U (Shurin)- - mid-September to mid-October

(7) Autumn - - - - - - - - - - mid-October through November

Korea, however, a country close to southern Japan, has four "traditional" seasons, but experiences a shortened autumn season and a longer winter season (U. S. Navy, 1965):

(1) Winter - - - - - - - - - - November through February

(2) Spring - - - - - - - - - - March through May

(3) Summer - - - - - - - - - - June through August

(4) Autumn - - - - - - - - - - September and October

2.2.1.2 Mei-Yu/Bai-U Spring Front of the Far East

The spring rainy season is a unique climatological feature. The circulation feature is known as the Mei-Yu front (plum rain) over China and Taiwan and as the Bai-U front in Japan. The front has a near stationary nature and occurs during the transition period between the Northeast Monsoon in the winter and the Southwest Monsoon in the summer. The front initially develops in mid to late May over southern China and Taiwan in response to the westward extension of the subtropical Pacific high. The duration of the rainy season is about one month over the southern areas and increases to about two months over central China and southern Japan. The nature of the precipitation is continuous or intermittent light rain mixed with frequent heavier rainshowers or thunderstorms. The entire cloud band and rainy area moves slowly northward throughout June and July and may influence areas of northern China and Japan until well into August. However, as pointed out by Kuo and Anthes (1982), the front tends to move back and forth, thus creating a difficult short-term forecasting problem.

The Mei-Yu/Bai-U front is a subtropical front and therefore has different characteristics than a Polar Front. The Mei-Yu/Bai-U front is characterized by a narrow steady precipitation zone, strong gradient of equivalent potential temperature, thick moist neutral layer, and a steady generation of convective instability (Ninomiya, 1984). However, model studies (Kuo and Anthes, 1982) as well as empirical studies by various far-east investigators indicate that the eastern section of the front (east of about 135°E) is similar to a mid latitude cold front while the western section (west of about 130°E) resembles a semi-tropical system. The Mei-Yu/Bai-U front is a relatively shallow feature and develops only in the lower troposphere, unlike the mid latitude fronts which typically have a supporting trough that extends to the upper troposphere.

The structure of the Mei-Yu/Bai-U front is marked by a significant low level jet (LLJ) which exhibits ageostrophic flow in the near surface to 600 mb layer. The winds are generally 20% to 50% stronger than indicated geostrophic winds. The LLJ maximums are located near the 700 mb level and are typically found about 180 n mi southeast of the areas of most active convection (Ushijima, 1968).

The circulation pattern of the frontal structure is composed of weak mesoscale cyclones with embedded clusters of convective cells. In the vicinity of Taiwan, the mesoscale disturbances have a periodicity on the order of 17 to 20 hours, a wavelength of about 180 n mi, and a phase speed of near 10 kt. The embedded convective clusters have periods of about 3 to 7 hours, wavelengths of 35 to 100 n mi, and speeds of 12 to 15 kt. In the vicinity of southern Japan, the wavelengths of the mesoscale features are on the order of 600 n mi or less, while the phase speeds increase to 30 to 40 kt (Chen and Tsay, 1978). The periodicity of the mesoscale remains near 20 hours (Matsumato et al, 1970) while the mesoscale disturbances are characterized by cyclonic circulation that show little tendency to deepen as they move eastward (Matsumato and Tsuneoka, 1970). Deepening is likely to occur if the Mei-Yu/Bai-U front is interacting with a mid latitude upper level trough east of about 135°E.

The Mei-Yu/Bai-U cloud band has different characteristics in its northern and southern portions. In the northern portion, low and/or middle clouds generally prevail while in the southern portion well organized cumulonimbus clusters are found, especially to the west of 130°E (Chen, 1980). The northern portion of the frontal zone is marked by a dry area with light winds in the mid troposphere (500 mb) and above.

2.2.1.3 Migratory Lows

Seasonal meteorological conditions affect the likelihood of cyclogenesis and cyclone trajectory cycle. Most discussions of migratory lows in the Far East identify six basic types, based on the location of their formation and/or track. Figure 2-6 depicts the tracks of the six types. The following descriptions are taken from the Area of Responsibility Forecasters Handbook, by NOCD, Atsugi, (1980).

The "northern lows" (Types A, B and C) generally form in northern China or southern USSR and move from their source region into the Sea of Okhotsk or into the northern Pacific. They are all formed by movement of short-wave troughs through the low pressure source region, and all are enhanced by downslope adiabatic warming as the systems traverse from their mountainous source regions to the Sea of Japan. Northern lows include:

Type A - Manchurian Low. Maximum occurrence is during the autumn and spring. The system generally tracks over Sakhalin Island and into the Sea of Okhotsk.

Type B - Lake Baikal Low. Maximum occurrence is during spring, but may occur throughout the year. The track is somewhat south of the Manchurian Low, moving instead over the Sea of Japan and northern Japan. Average speed of movement is 22 kt.

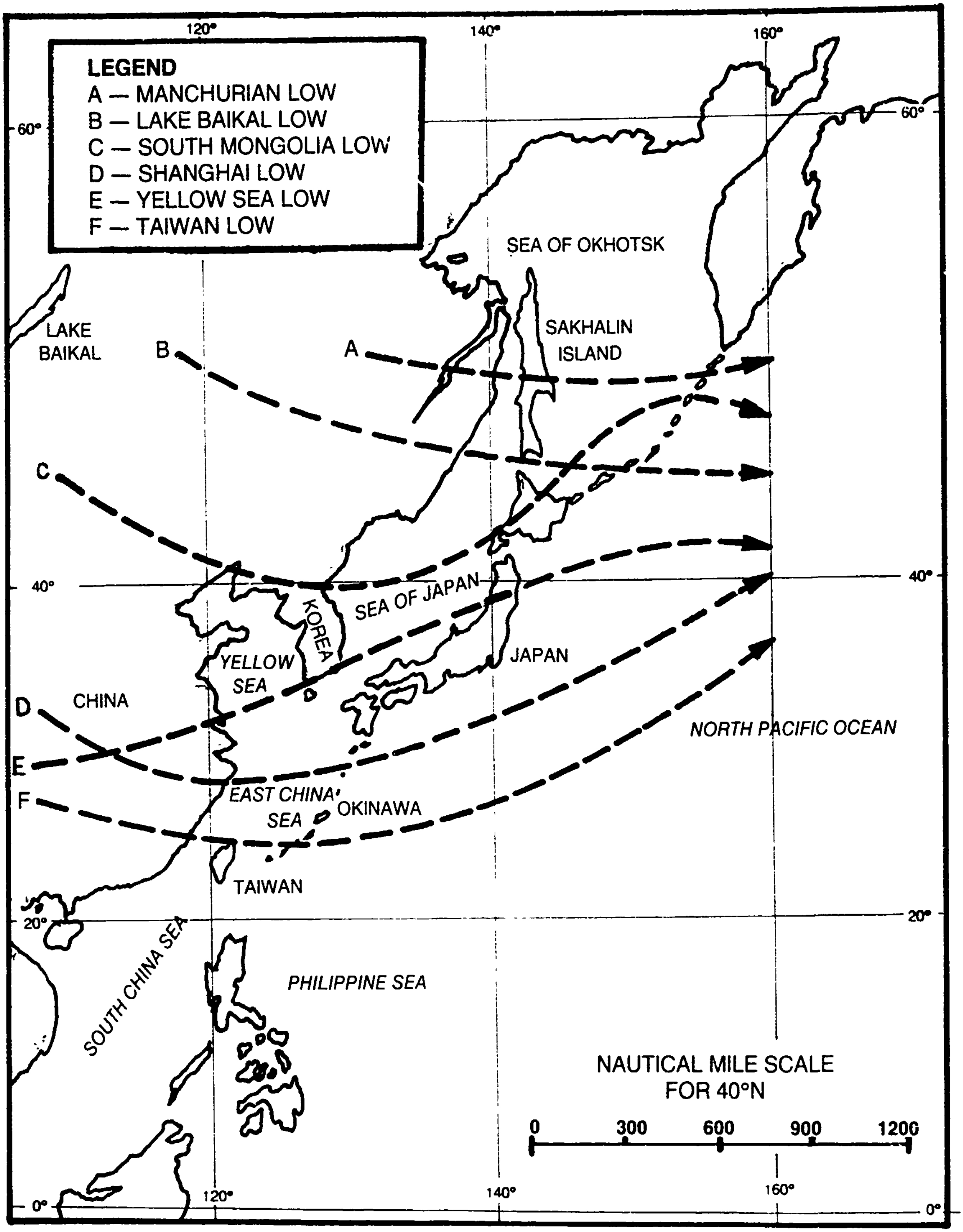

Figure 2-6. Storm tracks (adapted from Naval Oceanography Command Detachment, Atsgui, Japan, 1980).

Type C - <u>South Mongolia Low</u>. South Mongolia lows can occur during any season. The track is more southerly than the two previously discussed, and may generate a Yellow Sea Low (Type E) as it passes through that region. Its trajectory is normally over the Yellow Sea, Korea, the Sea of Japan, northern Japan, and into the southern Sea of Okhotsk with a mean speed of about 20 kt.

The "southern lows" (Types D, E, and F) generally form over central and southern China, then track over the Yellow Sea, Sea of Japan, and northern Japan, or track over the East China Sea and remain south of Japan. They occur year-round and produce widespread precipitation, low ceilings, poor visibility and occasional thunderstorms or high winds. There are three major systems in the southern group.

Type D - <u>Shanghai Low</u>. Also called the Hwang Ho Low, this system occurs most frequently during spring. Similar to the "Hatteras Low" of the United States' east coast, it is notorious for rapid intensification as it moves over the warm waters of the Kuroshio Current. Moving from its source region over central China, it tracks east to northeast at a mean speed of about 18 kt, and then eastward between the Japanese islands of Kyushu and Okinawa. This low is generated by a deepening of the China thermal low. If the thermal low is deepened by a short-wave trough moving north of the Himalaya Mountains, a central pressure of less than 1012 mb will generate a Shanghai Low. If the low is deepened by a short-wave trough moving from the south of the Himalayas, a central pressure of less than 1000 mb will generate a Shanghai Low. An empirical rule states that when a low is generated over China and passes 120°E south of 30°N, it will be a Shanghai Low and should pass south of the Japanese island of Honshu.

. Type E - Yellow Sea Low. Sometimes referred to as a Central Basin Low. Primarily a summer and autumn phenomena, Yellow Sea Lows move from their source region at a mean speed of 21 kt and track over South Korea into the Sea of Japan. They frequently produce a secondary low south of the Japanese islands of Khushu or Shikoku 12 to 18 hours after entering the Yellow Sea.

Type F - Taiwan Low. Sometimes called Yangtze Lows. Taiwan Lows are initially generated over China near 25°N 100°E, and occur most frequently from autumn through spring. They track northeastward from the Taiwan/China coast region at a mean speed of 24 kt, and will always track south of Japan.

2.2.1.4 Cold Fronts

The majority of cold fronts approaching the eastern coast of Asia are the result of old, occluded fronts coming from Europe. Circumventing the Tibetan Plateau, they follow a southeastward and eastward track toward Korea and Japan, causing invasions of intensely cold air. The flow pattern at 500 mb through 200 mb influences the direction the cold air will follow, and the availability of moisture determines weather in terms of precipitation and clouds. The document Forecaster's Handbook Volume 1 (FWC/JTWC, 1969) theorizes that in the Far East there are basically three types of cold fronts with respect to origin and movement (Figure 2-7). It was also found that anticyclones will follow the same trajectories as the cold fronts.

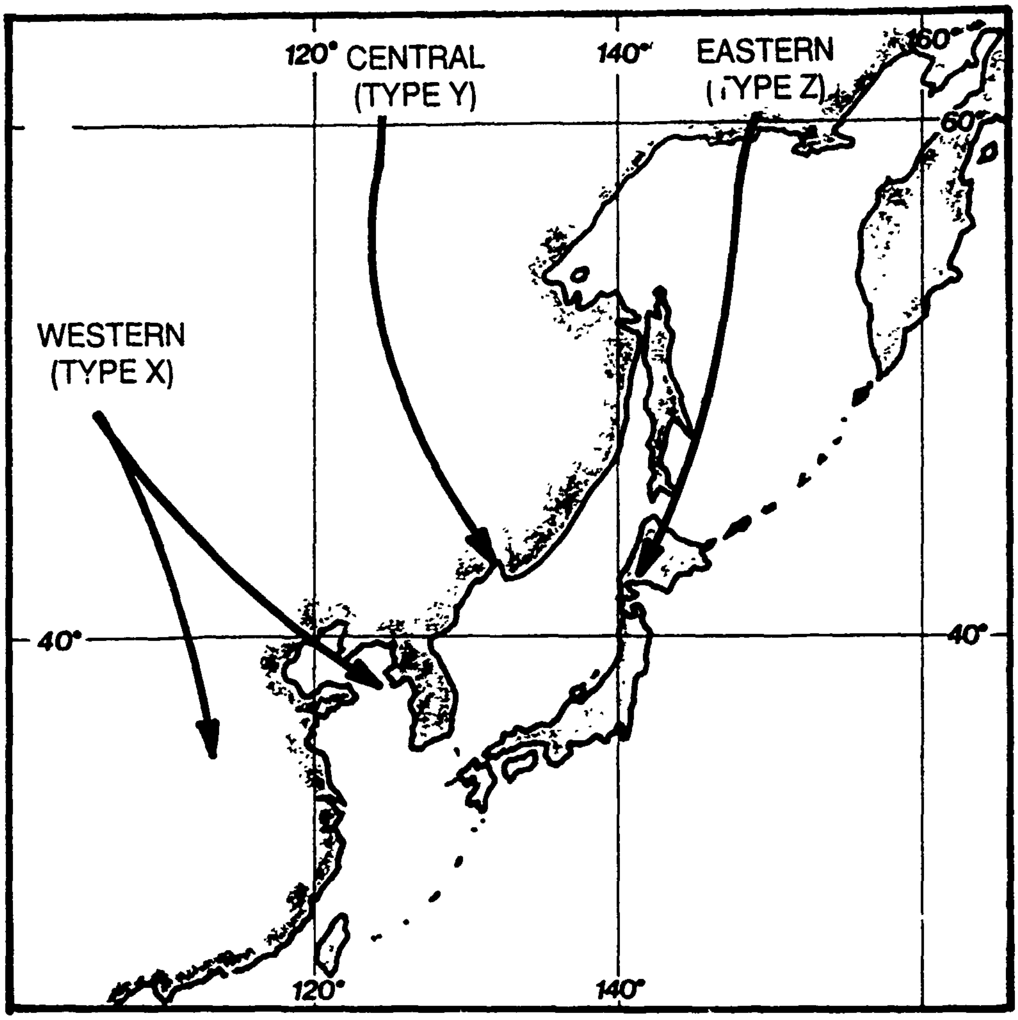

Figure 2-7. Tracks of cold fronts over Asia as categorized by Sjan-Zsi Li, adapted from Fleet Weather Central, Guam (1969).

The vertical extent of cold fronts is not believed to extend much above 6,500 ft (1,981 m). However, A. Lee in his study The Cold Waves of China, found that they may reach 10,000 ft (3,048 m) during a severe, cold outbreak.

Type X - Western Cold Front. Western cold fronts occur most frequently of the three types hypothesized, originating on the shores of the Arctic Ocean in the western USSR between 30°E and

90°E. They occur throughout the year and usually follow one of two trajectories. After leaving their source region, most Western fronts travel into north China, reaching the coast about 40°N. The other, less frequent, trajectory has the cold front moving southward as far as Indo-China. Western fronts are quite shallow and only in intermediate latitudes do they cause severe drops in temperature. Frontal precipitation is associated with them. Cyclogenesis along these fronts over the Shandong Peninsula in the western Yellow Sea will also cause widespread frontal weather. Western cold fronts are produced by relatively strong meridional flow at 500 mb with a long wave trough position over Korea.

Type Y - Central Cold Front. Central cold fronts occur frequently and are especially severe in northern and central China, Manchuria, Mongolia, Korea, and Japan. Originating in eastern Siberia between 100°E and 140°E at 55°N to 70°N, they have more vertical extent than the Western type, and are associated with very dry and cold air, resulting in pronounced drops in temperature. Central fronts are most often observed during mid-winter and are produced by strong meridional flow, or a block north of Mongolia and a long wave trough over Japan.

Type Z - Eastern Cold Front. Eastern cold fronts are formed from 140°E eastward between 55°N and 70°N and travel toward the south-southwest along the east coast of Siberia and into Korea. They do not occur as frequently Western and Central cold fronts and are primarily spring and summer phenomena, with a secondary frequency maximum in November.

2.2.1.5 Winter (mid-December to mid-March)

At the surface, Eastern Asia is under the influence of the Siberian high pressure cell which is resident in the Lake Baikal region of the USSR. This continental, cold high is at its maximum intensity in January and February. The Siberian high fluctuates in position and intensity in response to migratory mid-tropospheric disturbances and sends cold surges eastward from the Asian mainland. During winter, the oceanic, warm mid-Pacific high is at its weakest and has receded southeastward. The westward extension of this oceanic high is also weakened and shifted southeastward, resulting in an area of lower pressure between the two high pressure systems. The Polar Front lies between the two high pressure cells and is oriented east-west near 20°N over the waters adjacent to eastern Asia.

In the upper atmosphere, the jet stream is at its southernmost position and at its greatest strength in winter. A significant feature of the jet stream is that it splits as it passes the Tibetan Plateau in its eastward journey across western China. Murakami (1981) states that, based on a limited data study performed by Chinese scientists, during winter the low-level (below 500 mb) westerlies split into two branches (northern and southern) and flow around, rather than up and over, the high mountains of the Tibetan Plateau and that "a strong upper level (200-300 mb) jet stream flows along the southern periphery of the Tibetan Plateau...." The splitting effect is seen in Figure 2-8. The two branches of the jet stream then merge into a single flow over southwestern Japan.

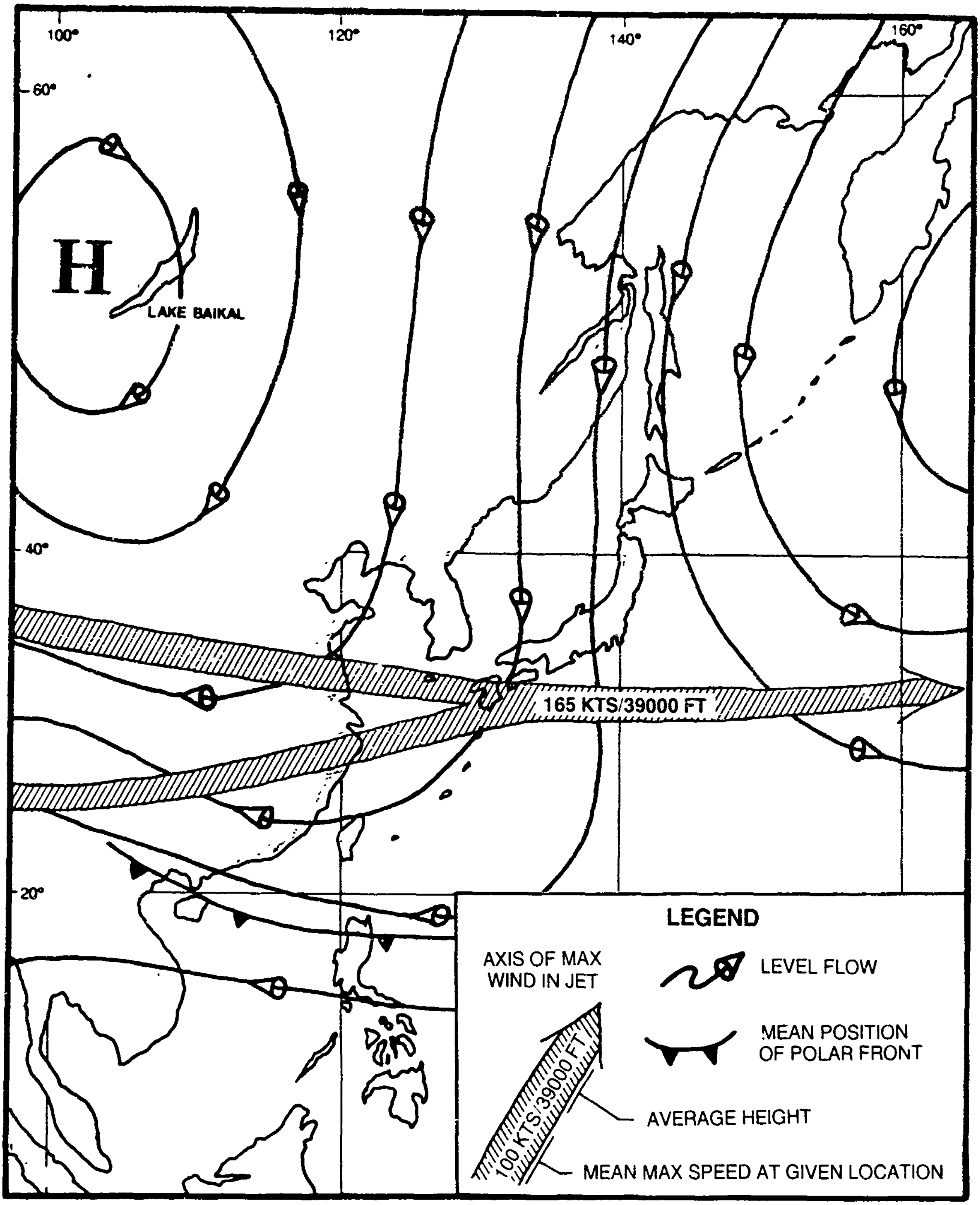

Figure 2-8. Typical atmospheric features during February: mean low level flow, mean position of polar front, and mean jet stream position (adapted from U S Marine Corps, 1967 and U S Air Force, 1968).

The Aleutian low is well established near 53N 170E and is at its strongest during the months of January and February. An area of low pressure, sometimes evident only as a trough, becomes a semi-permanent feature over the eastern Sea of Okhotsk during the winter and forms an anchor for a semi- permanent thermal trough that extends into the Sea of Japan. The thermally induced trough is a result of the temperature difference between the frigid air of the Asian landmass and the relatively warmer waters of the Sea of Japan.

The most probable winter migratory low pressure systems are Lake Baikal Lows, South Mongolia Lows, and Taiwan Lows. Records for the years 1951 and 1952 from Fleet Weather Facility, Yokosuka, Japan showed an average of about 57 cold fronts per year in the Far East. Of these, about 18 (32%) occurred during the winter (mid-December to mid-March) a frequency of about one every five days (FWC/JTWC,1969).

During the winter months, significant tropical cyclone activity is limited to the Philippine Sea and the western North Pacific Ocean south of about 20°N. Although tropical cyclones have been known to form during all months of the year, few form during winter, and of those that do, even fewer still reach typhoon strength. In the western Pacific approximately one typhoon per four years occurs in January and one per five years in February and March (Crutcher and Quayle, 1974). All of the storms of record during January and February have stayed well south of 30°N, with the primary track westward over the central Philippine Islands, or recurving northeastward and passing 140°E south of 20°N. Refer to Appendix B for tropical cyclone tracks.

Figures 2-9 through 2-21 depict various average climatic conditions that prevail over eastern Asia and adjacent waters during the month of February. A brief discussion of each of the parameters is presented in the climatology sections of the regional chapters in this handbook.

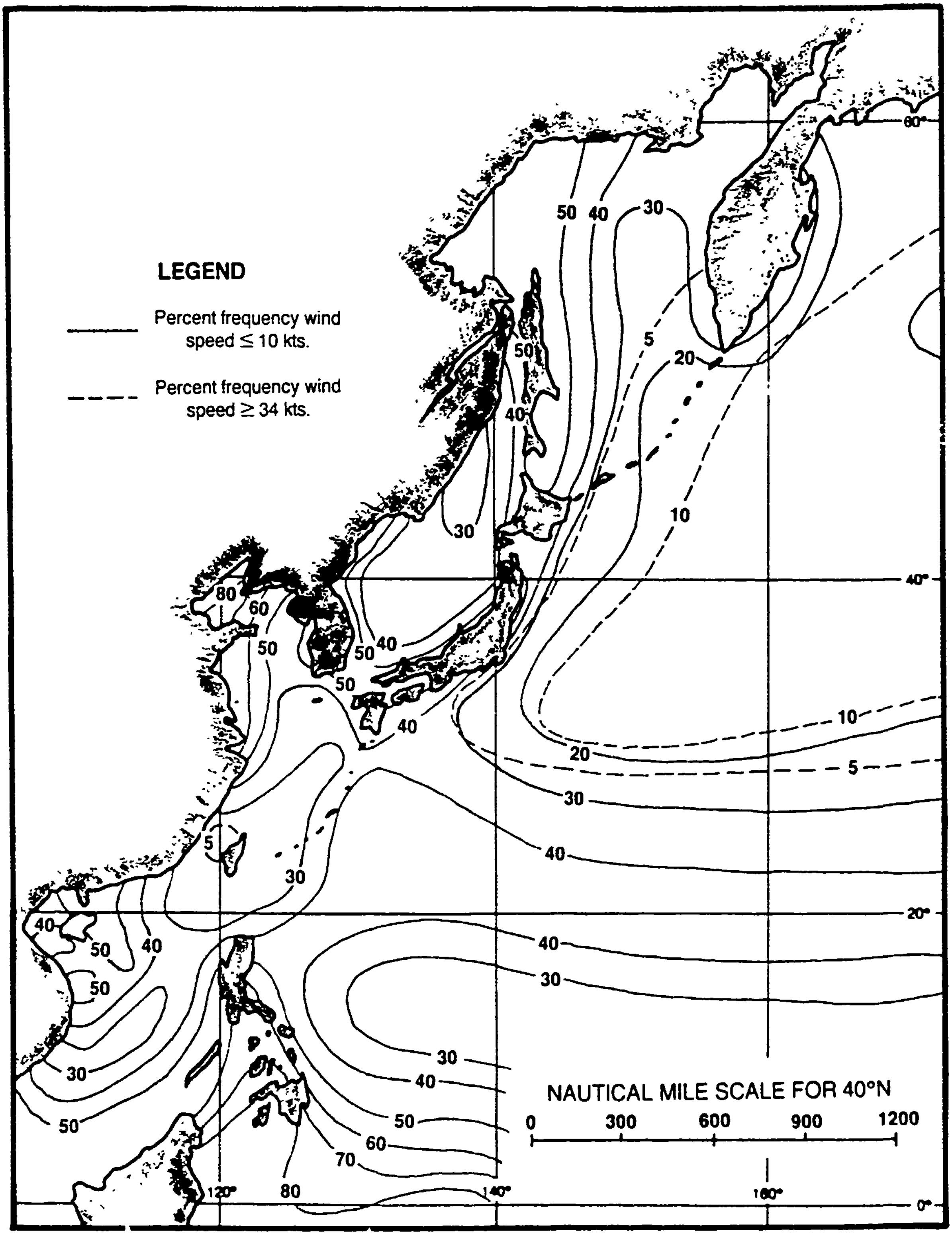

Figure 2-9. Surface winds during February (adapted from U S Navy, 1977).

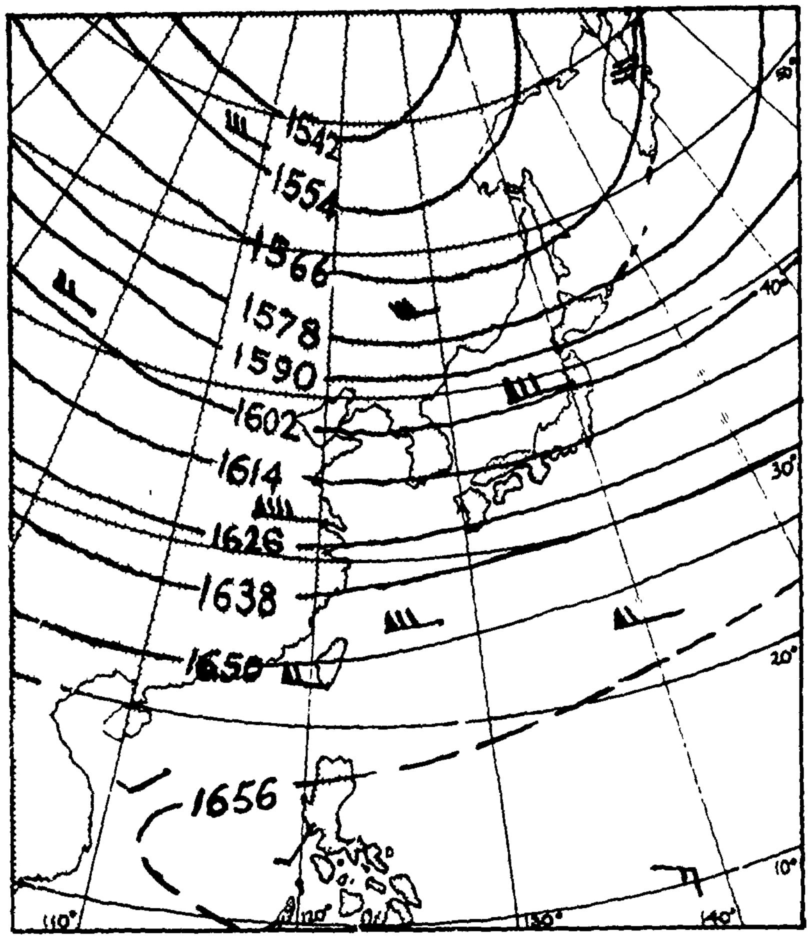

Figure 2-10. 100mb heights and winds for February. All heights in tens of gpm. (adapted from Crutcher & Meserve, 1970)

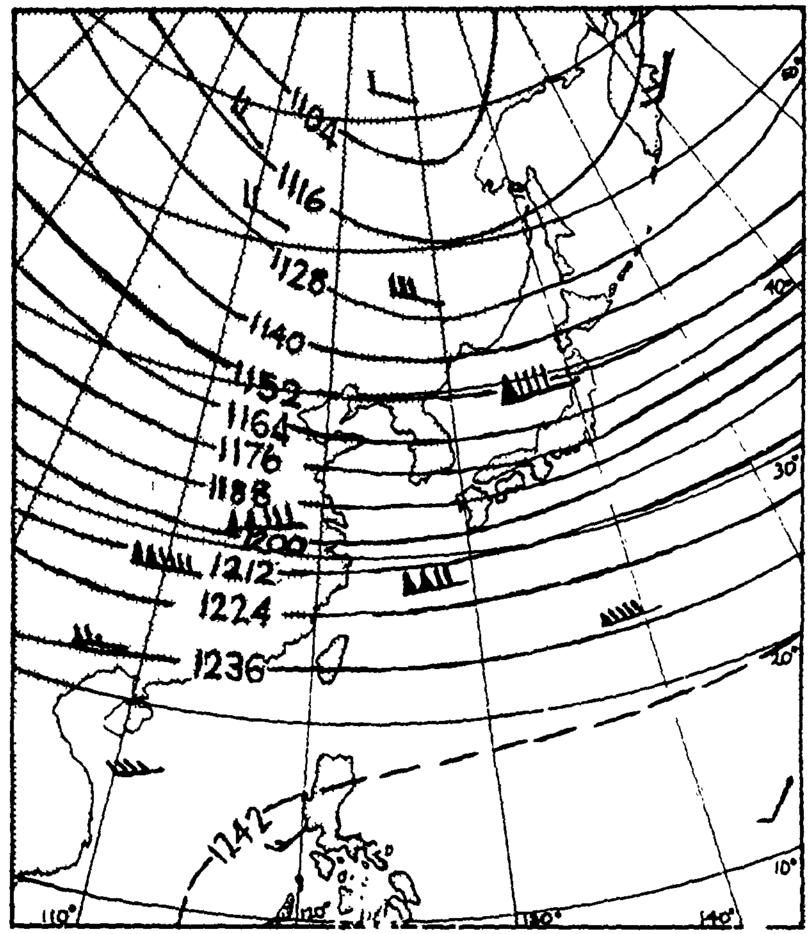

Figure 2-11 200mb heights and winds for February. All heights in tens of gpm (adapted from Crutcher & Meserve, 1970)

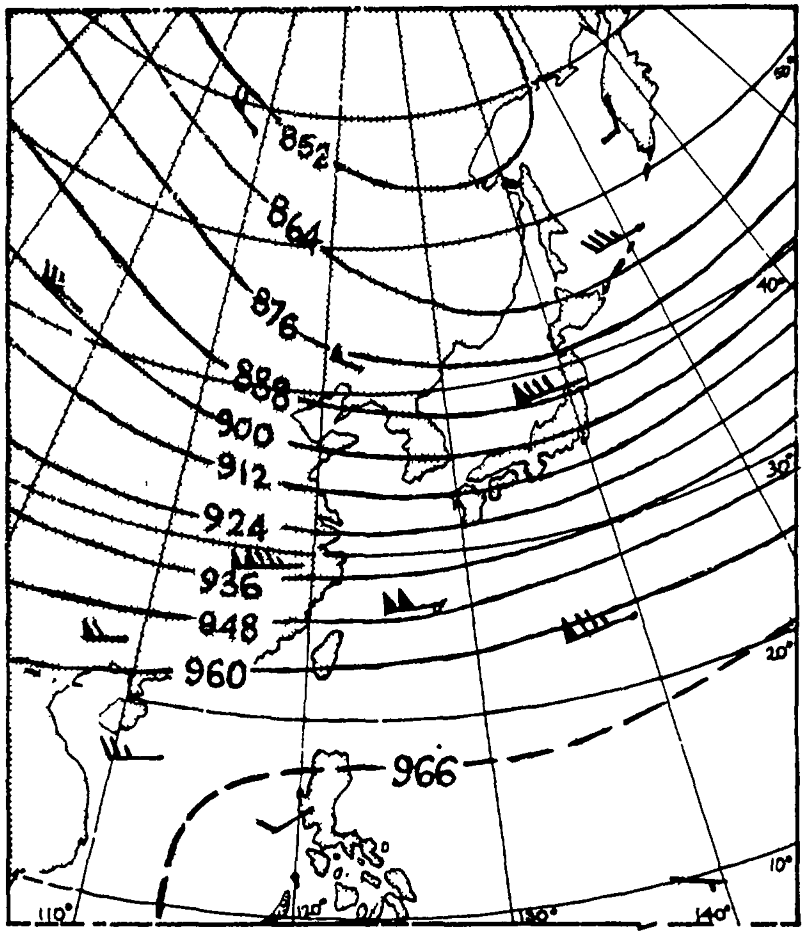

Figure 2-12 300mb heights and winds for February. All heights in tens of gpm. (adapted from Crutcher & Meserve, 1970)

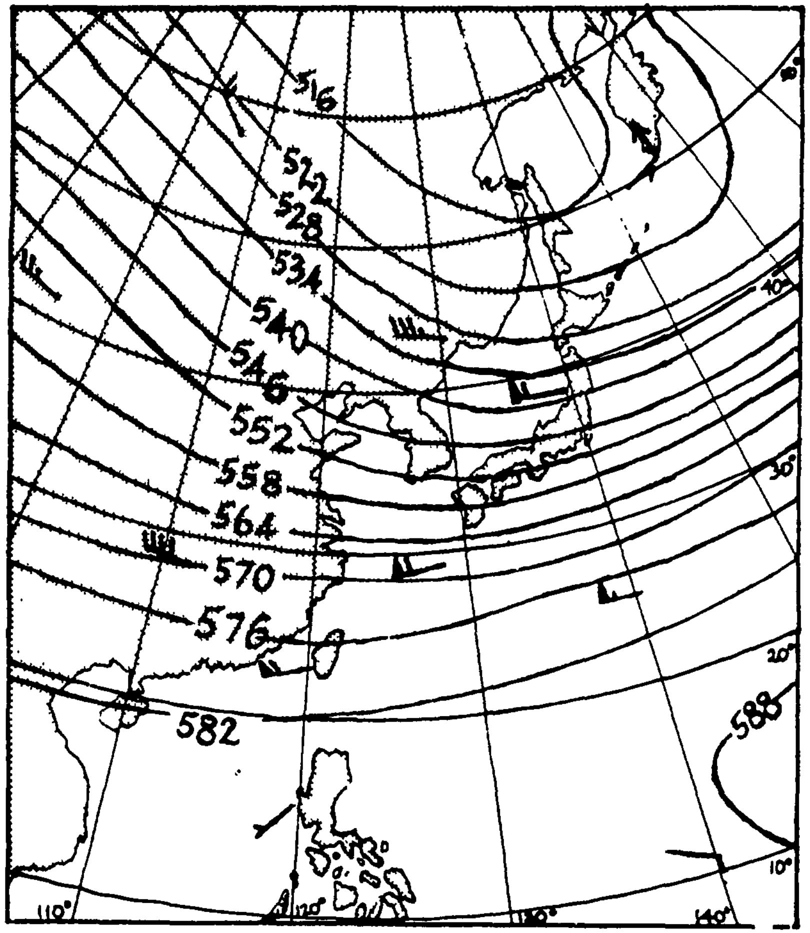

Figure 2-13 500mb heights and winds for February. All heights in tens of gpm (adapted from Crutcher & Meserve, 1970)

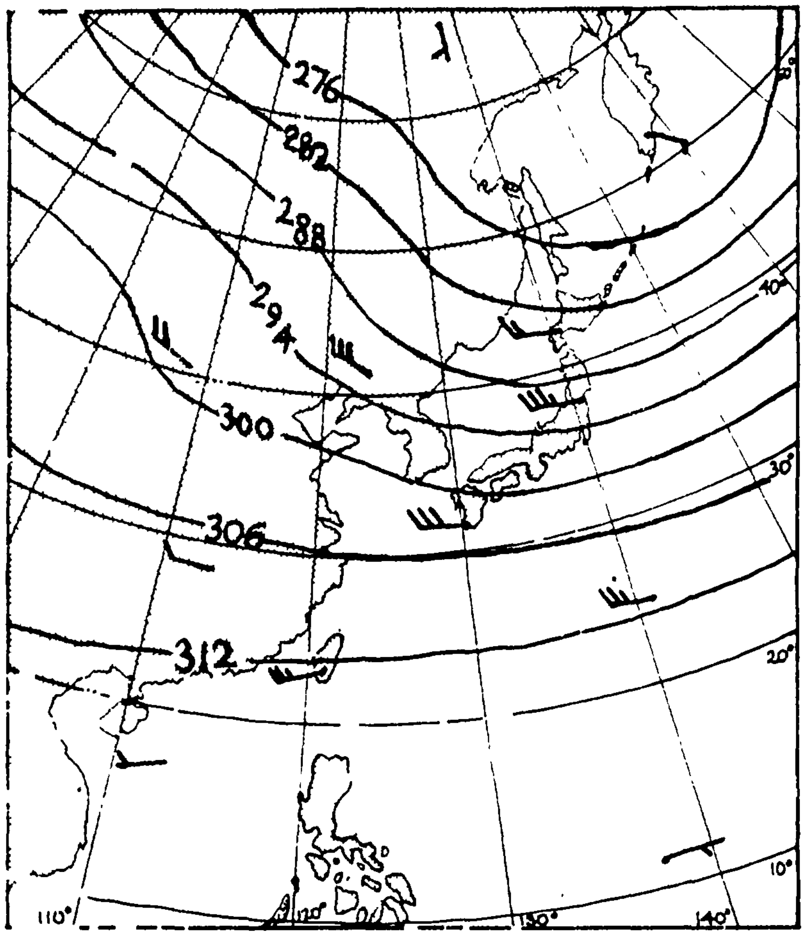

Figure 2-14. 700mb heights and winds for February. All heights in tens of gpm. (adapted from Crutcher & Meserve, 1970)

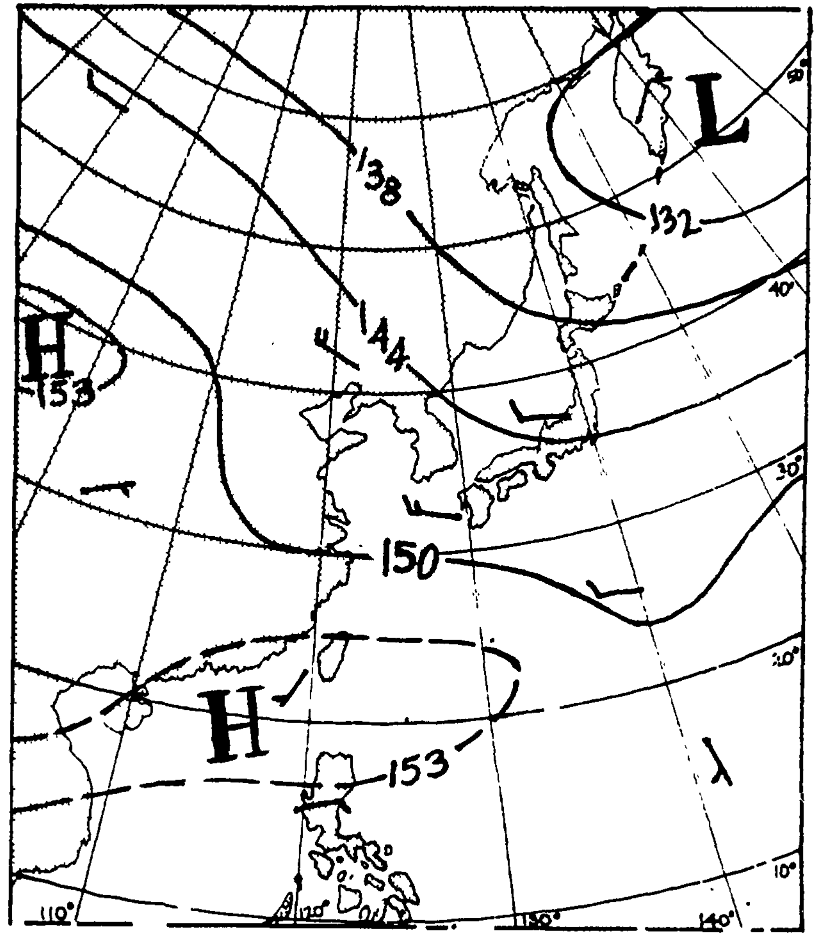

Figure 2-15 850mb heights and winds for February. All heights in tens of gpm. (adapted from Crutcher & Meserve, 1970)

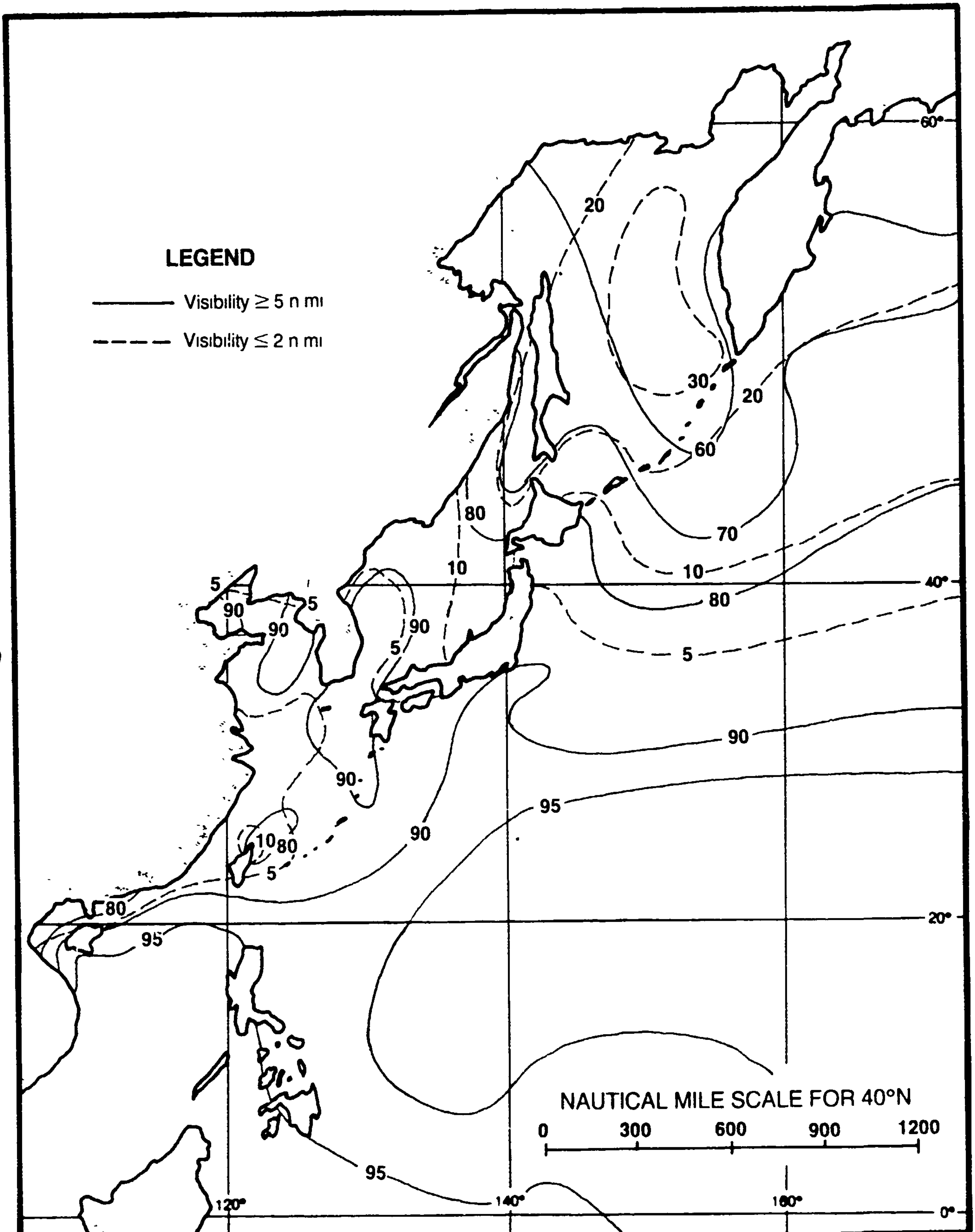

Figure 2-16. Percent frequency of occurrence of visibility limits during February (adapted from U S. Navy, 1977).

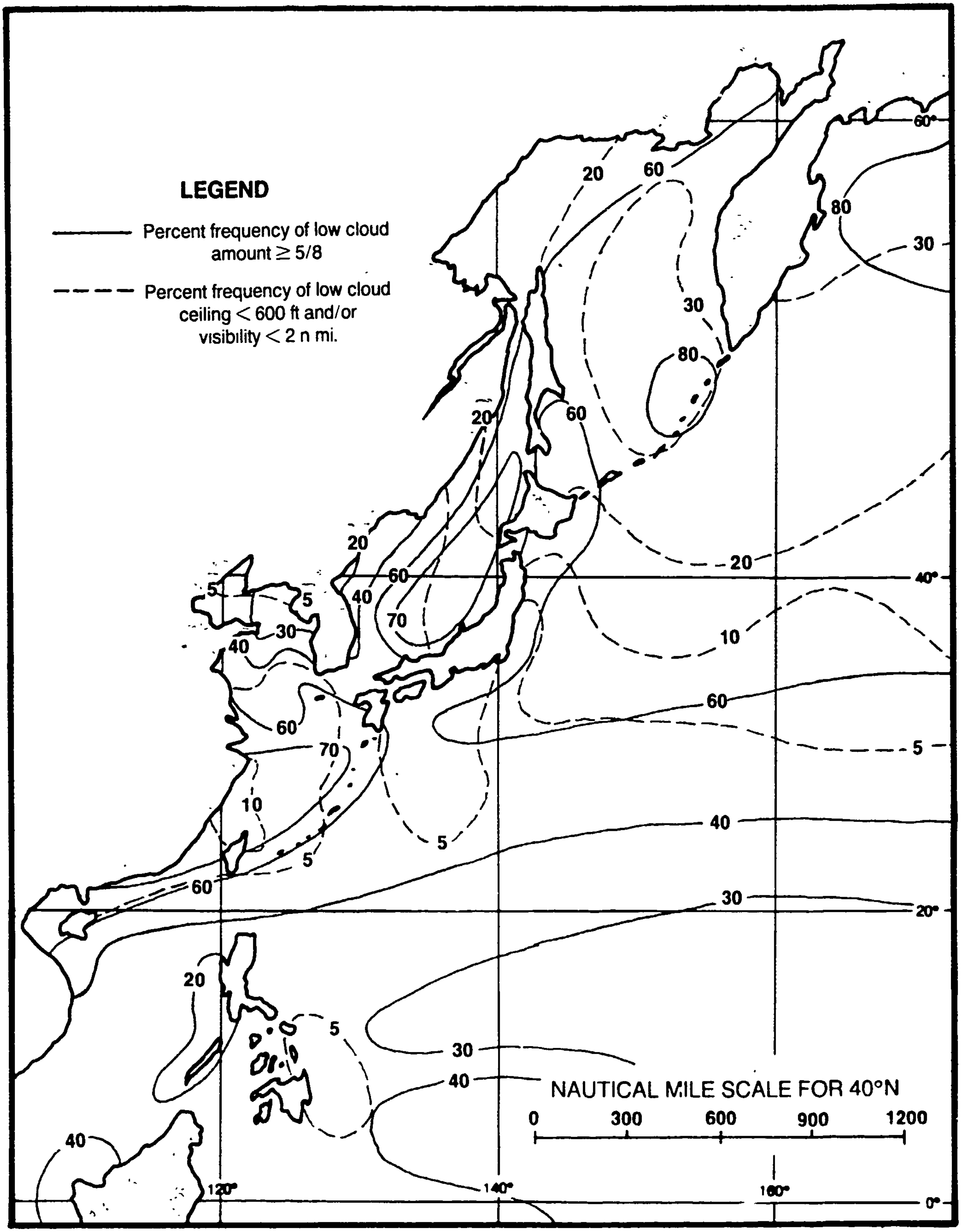

Figure 2-17. Low cloud amounts vs. ceiling and visibility during February (adapted from U.S. Navy, 1977).

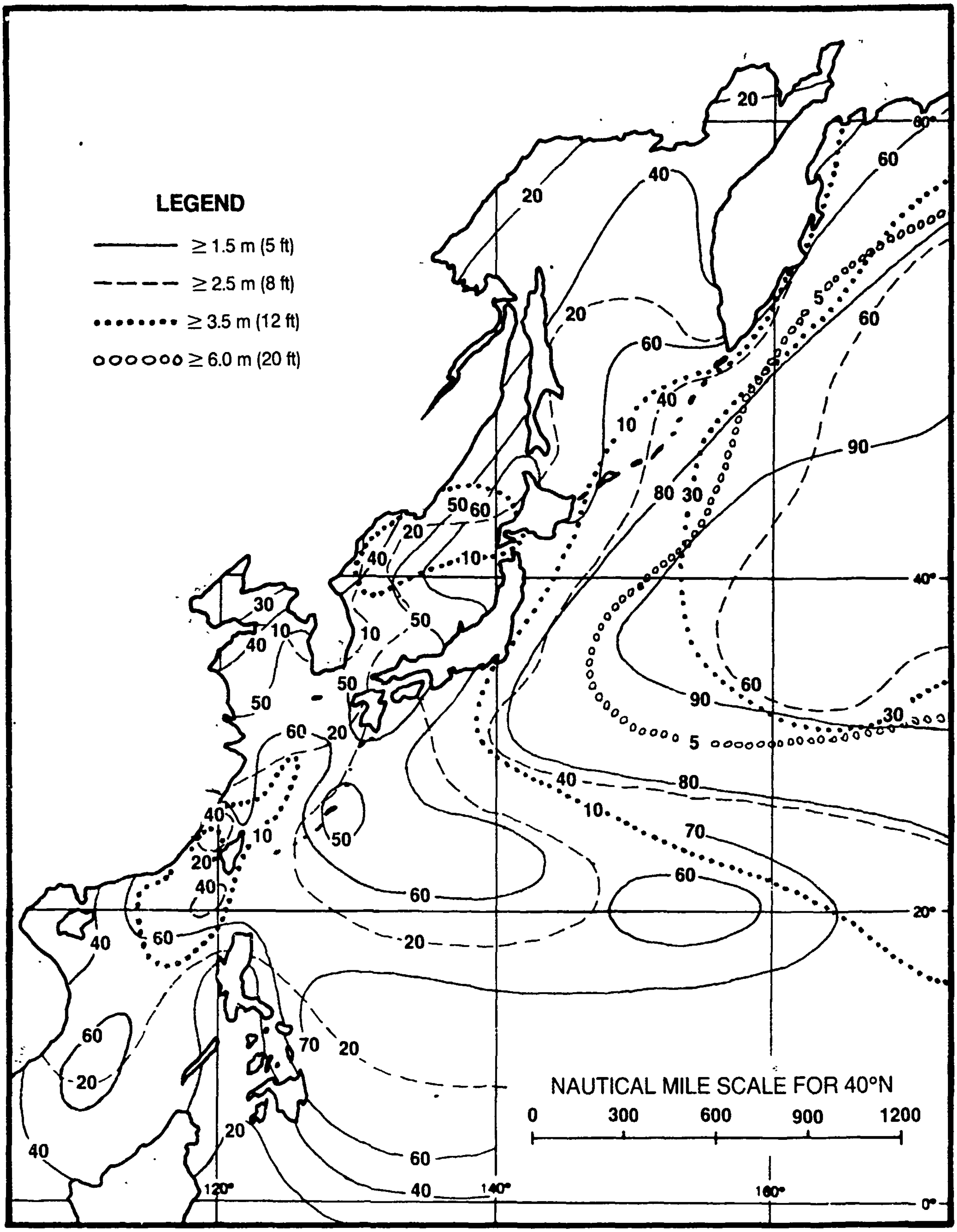

Figure 2-18. Percent frequency of occurrence of wave heights during February (adapted from U.S. Navy, 1977).

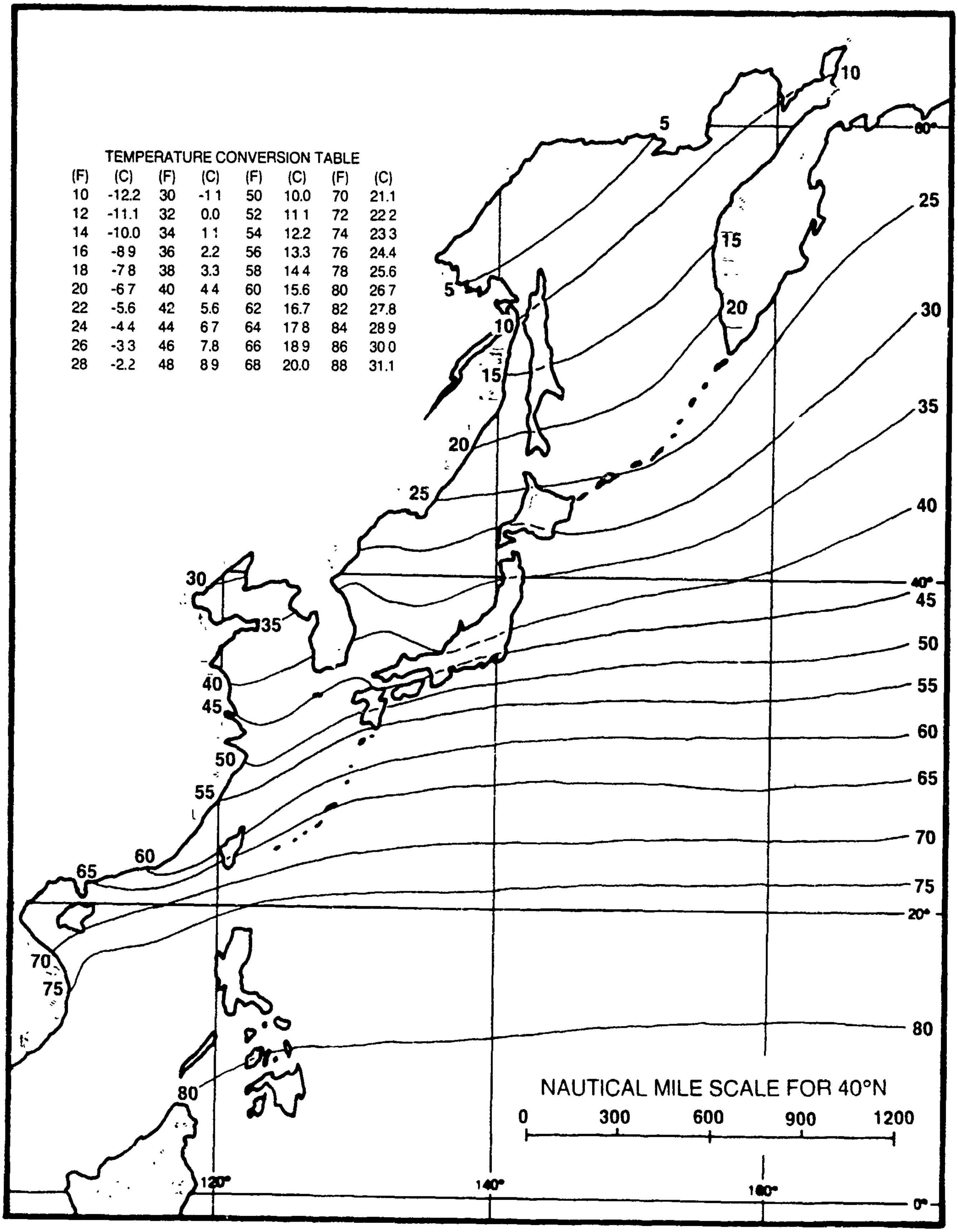

TEMPERATURE CONVERSION TABLE

(F)	(C)	(F)	(C)	(F)	(C)	(F)	(C)
10	-12.2	30	-1.1	50	10.0	70	21.1
12	-11.1	32	0.0	52	11.1	72	22.2
14	-10.0	34	1.1	54	12.2	74	23.3
16	-8.9	36	2.2	56	13.3	76	24.4
18	-7.8	38	3.3	58	14.4	78	25.6
20	-6.7	40	4.4	60	15.6	80	26.7
22	-5.6	42	5.6	62	16.7	82	27.8
24	-4.4	44	6.7	64	17.8	84	28.9
26	-3.3	46	7.8	66	18.9	86	30.0
28	-2.2	48	8.9	68	20.0	88	31.1

Figure 2-19. Mean surface air temperature in degrees Fahrenheit during February (adapted from Ownbey, 1973 and U.S Navy, 1977).

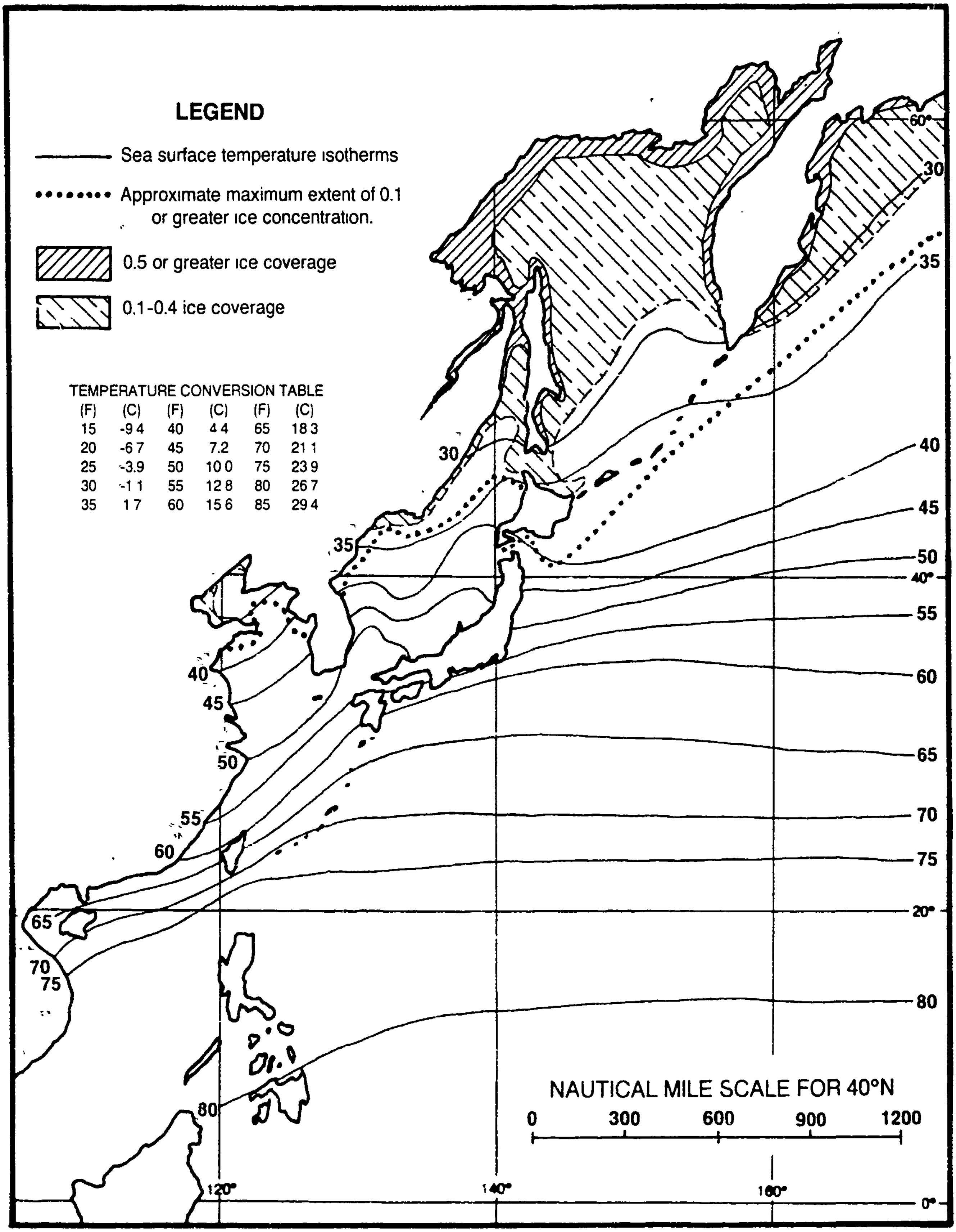

Figure 2-20. Mean sea surface temperature in degrees Fahrenheit during February, with approximate ice limits (adapted from U.S Navy, 1967 and U S. Navy. 1977)

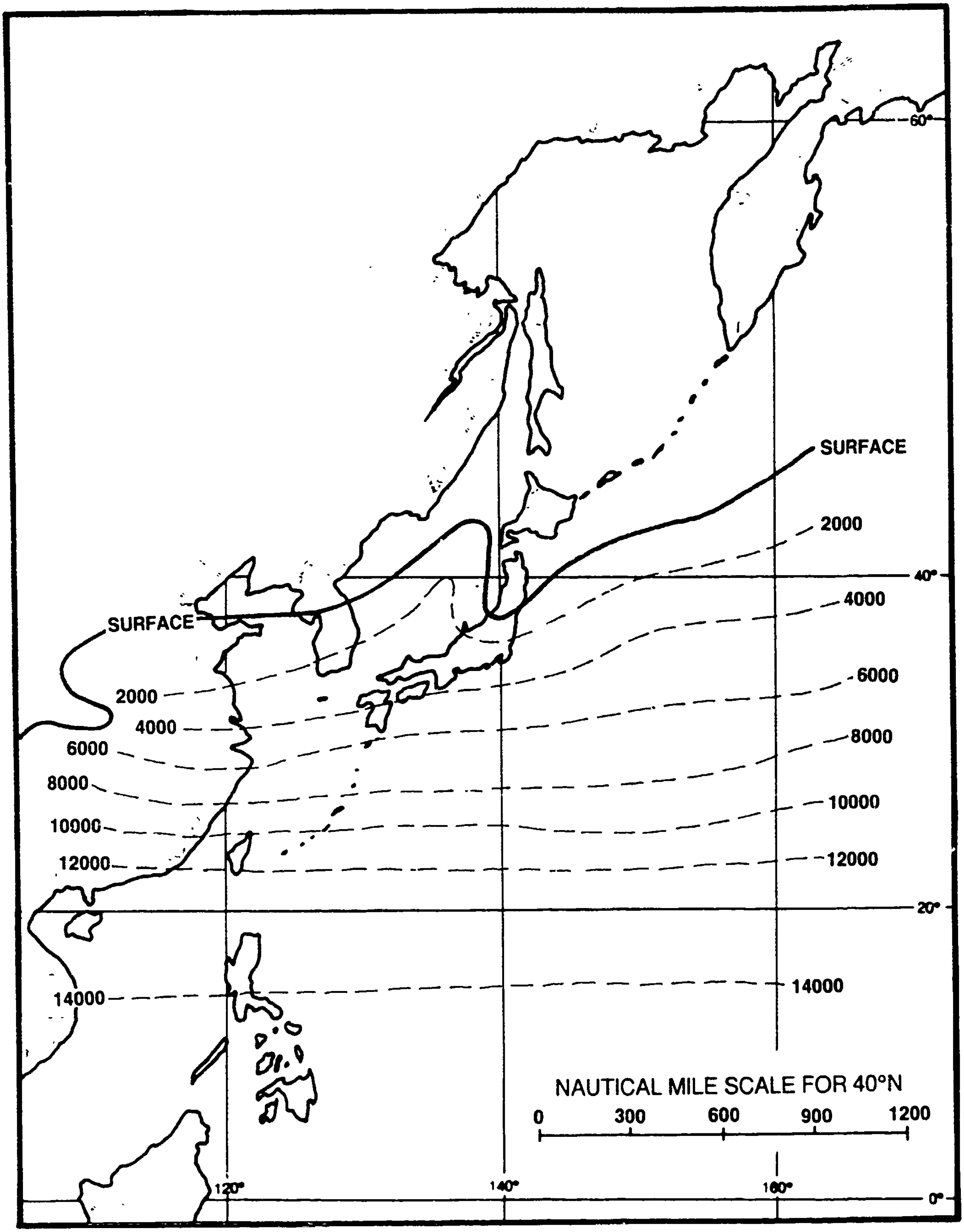

Figure 2-21. Mean altitude of the freezing level for February in feet (adapted from U.S. Air Force, 1965).

2.2.1.6 Spring (mid-March to mid-June)

The Siberian high weakens considerably and gradually shifts from the Lake Baikal position to near 45N 95E during spring. A low pressure area forms over Indochina and the low pressure center that is resident over the Sea of Okhotsk in winter retrogrades to a position over northern Mongolia. Thermal lows may begin to form over China and northeast Mongolia. As the Siberian high weakens, occasional "bubble highs" break off from the main high pressure cell and move eastward across the Sea of Japan. As the small high moves rapidly eastward it is usually followed by cyclogenesis and bad weather in the coastal Asian waters. As documented by George and Wolff (1953), "The reliability of this sequence of events leads directly to the adoption of the appearance of this surface bubble as the predictor for cyclogenesis and bad weather to follow."

The Aleutian low is still in evidence but, after April, is more diffuse and migratory in nature. The Polar Front starts to retreat northward, extending southwestward from the Aleutian low to a position south of Japan then westward across the Okinawa area and into China. Figure 2-22 shows the mean position of the front during May. It can be seen by comparing Figures 2-8 (page 2-29) and 2-22 that by May the jet stream has weakened and moved northward from its winter position. The north-south seasonal fluctuations of the Polar Front are directly tied to the movement of the southerly jet stream as it shifts from south of the Himalayan Plateau (winter position) to north of the plateau (summer position). Yoshino, (1965) shows

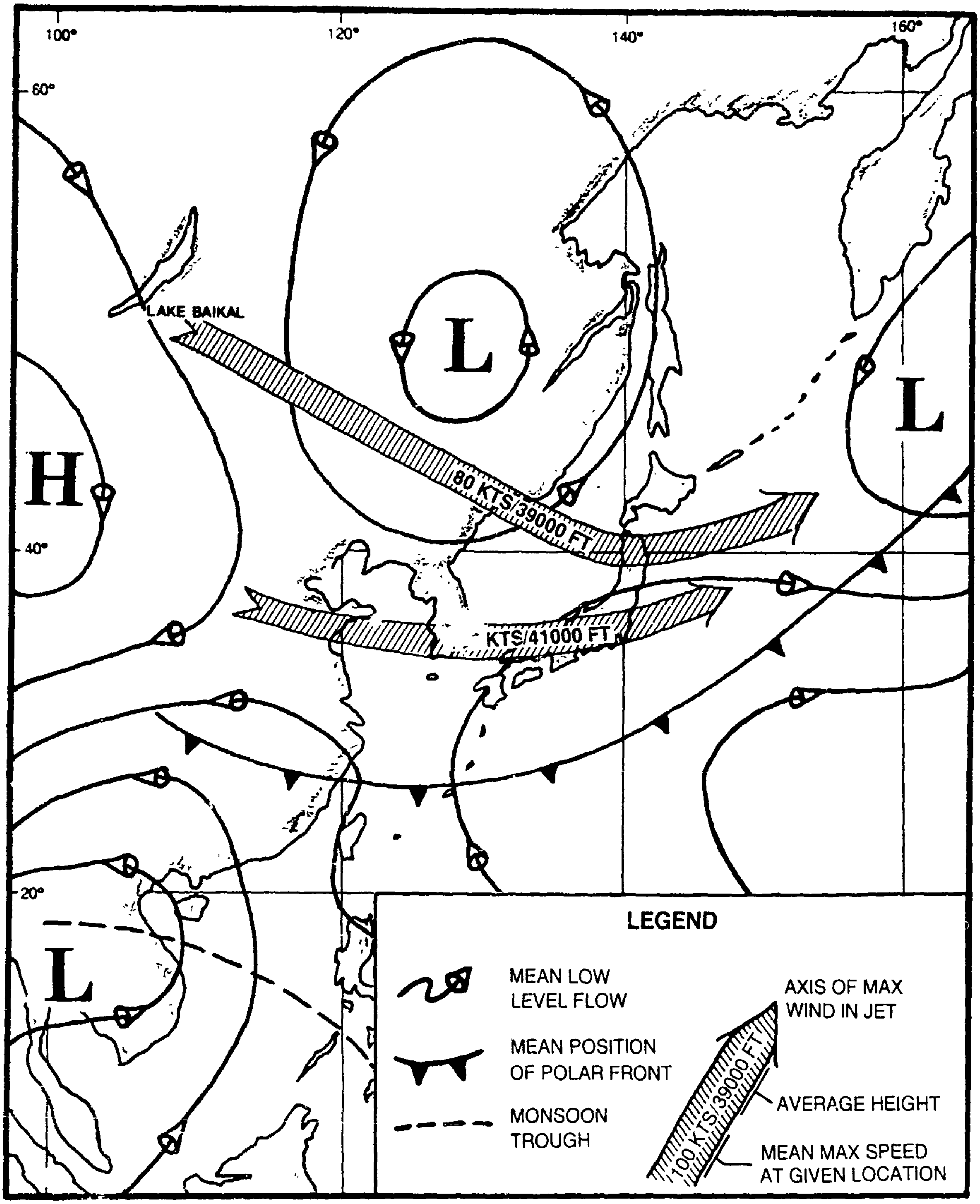

Figure 2-22. Typical atmospheric features during May: mean low level flow, mean position of polar front, mean position of monsoon trough and mean jet stream positon (adapted from U S. Marine Corps, 1967 and U S. Air Force, 1968)

the relationship of the latitude of the upper wind maximum to the beginning and end of the Bai-U season in Japan and the Mei-Yu season in the Yangtze (Changjiang) region of China, as the Polar Front moves northward in concert with the northward displacement of the upper wind maximums.

Figure 2-22 shows there are two mean jet stream cores. The southernmost core crosses the Yellow Sea, southern Korea and southern Honshu before proceeding east-northeastward across the Pacific Ocean. The northern core extends southeastward from Lake Baikal and crosses the northern tip of Honshu before moving eastward across the Pacific. Some studies show the two cores merging into a single core just east of Japan.

The most probable spring migratory low pressure systems include Manchurian Lows, Lake Baikal Lows, South Mongolia Lows, Shanghai Lows, and Taiwan Lows. The average tracks for each of the systems are presented in Figure 2-6 (page 2-23).

Of the yearly average of about 57 cold fronts occurring in the Far East, 14 (25%) occur during spring (mid-March to mid-June), a frequency of about one each six days (FWC/JTWC, 1969).

From a minimum in February, tropical cyclone activity starts to show a marked increase by June, although an average of only one typhoon can be expected to form in the western North Pacific during June. The northward limit of tropical cyclones during March and April (combined statistics) encompasses the East China Sea, extreme southern Sea of Japan, the western North Pacific Ocean south of 36°N, and the Philippine Sea. During June, the tracks start to show incursions across all of the water areas addressed in this handbook, except for the Sea of Okhotsk (Crutcher and Quayle, 1974). Refer to Appendix B for tropical cyclone tracks.

Figures 2-23 through 2-35 depict the average climatic conditions that prevail over eastern Asia and adjacent waters during the month of May. A brief discussion of each of the parameters is presented in the climatology sections of the regional chapters in this handbook.

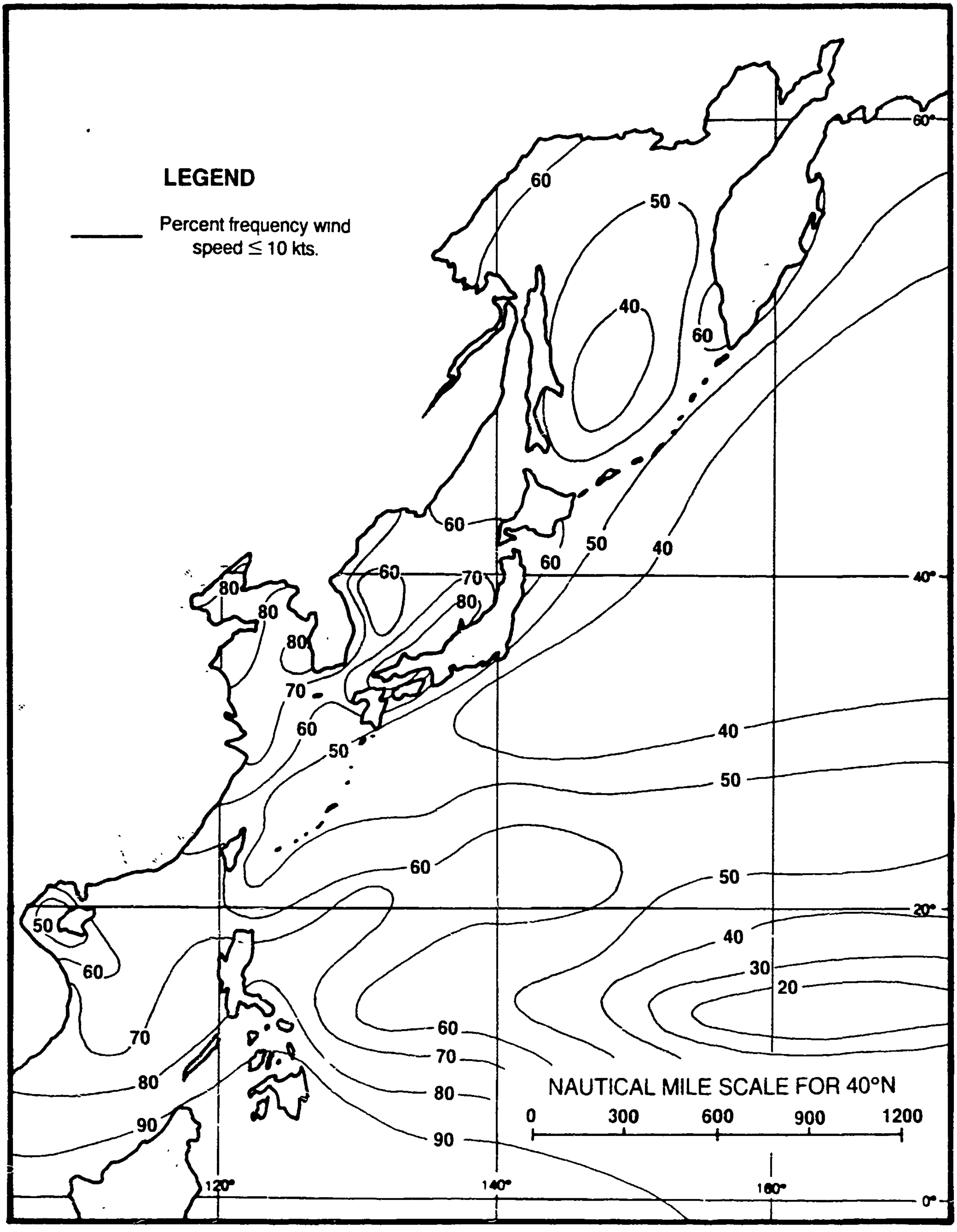

Figure 2-23. Surface winds during May (adapted from U.S Navy, 1977).

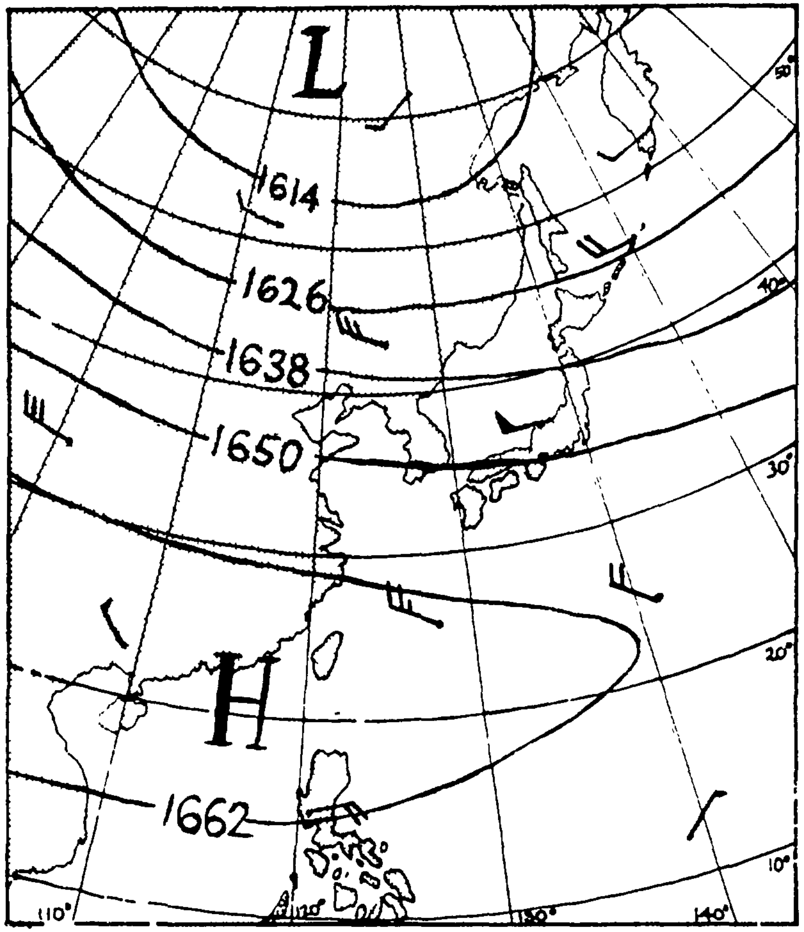

Figure 2-24 100mb heights and winds for May All heights in tens of gpm. (adapted from Crutcher & Meserve, 1970)

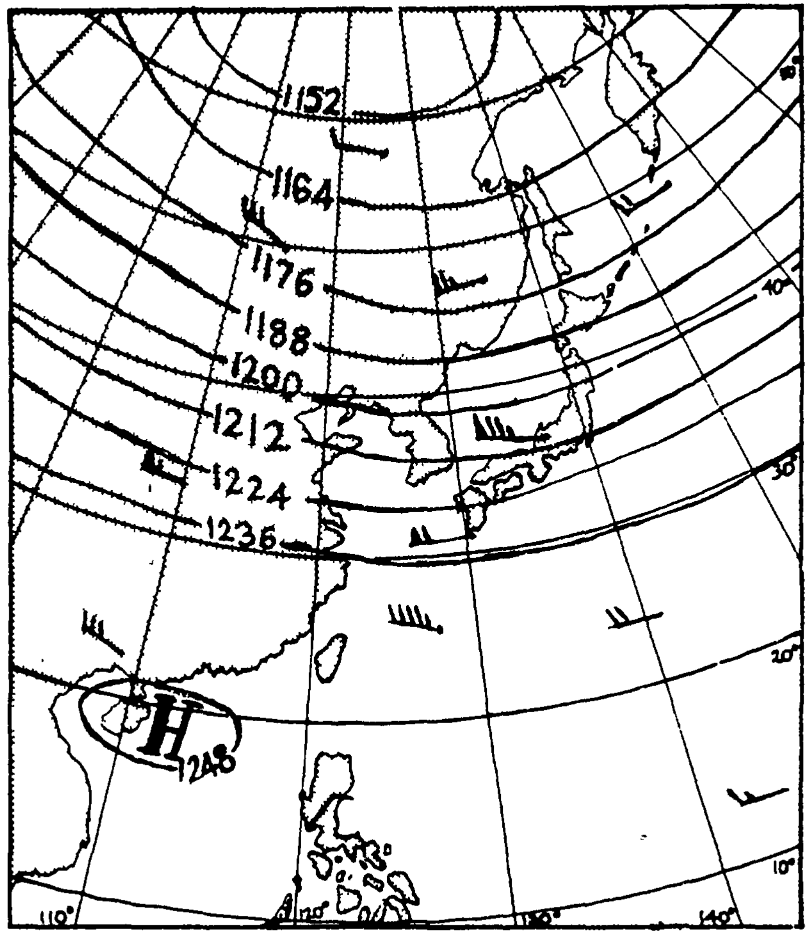

Figure 2-25 200mb heights and winds for May All heights in tens of gpm (adapted from Crutcher & Meserve, 1970)

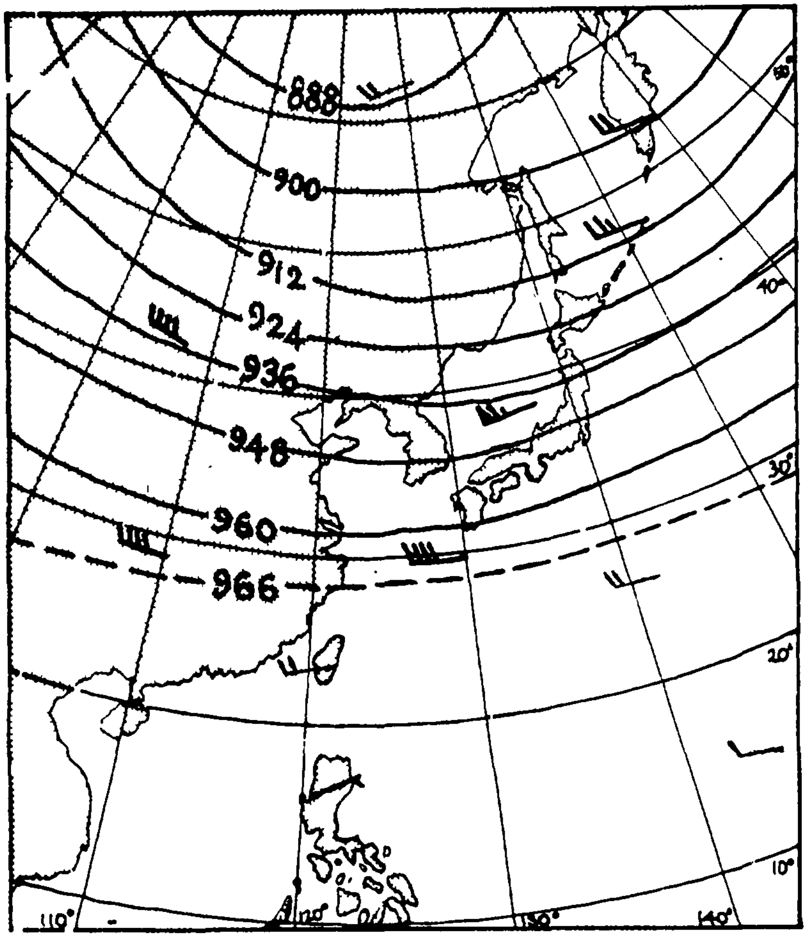

Figure 2-26 300mb heights and winds for May All heights in tens of gpm. (adapted from Crutcher & Meserve, 1970)

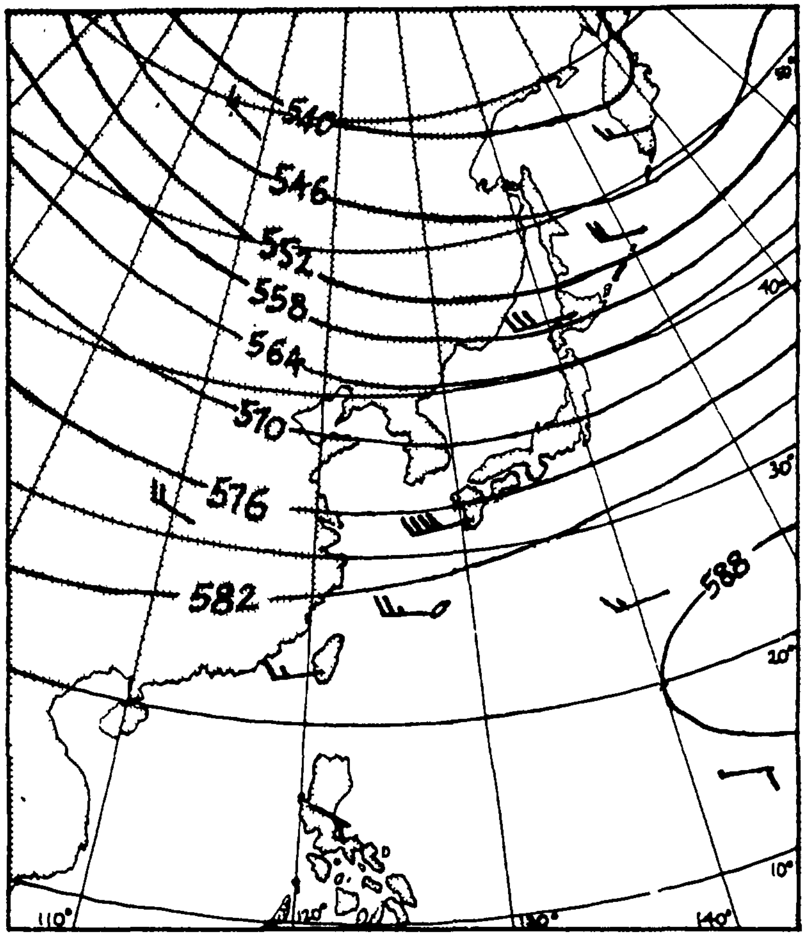

Figure 2-27 500mb heights and winds for May. All heights in tens of gpm (adapted from Crutcher & Meserve, 1970)

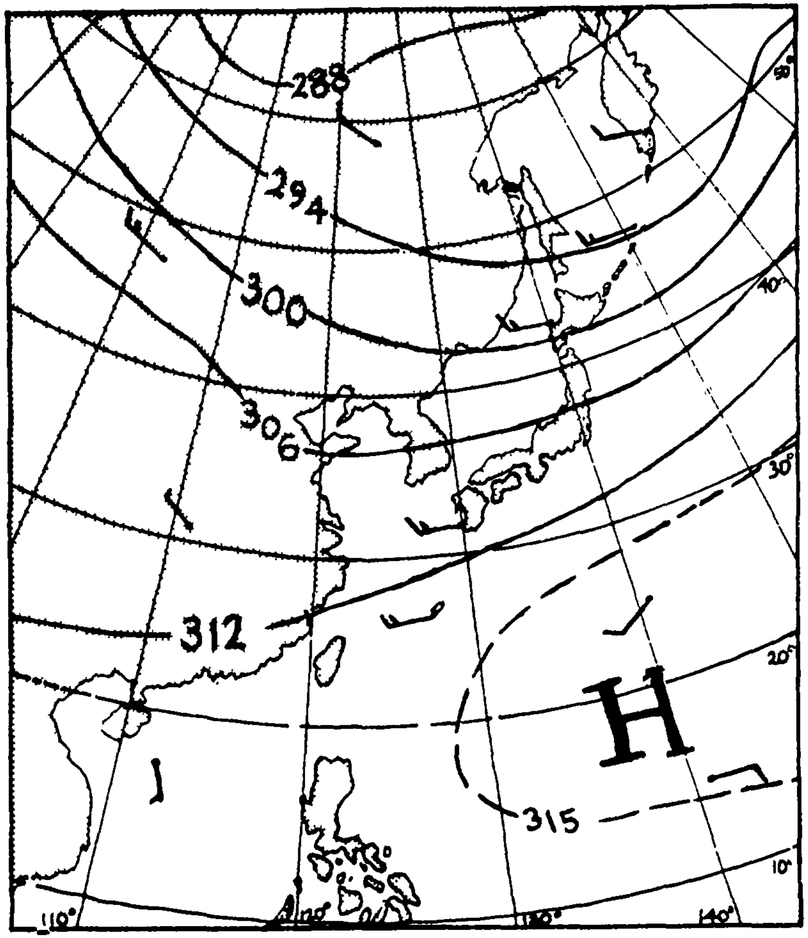

Figure 2-28. 700mb heights and winds for May. All heights in tens of gpm. (adapted from Crutcher & Meserve, 1970)

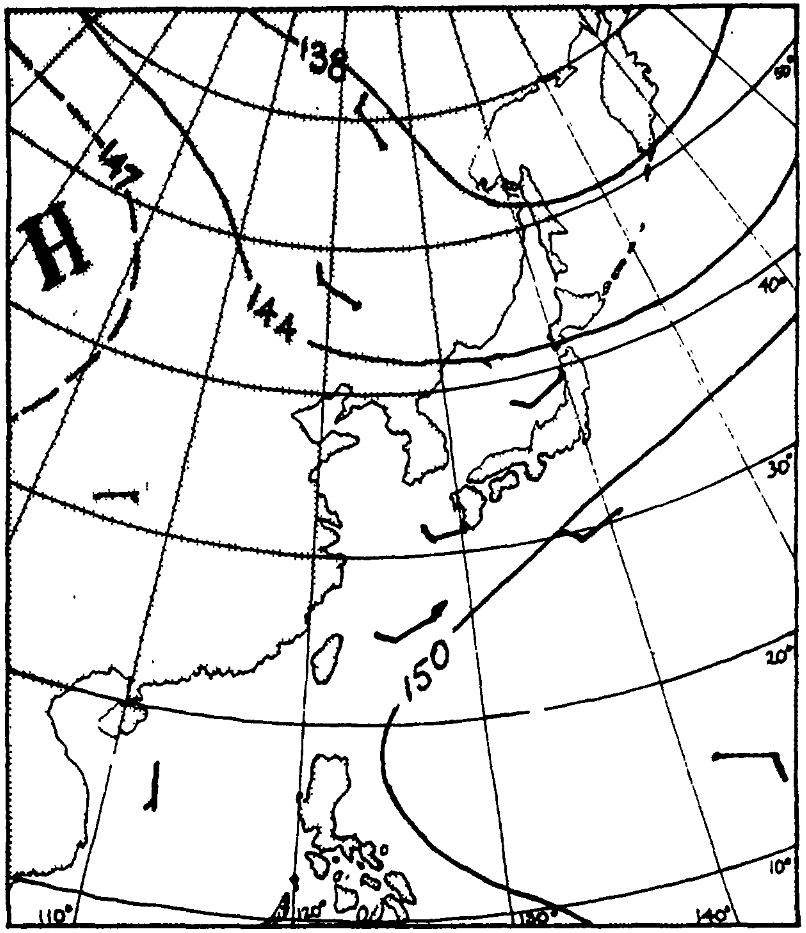

Figure 2-29. 850mb heights and winds for May. All heights in tens of gpm. (adapted from Crutcher & Meserve, 1970)

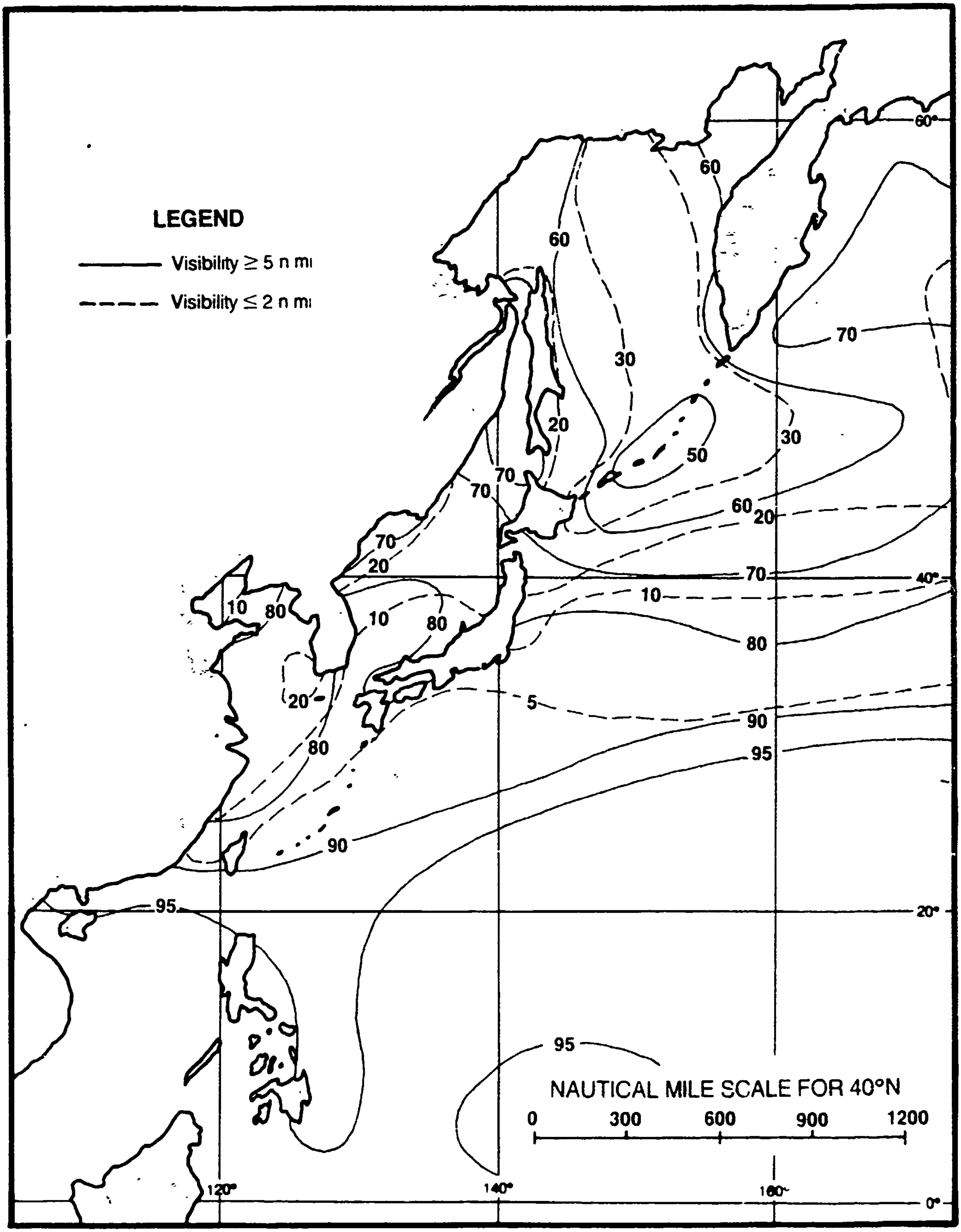

Figure 2-30. Percent frequency of occurrence of visibility limits during May (adapted from U.S. Navy, 1977).

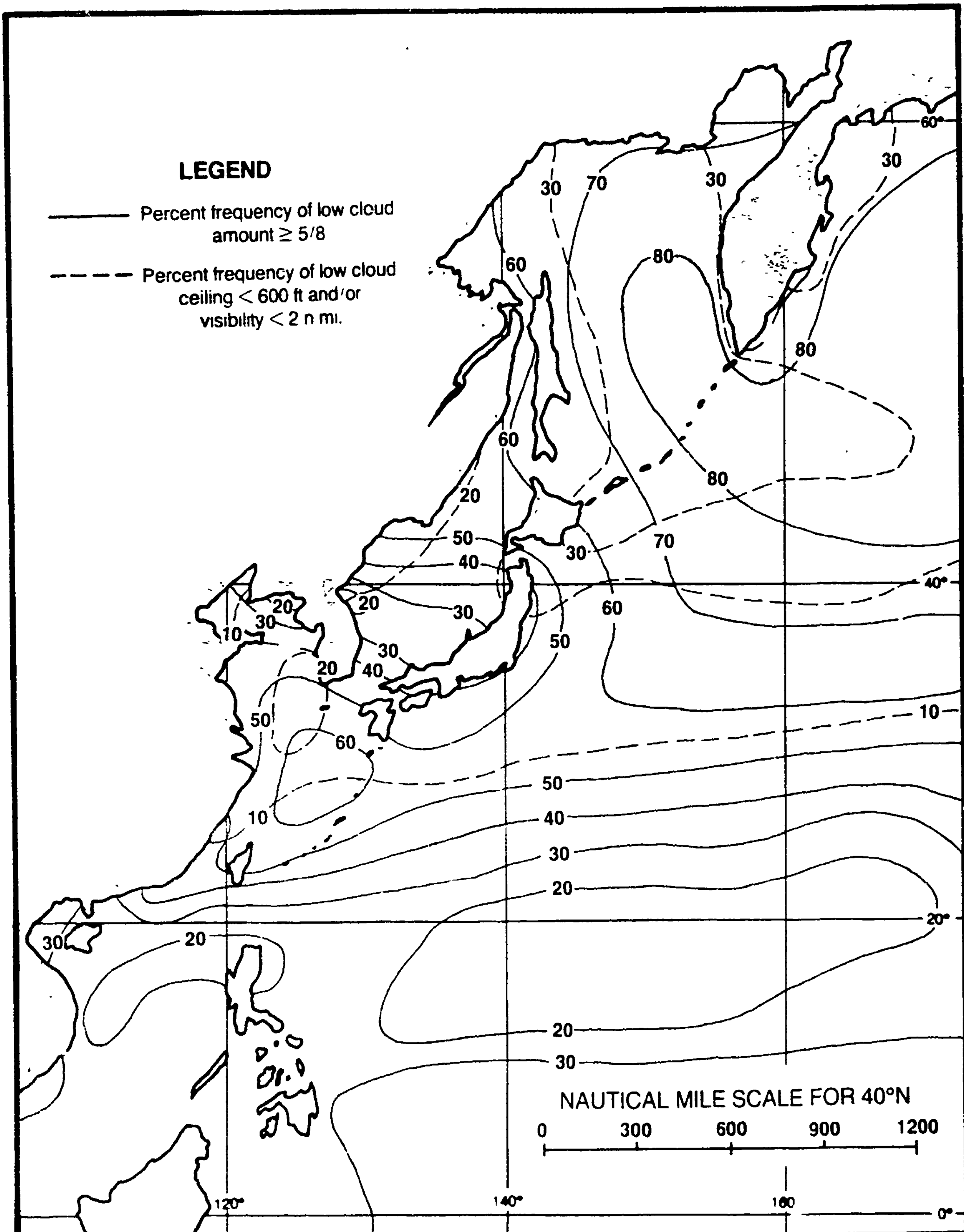

Figure 2-31 Low cloud amounts vs ceiling and visibility during May (adapted from U S. Navy, 1977)

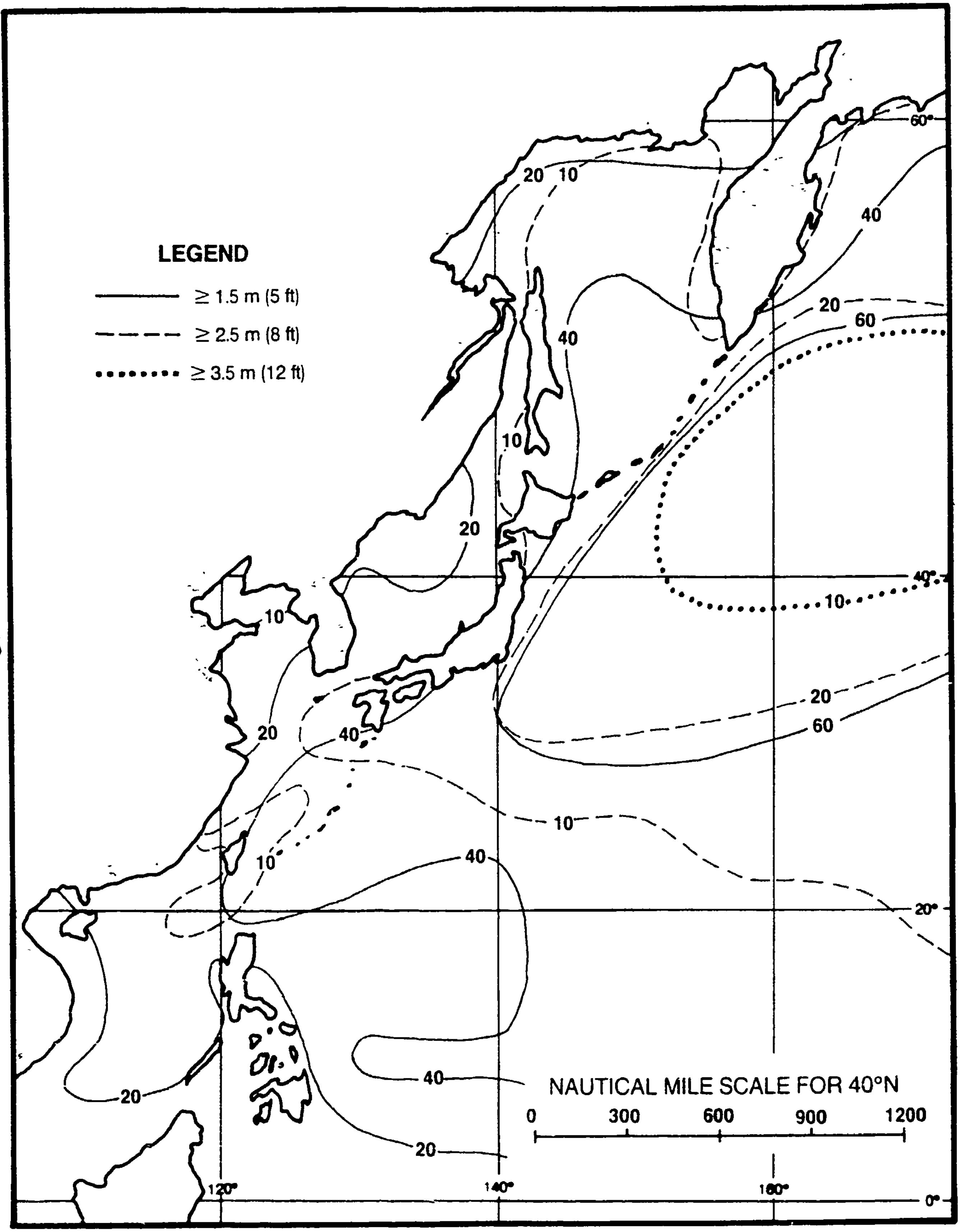

Figure 2-32. Percent frequency of occurrence of wave heights during May (adapted from U.S. Navy, 1977).

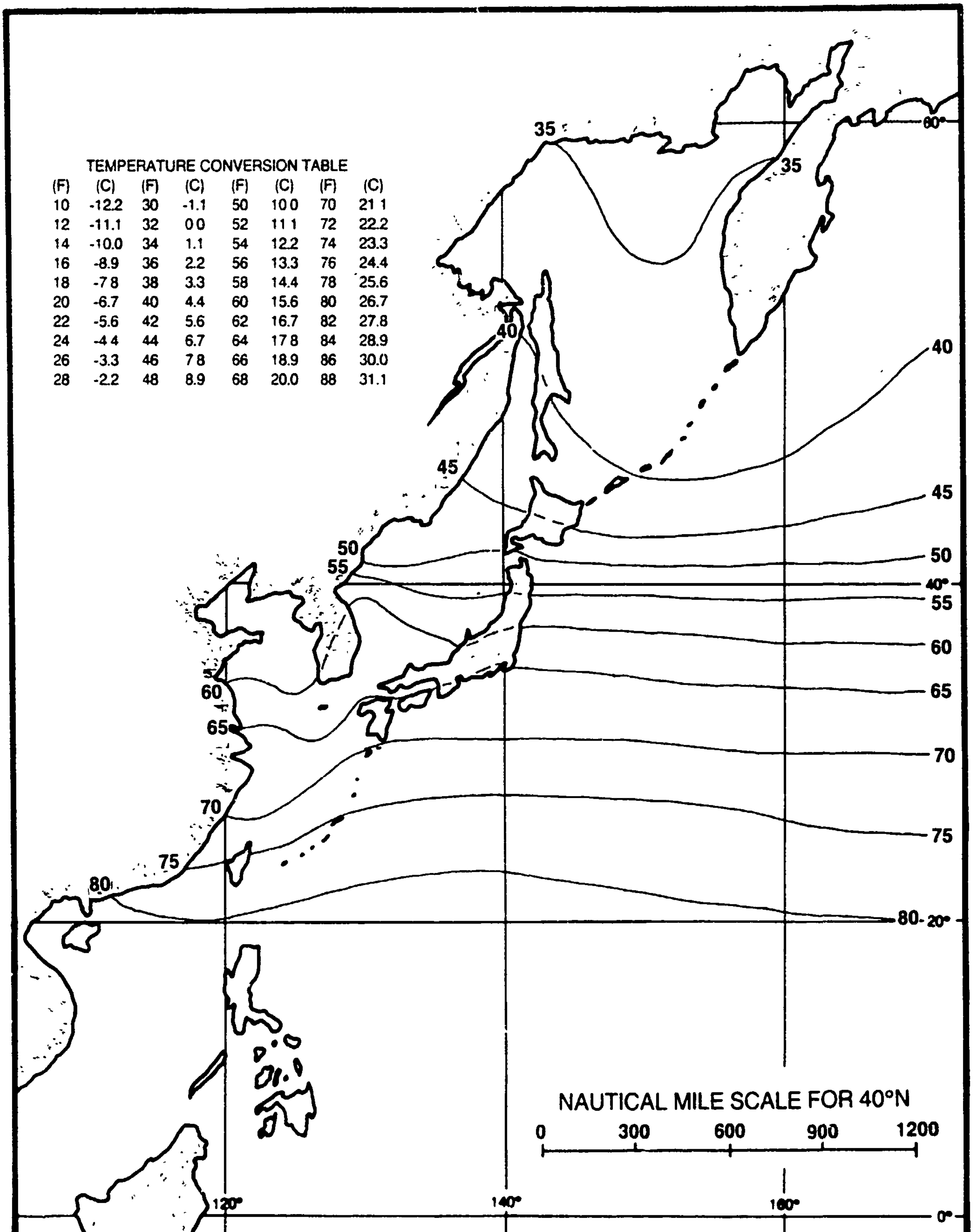

(F)	(C)	(F)	(C)	(F)	(C)	(F)	(C)
10	-12.2	30	-1.1	50	10 0	70	21 1
12	-11.1	32	0 0	52	11 1	72	22.2
14	-10.0	34	1.1	54	12.2	74	23.3
16	-8.9	36	2.2	56	13.3	76	24.4
18	-7 8	38	3.3	58	14.4	78	25.6
20	-6.7	40	4.4	60	15.6	80	26.7
22	-5.6	42	5.6	62	16.7	82	27.8
24	-4 4	44	6.7	64	17 8	84	28.9
26	-3.3	46	7 8	66	18.9	86	30.0
28	-2.2	48	8.9	68	20.0	88	31.1

Figure 2-33. Mean surface air temperature in degrees Fahrenheit during May (adapted from Ownbey, 1973 and U.S. Navy, 1977).

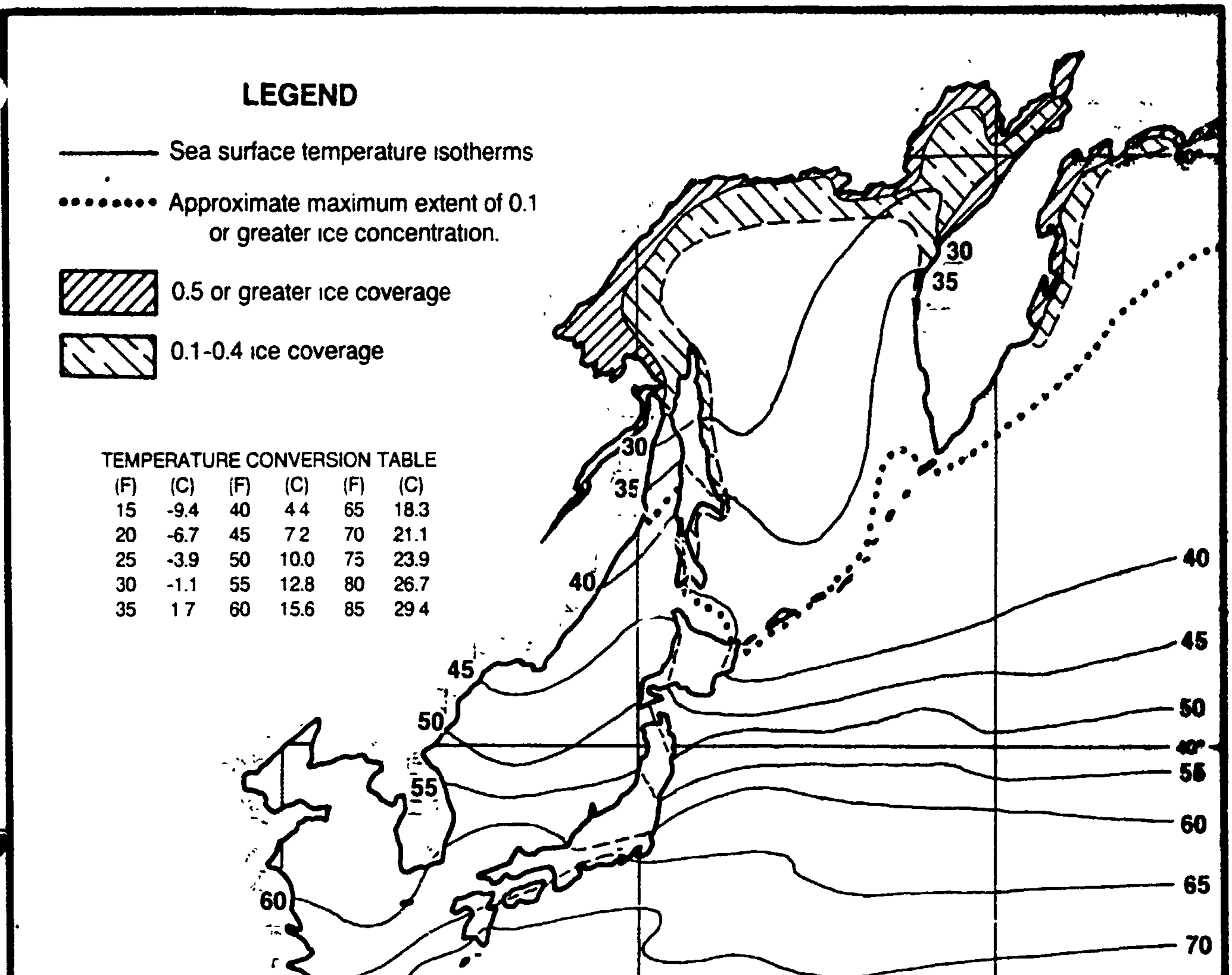

Figure 2-34. Mean sea surface temperature in degrees Fahrenheit during May, with approximate ice limits (adapted from U.S. Navy, 1967 and U.S. Navy, 1977).

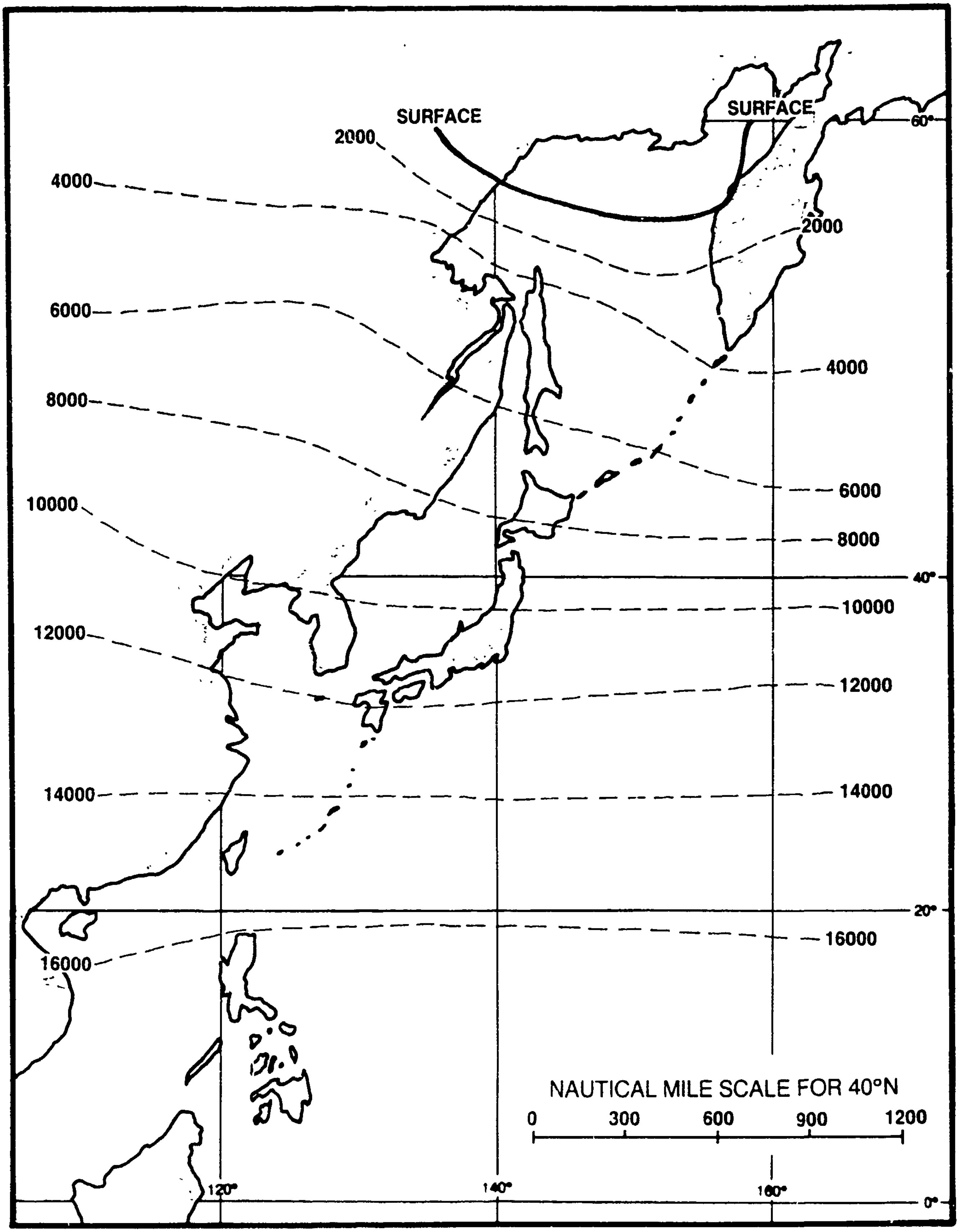

Figure 2-35 Mean altitude of the freezing level for May in feet (adapted from U S. Air Force, 1965).

2.2.1.7 Summer (mid-June to mid-September)

At the beginning of the traditional summer season, the Polar Front is oriented east-west along southern Honshu and extends west-southwestward into China. The warm, moist air being transported northward south of the front causes warm frontal-type overrunning and usually results in extensive precipitation over Japan. This situation, called the Bai-U (or Plum Rain) season, usually persists until mid-July when the Polar Front shifts northward and establishes its summer position northwest of the Sea of Japan.

The Siberian high is weak, and usually fractured into several small high pressure cells. Most migratory lows are relatively weak and move eastward north of the central portion of Honshu. The jet stream is at its weakest during the summer with a mean position across the northern Korean peninsula, Sea of Japan, and northern Honshu (see Figure 2-36).

The monsoon trough has migrated northward, extending northwestward from the tropical north Pacific waters east of the Philippines to the East China Sea north of Taiwan, thence westward into the interior of southern China.

The most probable summer migratory low pressure systems include Lake Baikal Lows, South Mongolia Lows, and Yellow Sea Lows. Average tracks for each of the systems are shown in Figure 2-6.

Of the yearly average of approximately 57 cold fronts occurring in the Far East, only 6 (11%) occur during summer (mid-June to mid-September), a frequency of about one every two weeks (FWC/JTWC, 1969).

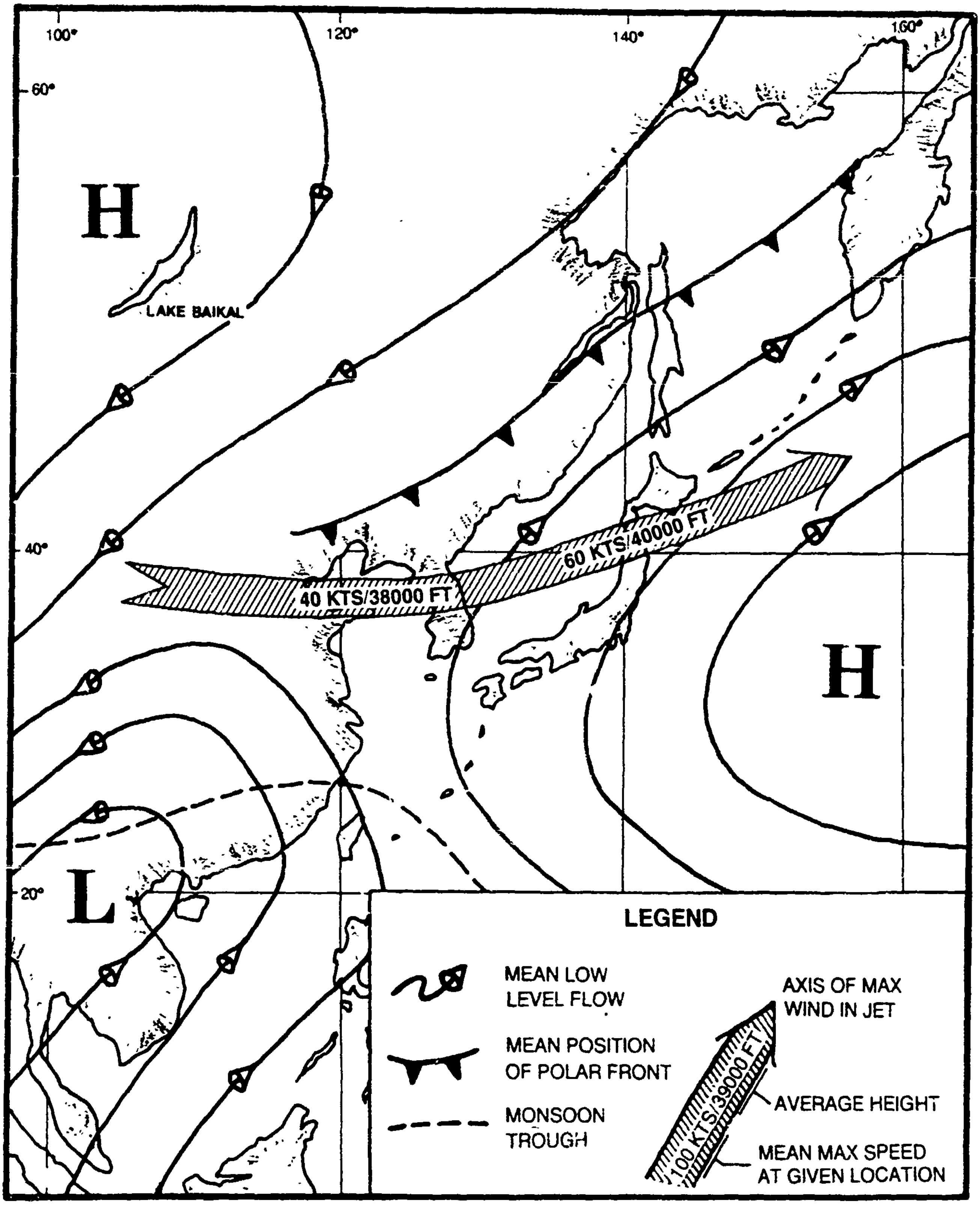

Figure 2-36. Typical atmospheric features during August: mean low level flow, mean position of polar front, mean position of monsoon trough and mean jet stream positon (adapted from U S. Marine Corps, 1967 and U S. Air Force, 1968).

Summer brings a maximum of <u>tropical cyclone</u> activity to the western North Pacific and eastern Asia. Approximately four typhoons per year form in each of the months of August and September, with three forming during July (Crutcher and Quayle, 1974). Of these, a large percentage can be expected to move northwestward across the waters of the Philippine Sea or western North Pacific. Some can be expected to recurve to the northeast while south of Japan, but a significant number will move into the waters of the East China Sea, Yellow Sea, or Sea of Japan. Refer to Appendix B for tropical cyclone tracks.

Figures 2-37 through 2-49 depict various average climatic conditions that prevail over eastern Asia and adjacent waters during the month of August. A brief discussion of each of the parameters is presented in the climatology sections of the regional chapters in this handbook.

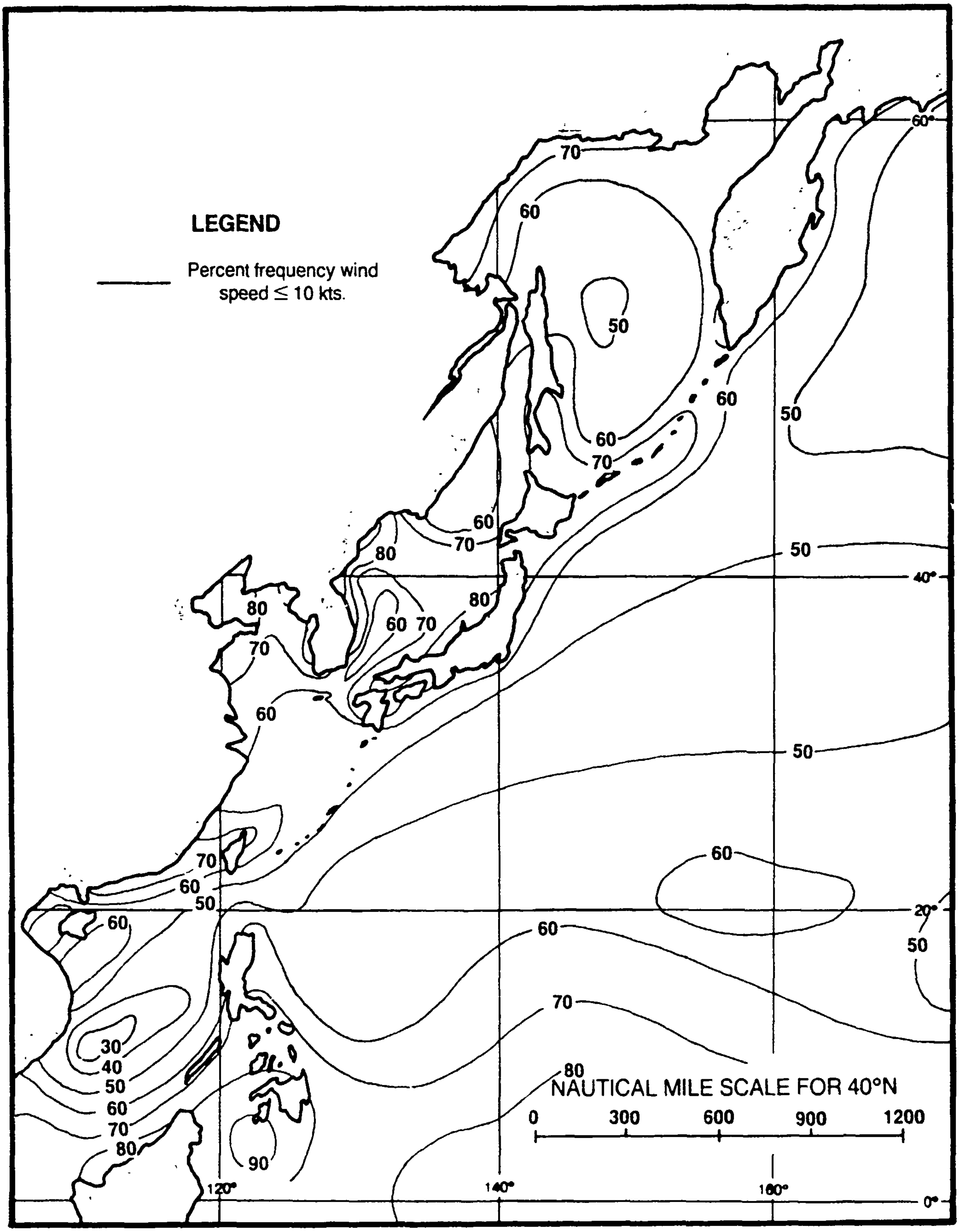

Figure 2-37 Surface winds during August (adapted from U.S Navy, 1977).

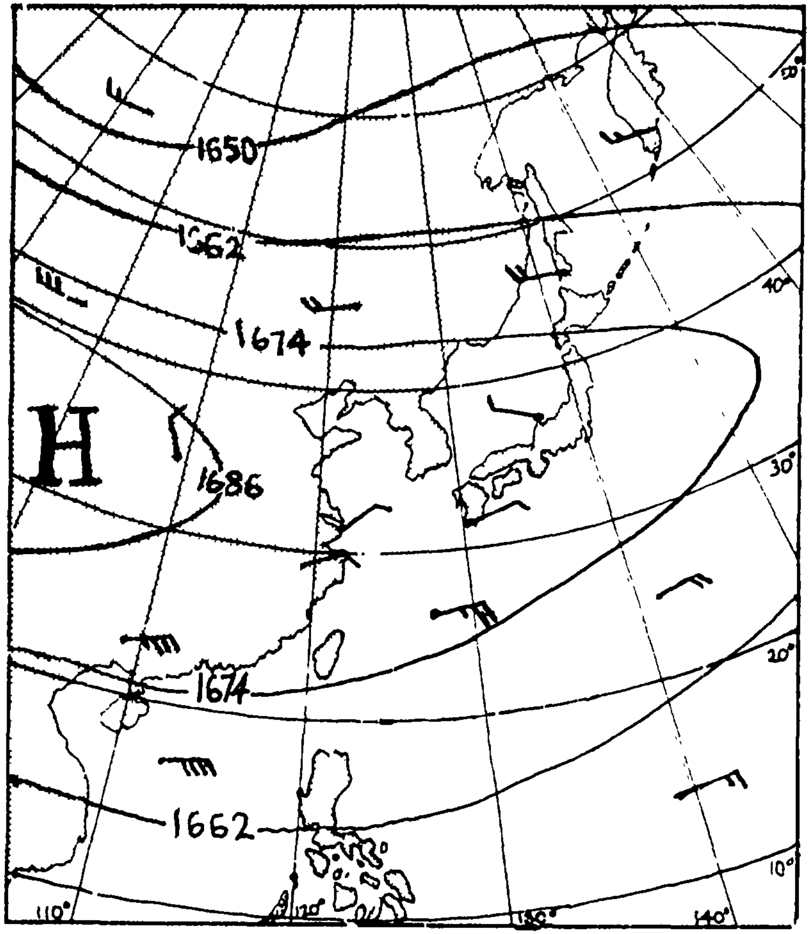

Figure 2-38 100mb heights and winds for August All heights in tens of gpm (adapted from Crutcher & Meserve, 1970)

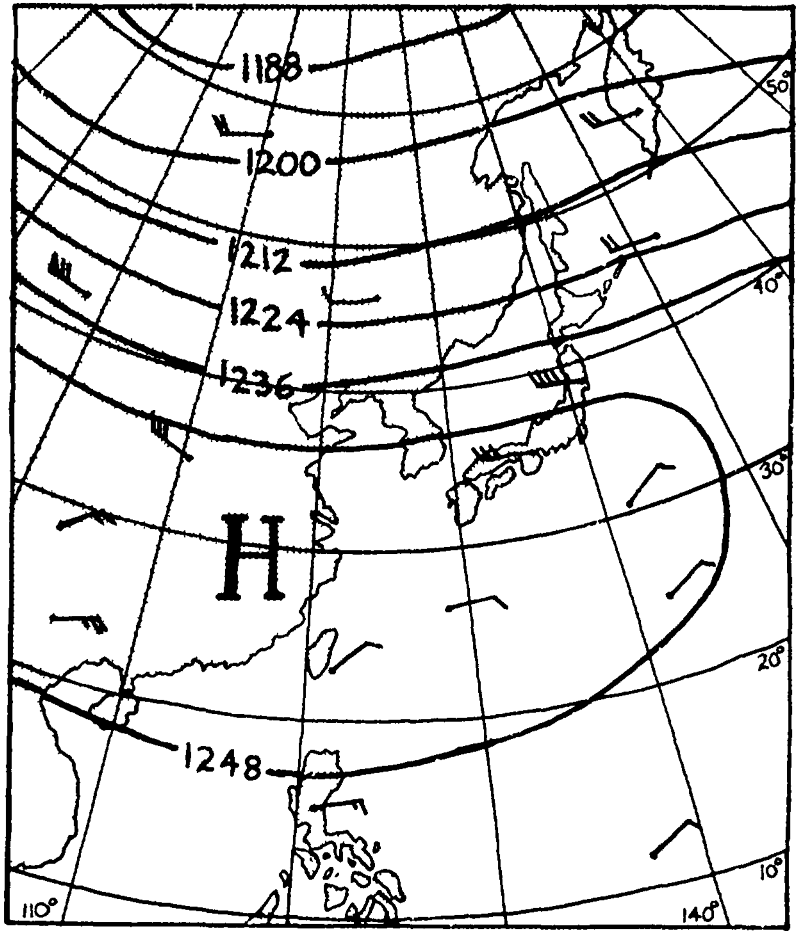

Figure 2-39 200mb heights and winds for August. All heights in tens of gpm (adapted from Crutcher & Meserve, 1970)

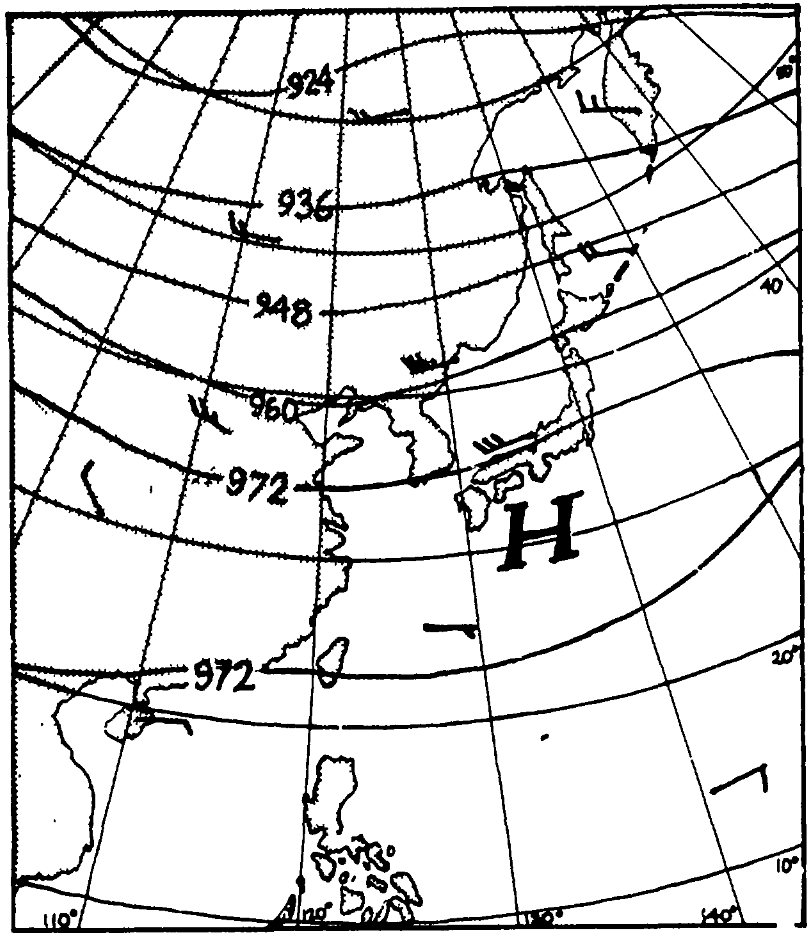

Figure 2-40 300mb heights and winds for August All heights in tens of gpm. (adapted from Crutcher & Meserve, 1970)

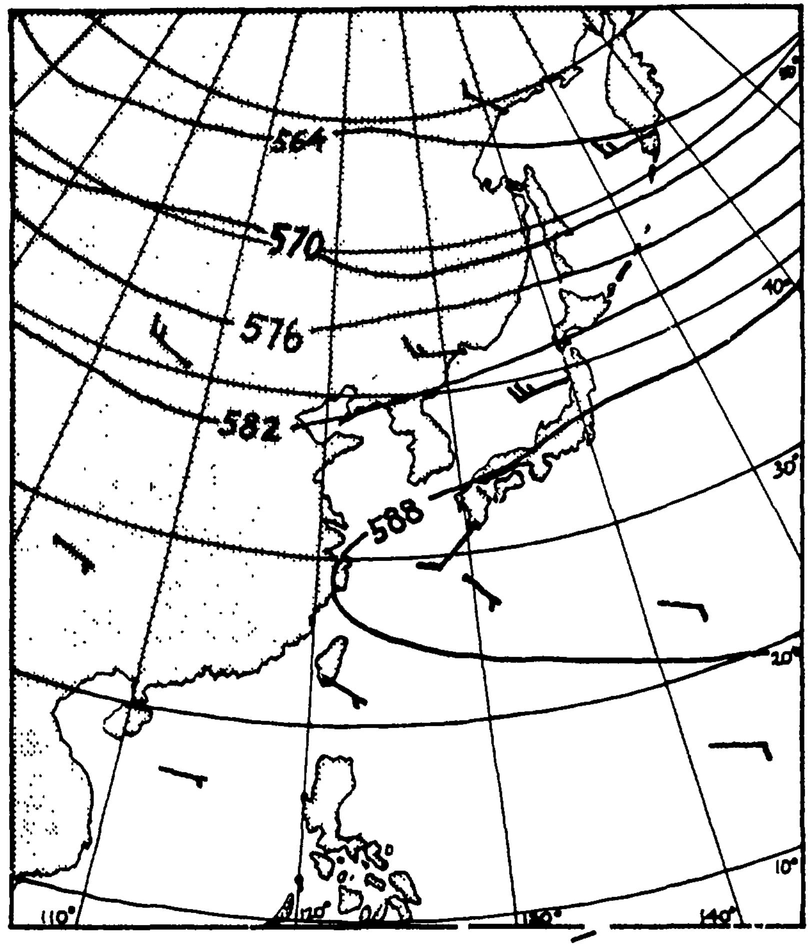

Figure 2-41. 500mb heights and winds for August. All heights in tens of gpm. (adapted from Crutcher & Meserve, 1970)

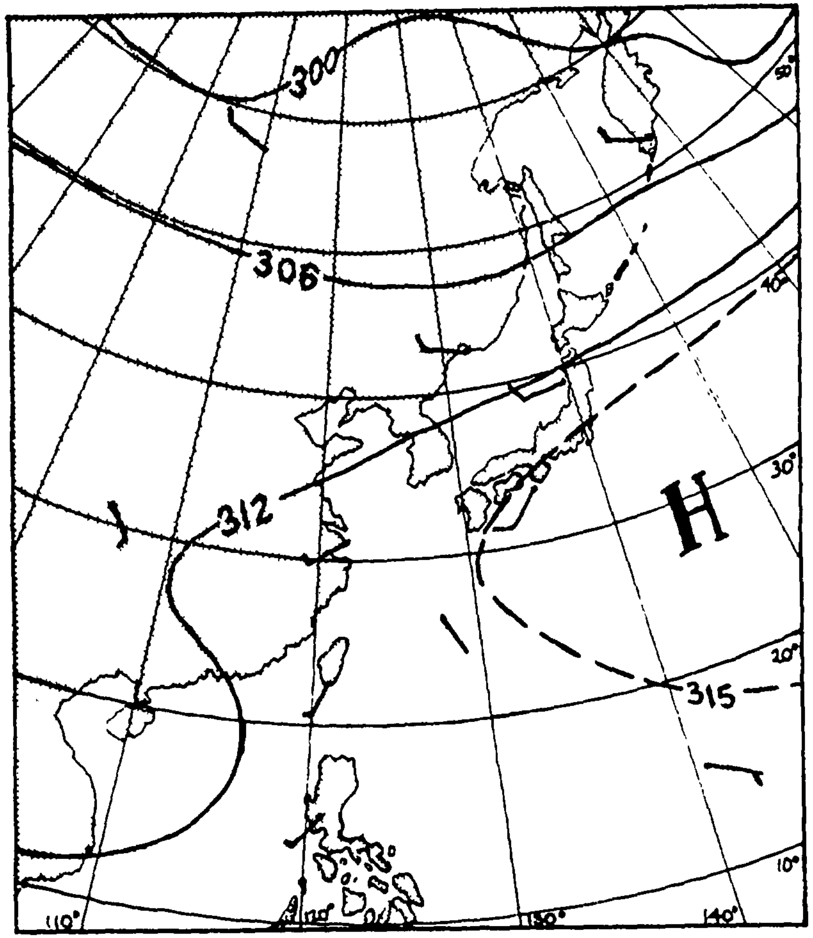

Figure 2-42. 700mb heights and winds for August All heights in tens of gpm. (adapted from Crutcher & Meserve, 1970)

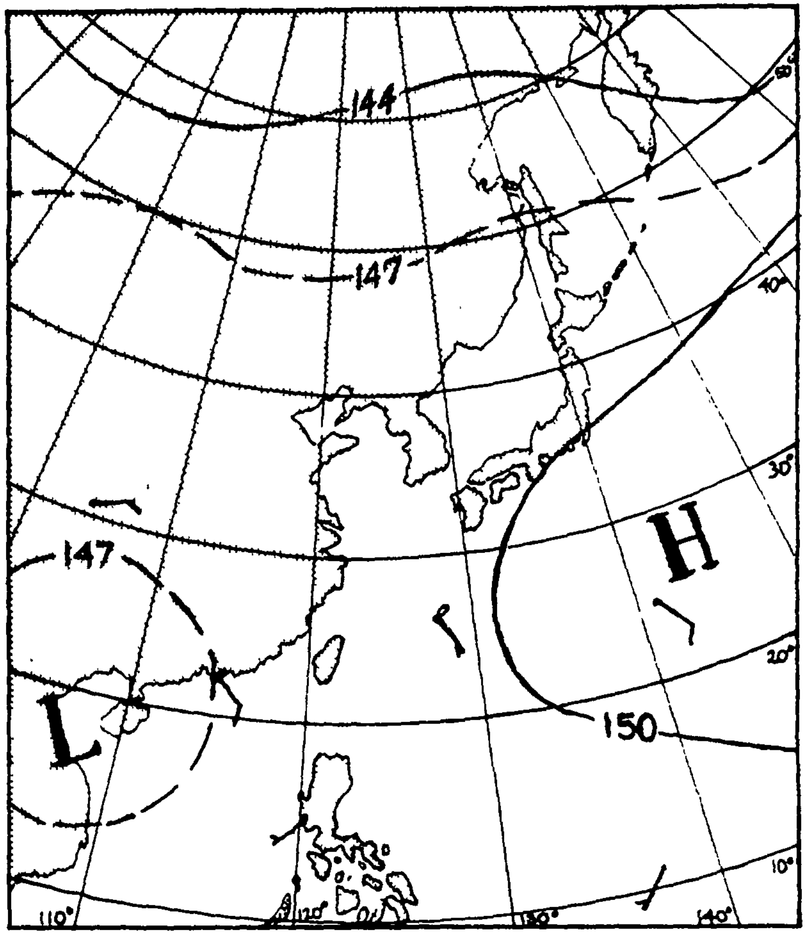

Figure 2-43. 850mb heights and winds for August. All heights in tens of gpm (adapted from Crutcher & Meserve, 1970)

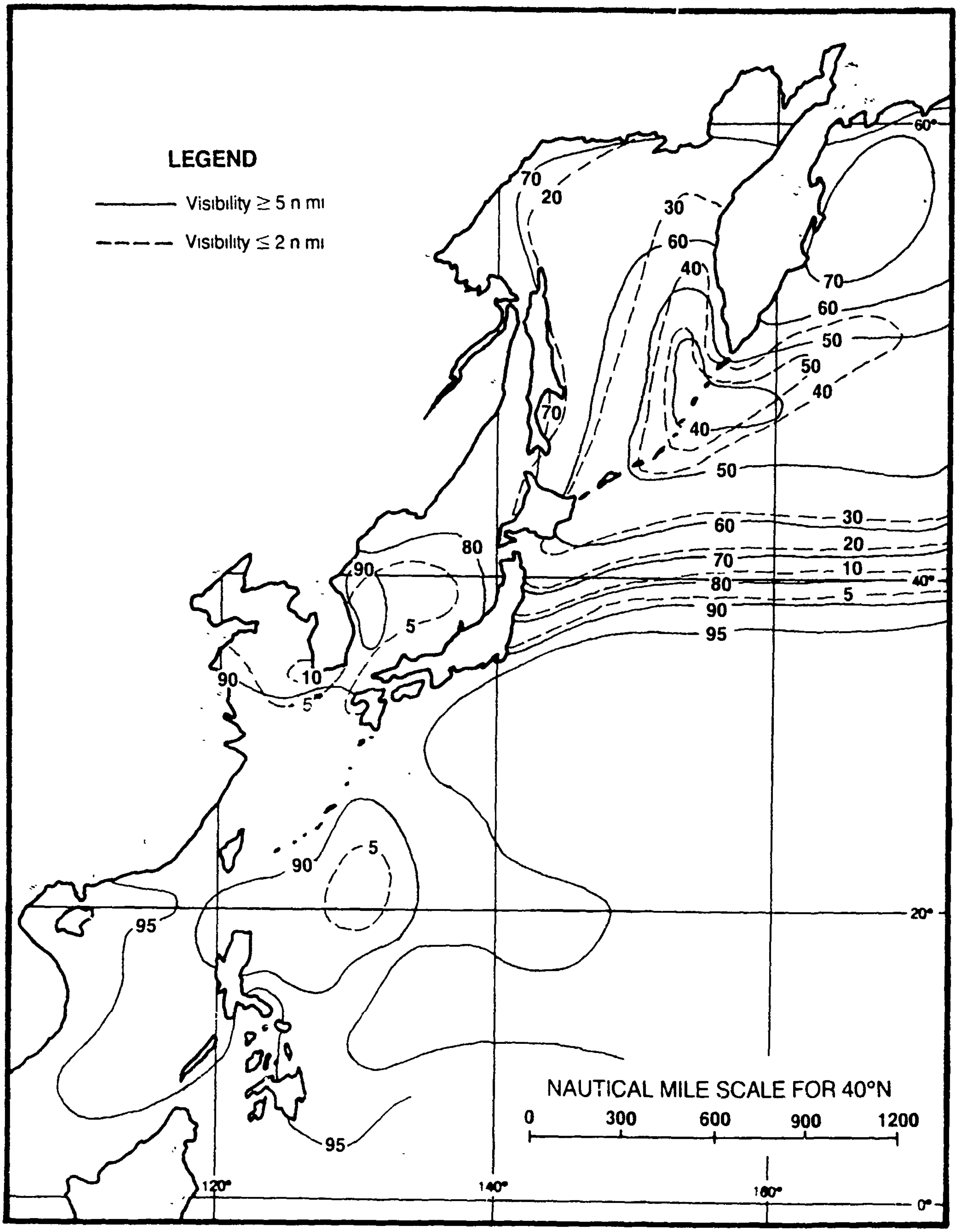

Figure 2-44 Percent frequency of occurrence of visibility limits during August (adapted from U S Navy, 1977)

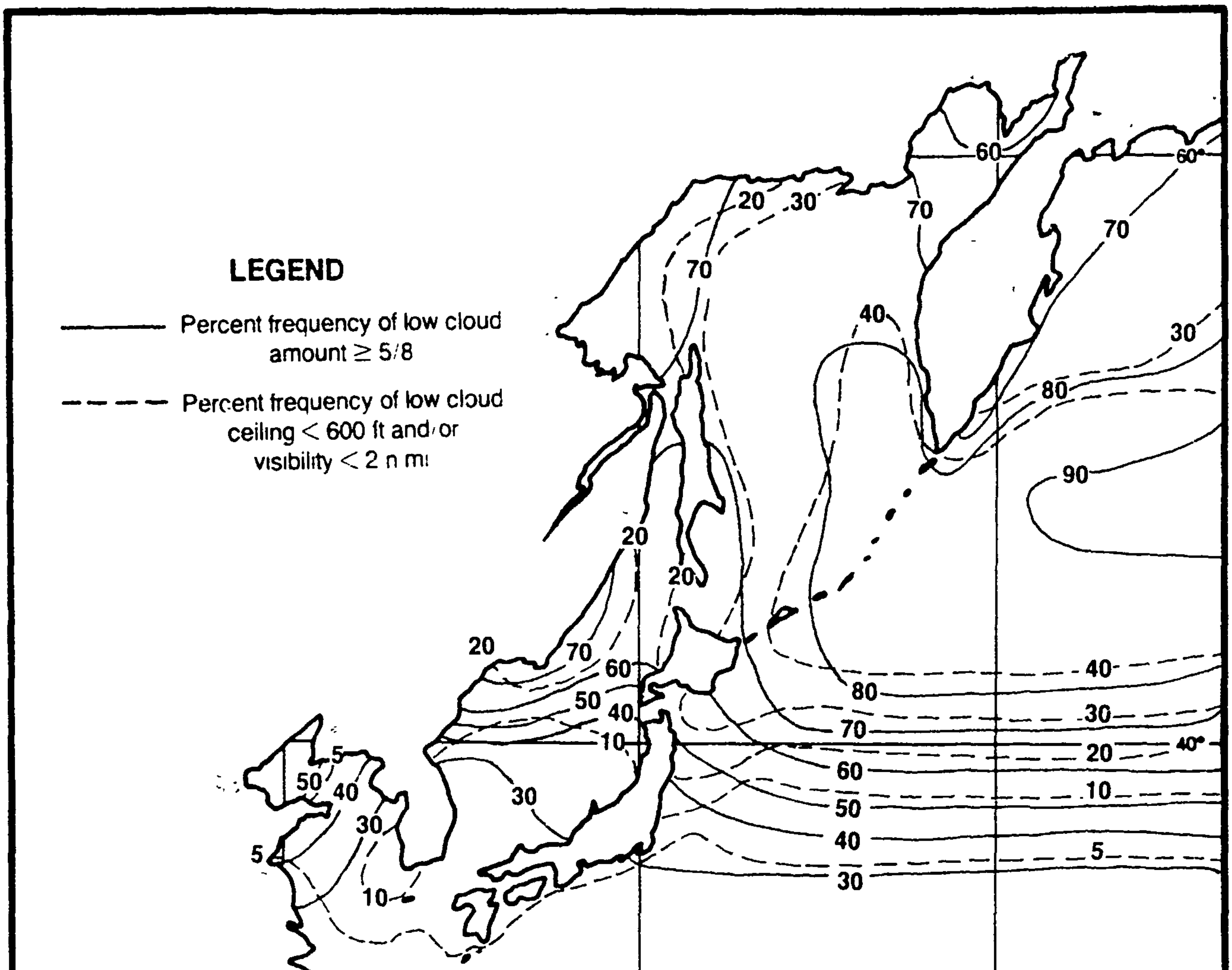

Figure 2-45 Low cloud amounts vs ceiling and visibility during August (adapted from U S Navy, 1977)

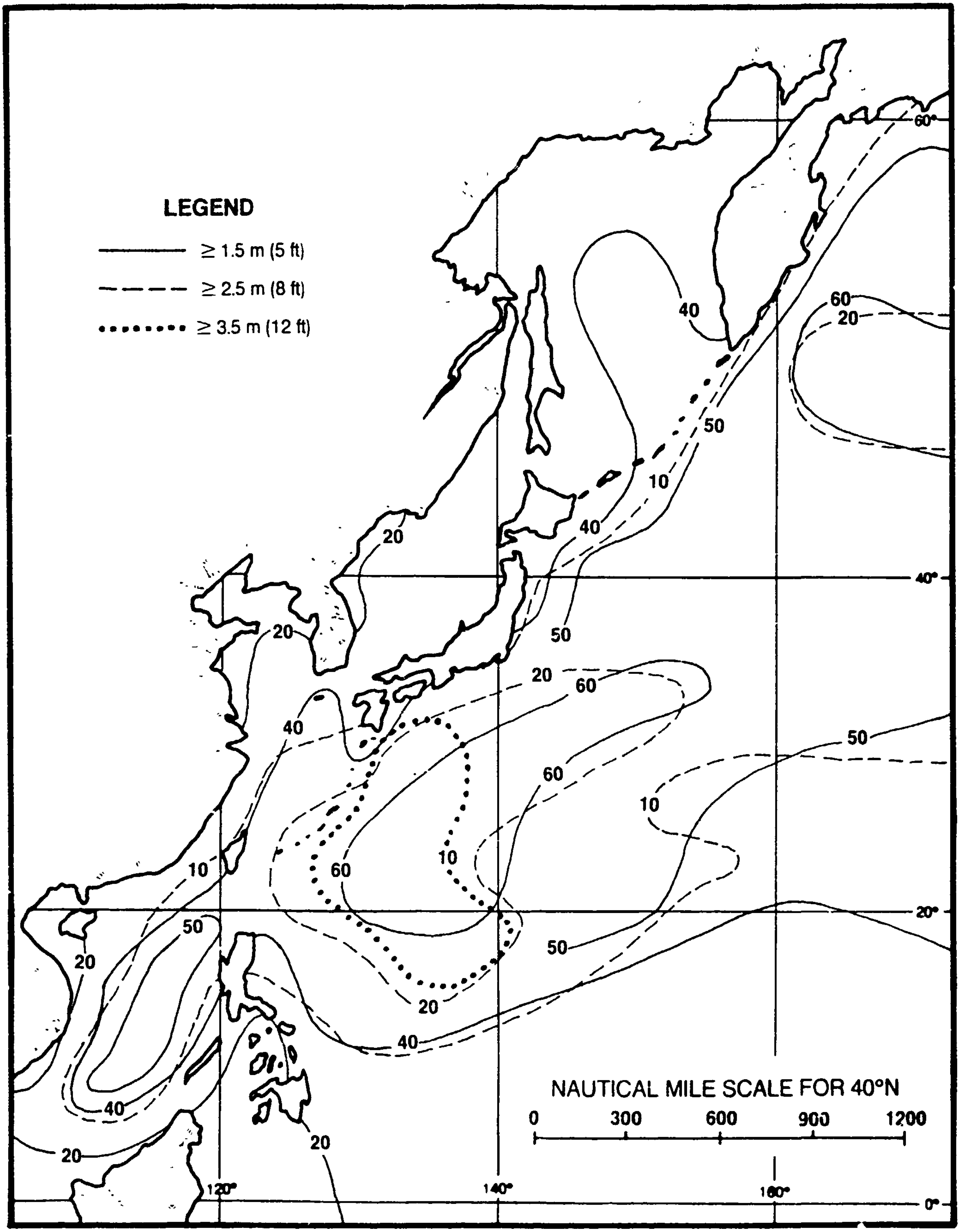

Figure 2-46 Percent frequency of occurrence of wave heights during August (adapted from U S. Navy, 1977).

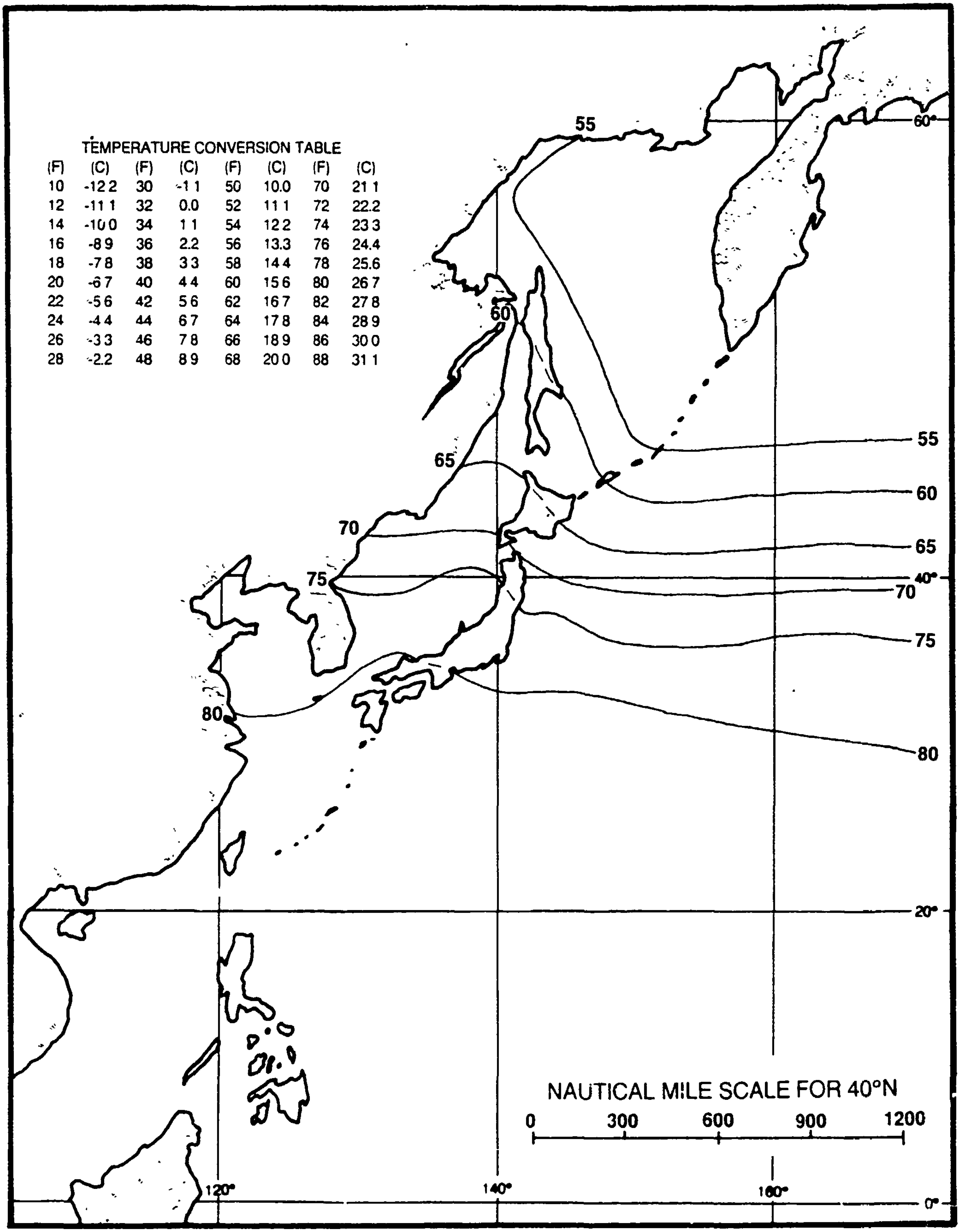

TEMPERATURE CONVERSION TABLE

(F)	(C)	(F)	(C)	(F)	(C)	(F)	(C)
10	-12.2	30	-1.1	50	10.0	70	21.1
12	-11.1	32	0.0	52	11.1	72	22.2
14	-10.0	34	1.1	54	12.2	74	23.3
16	-8.9	36	2.2	56	13.3	76	24.4
18	-7.8	38	3.3	58	14.4	78	25.6
20	-6.7	40	4.4	60	15.6	80	26.7
22	-5.6	42	5.6	62	16.7	82	27.8
24	-4.4	44	6.7	64	17.8	84	28.9
26	-3.3	46	7.8	66	18.9	86	30.0
28	-2.2	48	8.9	68	20.0	88	31.1

Figure 2-47. Mean surface air temperature in degrees Fahrenheit during August (adapted from Ownbey, 1973 and U.S Navy 1977).

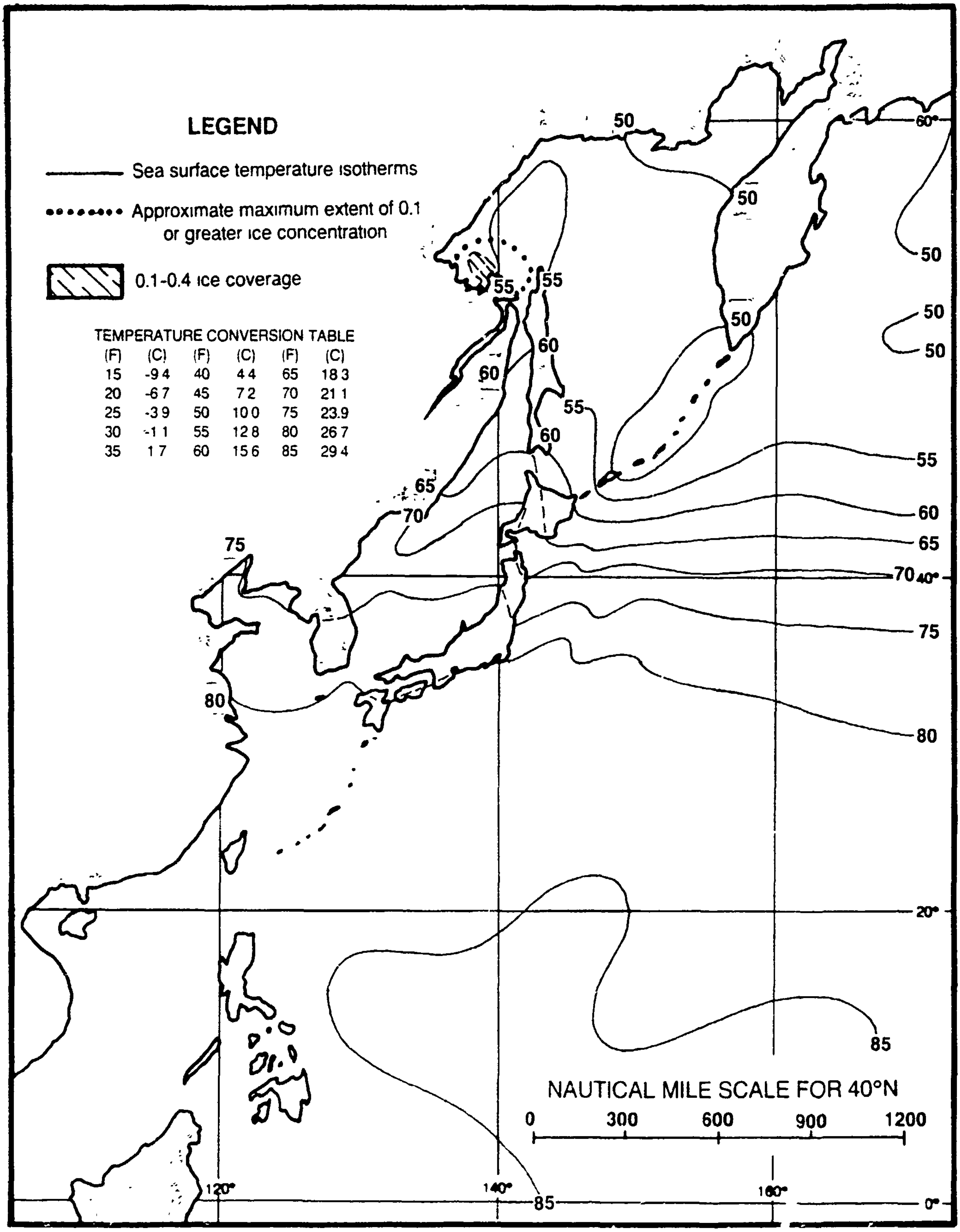

Figure 2-48. Mean sea surface temperature in degrees Fahrenheit during August, with approximate ice limits (adapted from U S Navy 1967 and U S Navy, 1977)

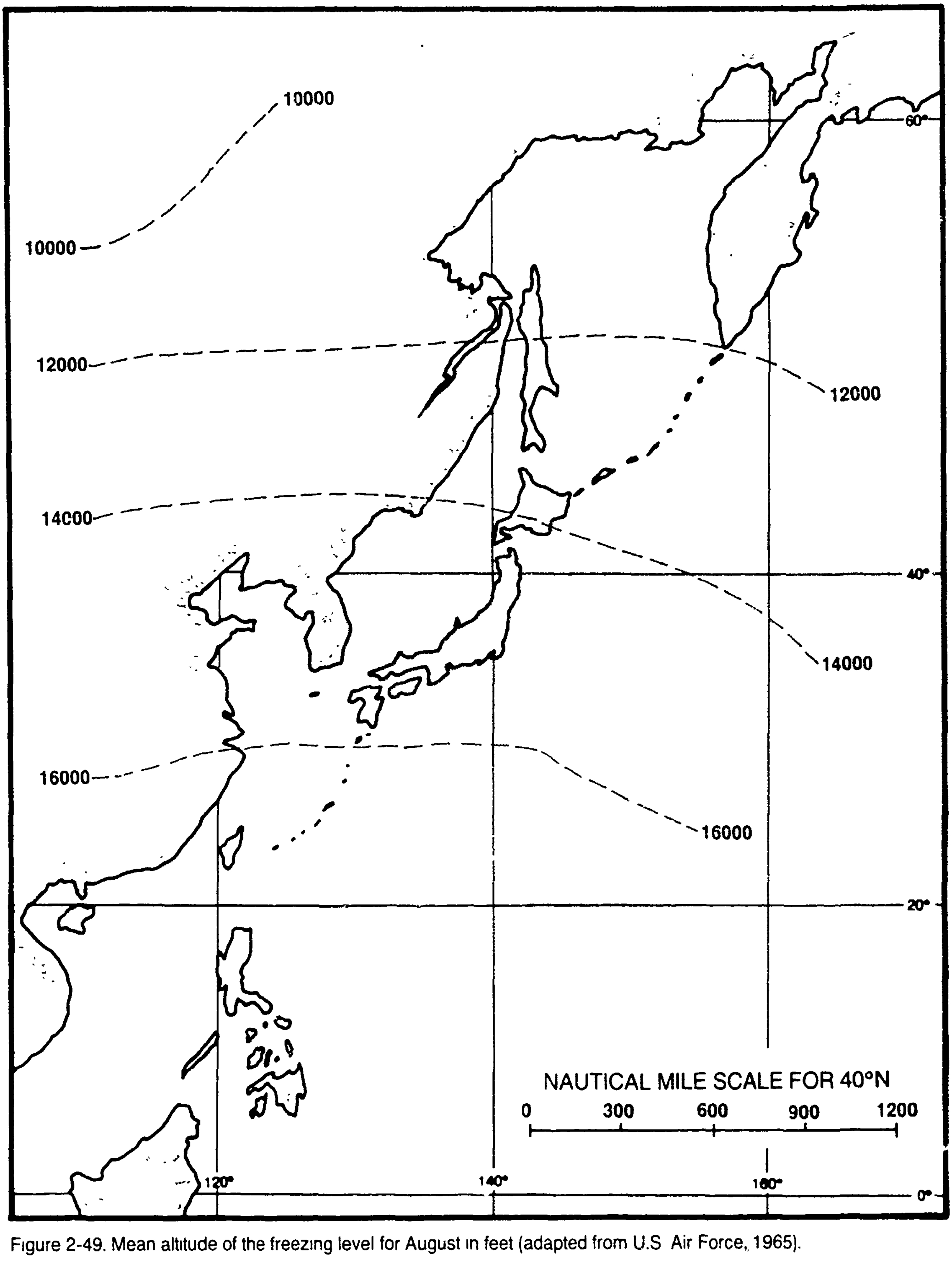

Figure 2-49. Mean altitude of the freezing level for August in feet (adapted from U.S Air Force, 1965).

2.2.1.8 Autumn (mid-September to mid-December)

The transition from the summer season to autumn occurs rapidly. The Polar Front moves rapidly from a position north of Korea to a location south of Japan as the Siberian high pressure cell becomes the dominant weather feature over Asia. Cool, dry air invades the offshore waters as northerly flow predominates at the surface.

The rapid movement of the Polar Front southward through Japan occurs during a period called the Autumn Bai-U (or Shurin). It is similar to the Spring Bai-U in that it usually brings a period of rain and cloudy weather to the southern half of Honshu and the East China Sea due to the overrunning of the warm tropical air over the colder polar air moving southeastward from the Asian landmass. The duration of the inclement weather is shorter during the Autumn Bai-U due to the rapid southward movement of the front.

The Aleutian Low strengthens and moves to a position close to its favored winter location, and the Sea of Okhotsk low re-establishes itself during the Autumn season.

The jet stream core velocities increase, with speeds of 140 kt common over the East China Sea and Japan. As shown in Figure 2-50, the jet stream once again is split over eastern Asia as a result of the influence of the Tibetan Plateau, with the two cores merging over central Japan.

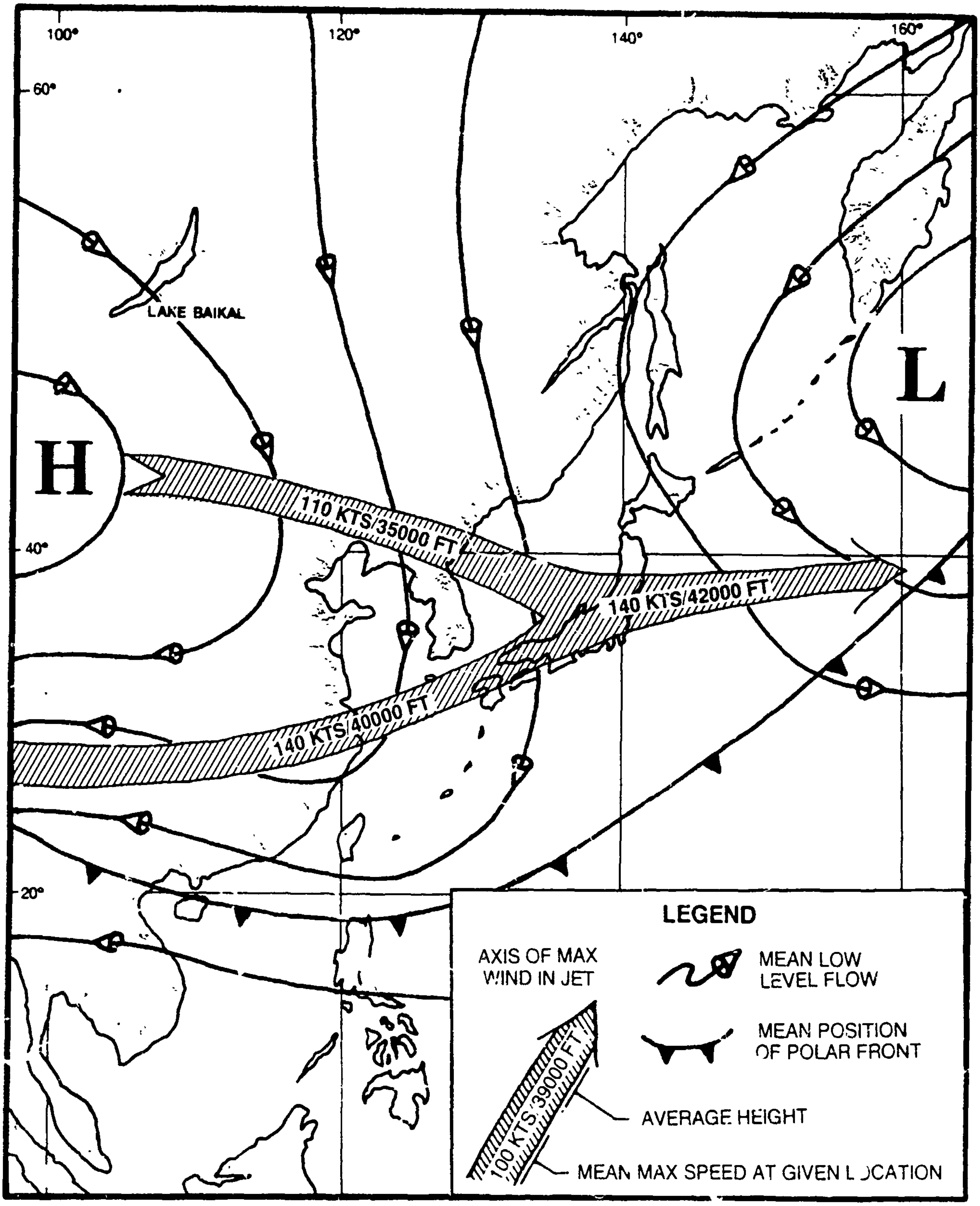

Figure 2-50. Typical atmospheric features during November: mean low level flow, mean position of polar front, and mean jet stream position (adapted from U.S. Marine Corps, 1967 and U.S. Air Force, 1968)

Figures 2-51 through 2-63 depict various average climatic conditions that prevail over eastern Asia and adjacent waters during the month of November. A brief discussion of each of the parameters is presented in the climatology sections of the regional chapters in this handbook.

The most probable types of migratory low pressure systems occurring during the autumn season include Manchurian Lows, Lake Baikal Lows, South Mongolia Lows, Yellow Sea Lows, and Taiwan Lows. Average tracks of each of the systems are depicted in Figure 2-6.

Of the yearly average of approximately 57 cold fronts occurring in the Far East, about 19 (33%) occurred during autumn (mid-September to mid-December), a frequency of about one every five days (FWC/JTWC, 1969).

From a maximum in August and September, tropical cyclone frequency declines during autumn, with an average of approximately six typhoons per year in the western Pacific (three in October, two in November, and only one during December) (Crutcher and Quayle, 1974). Early season storms pose the greatest threat to interests in the waters adjacent to eastern Asia. By December, typhoon activity is generally limited to latitudes south of 30°N. Those storms that do move north of that latitude recurve to the northeast well south of Japan. Refer to Appendix B for tropical cyclone tracks.

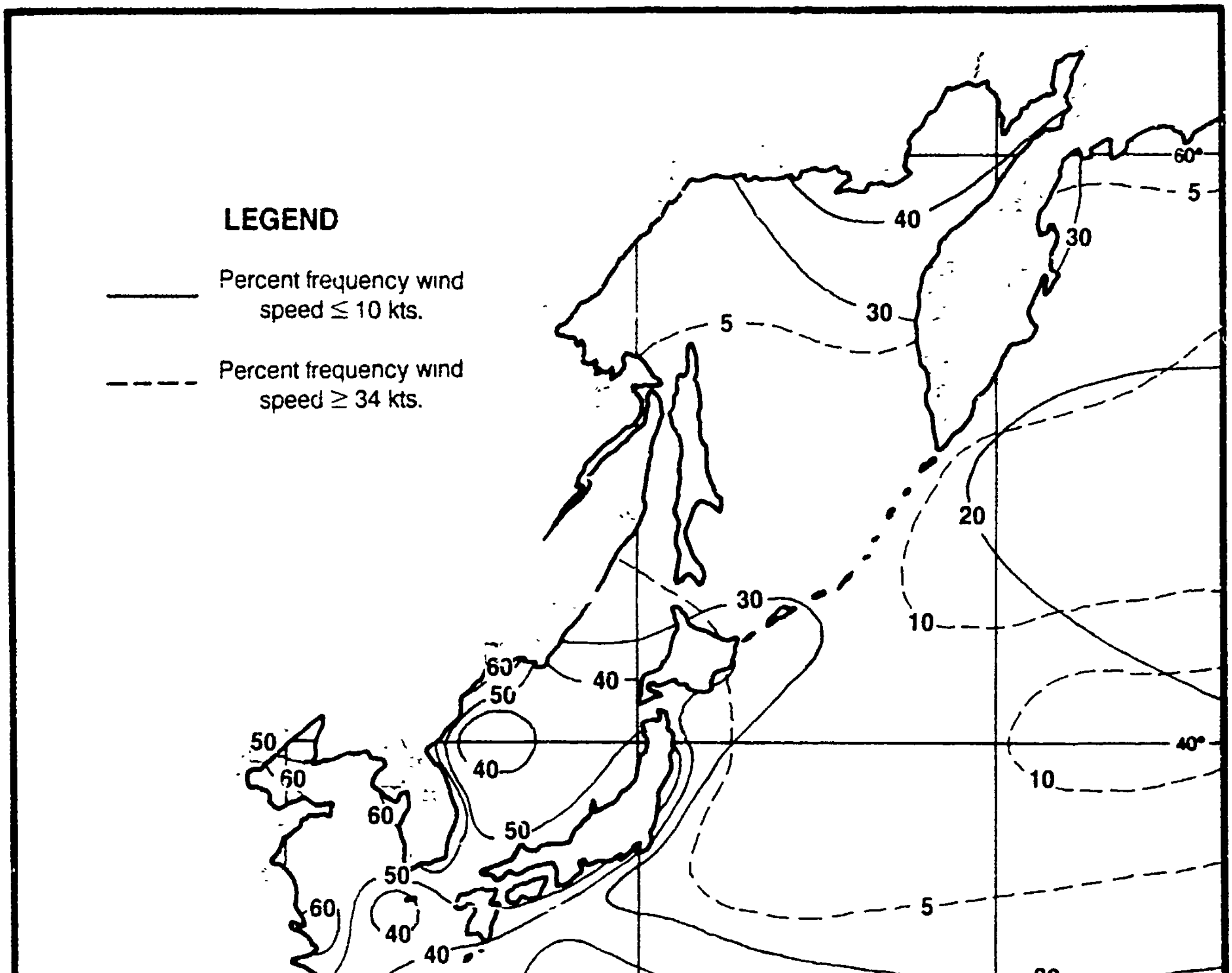

Figure 2-51 Surface winds during November (adapted from U.S Navy, 1977).

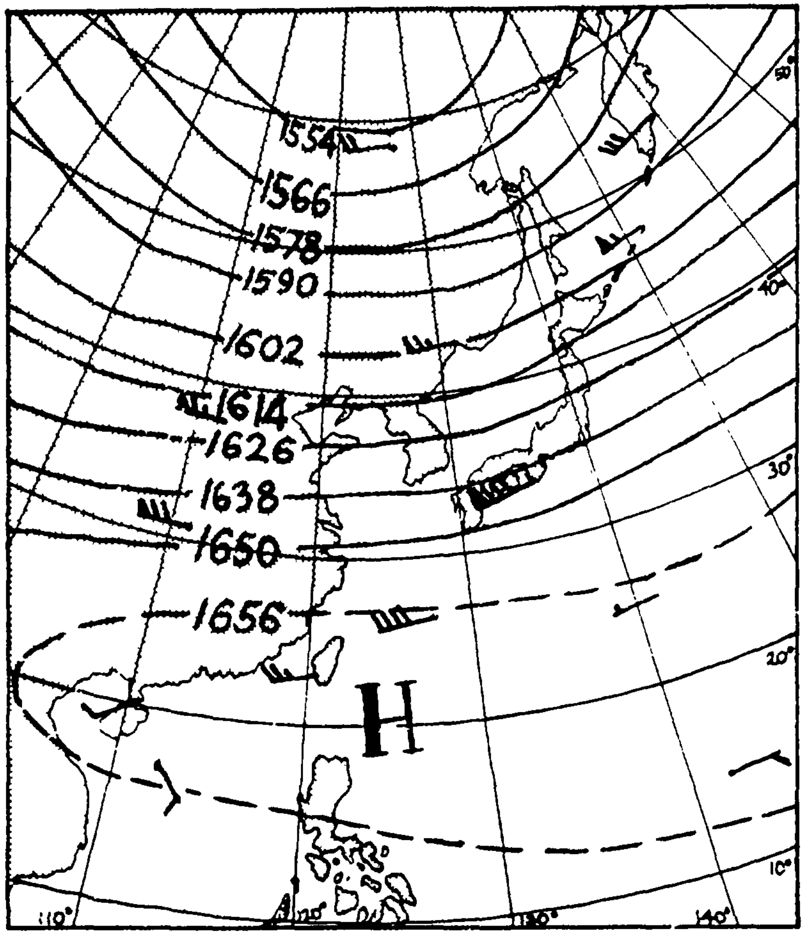

Figure 2-52. 100mb heights and winds for November All heights in tens of gpm. (adapted from Crutcher & Meserve, 1970)

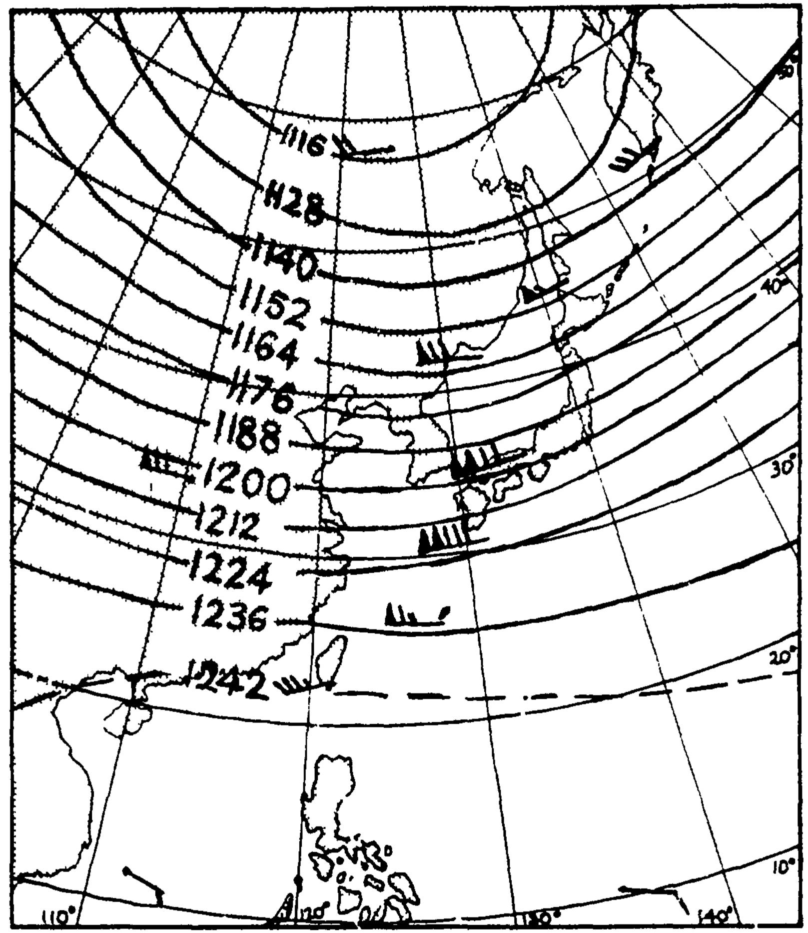

Figure 2-53. 200mb heights and winds for November. All heights in tens of gpm (adapted from Crutcher & Meserve, 1970)

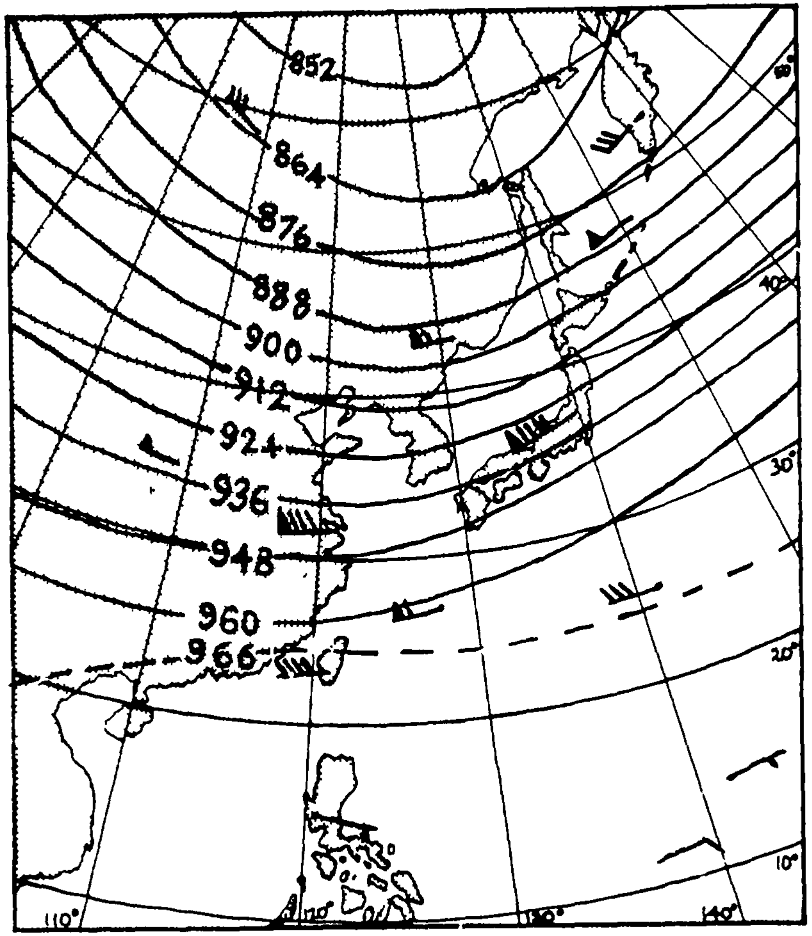

Figure 2-54. 300mb heights and winds for November. All heights in tens of gpm. (adapted from Crutcher & Meserve, 1970)

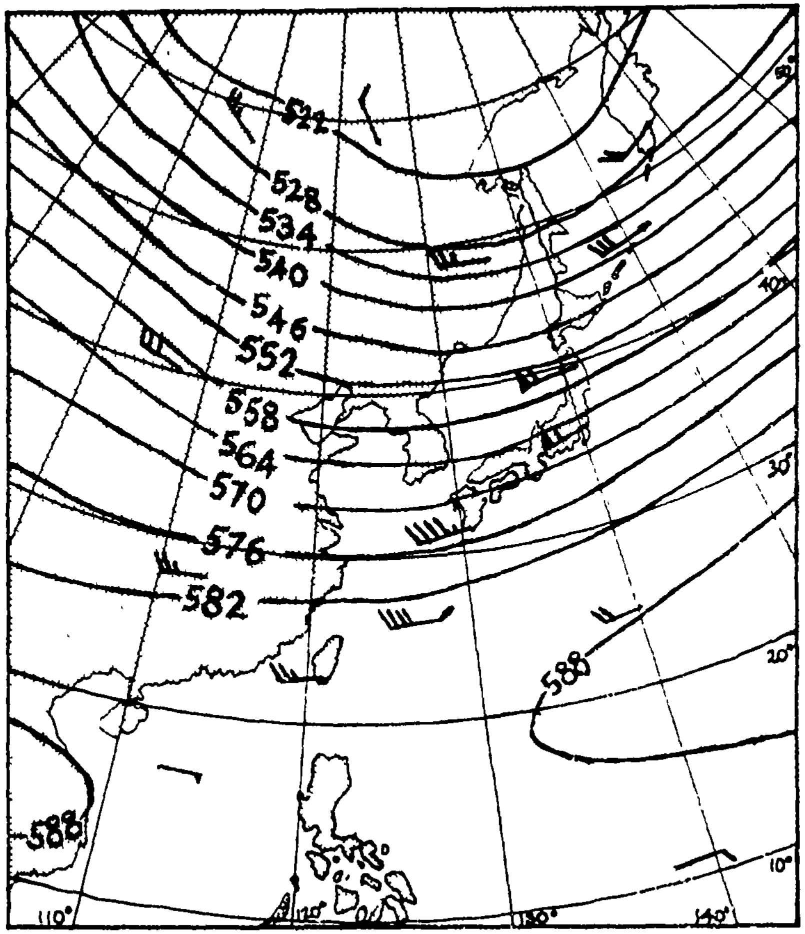

Figure 2-55. 500mb heights and winds for November. All heights in tens of gpm. (adapted from Crutcher & Meserve, 1970)

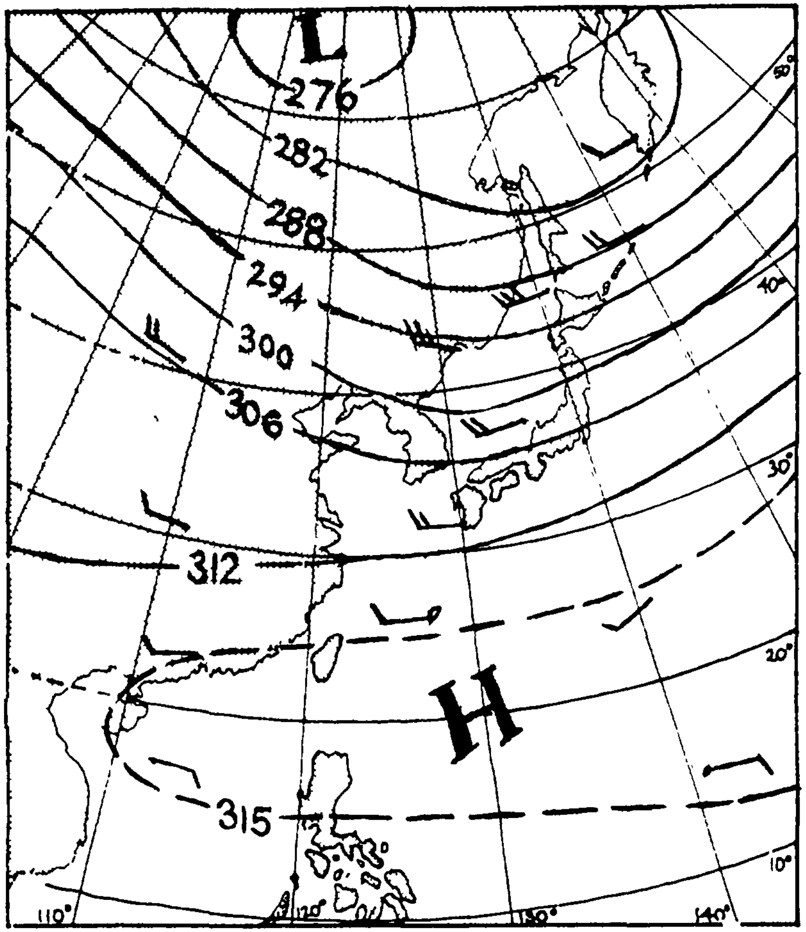

Figure 2-56 700mb heights and winds for November All heights in tens of gpm. (adapted from Crutcher & Meserve, 1970)

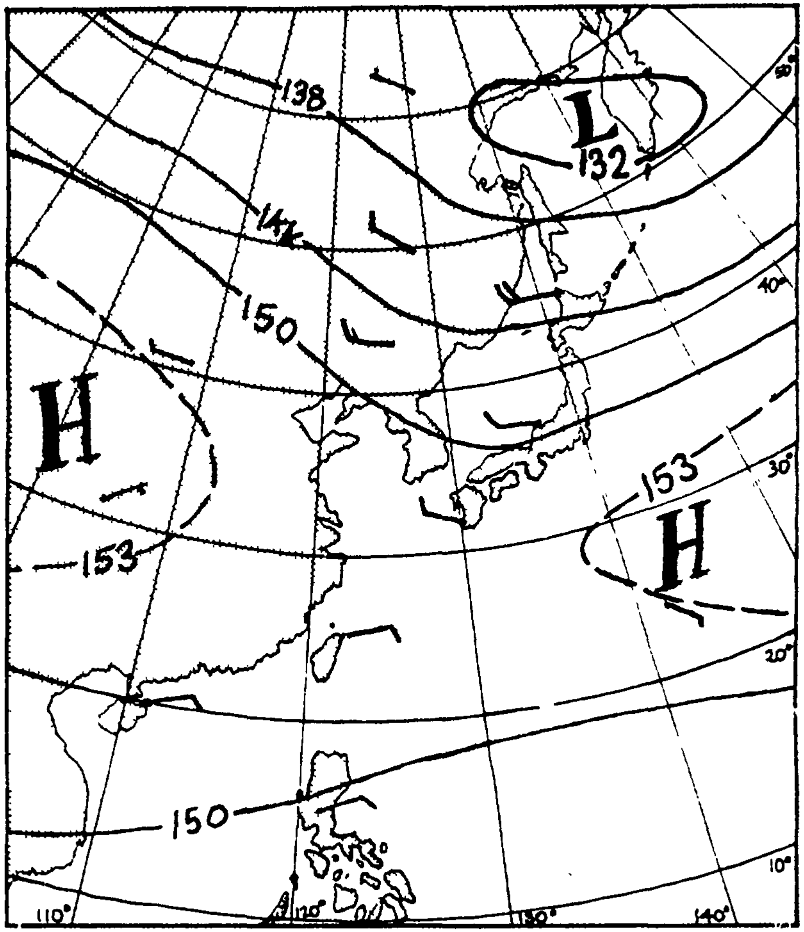

Figure 2-57. 850mb heights and winds for November. All heights in tens of gpm. (adapted from Crutcher & Meserve, 1970)

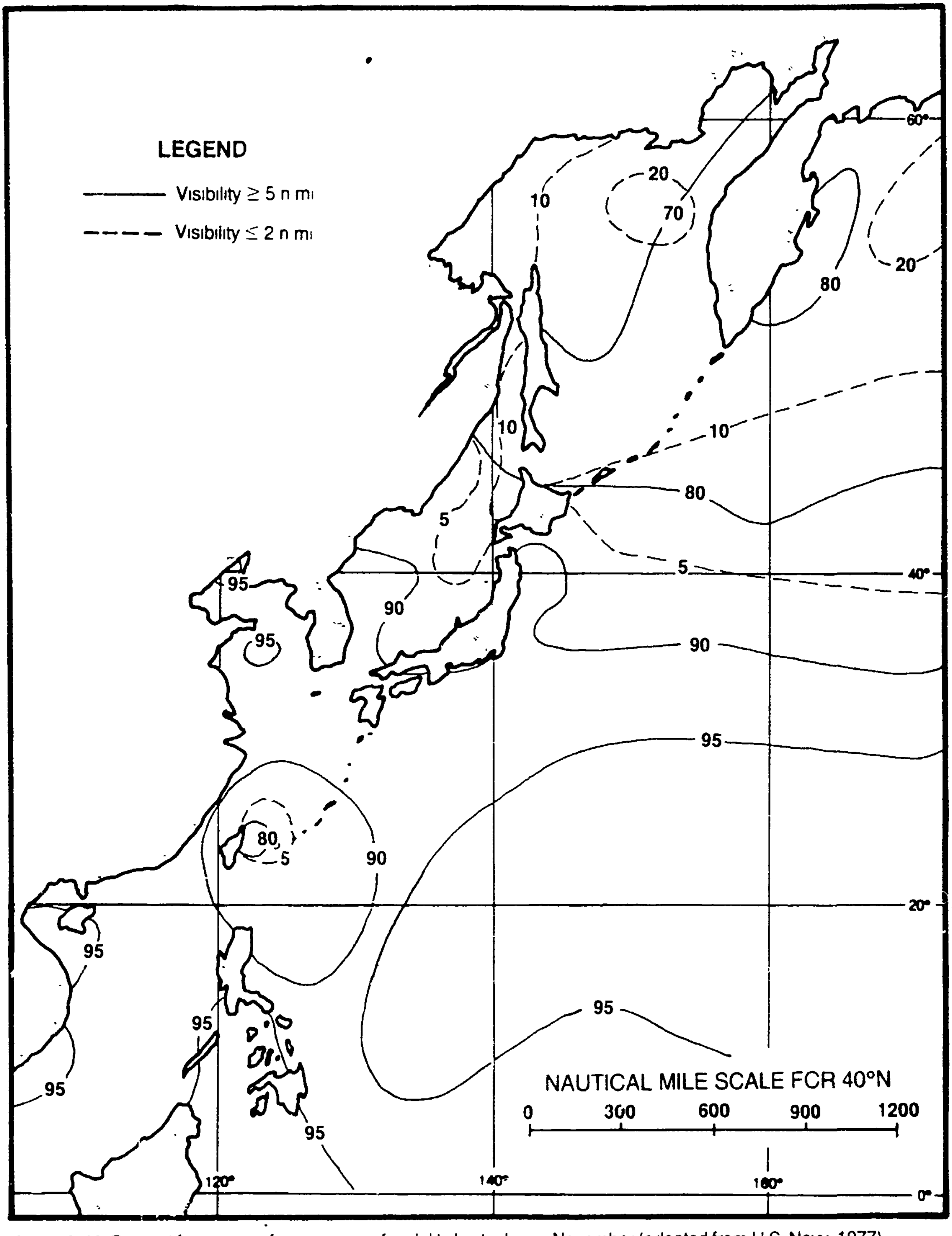

Figure 2-58 Percent frequency of occurrence of visibility limits during November (adapted from U S Navy, 1977).

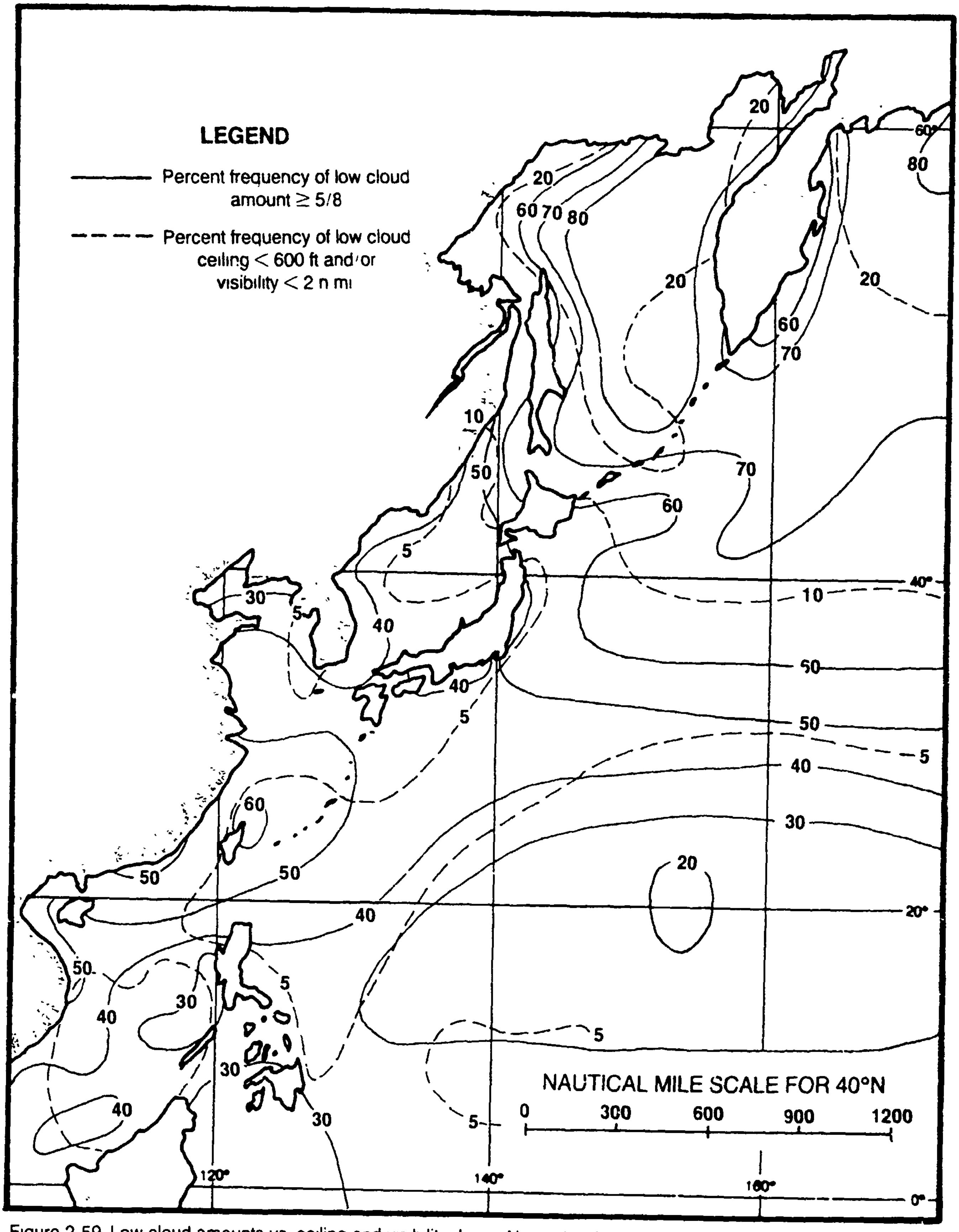

Figure 2-59. Low cloud amounts vs. ceiling and visibility during November (adapted from U.S. Navy, 1977).

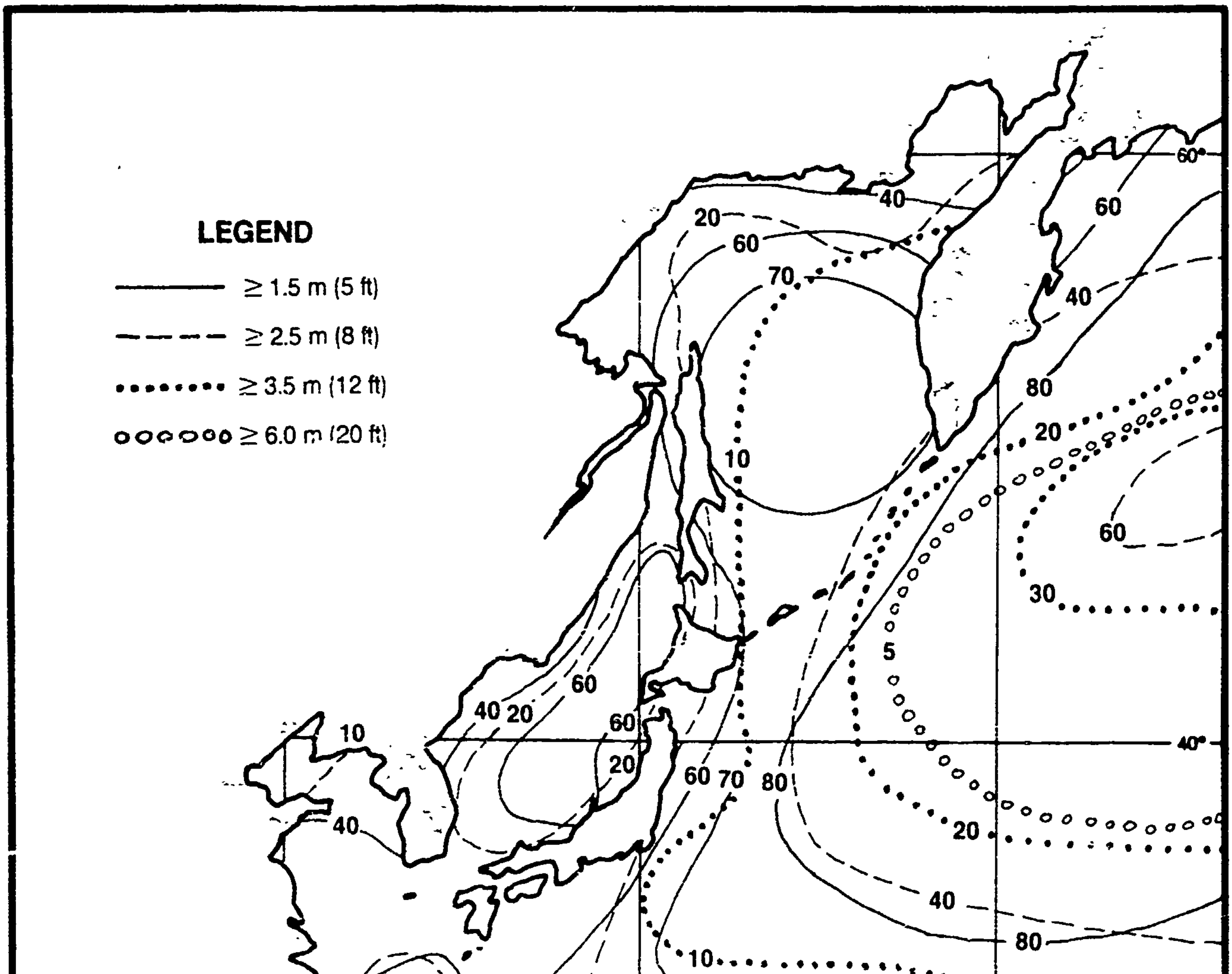

Figure 2-60. Percent frequency of occurrence of wave heights during November (adapted from U S Navy 1977)

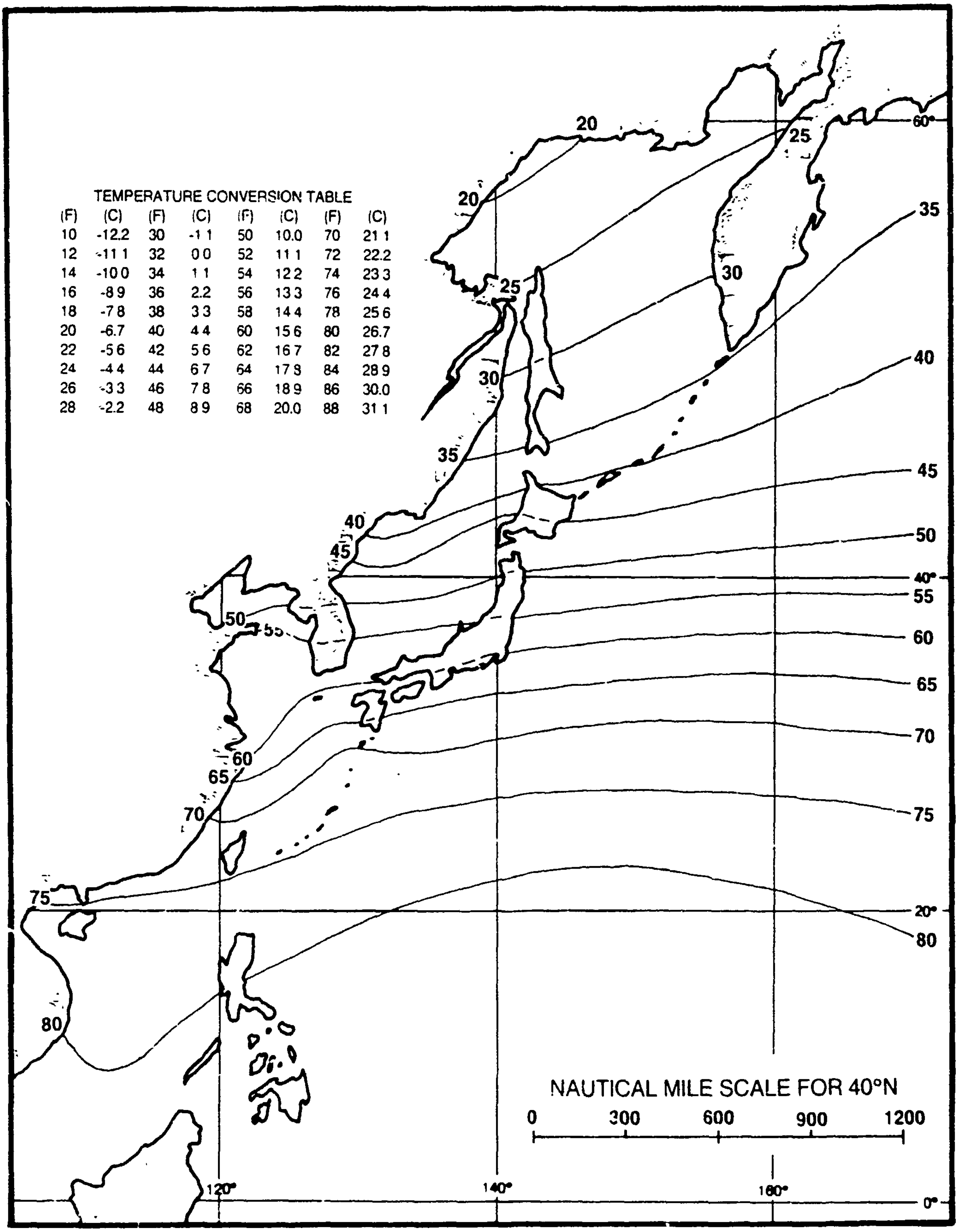

TEMPERATURE CONVERSION TABLE

(F)	(C)	(F)	(C)	(F)	(C)	(F)	(C)
10	-12.2	30	-1 1	50	10.0	70	21 1
12	-11 1	32	0 0	52	11 1	72	22.2
14	-10 0	34	1 1	54	12 2	74	23 3
16	-8 9	36	2.2	56	13 3	76	24 4
18	-7 8	38	3 3	58	14 4	78	25 6
20	-6.7	40	4 4	60	15 6	80	26.7
22	-5 6	42	5 6	62	16 7	82	27 8
24	-4 4	44	6 7	64	17 8	84	28 9
26	-3 3	46	7 8	66	18 9	86	30.0
28	-2.2	48	8 9	68	20.0	88	31 1

Figure 2-61. Mean surface air temperature in degrees Fahrenheit during November (adapted from Ownbey, 1973 and U.S Navy, 1977).

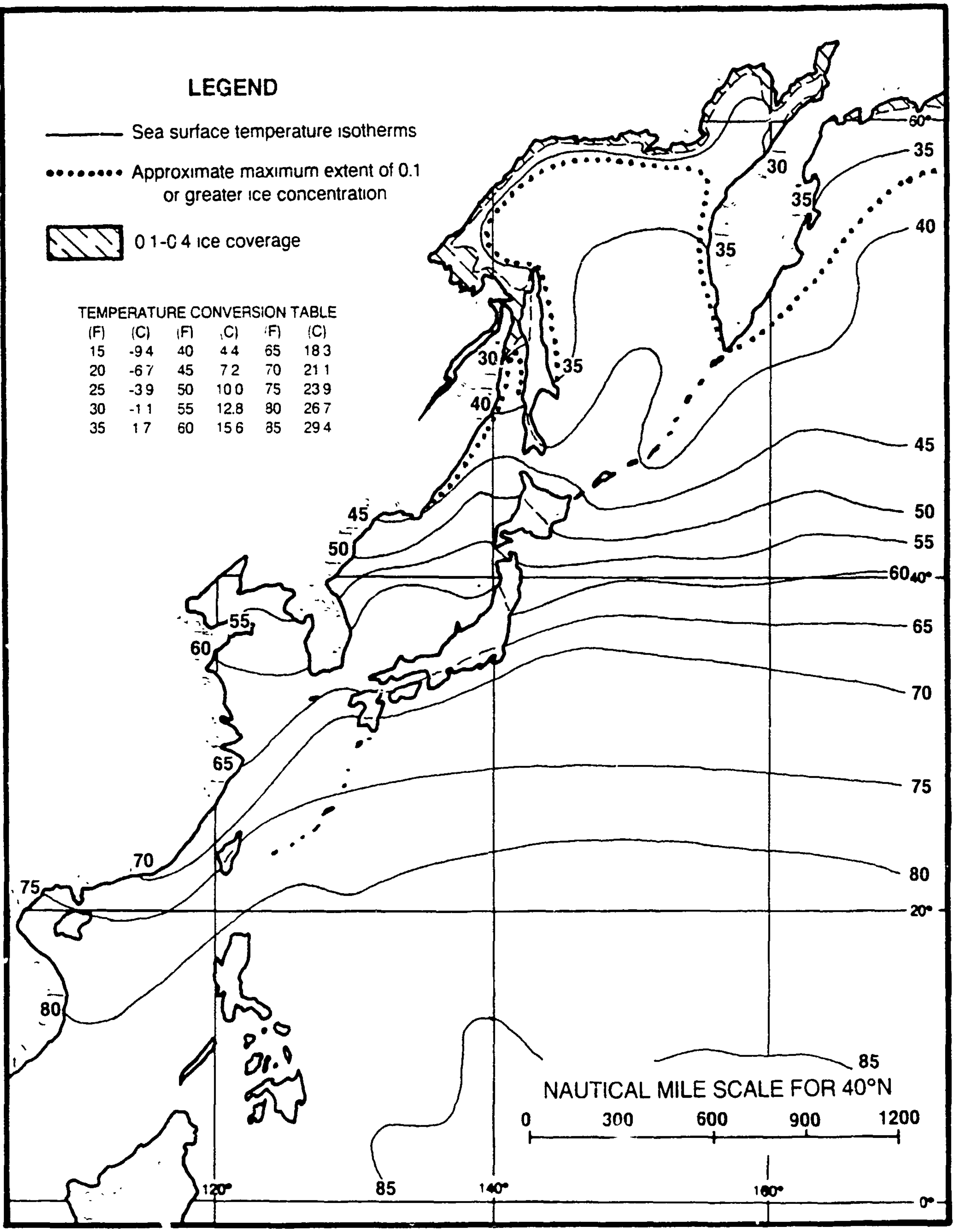

(F)	(C)	(F)	(C)	(F)	(C)
15	-9.4	40	4.4	65	18.3
20	-6.7	45	7.2	70	21.1
25	-3.9	50	10.0	75	23.9
30	-1.1	55	12.8	80	26.7
35	1.7	60	15.6	85	29.4

Figure 2-62. Mean sea surface temperature in degrees Fahrenheit during November, with approximate ice limits (adapted from U.S. Navy, 1967 and U.S. Navy, 1977)

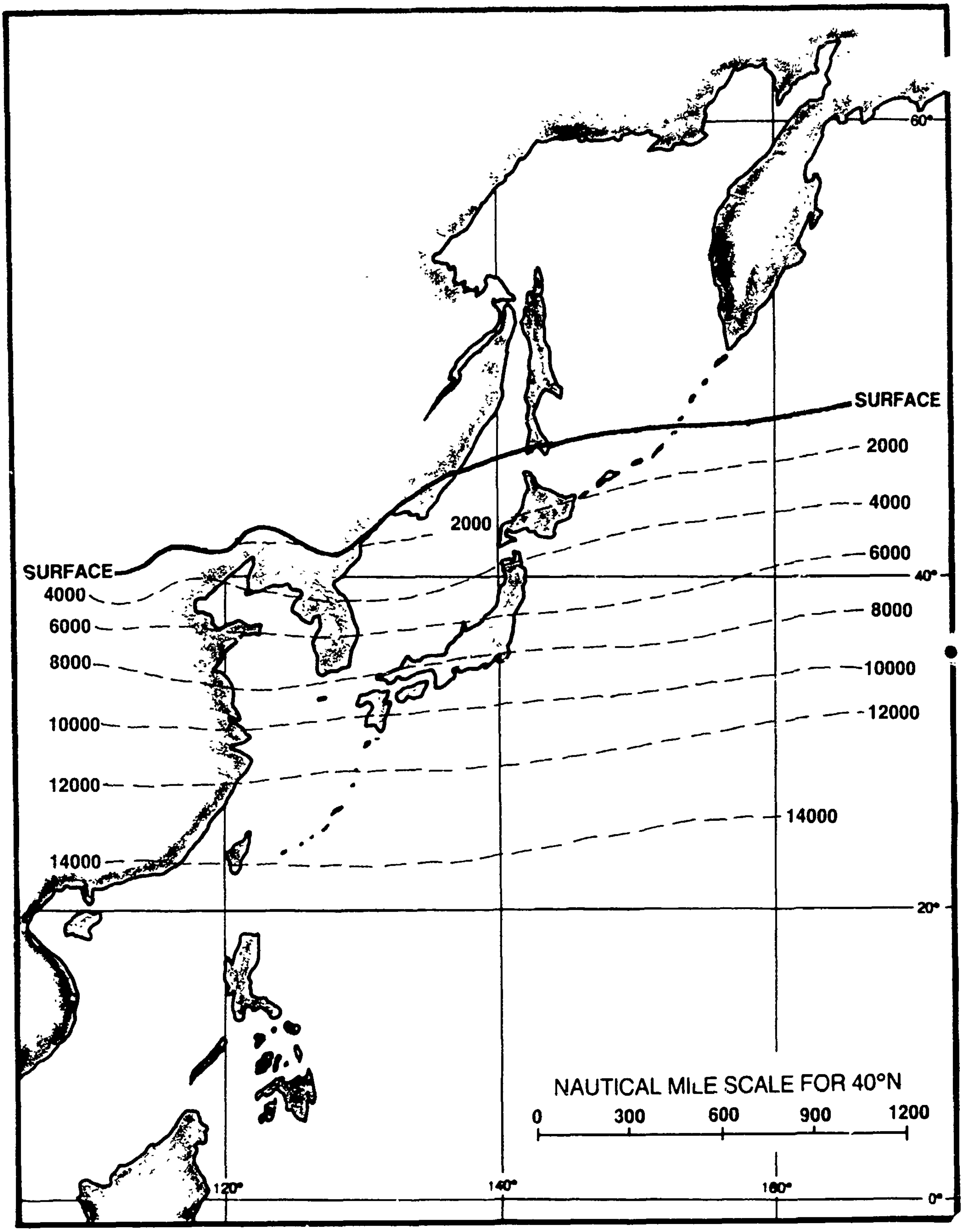

Figure 2-63. Mean altitude of the freezing level for November in feet (adapted from U.S Air Force, 1965).

2.3 Electro-Optical and Electromagnetic Conditions

Electro-Optical (E-O) systems are playing an increasing role in U.S. Navy operational activities. Fleet environmentalists have a growing requirement to support E-O systems and therefore a need for understanding the interactions between E-O systems and the marine environment. This introduction section provides some basic background material on electromagnetic (EM) radiation, its interaction with atmospheric constituents, and general types of E-O systems of concern to fleet environmentalists. The primary sources of the information provided here are: Electro-Optical Handbook Volume I, AWS/TR-79/002, Cottrell et al, 1979, and Proceedings of Workshop to Standardize Atmospheric Measurements in Support of Electro-Optical Systems, UDR-TR-83-71, Huffman et al, 1983.

2.3.1 E-O/EM and the Atmosphere as a Medium

E-O and EM systems respond to electro-magnetic radiation as a sensed stimulus. The atmosphere interferes to various degrees with these systems because it interacts with both the source and propagation of radiation. The interaction depends on the atmospheric constituents and the radiation wavelength. This handbook addresses portions of the magnetic spectrum from visible through microwave wavelengths (0.74 micrometers through 10.0 centimeters). Table 2-1 provides categories of sensor wavelengths, general types of systems, and significance of adverse weather elements.

Table 2-1. Electro-Optical and Electromagnetic Systems and Significance of Adverse Weather Elements as a Function of Sensor Wavelength Categories (after Cottrell et al, 1979).

	MICROWAVE		FLIR			VIDICON T.V.	
SYSTEMS	COMMUNICATIONS	RADAR	LASER				EYE T.V. CAMERA
WAVELENGTH CATEGORIES	MICROWAVE	MILLIMETER	INFRARED FAR FAR	FAR	MIDDLE	NEAR	VISIBLE
WAVELENGTH/ FREQUENCIES	10cm-1cm 3GHz-30GHz	1cm-0.1mm	0.1mm-15μm	15μm-6μm	6μm-2μm	2μm-0.74μm	0.74μm-0.4μm
WEATHER SENSITIVITY	GENERALLY INCREASES WITH DECREASING WAVELENGTH (TO THE RIGHT IN THIS TABLE)						
CLOUDS/FOG	SIGNIFICANT			EXTREMELY SIGNIFICANT			
DRY AEROSOLS	INSIGNIFICANT			SIGNIFICANT		EXTREMELY SIGNIFICANT	
PRECIPITATION	SIGNIFICANT		EXTREMELY SIGNIFICANT				
ABSORPTION	SIGNIFICANT		CAN BE EXTREMELY SIGNIFICANT			EXTREMELY SIGNIFICANT	
SCATTERING	SIGNIFICANT			EXTREMELY SIGNIFICANT			

There are four atmospheric physical processes which affect electromagnetic (EM) radiation: reflection, scattering, absorption, and emission. The type and size of the atmospheric constituents, gaseous molecules and particulates (dust, haze, smokes, fogs, other aerosols, cloud droplets, and precipitation) affect the propagation of radiation. The influence on various wavelengths is determined by the relationship between the size of the atmospheric constituents and the wavelength of the radiation. This relationship, referred to as the size parameter, is stated as:

$$\text{size parameter} = \frac{2\pi r}{\text{radiation wavelength}}$$

where r is the particle radius.

Reflection takes place when the size parameter is greater than approximately 10, that is, when the wavelength is much smaller than the particle radius. Scattering causes such phenomenon as the blue sky on clear days and the milky sky on hazy days. The blue sky results from preferential scattering of the short visual wavelengths (blue) of sunlight by molecules in the atmosphere, known as Rayleigh scattering. Larger particles such as cloud droplets, dust, haze, and smoke particles, which have a size parameter near one with respect to visible light, scatter all the visible wavelengths and cause the sky to appear white or milky. This scattering of the sunlight is called mie scattering. Absorption takes place on the molecular scale and occurs selectively with respect to wavelengths. Each absorbing constituent of the atmosphere (mainly water vapor, carbon dioxide, ozone, and oxygen) absorbs in specific wave length intervals, which are referred to as absorption bands. Radiation at other wavelengths is not significantly affected by that constituent. <u>Emission</u> is the emitting of electromagnetic radiation (for example, a flashlight beam or the heat from a household radiator). The process operates on the molecular scale, and every constituent of the atmosphere or earth emits radiation. However, emission occurs selectively with respect to wavelength, therefore the amount of energy emitted at a given wavelength may not be significant.

The <u>bulk or fundamental atmospheric parameters</u> of concern in E-O/EM forecasting are temperature, pressure, humidity, and wind. These elements determine the refractive index, absorption in the infrared, and the size and contribution to refractive index of atmospheric aerosols. Low-level profiles determine the atmospheric stability, which influences turbulence Weather elements such as drizzle, rain, and snow can severely limit the performance of all of the E-O/EM systems.

<u>Optical turbulence</u>, which degrades laser imaging systems, results from small-scale temperature and humidity fluctuations associated with atmospheric turbulence or mixing of air of different temperature and humidity. This turbulence causes fluctuations in the optical refractive index in the atmosphere. The turbulence parameter that is related to laser system performance is known as the refractive index structure parameter, labeled C^2_N, which is a function of temperature and humidity structure parameters. The turbulence or eddies that are of concern to lasers are very small, on the order of 10 to 20 cm.

The marine atmosphere can be divided into two layers: the <u>marine planetary boundary layer</u> (MPBL), and the <u>free atmosphere</u>. The MPBL is typically on the order of 1 km thick, well mixed, and topped by a stable marine inversion. The free atmosphere is controlled by large-scale highs and lows. The surface effects exert little influence on motion in the free atmosphere. With the exception of clear air turbulence, there is little turbulence and therefore only weak fluctuations in optical refractive index and consequently low values of C^2_N. In contrast, the MPBL is only weakly influenced by large scale patterns and is heavily influenced by surface effects. The primary surface effects are heating or cooling and friction. Surface effects cause the MPBL to be highly turbulent, and therefore large values of C^2_N are encountered. The larger the C^2_N value the greater the degradation of laser systems.

E-O systems in the visual through infrared wavelengths can be classified as either broadband or laser (narrow line) types. Broadband means to extend over a range of wavelengths, such as visual or infrared systems. A weapons system may combine both broadband and laser components e.g., a T.V. or forward looking infrared (FLIR) system used to locate a target that is then designated (illuminated and tracked) with a laser. Environmental support of combined systems would require consideration of the atmospheric parameters affecting the wavelengths of each of the systems.

2.3.2 Comments on E-O/EM Systems and Atmospheric Interactions

This section addresses some general E-O/EM systems and atmospheric interactions of concern to the fleet environmentalist.

Visual Systems: (E-O) Cameras and human eyeballs are visual systems that require cloud-free line-of-sight between the sensor and target. Furthermore, reduced visibility due to scattering and absorption by haze, fog, and precipitation limit the capabilities of visual systems. Also, each visible system requires a minimum level of illumination.

Infrared Systems:(E-O) Lasers and Forward Looking Infrared Radar (FLIR) are active and passive systems, respectively, that operate in the infrared wavelength and require cloud-free line-of-sight to the target. Some lasers can penetrate thin cloudiness, and passive infrared systems may detect hot targets through thin clouds. Haze, fog, and precipitation degrade the transmission of energy at near infrared wavelengths. Systems operating at longer infrared wavelengths are degraded by absorption of energy by atmospheric water vapor.

Millimeter/Microwave Systems: (E-M) Radar and microwave system performance is degraded by two main atmospheric factors: Heavy cloudiness (thick cloudiness with large droplet distributions of near-precipitation-sized particles), and precipitation.

2.3.3 Specific Categories of E-O/EM Systems

2.3.3.1 High Energy Laser

Atmospheric conditions degrade High Energy Laser (HEL) system performance by reducing fluence (energy density per unit time deposited on the target) on the target in a variety of ways: aerosols and water vapor absorb energy, atmospheric turbulence spreads the beam fluence, and atmospheric turbulence also causes the beam to wander off its intended target (Burk et al, 1979).

Environmental conditions such as heavy rainfall and fog-induced low visibility can reduce the effectiveness of HEL systems to a point that precludes operation of such systems. Goroch and Brown (1980) produced a climatology of the frequency of occurrence of adverse weather conditions which would preclude operations of the HEL system. They found that the area of the Yellow Sea, Korea, and the southern Sea of Japan experienced relatively high rates of limiting weather conditions, with fog being the most frequent factor. Their findings indicated limiting visibility conditions frequency of about 2% in winter and 10% in summer.

In general the highest rain rates occur in the tropical zones (short periods of intense rain under convection cells), while higher latitudes tend to experience longer periods of relatively light rain. The dense fog condition tendency is reversed with an increase in frequency with latitude (especially over the northwest Pacific). Local conditions related to upwelling and SST gradients, as well as the large-scale surface flow pattern, result in relatively high fog frequencies over the mid and sub-polar latitudes of the northwestern Pacific. Degraded HEL performance potential can be related to the climatology patterns of heavy rainfall and dense fog. Day-to-day performance will be influenced by these same conditions.

2.3.3.2 Forward Looking Infrared

The Forward Looking Infrared (FLIR) information presented in this handbook was taken from the Naval Environmental Prediction Research Facility (NEPRF) technical report 81-06, Climatology of Infrared Ranges in Pacific Ocean Regions of the Northern Hemisphere (Goroch and Brown, 1981). This climatology was computed for a nominal FLIR sensor attempting to detect a broadside cruiser target.

Expected range and standard deviations by month are available in this referenced report.

The basic concept of thermal sensing, such as FLIR, is the detection of a target by a thermal detector which senses or perceives a temperature difference (contrast) between the target and its background. The temperature differences result from solar heating (insolation) or cooling by the ambient wind. The sensed or perceived contrast by the detector is diminished by the atmosphere between the source (target and its background) and the receiver (the infrared detector). The loss of contrast is termed the transmittance. The strongest reduction in contrast occurs during fog or precipitation. When visibility is less than 1 km, FLIR ranges can be considered the same as the visibility.

These absorption characteristics give the FLIR ranges a close relationship to the general atmospheric circulation patterns. In general there is a latitude-FLIR range correlation (increasing range with increasing latitude) reflecting a change from the warm moist stable equatorial area, to the cooler drier but variable mid-latitudes, and finally the cold dry polar regions. Effects such as continental outbreaks, stratus and fog regimes, upwelling, and oceanic currents and associated areas of cyclogenesis result in extreme variability of FLIR ranges over near coastal waters.

In the infrared wavelengths (3.4 to 5 micrometers and 8-12 micrometers) the absorption by water vapor is generally the primary effect. Absorption by aerosol particles is normally of secondary importance. However, under conditions of atmospheric low water vapor content (low temperature and/or relative humidity) the aerosol absorption becomes dominant. The open north Pacific Ocean climatology of FLIR has the following general characteristics:

(1) Increases from equator northward through mid-latitudes.

Winter:	Equator	10-15 km
	40-50°N	30-35 km
Summer:	Equator	10-15 km
	near 60°N	30 km

(2) Summer equatorial type ranges extend into mid-latitudes in central and western Pacific. Reflects the northward advection of warm/moist equatorial air over western Pacific.

(3) The variability of ranges increases with latitude and near coastlines. Reflects the variation of the general weather patterns and specifically the associated variations in temperature, relative humidity, and pressure.

FLIR climatology for the area of Japan and surrounding seas is strongly influenced by coastal, as well as seasonal and latitudinal changes. The result is significantly large variations in FLIR ranges over most of this area on both seasonal and daily or synoptic time scales. FLIR ranges and variations over the area south of about 40°N correlate highly with the monsoon patterns. Equatorial values, near 15 km with about 2 km variations, occur during July and August under the fully developed Southwest Monsoon. Mid-latitude ranges of 25 to 30 km with variations of 10 to 20 km are found during December through March reflecting the Northeast Monsoon and migratory systems. North of about 40°N the FLIR ranges reflect the general middle and high latitude patterns averaging from 20 to 30 km, but are extremely variable with variations approaching the average values.

2.3.3.3 Radar and Microwave

The problems associated with atmospheric refraction and anomalous propagation of radar and radio waves have long been recognized by the U.S. Navy. The development of the computer-based

IREPS (Integrated Refraction Effects Prediction System) by the Naval Ocean System Center (NOSC), originally on Hewlett-Packard 9845 computers aboard selected ships, has significantly enhanced refraction index forecasting. General discussion of refraction and related conditions are addressed in several Navy standard training manuals including the Aerographic's Mate 1 & C training manual.

The refractive index N is defined as the ratio of the speed of propagation of an electromagnetic (EM) wave in a vacuum to that in the actual atmosphere. Refraction is the bending of waves due to a change in density of the medium through which they are passing, the atmosphere for our purposes. Under standard, or "normal", conditions the density of the atmosphere decreases at a gradual but continuous rate with altitude. This density change is a function of decreasing temperature, humidity, and pressure and results in a rate-of-change of N of 12 units/1000 ft. When non-standard temperature and humidity vertical distributions occur the rate-of-change of N becomes non-standard too.

The speed of propagation of an EM wave in a vacuum is greater than in air. Therefore, under normal conditions with decreasing density with height, EM waves travel faster at higher levels in the atmosphere than at lower. The result is that as a wave front, with some vertical extent, moves through the atmosphere the upper portion moves fastest and results in a downward bending or refraction of the wave front. The standard refraction rate however, is less than the curvature rate of the earth's surface. The end result is that under standard atmospheric conditions the wave front gradually moves away from (to higher altitude) the earth's surface but at a lesser rate than a line tangent to the earth's surface.

In the real world the atmosphere is seldom, if ever, standard. The actual refraction is typically slightly greater (super refraction) or less (subrefraction) than standard. Certain conditions occur which disrupt the standard temperature and humidity distributions to the extent that a significant degree of EM wave bending occurs and the wave becomes trapped within a layer of the atmosphere. This occurs under conditions of increasing temperature or sharply decreasing humidity with increasing altitude (as with an inversion). Anomalous propagation (AP) of the radar or microwave energy will then take place. The energy trapped within the layer will provide extended ranges in the layer or duct, but reduced ranges will result in the region which the waves were refracted away from.

There are three general types of ducts: 1) elevated ducts, 2) surface-based ducts that extend down from elevated trapping layers, and 3) evaporation ducts.

Elevated ducts primarily affect airborne operations. They are the result of moisture layers and/or elevated temperature inversions. They may be found anywhere from the surface to 20,000 ft or more, but are most common below 10,000 ft.

Surface-based-ducts can result in extended detection, intercept, and communication ranges for all frequencies above 100 MHz (Petit and Hamilton, 1984). These extended ranges presuppose that both the transmitter and receiver are in or near the duct. Surface ducts typically are found under the southeast quadrant (northern hemisphere), northeast quadrant (southern hemisphere) and near the center of high pressure systems.

Evaporation ducts are created by strong negative vertical water vapor gradients (i.e., water vapor rapidly decreases with height). Normally they occur within 100 ft of the surface and tend to extend ranges for surface-to-surface systems operating above 3 GHz.

Meteorological factors affecting evaporation duct height climatology for 10 Atlantic ocean weather stations was studied by Sweet (1980). Some general observations from this study are considered applicable to the general problem.

(1) Evaporation duct heights are normally within 100 ft of the sea surface.

(2) Evaporation duct heights increase as latitude decreases. Median annual duct heights (the height exceeded half the time during the year) ranged from about 50 ft at 35°N to about 20 ft at 55°N and remained nearly constant to 62°N, the northernmost station in the study.

(3) Increased air and sea surface temperatures result in higher duct heights.

(4) In mid-latitude, maximum duct heights occur during late fall and early winter. Minimum duct heights occur in late spring and early summer.

(5) Stronger winds result in higher duct heights.

(6) Sea surface temperatures greater than air temperatures result in higher duct heights.

Helvey and Rosenthal (1983) conducted a study to define ways of inferring refraction conditions from synoptic parameters. Considerable scatter or variation in duct conditions was found when attempting to correlate synoptic conditions with refractive conditions, resulting in an acknowledgement in the report that the procedures developed should be considered tentative interim guidance.

Seasonal histograms of duct heights (taken from the Tactical Environmental Support System (TESS) data base) are included for each geographic area.

2.3.4 Forecast Aids for Elevated and/or Surface Based Ducts

The following synoptic features and inferred elevated trapping layer (ETL) indicators are provided for assistance in forecasting ETL conditions for the current time at remote sites. When coupled with forecasting of synoptic or climatological patterns, these inferences can also be helpful in forecasting future ETL conditions.

(1) The strongest and most persistent inversions and associated refractive layers occur in the equatorward half of subtropical oceanic highs, particularly the southeast quadrant in the northern hemisphere and northeast quadrant in the southern hemisphere.

(2) Tracking westward under the equatorward half of the subtropical highs, convection related to warmer SST results in a progressively higher and weaker inversion (and refractive layer) with a correspondingly deeper marine layer.

(3) Changes from fog through low stratus areas to higher stratocumulus and cumulus areas infer a higher and weaker inversion.

(4) Ocean currents influence the thickness of the marine layer. Warm currents, such as the Kuroshio of the western north Pacific weaken and increase the thickness of the marine layer while the cold currents of the northwestern and eastern portion of the north Pacific intensify and reduce the thickness of the marine layer.

(5) Because inversions and ducting are associated with subsidence and stable layers, therefore highs rather than lows, the frequency of ducting shows a strong correlation with SLP. When the SLP is below 1000 mb, the probability of ducting is very low (<10%) while with SLP >1020 the probability approaches 50%.

(6) Duct frequency versus surface wind direction is at a minimum for S through WNW winds and a maximum for NNW through SE winds.

(7) Duct frequency increases as the temperature difference between the surface and 700 mb decreases. Small differences indicate a stable atmosphere (high frequency of inversion and ducts) and large differences indicate an unstable atmosphere and convective activity (low frequency of inversion and ducts).

Forecast Aids for Prediction of Standard Refractive Conditions

(1) Area of concern is located within the northwest quadrant of subtropical highs or northern half of migratory highs.
(2) Under or immediately following an active front.
(3) Area of cyclonically curved isobars.
(4) Close to a low pressure center.
(5) Surface pressure less than 1000 mb.
(6) Cold air aloft, 700 mb temperature less than -10C.
(7) Presence of cumulus and deep convective clouds.
(8) Unstable, windy conditions.
(9) Open celled clouds behind frontal systems.

Forecast Aids for Duct Height

(1) The maximum frequency of oceanic ducts occurs in the 4,000 to 6,000 ft layer.

(2) A secondary frequency maximum occurs between the surface and 2000 ft when the SLP is >1018 mb and surface winds are <6 kt (near centers of highs).

(3) When a migratory upper-level trough replaces a anticyclone, strong low-level ducts are likely to become weak ducts near 10,000 ft within a 48-hour period.

(4) Within oceanic anticyclones, duct heights vary by about 3000 ft from the lowest level in the SE quadrant to the highest in the NW quadrant.

(5) In addition to synoptic variations there are general latitude variations. On the average ducts are higher in lower latitude (over warmer water) and lower towards the poles (over colder water).

(6) There is a tendency for the mean elevated duct heights to increase with increasing SST. Table 2-2 provides approximate mean duct heights for areas within 300 n mi of the center of highs for SST intervals.

Table 2-2. Approximate Mean Elevated Duct Heights (Z_D) for areas within 300 n mi of highs for Specified Sea Surface Temperature Intervals (Helvey and Rosenthal, 1983).

Sea Surface Temperature (SST)		Height MSL (Z_D)	
(C)	(F)	(m)	(ft)
5- 7	41-45	1000	3300
8-10	46-50	1200	3900
11-12	51-55	1300	4300
13-15	56-60	1400	4600
16-18	61-65	1500	4900
19-21	66-70	1600	5200
22-24	71-75	1700	5600
25-27	76-80	1800	6200
>27	>80	2000	6600

(7) A best fit linear regression for optimum coupling height (OCHT), where OCHT is defined as the altitude at which electromagnetic energy is most effectively "coupled" into the duct, is:

$$\text{OCHT (m)} = 42 \text{ (SST in } ^{\circ}\text{C)} + 743$$

Example: SST = 20°C

OCHT = 1583 m

Based on 5 year study by Ortenburger, L. N. et al. (1978) of GTE, Sylvania, Electronic Systems Group, Western Division, Mountain View, California.

Forecast Aids Based on Satellite Interpretation

(1) The areas of open cells, to the rear of fronts, indicate unstable conditions and therefore are likely to have near-standard propagation conditions.

(2) Areas of closed cells indicate stable conditions, and inversions and ducting are probable.

(3) Areas of smooth low-level stratus are likely to be topped by a low-level inversion, and ducting is likely (may be surface-based).

(4) The appearance of ship condensation trails indicates a strong shallow marine layer and probable surface-based ducts.

(5) Frontal bands imply strong winds, well mixed atmosphere, and near-standard propagation conditions.

(6) Over the region where the closed cells become smaller and change to smooth continuous structures the inversions and duct heights will be lowering.

(7) In regions of offshore flow where clear conditions extend seaward and change to lighter gray shade areas and then smooth stratus type clouds, surface-based ducts are likely. These areas are under the influence of high pressure and subsidence.

(8) In regions of offshore flow where distinct cloudlines are seen forming, near-standard propagation conditions are probable. The areas generally have well mixed and unstable atmospheric conditions.

(9) Improved visibility, EM ranges, and weakened low level inversions are typically found in the lee of mountainous islands. In visual imagery then areas will appear darker than surrounding areas, unless they are in a sunglint area in which case very bright return will be seen if surface winds are light.

(10) Cornering effects result in increased winds, convergence, cloud development, and typically degraded visibility and EM conditions. Cornering effects occur where moderate or stronger winds blow around islands or points of land.

(11) Increasingly lighter gray shades over water areas imply increased atmospheric humidity and/or aerosols and reduced visibility and EM ranges.

(12) When smoke plumes from coastal facilities can be seen extending for some distance in satellite imagery or by eye, a temperature inversion is likely near the top of the smoke plume level.

(13) The SST pattern in shallow coastal water areas will exhibit a strong seasonal reversal relative to the deep water SST. Coastal waters tend to be hot in summer and cold in winter and will modify the atmosphere above it and the EM conditions. Summer heating provides well mixed and near normal conditions. Winter cooling will stabilize the lower levels resulting in low level inversions and generally reduced EM ranges.

2.4 Ocean Acoustics

A complete review of ocean thermal and acoustic properties and resulting sound propagation characteristics is beyond the scope of this handbook. The subjects are addressed in a number of training and information manuals, including general information in the Aerographer's Mate Training manuals and area specific information in Special Publication 3160-NP7. Application programs are also available on the Tactical Environmental Support System (TESS).

3.0 SEA OF JAPAN

3.1 Regional Features and Their Influence on Weather Phenomena

The Sea of Japan, with an areal extent of some 391,100 sq mi and average depth of 5,468 ft (1,667 m)(Newspaper Enterprise Association Inc., 1978), is nearly surrounded by mountainous terrain. Although not landlocked, the sea is accessible only by four narrow straits: the Tsushima (Korea) Strait between Japan and Korea, the Tsugaru Strait between the Japanese islands of Honshu and Hokkaido, the Soya (La Perouse) Strait between Hokkaido and Sakhalin Island, and the Tartar Strait between Sakhalin Island and the Asian continent (Figures 3-1 and S-3-1, page 3-3).

The coastal mountains of Korea and the USSR pose significant barriers to air flow along the western shoreline of the Sea of Japan. Beginning in the northern portions of eastern USSR with the Sikhote Alin Range, the coastal mountains extend southward through eastern Manchuria and into Korea. Elevations are in the 1,640 to 6,562 ft (500 to 2,000 m) range in the Sikhote Alin Range, with some peaks in the Nangnim Sanmaek Range of Korea exceeding 8,202 ft (2,500 m).

The mountains of Japan and Sakhalin Island border the eastern and southern shorelines of the Sea of Japan. Sakhalin Island has ridge lines oriented primarily north-south with elevations of 1,640 to 3,281 ft (500 to 1,000 m) predominating with a few peaks exceeding 3,281 ft (1,000 m). Japan has three mountain ranges which form a series of backbones running through the islands.

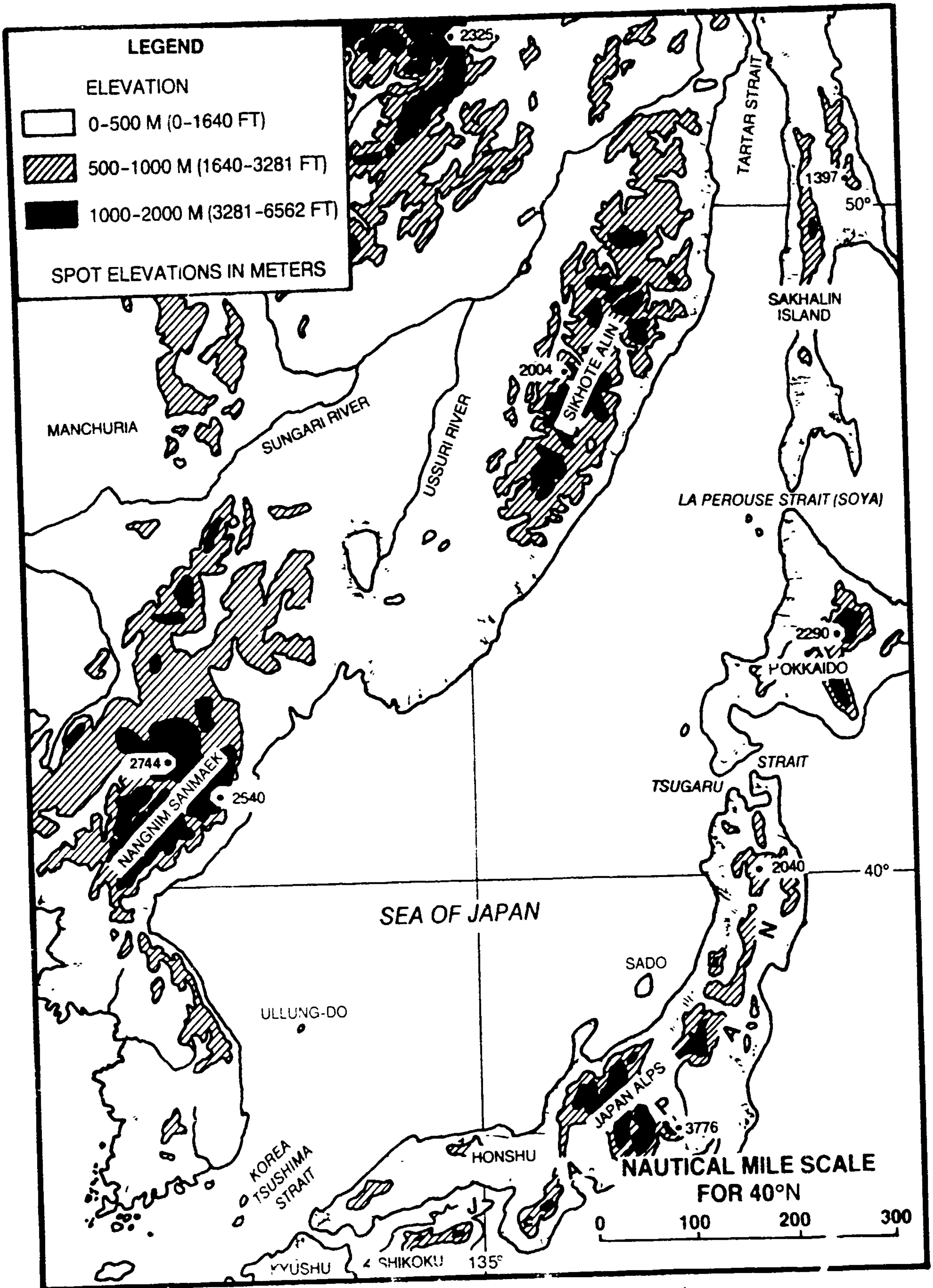

Figure 3-1 Major topographic features surrounding the Sea of Japan (adapted from Nestor, 1977)

Figure 9-I-1. Regional [illegible]

FIGURE S-3-1. REGIONAL VIEW, SEA OF JAPAN. 23 OCT 79
OSAN AB Visual DMSP: TN: 23/0137 GMT

Synoptic Features: An elongated bubble 1024 mb high encircles the Japanese Islands resulting in generally clear skies.

Satellite Features:

1. The general lack of organized cloud features throughout this field of view reflects the dominate high pressure system and area wide weak gradients. The ability to envision fair weather areas, because of the lack of cloud features, can sometimes be as useful as knowledge of bad weather (not labeled).

2. Increasing westerlies to the north are reflected by the lines of clouds off western Hokkaido and the upslope clouds and following wave clouds over the island.

3. The presence of a low level inversion over the colder waters east and north of Hokkaido are reflected by the wave patterns in the patches of stratus over that area.

4. The cloud lines extending northeastward from the Tsushima/Korea Strait reflect the land breeze fronts off Korea and Honshu. Ideal conditions for land breezes would have existed during the night before this late morning pass as the center of the bubble high with near calm gradient winds and clear skies passed over the southern Sea of Japan.

Forecast Aids:

1. When cloud patterns are widely scattered, disorganized, chaotic, and non-threatening appearing, weather conditions are generally fair and winds are light.

2. Local effects, such as land/sea breezes may in fact be enhanced during these periods of lack of large scale forcing.

3. Low level inversions are likely to exist over the cold water areas of the northwestern Pacific unless there is evidence of cold air advection (open celled cumulus) over the region.

4. If strong land breezes occurred during the late night/early morning, strong sea breezes are likely the next day unless the large scale forcing changes.

The principal mountain chain, the Japan Alps, is located in the central section of Honshu. The Alps average some 4,921 to 11,483 ft (1,500 to 3,500 m) in elevation, with Mt. Fuji, the highest peak in Japan, reaching 12,388 ft (3,776 m). The mountains of northern Honshu average 4,921 ft (1,500 m) with the highest peak reaching 6,693 ft (2,040 m). Southwestern Honshu is less rugged, with the highest peak reaching only 5,620 ft (1,713 m). The island of Shikoku, however, immediately adjacent to southwestern Honshu, has one peak reaching 6,496 ft (1,980 m). The second major mountain chain in Japan is comprised of the mountains of Hokkaido. They exceed 1,640 ft (500 m) with several areas exceeding 3,281 ft (1,000 m) and one peak reaching 7,513 ft (2,290 m). The third major chain is on the Japanese island of Kyushu. The mountains of Kyushu are not as impressive as those of the Japan Alps since the highest peak is only 5,866 ft (1,788 m), but they are significant. According to NOCD, Atsugi, (1980), "...the southern Honshu-Kyushu area is noted for its frontogenesis and cyclogenesis effects due in part to the mountains of Kyushu."

Most of the mountain barriers surrounding the Sea of Japan are oriented primarily north-northeast/south-southwest and have considerable influence on the climate and weather patterns of the Sea of Japan. Air masses, frontal systems and upper air features are all affected by the mountains, with some being significantly altered when passing over them. The veering of low level winds at land stations during frontal passage is frequently masked or delayed when the reporting station is in a valley with a northeast-southwest orientation, causing a misinterpretation of frontal velocity by the inexperienced environmentalist. The tracking and forecasting of any pressure system moving through eastern Asia is made difficult by the rugged terrain. Most surface wind directions reported by land stations throughout the area are unreliable when the speed is less than 15 kt. Temperatures and dew points can be misleading due to the complex topography. As documented by FWC/JTWC (1978), "Successful and accurate surface frontal analysis can only be achieved by careful analysis of the 850 mb level. At this level the elements of wind direction, temperature, dew point, etc., are relatively more accurate" and discontinuities between air masses are easily seen.

Other forecasting problems are caused by the geography and topography of the area. The barrier formed by the Sikhote Alin and Nangnim Sanmaek ranges affects all pressure systems moving southeastward to the Sea of Japan. Strong dynamic troughs are formed on the leeward side of the coastal ranges, becoming very intense with strong zonal flow aloft and strong northerly winds channeled through the Ussuri River Valley (west of the Sikhote Alin mountains).

The mountains of Japan have a profound effect on passing weather systems. Extratropical cyclones rarely cross the islands. Instead, they move up the northwest coast of Japan or skirt south of Japan before moving to the northeast. Frontal systems associated with these cyclones usually follow a definite pattern. A warm front will "hang up" in the mountains, causing an occlusion as the faster moving cold front overtakes it. Cold and occluded fronts are slowed on the up-slope of the Kyushu mountains and accelerate on the down slope, where they may lose almost all typical weather and cloud characteristics as the cold air is warmed by adiabatic compression. When these "dry" cold fronts reach the warm Kuroshio Current (Figure 2-4, page 2-11) they regain moisture and reintensify (FWC/JTWC, 1978).

The Sea of Japan itself exerts a strong influence on the air masses which pass over it. In winter, cold air from the Asian landmass gathers moisture as it moves over the relatively warm water, resulting in considerable instability, cumulus clouds and snow shower activity (Figure S-3-2). This sequence of events accounts for much of the snowfall on the windward shores of Japan. During summer, the warm tropical air brought northward by the monsoon is cooled, causing stable conditions such as fog and haze.

River drainage into the Sea of Japan is minimal. While several small rivers around its periphery contribute a small amount of fresh water runoff, no major rivers have mouths on the Sea of Japan. Two of the three largest rivers of Japan terminate in the sea, with one each on the west coasts of Honshu and Hokkaido. But the longest, the Shinano on Honshu, is only 229 mi long so the flow is not a significant influence on the climate of the region.

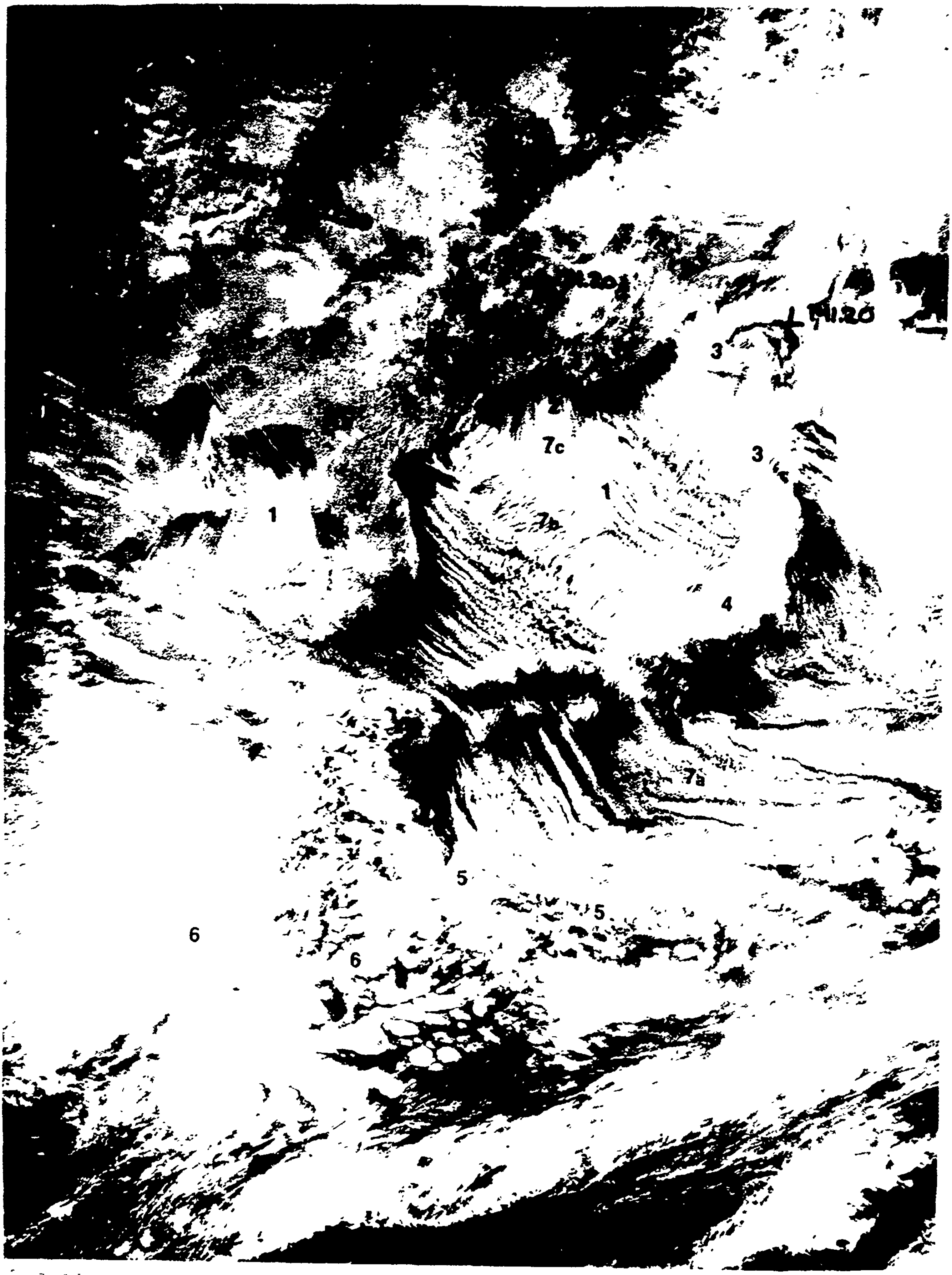

3
3
7c
1
1
7b
4
7a
5
5
6
6

FIGURE S-3-2. WINTER COLD OUTBREAK. 6 FEB 80
Visual DMSP: DN: 06/0006 GMT

Synoptic Features: A large 985 mb low centered about 900 n mi east of northern Japan and an intense 1064 mb Asian high are causing strong northerly flow and an outbreak of cold air over the Sea of Japan and adjacent seas.

Satellite Image Features:

1. The widespread numerous cloud lines vividly depict the intensity of this cold air outbreak. Air temperatures at or below freezing covered the entire Yellow Sea, Sea of Japan, Sea of Okhotsk, and portions of the open Pacific north of about 40°N on this day in February 1980. Ship observations report sustained surface winds were in the 20 to 40 kt range near the time of this image.

2. The local funneling patterns of valleys and breaks in the terrain are clearly indicated by the length of cloud free paths seaward and downwind from the terrain features. Cloud free paths are shorter downwind from valleys or low elevation terrain where minimum drying of the air occurs during flow down the terrain slope to sea level (Streten, 1975).

3. Small scale vortices, likely generated by terrain induced horizontal shear, are evident in the northern Sea of Japan.

4. The buildup of clouds on the windward side, and pronounced drying on the lee side is frequently seen over Japan and off the Asian continent.

5. A change in the cloud pattern south and east of Japan (extending east and west from a line between the two "5's") indicates the change in low level flow from cyclonic to anticyclonic curvature.

6. Continuing downwind in the area of anticyclonic flow, the clouds take on a flat topped, closed cellular pattern, becoming continuous smooth topped, layered, stratiform type.

7. Variations in the mean vertical wind shear through the cloud layer result in three convective cloud regimes: (7a) Cellular under light shear, (7b) transverse bands with moderate shear, and (7c) longitudinal bands with strong shear.

Additional Comments:

1. The cloud lines change from lines parallel (longitudinal bands) to the wind shear through the cloud layer (like area 1 and 2) to rows of clouds perpendicular (transverse bands) to the wind shear

(area 7b) in several areas of the image indicating weakening shear through the cloud layer (Tsuchiya and Fujita, 1967).

2. The length of the cloud free path increases with an increase in the upwind terrain height and decreases with the strength of the winter monsoon. These relationships are a result of increased drying of air during extended downslope flow and enhanced thermodynamic effects (moisture flux and heating from below) during extreme cold and high wind conditions of strong outbreaks.

Forecast Aids:

1. The intensity of cold air outbreaks is reflected in satellite imagery by the convective cloud regimes. Areas of strong outflow are marked by longitudinal bands, the stronger the outbreak the longer and wider the longitudinal bands.

2. Over the western Sea of Japan, the length of the cloud free path downwind from the western coastline will vary from less than 20 n mi under strong outbreaks to 180-240 n mi under weak outbreaks.

3. Opposite valleys and low terrain, the cloud free distances will be relatively short compared to areas opposite high terrain.

4. During winter outbreaks the dew points over USSR will be below -20°C, increase to about -10 to 0°C over Japan, and reach 10°C about 300 n mi south and east of Japan. Air temperatures will closely reflect the SST except near the coastlines and over terrain where lower air temperatures will reflect the source region and elevation factors (Tsuchiya and Fujita, 1967).

5. The change from longitudinal to transverse to cellular convective cloud patterns reflect decreasing wind shear through the cloud layer. Typical values are: Shear greater than 4-5 kt/1000 ft results in longitudinal bands, for 3-4 kt/1000 ft transverse bands, and for less than 3 kt/1000 ft cellular clouds.

6. Under moderate or stronger outbreaks, light snow showers will occur over the eastern Sea of Japan, increasing in intensity to heavy showers along western Japan. Two regions of frequent enhanced convective clouds and shower activity have been noted near 40°N, 135°E and off the northwest corner of Sado Island. These are likely associated with preferred regions of orographically induced and air-sea interaction enhanced mesoscale convergence zones, such as the band of clouds extending westward from near the number 4 across the Sea of Japan to just south of number 7b (Chou and Byerly, 1983) and (Uemura, 1981).

7. Generally the length of the cloud free path will increase from the northern to southern portion of the western Sea of Japan.

8. Heavy snow will fall over western Japan under cold outbreak regimes, with deposits measured in feet over the western slopes of mountainous areas.

9. For E/O forecasts the best ranges will be in the regimes of cloud free and shower free areas. Conditions will vary between the alternating longitudinal/transverse bands. These bands have width dimensions of 10 to 60 n mi with 20 to 30 n mi widths being typical.

10. Improved E/O ranges in coastal regions will be found downwind from high terrain, in the lee of island barrier effects, and in the clear slots between cold bands.

11. A lee side pressure trough will typically be found off the Asian coast during cold outbreaks, with pressure falls of 3-4 mb's typical.

12. During winter outbreaks the length of cloud free distances to the lee of the Japan Islands is near zero where the coastal $T_a = 0$ and temperature dew-point spreads are small. As the T_a decreases the cloud free path increases appreciably, reaching lengths of near 200 n mi where coastal T_a's are -15°C or less.

13. The wind profiles through the three convective cloud patterns all tend to show maximum speed shear in the layers below and immediately above the cloud layer. They differ in that through longitudinal regimes the <u>shear is near constant</u> from the surface to 3 to 5000 ft, increasing from surface speeds to 60 to 70 kt near 3000 ft. Through transverse banding the <u>speeds are near constant</u> through the cloud layer, while in cellular regimes the <u>speed may actually decrease</u> through the cloud layer. In the latter two cases (transverse and cellular) the resulting wind shears (just above and just below with little or no shear through the cloud) may be of greater threat to aircraft than the case of the continuous shear through the longitudinal cloud layers (Tsuchiya and Fujita, 1967)

14. The changes in convective cloud regimes shown in satellite imagery provides insights on forecasting low level turbulence due to wind shear.

3.2 Sea of Japan Oceanographic Features

The Sea of Japan is a marginal sea of the western north Pacific. It is nearly surrounded by the islands of Japan and coastal sections of Asia. Its openings to surrounding marginal seas and the Pacific Ocean are via the Tsushima (Korea) Strait to the south, Tsugaru Strait to the east, and the Soya (La Perouse) and Tartar Straits to the northeast and north respectively. The significance of the role played by these straits in both oceanographic and operational matters warrants special comments which are made in section 3.2.1 (page 3-31).

The oceanographic features of the Sea of Japan are strongly influenced by local bathymetry and physiography, climatic conditions, the shallow straits, and the character of the surrounding land masses. The surface waters show large variations in response to the monsoons, river runoff, and currents, while the deep waters display little change due to being cut off by the shallow sills from other deep water bodies. Figure 3-2, from Fett (1975), shows the major physical oceanographic features surrounding Japan and Korea. A notable convergence zone is the zone of mixing between the cold Liman Current and the warm Tsushima Current in the Sea of Japan.

Special Regional Characteristics

The following hydrographic phenomena are considered to have significant potential for impact on naval operations:

(1) complex bathymetric features,

(2) opposing warm and cold ocean currents,

(3) a persistent strong ocean thermal frontal zone,

(4) contrasting summer/winter stratified/destratified thermal properties north of the ocean front, and

(5) a general northeast-southwest alignment of features.

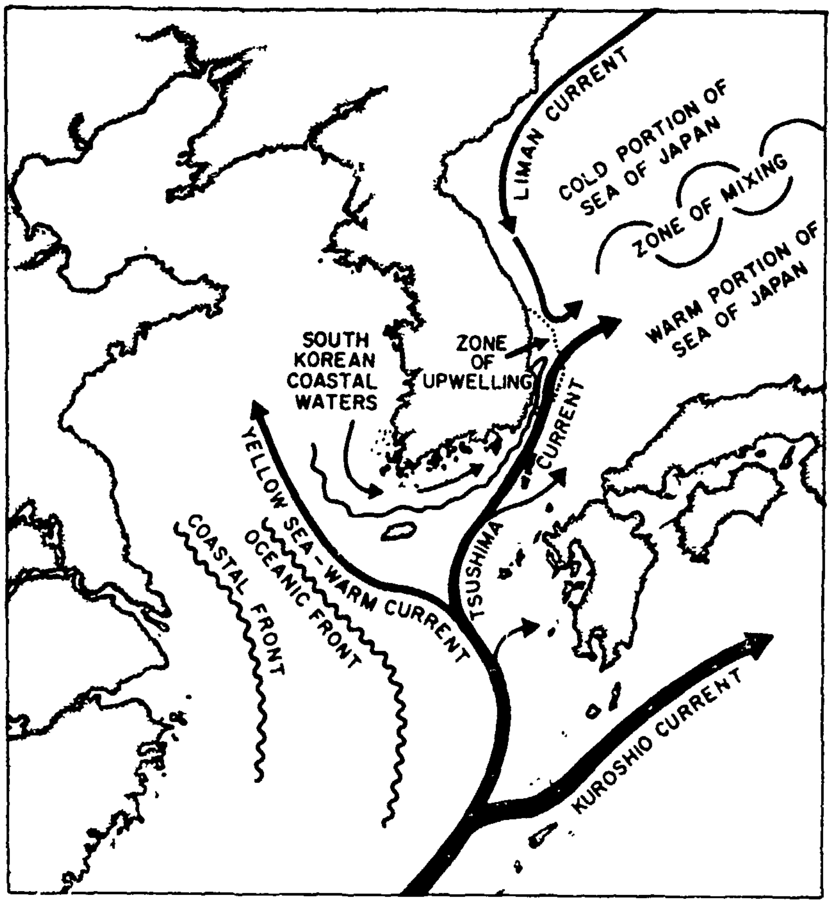

Figure 3-2 Shows the major physical oceanographic features surrounding Japan and Korea. A notable convergence zone is the zone of mixing between the cold Liman Current and the warm Tsushima Current in the Sea of Japan (from Fett, 1975).

Complex Bathymetric Features: The Sea of Japan bathymetry includes most of the major physiographic features of a major ocean. The Japan Basin and Abyssal Plain cover about one-quarter of the sea bottom.

Opposing Warm and Cold Ocean Currents: Circulation in the Sea of Japan is basically cyclonic. The cold Liman Current and the warm Tsushima Current are the chief components of the circulation. Both are rather slow (generally less than 1 knot) and broad. The Tsushima Current enters the sea through the Korea Strait, with the major branch flowing north along the Japanese Islands. Smaller branches move up the Korean peninsula (East Korean Warm Current) and, more diffusely, through the middle of the Sea of Japan. The currents coalesce at approximately 40°N on the eastern side of the Sea and continue northward along the Japanese coast. The greater portion of the flow in the sea subsequently leaves through Tsugaru and Soya Straits after mixing with cool water from Tartar Gulf. The Tartar Gulf water combines with Siberian runoff and forms the Liman Current flowing south along the Siberian coast. Cyclonic eddies are common in the region between the currents.

Persistent Ocean Frontal Zone: The Japan Sea is divided into a warmer sector on the Japanese side and a colder sector on the Korean and Siberian side (Figure 3-2, page 3-13 and Figure S-3-3). The boundary is marked by the oceanic "Polar Front", running approximately along 38-40°N. The warm sector water is related to the Tsushima Current and its extensions, the warm East Korea, Tsugaru and Soya Currents. The cold sector is comprised of three cold currents: Liman along the Siberian coast, North Korea from off Vladivostok to the central east Korean coast, and Mid-Japan Sea Cold Current which flows eastward into the central portion of the Sea of Japan.

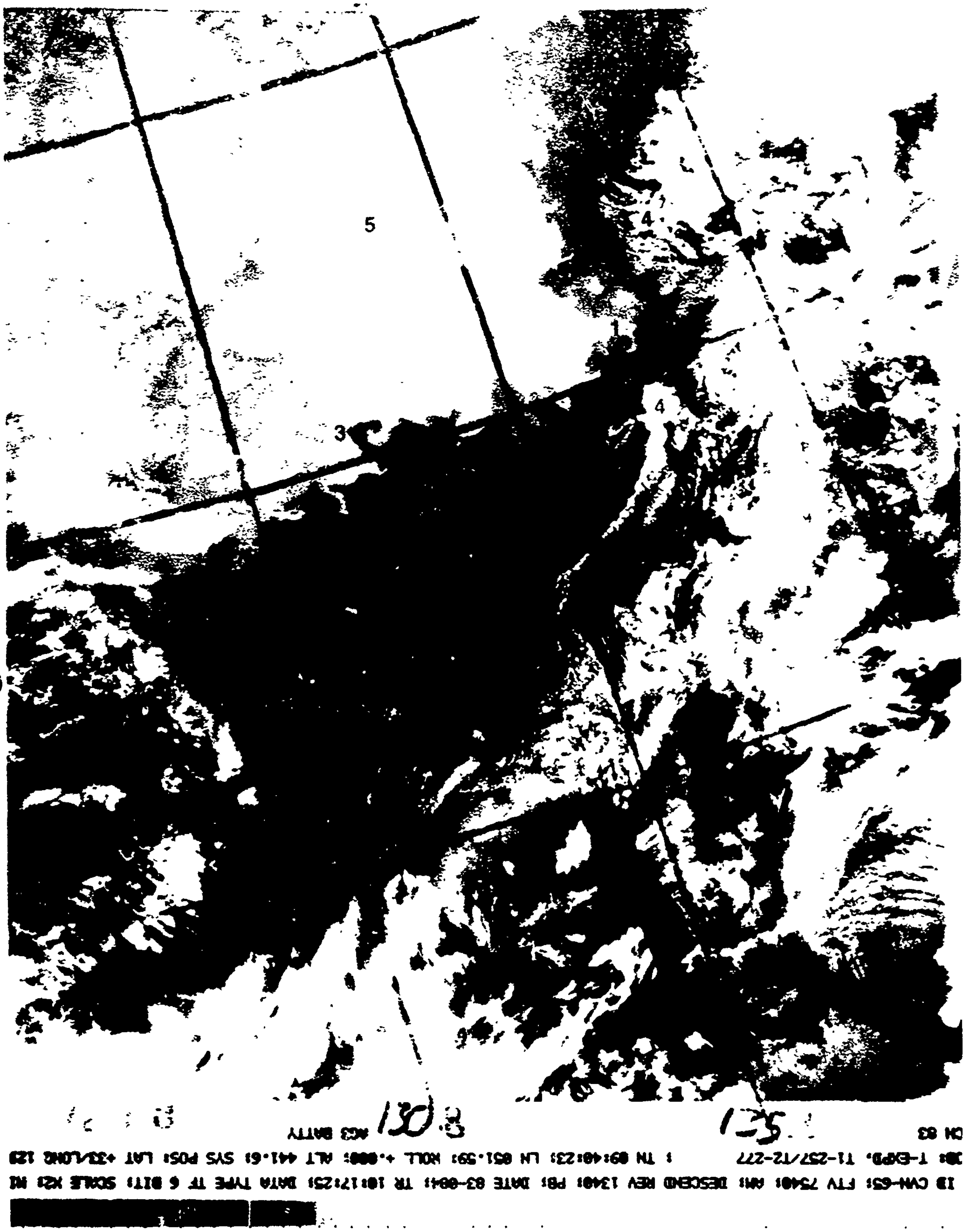

25 MAR 83 - Dm

Figure 5-3-?. Oceanic Polar Front, ... 25 March 198?.

FIGURE S-3-3. OCEANIC POLAR FRONT, SEA OF JAPAN. 25 MAR 83
USS ENTERPRISE (CVN 65) Infrared DMSP: TN: 25/1017 GMT

Synoptic Features: The major oceanic features are the Polar Front extending eastward from Korea across the Sea of Japan to near 139°E, the warm Tsushima Current that flows northeastward out of the Tsushima/Korea Strait and then northward along the western coast of Japan, and the cold Liman Current flowing southward along the coast of the USSR.

Satellite Image Features:

1. The diffuse oceanic Polar Front is indicated by the gray shade changes from near black (warm water) to medium gray (cold water). The front extends eastward across the Sea near 40°N and then turns sharply northward near 139°E.

2. There are about 6 shades of gray variations (representing a change of about 9°C across the approximately 100-200 n mi wide frontal zone (not labeled).

3. A cold core eddy is seen just east of Korea near 39°N, 129°E. Numerous filaments of warm and cold water intrusions are seen along the frontal zone.

4. Due to low level heating, atmospheric convection increases over the warm (dark) water. This is reflected by increased clouds and vertical development over the eastern part of the Sea of Japan.

5. The coldest water is seen in a narrow strip along the USSR coast north of the Vladivostok area (Liman Current).

Forecast Aids:

1. The larger scale oceanic thermal features, such as meanders, gyres, and eddies tend to persist longer and extend to greater depths than the smaller filament type features.

2. In oceanic frontal zones the warm water is likely to be a relatively thin layer over the cold water. An exception will occur where cold, low salinity outflow from rivers will override oceanic, high salinity water that is a few degrees warmer.

3. The oceanic Polar Front is a persistent year round feature. During the latter part of summer and into autumn surface heating will create a relatively shallow warm mixed layer and mask the feature at the surface.

4. The water north of the front, when the front is clearly evident in the infrared imagery, tends to be nearly isothermal. Half-channel conditions exist. See section 2.4 for description of half-channel.

The ocean frontal zone is found between these two contrasting thermal zones. The front is a persistent year-round feature located near 38-40°N, about the same latitude band as that of the oceanic "Polar Front" of the Pacific east of Japan. Eddy circulation patterns exist in the frontal zone with accompanying large horizontal variations of physical properties.

<u>Summer/Winter Stratified/Destratified Thermal Properties:</u> Large seasonal changes occur in the thermal properties of the Japan Sea near surface waters. During late summer and autumn a convectively mixed two-layer structure (stratified) condition prevails. The cold northerly air flow of winter removes heat from the near-surface layer destroying the seasonal mixed layer and thermocline and results in surface-to-bottom homogeneity in the cold sector north of the "Polar Front". In the warm sector a deep thermocline persists throughout the year, because winter cooling is not sufficient to completely remove the heat from the mixed layer and destroy the thermocline. Basically, the constant inflow of relatively warm water via the Tsushima Current and extensions overcomes the winter heat loss from the water to the atmosphere.

The impact on deep water ASW conditions is that full-channel conditions exist throughout the Japan Sea during summer and autumn and year-round in the warm sector. During the winter and spring half-channel conditions are found in the cold sector. Highly variable conditions exist in the frontal zone throughout the year. The frontal zone variability is in both the vertical and horizontal planes as well as temporal frame. The year-round persistence of the frontal zone and related SST gradient results in it being a feature that is observable in satellite infrared imagery throughout the calendar year.

Northeast-Southwest Alignment: In general the large-scale physiographic and thermal features of the Japan Sea are aligned northeast-southwest. At the surface this is reflected in the patterns of the ocean front, isotherms, and currents. The Yamato Rise (Figure 3-3), the most prominent topographic feature in the Sea of Japan, has a general northeast-southwest strike. This trend is typical of the physiographic features and reflects the alignment of the mountain ranges of the Japanese Archipelago on the east and Korea and Siberia on the west.

Tides: The tides of the Sea of Japan have a very small range. Along the west coast of Japan the tidal range is on the order of a foot; it approaches 2 feet along the Siberia coast. The maximum ranges occur in the Korea Strait and the Gulf of Tartar where they reach 6 to 8 feet.

Tidal currents are quite strong through the various straits when the tidal flow reinforces the normal easterly flowing ocean currents. Speeds approach 3 knots in the Tsushima Strait, 3 to 4 knots in Soya Strait, and 5 to 6 knots in the entrances to the Tsugaru Strait.

Bathymetry: The sea floor of the central Sea of Japan area between about 40-43°N is dominated by the Japan Basin and Japan Abyssal Plain (Figure 3-2, page 3-13). The Tartar Trough extends northward through the center of the Sea from 44° to near 50°N. South of about 40°N, ridge and trough topography is predominant. The continental shelf is very narrow throughout most of the Sea, except in the extreme northern portion (north of about 49-50°N)

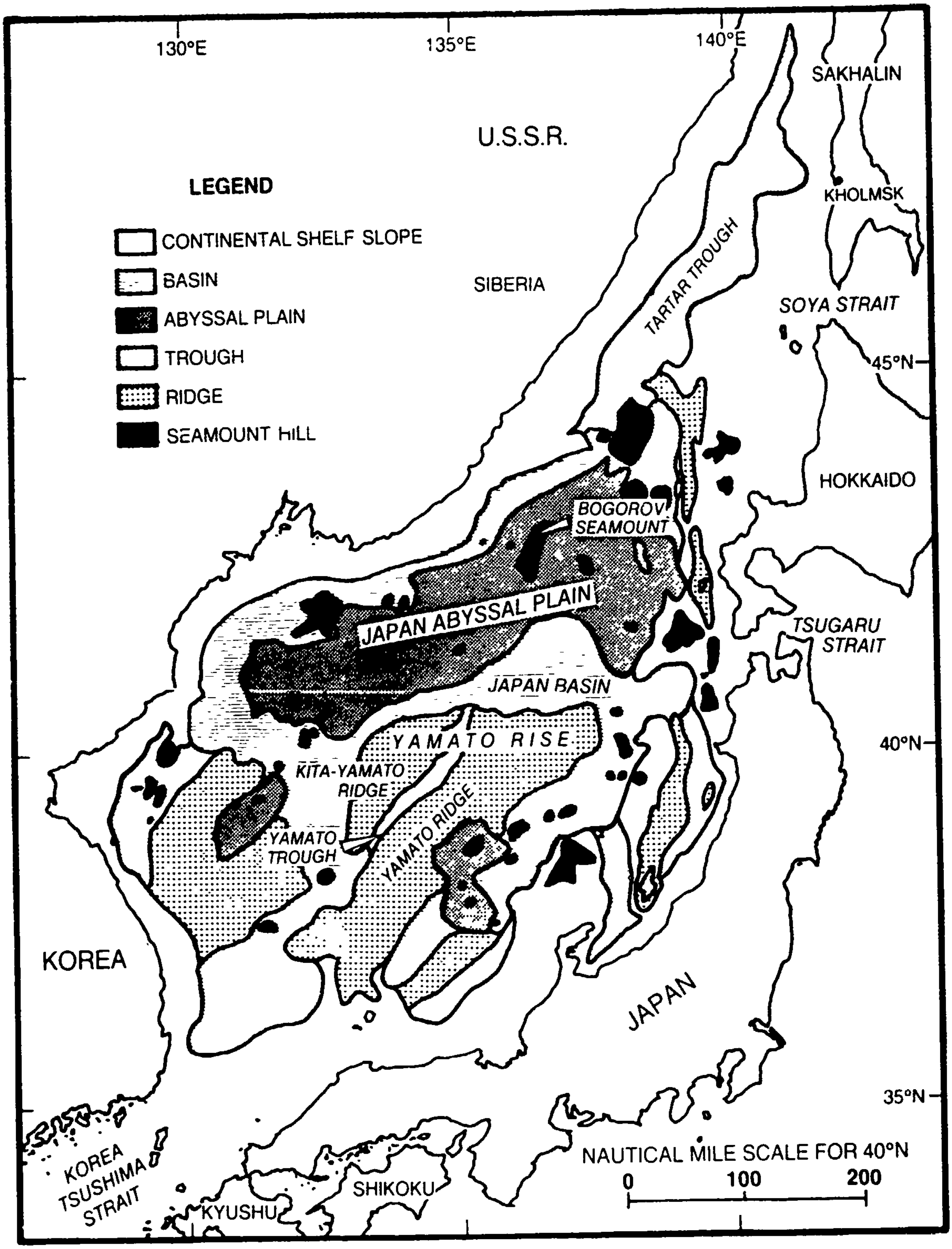

Figure 3-3. Bathymetry of the Sea of Japan (from NAVOCEANO SP PUB 133-18-1, 1974).

where the entire sea overlies the shelf. Steep bottom slopes (over 30°) bound the ridge and trough features. The prominent individual topographic feature in the Sea of Japan is Yamato Rise, which is divided into the Kita-Yamato Ridge and Yamato Ridge by Yamato Trough (Figure 3-2). All sides of the Rise are marked by steep slopes (>20°) except to the south which has small slopes. The majority of the bathymetric features of the Sea of Japan, like the mountain features of the bordering land areas, have a southwest/northeast strike.

Japan Abyssal Plain varies in depth from 1,700 fathoms (3,100 meters), near the coast of Siberia, to 1,990 fathoms (3,650 meters) at the base of the continental slope off southwestern Hokkaido. Large areas of the sea floor on the plain are nearly horizontal. Projecting through the sediment of the plain near 42.5°N, 136°E is Bogorov Seamount, a north-south oriented, 45-mile (75-km) long structure that is only 11 miles (18.5 km) wide.

Tartar Trough extends from the continental shelf near 49°N, between Sakhalin Island and Siberia, south to 44°N where it is terminated by a 500-fathom (900-meter) drop to the Japan Basin. The large, flat-topped seamount at 44°N, 138°15'E and other small peaks appear to be part of a structural dam holding back thick accumulations of sediment to the north. Tartar Trough is bowl shaped in the east-west cross section, and the division between the trough and continental slopes is arbitrary in some places.

Currents: The warm Tsushima Current (Figures 2-4 and 3-2 pages 2-11 and 3-13) is the major current of the Japan Sea. It originates southwest of Kyushu Island where it branches off from Kuroshio Current, flowing first through the eastern East China Sea and then entering the Sea of Japan through the Tsushima/Korea

Strait. As it leaves the strait a branch flows northward as the East Korea Warm Current. This branch continues up the Korean coast to near 38°N where it turns to the northeast and merges with the main flow. This main portion of the Tsushima current, about 200 km wide, flows northeastward through the eastern portion of the Sea of Japan. Near 41°N the current splits once more with one branch flowing eastward through the Tsugaru Strait, the warm Tsugaru Current, and the other branch continuing northward off western Hokkaido and then eastward through the Soya Strait as the the warm Soya current. Both the Tsugaru and Soya Currents tend to be deflected to the right as they exit the eastern end of the straits, following close to the eastern coast of Honshu and the northern coast of Hokkaido, respectively. However, the outflow portion of the warm Tsugaru Current is known to exhibit two principal circulation modes, a warm-core anticyclonic gyre during the warm season and the coastal flow mode during the colder months (Figure S-3-4). This phenomenon will be addressed in detail in the Pacific Ocean east of Japan section. The waters of the Tsushima Current are about 200 m thick, while those of the cold currents are limited to 50 m or less.

Figure S-3-4. Coastal mode, Tsugaru Strait. 26 April 1980

FIGURE S-3-4. COASTAL MODE, TSUGARU STRAIT. 26 APR 80
OSAN AB Infrared DMSP: TN: 26/0605 GMT

Synoptic Features: The oceanic features of interest are the outflow modes of the Tsugaru Strait and Soya (La Perouse) Strait and resulting SST patterns. Also of note is the large meander in the Kuroshio Current southeast of Honshu.

Satellite Image Features:

1. Warm water, indicated by a darker gray shade, extends southward along the coast from both the Tsugaru and Soya (La Perouse) Straits.

2. The cold waters (lighter gray shades) of the Oyashio Current, seen seaward of the warm coastal Tsugaru outflow, extend southward along the east coast of Honshu in about a 75 n mi wide strip to near 37-38°N.

3. East of the cold coastal strip, between about 37-42°N the warm Kuroshio and cold Oyashio waters mix and form the beginning of the eastward extending perturbed zone.

4. Convective cloud lines have formed over the warmer water east of Japan where the northerly flow is from over cold to warm water areas.

5. The large meander in the Kuroshio Current which periodically forms off southeast Honshu is evident in this image as a cool (light gray) wedge shaped area.

Forecast Aids:

1. The Tsugaru Strait has two outflow modes, a coastal mode during the weaker flow winter period and a warm cored anticyclonic eddy flow during the stronger flow summer period. During the coastal mode, as seen in this figure, the warm water is limited to a very narrow strip along the northeast coast of Honshu. During the gyre mode, the warm water extends eastward to near 143°E. Beyond the gyre position, throughout the year, the perturbed area between the cold Oyashio and warm Kuroshio displays a variety of eddy and filament configurations (Conlon, 1982).

2. The eastward flow through the Soya (La Perouse) Strait is through the southern side of the strait and curves southeastward along the Hokkaido coast once through the Strait. This results in the early clearing of ice from the north along that coast.

3. The SST patterns addressed in this image are below the resolution of numerical model analyses or forecasts and therefore must be detected in imagery or from local BT's.

4. Major characteristics of the large meander in the Kuroshio which forms southeast of Honshu include (Strommel and Yoshida, 1972):

A. The north-south translation of the Kuroshio is as much as 200 n mi. Near 137°E, the Kuroshio axis is found between 33°N and 34°N during periods without the meander and as far south as 30°N with the meander.

B. The meander develops in rather short time, i.e., in a few months.

C. The meander decays slowly, i.e, in several years.

D. The life of these meanders has been found to vary from 3 to 10 years.

Sea Ice: Sea ice begins to form in the Tartar Straits around mid-November. Sea ice starts to form in the northern part of the Japan Sea in early to mid-February. The ports of eastern USSR are ice bound for part of each winter. Vladivostok opens for activity about mid-April (Figure S-3-5). Along the northern coast of Korea sea ice is limited to coastal bays and harbors and in general does not restrict shipping activity.

The duration of sea ice ranges from about 200 days in the Tartar Strait ports, to around 120 days along the Siberian coast, and 90 days along the west coast of Sakhalin. The only year-round ice free port on western Sakhalin is Kholmsk (see Figure 3-2, page 3-13) which is kept ice free by the influence of an extension of the Tsushima Current.

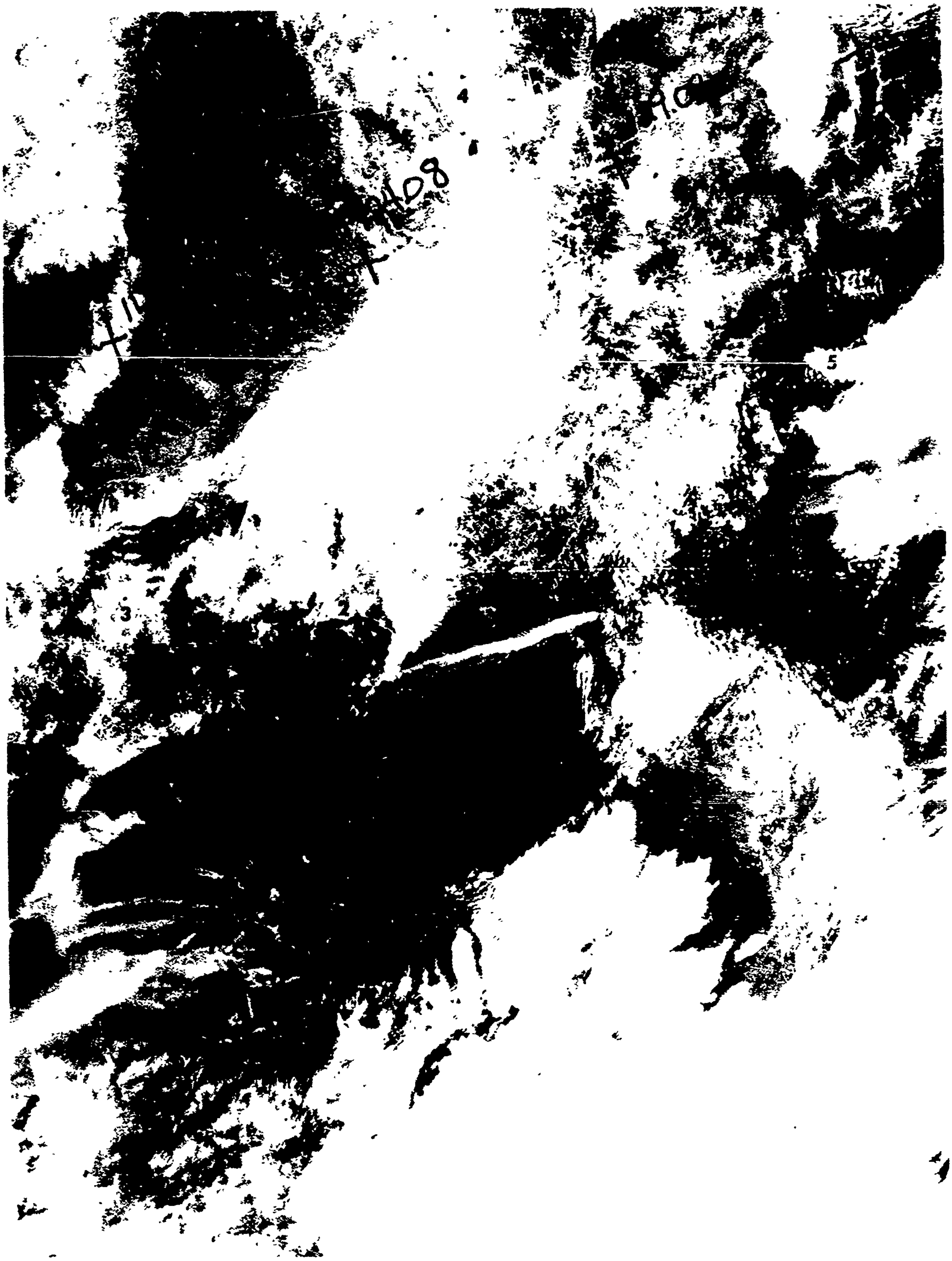

Figure S-3-5. Vladivostok Harbor, ice covered. 26 February 1980

FIGURE 3-3-5. VLADIVOSTOK HARBOR, ICE COVERED. 26 FEB 80
OSAN AB Visual DMSP: TN: 26/0307 GMT (Expanded image)

Synoptic Features: Winter time offshore flow.

Satellite Image Features:

1. The harbor of Vladivostok is ice covered.

2. A narrow strip of coastal ice exists in the northwestern Yellow Sea.

3. The snow cover over mountainous areas is dendritic in pattern, resulting from the varying coverage over adjacent ridgelines and valleys.

4. The snow cover over grasslands is of a dull gray nature, the newer the snow the whiter, and cities and centers of activity are seen as dark snow free areas. In forested areas, the snow cover can not be determined.

5. The wave patterns seen in flow when an inversion exists can be seen in both the cloud patterns and the gray shades which reflect atmospheric moisture content at levels below that needed for cloud formation.

Forecast Aids:

1. The ice conditions of harbors, straits, and other points of interest can be monitored in polar orbiting satellite imagery.

2. Knowledge of the underlying surface conditions, flat, grass covered, forest, etc. must be known before correct interpretations of snow cover can be made.

3. The wave patterns seen in clouds and gray shade areas, imply the flow direction and the existence of an inversion.

4. Pin-point accuracy in gridding satellite imagery can be achieved by utilizing known positions of city locations in snow covered, cloud free regions.

Temperature and Salinity: The Japan Sea is divided into contrasting warm and cold sections which are determined by the source of the two water masses. The warm sector, on the Japanese side, originates from the Tsushima Current which is an extension of the Kuroshio Current. Following passage through the Tsushima Strait, the warm water flows east and north along western Japan. It influences oceanographic, atmospheric, and ice conditions as far north as Soya Strait (near 46°N). The cold sector, on the Korean and Siberian side, is formed due to the extreme loss of heat to the atmosphere during winter plus the influx of river runoff and ice melt. The boundary of these two contrasting thermal sections, typically located near 38-40°N, is referred to as the "Polar Front". The SST gradient of the frontal zone is a distinct feature in infrared satellite imagery throughout the winter and spring portion of the year (See Figure S-3-3, page 3-15).

The waters of the Sea of Japan can be classified as surface, middle, and deep water. The surface water extends to about 25 m and during summer displays a strong thermocline between it and the deeper waters. The temperature and salinity fluctuate widely in the surface waters, in response to seasonal and areal factors. In the Korea Strait salinity exceeds 35.0‰ in April and May and decreases to 32.5‰ in August and September. Off the coast of Hokkaido it only varies from 33.7 to 34.1‰. The summer sea surface temperature (SST) is about 25°C over the southern portion, south of the Polar Front, and decreases to about 18°C over the northern region; in winter it varies from 15°C in the Korea Strait to 5°C off Hokkaido, and near 0°C along the Siberian coast. During all seasons, the isotherms trend approximately northeast-southwest.

The middle water is best defined in the warmer sector as a layer of high temperature and high salinity below the surface water. It originates from the Kuroshio Current intermediate layer and enters the Sea of Japan during the period from the winter to early summer. The middle water has a rather strong vertical decrease in temperature. Throughout the Japan Sea there is a decrease in temperature from about 17°C at 25 m to near 2°C at 200 m. The thickness of the middle warm layer decreases from the warm to cold sector, with the steeper vertical gradient of temperature found in the cold sector. Middle water is the most saline water of the Japan Sea, ranging from 34.5-34.8‰ in the warm sector and about 34.1‰ in the cold sector.

The deep water is of extremely uniform nature. Temperatures range from 0 to 0.5°C and salinity from 34.0 to 34.1‰. The source of the deep water is cold sinking surface water that forms in the northern part of the Sea of Japan during February and March. The shallow sill depths isolate the Sea of Japan deep water from other oceanic basins. This isolation contributes to the uniform characteristics of this water.

The surface and middle waters comprise a seasonal zone that exhibits pronounced change in physical properties such as temperature, salinity, density and therefore sound velocity. The seasonal zone varies in thickness from about 50 to 500 m. Its maximum vertical extent occurs in the warm waters in the southern and eastern parts of the sea. The deepest penetration of the zone is found in the Tsushima Current. North of the Polar Front the seasonal zone is wiped out during the winter season. The largest seasonal variations in surface water physical properties and sound velocities occur in the northern and western portions where the seasonal zone has minimum summer thickness and totally disappears in winter.

Sound Velocity Channel: The gross features of the sound channel axis depth distribution are fairly persistent. A general decrease in depth occurs from east to west and south to north. The deepest axis of 500-600 m occurs in the Korea Strait; in the area of the Tsushima Current near the central Japan Islands the axis is found near 300 to 400 m, and values off the Siberian coast range from 0 to 200 m. The areal distribution of the sound channel axis generally follows that of the isotherms, trending roughly northeast-southwest. Pronounced changes in sound velocity occur in the seasonal zones. Off Siberia and North Korea the large temperature changes cause 4 to 5 m/sec differences in winter and summer sound velocities. The sound channel axis and velocity are strongly affected by the seasonal changes north of the Polar Front. South and east of the front the sound channel axis lies essentially below the seasonal zone. In this area the major cause of change in sound channel axis depth or velocity is largely dependent on the volume of flow of the Tsushima Current. Increased flow (spring/summer) causes deeper axis depth and increased velocity. The local maximums occur later in the northern portions.

3.2.1 Sea Straits of the Sea of Japan

The Sea of Japan is a marginal sea that is bounded by the Islands of Japan and portions of the Asian mainland. The sea communication with the waters of the bordering marginal seas and Pacific Ocean is limited to that through several shallow straits. These straits may also play critical roles during naval operations. In light of their importance from both an operational and oceanographic view the straits of the Sea of Japan are addressed in this special section.

The Sea of Japan waters interact with the East China and Yellow Seas through the Tsushima/Korea Strait, with the main Pacific Ocean through the Tsugaru Strait, and with the Sea of Okhotsk through the Soya (La Perouse) and Tartar Straits.

The Tsushima/Korea, Tsugaru, and Soya/La Perouse Straits are the primary straits in regards to oceanographic conditions. All three have a common aspect in that they are the principal passages of the warm Tsushima Current. The Tsushima Warm Current enters into the Sea of Japan from the East China Sea through the Tsushima Strait. After flowing into the Sea of Japan and subsequently moving northward along the northwestern coast of Honshu (the main island of Japan), the Tsushima Warm Current discharges much of its transport into the Pacific Ocean through the Tsugaru Strait and the remainder into the Sea of Okhotsk through the Soya Strait.

Technical Report No. 1, Survey of Sea Strait Data Around Japan by C.J. Sonu under ONR contract N00014-80-C-0039 is the primary source of information for this section.

The Tsushima Current is considered to be an extension of the

Kuroshio Current that branches off south of Kyushu Island and then moves northward as the Tsushima Warm Current along the west coast of Kyushu. The sea surface temperature pattern seen in the satellite image supports this concept (Figure S-3-6 and simultaneous visual image Figure S-3-7, page 3-36).

Developing the branching concept, the Tsushima Current can be followed northward from its source area, past the west side of the Goto Retto (Goto Islands or Archipelago), to a point south of Cheju-do Island. Upon reaching this point the current splits into two: the Yellow Sea Warm Current which veers northwest toward the west coast of Cheju-do and the Korean Peninsula, and the Tsushima Warm Current which veers eastwa.d bound for the East and West Channels of Tsushima Strait. As it approaches and subsequently enters the strait, the Tsushima Warm Current mixes with coastal waters on both of it flanks. Because the Tsushima mixes with water masses of contrasting densities, the formation of fronts and rips is typical of the mixing zones. Further, because the distribution and characteristics of these coastal waters are highly seasonal, the water mass composition of the Tsushima Current fluctuates considerably by season.

Figure 5-3-6. Kuroshio Split. Infrared 18 May 1980.

FIGURE S-3-6. KUROSHIO SPLIT, SIMULTANEOUS VISUAL (S-3-7) AND INFRARED IMAGES (S-3-6). 18 MAY 80
OSAN AB Infrared DMSP: TN: 18/0136 GMT

Synoptic Features: The large scale oceanic surface thermal features include: the Kuroshio split, the Tsushima Current flowing northward from the split and then northeast through the Tsushima/Korea Strait, the warmer waters of the Tsushima continue northward along the eastern Sea of Japan with outflow occurring through first the Tsugaru and farther north the Soya Straits. The warm outflow through these two straits turns sharply southward along the northeast coasts of Honshu and Hokkaido, respectively, in what is referred to as coastal modes. East of Tsugaru Strait a small portion of the perturbed area created by the converging cold Oyashio and warm Kuroshio Currents can be seen.

Satellite Image Features:

1. The Kuroshio split just south of the southern most part of Japan.

2. The northward flow from the split area of the Tsushima Current.

3. The thermal contrast across the Tsushima/Korea Strait, cold on the Korean side, warm on the Japan side.

4. The relatively warm waters on the east and south sides of the Sea of Japan and cold on the north and west sides. The minimum contrast of gray shades across the south central Sea of Japan in this image is likely caused by masking of the surface temperatures by the high level return from a cirrus band (Huh et al, 1982).

5. The outflow through the Tsugaru and Soya Straits. Note that the thermal pattern from north to south across these two straits is similar to that across the Tsushima, cold on the north, warm on the south.

6. The warm water turns southward after exiting the Tsugaru and Soya Straits and is confined to a narrow band along the coastline.

7. The western end of the perturbed areas resulting from the confluence of the cold Oyashio and warm Kuroshio Currents east of Japan is seen east of the Tsugaru Strait. This pattern extends eastward beyond 160°E.

Forecast Aids:

1. The major features of the Kuroshio and Tsushima Currents will persist over extended periods of time. The latest available positioning view should be retained until direct evidence of a change becomes known or a new satellite view is available. Neither the large scale numerical analyses and forecasts, nor products derived from them will reflect the strong thermal boundaries that are evident in the imagery.

2. The infrared temperature sensed by the satellite sensor is an integrated value from the entire atmospheric column. The best SST readings are obtained through cold and dry atmospheric conditions. The normal strong gray shade contrast across the southern Sea of Japan caused by the cold water of the Liman Current along the north and west sides and warm Tsushima Current along the south and east side, are largely masked in this image due to the added high level moisture associated with the cirrus shield approaching from the west. The effects of increased atmospheric moisture include both attenuation which lowers all temperature values sensed and suppression of temperature differences because of increasing attenuation with increasing surface temperatures which reduce the real temperature differences or gradients (Huh et al, 1982).

3. The surface water of the northern parts of the Tsushima, Tsugaru, and Soya Straits will be colder than the southern side where the warm outflow is located. There are known variations to this, including:

A. The cold water flowing south and east around southern Korea sinks under the warm Tsushima water during winter. In spring and into summer when heavy run-off reduces the cold water salinity, it overrides the Tsushima waters and produces a frontal zone near a line between the islands of Cheju-do and Tsushima.

B. During the summer when surface heating results in uniform sea surface temperature values and a mixed layer (full-channel conditions), even though it is quite thin over the northern waters, the obvious thermal contrast is not there.

C. The inflow (Tsushima) and outflow (Tsugaru and Soya) are strongest during summer and therefore increasing portions of the Straits will be covered by warm water as the summer season approaches and also following it. During winter the cold water portion is largest.

4. The coastal mode outflow is a year-round feature of the Soya Strait. The outflow of the Tsugaru changes to a warm gyre mode that extends eastward to near 143°E during the summer strong outflow period.

5. The perturbed area east of the Tsugaru Strait and the main Japan island of Honshu is a year-round feature. A series of gyres are typically aligned east-west along it and its north-south extent is on the order of 300 n mi. Little evidence of this general feature is reflected in numerical products and the gyres are not likely to be reflected at all.

Figure S-3-7. Kuroshio Split. Visual 18 May 1980.

FIGURE S-3-7. KUROSHIO SPLIT, SIMULTANEOUS VISUAL (S-3-7) AND INFRARED IMAGES (S-3-6). 18 MAY 80
OSAN AB Visual DMSP: TN: 18/0136 GMT

Synoptic Features: The Polar Front extends from east of Japan to southern China. The Sea of Japan and bordering Seas to the north and south are nearly clear of clouds.

Satellite Image Features:

1. The region of the Kuroshio split is largely cloud free.

2. The northerly surface flow over the split area is indicated by the clouds on the upwind side of Yaku Island (the small bright white feature north of the number 2) and the formation of convective clouds over the warm water. Compare the northern edge of the convective cloud pattern with the warm/cold water boundary seen in the infrared (near satellite image feature 1).

3. A weakly curved anticyclonic shaped cirrus band over Korea indicates the location of the upper level ridge. The cirrus extends over the south central Sea of Japan. The radiation from this high level (cold) moisture will result in reduced infrared sensed outgoing radiational temperatures from this area and mask lower level warm properties such as the SST.

4. A cloud plume exhibiting a series of waves extends due north from the Vladivostok area, on close inspection it is evident in both the visual and infrared. This plume pattern implies a low level inversion. The infrared data indicates that the plume emanates from Ostrov Russkiy, an island slightly southwest of Vladivostok. This implies a low level wind direction from the southeast. At 0000Z on this date, Vladivostok reported a surface wind of 20 kt from 140°.

5. Through comparison of the visual and infrared it can be determined that the cloud pattern over the central Sea of Japan, between Vladivostok and the Tsugaru Strait, is clearly fog and/or stratus. Note there is little or no indication of this feature in the infrared which implies that the cloud tops temperatures are near the temperature of the surrounding water. This is a typical characteristic of fog/stratus decks under low level inversions.

6. Some pack ice still exists east of Sakhalin Island. A time sequence of satellite images is a useful aid in differentiating between clouds and pack ice.

7. Land fast ice around northern Sakhalin Island continues to block the Tartar Strait.

8. The north-south sunglint pattern parallels the land of northern Japan and Sakhalin. Coastal areas around the Tsugaru

Strait that show up as dark shades of gray indicate near calm wind conditions. Areas where the sunglint related gray shade patterns are very uniform, like over the northern Sea of Japan, indicate regions of uniform wind speed and sea roughness.

Forecast Aids:

1. A daily (optimally every 6 hours) set of simultaneous infrared and visual images are necessary for maximum utilization of imagery.

2. The normal modes and persistence characteristics of oceanic surface thermal patterns if known will assist in improving the knowledge of SST features during periods when cloud cover or other factors limit the availability of current infrared images.

3. Low level cloud features, such as the formative area of convective clouds, provides information on the location of warm water areas.

4. Over areas of wind flow from cold to warm water the change in atmospheric stability due to the heating from below will result in changes in several surface and low level conditions, including:

A. Surface wind speeds will increase and seas will be rougher.

B. The marine layer will thicken and the flux of moisture from the sea surface to the atmosphere will increase. Clouds may form and if the flow continues over an extended length (on the order of 100 n mi or more) light showers will occur.

C. The increased turbulence, atmospheric moisture content, and possible showers will degrade E/O ranges.

D. The low level inversion will rise and tend to weaken downstream, changing the low level ducting/trapping characteristics.

5. Wind flow from over warm to over cold water areas will result in increased stability and a general reversal of the above processes. Note that some of the processes are complex and can not simply be reversed. The warm moist air when cooled may result in widespread fog/stratus/drizzle and reduced E/O ranges and visibility. The wind/sea conditions are the best case of simple reversal properties.

6. Knowledge of power plant locations that give rise to smoke/exhaust plumes is useful information under low level inversion conditions, since plume alignment closely correlates with low level wind directions.

Tsushima/Korea Strait: The Tsushima/Korea Strait (Figure 3-1, page 3-2), centered near 34.5°N, 129.5°E, is oriented northeast-southwest between the southern coast of Korea and western Japan. The strait is comprised of the East and West Channels, which are located on either side of Tsushima Island. The narrowest widths are about 27 n mi across the entire strait.

The bottom topography of the strait is basically a continuation of the continental shelf of the East China Sea. The bottom is relatively flat with an average depth of about 100 m. The major topographic features are:

(1) Tsushima Island located approximately in the middle of the strait,
(2) the irregular coastlines on both the Korean and Japanese coasts flanking the north and south sides of the strait, and
(3) a local depression about 200 m deep centered just off the northwest coast of Tsushima Island in the West Channel.

In the vicinity of the depression the West Channel bottom slope is fairly steep. On the Japan side of the strait, there is a broad shallow (100-140 m) bed extending some 70 n mi beyond Tsushima Island to the northeast. The West Channel continues for about 60 n mi north of Tsushima Island where it encounters a steep slope descending into the Tsushima Basin.

Surface currents alternate in direction with tidal action, northeastward with ebb and southwest with flood, and average 1 to 2 kt with maximums in both directions about 3.5 kt.

A warm season thermocline is typically found near 50 to 100 m below the surface. During winter the water column is well-mixed from surface to bottom. The isotherm values of the East Channel resemble those of the Tsushima Current west of the Goto Islands, while those of the West Channel reflect the pattern found west of Cheju-do Island.

The relatively cold and low-salinity waters found along the southern coast of Korea converge with the Tsushima Warm currents and result in extensive frontal structures and meso-scale eddies. During winter these Korean source waters are very cold and tend to sink under the warm Tsushima water, thus reducing the clear thermal signature seen in infrared imagery during the autumn season. Two other features contribute to the formation of thermal fronts on the Korean side of the strait:

(1) the North Korea Cold Current moving southward along the east coast of Korea, and
(2) upwelling (most prevalent during summer) along the coast of Korea facing the West Channel.

Tsugaru Strait: The Tsugaru Strait is located near 41.5°N, 140°E between the main Japan island of Honshu to the south and Hokkaido to the north (Figure 3-1, page 3-2). The strait provides the primary exchange of water between the Sea of Japan and the Pacific Ocean east of the Japanese Islands. The Tsushima Current flowing northward through the eastern portion of the Sea of Japan splits to the west of the Tsugaru Strait with one branch entering the strait and the other continuing northward off western Hokkaido.

The coastlines surrounding the strait are quite irregular. The minimum width of the strait is about 11 n mi at its western entrance and 9 n mi at the eastern end. The channel length between the two narrows is about 38 n mi, while the total length of the channel is about 65 n mi. The shallowest portion of the strait is about 130 m in the western narrows which form the limiting sill depth. Eastward through the channel the maximum depth exceeds 200 m, with the 200 m channel width becoming extremely narrow in the vicinity of the eastern entrance before opening to the Pacific Ocean.

The Tsushima Current exhibits a complex pattern across the Sea of Japan as it interacts with the Polar Front. Near 40°N, about 70 n mi south of the Tsugaru Strait, the Tsushima Current becomes consolidated and exhibits a sharper western boundary or front. The minimum sill deptn (130 m) of the Tsugaru Strait limits the outflow from the Sea of Japan.

The current through the channel forms a core only about 11 n mi wide. The current is flanked on either side by eddies which appear to be trapped due to the configuration of the channel boundary. Maximum current speeds occur during the tidal spring phase in summer and winter, reaching 4.5 to 5.5 kt at the western entrance and near 5 to 6.5 kt at the eastern exit. The maximum speeds are directed to the east due to the combined tidal and ocean currents. The maximum speeds are found along the southern side of the current core.

The Tsugaru Current extension into the Pacific Ocean displays distinct variations in pattern between periods of strong and weak transport. During strong outflow an extensive anticyclonic gyral motion is formed while during weak outflow a coastal flow pattern is observed. These patterns are naturally referred to as gyre and coastal modes. The gyre mode is exhibited during summer and fall and the coastal mode during winter and spring (See Figure S-3-4, page 3-22).

Soya/La Perouse Strait: The Soya/La Perouse Strait, centered near 45.5°N, 142°E, separates the islands of Hokkaido to the south and Sakhalin to the north (Figure 3-1, page 3-2). The international boundary between Japan and USSR is located along the centerline of the strait.

The narrowest point of the strait is about 23 n mi wide with a channel minimum depth of near 75 m occurring in the narrows. Depths less than 100 m extend east and west from the narrows for about 16 n mi; the distance to the 200 m isobath is an additional 45 n mi eastward and only 20 n mi westward.

The portion of the Tsushima Current that continues northward beyond the Tsugaru Strait encounters a complex coastline and as it approaches the Soya (La Perouse) strait, an area of extended shelf with depths less than 200 m plus islands. The weakened warm current plus this complex topography results in large fluctuations in volume, speed, and path of the warm current flowing into the strait. The warm current is further hindered by the Japan Sea Polar Front and the cold waters to the west and north. The result is that the water from the Tsushima Warm Current s not always reach the Soya/La Perouse Strait. Infrequently the warm water will extend well north of the strait, in fact as far north as the entrance to the Tartar Strait. Even during the heaviest warm flow through the Soya/La Perouse Strait the warm water only occupies part of the strait on the Hokkaido side. The northern part of the strait is usually occupied by cold water, with a front that is quite sharp at times separating the warm and cold waters. The strongest surface currents of 1 to 2 kt occur in the warm water side. Exiting the strait, the current curves southeastward and hugs the northeast coast of Hokkaido. This portion of the warm current is strongest in late summer and disappears at the surface during winter, during which time the area is ice covered. This warm and cold water pattern can be clearly seen in satellite infrared imagery (See

Figure S-3-4, page 3-22). The Hokkaido coastline southeastward from the strait is the first area to become ice free in the spring. Other features frequently seen in infrared imagery are: An area of upwelling along the extreme southwest coast of Sakhalin, just above the strait and a long cold water belt extending southeastward from the northern region of the narrows. This belt is 150 to 200 n mi long and is typically comprised of three instability waves. The wave pattern is located just eastward of the coastal warm current with turbulent instability patterns along the boundary.

3.3 Winter (December to mid-March) (See section 2.2.1.5)

Although winter does not normally begin in the mid-latitudes until mid-December, the winter season has an early onset for much of the region adjacent to eastern Asia. The coastal water areas which border the Asian mainland north of about 35°N feel the effects of a strengthening Siberian high pressure cell by early autumn (late September), and the onset of winter is accelerated. The Sea of Japan lies within the area of early winter onset. Refer to Figure 2-8 (page 2-29) which depicts a generalized winter synoptic pattern.

3.3.1 Climatology

During winter, December to mid-March, a continental polar (cP) air mass dominates the weather over the Sea of Japan. Originating in Siberia as part of the Siberian high, the cold, dry air over land is characterized by a strong, low level temperature inversion. The Siberian high fluctuates both in position and intensity in response to atmospheric changes aloft caused by migratory mid-tropospheric disturbances. Surface temperatures at the source region range generally from 15°F to -40°F. The trajectory of the air as it leaves Siberia and Mongolia is primarily downslope, causing adiabatic temperature rises of as much as 25°F over land. Cold air surges caused by the mid-tropospheric disturbances are preceded through the Sea of Japan by strong cold fronts, with accompanying warm fronts only rarely seen.

3.3.1.1 Synoptic Patterns

Figure 2-6 (page 2-23) depicts the tracks of typical migratory extratropical cyclones occurring throughout the year. Of the six tracks depicted, only two typically affect the Sea of Japan during the winter: the Lake Baikal Low (track B) and the South Mongolia Low (track C).

Cold frontal activity starts to increase during the autumn season, and continues throughout the winter. A very severe cold outbreak can be expected in the latter part of January or early February. While velocities of the cold fronts are greatly influenced by the topography of the land, speeds average about 25 kt and may vary from 45 to 60 kt down mountain slopes during the winter.

3.3.1.2 Surface Wind

Figure 2-9 (page 2-31) presents wind statistics for the month of February. According to the U.S. Navy (1977), January is the windiest month in the Sea of Japan. Mean wind speeds north of 40°N average 20 kt, decreasing to about 10 kt near the Japan coast between 35°N and 40°N. Gale (≥34 kt) frequency of occurrence is between 5 and 10 percent in a five-degree square centered at 40°N 135°E. February mean wind speeds are decreased only slightly from January, and frequency of occurrence of gale force winds is less than 5 percent in all sectors of the sea. Prevailing wind direction is north-northwest during the winter.

3.3.1.3 Upper Level Winds

The area near southern Japan is known to have the strongest and most persistent jet stream speeds in the world, with velocities commonly exceeding 200 kt during the winter months. Figures 2-10 through 2-15 (pages 2-32 to 2-34) depict the upper level flow patterns for the month of February. The strongest winds for February (at the specified pressure surfaces) are found over southern Japan at 200 mb with a mean speed of 145 kt. The winds at 200 mb diminish to about 30 kt at the north end of the Sea of Japan.

3.3.1.4 Visibility

Figure 2-16 (page 2-35) depicts the frequency of occurrence of visibility limits during February. Winter is a relatively good season for visibility in the region, with average frequency of occurrence of ≥5 n mi about 70 percent in the northern portion of the sea, increasing to about 90 percent in the south, with each of the winter months approximately the same. In general, visibilities are better in the western portions of the sea than they are in the east, largely due to the increasing sea surface temperature from west to east and typical enhanced cloud cover and shower activity over the warmer water.

3.3.1.5 Cloud Heights/Ceilings

Figure 2-17 (page 2-36) presents combined low cloud ceiling and visibility limits for the month of February. Of the winter months, January is the cloudiest in the Sea of Japan, with an average frequency of low cloud amount ≥5/8 exceeding 80 percent in the southeastern portion, compared to over 70 percent during December and February. In each of the winter months, the percentage decreases with westward progression, with about a 20 percent frequency of occurrence along the coast of North Korea. As one might expect, since January is the cloudiest of the winter months, it also has a slightly higher frequency of occurrence of low cloud ceiling <600 ft and/or visibility <2 n mi than do the other winter months.

3.3.1.6 Precipitation

During the winter months, a precipitation maximum (30% frequency during February) occurs in the eastern portions of the Sea of Japan, probably due to the cold air from Siberia picking up moisture in its transit across the sea and then moving over warm SST areas resulting in low level instability and cloud development enhancement. While minor differences exist between the winter months, the precipitation patterns are similar. About 40 percent of the precipitation occurring during February in the southern Sea of

Japan falls as snow, with the figure increasing to about 90 percent near 40°N.

3.3.1.7 Sea State

Figure 2-18 (page 2-37) presents wave height statistics for the month of February. Reflecting the prevailing north-northwesterly surface wind flow, the frequencies of occurrence of wave heights ≥5 ft (1.5 m) and ≥8 ft (2.5 m) increase from northwest to southeast as the fetch length increases. However, the 10 percentile isoline for waves ≥12 ft (3.5 m) does not fit this pattern, because of the increased wind velocities associated with extratropical cyclones as they transit the Sea of Japan.

3.3.1.8 Surface Air Temperature

As shown in Figure 2-19 (page 2-38), the winter surface air temperatures over the Sea of Japan reflect the extreme cold of the Siberian high. The mean air temperature near the southern Sea of Japan averages about 43°F (6°C), while it lowers to near 10°F (-12°C) in the extreme northern reaches of the sea.

During February the extreme maximum temperature for the southern part of the sea is 61°F (16°C) while the extreme minimum temperature for the northern areas is about 2°F (-17°C).

3.3.1.9 Freezing Level

The altitude of the mean freezing level during winter varies from approximately 3,000 ft in the southern Sea of Japan to the surface in the northern areas. Due to the warming effect of the sea surface and trajectory of Tsushima Current, the surface freezing level is considerably farther north in the central and eastern portions of the sea than it is along the coastlines of Asia and Japan. Figure 2-21 (page 2-40) depicts the mean altitudes of the freezing level during February.

3.3.1.10 Aircraft Carrier Operating Conditions

Optimum aircraft carrier operating conditions, defined as having a low cloud ceiling ≥5,000 ft (or no low cloud ceiling), visibility ≥5 n mi, and wind 11-21 kt, occur between 10 and 40 percent of the time over the major portions of the Sea of Japan during February, with the best percentages occurring near the coast of the Asian landmass.

Poor conditions, defined as having a low cloud ceiling <300 ft, or visibility <1 n mi, or wind <6 kt or ≥34 kt, occur between 10 and 20 percent of the time over most of the sea, increasing to over 20 percent north of about 45°N and east of 140°E.

3.3.1.11 Seasonal Oceanographic Features

January and February are the months of the coldest sea surface temperatures in the Sea of Japan, with water below 30°F (-1°C) being recorded in the northern sea. Temperatures in the southern areas of the sea reduce to near 50°F (10°C) during February, as depicted in Figure 2-20 (page 2-39).

Sea ice is observed in the northern Sea of Japan as early as

November. Average ice limits for February are shown in Figure 2-20 (page 2-39)

3.3.1.12 Electro-Optical Conditions (See section 2.3.1)

Under the winter Northeast Monsoon flow pattern cold dry continental polar air from off Asia dominates over the Sea of Japan. These conditions result in generally improving E/O range as the Northeast Monsoon intensifies. The well mixed atmosphere resulting from heating from below by the relatively warm ocean minimizes inversions and stable layers and results in an annual minimum of ducting and superrefraction layers.

The large scale and seasonal trends are for improved E/O conditions when progressing from south to north and from autumn to winter. The local conditions of an area frequently modify these large scale considerations and may in fact reverse them.

The local conditions of the Sea of Japan during winter result in the following mean patterns. The E/O conditions are gradually degraded from west to east in response to the increasing cloud cover and precipitation. Due to the extreme cold air moving over the northern part of the Sea of Japan from off the USSR, the cloud free paths tend to be shorter than to the south. This results in a degradation of E/O conditions from south to north and a reversal from the large scale general pattern. The mean elevation of elevated ducts increases from 1200 m in the south to 1800 m in the north. Surface based ducts are most likely to occur in the offshore flow area and where the cloud lines do not form until some distance offshore.

Precipitation patterns are dominated by shower activity with the majority of frontal systems passing to the south and east. Under the prevailing northerly flow of the winter the large scale variations are small, but the small scale variations between cloud lines and shower/non-shower areas will be large.

The coastal terrain of Asia is mountainous and results in areas of low level funneling of winds out of valleys and off river mouths. This results in marked local scale variations in E/O conditions. Generally degraded ranges occur where the offshore flow is strongest and improved ranges are found where terrain barriers block the low level winds. The formation of cloud lines and associated lighter gray shade areas as seen in visual satellite imagery provide information on the low level wind patterns.

The following table presents statistical information on duct heights for the regional area and season of interest:

CENTER OF AREA: 40°N 135°E SEASON: WINTER

EVAPORATION DUCT HISTOGRAM IN PERCENT OCCURRENCE

Height (m)	December day	December nite	December both	January day	January nite	January both	February day	February nite	February both
0 to 4	2	2	2	2	1	1	4	3	4
4 to 8	4	6	5	6	9	8	8	11	10
8 to 12	14	15	14	18	17	18	18	20	19
12 to 16	22	23	23	25	27	26	25	25	25
16 to 20	28	29	28	27	28	28	26	27	26
20 to 24	20	19	19	14	12	13	10	8	9
24 to 28	6	6	6	4	4	4	6	6	6
28 to 32	1	1	1	1	0	1	1	1	1
32 to 36	1	0	0	0	0	0	1	0	0
36 to 40	0	0	0	0	0	0	0	0	0
above 40	3	1	2	2	1	1	3	2	3
Ave. Ht.	18	17	17	16	15	16	16	15	16

3.4 Spring (mid-March to mid-June) (See section 2.2.1.6)

Spring is a season of major changes over the coastal waters of eastern Asia. The Siberian high begins to lose strength, resulting in a weakening of the winter monsoon and a gradual northward migration of the Polar Front as the Southwest Monsoon strengthens. Refer to Figure 2-22 (page 2-42) which depicts a generalized spring synoptic pattern. Figure S-3-8 provides a view of the spring cloud patterns on 18 May 1980.

3.4.1 Climatology

During the months of spring (mid-March to mid-June) significant changes occur in the weather over the Sea of Japan as the intense Siberian high of winter weakens. Migratory upper atmospheric disturbances transit the area allowing "bubble highs" to break off from the weakened Siberian high and move eastward across the Sea of Japan. Typically a trough follows the bubble high resulting in cyclogenesis, inclement weather and precipitation over the region. The mid-Pacific high begins to intensify and move northwestward and, in concert with the weakened Siberian high, allows the Polar Front to start its northward migration from Taiwan to the southern coast of Honshu. See Figure 2-5 (page 2-18). The winter Sea of Okhotsk low moves to a position over northern Mongolia, and the Aleutian low weakens. Thermal lows may be expected to form over China and northeastern Manchuria by the end of the season.

Figure S-3-8. Spring regional view, Sea of Japan. 18 May 1980.

FIGURE S-3-8. SPRING REGIONAL VIEW, SEA OF JAPAN. 18 MAY 80
OSAN AB Visual DMSP: TN: 18/0136 GMT

Synoptic Features: The Polar Front is south of the area and low pressure dominates the land area to the west. Surface winds are generally southerly, north of a synoptic scale ridge which extends from southern Korea eastward across northern Honshu.

Satellite Image Features:

NOTE: See Figure S-3-7 for additional comments relative to labels 1-8.

3 and 5. The Sea of Japan area is nearly cloud free, except for some cirrus off central Korea and a patch of fog/stratus over the central sea.

4. The low level southerly flow and the existence of a low level inversion are indicated by the northward extending cloud plume composed of wave clouds emanating from near Vladivostok. This cloud plume is frequently evident in the imagery and is likely caused by a large industrial smoke stack.

8. The light wind conditions near the ridgeline are indicated by the dark gray shades seen in coastal areas around the Tsugaru Strait region.

Forecast Aids:

1. The spring transition is a gradual one and a period of fair weather and light winds as long as the front remains to the south.

2. Under light wind conditions local effects tend to dominate. At such times the small scale features of satellite images take-on added significance. The gray shade patterns within the sunglint band are useful in detailed wind forecasting.

3.4.1.1 Synoptic Patterns

Figure 2-6 (page 2-23) depicts the tracks of typical migratory extratropical cyclones. Of those depicted, four would typically impact the weather over the Sea of Japan during spring: the Manchurian Low (Track A), the Lake Baikal Low (track B), the South Mongolia Low (track C), and the Shanghai Low (track D).

Of the three types of cold fronts discussed in section 2.2.1, two can be expected to occur during the spring: Western and Eastern.

3.4.1.2 Surface Wind

Average wind speeds over the Sea of Japan decrease gradually throughout spring, with the percent frequency of occurrence of wind speeds of 10 kt or less increasing throughout the period. Figure 2-23 (page 2-45) presents wind statistics for the month of May. The frequency of occurrence of gale velocities (≥34kt) over the Sea of Japan during spring is less than 5 percent and therefore is not represented in Figure 2-23. Prevailing directions show significant changes during the period and reflect the seasonal monsoonal shift, with north-northwest dominant in March becoming south to southwest by May.

3.4.1.3 Upper Level Winds

Figures 2-24 through 2-29 (pages 2-46 to 2-48) depict the upper level flow patterns for the month of May. The strongest winds (at the specified pressure surfaces) are found over the southern Sea of Japan at 200 mb with a mean speed of about 80 kt.

3.4.1.4 Visibility

Figure 2-30 (page 2-49) depicts the frequency of occurrence of visibility limits during May. There is some deterioration in visibility during spring because of fog. March has a percent frequency of occurrence of visibilities ≥5 n mi of between 80 and 90 percent, while June shows a frequency of occurrence of between 60 and 80 percent. March has a percent frequency of occurrence of visibilities <2 n mi of about 10 percent over most of the sea while June's percentages increase to between 10 and 30 percent, with over 30 percent recorded along the North Korean and adjacent USSR coastlines.

3.4.1.5 Cloud Heights/Ceilings

Figure 2-31 (page 2-50) depicts low cloud ceiling statistics combined with visibility limits. The percent frequency of occurrence of low cloud amounts ≥5/8 gradually decreases between March and May over the major portion of the Sea of Japan, but increases significantly between May and June as the Polar Front moves northward into the area south of Japan (Figure 2-5, page 2-18). The amounts for March range from 30 to 60 percent, while May shows a range of 20 to 60 percent and June a range of 55 to 65 percent. The major difference between March and May is not the percentages of occurrence, however, but the areal extent, with May showing the lower percentages over a broader area of the sea.

Frequencies of occurrence of low cloud ceiling <600 ft and/or visibility <2 n mi show an increase during the spring. March has an average of 10 percent over most of the Sea of Japan, increasing to 20 percent in the northern part of the Sea. June has between 15 and 30 percent frequency of occurrence of low cloud ceilings <600 ft and/or visibility <2 n mi increasing to over 30 percent along the coastal areas in the southwestern and western portions of the sea.

3.4.1.6 Precipitation

The spring season shows a significant change in the precipitation statistics over the Sea of Japan. In March there is a minimum of precipitation (5 percent frequency of occurence) near the coastline in the extreme western portion of the sea, increasing eastward and reaching a maximum of 20 to 25 percent in an elongated area stretching north-south along 139°E between 37°N and 47°N. By May, the frequency of occurrence of precipitation is less than 10 percent over most of the sea west of 140°E, and between 10 and 15 percent over the remainder of the area. The 10 percentile snow line (10 percent of precipitation observations report snow) reaches as far south as the extreme southern Sea of Japan in March, but is limited to north of 45°N by May and is north of the Sea of Japan by June.

3.4.1.7 Sea State

As the surface winds decrease during the spring over the Sea of Japan (see section 3.4.1.2), the sea heights also decrease. In

March, waves ≥5 ft (1.5 m) have a frequency of occurrence of less than 60 percent over the central portion of the sea. By May, the percentage has decreased to near 20 percent (Figure 2-32, page 2-51), and is 10-20 percent by June. Waves ≥8 ft (2.5 m) occur some 20 percent of the time during March in the central Sea of Japan, decreasing to less than 10 percent during May and June.

3.4.1.8 <u>Surface Air Temperature</u>

The months of spring show significant surface air temperature increases over the Sea of Japan. The temperature during March ranges from about 50°F (10°C) in the southern reaches of the sea to near 21°F (-6°C) in the northern areas, warming to 68°F (20°C) and 48°F (9°C) in June. Figure 2-33 (page 2-52) depicts the mean surface air temperatures for the month of May.

During May, the extreme maximum temperature for the southern area of the sea is 75°F (24°C) while the extreme minimum temperature for the northern area is about 27°F (-3°C).

3.4.1.9 <u>Freezing Level</u>

The altitude of the freezing level increases significantly during the spring months. The March altitude of about 5,000 ft in the southern Sea of Japan increases to about 13,000 ft by June, while the freezing level in the northern sea increases from the surface to approximately 9,000 ft during the same period. Figure 2-35 (page 2-54) depicts the mean altitude of the freezing level during May.

3.4.1.10 Aircraft Carrier Operating Conditions

Optimum aircraft carrier operating conditions, defined as having a low cloud ceiling ≥5,000 ft (or no low cloud ceiling), visibility ≥5 n mi, and wind 11-21 kt, occur between 20 and 30 percent of the time over the major portions of the Sea of Japan during May. A circular area with an approximate radius of 150 n mi ntered near 38°N 131°E has a frequency of occurrence of greater than 30 percent, while most of that portion of the sea north of about 47°N has less than 20 percent.

Poor conditions, defined as having a low cloud ceiling <300 ft, or visibility <1 n mi, or wind <6 kt or ≥34 kt, occur more than 30 percent of the time north of about 42°N. South of the same line, poor conditions occur less frequently, reducing to below 20 percent in the southwestern portion of the sea.

3.4.1.11 Seasonal Oceanographic Features

By the end of spring the waters of the Sea of Japan have started to show considerable warming when compared to the winter temperatures. The coldest water during June in the northern areas is still quite cold, with temperatures near 36°F (2°C), but the sea has warmed to near 68°F (20°C) in the southern sea. Figure 2-34 (page 2-53) depicts sea surface temperatures during May.

By May, sea ice has disappeared south of about 49°N. An approximation of the ice limit during May is shown in Figure 2-34. The Sea of Japan is essentially ice free by the end of June.

3.4.1.12 Electro-Optical Conditions (See section 2.3)

The gradual northward migration of the Polar Front during spring results in a major change of E/O environments over the Sea of Japan. North of the Polar Front conditions similar to winter prevail and south of the frontal zone, summer and tropical type conditions will exist. Under the frontal band, the conditions will differ from both of those found in the north and the south, and in general will exhibit a major reduction in E/O ranges due to precipitation. Elevated ducts will prevail in the northern sector of the frontal band and to the rear of the cloud band where large scale subsidence prevails.

The local conditions of the Sea of Japan during spring result in the following mean patterns. The E/O conditions will vary from the earlier patterns of winter to that of summer late in the period. The summer type pattern is generally in agreement with the large scale patterns, i.e., a general increase in E/O ranges from the tropics poleward as atmospheric humidity decreases. The mean height of elevated ducting layers decrease from about 1400 m in the south to 600 m in the extreme north.

The occurrence of precipitation is generally around 10% with the higher values along the eastern and northern portions. The occurrence of fog will increase over the colder waters of the western and northern sectors as the season progresses and the warm, moist southerly flow pattern advances northward.

The following table presents statistical information on duct heights for the regional area and season of interest:

CENTER OF AREA: 40°N 135°E SEASON: SPRING

EVAPORATION DUCT HISTOGRAM IN PERCENT OCCURRENCE

Height (m)	March day	March nite	March both	April day	April nite	April both	May day	May nite	May both
0 to 4	6	5	5	13	13	13	15	13	14
4 to 8	8	11	10	11	15	13	10	15	12
8 to 12	19	20	19	14	19	16	12	19	16
12 to 16	20	26	23	16	22	19	13	18	16
16 to 20	23	23	23	13	14	13	11	11	11
20 to 24	11	9	10	8	7	7	7	8	8
24 to 28	4	2	3	4	3	4	6	4	5
28 to 32	2	1	1	2	1	1	3	2	2
32 to 36	1	0	0	1	1	1	1	1	1
36 to 40	0	0	0	1	1	1	1	1	1
above 40	6	3	5	16	6	11	21	8	14
Ave. Ht.	17	15	16	20	15	18	23	16	19

3.5 Summer (mid-June to mid-September) (See section 2.2.1.7)

The summer monsoon is not as evident over the Sea of Japan as it is over waters to the south. During the first 30 days or so of the season the Polar Front moves northward from a position south of Japan to its August position in Mongolia, a transit which carries it through the Sea of Japan. The remainder of the season sees light southerly flow generally dominating the weather over the sea. Figure 2-36 (page 2-56) depicts a generalized summer synoptic pattern.

3.5.1 Climatology

The period of the traditional summer season (mid-June to mid-September) actually spans two seasons in much of the Far East. The first period, known as the Mei-Yu/Bai-U (Plum Rain) season in Japan, normally commences in the middle of June and continues until mid-July. During this period the Polar Front migrates from a position south of Japan to its summer position over Sakhalin Island and Mongolia (Figure 2-5, page 2-18). As the front moves northward through the area, the Mei-Yu/Bai-U season ends and summer begins, characterized by relatively warm, moist air that is transported northward around the western periphery of the strengthened mid-Pacific ridge.

3.5.1.1 Synoptic Patterns

Figure 2-6 (page 2-23) depicts the tracks of typical migratory extratropical cyclones that occur throughout the year. Of the tracks depicted, three typically affect the weather over the Sea of Japan during the summer: the Lake Baikal Low (track B), the South Mongolia Low (track C) and the Yellow Sea Low (track E).

During the Mei-Yu/Bai-U season an extension of the Polar Front lies roughly parallel to the south coast of Honshu. This frontal extension does not have the classic structure of the mid-latitude Polar Front. Warm, moist air south of the front is forced aloft over the cooler air north of the front. This overrunning and resultant cloudiness and rain is similar to conditions one would expect north of a classic warm front. The slope of the front results in the effects of the overrunning being felt as much as 200 mi north of the surface front (Naval Oceanography Command Detachment, Atsugi, Japan, 1980).

A typical Mei-Yu/Bai-U synoptic pattern is characterized by a series of weak low pressure centers on the extension of the Polar Front extending from China, along the south coast of Japan, and into the North Pacific Ocean. In some years the front will pass quickly over southern Japan but remain stationary through central Honshu and the Sea of Japan. Under these anomalous conditions, the warm-frontal weather is still produced by overrunning, but it is confined to an area north of its traditional position, resulting in a Kara Tsuyu, or "dry rainy season" over central Japan.

After the Mei-Yu/Bai-U season has ended, the more typical summer season begins as the Polar Front completes its northward migration to a position between Sakhalin Island and Mongolia.

Cold frontal activity is at a minimum during summer. Of those fronts that do occur, the Western type is found to occur most frequently throughout the year, but a frequency vs. seasonal breakdown by frontal type is not available. In general, Western and Central type fronts pose little threat to the Sea of Japan during the summer. Eastern type fronts are more frequent in spring and early summer than during other times of the year and may impact the weather over the northern Sea of Japan.

3.5.1.2 Surface Wind

As shown in Figure 2-37 (page 2-58), surface wind velocities average 10 kt from near 60 to 90 percent of the time in the Sea of Japan during August, with the higher frequencies occurring in the coastal waters of the western sea from 37°N to 43°N and in the southeastern sea between 35°N and 39°N. Winds of gale force (≥34 kt) seldom occur during summer. Prevailing directions are southwest north of 40°N, and northeast south of 40°N.

3.5.1.3 Upper Level Winds

Figures 2-38 through 2-43 (page 2-59 to 2-61) depict the upper level flow patterns for the month of August. The strongest winds (at the specified pressure surfaces) are found at both 200 mb and 300 mb over the northern Sea of Japan with a mean speed of about 40 kt.

3.5.1.4 Visibility

Figure 2-44 (page 2-62) depicts the frequency of occurrence of visibility limits during August. Visibilities of ≥5 n mi occur over 70 percent of the time over the entire sea.

3.5.1.5 Cloud Heights/Ceilings

During the summer months, average low cloud amounts ≥5/8 over the Sea of Japan are about 30 to 50 percent over the southern areas ranging to 60 to 80 percent over the northern reaches of the sea. The month of September has the least amount of low cloudiness of the season, with less than 30 frequency percent reported over the southern waters and just over 50 percent in the extreme northern sea. Figure 2-45 (page 2-63) presents average low cloudiness statistics for the month of August.

3.5.1.6 Precipitation

The months of summer are relatively dry over the Sea of Japan, with overall frequency of occurrence of precipitation averaging 7-15 percent. The lower percentages occur in the southwestern areas while the highest percentages are seen near the northern portion of the sea. No significant differences are noted between the individual months of summer.

3.5.1.7 Sea State

Frequencies of occurrence of wave heights ≥ 5 ft (1.5 m) during August for the Sea of Japan are depicted in Figure 2-46 (page 2-64). Whereas, during the month of June, waves ≥5 ft (1.5m) are observed 10-20 percent of the time over much of the central and southern Sea of Japan, by September an increase to 25-40 percent is observed. Waves ≥8 ft (2.5 m) occur less than 10 percent of the time during all summer months over all areas of the sea.

3.5.1.8 Surface Air Temperature

Surface air temperatures over the Sea of Japan during August (Figure 2-47, page 2-65) are the warmest of the year, ranging from near 61°F (16°C) in the northern areas to near 80°F (27°C) in the south, a warming since May of 22°F (12°C) and 16°F (9°C) respectively.

During August, the extreme maximum temperature for the southern sea is about 88°F (31°C) while the extreme minimum temperature for the northern sea is about 48°F (9°C).

3.5.1.9 Freezing Level

Figure 2-49 (page 2-67) depicts the altitude of the mean freezing level during August. Over the northern portion of the sea the altitude of the lowest freezing level increases from about 9,000 ft in June to near 12,000 ft in August. Altitudes in the southern areas increase from 14,000 ft in June to approximately 15,000 ft in August, the maximum altitude of the year over the Sea of Japan.

3.5.1.10 Aircraft Carrier Operating Conditions

Optimum aircraft carrier operating conditions, defined as having a low cloud ceiling ≥5,000 ft (or no low cloud ceiling), visibility ≥5 n mi, and wind 11-21 kt, occur between 10 and 30 percent of the time over the major portion of the sea during August, with a small area of over 30 percent frequency of occurrence in the southwest Sea of Japan.

Poor conditions, defined as having a low cloud ceiling <300 ft, or visibility <1 n mi, or wind <6 kt or ≥34 kt have a frequency of occurrence of over 40 percent between about 42°N and 45°N and east of 137°E, and less than 20 percent in a circular area between 36°N to 40°N and 129°E to 135°E. The remainder of the sea has a poor condition frequency of occurrence of 20-40 percent.

3.5.1.11 Seasonal Oceanographic Features

As shown in Figure 2-48 (page 2-66), August is the month of warmest sea surface temperatures in the Sea of Japan. Temperatures range from a high of 79°F (26°C) in the southern part of the sea to about 59°F (15°C) in the northern waters.

No sea ice is observed in most of the Sea of Japan during summer. The last remnants of ice are seen during June in the extreme northern sea and are gone by July.

3.5.1.12 Electro-Optical Conditions (See section 2.3)

The Southeast Monsoon dominates the majority of the Sea during summer resulting in tropical like conditions. The large scale E/O conditions therefore take on the characteristics of the tropics, generally reduced E/O ranges due to increased atmospheric aerosols but fewer elevated ducts due to stronger vertical mixing. The northern part of the sea, which is likely to be affected by the Polar Front and migratory highs will differ from the area under the Southeast Monsoon flow. E/O conditions will have large variations in the northern area that reflect the synoptic scale influence.

The following table presents statistical information on duct heights for the regional area and season of interest:

CENTER OF AREA: 40°N 135°E SEASON: SUMMER

EVAPORATION DUCT HISTOGRAM IN PERCENT OCCURRENCE

Height (m)	June			July			August		
	day	nite	both	day	nite	both	day	nite	both
0 to 4	21	20	21	17	17	17	7	7	7
4 to 8	13	19	16	11	16	14	6	12	9
8 to 12	15	23	19	13	19	16	11	18	14
12 to 16	14	17	16	11	18	15	14	22	18
16 to 20	9	8	8	9	11	10	15	19	17
20 to 24	5	5	5	6	6	6	10	9	9
24 to 28	3	2	3	4	3	4	5	4	5
28 to 32	2	1	1	2	1	2	3	1	2
32 to 36	1	1	1	2	1	2	2	1	1
36 to 40	1	0	1	1	0	1	1	0	1
above 40	16	5	10	21	7	14	26	8	17
Ave. Ht.	18	13	15	22	15	18	27	17	22

3.6 Autumn (mid-September through November) (See section 2.2.1.8)

The onset of the autumn season over the Sea of Japan is abrupt. The strengthening Siberian high pressure cell forces the Polar Front rapidly southward to a position south of Japan by late September, resulting in the establishment of the Northeast Monsoon by mid-October. Figure 2-50 (page 2-69) depicts a generalized synoptic pattern during autumn.

3.6.1 Climatology

The first month of autumn brings significant changes to the weather of the Far East. In the region of southern Honshu and the southern Sea of Japan (Figure 3-1, page 3-2), the period is called the Autumn Bai-U (or Shurin). During this time the Siberian high begins to strengthen as the mid-Pacific high weakens, resulting in the rapid southward migration of the Polar Front through the Sea of Japan to a position well south of Japan (Figure 2-5, page 2-18). It is accompanied by a wide band of rain, reduced visibilities and low ceilings. A quasi-stationary, upper level low center forms over the Sea of Okhotsk and spawns short wave troughs that move through the Sea of Japan. The area comes under the influence of cool air forced southward by the strengthening Siberian high pressure cell.

By November, the Polar Front is forced southward to a position just north of the Philippine Islands (Figures 2-5 and 2-50, pages 2-18 and 2-69) and cool, dry air covers the Sea of Japan. As autumn progresses, the Siberian high becomes the dominant weather feature over eastern Asia and adjacent waters. High pressure cells routinely break off from the Siberian high and move across the Sea of Japan and northern Honshu (Figure S-3-9). Frontal activity and cyclogenesis typically occur over Eastern Asia and adjacent waters in the induced trough between the stationary Siberian high and the migratory high. The semipermanent low over the Sea of Okhotsk continues to strengthen throughout the period.

3.6.1.1 Synoptic Patterns

Figure 2-6 (page 2-23) depicts the tracks of extratropical cyclones that normally occur throughout the year. Of the six tracks depicted, four will typically affect the weather over the Sea of Japan during autumn: the Manchurian Low (track A), Lake Baikal Low (track B), South Mongolia Low (track C), and Yellow Sea Low (track E).

Because of its rapid movement, the southward migration of the Polar Front during the Autumn Bai-U affects the Sea of Japan for a short period relative to the Spring Bai-U. Once the front is south of Japan, frontal activity in the Sea of Japan is generally limited to those typed by Sjan-Zsi Li in the document Forecasters Handbook Volume 1 (FWC/JTWC, 1969) Climate of China. The tracks are depicted in Figure 2-7 (page 2-26).

The first series of "noticeable" cold fronts, usually of the Western or Central types, occur with great regularity during the autumn between the latter part of October and early November, with a second and more severe series occurring in early December.

Figure S-3-9. Local conditions, Autumn. 22 October 1979.

FIGURE S-3-9. LOCAL CONDITIONS, AUTUMN. 22 OCT 79
OSAN AB Visual DMSP: TN: 22/0035 GMT

Synoptic Features: A bubble high center over coastal central China is moving eastward. Northerly flow extends to the northern Philippine Islands. A surge line extends northeastward from northern Luzon to south of the Japan Islands.

Satellite Image Features:

1. A surge line (cold front) cloud band extends from the South China Sea across Luzon and northeastward beyond Japan.

2. The bathymetric features of the shallow shelf area along the central China coast are clearly depicted by variations in gray shades. The features include the fan shaped sub-surface delta formation off the old mouth of the Yangtze (Changjiang) River, which is north of the current mouth position. These bathymetric features can be recognized by their persistence and should not be confused with gray shades that are associated with atmospheric aerosols. This same feature can be seen in Fett (1977) which includes a DMSP image from 30 January 1973.

3. The dark areas downwind from southern Taiwan and northwestern Luzon are areas of atmospheric drying resulting from flow over the upwind terrain.

4. Cloud lines extending downwind from the end of northern Luzon, northern and southern Taiwan, and eastern and western Cheju-do Island are examples of cornering effects. Winds are accelerated around the corners and significant changes in aerosols, humidity and cloud cover will occur across these cloud lines.

5. The gray shade cap around the tip of Shandong Peninsula may reflect an area of higher relative humidity associated with a region of upwelling caused by tidal actions (Guo and Xia, 1984)

Forecast Aids:

1. In the vicinity of surge lines winds will be stronger, gusty, and shifting in direction. Showers are likely along the line.

2. E/O conditions will generally improve in the lee side dark areas seen in satellite imagery, also visibility increases, and winds decrease. Conditions will be degraded in areas of lighter gray shades caused by atmospheric aerosols or increased relative humidity.

3. Persistent gray shade patterns in shallow water due to bathymetric features must be known so as not to mistake them for aerosol related gray shades in visual images and SST features in IR images.

4. The thin cloud lines flowing southwestward out of the western Taiwan Strait reflect the stronger surface winds due to funneling in this area. On this day the winds in the Strait were 20 kt or more and around the area they were 10-15 kt.

3.6.1.2 Surface Wind

Prevailing winds increase in speed and change directions with the onset of autumn over the Sea of Japan. By late September the prevailing directions are northeast with a speed of 10-15 kt becoming north-northwest 15-20 kt by November. As shown in Figure 2-51 (page 2-71), the frequencies of occurrence of winds ≤10 kt reduce sharply during autumn, with 40-50 percent predominating over much of the central area of the sea, and less than 30 percent north of 39°N. Gale (≥34 kt) frequency of occurrence is less than 5 percent over the major portion of the sea, increasing to 5-10 percent north of about 47°N.

3.6.1.3 Upper Level Winds

Figures 2-52 through 2-57 (page 2-72 to 2-74) depict upper level flow patterns for the month of November. The strongest winds (at the specified pressure surfaces) are found over southern Japan at 200 mb with a mean speed of 120 kt. The winds diminish to about 35 kt over the northern Sea of Japan.

3.6.1.4 Visibility

Figure 2-58 (page 2-75) depicts the frequency of occurrence of visibility limits during November. The frequency of occurrence of visibility ≥5 n mi is slightly improved over August due to less fog: 80-90 percent over most of the central portion of the sea, and over 90 percent along the southwestern coast. The percentage lowers to under 80 percent north of about 45°N. A corresponding reduction in frequency of occurrence of visibilities <2 n mi is also seen in November.

3.6.1.5 Cloud Heights/Ceilings

There is a significant decrease in percent frequency of occurrence of low cloud amount ≥5/8 from August to September. However, as shown in Figure 2-59 (page 2-76), there is an increase in low cloud amounts ≥5/8 from September to November. The percent frequency of occurrence of low cloud ceiling <600 ft and/or visibility <2 n mi is less than 5 percent in the southern Sea of Japan, and over 10 percent in the northern sea.

3.6.1.6 Precipitation

The months of autumn see a gradual increase in precipitation frequency throughout the period from a minimum of 8-17 percent in September to about 8-25 percent in November.

Snow frequency (as a percent of observations reporting precipitation) becomes a factor in October with a maximum of about 20 percent in the extreme northern part of the sea and the snow limit line north of 45°N. By November however, as the cold air of the Siberian high invades the area, the snow limit line has reached the southern limit of the sea, and the 60 percentile isoline extends east-west along 45°N.

3.6.1.7 Sea State

The wave height statistics for the Sea of Japan during November as depicted in Figure 2-60 (page 2-77) reflect the increased wind speeds and north to northwest directions discussed in section 3.6.1.2. The frequency of occurrence of waves ≥5 ft (1.5 m) is over 60 percent in the central and eastern portions of the sea, decreasing to less than 40 percent along the western coastline between 38°N and 46°N. Waves ≥8 ft (2.5 m) occur more than 20 percent of the time over the central and eastern areas of the sea and less than 20 percent elsewhere.

3.6.1.8 Surface Air Temperature

By November (Figure 2-61, page 2-78) the surface air temperatures over the Sea of Japan have cooled considerably from the warm temperatures of summer. The mean temperature in the extreme northern section is less than 30°F (-1°C), while the southern sea has a mean temperature of about 59°F (15°C).

The extreme maximum temperature for the southern area is about 72°F (22°C) while the extreme minimum temperature for the northern sea is about 3°F (-16°C).

3.6.1.9 Freezing Level

The altitude of the freezing level lowers drastically between August and November (Figure 2-63, page 2-80). The freezing level is at the surface north of about 46°N during November, increasing to 8,000 ft in the southern sea.

3.6.1.10 Aircraft Carrier Operating Conditions

Optimum aircraft carrier operating conditions, defined as having a low cloud ceiling ≥5,000 ft (or no low cloud ceiling), visibility ≥5 n mi, and wind 11-21 kt, occur 20-35 percent of the time over most of the sea during November, with less than 20 percent frequency occurring east of 140°E between 45°N and 49°N.

Poor conditions, defined as having a low cloud ceiling <300 ft, or visibility <1 n mi, or wind <6 kt or ≥34 kt, have a frequency of occurrence of less than 20 percent over most of the sea.

3.6.1.11 Seasonal Oceanographic Features

Figure 2-62 (page 2-79) depicts the mean sea surface temperatures during November. The onset of the colder autumn air temperatures is evident, as the sea surface temperatures show a significant decrease from the summer temperatures shown in Figure 2-48 (page 2-66).

Sea ice is again observed in the Sea of Japan during November, but the approximate maximum extent of 0.1 or greater ice concentration is limited to the coastal waters north of about 43°N and the non-coastal waters north of about 51°N.

3.6.1.12 Electro-Optical Conditions (See section 2.3)

The large scale pressure patterns will change rapidly over the Sea during the autumn period. The southward passage of the Polar Front and return of the Northeast Monsoon will develop within a span of a couple of weeks. The result is a major change in all weather conditions including E/O conditions.

The local forcing will likewise change from summer patterns to winter patterns within a few weeks period. In general the lee side windward side patterns will reverse as well as the changes in air mass and air sea temperatures differences. Forecasters should be aware of these reversal and change patterns when returning to the area following a short absence during which the transition occurred.

The following table presents statistical information on duct heights for the regional area and season of interest:

CENTER OF AREA: 40°N 135°E SEASON: AUTUMN

EVAPORATION DUCT HISTOGRAM IN PERCENT OCCURRENCE

Height (m)	September day	September nite	September both	October day	October nite	October both	November day	November nite	November both
0 to 4	7	13	10	9	7	8	7	6	7
4 to 8	12	15	13	9	12	11	20	25	22
8 to 12	12	15	14	15	22	19	37	35	36
12 to 16	15	20	17	17	25	21	21	23	22
16 to 20	11	9	10	21	17	19	9	7	8
20 to 24	9	7	8	7	9	8	2	1	1
24 to 28	4	7	5	6	3	4	1	1	1
28 to 32	4	1	3	1	0	1	0	1	0
32 to 36	2	1	2	1	0	1	0	0	0
36 to 40	2	1	2	0	0	0	0	1	1
above 40	22	11	16	13	3	8	5	1	3
Ave. Ht.	24	18	21	20	15	17	13	11	12

4.0 EAST CHINA SEA

4.1 Regional Features and Their Influence on Weather Phenomena

The East China Sea is bordered on the west by The People's Republic of China, and on the east and south by the arc of the Ryukyu Islands and Taiwan. To the north, the sea is bounded by the Japanese island of Kyushu, South Korea, and the Yellow Sea (Figures 4-1 and S-4-1). The East China Sea has a surface area of approximately 256,600 sq mi and an average water depth of about 620 ft (189 m) (Newspaper Enterprise Association Inc., 1978).

The sea is accessible from the Philippine Sea/North Pacific Ocean through many passages between the islands of the Ryukyu chain. Access from the South China Sea is gained through the Taiwan Strait between Taiwan and the Chinese mainland. To the north, the Tsushima (Korea) Strait between Korea and Japan leads to the Sea of Japan, while the Yellow Sea is accessible from the East China Sea through a common 240 n mi boundary extending from the Yangtze (Changjiang) River delta on mainland China to the South Korean island of Cheju-do.

The topography of the land areas adjacent to the East China sea is generally unremarkable. The coastal areas of eastern mainland China are characterized by extensive low lying mountain ranges, which have elevations commonly below 3,018 ft (920 m). A few peaks exceeding 5,906 ft (1,800 m) are found 150-200 mi inland,

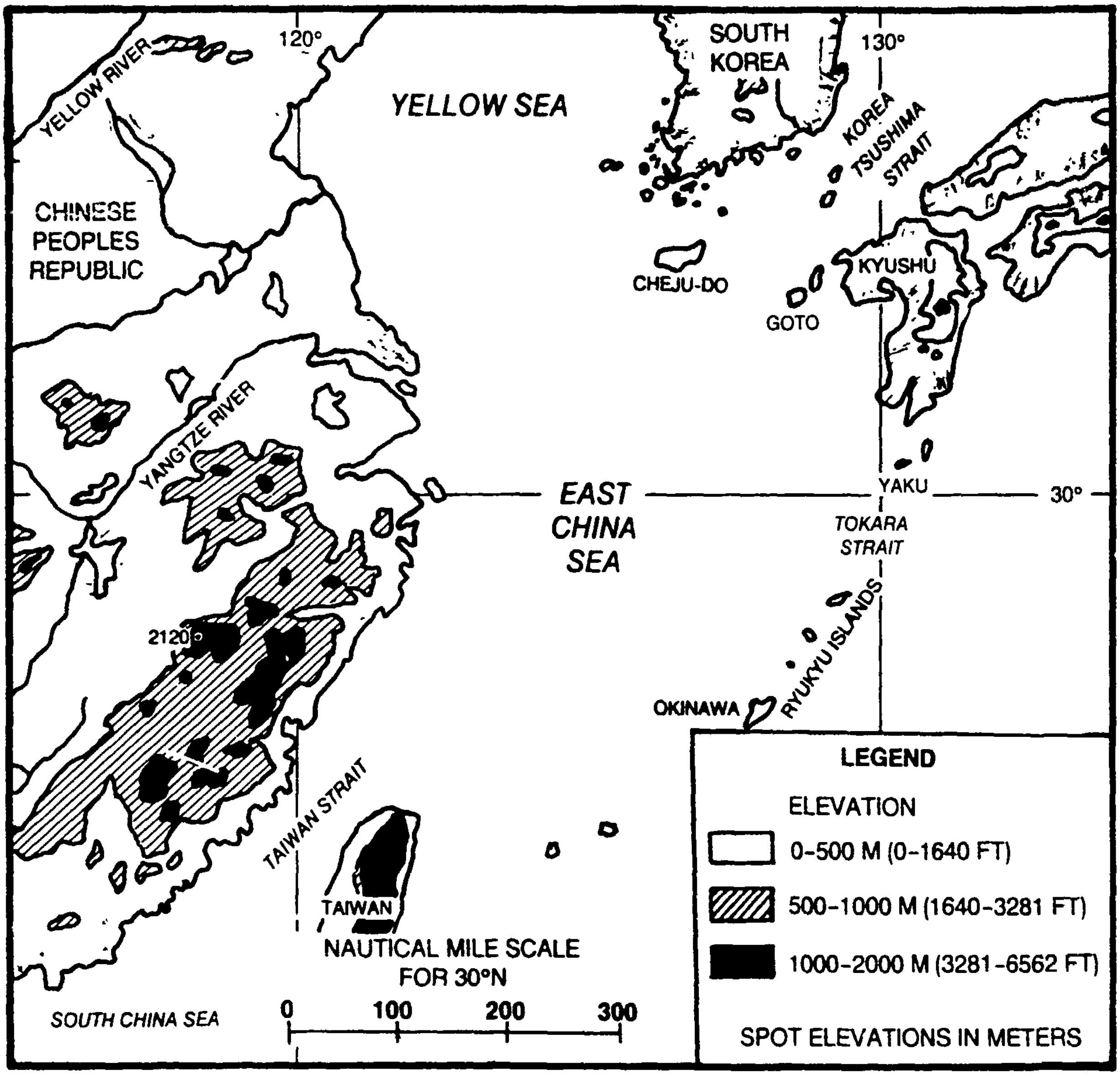

Figure 4-1. Major topographic features surrounding the East China Sea (adapted from Nestor, 1977)


2
3

FIGURE S-4-1. OCEAN FEATURES, YELLOW SEA AND EAST CHINA SEA.
19 MAR 80
Simultaneous Visual (S-4-1) and Infrared Images (S-4-2)
OSAN AB Visual DMSP: TN: 19/0242 GMT

<u>Synoptic Features</u>: A migratory high cell is resulting in clear sky conditions over the southern Yellow Sea and northern East China Sea, providing an opportunity for viewing oceanic features of the area.

<u>Satellite Image Features</u>:

1. The major gray shade pattern seen off the coast of China is caused by bathymetry features. Note that the pattern does not correspond with the gray shades seen in the infrared image (see Figure S-4-2). This delta fan like pattern is related to the sediment deposits from the Yangtze River outflow. The pattern appears to emanate from a point about 60 n mi north of the current river mouth location (Huh, 1983).

2. The cloud pattern north of the Yellow Sea is associated with a developing 1016 mb low. Comparing the visual and infrared images aids in identifying the various types/levels of clouds.

3. The cirrus pattern has been defined as a baroclinic leaf and has been shown to proceed low level cyclogenesis.

<u>Forecast Aids</u>:

1. There are several causes of gray shades in visual imagery: sunglint area surface roughness, atmospheric aerosol content, and bathymetry features. The majority of the gray shade variations seen in this image are likely related to the light wind situation in the ridgeline that extends from the coast of China, across Korea, to northern Japan. One obvious exception is the bathymetry feature of the Yangtze River, other possible exceptions are the light gray shape cap around the tip of Shandong Peninsula and the dark strip extending southwestward from Goto Island, east of Cheju-do Island. The dark strip downwind from Goto is probably due to barrier effect drying. These subtle gray shade patterns can provide significant insight to atmospheric conditions. But a thorough understanding of the complexities of satellite imagery is necessary for proper interpretation. See the NEPRF NTAG series by Fett.

2. The migratory high and developing low in combination is an example of the bubble high forecast rule provided elsewhere.

but the highest elevations near the coast are limited to 3,281-4,101 ft (1,000-1,250 m).

Taiwan is mostly mountainous, with peaks of 12,743 ft (3,884 m) and 13,114 ft (3,997 m) found in the northern and central areas of the island.

The Ryukyu Islands are generally low in elevation, with 1,634 ft (498 m) on the northern end of Okinawa being the highest point.

The Japanese island of Kyushu borders the northeast portion of the East China Sea. Mountainous over most of its extent, it's highest peaks are 5,866 ft (1,788 m), 5,577 ft (1,700 m), and 5,223 ft (1,592 m).

The southern part of South Korea adjacent to the East China Sea is mountainous, with one peak of 6,283 ft (1,915 m) close to its southern coast. Cheju-do, a prominent South Korean island located some 50 n mi south of the Korean peninsula at the southwestern end of the Tsushima (Korea) Strait, is essentially one large mountain, with a maximum elevation of 6,398 ft (1,950 m).

Because of the generally low elevations of the larger adjacent land areas, the topography exerts a rather small influence on the weather over the East China Sea. One notable exception, however, is found in the Taiwan Strait. Because of the mountainous terrain of Taiwan and the coastal range on the adjacent Chinese mainland, winds channeled through the strait experience an acceleration due to a Venturi effect. The increase in velocity is especially evident during periods of strong northeast or southwest monsoonal flow or when a tropical cyclone is in the vicinity. The accelerated wind phenomenon is discussed later in section 4.7.3.

Perhaps the most significant feature of the region with respect to its influence on weather phenomena is not the surrounding topography, but the sea itself. The bathymetry of the East China Sea will be addressed in more detail later, but since the sea profoundly influences the meteorology of the region, it will be briefly addressed here.

The North Equatorial Current flows westward at tropical latitudes in the western North Pacific Ocean until it reaches the Philippine Sea east of the Philippine Islands. It then curves northward as the Kuroshio Current and flows to southwestern Japan, where it splits into subcurrents. As it moves northward from the Philippine Sea its path takes it just to the east of Taiwan, over the eastern part of the East China Sea, approximately following the Okinawa trough (Figures 2-3, page 2-7 and S-4-2, page 4-7). The Kuroshio is a warm current, like the Gulf Stream off of the United States' east coast, and the Kuroshio Current exerts a similar influence on passing weather systems. Seemingly innocuous weather systems moving offshore from the Chinese mainland may develop into major storms after encountering the warm waters of the Kuroshio Current. The disturbances, known as Shanghai and Taiwan lows (Figure 2-6, page 2-23), are particularly evident in the spring and autumn and the environmentalist must be aware of their potential for development. They are discussed more fully in section 2.2.1.

Several small rivers from the extensive eastern watershed of The People's Republic of China drain into the East China Sea, all are insignificant compared to the runoff provided by the 3,400 mi Yangtze (Changjiang) River, which drains into the sea near its interface with the Yellow Sea. The overall effect of riv r outflow on the climate of the East China Sea region is not signif cant.

Figure S-4-2. SST patterns, Yellow and East China Seas. Infrared 19 March 1980.

FIGURE S-4-2. SST PATTERNS, YELLOW AND EAST CHINA SEAS. 19 MAR 80
Simultaneous Visual (S-4-1) and Infrared Images (S-4-2)
OSAN AB Infrared DMSP: TN: 19/0242 GMT

Synoptic Features: The large scale oceanic features include the Tsushima Current which flows northward from the Kuroshio Split (near 30°N, 130°E) to the vicinity of Cheju-do Island where it in turn splits. The left branch continues northward into the central basin area of the Yellow Sea and the right branch flows northeastward into the southern Sea of Japan.

Satellite Image Features:

1. The warm Tsushima and Yellow Sea Currents are evident as darker gray tones in the cloud free areas (see simultaneous visual image Figure S-4-1). Note: The labels are actually on cloud features.

2. The lighter gray shades seen in the shallow bays along southern Japan and over the coastal shallows and shelf areas of the Yellow and East China Seas indicate relatively cold surface waters.

3. The cold fresh (low salinity) outflow from the Yangtze River flows over the denser more saline sea water and is seen as lighter gray ribbons near the river mouth. Note that there are some low stratus/fog just to the southeast of the river mouth.

4. Cold coastal water is seen along western Korea. Relatively warm water (darker gray) is seen between Cheju-do Island and the southern coast of Korea.

Forecast Aids:

1. The areal distribution of warm and cold surface water is evident in a properly enhanced infrared image. The major current patterns and areas of warm or cold water are relatively persistent and once defined will provide useful information for several days.

2. The cold coastal waters flowing south and east around southwestern Korea sink under the warm Tsushima Current warms during winter. During spring and autumn the cold surface boundary will extend southward to a line between Cheju-do and Tsushima Islands.

3. Cold but low salinity waters from the rivers feeding into the Yellow and East China Seas will flow over the ocean coastal waters.

4.2 East China Sea Oceanographic Features

The East China Sea (ECS) oceanographic features reflect the combined influences of regional atmospheric forcing and bathymetry, plus the interaction with large-scale hydrographic (current) patterns.

The atmospheric monsoon regime that prevails over the ECS provides cyclic seasonal forcing that dominates the regional oceanographic processes. Atmospheric forcing occurs in two modes: in winter by cooling and destratification due to strong cold and dry northerly winds, and in summer by extensive precipitation, river runoff, and solar heating, which produce a well-stratified water column with a warm, low-salinity surface layer. (Huh, 1982). Understanding the variations in seasonal atmospheric forcing and sources of water are critical to understanding the seasonal variability in oceanographic conditions throughout the ECS. Seasonal conditions are further agitated by strong winter cold outbreaks and by summer typhoon passage.

The ECS hydrographic conditions are influenced on the western side by the discharge of the Yangtze (Changjiang) River. On the east side, the Kuroshio Current and its branches and extensions exert strong influences. The main body of the Kuroshio does not flow over the continental shelf; however, its effect is felt through its branches and extensions, which flow over the shelf area and mix with the continental coastal water.

The ECS bathymetry is divided into two contrasting provinces: the shallow water, broad continental shelf and the deep water Okinawa trough. The shelf area is relatively narrow and elongated, extending from near 22°N to 40°N. The depth contours (isobaths) generally parallel the north-south coast. The trough extends from Taiwan to Kyushu along the inner Ryukyu Island arc.

Special Regional Characteristics

The following hydrographic phenomena of the shallow water area are considered to have significant potential for impact on naval operations:

(1) the diluted water of the Yangtze (Changjiang) River,
(2) coastal upwelling off Zhyiang,
(3) eddies on the continental shelf,
(4) an "against-the-wind current" in winter off the SE coast of China,
(5) the direct relationship between winter winds and ocean currents, and
(6) vigorous tidal action.

Yangtze (Changjiang) Inflow: Initially, the Yangtze (Changjiang) discharge water flows southeastward along the direction of its mouth. A short distance from shore it turns cyclonically to the east and northeast. In the flood season the water tongue of the Yangtze (Changjiang) diluted water may extend as far as the area of Chyu Island (Figure S-4-3). In the diluted water region salinity as low as 5‰ are found near the river mouth and the 31‰ isopleth may extend eastward as far as 125°E.

Coastal Upwelling off Zhejiang (China coast north of Taiwan to near 30°N): This is generally a summer condition. The short-term variability relates to the intensity of the Southwest Monsoon surface wind. In the region of upwelling the temperature increases and the salinity decreases from west to east in the upper layer of the ocean. Summer upwelling has also been noted along the northeastern and southeastern coasts of Taiwan.

Figure S-4-3. Yellow Sea Spring. 9 April 1980.

FIGURE S-4-3. YELLOW SEA SPRING. 9 APR 80
OSAN AB Infrared DMSP: DN: 09/0235 GMT (TS (T=285°K))

Synoptic Features: The Yellow Sea Warm Current extends northwestward from the Tsushima Current near the Tsushima/Korea Strait and then northward over the deep basin portion of the Yellow Sea (YS) (Figure 2-4, page 2-11). The cold coastal current flows southward around the Shandong Peninsula and over the shelf area of the East China Sea (ECS). A portion of the oceanic Polar Front can be seen in the cloud free part of the west central Sea of Japan (SOJ). The corresponding visual image of this pass is seen in Figure S-5-5 (page 5-25).

Satellite Image Oceanographic Features:

1. The warm Yellow Sea Current.

2. The oceanic Polar Front of the SOJ.

3. The cold coastal current flowing southward around the Shandong Peninsula and along the China coast.

4. The warmer waters of the Tsushima Current flowing through the Tsushima/Korea Strait, primarily on the Japanese side, is only partially evident because of cloud cover.

5. The cold water of the Yangtze (Changjiang) River is in clear contrast with the warmer land. There is evidence of the offshore path of the cold water in the form of a faint light gray shade cyclonically curved plume extending eastward from the southern outflow point of the river.

Forecast Aids:

1. Near iso-thermal, half-channel conditions dominate the YS and the shelf portion of the ECS during the cold seasons. The warm Yellow Sea Current will result in some vertical stratification over the southern YS.

2. The oceanic Polar Front is a year round feature of the central SOJ. A change from half-channel to full-channel conditions occurs across this feature during the winter.

3. The warm water features along the Polar Front are generally shallow lens or wedge shaped in the vertical. When well developed warm eddies or well defined current boundaries are evident, the warm water will extend to greater depths.

4. The thermal structure across the Tsushima/Korea Strait typically reflects a frontal discontinuity pattern, cold on the Korean side, warm on the Japanese side.

Eddies on the Continental Shelf: Several eddies have been found that appeared frequently in the past. The majority are cold cyclonic eddies which tend to be more stable than warm anticyclonic eddies (Figure S-4-4).

Cold cyclonic eddies:

(1) north of Taiwan, near surface (26°N, 122°E)
(2) south of Cheju-do Island to the left side of the Tsushima Current in the near bottom layer (32°N, 126°E)
(3) northeast of the Yangtze (Changjiang) River mouth in summer at the surface (33°N, 123°E)

Warm anticyclonic eddy:

(1) northeast of Taiwan to west of the Kuroshio in summer at the surface (27°N, 123°E)

"Against-the-Wind" Current in Winter: In winter a southerly current driven by the northeasterly monsoon flow exists along the China coast. However, once away from the coastal zone and at depths below about 5 m, there is a northeast (against-the-wind) current. A similar pattern of currents exists through the Taiwan Strait and southward into the South China Sea during winter.

Winter Winds and Responding Currents and SST Gradients: Cold coastal currents off eastern China and western Korea are enhanced by prolonged strong northerly winter winds. In response, as a return flow current, the northwesterly extension of the Tsushima Current (the Yellow Sea Warm Current) also is enhanced. The result is intensified SST gradients in the boundary regions of these juxtaposed but thermally, as well as directionally, opposite currents.

Figure 5-4-4. Kuroshio Split. Infrared 12 May 1980.

FIGURE S-4-4. KUROSHIO SPLIT, SIMULTANEOUS VISUAL AND INFRARED IMAGES. 18 MAY 80
OSAN AB Infrared DMSP: TN: 18/0136 GMT

Synoptic Features: The large scale oceanic surface thermal features include: the Kuroshio split, the Tsushima Current flowing northward from the split and then northeast through the Tsushima/Korea Strait, the warmer waters of the Tsushima continue northward along the eastern Sea of Japan with outflow occurring through first the Tsugaru and farther north the Soya Straits. The warm outflow through these two straits turns sharply southward along the northeast coasts of Honshu and Hokkaido, respectively, in what is referred to as coastal modes. East of Tsugaru Strait a small portion of the perturbed area created by the converging cold Oyashio and warm Kuroshio Currents can be seen.

Satellite Image Features:

1. The Kuroshio split just south of the southern most part of Japan.

2. The northward flow from the split area of the Tsushima Current.

3. The thermal contrast across the Tsushima/Korea Strait, cold on the Korean side, warm on the Japan side.

4. The relatively warm waters on the east and south sides of the Sea of Japan and cold on the north and west sides. The minimum contrast of gray shades across the south central Sea of Japan in this image is likely caused by masking of the surface temperatures by the high level return from a cirrus band.

5. The outflow through the Tsugaru and Soya Straits. Note that the thermal pattern from north to south across these two straits is similar to that across the Tsushima, cold on the north, warm on the south.

6. The warm water turns southward after exiting the Tsugaru and Soya Straits and is confined to a narrow band along the coastline.

7. The western end of the perturbed areas resulting from the confluence of the cold Oyashio and warm Kuroshio Currents east of Japan is seen east of the Tsugaru Strait. This pattern extends eastward beyond 160°E into the Central Pacific.

Forecast Aids:

1. The major features of the Kuroshio and Tsushima Currents will persist over extended periods of time. The latest available positioning view should be retained until direct evidence of a change becomes known or a new satellite view is available. Neither

the large scale numerical analyses and forecasts, nor products derived from them will reflect the strong thermal boundaries that are evident in the imagery.

2. The infrared temperature sensed by the satellite sensor is an integrated value from the entire atmospheric column. The best SST readings are obtained through cold and dry atmospheric conditions. The normal strong gray shade contrast across the southern Sea of Japan caused by the cold water of the Liman Current along the north and west sides and warm Tsushima Current along the south and east side, are largely masked in this image due to the added high level moisture associated with the cirrus shield approaching from the west. The effects of increased atmospheric moisture include both attenuation which lowers all temperature values sensed and suppression of temperature differences because of increasing attenuation with increasing surface temperatures which reduce the real temperature differences or gradients.

3. The surface water of the northern parts of the Tsushima, Tsugaru, and Soya Straits will be colder than the southern side where the warm outflow is located. There are known variations to this, including:

A. The cold water flowing south and east around southern Korea sinks under the warm Tsushima water during winter. In spring and into summer when heavy run-off reduces the cold water salinity, it overrides the Tsushima waters and produces a frontal zone near a line between the islands of Cheju-do and Tsushima.

B. During the summer when surface heating results in uniform sea surface temperature values and a mixed layer (full-channel conditions), even though it is quite thin over the northern waters, the obvious thermal contrast is not there.

C. The inflow (Tsushima) and outflow (Tsugaru and Soya) are strongest during summer and therefore increasing portions of the Straits will be covered by warm water as the summer season approaches and also following it. During winter the cold water portion is largest.

4. The coastal mode outflow is a year round feature of the Soya Strait. The outflow of the Tsugaru changes to a warm gyre mode that extends eastward to near 143°E during the summer strong outflow period.

5. The perturbed area east of the Tsugaru Strait and the main Japan island of Honshu is a year round feature. A series of gyres are typically aligned east-west along it and its north-south extent is on the order of 300 n mi. Little evidence of this general feature is reflected in numerical products and the gyres are not likely to be reflected at all.

Tides: The tidal range over the ECS increases from east to west. Maximum heights of 2 to 3 ft occur in the Ryukyu Islands, increasing to 15 to 20 ft around Taiwan and to over 30 ft in the mainland Hangchow Bay southwest of Shanghai. Maximum tides occur during summer and winter.

The combination of tidal action and ocean currents (Kuroshio) result in some strong local tidal currents in the vicinity of islands and narrow channels. Tidal currents of 2 to 3 kt are not unusual along the Ryukyu Island chain and speeds of 5 kt have been reported in the Tokara Strait (near 30°N, 130°E).

Bathymetry: The continental shelf varies in width from about 150 n mi near Taiwan to 400 n mi near the northern boundary (33°N). The shelfbreak occurs at depths from 150 to 170 m. There are a few scattered islands near the outer edge of the shelf. Terrigenous sediment deposited from the outflow of the Yangtze (Changjiang) River is the primary origin of the shelf material. The general composition is comprised of a 75 n mi wide belt of mud out from the shore with a broader paralleling zone of fine-grained sediments changing to sand over the outer shelf zone. There is a large submerged mud delta off the mouth of the Yangtze (Changjiang) River which spreads over a radius of about 180 n mi. Water depths over this delta are only about 30 m. The turbidity associated with this delta is visible in satellite imagery (see Figure S-4-1, page 4-3).

The Okinawa trough, with depths to near 2270 m near Taiwan, borders the continental shelf. The steep western slope of the trough is the continental slope.

Currents: The circulation pattern of the ECS consists of two systems: the warm saline current of oceanic origin, and the less saline coastal current. This results in a cyclonic gyre with the Kuroshio-Tsushima warm current and its extension on the east side, and the ECS coastal current on the west side. This closed circle circulation is strongest in the winter when the ECS coastal current is best developed. During summer the southern portion of the ECS circulation is more a band of predominant northeast flow than a closed gyr~ flow.

Temperature and Salinity: The near surface temperature and salinity values over the continental shelf area show marked seasonal variations, while the region of the warm currents, Kuroshio over the Okinawa trough and the extension of the Tsushima Current through the Tsushima Strait, is more stable. During the cold season isothermal (half-channel) conditions exist from the surface to the bottom in the shallow coastal area. In winter the pattern of the isotherms throughout the vertically homogeneous layer and the isobaths are very similar. During all seasons a two-layer ocean structure and thermocline are found over the deeper shelf and trough areas, and wherever a warm surface current occurs.

Sea Ice: Sea ice does not occur in the ECS area.

4.3 Winter (mid-December to mid-March) (See section 2.2.1.5)

The weather over the East China Sea is under the influence of the Northeast Monsoon during the winter. The Polar Front lies well south of the southern limit of the sea throughout the season (Figure 2-5, page 2-18). A generalized winter synoptic pattern is depicted in Figure 2-8 (page 2-29).

4.3.1 Climatology

With the Polar Front south of the area, the weather over the East China Sea is dominated by modified continental polar (cP) air forced southward by the Siberian high. The Siberian high, at its greatest strength during the winter, fluctuates both in intensity and position in response to atmospheric changes aloft (Figure S-4-5). These changes are caused by migratory mid-tropospheric disturbances which cause cold surges to move through the area. Surface temperatures at the source region range generally from 15°F to -40°F, but the air is adiabatically warmed as much as 25°F in its primarily downslope trajectory toward the coastal waters. By the time the air reaches the East China Sea, it has been further modified by its marine trajectory so that the temperatures experienced are markedly warmer than those seen over the Sea of Japan and the Yellow Sea.

Figure S-4-5. Winter cold outbreak. 6 February 1980.

FIGURE S-4-5. WINTER COLD OUTBREAK. 6 FEB 80
Visual DMSP: DN: 06/0006 GMT

Synoptic Features: A large 985 mb low near 39°N, 155°E and an intense 1064 Asian high are causing a strong northerly flow and an outbreak of cold air over the Sea of Japan and adjacent seas.

Satellite Image Features:

1. The widespread numerous cloud lines vividly depict the intensity of this cold air outbreak. Air temperatures at or below freezing covered the entire Yellow Sea, Sea of Japan, Sea of Okhotsk, and portions of the open Pacific north of about 40°N on this day in February 1980. Sustained surface winds were in the 20 to 40 kt range.

2. The local funneling patterns of valleys and breaks in the terrain are clearly indicated by the length of cloud free paths seaward and downwind from the terrain features. Cloud free paths are shorter downwind from valleys or low elevation terrain where minimum drying of the air during flow down the terrain slope to sea level has occurred.

3. Small scale vortices, likely terrain induced, are evident in the northern Sea of Japan.

4. The buildup of clouds on the windward side, and pronounced drying on the lee side is frequently seen over Japan and off the Asian continent.

5. A change in the cloud south and east of Japan indicates the change in low level flow from cyclonic to anticyclonic curvature.

6. Continuing downwind in the area of anticyclonic flow, the clouds take on a flat topped, closed cellular pattern, becoming continuous smooth topped, layered, stratiform type.

7. Variations in the mean vertical wind shear through the cloud layer result in three convective cloud regimes: (7a) Cellular under light shear, (7b) transverse bands with moderate shear, and (7c) longitudinal bands with strong shear.

8. The cloud lines change from lines parallel (longitudinal bands) to the wind shear through the cloud layer to rows of clouds perpendicular (transverse bands) to the wind shear in several areas of the image indicating weakening shear through the cloud layer (not labeled).

9. The length of the cloud free path increases with an increase in the upwind terrain height and decreases with the strength of the winter monsoon. These relationships are a result of increased drying of air during extended downslope flow and enhanced

thermodynamic effects (moisture flux and heating from below) during extreme cold and high wind conditions of strong outbreaks (not labeled).

Forecast Aids:

1. The intensity of cold air outbreaks is reflected in satellite imagery by the convective cloud regimes. Areas of strong outflow are marked by longitudinal bands, the stronger the outbreak the longer and wider the longitudinal bands.

2. Over the western Sea of Japan, the length of the cloud free path downwind from the western coastline will vary from less than 30 n mi under strong outbreaks to 180-240 n mi under weak outbreaks.

3. Opposite valleys and low terrain, the cloud free distances will be relatively short compared to areas opposite high terrain.

4. During winter outbreaks the dew points over USSR will be below -20°C, increase to about -10 to 0°C over Japan, and reach 10°C about 300 n mi south and east of Japan. Air temperatures will closely reflect the SST except near the coastlines and over terrain where lower air temperatures will reflect the source region and elevation factors.

5. The change from longitudinal to transverse to cellular convective cloud patterns reflect decreasing wind shear through the cloud layer. Typical values are: Shear greater than 4-5 kt/1000 ft results in longitudinal bands, for 3-4 kt/1000 ft transverse bands, and for less than 3 kt/1000 ft cellular clouds.

6. Under moderate or stronger outbreaks, light snow showers will occur over the eastern Sea of Japan, increasing in intensity to heavy showers along western Japan. Two regions of frequent enhanced convective clouds and shower activity have been noted near 40°N, 135°E and off the northwest corner of Sado Island. These are likely associated with SST pattern boundary regions.

7. Generally the length of the cloud free path will increase from the northern to southern portion of the western Sea of Japan.

8. Heavy snow will fall over western Japan under cold outbreak regimes, with deposits measured in feet over the western slopes of mountainous areas.

9. For E/O forecasts the best ranges will be in the regimes of cloud free and shower free areas. Conditions will vary between the alternating longitudinal/transverse bands. These bands have width dimensions of 10 to 60 n mi with 20 to 30 n mi widths being typical.

10. Improved E/O ranges in coastal regions will be found downwind from high terrain, in the lee of island barrier effects, and in the clear slots between cold bands.

11. A lee side pressure trough will typically be found off the Asian coast during cold outbreaks, with drops of 3-4 mb's typical.

12. During winter outbreaks the length of cloud free distances to the lee of the Japan Islands is near zero where the coastal $T_a = 0$. As the T_a decreases the cloud free path increases appreciably, reaching lengths of near 200 n mi where coastal T_a's are -15°C or less.

13. The wind profiles through the three convective cloud patterns all tend to show maximum speed shear in the layers below and immediately above the cloud layer. They differ in that through longitudinal regimes the shear is near constant from the surface to 3 to 5000 ft, increasing from surface speeds to 60 to 70 kt near 3000 ft. Through transverse banding the speeds are near constant through the cloud layer, while in cellular regimes the speed may actually decrease through the cloud layer. In the latter two cases (transverse and cellular) the resulting wind shears (just above and just below with little or no shear through the cloud) may be of greater threat to aircraft than the case of the continuous shear through the longitudinal cloud layers.

14. The changes in convective cloud regimes shown in satellite imagery provides insights on forecasting low level turbulence due to wind shear.

4.3.1.1 Synoptic Patterns

Figure 2-6 (page 2-23) depicts the tracks of extratropical cyclones that normally occur throughout the year. Of the six types depicted, only one -- the Taiwan Low (track F) -- will significantly affect the weather over the East China Sea during winter.

Of the frontal types, only the Western and Central types may significantly impact the weather over the East China Sea.

4.3.1.2 Surface Wind

January is the windiest of the winter months over the East China Sea, with February's winds (Figure 2-9, page 2-31) only slightly lower. Northerly winds prevail, reflecting the flow of the winter monsoon. The only significant incidence of gale force (≥34 kt) wind occurs in the Taiwan Strait (identified in Figure 2-3 page 2-7), where the northerly winds are accelerated due to a Venturi effect between the mountains of Taiwan and the Chinese mainland.

4.3.1.3 Upper Level Winds

Figures 2-10 through 2-15 (pages 2-32 to 2-34) depict upper level flow patterns for the month of February. Maximum velocities (at the specified pressure surfaces) over the East China sea occur at 200 mb and 300 mb where winds of 125-140 kt are indicated. The area near southern Japan is known to have the strongest and most persistent jet stream speeds in the world, with velocities exceeding

200 kt not uncommon. Such winds may be observed over the northern part of the East China Sea during the winter months.

4.3.1.4 Visibility

Winter visibilities over the East China Sea are generally good, with visibilities ≥5 n mi occurring between 80 and 90 percent of the time over most of the sea. Figure 2-16 (page 2-35) depicts visibility statistics for February. More favorable visibilities are observed over the northeast portion of the sea, while the greatest incidence of reduced visibility is found in the southwest portion.

4.3.1.5 Cloud Heights/Ceilings

Figure 2-17 (page 2-36) is an example of combined low cloud and visibility statistics for February. There is some variation between the individual months of winter, but for each month, low cloud ceilings (low cloud amount ≥5/8) generally exist between 60 and 75 percent of the time over most of the sea, with the greatest incidence occurring over the southwest portion of the sea. Statistics of combined low cloud ceiling and visibility limits of <600 ft and/or <2 n mi show deteriorating conditions throughout the winter, with the higher frequencies of occurrence seen south of 30°N and west of about 123°E.

4.3.1.6 Precipitation

During winter, a maximum precipitation frequency of 20-25 percent occurs near the Taiwan Low track in the southwestern portion of the sea in an elongated area roughly bounded by 24°N to 29°N and 122°E to 124°E. The remainder of the East China Sea has precipitation occurrences of less than 20 percent, except less than 15 percent north of about 31°N. The approximate southern limit of snow observations for the year is about 28°N in February.

4.3.1.7 Sea State

Wave height frequencies of occurrence are depicted in Figure 2-18 (page 2-37). The wave height statistics reflect the northerly winds of winter, as the percentile isolines for waves ≥5 ft (1.5 m), ≥8 ft (2.5 m) and ≥12 ft (3.5 m) increase from north to south. The greatest incidence (about 20 percent frequency of occurrence) of the higher wave heights is seen in the Taiwan Strait.

4.3.1.8 Surface Air Temperature

January and February are the coldest months of the year over the East China Sea but the surface air temperatures (Figure 2-19, page 2-38) are relatively mild when compared to adjacent waters to the north. The mean air temperature is about 43°F (6°C) in the northern part of the sea near the Tsushima Strait and 66°F (19°C) in the southeastern part near the Ryukyu Islands. The extreme maximum temperature near the southern Ryukyu Islands is 77°F (25°C) and the extreme minimum temperature near the Tsushima Strait is about 32°F (0°C).

4.3.1.9 Freezing Level

As depicted in Figure 2-21 (page 2-40), winter freezing levels range from a low of about 3,000 ft over the northern East China Sea to over 10,000 ft in the southern areas. Little difference is seen between January and February, the months with lowest freezing levels. By March the levels increase by approximately 2,000 ft as they begin their rise to summer levels.

4.3.1.10 Aircraft Carrier Operating Conditions

Each of the winter months has approximately 10 to 20 percent frequency of occurrence of optimum aircraft carrier operating conditions (defined as having a low cloud ceiling ≥5,000 ft (or no low cloud ceiling), visibility ≥5 n mi, and wind 11-21 kt) over the East China Sea.

Poor conditions (defined as having a low cloud ceiling <300 ft, or visibility <1 n mi, or wind <6 kt or ≥34 kt) occur with about the same frequency -- 10 to 20 percent -- except less than 10 percent in the southern sea during February and more than 20 percent along the coastal areas of the western sea during March.

4.3.1.11 Seasonal Oceanographic Features

January and February are the months of coldest sea surface temperatures for the East China Sea. As shown in Figure 2-20 (page 2-39), February temperatures range from an approximate high of 68°F (20°C) in the southern waters to a low of about 50°F (10°C) in the northern areas. Little warming of the sea surface is seen until April.

The strong cold and dry winter northerly winds induce vigorous convective activity. The shallow areas over the continental shelf (generally less than 50 m depths) become vertically homogeneous. This creates a half-channel condition for sound propagation. On the other hand, horizontal temperature gradients become strong, resulting in rapidly changing sound speed conditions. The horizontal temperature and salinity gradients are enhanced by southward flowing coastal currents of cold, low-salinity, high-turbidity waters along the China coast and west coast of Korea. The cold coastal water extends southward beyond Taiwan. The width and shape of the cold current closely resembles the area between the coast and the 50 m isobath. The warm Kuroshio and Tsushima Currents, while at their minimum annual flow volume, are maintained seaward of the continental break. An area of warmer water extends northwestward from around Cheju-do Island toward the Shandong Peninsula. The warm and high salinity water of the Tsushima overruns the cold and low salinity Yellow Sea water and extends northward to near the South Korea coast. Note that this is in contrast to the fall conditions where a strong surface thermal front is found between Cheju-do and Tsushima Islands. Wave and swell heights are at seasonal maximum and reflect the prevailing strong northerly winds.

4.3.1.12 <u>Electro-Optical Conditions</u> (See section 2.3)

Under the winter Northeast Monsoon flow pattern cold dry continental polar air from off Asia dominates over the East China

Sea. These conditions result in generally improving E/O range as the Northeast Monsoon intensifies. The well mixed atmosphere resulting from heating from below by the relatively warm ocean minimizes inversions and stable layers and results in an annual minimum of ducting and superrefraction layers.

The large scale and seasonal trends are for improved E/O conditions when progressing from south to north and from autumn to winter. The local conditions of an area frequently modify these large scale considerations and may in fact reverse them.

The local conditions of the East China Sea (ECS) during winter result in the following mean pattern. The E/O conditions are gradually degraded from west to east and north to south in response to the warmer sea surface temperatures and resulting flux of moisture into the marine layer. Cloud cover and shower activity increases over the warm ocean current areas. Surface winds also increase over the warmer waters due to increased convective activity. The marine layer thickness will increase from west to east and north to south resulting in a lowering of elevated inversions from the open sea (over warm current areas) toward the Asian coast and northern ECS. The mean height of elevated ducting layers increases from about 1400 m in the north to 2200 m over southern Taiwan.

During strong cold air outbreaks convective cloud lines will form aligned with the direction change (shear) through the cloud layer (marine layer). Transiting across these cloud lines will result in marked changes of E/O conditions between the cloudy regions and clear zones. In general E/O conditions will be degraded in the cloudy areas and improved in the clear. Marine layer thickness and therefore elevated inversion heights will increase in the cloudy areas and be at a minimum in the clear zones.

Terrain features are not as significant along the coast of China as off the USSR in the Sea of Japan, but island barrier effects will cause lee side drying and enhanced E/O conditions. Ocean current boundaries are significant during the cold season over the ECS and will causes marked local variations in low level atmospheric conditions.

Northward movement of the Polar Front during weak Northeast Monsoon periods will result in large variations in weather conditions in general and E/O ranges in specific over the extreme southern ECS during winter.

The following table presents statistical information on duct heights for the regional area and season of interest:

CENTER OF AREA: 27°N 125°E SEASON: WINTER

EVAPORATION DUCT HISTOGRAM IN PERCENT OCCURRENCE

Height	December			January			February		
(m)	day	nite	both	day	nite	both	day	nite	both
0 to 4	2	2	2	2	2	2	5	4	5
4 to 8	3	4	4	4	5	4	6	8	7
8 to 12	8	10	9	9	11	10	11	15	13
12 to 16	15	18	17	20	23	22	19	24	21
16 to 20	21	28	24	25	27	26	22	23	23
20 to 24	21	20	20	18	18	18	16	14	15
24 to 28	12	10	11	9	8	8	7	5	6
28 to 32	5	4	4	4	3	3	2	1	2
32 to 36	2	1	1	2	1	1	1	1	1
36 to 40	1	0	1	1	0	0	1	0	1
above 40	9	3	6	7	2	4	11	4	7
Ave. Ht.	22	19	21	21	18	19	21	17	19

4.4 Spring (mid-March to mid-June) (See section 2.2.1.6)

Spring is a season of major changes in the coastal waters of eastern Asia. The Siberian high begins to lose strength, resulting in a weakening of the winter monsoon and a gradual northward migration of the Polar Front. The Southwest Monsoon begins to establish itself. Figure 2-22 (page 2-42) depicts a generalized synoptic pattern for May, a typical spring month. Figure S-4-6 provides a satellite view of the East China Sea in Spring.

4.4.1 Climatology

Spring (mid-March to mid-June) is a transition season for the East China Sea. As the Siberian high weakens, the Polar Front begins the annual northward migration from its winter position between Taiwan and the Philippine Islands, as shown in Figure 2-5 (page 2-18). As the Polar Front moves northward, extratropical waves develop along the frontal zone -- typically near Taiwan and in eastern China. Upper atmospheric disturbances (short wave troughs) transit the northern part of the sea. Associated "bubble highs" break off from the weakened Siberian high and move eastward. Cyclogenesis in the induced trough between the "bubble high" and Siberian high occurs over the region during this season. Thermal lows may be expected to form over China and northeastern Manchuria by the end of the period.

Figure S-4-6. Spring regional view, East China Sea. 18 May 1980.

FIGURE S-4-6. SPRING REGIONAL VIEW, EAST CHINA SEA. 18 MAY 80
OSAN AB Visual DMSP: TN: 18/0136 GMT

Synoptic Features: The northward migration of the Polar Front (Mei-Yu/Bai-U Front) and the threat of tropical storm activity are evident in this image. Weather north of the front is generally fair with light to moderate winds.

Satellite Image Features:

NOTE: See figure S-7-4 (page 7-26) for additional comments relative to labels 1-4.

1. The Mei-Yu/Bai-U front extends from southern China to south and east of Japan.

2. A tropical cyclone is approaching Taiwan with a second one less than 1000 n mi to the east.

3. A small scale convective cloud pattern forms south of Japan where the northerly surface winds flow over the warm Kuroshio Current.

Forecast Aids:

1. The daily movement of the Mei-Yu/Bai-U front and embedded weak lows with enhanced convective activity are best monitored by satellite imagery.

2. Both large scale (fronts, etc.) and small scale (local wind patterns) can be detected in satellite imagery. The large scale features are generally well handled by numerical guidance, but the small scale features must be detected by local observations or satellite imagery. Knowledge of both the large scale and small scale patterns and seasonal changes as obtained from climatological studies is necessary in order to properly interpret imagery and develop the best possible analyses and forecasts.

3. The E/O conditions will vary from tropical in nature south of the Mei-Yu/Bai-U front to mid-latitude characteristics to the north. Generally south of the front the conditions are, unstable, moist, and warm. North of the front they are, stable cool, and dry. The underlying oceanic thermal and current patterns will cause local modifications of the general atmospheric conditions.

4.4.1.1 <u>Synoptic Patterns</u>

Figure 2-6 (page 2-23) depicts the tracks of extratropical cyclones that normally occur throughout the year. Of the six shown, two have tracks which impact the weather over the East China Sea during spring: the Shanghai Low (track D), and the Taiwan Low (track F).

The location and northward migration of the Polar Front is depicted in Figure 2-5 (page 2-18). An examination of the figure reveals that the mean position of the front during March -- the start of the spring season -- is well south of Taiwan and the East China Sea. By April it has moved northward to a position at the extreme south end of the sea, and by June has reached the southern extremity of Kyushu (Figure 4-1, page 4-2), the southernmost of the four largest Japanese islands. The slow northward migration of the front positions it over the East China Sea from April to June. The spring season also sees the Mei-Yu/Bai-U front form over southern China and the southern East China Sea (Figure S-4-7, page 4-35). Both fronts bring extensive cloudiness and precipitation to the area and make spring the "rainy season" of the region.

Of the frontal types discussed, only the Western type is considered a threat to the weather over the East China Sea during spring.

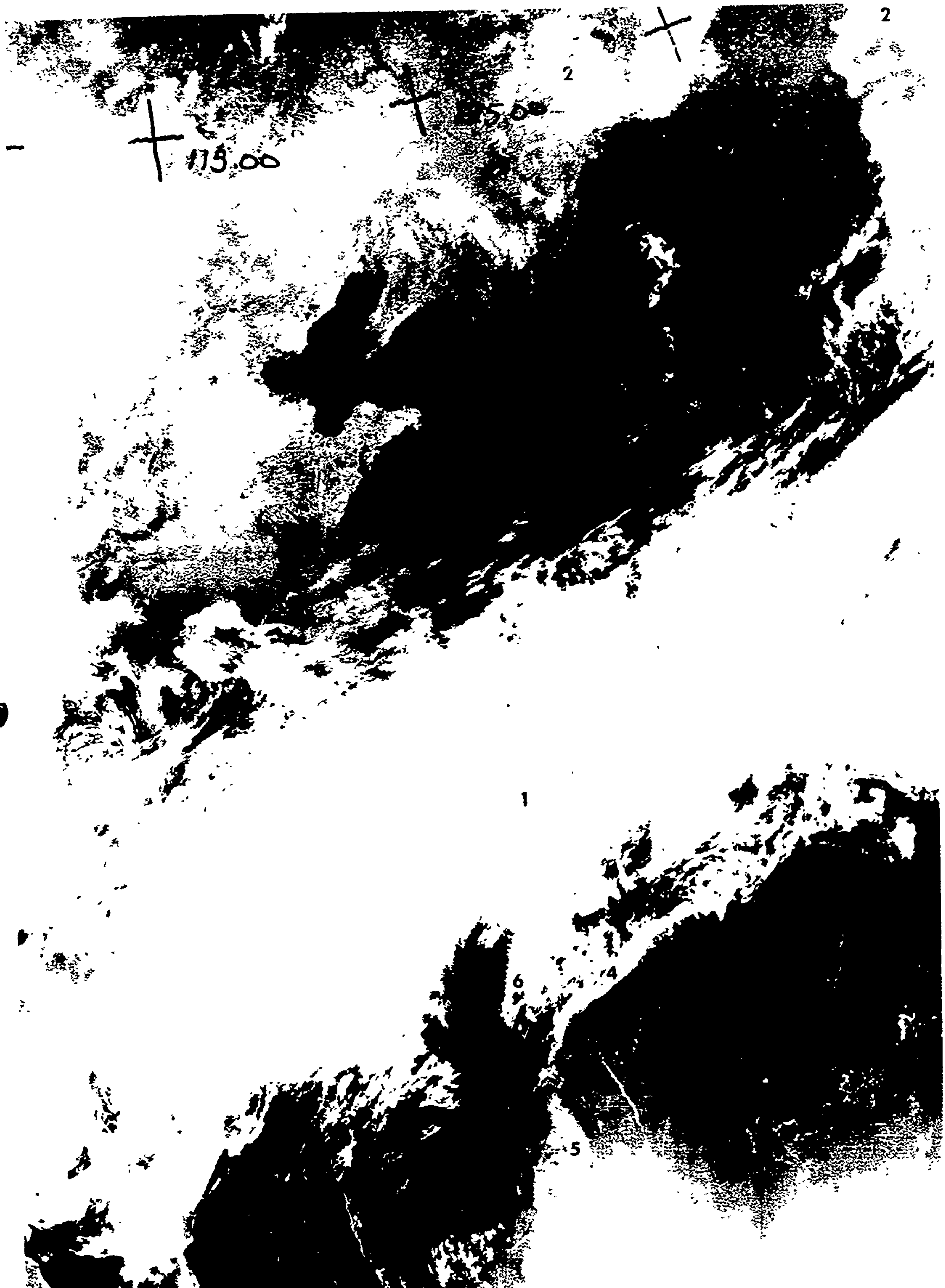

Figure S-4-7. Spring, Mei-Yu/Bai-u Front. [illegible]

FIGURE S-4-7. SPRING, MEI-YU/BAI-U FRONT. 25 APR 80
OSAN AB Visual DMSP: TN: 25/0224 GMT

Synoptic Features: The Mei-Yu/Bai-U front extends from south central China east-northeastward to just south of Japan. A 1024 mb high is centered southwest of the Shandong Peninsula.

Satellite Image Features:

1. The Mei-Yu/Bai-U frontal band dominates the picture.

2. Convective cumulus is widespread over the USSR and northern Japan land areas in this late morning/mid day local time image. The cumulus buildups are just starting to show cirrus plumes. Surface observations at 0300 GMT indicate widespread low type 2 clouds with scattered reports of low 3 and 9 and occasional rain showers.

3. Clear skies prevail over the water areas clear of the Mei-Yu/Bai-U front, except for the remains of a land breeze front off eastern Korea.

4. The rope cloud along the leading edge of the cloud band east of Taiwan indicates the area of surface wind shifts. South of it surface winds are southwesterly, to the north they are northeasterly.

5. Brilliant sunglint around Luzon and on the Cagayan River of eastern Luzon implies light surface winds at this late morning pass time.

6. Low clouds along eastern Taiwan are filling the coastal valleys and provide evidence of the northeasterly low level flow and cloud levels of that area.

7. Thin cloud lines, as seen over the South China Sea, have been found to be aligned within 20 to 30° of the surface winds in the tropics. In this case indicating the southerly flow of the tropical circulation.

Forecast Aids:

1. The Mei-Yu/Bai-U front is the major weather producer over the waters off eastern Asia during the spring season. While it is an annual event, there are variations from year to year relative to time of passage and intensity. At any given time the front will have areas of enhanced convection and more intense weather migrating along it. These so called pulses generally have cyclic periods of about 18 hours.

2. When rows of small cumulus are seen over land in morning satellite passes, afternoon thunderstorms are likely.

3. Clear of the Mei-Yu/Bai-U front, the over water areas of the inland seas generally experience mostly clear skies, light winds, and fair weather during the spring period.

4. The shift of surface winds associated with the Mei-Yu/Bai-U front typically occurs near the leading edge of the cloud band. If a rope cloud is present it is a strong indicator of the location of the surface wind shift.

5. A number of image features provides evidence of the surface wind pattern including: Sunglint patterns, rope clouds, thin cloud lines over tropical oceans, and land/sea breeze fronts.

4.4.1.2 Surface Wind

Surface winds over the East China Sea gradually diminish as the Siberian high begins to weaken. Wind speeds average about 10 kt during May (Figure 2-23, page 2-45). Southeasterly directions predominate north of 28°N during May, with northeasterly prevailing south of that latitude, apparently a result of inflow along the trough of the Polar Front. By June, the prevailing winds are southerly over the entire sea.

4.4.1.3 Upper Level Winds

Figures 2-24 through 2-29 (pages 2-46 to 2-48) depict upper level flow patterns for the month of May. The maximum winds at the specified pressure surfaces over the East China Sea are about 75-80 kt, observed at the 200 mb level in the extreme northern part of the sea as the jet stream shifts north of the Tibetan Plateau and moves northward for the summer.

4.4.1.4 Visibility

Spring visibilities over the East China Sea are generally good. Visibilities ≥5 n mi are observed between 80 and 90 percent of the time over most of the sea, except less than 80 percent along the coast of the Chinese mainland. Figure 2-30 (page 2-49) depicts visibility statistics for May. The other months of spring vary only slightly from the May percentages, showing a slight deterioration as spring progresses.

4.4.1.5 Cloud Heights/Ceilings

Figure 2-31 (page 2-50) depicts low cloud statistics for the

East China Sea during May. There is little significant variation between the months of spring except in the extreme northern part of the sea, where the frequency of low cloud ceiling <600 ft and/or visibility <2 n mi exceeds 20 percent during May and June. Overall cloudiness has decreased somewhat from winter, with low-cloud ceilings (low cloud amounts ≥5/8) occurring between 50 and 65 percent of the time vs. 60 and 75 percent for winter.

4.4.1.6 Precipitation

Spring precipitation occurrence percentages for the East China Sea are similar to those for winter (comparing February and May). The May frequencies are about 15 to 20 percent over the east-central portion of the sea, decreasing to 10 percent along the western and northern boundaries.

4.4.1.7 Sea State

As wind velocities decrease during spring as discussed in section 4.4.1.2, so do the wave heights. By May (Figure 2-32, page 2-51) waves ≥8 ft (2.5 m) have a frequency of occurrence of less than 10 percent over most of the East China Sea, and waves ≥5 ft (1.5 m) are observed about 30-45 percent of the time over most of the sea. Observations of waves ≥12 ft (3.5 m) during May are infrequent.

4.4.1.8 Surface Air Temperature

The warming trends of spring are evident when comparing February temperatures (Figure 2-19, page 2-38) to the temperatures of May (Figure 2-33, page 2-52). Mean temperatures increase by about 10°F (6°C) in the southern areas to 75°F (24°C) and by about

15°F (8°C) in the northern sea to 65°F (18°C). The difference in increase is due to the moderating effects of the Kuroshio Current on winter temperatures in the southern areas. During May, the extreme maximum temperature in the southern sea is near 88°F (31°C). The extreme minimum temperature is about 54°F (12°C) in the northern areas.

4.4.1.9 Freezing Level

The altitude of the freezing level shows dramatic changes over the East China Sea when one compares winter values (Figure 2-21, page 2-40) to those of spring (Figure 2-35, page 2-54). The more significant changes are seen in the northern areas, where the 3,000 ft winter level increases to almost 12,000 ft by May. In the southern East China Sea, the May freezing level exceeds 14,000 ft.

4.4.1.10 Aircraft Carrier Operating Conditions

Optimum aircraft carrier operating conditions (defined as having a low cloud ceiling ≥5,000 ft (or no low cloud ceiling), visibility ≥5 n mi, and wind 11-21 kt) occur less than 20 percent of the time over the central portion of the sea, and between 20 and 30 percent elsewhere.

Poor conditions (defined as having a low cloud ceiling <300 ft, or visibility <1 n mi, or wind <6 kt or ≥34 kt) occur less than 20 percent of the time in the eastern portion of the sea but have a frequency of occurrence of over 30 percent along the Chinese coast (Figure S-4-8).

Figure S-4-8. Local effects, East China Sea. 2? March 1980.

FIGURE S-4-8. LOCAL EFFECTS, EAST CHINA SEA. 23 MAR 80
OSAN AB Visual DMSP: DN: 23/0305 GMT

Synoptic Features: A ridge of high pressure extends southeastward from the 1044 mb Asian high just southwest of Lake Baikal to the Taiwan area. A weak 1012 mb low is located just leeward of the Himalayas over southwest China.

Satellite Image Features:

1. The ridge line extending seaward off China north of Taiwan is reflected in a change of cloud patterns from cellular to stratified.

2. The subsidence regime under the southeastern portion of the high (Taiwan area) is reflected by the inversion capped flat topped stratiform clouds.

3. Fog and low stratus are filling the valleys of eastern Taiwan where the pattern of the higher terrain (dark shade) is clearly seen in contrast to the fog/stratus (light shades).

4. The funneling of low level flow through the Taiwan Strait is indicated by the low level convective cloud lines.

5. The thin, closely spaced convective cloud lines over the southeastern Yellow Sea, the clear wake with a central enhanced cloud line downwind from Cheju-do Island, and the near classic gravity wave (Kelvin ships wave) seen downwind from Cheju-do all imply a shallow, inversion capped marine layer.

6. The light gray shades around the seaward tips of the Liaoning and Shandong Peninsulas of the Yellow Sea indicate regions of enhanced winds (cornering effects) and increased aerosol and water vapor content.

Forecast Aids:

1. The cloud patterns and gray shade features seen in imagery for the region around the southeastern sector of high pressure cells provide evidence of low level wind directions, areas of enhanced winds, low level inversions, and areas of reduced visibility, low ceilings/fog, and reduced E/O ranges.

2. Near the time of this image a ship reported 30 kt northerly winds in the Taiwan Strait while another about 100 n mi east of northern Taiwan reported 15 kt.

3. Reports near the tips of Liaoning and Shandong reported 20 and 25 kt respectively, 10 to 20 kt higher than nearby reports.

4. The cirrus band across China indicates the jet stream position.

5. Visibility and E/O ranges would be significantly lower east of Taiwan as compared to through the Taiwan Strait.

6. A low level inversion and probable ducting/trapping is likely just above the cloud deck over the Yellow Sea/East China Sea area. Near Cheju-do Island, the inversion height as implied by the cloud pattern is below the highest elevation on the island (1950 m).

4.4.1.11 Seasonal Oceanographic Features

Figure 2-34 (page 2-53), which depicts mean sea surface temperatures during May, reflects the warming air temperatures discussed in the previous section. Average increases over the sea during the season are approximately 10°F (6°C).

The early spring physical properties are similar to late winter and near one extreme of their annual cycles; waters are the coldest, most saline, densest, and least stratified. The increasing cloudiness, fog, and dust-storm activity of spring creates progressively poorer conditions for determining SST patterns from infrared satellite imagery. Therefore, knowledge of the typical SST and current change during this period of rapidly changing patterns is crucial to making accurate ASW forecasts.

During the early spring, the warmest waters are limited to the Kuroshio core which, except for minor excursions to the northwest as the Tsushima Current, flows eastward through the Ryukyu Islands and south and east of Japan. The coldest water over the shelf regions has expanded to near the 100 m isobath. A region of intermediate temperature water, composed of a mixture of shelf and Kuroshio waters, is formed between the 100 m isobath region and the Kuroshio core region.

Rapid transitions occur by late spring. SST rise most rapidly in May of any period of the year. Salinities drop in the shallow coastal regions, particularly the mouth of rivers, due to the spring thaw runoff. The Tsushima Current volume increases and the Yellow Sea Warm Current sets up. The cold turbid water along the China coast continues to exist but over a smaller and smaller portion of the shelf. Stratification begins to develop as a combined result of increased solar radiation, fresh water sources, and warm current transport increases. Wave and swell conditions change significantly during the spring period in response to the change from the winter northerly to summer southerly prevailing wind patterns. The slow transition from the Northeast to Southwest Monsoon results in an extended period of slight sea conditions.

4.4.1.12 <u>Electro-Optical Conditions</u> (See section 2.3)

The gradual northward migration of the Polar Front during spring results in a major change of E/O environments over the East China Sea. North of the Polar Front conditions similar to winter prevail and south of the frontal zone, summer and tropical type conditions will exist. Under the frontal band, the conditions will differ from both of those found in the north and the south, and in general will exhibit a major reduction in E/O ranges due to precipitation. Elevated ducts will prevail in the northern sector of the frontal band and to the rear of the cloud band where large scale subsidence prevails.

The local conditions of the East China Sea during spring result in the following mean patterns. The E/O conditions will vary from the earlier patterns of winter to that of summer late in the period. The summer type pattern is generally in agreement with the large scale patterns, i.e., a general increase in E/O ranges from the tropics poleward as atmospheric humidity decreases. The mean height of elevated ducting layers increase from about 1400 m in the north to 1900 m over the southern portion.

The following table presents statistical information on duct heights for the regional area and season of interest:

CENTER OF AREA: 27°N 125°E   SEASON: SPRING

EVAPORATION DUCT HISTOGRAM IN PERCENT OCCURRENCE

Height (m)	March day	March nite	March both	April day	April nite	April both	May day	May nite	May both
0 to 4	6	5	6	12	11	11	10	10	10
4 to 8	7	9	8	7	12	9	7	11	9
8 to 12	13	16	14	11	19	15	12	18	15
12 to 16	18	26	22	15	20	18	14	22	18
16 to 20	19	23	21	15	17	16	14	15	15
20 to 24	13	11	12	10	9	10	9	8	9
24 to 28	5	4	5	5	4	5	6	4	5
28 to 32	3	1	2	3	2	2	3	2	2
32 to 36	1	1	1	2	1	1	2	1	2
36 to 40	1	0	1	1	1	1	1	1	1
above 40	13	4	8	18	5	11	23	8	15
Ave. Ht.	21	16	19	22	16	19	25	17	21

4.5 Summer (mid-June to mid-September) (See section 2.2.1.7)

As shown in Figures 2-5 (page 2-18) and S-4-9, the Polar Front lies across the northern one-third of the East China Sea at the start of the summer season, but is usually well north of the area by July. The summer monsoon becomes well established over the sea once the front has moved north, and maritime tropical (mT) air dominates the weather. Figure 2-36 (page 2-54) depicts a generalized summer synoptic pattern.

Figure 3-4-9. Summer local effects. 12 July 81.

FIGURE S-4-9. SUMMER LOCAL EFFECTS. 18 JUL 81
Scripps NOAA 6 Visual: DN: 18/2349 GMT

Synoptic Features: A period of weak surface winds during the summer monsoon is occurring. The subtropical ridge of high pressure extends westward across Kyushu, the southern island of the Japanese chain.

Satellite Image Features:

1. The marked variations from dark areas to brilliant reflection within the sunglint band (right 1/3 of image) indicate the predominance of local, small scale wind features. This implies a lack of large scale forcing, a typical condition during mid latitude summer periods.

2. The subtropical ridge line is clearly indicated by the dark east-west stripes intruding into the north-south sunglint band near the southern end of Kyushu.

Forecast Aids:

1. When the sunglint pattern shows widespread marked variations with juxtaposition dark and brilliant areas, weak large scale forcing is implied and local conditions are dominate. These include land/sea breezes, strong diurnal variations, and afternoon convective activity over land areas.

2. Land/sea breeze fronts will cause local variations in E/O performances in coastal areas, nearly uniform conditions will occur over sea areas free of scattered showers.

3. Sea surface temperature gradients are minimized during the summer monsoon season. Afternoon effects (1 to 3°C rises in water skin temperatures) are likely under near calm conditions.

4.5.1 Climatology

The summer season (mid-June to mid-September) begins in the East China Sea under two weather regimes -- the Mei-Yu/Bai-U (Plum Rain) weather over the northern portion of the sea north of the Polar and Bai-U Fronts, and the warm summer monsoonal weather south of the Polar Front. The northward migration of the Polar Front allows the summer monsoon to dominate the weather over the entire sea by mid-July. Until early September, the climate is characterized by the relatively warm, moist air that is transported northward around the western periphery of the strengthened mid-Pacific ridge.

As shown in Figure 2-5 (page 2-18), in early September the Polar Front once again starts to affect the weather over the northern East China Sea as it makes its swift southward migration in response to a strengthening Siberian high pressure cell.

4.5.1.1 Synoptic Patterns

Summer is a season of reduced extratropical storm activity over the East China Sea. Figure 2-6 (page 2-23) depicts the tracks of typical migratory extratropical cyclones that normally occur throughout the year. Of the six tracks depicted, only one -- the Yellow Sea Low (track F) -- has the potential to significantly affect the weather over the East China Sea during the summer.

Cold frontal activity in the Far East is at a minimum during the summer and, in general, is not a significant problem over the East China Sea.

4.5.1.2 Surface Wind

As depicted in Figure 2-37 (page 2-58), surface winds over the East China Sea are generally light in August. The same conditions prevail during June and July, but significant changes occur in September. The prevailing direction during June through August is southerly, but changes to northeast in September reflecting the rapid southward movement of the Polar Front through the region. September's mean wind speed over the southern sea increases to about 15 kt. As can be seen in Figure 2-37, the mean wind speed over most of the sea is 10 kt or less about 50 to 60 percent of the time during August.

4.5.1.3 Upper Level Winds

Figures 2-38 through 2-43 (pages 2-59 to 2-61) depict upper level flow patterns for the month of August. The band of strongest winds moves well north of the area during summer, and the flow over the East China Sea is light as the upper level subtropical ridge lies east-west over the sea.

4.5.1.4 Visibility

Surface visibility is generally good over the East China Sea during the summer, with visibilities ≥5 n mi occurring 80 to 90 percent of the time during June, increasing to 90 to 95 percent from July through September. Figure 2-44 (page 2-62) presents visibility statistics for August.

4.5.1.5 Cloud Heights/Ceilings

Of the months of June through September, June is the cloudiest over the East China Sea. Low cloud ceilings are evident between 40 and 60 percent of the time, with the higher percentages seen in the northeast section of the sea, reflecting the location of the Polar Front as it migrates northward. By July, however, when the Polar Front has cleared the area, low cloud ceilings occur only about 20 to 30 percent of the time over most of the sea, and about 40 percent near the Tsushima Strait. Low cloud ceiling statistics for August (Figure 2-45, page 2-63) are the best of the season, with only 20-30 percent frequency of occurrence evident over the entire sea. Combined ceiling and visibility limits for the same period show similar trends, with the higher percentages of low cloud ceilings and reduced visibilities seen in June, and the lowest percentages occurring in August and September.

4.5.1.6 Precipitation

Frequencies of occurrence of precipitation over the East China Sea during the summer are at a maximum during June, varying from 10 to over 20 percent. The higher percentages are evident in the northern sea and coincide with the cloudiness discussed in section 4.5.1.5. By July, precipitation frequency of occurrence has decreased to less than 5 percent over most of the sea, the lowest of the season. August and September occurrences are generally in the 5 to 10 pe cent range.

4.5.1.7 Sea State

The wave heights of summer reflect the relatively light surface winds discussed in section 4.5.1.2. August wave height frequency of occurrence (Figure 2-46, page 2-64) is typical of the summer months. September percentages start to show the increasing winds related to the rapid southward migration of the Polar Front.

4.5.1.8 Surface Air Temperature

Summer temperatures over the East China Sea are quite warm. In June the mean temperatures range from just over 80°F (27°C) in the southern areas to about 70°F (21°C) in the north. By August, the warmest month (Figure 2-47, page 2-65), temperatures have increased to 80°F (27°C) or above over the entire sea. September sees a decrease to 75°F (24°C) over the northern sea. In August, the extreme maximum temperature over the southern sea is about 92°F (33°C) while the extreme minimum temperature in the northern sea is near 70°F (21°C).

4.5.1.9 Freezing Level

Figure 2-49 (page 2-67) depicts the altitude of the mean freezing level over the East China Sea during August. The 16,000 ft isoheight contour progresses northward during the season, from a position south of the sea in June to about 30°N in August, its northernmost position of the year. By September, the contour has retreated southward to near its June position.

4.5.1.10 Aircraft Carrier Operating Conditions

Optimum aircraft carrier operating conditions (defined as having a low cloud ceiling ≥5,000 ft (or no low cloud ceiling), visibility ≥5 n mi, and wind 11-21 kt), have a frequency of occurrence of 25-30 percent during the summer, with each of the months approximately the same.

The occurrence of poor aircraft carrier operating conditions (defined as having a low cloud ceiling <300 ft, or visibility <1 n mi, or wind <6 kt or ≥34 kt), is approximately equal for all of the summer months, but July's occurrence frequency of less than 20 percent over most of the sea is a slight improvement on the 20 to 30 percent values of the other months.

4.5.1.11 Seasonal Oceanographic Features

The sea surface temperature of the East China Sea is at its yearly maximum during August (Figure 2-48, page 2-66). Only near the extreme northern boundary are values below 80°F (27°C) and values above 84°F (29°C) occur in the southeastern section. By September, the temperatures begin to decrease, reducing to about 74°F (23°C) in the northern waters and 83°F (28°C) in the southern areas.

Solar heating, fresh water runoff, and the prevailing southerly winds result in markedly modified physical properties in the ECS from the winter and early spring patterns. Stratification continues to intensify throughout summer resulting in stronger and stronger thermocline structures. The vertical thermal gradients reach maximum strengths in late summer. Changes in this vertical structure are most pronounced in the shelf and intermediate water. Because the Kuroshio Current retains its basic structure and position throughout the year there are smaller season to season variations of all ocean physical properties in the vicinity of the Kuroshio or any other major current.

A second peak in river discharge, resulting from the summer monsoon (Mei-Yu/Bai-U front) rains further increases the supply of low saline surface water in coastal regions. The Kuroshio, Tsushima, and Yellow Sea warm currents advect relatively saline tropical waters into the eastern portion of the ECS. A northward flowing warm coastal current is set up along the China coast, in response to the southerly winds. Wave and swell conditions increase in height from spring conditions in response to the prevailing southerly flow, but are relatively low in comparison to winter conditions.

4.5.1.12 Electro-Optical Conditions (See section 2.3)

The Southwest Monsoon dominates the entire ECS during summer. Tropical conditions , hot and humid, result in reduced E/O ranges. The local variations due to precipitation will be generally disorganized. The strong horizontal gradients of SST along ocean fronts that create large local changes during winter and spring are totally masked by the heating of surface waters. Night and early morning land breeze fronts will result in diurnal variations of E/O ranges in coastal areas. The occurrence of elevated ducts is at an annual minimum in summer occurring about 20-30% of the time.

Heights are also at a minimum, around 1000 m, and the ducts are typically related to night time cooling over land and therefore largely coastal in nature.

The following table presents statistical information on duct heights for the regional area and season of interest:

CENTER OF AREA: 27°N 125°E SEASON: SUMMER

EVAPORATION DUCT HISTOGRAM IN PERCENT OCCURRENCE

Height (m)	June			July			August		
	day	nite	both	day	nite	both	day	nite	both
0 to 4	10	9	9	6	5	5	5	4	4
4 to 8	7	11	9	4	8	6	4	7	6
8 to 12	11	20	15	7	13	10	8	13	10
12 to 16	14	21	17	11	20	16	12	22	17
16 to 20	13	17	15	14	22	18	15	23	19
20 to 24	8	8	8	10	11	10	12	12	12
24 to 28	5	4	4	7	5	6	8	6	7
28 to 32	4	1	2	4	3	3	5	2	3
32 to 36	2	1	2	3	2	2	3	1	2
36 to 40	2	1	1	2	1	1	2	1	1
above 40	25	8	17	32	10	21	27	8	17
Ave. Ht.	26	17	22	31	20	25	29	19	24

4.6 Autumn (mid-September to mid-December) (See section 2.2.1.8)

The transition from summer to autumn occurs quickly in the East China Sea as the Polar Front makes its rapid transit southward (Figures 2-5, page 2-18 and S-4-10). The front moves south of the sea by early October, as the Northeast Monsoon establishes itself in response to a strengthening Siberian high pressure cell. Figure 2-50 (page 2-69) depicts a generalized autumn synoptic pattern.

Figure S-4-10. Autumn regional view. 21 October 79.

FIGURE S-4-10. AUTUMN REGIONAL VIEW. 21 OCT 79
OSAN AB Visual DMSP: DN: 21/0215 GMT

Synoptic Features: A 1032 mb high center 450 n mi west of the Yellow Sea,' combined with a 992 mb low over the northern Sea of Japan with a trailing weak frontal band over Japan and southwestward to Taiwan, are resulting in northerly flow over the Sea of Japan, Yellow Sea and East China Sea.

Satellite Image Features:

1. The cloud patterns over the inland seas imply a relatively weak cold air outbreak, compared to winter conditions. Only a few areas of cloud lines have formed and then only after quite a long cloud free path.

2. Lighter gray shades extending out from various regions of the USSR coast into the Sea of Japan indicate areas of relatively strong offshore flow and increased atmospheric aerosol content. Note how these lighter gray shade areas generally evolve into the cloud line conditions.

3. The closely spaced wave clouds off southern Korea are evidence of relatively light winds through the cloud layer.

4. Areas of fresh snow fall can be seen over northern Korea and the USSR.

5. The worst weather conditions are occurring along the western slopes of central and northern Japan where overcast terrain related cloudiness is seen.

Forecast Aids:

1. The strength of the flow behind cold fronts can be estimated based on the length of the cloud free path of offshore flow and the type of cloud pattern that forms (cloud lines imply winds greater than 20 kt, parallel bands and cellular imply 10-20 kt).

2. The spacing between wave clouds relates to mean wind speed through the cloud layer, the fewer waves per unit distance the stronger the wind.

3. Areas of reduced visibility and degraded E/O ranges are indicated in cloud free offshore flow areas by lighter gray shades which indicate increased aerosol content.

4. Prior to river freeze up, the detection of areas of fresh snow is aided by the path of the rivers which show up as dark meandering lines. In mountainous areas snowfall has a dendritic pattern (branching pattern) related to alternating ridgelines (snow covered) and valleys (snow free).

4.6.1 Climatology

The autumn season (mid-September to mid-December) brings significant changes to the weather of the Far East. The rapid southward movement of the Polar Front in the first month of the season is in contrast to its slow and sometimes erratic northward migration in the spring (Figure 2-5, page 2-18). Because of the rapid movement, prolonged periods of frontal precipitation are unusual. Except for periods of precipitation associated with tropical cyclones, the months of autumn are the driest of the year.

The northeast flow of the winter monsoon is established over the East China Sea in October, with the Polar Front pushed southward to a position between Taiwan and the Philippine Islands. As autumn progresses, the Siberian high becomes the dominant weather feature over eastern Asia and adjacent waters. Small high pressure cells break off from the main cell as upper tropospheric disturbances transit the region and cause cold outbreaks over the East China Sea.

4.6.1.1 Synoptic Patterns

Figure 2-6 (page 2-23) depicts the tracks of migratory extratropical cyclones that normally occur throughout the year. Of the six tracks depicted, two can be expected to affect the weather over the East China Sea during the autumn season: the Yellow Sea Low (track E), and the Taiwan Low (track F).

Cold frontal activity in the Far East starts to increase during autumn after being at a minimum during the summer. Once the Polar Front has moved south of the East China Sea in October, frontal activity of the Western and Eastern types may occur.

4.6.1.2 Surface Wind

Autumn is windy over the East China Sea with the winter monsoon becoming well established as the season progresses. By November (Figure 2-51, page 2-71) the mean wind speed has increased to about 20 kt over the central portion of the sea, and gale (≥34 kt) frequency of occurrence reaches 10 percent in the Taiwan Strait.

4.6.1.3 Upper Level Winds

Figures 2-52 through 2-57 (pages 2-72 to 2-74) depict the upper level flow patterns for November. The subtropical ridge that dominated the upper levels of the atmosphere in August has moved southward. At the same time, the core of the jet stream again splits around the Himalaya Mountains and strong westerlies again prevail over the East China Sea. Winds at the specified pressure surfaces are strongest at 200 mb, where 125 kt are seen over the northern part of the East China Sea.

4.6.1.4 Visibility

Visibility over the East China Sea during autumn is generally good. Visibility conditions of ≥5 n mi are seen over the entire sea 90 percent of the time in September and October, and over the northern half of the sea in November (Figure 2-58, page 2-75). Reduced limits of <2 n mi are seen less than 5 percent of the time over the entire East China Sea in September and October. The same holds true for November except for the small area near Taiwan as shown in Figure 2-58. December's statistics approximate those of November.

4.6.1.5 Cloud Heights/Ceilings

As shown in Figure 2-59 (page 2-76), low cloud ceilings (low cloud amount ≥5/8) exist 50 to 60 percent of the time over the East China Sea during November, except for the northern third of the sea where the percentage is less than 50 percent and a small area in the southern sea where the percentage exceeds 60 percent. The November percentages are higher than the 30 to 40 percent of September, but less than the 60 to 70 percent of December, as cloudiness increases with the progression of the autumn season. The occurrence frequency of low cloud ceiling <600 ft and/or visibility <2 n mi remain nearly constant at about 5 percent during the entire season.

4.6.1.6 Precipitation

The frequency of occurrence of observations reporting precipitation over the East China Sea does not change appreciably early in the autumn season, with the months of September and October each having a precipitation frequency of between 5 and 10 percent. By November the percentages increase to 5 to 20 percent, with the higher amounts seen in the southern half of the sea. December's percentages are similar to November's.

4.6.1.7 Sea State

The increased surface winds of autumn discussed in section 4.6.1.2 are reflected in increased wave heights. By November (Figure 2-60, page 2-77) frequency of wave heights of ≥12 ft (3.5 m) has reached 20 percent in the Taiwan Strait (identified in Figure 2-3, page 2-7), and 10 percent over the central portion of the East China Sea. Other wave heights show similar trends.

4.6.1.8 Surface Air Temperature

Figure 2-61 (page 2-78) depicts the mean surface air temperature over the East China Sea during November. Temperatures have decreased markedly since August (Figure 2-47, page 2-65), but remain near 73°F (23°C) over the southern sea and about 59°F (15°C) in the north. During November the extreme maximum temperature over the southern sea is near 83°F (28°C), while the extreme minimum temperature over the northern East China Sea is about 40°F (4°C).

4.6.1.9 Freezing Level

By November, freezing levels over the East China Sea have lowered appreciably. As shown in Figure 2-63 (page 2-80), the freezing level over the northern sea is about 8,000 ft and about 13,000 ft in the southern areas.

4.6.1.10 Aircraft Carrier Operating Conditions

During November, optimum aircraft carrier operating conditions (defined as having a low cloud ceiling ≥5,000 ft (or no low cloud ceiling), visibility ≥5 n mi, and wind 11-21 kt), occur between 20 and 30 percent of the time over most of the sea, except less than 20 percent in the extreme southern area of the sea.

Poor conditions (defined as having a low cloud ceiling <300 ft, or visibility <1 n mi, or wind <6 kt or ≥34 kt), have a frequency of occurrence of 10 percent or less over the central area of the sea, increasing to 10 to 20 percent elsewhere.

4.6.1.11 Seasonal Oceanographic Features

Figure 2-62 (page 2-79) depicts the mean sea surface temperature of the East China Sea during November. The temperatures have decreased some 16°F (9°C, in the northern areas and about 8°F (4°C) in the south since August.

Physical properties of the ECS in autumn most closely resemble those of summer. However, from early September on the periodic passage of Polar Fronts and the onset of the winter northerly monsoon winds start to remove heat from the ocean, produce opposing cold surface currents to the summer predominate warm northward flowing currents, and reverse the mean wave and swell directions. Destratification of the water column due to convective and wind generated mechanical mixing progressively advances from shallow coastal regions in the north to deeper and more southerly locations. Cold low saline coastal waters from the eastern Yellow Sea flows south and eastward through the Korea Strait and converges with the Tsushima Current. This forms a strong temperature, salinity, and density boundary known as the South Korean Coastal front. This front closely parallels the 100 m isobath from west of Cheju-do to Tsushima Island. The onset of the winter monsoon is much faster than the spring transition, therefore the change from summer-like to winter-like conditions occurs rapidly. The ocean response of course is typically slower and lags the atmospheric changes. Note that by mid and late autumn wind speeds and wave heights have increase throughout the ECS with the most pronounced changes occurring in the southern portions. The change from summer to winter in the Taiwan Strait region is particularly significant.

4.6.1.12 Electro-Optical Conditions (See section 2.3)

The major large scale forcing will change rapidly over the Sea during the autumn period. The southward passage of the Polar Front and return of the Northeast Monsoon will develop within a span of a couple of weeks. The result is a major change in all weather conditions including E/O conditions.

The local forcing will likewise change from summer patterns to winter patterns within a few weeks period. In general the lee side windward side patterns will reverse as well as the changes in air mass and air sea temperatures differences. Forecasters should be aware of these reversal and change patterns when returning to the area following a short absence during which the transition occurred.

The following table presents statistical information on duct heights for the regional area and season of interest:

CENTER OF AREA: 27°N 125°E SEASON: AUTUMN

EVAPORATION DUCT HISTOGRAM IN PERCENT OCCURRENCE

Height (m)	September			October			November		
	day	nite	both	day	nite	both	day	nite	both
0 to 4	3	3	3	4	3	3	3	2	2
4 to 8	4	7	5	3	5	4	3	4	3
8 to 12	7	11	9	7	10	8	6	7	6
12 to 16	12	21	17	11	18	14	11	14	12
16 to 20	13	22	18	14	19	16	17	22	20
20 to 24	11	15	13	13	18	15	21	24	22
24 to 28	9	7	8	13	14	13	16	16	16
28 to 32	5	3	4	7	6	7	9	6	8
32 to 36	3	1	2	5	3	4	4	2	3
36 to 40	2	1	2	3	1	2	2	1	1
above 40	30	8	19	21	6	13	10	3	6
Ave. Ht.	31	20	26	28	21	25	24	21	22

5.0 YELLOW SEA

5.1 Regional Features and Their Influence on Weather Phenomena

The Yellow Sea is bounded on three sides by the coastlines of the Chinese Peoples' Republic, North Korea, and South Korea. Its southeastern limit borders the East China Sea, with which it shares a common boundary of some 240 n mi between the Yangtze (Changjiang) River delta and the Korean island of Cheju-do (Figure 5-1 and S-5-1, page 5-3). Less than half as large as the adjacent East China Sea, the Yellow Sea has an areal extent of about 113,500 sq mi and a relatively shallow average depth of only 121 ft (37 m) (Newspaper Enterprise Association Inc., 1978).

The geographic configuration of the Yellow Sea divides it roughly into three parts: the Gulf of Pohai to the west, the central part of the sea of which Korea Bay comprises a major portion, and the largest segment located west and southwest of South Korea.

The topography of the landmass bordering the Yellow Sea is generally low and unremarkable, with elevations of 3,028 ft (923 m) on the Shandong Peninsula, 4,167 ft (1,270 m) about 80 n mi inland west of the Gulf of Pohai, and 3,711 ft (1,131 m) on the Liaodong Peninsula. The Korean Peninsula is mountainous by comparison, but most of the mountains are on the east side, away from the Yellow Sea. One peak of 6,283 ft (1,915 m) is located near the southern end of the peninsula about 60 n mi from the Yellow Sea.

The island of Cheju-do, on the border between the Yellow Sea and East China Sea, is essentially one large mountain, with a maximum elevation of 6,398 ft (1,950 m).

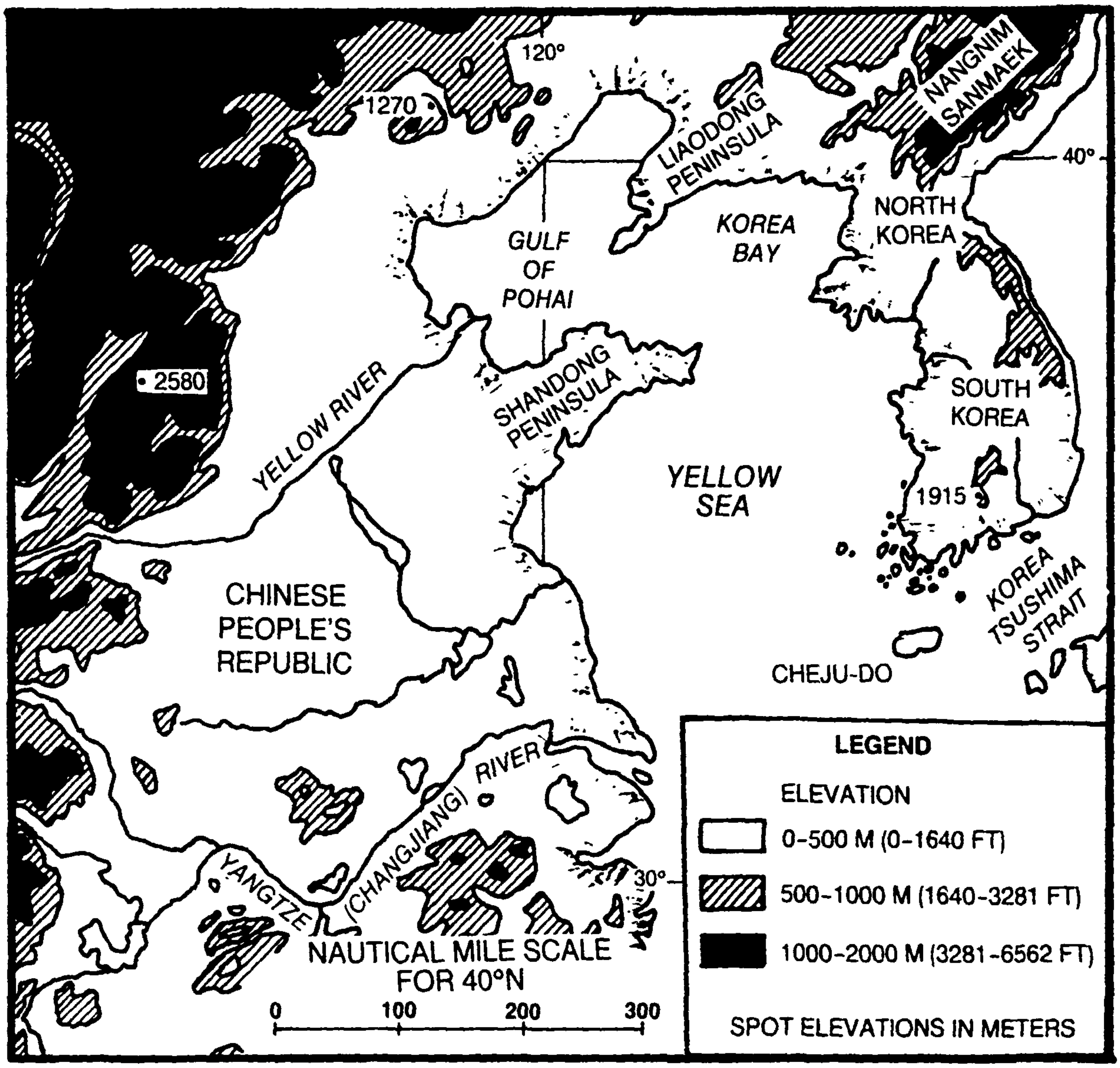

Figure 5-1. Major topographic features surrounding the Yellow Sea (adapted from Nestor, 1977).

Figure S-5-[illegible]. Autumn regional view [illegible] 197[illegible].

FIGURE S-5-1. AUTUMN REGIONAL VIEW. 21 OCT 79
OSAN AB Visual DMSP: DN: 21/0215 GMT

Synoptic Features: A 1032 mb high center 450 n mi west of the Yellow Sea, combined with a 992 mb low over the northern Sea of Japan with a trailing weak frontal band over Japan and southwestward to Taiwan, are resulting in northerly flow over the Sea of Japan, Yellow Sea and East China Sea.

Satellite Image Features:

1. The cloud patterns over the inland seas imply a relatively weak cold air outbreak, compared to winter conditions. Only a few areas of cloud lines have formed and then only after quite a long cloud free path.

2. Lighter gray shades extending out from various regions of the USSR coast into the Sea of Japan indicate areas of relatively strong offshore flow and increased atmospheric aerosol content. Note how these lighter gray shade areas generally evolve into the cloud line conditions.

3. The closely spaced wave clouds off southern Korea are evidence of light winds through the cloud layer.

4. Areas of fresh snow fall can be seen over northern Korea and the USSR.

5. The worst weather conditions are occurring along the western slopes of central and northern Japan where overcast terrain related cloudiness is seen.

Forecast Aids:

1. The strength of the flow behind cold fronts can be estimated based on the length of the cloud free path of offshore flow and the type of cloud pattern that forms (cloud lines imply winds greater than 20 kt, parallel bands and cellular imply 10-20 kt).

2. The spacing between wave clouds relates to mean wind speed through the cloud layer, the fewer waves per unit distance the stronger the wind.

3. Areas of reduced visibility and degraded E/O ranges are indicated in cloud free offshore flow areas by lighter gray shades which indicate increased aerosol content.

4. Prior to river freeze up, the detection of areas of fresh snow is aided by the path of the rivers which show up as dark meandering lines. In mountainous areas snowfall has a dendritic pattern (branching pattern) related to alternating ridgelines (snow covered) and valleys (snow free).

Because of the low elevations, the topography of the adjacent land areas exerts a rather small influence on the weather of the Yellow Sea. But the sea itself exerts a significant influence on passing weather systems, especially during winter, spring, and autumn when outbreaks of cold, arctic air are common. The relatively warm water surfacc yields moisture to the drier, cold air moving offshore from the Asian mainland, resulting in extensive instability, cumulus clouds, and shower activity over the windward areas of the sea.

River drainage into the Yellow Sea is considerable. Although it affects the climate of the region very little, it contributes significantly to the composition of the sea floor. Section 2.1.3.1 discusses the subject more fully.

5.2 Yellow Sea Oceanographic Features

The Yellow Sea (YS) is a shallow marine embayment which is encircled by the mainland of northern China and peninsula of Korea. Two major peninsulas extend into the Sea: The Liandong (Shan-Tung) from the northeast coastline and the Shandong from the southwestern side. The inner portion of the Sea, northwest of the extension of the two peninsulas, is called the Gulf of Pohai (Pwok Hai). The remainder of the Sea is referred to as the Yellow Sea proper.

The circulation of the YS, like that of the East China Sea (ECS), is strongly influenced by the regional atmospheric forcing and the bathymetry. Unlike the ECS, the major ocean currents play only a limited indirect role in the circulation.

The atmospheric monsoon regime that prevails over the YS provides cyclic seasonal changes that dominate the regional oceanographic processes. Atmospheric forcing occurs in two modes: in winter by cooling and destratification due to strong cold and dry northerly winds, and in summer by extensive precipitation, river runoff, and solar heating, which produces a well-stratified water column with a warm, low-salinity surface layer (Huh, 1982). Understanding the variations in seasonal atmospheric forcing and sources of water are critical to understanding the seasonal variability in oceanographic conditions throughout the YS. Seasonal conditions are further agitated by strong winter cold outbreaks and occasionally by summer typhoons.

The surface temperatures and salinity values of the YS show marked seasonal variations. The temperature is controlled by radiational gains and losses of summer and winter, with the winter losses being accentuated by the persistent flow of cold air off the land mass. The surface salinity in the Gulf of Pohai and YS proper is markedly reduced by runoff from the Yellow River. The northeastward advection of runoff water from the Yangtze River sometimes reaches the southern boundary regions of the YS. Surface salinity values in the outflow areas is reduced to near 20‰ during the spring and early summer heavy runoff. The combined influence of the monsoon winds, especially the winter northerly flow, the fresh water from river runoffs, and the intrusion of an extension of the Tsushima Current (Warm Yellow Sea Current) result in several special regional features that could affect naval operations. They include:

(1) The low salinity river runoff water which forms a surface lens over oceanic water,
(2) upwelling off peninsulas,
(3) the cold water mass of the Yellow Sea,
(4) current and SST responses to strong northerly wind, and
(5) large tidal ranges.

<u>River Inflow:</u> The major source of fresh water (low salinity) for the YS is the Yellow River which flows into the southwest region of the Pohai. Other sources of fresh water include: the Luanhe and Liaohe Rivers entering the western and northern Pohai and the Yalu, Han, and lesser rivers of western Korea. This results in a general reduction of surface salinity to 31-33°/oo throughout the entire YS. Within Pohai near the mouth of the Yellow River, salinity approaches 20°/oo. During July the combined results of heavy local rain plus river runoff typically results in reductions of surface salinity to around 20°/oo, even over the extreme southern portions of the YS, around 33°N, and 123 to 125°E.

<u>Upwelling off Peninsulas:</u> Upwelling induced by tidal current past a peninsula has been found in many places throughout the world. Two such regions are found in the YS during the summer. One off the eastern tip of the Shandong Peninsula and a second off the southern tip of the Liaodong Peninsula. Water temperatures off the tips of these two peninsulas are found to be 3-5°C lower than surrounding areas during May through August. Off the Shandong Peninsula the cold water extends seaward 30-50 km, while off the Liaodong Peninsula it is limited to about 20 km. Cold water is favorable to sea fog formation and both of these areas have relatively high frequencies of local fog.

Yellow Sea Cold Water Mass: During the winter the surface water of the YS undergoes extreme cooling and sinks to the bottom. When summer incoming radiation warms the upper layers to the 24-28°C range the bottom water near depths of 50 m remains around 5°C. This results in the region being characterized by the greatest vertical temperature gradient and the most intense thermocline of any of the seas covered in this handbook. The temperature difference between 10 and 25 m reaches values of 7 to 11°C. This cold summer deep water mass is most pronounced in the northern and central portions of the YS proper.

Current and SST Responses to Strong Northerly Winds: With the return of the Northeast Monsoon periodic outbreaks of polar continental air flow over the YS. The convective forcing of the cooled surface water plus mechanical mixing due to wind begins to breakup the surface layer and destratifies the water column. The shallow waters of the northern and eastern YS cool most rapidly, while the region south of the Shandong Peninsula has been observed to remain relatively warm. Southerly flowing cold coastal currents are established on both sides of the YS. The flow along the west coast of Korea is discharged southward and eastward through the Tsushima/Korea Strait into the Sea of Japan (Figure S-5-2, page 5-9). Along the convergence with the Tsushima Current, a strong temperature, salinity, and density boundary (South Korean Coastal Front) is formed. This feature disappears in winter, probably due to sinking of the cold coastal water and overrunning by the warm Tsushima Current water. During winter the area of warmest water is found as a northward extension of the Tsushima Current in the east-

Figure 5-5-2. SST patterns, Yellow and East China Seas. 19 March 1980.

FIGURE S-5-2. SST PATTERNS, YELLOW AND EAST CHINA SEAS. 19 MAR 80
Simultaneous Visual (S-5-2) and Infrared Images (S-5-3)
OSAN AB Infrared DMSP: TN: 19/0242 GMT

Synoptic Features: The large scale oceanic features include the Tsushima Current which flows northward from the Kuroshio Split (near 30°N, 130°E) to the vicinity of Cheju-do Island where it in turn splits. The left branch continues northward into the central basin area of the Yellow Sea and the right branch flows northeastward into the southern Sea of Japan.

Satellite Image Features:

1. The warm Tsushima and Yellow Sea Currents are evident as darker gray tones in the cloud free areas (see simultaneous visual image Figure S-5-3). Note: The labels are actually on cloud features.

2. The lighter gray shades seen in the shallow bays along southern Japan and over the coastal shallows and shelf areas of the Yellow and East China Seas indicate relatively cold surface waters.

3. The cold fresh (low salinity) outflow from the Yangtze River flows over the denser more saline sea water and is seen as lighter gray ribbons near the river mouth. Note that there are some low stratus/fog just to the southeast of the river mouth.

4. Cold coastal water along western Korea. Relatively warm water (darker gray) is seen between Cheju-do Island and the southern coast of Korea.

Forecast Aids:

1. The areal distribution of warm and cold surface water is evident in a properly enhanced infrared image. The major current patterns and areas of warm or cold water are relatively persistent and once defined will provide useful information for several days.

2. The cold coastal waters flowing south and east around southwestern Korea sink under the warm Tsushima Current warms during winter. During spring and autumn the cold surface boundary will extend southward to a line between Cheju-do and Tsushima Islands.

3. Cold but low salinity waters from the rivers feeding into the Yellow and East China Seas will flow over the ocean coastal waters.

central YS. By late winter early spring, the warm water intrusion is at a minimum, and the coldest coastal waters extend seaward to near the 100 m isobath. Waters are coldest, most saline, densest, and least stratified of the annual cycle. The surface water temperatures rise most rapidly in May. Salinities drop in the shallows as they receive runoff from spring thaw in the highlands. Cold YS deep water moves southward into the deepest part of the YS proper. Stratification begins to develop from combined effects of solar warming, fresh water runoff, and renewed influx of Kuroshio water via the Tsushima and Yellow Sea warm currents. During summer stratification reaches a maximum. Strong thermoclines are established, particularly in the YS and south coast region off Korea.

Tidal Ranges: The tidal range along the west coast of Korea are some of the largest in the world. The difference between high and low tide at Inchon averages 19 ft (5 m) and reaches extremes of 33 ft (10 m). The tidal range along the entire west coast of Korea varies from 12-24 ft (4-8 m), while along the coast of China it ranges from 3-9 ft (1-3 m). The inner most part of Pohai experiences tidal ranges over 9 ft (3 m). Most of the tidal currents average 2-3 kt, but speeds to 9-10 kt occur near the southwest tip of Korea.

Bathymetry: The Yellow Sea proper and Pohai form a partly enclosed, wide, flat, and shallow marine embayment. The entire sea bottom is part of the continental shelf. Table 5-1 provides information on the portions of the sea covered by various water depths.

Table 5-1. Water Depths of the Yellow Sea (after Fairbridge, 1966)

	Yellow Sea Proper	Pohai
Depth (m)	Area (km²)	Area (km²)
0-20	93,600	42,900
20-40	101,900	36,700
40-60	78,200	2,100
60-80	90,500	1,000
>80	39,800	--
Total	404,000	82,700
Mean depth, m	44	21
Maximum depth, m	103	72

The central portion of the YS is comprised of an elongated north-south oval-shaped basin with depths of 60-80 m. The sides slope gently up to the coasts of Korea and China. There are numerous sand ridges and channels running perpendicular to the coast lines. Strong tidal currents flow over this coastal feature resulting in a sandy bottom due to sorting by the currents. The bottom of the central basin, as well as the China side of Pohai, is composed of muddy silt. The Great Yangtze Sand Bank lies in the southern portion of the sea near the boundary with the East China Sea (Figure S-5-3). In general sandy bottoms are found where tidal currents are strong and/or bottom slopes are large.

Figure 5-5-3. Ocean features, Yellow Sea and East China Sea.
19 MAR 80

FIGURE S-5-3. OCEAN FEATURES, YELLOW SEA AND EAST CHINA SEA.
19 MAR 80
Simultaneous Visual (S-5-3) and Infrared Images (S-5-2, page 5-9)
OSAN AB Visual DMSP: TN: 19/0242 GMT

Synoptic Features: A migratory high cell is resulting in clear sky conditions over the southern Yellow Sea and northern East China Sea, providing an opportunity for viewing oceanic features of the area.

Satellite Image Features:

1. The major gray shade pattern seen off the coast of China is caused by bathymetry features. Note that the pattern does not correspond with the gray shades seen in the infrared image. This delta fan like pattern is related to the sediment deposits from the Yangtze River outflow. The pattern appears to emanate from a point about 60 n mi north of the current river mouth location (Huh, 1983).

2. The cloud pattern north of the Yellow Sea is associated with a developing 1016 mb low. Comparing the visual and infrared images aids in identifying the various types/levels of clouds.

3. The cirrus pattern has been defined as a baroclinic leaf and has been shown to proceed low level cyclogenesis.

Forecast Aids:

1. There are several causes of gray shades in visual imagery: sunglint area surface roughness, atmospheric aerosol content, and bathymetry features. The majority of the gray shade variations seen in this image are likely related to the light wind situation in the ridgeline that extends from the coast of China, across Korea, to northern Japan. One obvious exception is the bathymetry feature of the Yangtze River, other possible exceptions are the light gray shape cap around the tip of Shandong Peninsula and the dark strip extending southwestward from Goto Island, east of Cheju-do Island. The dark strip downwind from Goto is probably due to barrier effect drying. These subtle gray shade patterns can provide significant insight to atmospheric conditions. But a thorough understanding of the complexities of satellite imagery is necessary for proper interpretation. See the NEPRF NTAG series by Fett.

2. The migratory high and developing low in combination is an example of the bubble high forecast rule provided elsewhere.

5.3 Winter (December to mid-March) (See section 2.2.1.5.)

The Yellow Sea experiences the four more-or-less normal seasons one would expect in the middle latitudes, except that the autumn season is shortened as the region feels the early effects of the strengthening Siberian high pressure cell. Because of the abbreviated autumn season, the winter season commences by late November (FWF, Yokosuka, 1965). Refer to Figure 2-8 (page 2-29) which depicts a generalized winter synoptic pattern.

5.3.1 Climatology

During the winter months of December to mid-March, a continental polar (cP) air mass dominates the weather over the Yellow Sea. Mid-tropospheric disturbances transiting the area cause position and intensity changes in the Siberian high, resulting in periodic surges of cold, dry air throughout the region. Although surface temperatures at the source region generally range from 15°F (-9°C) to -40°F (-40°C), the trajectory of the air as it leaves Siberia and Mongolia is primarily downslope, causing adiabatic warming of as much as 25°F (14°C) over land. The cold surges are preceded through the Yellow Sea by strong cold fronts.

5.3.1.1 Synoptic Patterns

Figure 2-6 (page 2-23) depicts the tracks of migratory extratropical cyclones that normally occur throughout the year. Of the six tracks depicted, only the South Mongolia Low (track C) typically affects the weather over the Yellow Sea during winter. Although more commonly occurring during other seasons, two other migratory extratropical cyclones may also affect the Yellow Sea area during winter -- the Shanghai Low (track D), and Yellow Sea Low (track E).

Cold frontal activity in the Far East starts to increase during autumn and continues throughout winter. According to FWF, Yokosuka, (1965), the first series of noticeable cold waves occur with "great regularity" between late October and early November; the second, more severe, in early December; and a third, very severe cold outbreak in late January or early February. Frontal velocity varies greatly due to the influence of topography but, on the whole, averages about 25 kt. Downslope velocities can reach 45 to 60 kt in winter.

5.3.1.2 Surface Wind

Winter surface winds over the Yellow Sea are predominantly northerly, with a mean speed of about 15 kt. Little variation between the individual months of winter is noted. Figure 2-9 (page 2-31) depicts surface wind statistics during February.

5.3.1.3 Upper Level Winds

The jet stream is at its strongest during winter and, like southern Japan (see section 3.3.1.3), the southern Yellow Sea experiences some of the strongest and most persistent jet stream speeds in the world, with velocities commonly reaching 200 kt.

Figures 2-10 through 2-15 (pages 2-32 to 2-34) depict upper level flow patterns for February. The strongest winds (at the specified pressure surfaces) are found over the extreme southern portion of the sea at 200 mb, with a mean speed of about 130 kt.

5.3.1.4 Visibility

During winter visibility is relatively good over the Yellow Sea. As shown in Figure 2-16 (page 2-35), visibility ≥5 n mi occurs over 90 percent of the time over most of the eastern and western sea, and 80-90 percent over the remainder of the sea. The visibility limit of <2 n mi has a frequency of occurrence of less than 5 percent over most of the sea except for a small area adjacent to the Yangtze (Changjiang) River delta where it is 5 percent.

5.3.1.5 Cloud Heights/Ceilings

Frequencies of occurrence of low cloud ceilings (cloud amount ≥5/8) gradually diminish during winter from a range of 30-60 percent (lowest percentages in the northwest, highest in the southeast) in December to 10-50 percent (lowest percentages in the northwest, highest in the southeast) in March. Similar trends are seen in frequencies of occurrence of low cloud ceiling <600 ft and/or visibility <2 n mi with less than 5 percent frequency seen in December, increasing to 5-20 percent in March, with the 20 percentile isoline encircling the mouth of the Yangtze (Changjiang) River. Figure 2-17 (page 2-36) depicts combined low cloud ceiling and visibility statistics for February.

5.3.1.6 Precipitation

January has a slightly higher frequency of occurrence of precipitation over the Yellow Sea than do the other months of winter, with a range of about 5-15 percent. The highest percentages occur over the central sea west of Korea. About 90 percent of the precipitation in the northern areas falls as snow, while about 5-10 percent of the precipitation over the southern sea near the Yangtze (Changjiang) River delta is snow. By March, the precipitation frequency decreases to 5-10 percent, with about half occurring as snow in the northern sea, and less than 10 percent in the south.

5.3.1.7 Sea State

Figure 2-18 (page 2-37) depicts wave height statistics for the month of February. Wave heights are generally low, heights ≥5 ft (1.5 m) occurring between 25 and 55 percent of the time, with the higher percentages seen in the southeast portion of the sea. Occurrence percentages for waves ≥8 ft (2.5 m) are less than 20 percent over the entire sea. All months of winter are approximately the same.

5.3.1.8 Surface Air Temperature

Figure 2-19 (page 2-38), which depicts mean surface air temperatures during the month of February, reflects the cold temperatures of winter in eastern Asia. While January's temperatures are slightly colder in the extreme northern sea, the overall temperature distribution is approximately the same for both months. Slight warming is seen in March.

During February, the extreme maximum temperature for the southern part of the sea is about 61°F (16°C) while the extreme minimum temperature for the northern sea is about 10°F (-12°C).

5.3.1.9 Freezing Level

As shown in Figure 2-21 (page 2-40), the freezing level during February varies from the surface in the northern Yellow Sea along about 38°N, to near 4,000 ft in the southern sea.

5.3.1.10 Aircraft Carrier Operating Conditions

Optimum aircraft carrier operating conditions, defined as having a low cloud ceiling ≥5,000 ft (or no low cloud ceiling), visibility ≥5 n mi, and wind 11-21 kt, occur 15 to 35 percent of the time over the Yellow Sea during February, with the higher percentages occurring along the Korean coast.

Poor conditions, defined as having low cloud ceiling <300 ft, or visibility <1 n mi, or wind <6 kt or ≥34 kt, occur between 15 and 25 percent of the time, with the greatest incidence seen in the Gulf of Pohai.

5.3.1.11 Seasonal Oceanographic Features

February is the month of coldest sea surface temperatures in the Yellow Sea (Figure 2-20, page 2-39), with water colder than 32°F (0°C) recorded in the Gulf of Pohai. Temperatures in the southern areas are in the 45°F to 48°F (7°C to 9°C) range.

Sea ice is observed as far south as about 36°N along the Korean coast and south of the Shandong Peninsula, but the major concentration (0.1 to 0.4 ice coverage) is limited to the western and northern Gulf of Pohai and eastern Korea Bay (Figure S-5-4). Average ice limits for February are shown in Figure 2-20.

The strong cold and dry northerly flow of the winter Northeast Monsoon produces an oceanic temperature distribution that is vertically homogeneous, but with strong horizontal gradients. The shallow water areas of the northern and eastern YS cool most rapidly. The region south of the Shandong Peninsula has been observed to remain relatively warm through late autumn/early winter. Cold southerly-flowing coastal currents are established along both sides of the YS. By mid-winter the warmest surface water is typically found over the deepest portion of the YS proper and reflects the winter limited northwest extension of the warm current (see Figure S-5-2, page 5-9). The cold water flowing south and then east around western Korea sinks under the warm Tsushima Current water in the northern portions of the Tsushima (Korea) Strait. This is in contrast to the autumn condition when a strong SST front is typically found between Cheju-do and Tsushima Islands. By late winter the cold, vertically homogeneous water extends seaward to near the 100 m isobath. At this time the YS water is at its coldest, most saline, densest, and least vertically stratified condition of the annual cycle.

The winter conditions result in half-channel conditions for sound propagation. The limited water depth throughout the YS necessitates shallow water ASW operations year round. Infrared satellite imagery is at its maximum value in depiction of SST and current patterns due to the strong horizontal SST gradients.

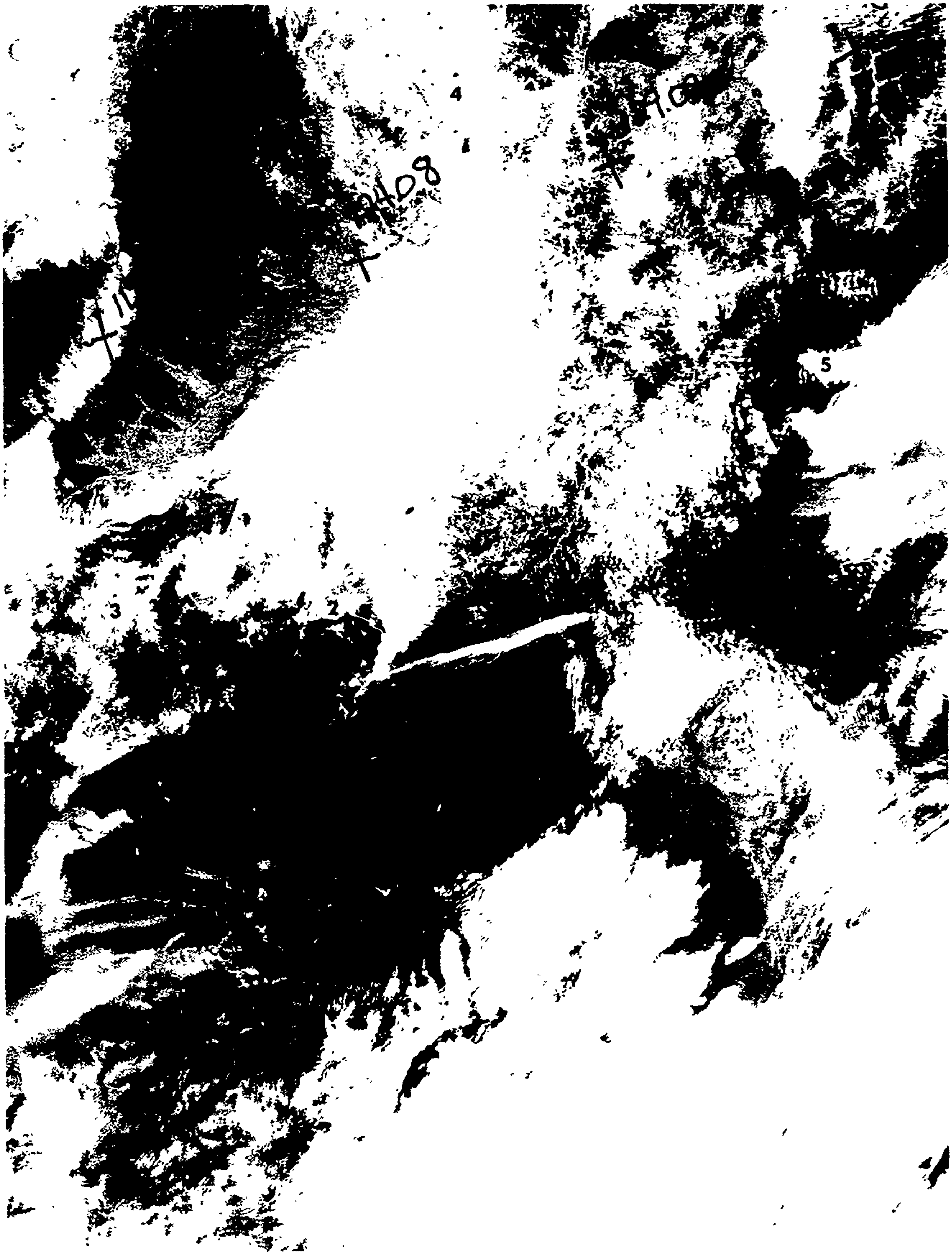

Figure 5-5-4. Winter ice and snow patterns. 26 February 1980.

FIGURE S-5-4. WINTER ICE AND SNOW PATTERNS. 26 FEB 80
OSAN AB Visual DMSP: TN: 26/0307 GMT (Expanded image)

Synoptic Features: Winter time offshore flow.

Satellite Image Features:

1. The harbor of Vladivostok is ice covered.

2. A narrow strip of coastal ice exists in the northwestern Yellow Sea.

3. The snow cover over mountainous areas is dendritic in shape, resulting from the varying coverage over adjacent ridgelines and valleys.

4. The snow cover over grasslands is of a dull gray nature, the newer the snow the whiter, and cities and centers of activity are seen as dark snow free areas. In forested areas, the snow cover can not be determined.

5. The wave patterns seen in flow when an inversion exists can be seen in both the cloud patterns and the gray shades which reflect atmospheric moisture content at levels below that needed for cloud formation.

Forecast Aids:

1. The ice conditions of harbors, straits, and other points of interest can be monitored in polar orbiting satellite imagery.

2. Knowledge of the underlying surface conditions, flat, grass covered, forest, etc. must be known before correct interpretations of snow cover can be made.

3. The wave patterns seen in clouds and gray shade areas, imply the flow direction and the existence of an inversion.

5.3.1.12 Electro-Optical Conditions (See section 2.3.)

Under the winter Northeast Monsoon flow pattern cold dry continental polar air from off Asia dominates over the Yellow Sea. These conditions result in generally improving E/O range as the Northeast Monsoon intensifies. The well mixed atmosphere resulting from heating from below by the relatively warm ocean minimizes inversions and stable layers and results in an annual minimum of ducting and superrefraction layers.

The large scale and seasonal trends are for improved E/O conditions when progressing from south to north and from autumn to winter. The local conditions of an area frequently modify these large scale considerations and may in fact reverse them.

The local conditions over the Yellow Sea during winter are influenced by the SST/current patterns and coastal terrain. The warm Yellow Sea Current influences the area over the deep basin west of South Korea. The shallow coastal waters become quite cold, with sea ice forming along sections of the northern and western coastlines. The areas around the ends of the Shandong and Liaodong Peninsulas are known to be regions of upwelling and frequent fog occurrence.

Shallow surface ducts are formed when the cold dry continental air flows over the water areas. The duct thickness will increase from north to south and be at a maximum over the warmer water areas. The frequency of elevated ducts is less than 10% over the sea except over the extreme southeast sector where the frequency is around 20%. The average height of elevated ducts is near 1400 m.

The following table presents statistical information on duct heights for the regional area and season of interest:

CENTER OF AREA: 36°N 124°E   SEASON: WINTER

EVAPORATION DUCT HISTOGRAM IN PERCENT OCCURRENCE

Height (m)	December day	December nite	December both	January day	January nite	January both	February day	February nite	February both
0 to 4	7	6	6	5	4	5	6	8	7
4 to 8	7	9	8	11	12	11	11	18	15
8 to 12	15	12	14	20	29	25	24	27	25
12 to 16	18	22	20	30	29	29	29	26	28
16 to 20	19	18	19	19	17	18	16	14	15
20 to 24	7	9	8	9	3	6	5	4	4
24 to 28	3	2	2	2	1	2	1	1	1
28 to 32	2	1	2	1	0	0	0	0	0
32 to 36	0	1	0	0	0	0	0	0	0
36 to 40	0	0	0	0	0	0	0	0	0
above 40	22	20	21	3	3	3	7	2	4
Ave. Ht.	24	23	23	15	14	14	16	12	14

5.4 Spring (mid-March to mid-June) (See section 2.2.1.6.)

As discussed in section 3.4, spring is a season of major changes over the coastal waters of eastern Asia. As the Siberian high pressure cell weakens, the winter monsoon also loses strength and the Polar Front begins its rather slow and erratic northward migration. Refer to Figure 2-22 (page 2-42) which depicts a generalized spring synoptic pattern and S-5-5, an early spring visual satellite image.

Figure 5-5-5. Yellow Sea Spring. 9 April 1980.

FIGURE S-5-5. YELLOW SEA SPRING. 9 APR 80
OSAN AB Visual DMSP: DN: 09/0235 GMT

Synoptic Features: A frontal band extends from southern China east-northeastward just below the southern extent of this enlarged portion of the image. Within the area shown the low level flow is dominated by a high cell centered over the extreme northwestern Yellow Sea. Northerly surface flow of 15-20 kt dominates over the water areas. At upper levels the flow is southwesterly, a jet core is located over southern Korea.

Satellite Features:

1. The lighter gray oval shaped pattern around the tip of the Shandong Peninsula is caused by increased northerly surface winds (corner effect), resulting in higher seas and low level aerosol concentrations and higher relative humidity. Near image time a 20 kt wind was reported just off the peninsula while winds of less than 5 kt were reported over the waters of the northern Yellow Sea.

2. The wave clouds over the Liaodong Peninsula and the wave shapes in the gray shade pattern just to the east indicate the presence of a low level inversion.

3. The stratus cloud bank along the northeastern coast of Korea implies northeasterly surface winds. The winds aloft are 180° out of phase with low level flow in this area.

4. The acceleration of the surface winds around southeastern Korea is indicated by a pattern of low level cloud lines.

5. Upslope terrain forced clouds are seen on the northeastern side of Cheju-do Island indicating the direction of the low level flow.

Forecast Aids:

1. Reduced E/O ranges are likely in the lower levels where lighter gray shades are evident, such as around the tip of Shandong Peninsula.

2. Stronger surface winds, rougher seas, and reduced visibility occur in areas where surface winds accelerate, such as the Shandong Peninsula and eastern Tsushima/Korea Strait in this case.

3. Strong low level (near surface) inversion are likely in the southeast quadrant of high pressure cells. In this case there is strong evidence of such conditions: clear skies free of terrain features, wave clouds over low terrain and in the gray shade pattern of cloud free areas, and evidence of low level flow around terrain barriers.

4. Reduced visibility, overcast skies with fog and drizzle are likely on the windward side of terrain under inversion capped flow. E/O ranges will be further reduced in these areas of precipitation.

5. Above the low level inversion, and in the leeside of islands and terrain, marked extended E/O ranges are likely. Significant variations will result from relatively small vertical and/or horizontal position changes.

5.4.1 Climatology

The spring season is a transition period for the Yellow Sea which sees many changes occurring in the weather patterns over the region. The gradual warming of the Asian continent begins to weaken the Siberian high pressure cell, causing a commensurate weakening of the winter monsoon. At the same time, the mid-Pacific high pressure ridge strengthens, resulting in the annual northward progression of the Polar Front. See Figure 2-5 (page 2-18). Migratory upper tropospheric disturbances transit the area, allowing "bubble highs" to break off from the weakened Siberian high and move eastward. Cyclogenesis typically occurs in the induced trough between the "bubble high" and the Siberian high, resulting in inclement weather and precipitation over the region. Thermal lows may be expected to form over China and northeastern Manchuria by the end of the season.

5.4.1.1 Synoptic Patterns

Figure 2-6 (page 2-23) depicts the tracks of typical migratory extratropical cyclones. Of those depicted, two would typically impact the weather over the Yellow Sea during spring: the South Mongolia Low (track C) and the Shanghai Low (track D). Yellow Sea Lows (track E) may form during late spring, but are primarily summer and autumn phenomena.

The location and northward migration of the Polar Front is depicted in Figure 2-5 (page 2-18). It can be seen that the front remains well south of the Yellow Sea during spring.

Of the frontal types discussed, only the Western type is considered a threat to the weather over the Yellow Sea during Spring.

5.4.1.2 Surface Wind

Average surface wind speeds over the Yellow Sea show a marked decrease between March and April and the northerly winds of winter give way to the Southwest Monsoon of summer by May. Figure 2-23 (page 2-45) depicts wind statistics for May, showing that wind speeds ≤10 kt occur between 70 and 85 percent of the time. The incidence of gale force (≥34 kt) winds is negligible.

5.4.1.3 Upper Level Winds

Figures 2-24 through 2-29 (pages 2-46 to 2-48) depict upper level flow patterns for May. The strong jet stream speeds of winter have moderated considerably with a maximum wind (at the specified pressure surfaces) over the Yellow Sea found at 200 mb with a mean speed of about 75-80 kt.

5.4.1.4 Visibility

There is little variation in visibility statistics between the individual months of spring over the Yellow Sea, with visibility ≥5 n mi occurring 75 to 90 percent of the time for all months. Frequency of occurrence of visibility limits <2 n mi generally ranges from 5 to 20 percent. Visibility restrictions occur with greatest frequency southwest of the Korean peninsula while the best visibility is observed in the Gulf of Pohai. Figure 2-30 (page 2-49) depicts visibility statistics for the month of May.

5.4.1.5 Cloud Heights/Ceilings

Low cloud ceilings (low cloud amount ≥5/8) occur generally 15 to 60 percent of the time over the Yellow Sea from March through June, with the lowest percentages occurring in the eastern Korea Bay in April and May and in the Gulf of Pohai in March and June. The highest percentages occur in the southern sea. In all months, the frequency of occurrence of low cloud ceiling <600 ft and/or visibility <2 n mi is approximately 5 to 20 percent. Figure 2-31 (page 2-50) depicts combined cloud and visibility statistics for May.

5.4.1.6 Precipitation

Precipitation patterns remain remarkably consistent over the Yellow Sea during spring, with a frequency of occurrence of about 3 to 10 percent. The lowest percentages are seen in the Gulf of Pohai and the highest in the southern sea. Little snowfall is recorded after March.

5.4.1.7 Sea State

Wave heights show a significant decrease between March and April and then remain essentially constant through June. After March, waves ≥5 ft (1.5 m) are seen about 5 to 30 percent of the time, with the smaller percentages observed in the Gulf of Pohai.

Waves ≥8 ft (2.5 m) are observed less than 10 percent of the time after March, and waves ≥12 ft (3.5 m) are seldom seen. Figure 2-32 (page 2-51) depicts wave height statistics for May.

5.4.1.8 Surface Air Temperature

Significant surface temperature rises are seen during the months of spring as March temperatures of 35°F to 48°F (2°C to 9°C) increase to 66°F to 72°F (19°C to 22°C) in June. Figure 2-33 (page 2-52) depicts the mean surface air temperatures for May.

During May the extreme maximum temperature for the southern area of the sea is about 82°F (28°C) while the extreme minimum temperature for the northern sea is about 50°F (10°C).

5.4.1.9 Freezing Level

The altitude of the freezing level over the Yellow Sea increases significantly during spring, lifting to over 14,000 ft in the southern areas and over 12,000 ft in the north by June. Figure 2-35 (page 2-54) depicts the mean freezing level altitudes during May.

5.4.1.10 Aircraft Carrier Operating Conditions

Optimum aircraft carrier operating conditions, defined as having a low cloud ceiling ≥5,000 ft (or no low cloud ceiling), visibility ≥5 n mi, and wind 11-21 kt, occur between 20 and 30 percent of the time over the Yellow Sea during May. Poor aircraft carrier operating conditions, defined as having a low cloud ceiling

<300 ft, or visibility <1 n mi, or wind <6 kt or ≥34 kt, occur from 30 to 45 percent of the time during May, with the higher percentages occurring in the areas west of about 124°E.

5.4.1.11 Seasonal Oceanographic Features

The waters of the Yellow Sea show considerable warming during the months of spring. June temperatures are approximately 7°F warmer than those depicted for May in Figure 2-34 (page 2-53). The last remnants of sea ice are seen in April in the Gulf of Pohai and northeastern Korea Bay.

During spring a rapid transition from the late winter conditions to summer conditions occurs. The vertically homogeneous and strong horizontal SST gradient pattern reverse. The most rapid SST increase occurs during May. The high-salinity, dense surface water is replaced by low-salinity, less-dense water due to heavy rainfall and river runoff. The cold coastal water regimes shrink from the late winter extent of near the 100 m isobath to become non-existent by mid to late spring. The cold coastal currents of winter also disappear, while the warm Tsushima Current increases in flow volume. By late spring the Yellow Sea Warm Current flow has increased significantly from the winter volume and begins to advance northwestward toward the Gulf of Pohai.

The cold YS bottom water stagnates in the deeper portions of the YS proper, and coupled with the increased solar warming, influx of the warm currents, and freshwater runoff, the stratification of the YS water develops rapidly. Sea states decrease rapidly with the weakening Northeast Monsoon; long-period southerly swell will begin reaching the area as the Southwest Monsoon flow advances from the tropical regimes.

5.4.1.12 <u>Electro-Optical Conditions</u> (See section 2.3.)

The gradual northward migration of the Polar Front during spring results in a major change of E/O environments over the Yellow Sea. North of the Polar Front conditions similar to winter prevail and south of the frontal zone, summer and tropical type conditions will exist. Under the frontal band, the conditions will differ from both of those found in the north and the south, and in general will exhibit a major reduction in E/O ranges due to precipitation. Elevated ducts will prevail in the northern sector of the frontal band and to the rear of the cloud band where large scale subsidence prevails.

The local conditions over the Yellow Sea during spring will vary in relationship to the large scale pattern. The windward/leeward patterns reverse with the change of monsoons. The basic air masses change from dry/cold continental to moist/warm tropical. Between these two extremes, a prolonged period of frontal activity will exist as the Polar Front moves slowly northward.

Elevated stable layers and potential ducting are typically found from the center of the frontal cloud band poleward for 200-300 n mi. This is an area of subsidence and smooth topped cloud layers are generally seen in satellite imagery. The average height of elevated ducts is near 2000 m, an annual maximum, and the frequency of occurrence is about 10%. The majority of occurrences will be related to subsidence on the back side of the Polar Front. Surface based inversions will rarely occur under Southwest Monsoon flow, but will be found under migratory high cell circulations. Due to the deep layer of moist air associated with the Southwest Monsoon flow, evaporation ducts are also rare.

The following table presents statistical information on duct heights for the regional area and season of interest:

CENTER OF AREA: 36°N 124°E SEASON: SPRING

EVAPORATION DUCT HISTOGRAM IN PERCENT OCCURRENCE

Height (m)	March day	March nite	March both	April day	April nite	April both	May day	May nite	May both
0 to 4	9	9	9	20	20	20	27	22	25
4 to 8	11	16	14	10	17	14	11	16	14
8 to 12	20	24	22	17	20	18	14	20	17
12 to 16	23	26	25	16	19	17	13	13	13
16 to 20	15	13	14	10	9	10	8	9	8
20 to 24	6	5	5	4	5	4	4	4	4
24 to 28	3	1	2	4	2	3	3	2	3
28 to 32	2	1	1	1	1	1	3	1	2
32 to 36	1	1	1	1	1	1	1	1	1
36 to 40	0	0	0	1	0	1	1	1	1
above 40	10	5	7	15	7	11	15	11	13
Ave. Ht.	17	14	16	18	14	16	18	15	16

5.5 <u>Summer</u> (mid-June to mid-September) (See section 2.2.1.7.)

As indicated in Figure 2-5 (page 2-18), the Polar Front is south of the Yellow Sea at the start of the summer season, moving into the sea in July, and north of the sea by August (Figure S-5-6). It remains north until the first 10 days of September, when it shifts rapidly southward to a position south of the Yellow Sea. During the relatively short period when the front is north of the area, the weather over the sea is dominated by the Southwest Monsoon. Figure 2-36 (page 2-56) depicts a generalized summer synoptic pattern.


L
1
1
2
2
5
5
4
4
4

FIGURE S-5-6. SUMMER POLAR FRONT. 1 AUG 81
Scripps NOAA 6 Visual: DN: 01/2331 GMT

Synoptic Features: The Polar Front is located near the mean August position (Figure 2-36, page 2-56). The Pacific subtropical ridge line is near 35°N a few degrees north of its mean position. A tropical cyclone is centered near 19°N, 145°E, south of the area covered by this visual image. An area of 30-35 kt surface winds extends northward from the T.C. to near 30°N.

Satellite Image Features:

1. The Polar Front cloud band extends from north of the Yellow Sea to a low over the southern Sea of Okhotsk.

2. Striated cloud plumes extending perpendicular to the main frontal cloud band along its southeastern edge indicate a region of strong horizontal shear.

3. Wave clouds over Siberia reflect the flow pattern over the terrain feature of the area.

4. The surface wind patterns over the water areas are reflected by:

   A. clouds on the southern slopes of Cheju-do Island, indicating southerly flow,

   B. cloud lines over the north Philippine Sea, East China Sea, and southern Yellow Sea, indicating the general veering from easterly to southerly,

   C. lack of clouds over the Sea of Japan indicating very weak surface winds,

   D. and, an offshore land breeze convergence cloud line extending northward from the Yangtze (Changjiang) River Delta, reflects the effects of a land breeze in this morning pass.

5. Within the sunglint area the brilliant reflection along eastern Honshu as well as the dark areas seen along western Honshu indicate areas of near calm surface winds.

Forecast Aids:

1. Cloud features of the Polar Front provide information on upper level wind conditions, areas of shear and turbulence, and convective activity in the vicinity of the front.

2. Low level cloud features and sunglint patterns indicate the near surface wind directions and relative speeds. This provides information on the location of the subtropical ridge line.

3. Image features that reflect local effects/conditions from which environmental conditions can be deduced include.

A - The low level cloud lines imply a marine layer of sufficient thickness to allow vertical cloud development.

B - The cloud free Sea of Japan, in advance of the Polar Front position indicates a suppressed marine layer. The cloud topped island of Ullung-do (station 47115) reporting 20 kt winds in a region where the imagery as well as surrounding near sea level reports indicate light surface winds, provides evidence on the inversion capped marine layer thickness. The reporting site elevation at 47115 is 663 ft above MSL. Its 20 kt wind compared to the near calm sea level conditions around it indicates the reporting site is above the inversion.

4. The following features are likely to effect E/O conditions and should be considered in short term forecasts:

A - the marine layer height reduction from the southern portions of the image to the central portion,

B - the light wind conditions near the ridge line and associated low level stable conditions (reduced E/O range),

C - likely barrier effects in the lee of islands that penetrate the marine layer (enhanced E/O to lee),

D - and, the land breeze convective cloud line and changes in vertical mixing (increased shoreward) across the convergence area (enhanced E/O to shoreward)

5.5.1 Climatology

Because of its unique position with respect to the location and movement of the Polar Front, the Yellow Sea does not experience a lengthy period of warm, humid (i.e. tropical) weather. Even when the front is north of the area, its trailing edge lies close to the Gulf of Pohai (Figure 5-1, page 5-2) and brings increased cloudiness to the western portion of the sea.

5.5.1.1 Synoptic Patterns

As is the case for most of the waters adjacent to eastern Asia, summer is a period of reduced extratropical storm activity over the Yellow Sea. Figure 2-6 (page 2-23) depicts the tracks of typical migratory extratropical cyclones that occur throughout the year. Of the six tracks depicted, two -- the South Mongolia Low and the Yellow Sea Low -- would normally be expected to occur during summer and have the potential to significantly affect the weather over the Yellow Sea.

Cold frontal activity is at a minimum during summer. Of those fronts which do occur, the Western type is found to occur most frequently throughout the year but, unfortunately, a frequency vs. seasonal breakdown by frontal type is not available.

5.5.1.2 Surface Wind

As shown in Figure 2-37 (page 2-58), surface winds are relatively light over the Yellow Sea during the summer, with winds ≤10 kt occurring from 60 to 90 percent of the time in all months except September, when the figures drop to 60 to 75 percent. Gale (≥34 kt) frequency is less than 1 percent. The prevailing wind direction is southeasterly from June through August, but becomes north-northeasterly in September as the Polar Front again moves south of the Yellow Sea.

5.5.1.3 Upper Level Winds

Figures 2-38 through 2-43 (pages 2-59 to 2-61) depict upper level flow patterns during the month of August. The strongest winds (at the specified pressure surfaces) are found at 200 mb, with velocities of 40 to 50 kt indicated across the northern limits of the sea. The upper-level subtropical ridge is at its northernmost position of the year, oriented east-west along 30°N at levels below 100 mb, and about 34°N at 100 mb.

5.5.1.4 Visibility

Surface visibilities over the Yellow Sea during summer are generally good, with ≥5 n mi occurring about 90 percent of the time. Figure 2-44 (page 2-62) depicts visibility statistics during August.

5.5.1.5 Cloud Heights/Ceilings

Low cloudiness over the Yellow Sea remains approximately constant during the months of June through August with low cloud ceilings (cloud amount ≥5/8) occurring about 25 to 55 percent of the time. In June, however, the lower percentages occur in the Gulf of

Pohai, while in August, they are in the southeastern portion of the sea. By September, the frequencies have decreased to 20 to 30 percent.

The frequency of occurrence of low cloud ceiling <600 ft and/or visibility <2 n mi is about 5 to 20 percent in June and July, decreasing to 5 to 10 percent in August and September. Figure 2-45 (page 2-63) depicts combined cloud height and visibility statistics for August.

5.5.1.6 Precipitation

The frequency of occurrence of precipitation during each of the summer months remains more-or-less constant with about 5 to 10 percent of the observations reporting precipitation.

5.5.1.7 Sea State

Wave heights over the Yellow Sea during the summer reflect the relatively light winds discussed above. (See Figure 2-46, page 2-64). Wave heights ≥5 ft (1.5 m) occur from 5 to 30 percent of the time during most of the summer, with the lower percentages occurring in the western portion of the sea. In September the percentages increase to 25 to 45 percent, with that part of the sea north of about 37°N in the 25 to 30 percent range. Wave heights ≥8 ft (2.5 m) and ≥12 ft (3.5 m) have a frequencies of occurrence of less than 10 percent.

5.5.1.8 Surface Air Temperature

Surface air temperatures show gradual warming trends until August, the warmest month of the year (Figure 2-47, page 2-65). During August, mean surface air temperatures range from 77°F to 79°F (25°C to 26°C) over the entire sea. The extreme maximum temperature in August over the southern sea is about 88°F (31°C). The extreme minimum temperature over the northern sea is about 63°F (17°C).

5.5.1.9 Freezing Level

Figure 2-49 (page 2-67) depicts the altitude of the mean freezing level over the Yellow Sea during August. In June the average height over the Yellow Sea is about 13,000 ft, rising to about 15,000 ft in August -- the highest of the season. By September, the average freezing level height has lowered to near 13,000 ft.

5.5.1.10 Aircraft Carrier Operating Conditions

Optimum aircraft carrier operating conditions (defined as having a low cloud ceiling ≥5,000 ft (or no low cloud ceiling), visibility ≥5 n mi, and wind 11-21 kt), have a frequency of occurrence of about 20 to 30 percent during the summer, with each of the months from June through September approximately the same.

Poor aircraft carrier operating conditions (defined as having a low cloud ceiling <300 ft, or visibility <1 n mi or wind <6 kt or ≥34 kt), show considerable variation during the months of summer: 40 to 50 percent in June, 20 to 35 percent in July, 30 to 45 percent in August, and 15 to 25 percent in September.

5.5.1.11 Seasonal Oceanographic Features

The temperature of the sea surface of the Yellow Sea is at its yearly maximum in August. June temperatures range from 63°F (17°C) in the north to 68°F (20°C) in the south; August temperatures (see Figure 2-48, page 2-66) range from 75°F (24°C) to 80°F (27°C).

Summer solar heating, freshwater runoff, and the prevailing Southwest Monsoon flow result in markedly modified oceanographic properties throughout the YS from the winter conditions. The summer conditions are marked by continuously intensifying thermal stratification. The surface waters reach temperatures of 24-28°C, while the water deeper than about 50 m remains near 5°C. This results in an intense thermocline throughout all but the shallowest coastal areas. The early summer rainy period results in increased river runoff and additional influx of fresh water. Near-surface salinity values near the mouth of the Yellow River within Pohai are reduced to near 20‰. Plumes of this low-salinity water sometimes extend to near 33°N, 123-125°E in the southern extent of the YS proper region. Maximum near-surface salinity throughout the YS is reduced to the 31-33‰ range.

Upwelling induced by tidal currents develops off the eastern tip of Shandong and southern tip of Liaodong Peninsulas. Water temperatures 3-5°C colder than those of surrounding areas are found up to 50 km seaward of Shandong Peninsula and about 20 km of Liaodong Peninsula. These regions experience high frequencies of summer fog and/or low stratus conditions.

The Kuroshio, Tsushima, and Yellow Sea warm currents reach their seasonal maximum flow limits. In the boundary regions between the waters advected by these currents and the source waters of the YS, significant variations in oceanographic properties will occur. The waters advected by the currents tend to reflect stable properties with limited seasonal variations while the YS water shows marked seasonal variations.

ASW conditions in summer within the YS waters include strong, shallow thermoclines, strong salinity gradients, regions of upwelling, and interfaces between regional and large current water masses.

5.5.1.12 Electro-Optical Conditions (See section 2.3.)

The Southwest Monsoon dominates the majority of the Sea during summer resulting in tropical like conditions. The large scale E/O conditions therefore take on the characteristics of the tropics, generally reduced E/O ranges due to increased atmospheric aerosols but fewer elevated ducts due to stronger vertical mixing. The northern part of the sea, which is likely to be affected by the Polar Front and migratory highs will differ from the area under the Southwest Mon.oon flow. E/O conditions will have large variations in the northern area that reflect the synoptic scale influence.

Elevated ducts are at a local maximum over the northern Yellow Sea, likely reflecting the presence of the Polar Front and subsidence on the back side of the cloud band. The percent occurrence is still relatively low, around 10%, and the height averages near 1200 m.

The horizontal variations in SST become very small during summer. Tidal action forced upwelling is still found off the major peninsulas.

The following table presents statistical information on duct heights for the regional area and season of interest:

CENTER OF AREA: 36°N 124°E SEASON: SUMMER

EVAPORATION DUCT HISTOGRAM IN PERCENT OCCURRENCE

Height	June			July			August		
(m)	day	nite	both	day	nite	both	day	nite	both
0 to 4	37	38	38	24	28	26	12	10	11
4 to 8	16	22	19	11	16	13	7	12	9
8 to 12	14	16	15	13	18	15	8	15	12
12 to 16	8	10	9	13	12	13	12	20	16
16 to 20	5	4	5	8	10	9	10	14	12
20 to 24	3	2	3	5	4	4	10	9	9
24 to 28	2	1	2	3	2	3	5	5	5
28 to 32	1	0	1	2	1	2	4	2	3
32 to 36	1	0	1	2	1	1	3	1	2
36 to 40	1	1	1	1	1	1	2	1	1
above 40	12	6	9	19	7	13	29	12	20
Ave. Ht.	14	10	12	20	13	16	27	19	23

5.6 Autumn (mid-September through November) (See section 2.2.1.8.)

Because of the rapid southward shift of the Polar Front, the onset of the autumn season is early and abrupt over the Yellow Sea. The strengthening Siberian high pressure cell begins to influence the weather in the area as the northeast monsoonal winds become established in September. Figure 2-50 (page 2-69) depicts a generalized autumn synoptic pattern over the Far East.

5.6.1 Climatology

As is the case with other regions of eastern Asia, the autumn season brings significant changes to the weather of the Yellow Sea (Figure S-5-7). The swift southward movement of the Polar Front in September causes an almost overnight transition from summer to the cooler weather of autumn as the region comes under the influence of air forced southward by the strengthening Siberian high pressure cell. Small high pressure cells break off from the main cell as upper tropospheric disturbances transit the region and spawn cold outbreaks over the Yellow Sea during the autumn season.

5.6.1.1 Synoptic Patterns

Figure 2-6 (page 2-23) depicts the tracks of migratory extratropical cyclones that normally occur throughout the year. Of the six tracks depicted, two -- the South Mongolia Low (track C) and the Yellow Sea Low (track E) -- can be expected to effect the weather over the Yellow Sea during the autumn season.

Cold frontal activity in the Far East begins to increase in autumn after being at a minimum during the summer months. Once the Polar Front has moved south of the Yellow Sea in September, frontal activity is usually associated with cold outbreaks from the Siberian high.

Figure 5-5-7. Yellow Sea Autumn. 29 September 1981.

S-5-7. YELLOW SEA AUTUMN. 29 SEP 81
Scripps NOAA 6 Visual: DN 29/0025 GMT

Synoptic Features: The Polar Front has commenced its rapid southward movement from the summer position north of the Yellow Sea and is now over the Yellow Sea. A 1022 mb high center located over China is causing northerly flow over the entire Yellow Sea and East China Sea area. This is a marked reversal from the recent summer Southwest Monsoon flow pattern. The convergence of the mid-latitude northerly flow and tropical southerly flow is marked by the convective cloud line over the South China Sea near 20°N.

Satellite Features:

1. The weak Polar Front extends from a low over southwest China, east-northeastward to Japan.

2. The uniform sunglint pattern over the East China Sea indicates an unchanging wind field, in this case northerly, 10-15 kt.

3. The cloud lines around Taiwan, across the Taiwan Strait, and along the coast of China provide evidence of the general northerly flow and interaction with land breeze convergence cloud lines off Taiwan.

4. The enhanced cloud line through the Taiwan Strait area is evidence of the increased low level winds, vertical mixing, and increased depth of the marine layer.

Forecast Aids:

1. The Polar Front and northeasterly monsoon conditions migrate rapidly southward during Autumn. The conditions over the Yellow Sea, Sea of Japan, and East China Sea change from summer (Southwest Monsoon) to winter (Northeast Monsoon) in about a one month period, typically late September through middle October.

2. An area of diffuse sunglint pattern implies a uniform surface wind pattern.

3. The northeasterly monsoon flow is accelerated through the Taiwan Strait.

4. The existence of offshore land breeze convergence cloud lines indicate that the local effects are stronger than the synoptic scale effects. In this case it implies that the Northeast Monsoon is still quite weak.

5.6.1.2 Surface Wind

Mean wind velocities over the Yellow Sea gradually increase throughout the autumn season. Wind speeds ≤10 kt occur with a 60 to 75 percent frequency in September but, during November (Figure 2-51, page 2-71), the numbers decrease to about 40 to 65 percent. Gale occurrence is less than 5 percent during all autumn months. The prevailing wind direction is north-northeasterly throughout the entire autumn season.

5.6.1.3 Upper Level Winds

Figures 2-52 through 2-57 (pages 2-72 to 2-74) depict upper level flow patterns for November. The westerlies are reestablished over the Yellow Sea and jet stream velocities are approaching those of winter, with over 100 kt seen over the southern Yellow Sea at 200 mb.

5.6.1.4 Visibility

Autumn is a season of relatively good visibility over the Yellow Sea. As can be seen in Figure 2-58 (page 2-75), November visibility ≥5 n mi has an occurrence frequency of 90 to 95 percent. September and October frequencies are approximately the same. In each of the autumn months, the frequency of occurrence of visibility <2 n mi is 5 percent or less.

5.6.1.5 Cloud Heights/Ceilings

As shown in Figure 2-59 (page 2-76), low cloud ceilings (low cloud amount ≥5/8) exist some 25 to 45 percent of the time over the Yellow Sea during November. The November percentages are somewhat higher than the 20 to 30 percent of September and 5 to 30 percent of October. In all months, the lower percentages are seen in the northwestern portion of the sea.

The frequency of occurrence of low cloud ceiling <600 ft and/or visibility <2 n mi is from 5 to 10 percent during September and November, and less than 5 percent during October.

5.6.1.6 Precipitation

The frequency of occurrence of observations reporting precipitation over the Yellow Sea ranges from about 5 to 10 percent during the months of September and November. During October, the driest month of the year over the Yellow Sea, the range is about 2 or 3 to 6 percent. The northern and western areas of the Yellow Sea have the lowest percentages during each month.

5.6.1.7 Sea State

Mean wave heights remain essentially unchanged during autumn. Figure 2-60 (page 2-77), which depicts wave height statistics for November, shows that wave heights ≥5 ft (1.5 m) occur about 35 to 50 percent of the time on the Yellow Sea, while waves

≥8 ft (2.5 m) have an occurrence frequency of about 5 to 15 percent. September and October statistics differ only slightly from November's.

5.6.1.8 Surface Air Temperature

Figure 2-61 (page 2-78) depicts the mean surface air temperatures over the Yellow Sea during November. Temperatures have decreased markedly since August as they progress towards the low temperatures of winter, but remain near 45°F (7°C) over the northern sea and 59°F (15°C) in the south.

The extreme maximum temperature over the southern part of the sea during November is about 73°F (23°C). The extreme minimum temperature over the northern sea is about 28°F (-2°C).

5.6.1.9 Freezing Level

The altitude of the freezing level over the Yellow Sea is shown in Figure 2-63 (page 2-80). The heights have decreased markedly since August to about 2,000 ft in the northern Gulf of Pohai and near 10,000 ft over the extreme southern sea.

5.6.1.10 Aircraft Carrier Operating Conditions

During November, optimum aircraft carrier operating conditions (defined as having a low cloud ceiling ≥5,000 ft (or no low cloud ceiling), visibility ≥5 n mi, and wind 11-21 kt), occur between 20 and 35 percent of the time. Little variation is seen between the individual months of autumn.

Poor aircraft carrier operating conditions (defined as having a low cloud ceiling <300 ft, or visibility <1 n mi, or wind <6 kt or ≥34 kt) occur with approximately the same frequency during each of the autumn months, about 20 to 25 percent over most of the sea.

5.6.1.11 Seasonal Oceanographic Features

Figure 2-62 (page 2-79) depicts sea surface temperatures for the Yellow Sea during November. While the indicated temperatures range from about 50°F (10°C) to 63°F (17°C), sea ice is observed in the northern and western areas of the Gulf of Pohai, the northeast part of Korea Bay, and along the west coast of Korea near about 38°N. No ice is observed in October.

The autumn properties tend to closely resemble the summer pattern. However, the change from summer to winter conditions occurs rapidly once it commences.

With the onset of the winter Northeast Monsoon, periodic outbreaks of cold dry continental air sweep over the YS. The sea surface rapidly loses heat to the atmosphere, and convective as well as mechanical mixing begins to break up the near-surface layer of warm water. The destratification process advances progressively from north to south over deeper and deeper water. The coastal waters of the northern and eastern YS cool most rapidly.

An autumn thermal anomaly is reflected by warmer SSTs which remain in the region south of the Shandong Peninsula. This and other SST and current patterns become more readily recognizable in infrared satellite imagery as the horizontal SST gradients intensify. A second thermal anomaly is formed south of Korea where low-salinity, cool water flows south and east around southern Korea and converges with the Tsushima current waters. This convergence forms the so-called South Korea Coastal Front. The front typically extends from west of Cheju-do Island eastward to near Tsushima Island.

The sea and swell heights change to northerly and increase in response to the cold air outbreaks associated with the Northeast Monsoon flow. Swell periods will decrease, and with the typically stronger surface winds associated with the outbreaks, the sea conditions will also show rapid deterioration in late autumn.

ASW conditions will change quickly to the winter condition of vertical homogeneous and horizontal variability of temperatures. A shallow water mode is dictated by the YS bathymetry.

5.6.1.12 Electro-Optical Conditions (See section 2.3.)

The major large scale forcing will change rapidly over the Sea during the autumn period. The southward passage of the Polar Front and return of the Northeast Monsoon will develop within a span of a couple of weeks. The result is a major change in all weather conditions including E/O conditions.

The local forcing will likewise change from summer patterns to winter patterns within a few weeks period. In general the lee side windward side patterns will reverse as well as the changes in air mass and air sea temperatures differences. Forecasters should be aware of these reversal and change patterns when returning to the area following a short absence during which the transition occurred.

Following the southward passage of the Polar Front, clear skies and light winds will frequently be found over this area. The diurnal radiational cycle will frequently result in low level inversions, particularly over the coastal areas. Night time land breezes will be relatively strong and well developed land breeze fronts will occur. Low level E/O conditions and inversions will show large variations across these fronts and from day to night. Satellite imagery can provide evidence of these local day/night variations (see Figure S-3-1, page 3-3). The occurrence of elevated ducts is near a maximum (about 10%) in early autumn and decreases rapidly once the Polar Front moves southward out of the area. Average heights are about 1000 m. Shallow surface based ducts as well as evaporation ducts will become more frequent late in the season once the sea surface temperatures begin to cool.

The following table presents statistical information on duct heights for the regional area and season of interest:

CENTER OF AREA: 36°N 124°E SEASON: AUTUMN

EVAPORATION DUCT HISTOGRAM IN PERCENT OCCURRENCE

Height (m)	September			October			November		
	day	nite	both	day	nite	both	day	nite	both
0 to 4	6	6	6	4	3	3	4	3	4
4 to 8	5	7	6	4	4	4	5	7	6
8 to 12	5	12	9	7	9	8	9	11	10
12 to 16	10	13	12	9	13	11	11	15	13
16 to 20	12	19	16	13	16	14	18	18	18
20 to 24	12	11	12	14	14	14	14	15	14
24 to 28	6	8	7	7	8	8	6	5	6
28 to 32	5	3	4	4	4	4	3	2	2
32 to 36	2	2	2	2	1	1	2	0	1
36 to 40	1	0	1	1	1	1	1	1	1
above 40	34	18	26	35	26	31	26	23	25
Ave. Ht.	31	24	28	33	29	31	28	26	27

6.0 SEA OF OKHOTSK

6.1 Regional Features and Their Influence on Weather Phenomena

The Sea of Okhotsk is a semi-enclosed marginal sea located in eastern Siberia north of Japan. It is formed where the continent of Asia is separated from the Pacific Ocean by the Kuril Island arc and the Kamchatka Peninsula (Figures 2-1, page 2-2 and 6-1). Its western boundary south of 54°N is formed by Sakhalin Island. Roughly one-third larger than the Sea of Japan, the Sea of Okhotsk has an areal extent of about 537,500 sq mi and an average depth of 3,192 ft (Newspaper Enterprise Association Inc., 1978). Landlocked on three sides, the sea is accessible from the Sea of Japan through two major straits: the Tartar Strait between Sakhalin Island and the Asian continent, and the La Perouse (Soya) Strait between Sakhalin Island and the northern Japanese island of Hokkaido (Figure 6-1). The southeastern limit of the Sea of Okhotsk is defined by the arc of the Kuril Islands. Several straits between the islands permit access to/from the western North Pacific Ocean.

The land areas bordering the Sea of Okhotsk are mostly mountainous. To the east, the southern extension of the Koryak Range extends the length of the Kamchatka Peninsula, with elevations commonly exceeding 8,202 ft (2,500 m). Individual peaks on the peninsula range from 11,339 ft (3,456 m) to 15,584 ft (4,750 m). Forty volcanos are known to exist on the peninsula, with 14 being active. Almost all of the volcanoes are located on the eastern side.

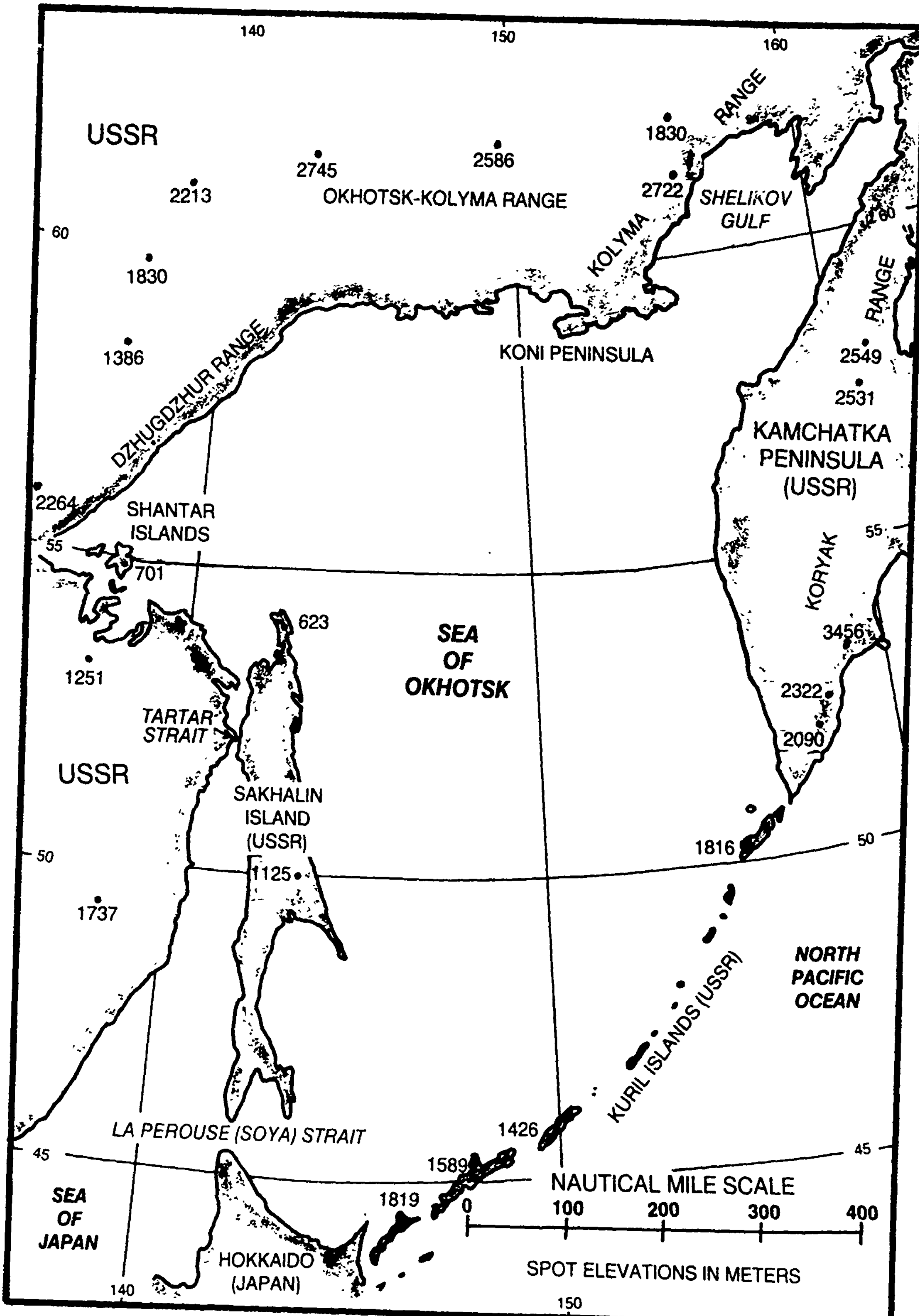

Figure 6-1. Sea of Okhosk.

The southwestern portion of the Kolyma Range, with elevations ranging from 5,906 to 7,480 ft (1,800 to 2,280 m), borders the northern shore of the Shelikov Gulf. The Dzugdzhur Range lies along the northwestern coast of the sea, with elevations mostly below 3,000 ft (914 m). To the north, the Okhotsk-Kolyma range lies east-west about 120 mi inland. Some elevations of the Okhotsk-Kolyma range exceed 8,400 ft (2,560 m), with the elevations of the southern slope of the range gradually decreasing toward the sea.

The southern half of the west shore of the Sea of Okhotsk is formed by Sakhalin Island. Sakhalin is a 510 n mi (approximate) long island marked by a north-south ridge of mountains with elevations of 1,640 to 2,953 ft (500 to 900 m) predominating. The highest peak reaches 3,691 ft (1,125 m). The Kuril Islands form the southeastern limit of the sea. They are primarily of volcanic origin with over 100 volcanic cones in the island chain, of which 38 are active. Three of the islands have peaks exceeding 4,921 ft (1,500 m).

As is true for other regions of eastern Asia, accurate tracking and forecasting of weather systems over the land areas adjacent to the Sea of Okhotsk is complicated by the irregular terrain. In the mountainous areas, few of the surface reporting stations can be considered representative, so the 850 mb chart is an important tool in analysis and forecasting. It is often true that successful and accurate analysis of surface frontal systems in eastern Asia can be achieved only by careful and thorough scrutiny of 850 mb data.

Although not usually as intense as those occurring over the Sea of Japan, induced troughs form over the Sea of Okhotsk in the lee of the Dzugdzhur Mountains and Sakhalin Island. They are relatively less frequent because the normal location of the strong upper level westerlies which are usually associated with lee troughs lies south of the area.

The latitudes spanned by the Sea of Okhotsk (about 44°N to 62°N), its proximity to Siberia, and its semi-enclosed configuration make it a relatively cold sea. During late February to mid-March, the period of maximum ice extent, approximately 75 to 80 percent of the sea is covered by at least 0.1 to 0.4 ice concentration (See Figure S-6-1, page 6-5). The sea is never ice-free. During September, when ice is at a minimum, small amounts of ice in concentrations less than 0.1 exist around the Shantar Islands in the western corner of the sea, and along the adjacent shorelines of the Asian mainland and northern Sakhalin Island (See Figure S-6-2, page 6-7). Because of the low temperatures of the water surface and extensive ice coverage, there is relatively little thermal heating of the atmosphere. Low pressure systems transiting the sea in autumn before ice concentrations increase are affected most strongly by air-sea interaction. Once the sea surface temperature decreases to 30°F (-1°C) or lower, ice quickly forms and air-sea interaction is minimized.

Figure S-6-1. Winter, Sea of Okhotsk. Visual 24 February 1980.

FIGURE S-6-1. WINTER, SEA OF OKHOTSK. 24 FEB 80
Simultaneous Visual and Infrared Images (IR: S-6-3)
OSAN AB Visual DMSP: TN: 24/0205 GMT

Synoptic Pattern: Northerly flow dominates the Sea of Okhotsk area. Pack ice covers the majority of the Sea, with open water limited to the extreme eastern and southern portions.

Satellite Image Features:

1. Typically, the openings in the pack ice reflect the bathymetry features, more numerous over the deep basins, near solid cover over the shelf areas.

2. Land fast ice surrounds northern Sakhalin Island.

3. The northeast coast of Hokkaido is ice bound.

4. Strong low level circulation is implied by the convective cloud lines forming at the ice edge and remaining as cloud lines for some distance off-shore.

5. Dark areas off coastlines indicate ice free coastal leads or areas of snow free new ice.

6. Urban areas in snow covered grass lands show up as dark spots.

7. A small scale polar vortex centered over the southern Kuril Islands is reflected in the low level cloud lines. Enhanced cloud development is seen north and east of the vortex.

Forecast Aids:

1. In winter the area is ice covered, the maximum extent normally occurs about one month after this date.

2. The pack ice concentration reflects the bathymetry features and ocean current patterns.

3. Land fast ice appears as smooth white areas, there are no leads or breaks apparent.

4. Along the western coastline where offshore winds typically advect the new ice out of the growth area, the continuously forming new ice is of a darker shade.

5. Coastal leads show up as dark areas. But these dark areas are not necessarily ice free. One to two feet of new ice that is snow free will appear as dark as open water in satellite imagery.

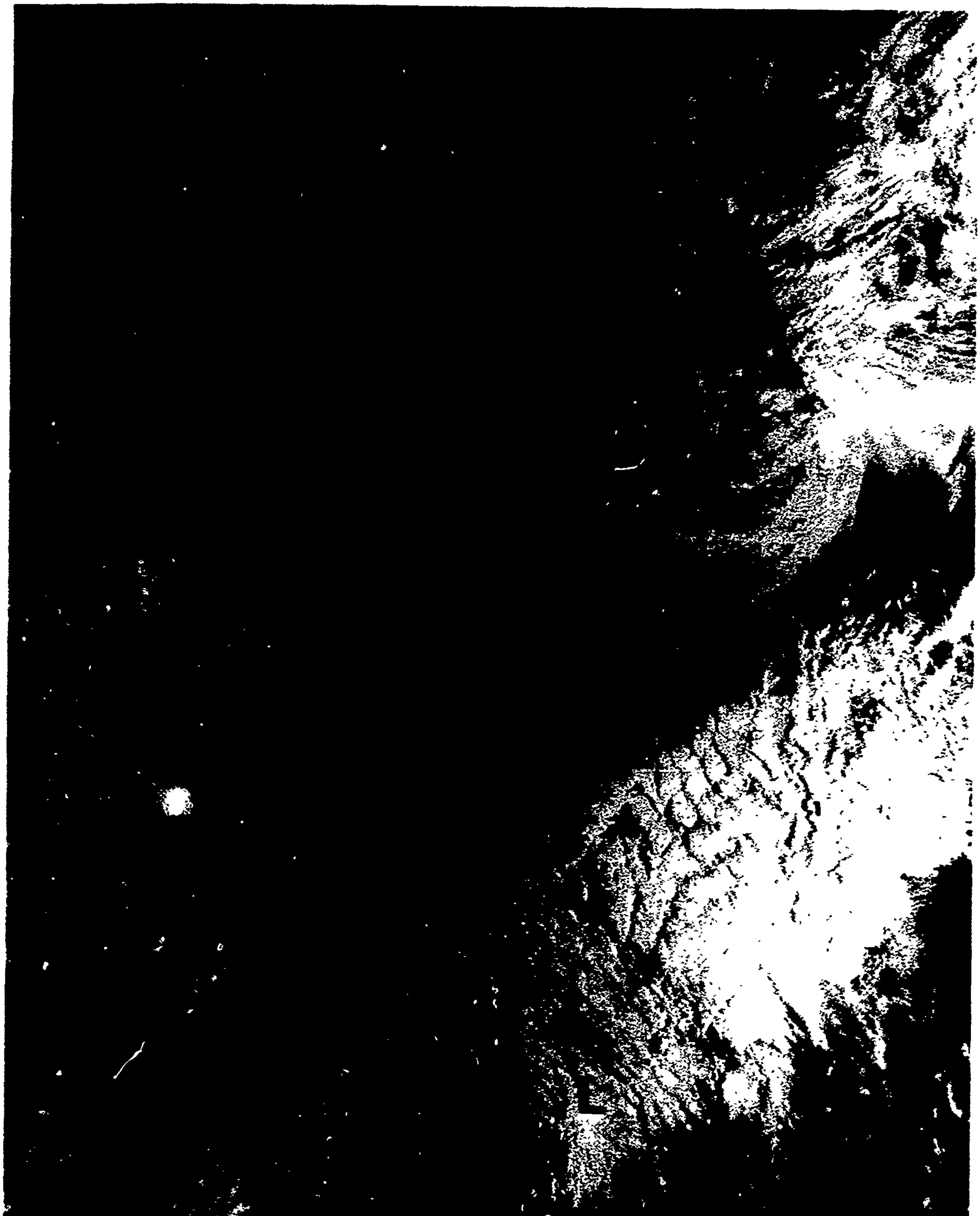

Figure S-6-2. Autumn frontal activity. 11 September 1981.

FIGURE S-6-2. AUTUMN FRONTAL ACTIVITY. 11 SEP 81
Scripps NOAA 6 Visual: DN: 11/2256 GMT

Synoptic Features: The autumn southward advance of the Polar Front has reached the area of Japan. A typically autumn front with a series of lows forming along it from the China coast to east of Japan is resulting in multi-layered clouds and overcast conditions over Japan and coastal areas, especially to the south and east.

Satellite Image Features:

1. A well developed frontal cloud band from 300 to 450 n mi wide dominates the image. The Polar Front has moved southward out of the Sea of Okhotsk area.

2. Lines of convective activity are embedded within the frontal band and are most predominate in the leading one-third of the cloud band.

3. Transverse banding along the trailing edge of the frontal band implies an active jet and strong shear.

4. The wave clouds east of the Kuril Islands.

5. A clear zone over the southern Sea of Japan between the main frontal band and the cloud band associated with a low over Siberia indicates that the two systems are not interacting at this time. The numerical analysis may not depict this well in that it may combine the two systems into one large low.

Forecast Aids:

1. The major convective activity and highest surface winds typically occur in the vicinity of the leading one-third of frontal bands in this region. Surface wind direction shifts occur along these enhanced convective lines.

2. The closed lows along this frontal zone south of Japan seldom have central pressures below 1002-1006 mbs, but surface winds of 30-40 kt within 200-300 n mi of their centers are not unusual. When and if these lows move north of the jet stream position, major cyclogenesis may occur.

3. When a front l system of this type moves off southern Japan and the northerly flow behind the front flows over the area of the Kuroshio Current, particularly dangerous sea conditions can develop. The cold unstable air allows high winds to descend down to the sea surface where they are aligned opposite to the warm ocean current. These two factors make this a region of potentially dangerous high sea conditions. There is maximum transfer of energy from the wind to the ocean, and the wave direction is opposite to

the ocean current. The results are anomalously steep and high waves. Forecasters Beware. This local high wave condition is generally not accurately depicted in numerical products, because: 1) wind/current interactions are not included in the models and 2) the area affected is likely to be below the model resolution (Earle and Bishop, 1984).

An example of very high seas with a rapid increase in height near the north wall was experienced by the USS St. Louis (LKA-16) on a Kushiro to Okinawa transit of 10-14 October 1984. Winds and seas increased from 12 kt and 8-9 ft at 11/1200Z to 41 kt and 13 ft by 11/2300Z with seas to 15-16 ft between these observation times (COMAMPGRPONE, 1984)

4. The jet stream core is typically located in the clear zone just west and north of the frontal cloud band. Regions of transverse banding indicate areas of jet maxima and strong horizontal shear.

5. The E/O and ducting conditions in the region south of the frontal band is generally well mixed and tropical in nature. West and north of the region of convective activity elevated stable layers are likely near cloud tops, the smoother the cloud top the more likely it is under a suppressing stable layer.

6. Terrain induced wave clouds imply the existence of a stable layer. The wind direction and speed are implied by the wave pattern. The waves are seen downwind from the terrain features and the wave lengths (distance from cloud line to cloud line is related to wind speed). This is not an exact relationship but a reasonably representative estimate of the mean wind through the layer from near the top of the terrain to near the top of the wave clouds. An empirically derived equation for this computation is: $U = 6L + 10$ where L is the wave length in nautical miles and U is the mean wind. The suggested method is to measure the wave length over several wave lengths to get a representative single wave length. Using this method and measuring over 10-12 wave lengths the implied speeds for the wave clouds west of the Sea of Okhotsk is 53 to 63 kt and those over the Kuril Islands are about 30 kt. When the wave or billow clouds are associated with a jet stream, rather than lee wave clouds from terrain, the empirically derived equation is: $U = 18L + 16$.

6.2 Sea of Okhotsk Oceanographic Features

The Sea of Okhotsk is a marginal sea of the northwest part of the North Pacific. It is bounded by Asia on the west and north sides, by the peninsula of Kamchatka and Kuril Island Chain on the east and southeast, and the Japanese Island of Hokkaido and Sea of Japan on the south. The extreme latitudes are 44°N and 63°N between 135°E and 165°E longitude. The greatest stretch of sea is about 1330 n mi (SW-NE) and about 300 n mi in the transverse direction (SE-NW). The Kuril Straits connect the Sea with the Pacific Ocean, and the shallow water Tartar and Soya (La Perouse) Straits with the Sea of Japan. Information on the significance of these two straits is addressed in section 3.2.1.

The Okhotsk Sea is surrounded by mountainous terrain. The mountain features are close to the coast in the south, northwest, and north and separated from the Sea by extensive lowlands in the east (western Kamchatka) and west (northern part of Sakhalin Island).

Islands are scarce and mainly near shore. The Kuril Archipelago, about 640 n mi in length is composed of 28 relatively big islands and many small islands and rocks.

Special Regional Features

The following hydrographic phenomena are considered to have significant potential for impact on naval operations:

(1) seasonal ice conditions,
(2) bottom topography, and
(3) a cold layer of intermediate water.

Seasonal Ice Conditions: The Sea of Okhotsk begins to freeze over in a few coastal locations in November, reaches its maximum coverage in mid-March, and is nearly ice free by June. The areas of preferred ice formation are those of cold, low salinity, shallow water in sheltered coastal areas that are some distance from the Pacific inflow. The inflow is largely through the central Kuril Islands, northward off western Kamchatka and then continues counterclockwise within the Sea. The large scale ice drift follows this general circulation which results in the counterclockwise Okhotsk Gyre. Coastal ice forms first in the northeastern and northwestern extremes and then along the remainder of the northern and western boundaries, and last along the Kamchatka Peninsula. By early January, the western third of the Sea is ice covered and by late January some ice is found along the major (west, north, east) coastlines. The ice edge then advances inward toward the center of the basin, reaching maximum coverage sometime in March. Ice retreat proceeds in a reverse pattern from the growth, first disappearing from the center of the sea, then along the eastern side and last in the northwest and northeast. The ice retreat differs from the growth in that it is continuous once started while the growth tends to pulsate in growth/retreat cycles. A second difference is the tendency for the growth season to be longer than the decay season. The decay season tends to show large retreats during the first couple of weeks, then slower retreat for a couple of months. There are significant year to year variations in ice coverage which is largely determined by atmospheric forcing. The stronger and more persistent the Siberian High (stronger, cold, northerly flow off Asia across the Sea), the more extensive the ice coverage. The severity of ice conditions for the Sea of Okhotsk has been noted to be out-of-phase with the Bering Sea and other Arctic region ice coverages.

Bottom Topography: The Sea of Okhotsk has three main categories of bottom topography: (a) continental and island shelves, (b) the bottom of the central part of the sea, and (c) the bottom of the southern deep-water basin. The shelf area occupies more than 40% of the entire sea area and is composed primarily of sands or silts. The widths, outer margin depths, and slopes toward the basins vary widely. The central floor area has several systems of elevations and troughs. Depths over the systems range from 200 m to near 1,750 m. The Kuril Basin runs along the inner side of the Kuril Islands and has a greatest depth of over 3,000 m. The basin is surrounded on all sides by steep slopes (15-20°). The sediments range from pebbly gravel and sand in the nearshore and over open sea summits and slopes, through bands of silts and clays to ooze over the majority of the central part and abyssal plain of the Kuril Basin. In contrast to the Sea of Japan, which is nearly landlocked, the Sea of Okhotsk has free exchange of water with the Pacific. Bussol (Boussole) Strait accounts for over 40 percent of the cross sectional opening of the straits and has a sill depth of over 2,300 m. Kruzenshtern Strait accounts for about 25 percent more of the total opening and has a sill depth over 1,900 m.

Cold Intermediate Layer: The surface waters of the Sea of Okhotsk have temperatures of -1.8 to 2.0°C in the winter and about 10-18°C in summer. Summer heating extends down to 30-75 m but may not reach the lower levels of the water cooled in winter. Consequently, there is a cold intermediate layer with negative temperatures (to -1.6°C) at depths of about 150 m. Below this layer, the basin is filled with warmer Pacific waters of 2 to 2.5°C at depths of 750-1500 m. Bottom waters in the regions of maximum depths are about 1.8°C.

Tides: The tides, mainly related to the entry of the Pacific tide, have a mixed character with the diurnal type predominating. Semi-diurnal types occur along the northern and northwestern coasts. The coastal tidal range varies from 10 to 12 feet at springs and about half of that at neaps. Inside the bays the ranges increase considerably, being near 40 feet at springs in the northeastern most bay. Tidal currents tend to be strong in the coastal areas, reportedly up to 5-8 kt in bays and narrows. The large tidal range and strong coastal currents result in areas of strong rip tides that are known to extend as far as 15 n mi seaward in the vicinity of capes on Kamchatka.

Bathymetry: See comments on bottom topography above.

Currents: The basic circulation is one of cyclonic rotation (Okhotsk Gyre) which is forced by the inflow from the Pacific through the northern Kuril Island Straits. Additional inflow occurs through the Soya (La Perouse) Strait from the Sea of Japan.

Sea Ice: See comments on seasonal ice conditions above.

Temperature and Salinity: Mean sea surface temperatures range from less than 29°F (-1.6°C) over much of the Sea in February to more than 64°F (18°C) near the Soya (La Perouse) Strait and 58°F (14°C) north of the Tatar Strait in August. See comments above on cold layer of intermediate water for subsurface temperature information.

The maximum salinities occur during winter when freezing and evaporation are at a maximum. In summer and autumn, when river runoff and precipitation are at a maximum, salinity values are at a minimum. Thin layers of low salinity water (50 feet or less) extend seaward from major rivers, such as the Amur in the northwest sector.

Sound Velocity Channel: The sound channel axis is at the surface during the colder months and half-channel mode conditions prevail. In the warmer months, the surface heating results in a near surface sound speed maximum and a resultant shallow sound channel axis.

6.3 Winter (mid-November through March) (See section 2.2.1.5.)

Because of its northern location, winter weather comes early to the Sea of Okhotsk and lasts longer than over more southern waters. The strengthening Siberian high pressure cell starts to influence the regional weather as early as September, resulting in a short, transitional autumn season and an early winter onset. Figure 2-8 (page 2-29) depicts a generalized wintertime synoptic pattern (see Figure S-6-1, page 6-5).

6.3.1 Climatology

The Siberian High, a continental polar (cP) air mass, is the dominant feature of the weather patterns over the Sea of Okhotsk during winter. Resident in the Lake Baikal region of the USSR, the Siberian high reaches its maximum intensity during January and February. The Aleutian low is well established east of the Kamchatka Peninsula near 53°N 170°E, and is also at its strongest during January and February. A semi-permanent area of low pressure, sometimes evident only as a trough, becomes established over the eastern Sea of Okhotsk. It forms an anchor for a semi-permanent thermally induced trough which normally extends southwestward into the Sea of Japan.

The following sections address the average conditions which prevail over the Sea of Okhotsk during the winter months.

6.3.1.1 Synoptic Patterns

Figure 2-6 (page 2-23) depicts the tracks of typical migratory extratropical cyclones that normally occur throughout the year. Of the six tracks shown, two would be expected to affect the weather over the Sea of Okhotsk during winter: the Lake Baikal Low (track B) and the South Mongolia Low (track C).

Because of its location adjacent to intensely cold eastern Siberia where winter weather is dominated by the Siberian high, the arctic front influences weather in the northern Sea of Okhotsk. The atmosphere south of the front - over the frozen sea - gains some heat from the water beneath the ice. North of the front - over land - air flow from the north piles up behind the coastal mountains and creates a stong pressure gradient. On occasion, an old occluded low pressure system will move into the influence of the arctic front and regenerate, leading to thawing along coastal areas.

6.3.1.2 Surface Wind

Figures 2-9 and 2-51 (pages 2-31 and 2-71) show that surface wind speeds over the Sea of Okhotsk vary slightly between November and February, with higher winds occurring in November. Lighter winds occur more frequently in the western and northern areas of the sea. The higher winds occur near the Kuril Islands, a circumstance that is to be expected since the southeastern part of the sea is closer to the extratropical storm tracks discussed in section 6.3.1.1 above.

6.3.1.3 Upper Level Winds

Figures 2-10 through 2-15 and 2-52 through 2-57 (pages 2-32 to 2-34 and 2-72 to 2-74) depict mean upper level flow patterns during the months of February and November. As shown in the figures the mean position of the winter jet stream is south of Japan, with velocities decreasing rapidly north of the jet stream core. The extreme southern part of the Sea of Okhotsk is on the fringe of higher winds, but most of the sea has relatively low wind velocities at all levels above the surface.

6.3.1.4 Visibility

Figures 2-16 (page 2-35) and 2-58 (page 2-75) depict the frequency of occurrence of visibility limits during February and November. In general, visibility is better in the southern portion of the sea than it is in the north and the prevailing visibility is better early and late in the season than it is during mid-winter, likely due to steam fog or ice fog conditions.

6.3.1.5 Cloud Heights/Ceilings

Generally cloudy conditions prevail during the winter over the Sea of Okhotsk, with low cloud ceilings (cloud amount $\geq 5/8$) existing over 80 percent of the time over a major portion of the sea in November (Figure 2-59, page 2-76). By February (Figure 2-17, page 2-33) the percentage lowers slightly, but there is an increase in frequency of occurrence of ceilings <600 ft and/or visibility <2 n mi.

6.3.1.6 Precipitation

During the early winter months, a precipitation maximum of 35-40 percent frequency of occurrence exists over the central portion of the sea, decreasing to about 20-30 percent in the coastal regions. By January, a large maximum of 40-45 percent has moved southeastward to a position over the Kuril Islands (closer to the migratory extratropical storm track) while the coastal regions of the northwest Sea of Okhotsk have occurrences below 20 percent. March is the driest month of the season with a 30 percent frequency of occurrence near the southern tip of the Kamchatka Peninsula, decreasing to below 15 percent along the western coast.

Precipitation occurs as snow over 90 percent of the time during the period January-March. In November the 90 percentile isoline bisects the sea east-west at about 55°N, with the occurrence frequency decreasing to about 60 percent near Hokkaido. The December 90 percentile isoline is near the Kuril Islands.

6.3.1.7 Sea State

Figures 2-18 (page 2-37) and 2-60 (page 2-77) present wave height statistics for February and November. The figures show an increased incidence of higher waves during November, reflecting the somewhat higher winds as discussed in section 6.3.1.2 above.

6.3.1.8 Surface Air Temperature

Winter temperatures over the Sea of Okhotsk reflect the extreme cold of the Siberian high. As early as November (Figure 2-61, page 2-78), freezing temperatures cover much of the sea. By February (Figure 2-19, page 2-38), mean temperatures are below freezing over the entire sea, and temperatures along the northwest coast are approaching 0°F (-18°C).

During January, the coldest month, the extreme minimum temperature for the northwestern corner of the sea is -18°F (-28°C). The extreme maximum temperature in the southern portion of the sea during the same month is 46°F (8°C).

6.3.1.9 Freezing Level

Except during November (Figure 2-63, page 2-80) when a small area in the extreme southern portion of the sea has a mean freezing level between the surface and 2,000 ft, the winter season brings surface freezing levels to the entire Sea of Okhotsk.

6.3.1.10 Aircraft Carrier Operating Conditions

Optimum aircraft carrier operating conditions, defined as having a low cloud ceiling ≥5000 ft (or no low cloud ceiling), visibility ≥5 n mi, and wind 11-21 kt, occur between 20 and 30 percent of the time over most of the sea during the entire season except greater than 30 percent in the northeast section, including Shelikov Gulf.

Poor conditions, defined as having a low cloud ceiling <300 ft, or visibility <1 n mi, or wind <6 kt or ≥34 kt, occur between 10 and 20 percent of the time, except early in the season. During November the percentages range from about 5 to 25 percent, with a large area encompassing most of the central part of the sea being less than 10 percent. Ice coverage will limit the regions of carrier operations.

6.3.1.11 Seasonal Oceanographic Features

As winter begins, the mean sea surface temperature over the extreme southern portion of the sea is only about 45°F (7°C), while the temperature of the coastal waters along the western and northern areas is already below 30°F (-1°C) (Figure 2-62, page 2-79). As the winter season progresses, temperatures decrease, resulting in the warmest water during February being only about 35°F (2°C) near Japan and the southern Kuril Islands (Figure 2-20, page 2-39).

By February, 0.6 to 0.8 ice coverage covers about 75 to 80 percent of the sea, with higher concentrations in the coastal waters. Little change occurs between February and March. Figure S-6-3 is an infrared image for 24 February 1980 which indicates a condition of 0.6 to 0.8 ice coverage over the majority of the sea. Figure S-6-1 (page 6-5) is a simultaneous visual image of this area.

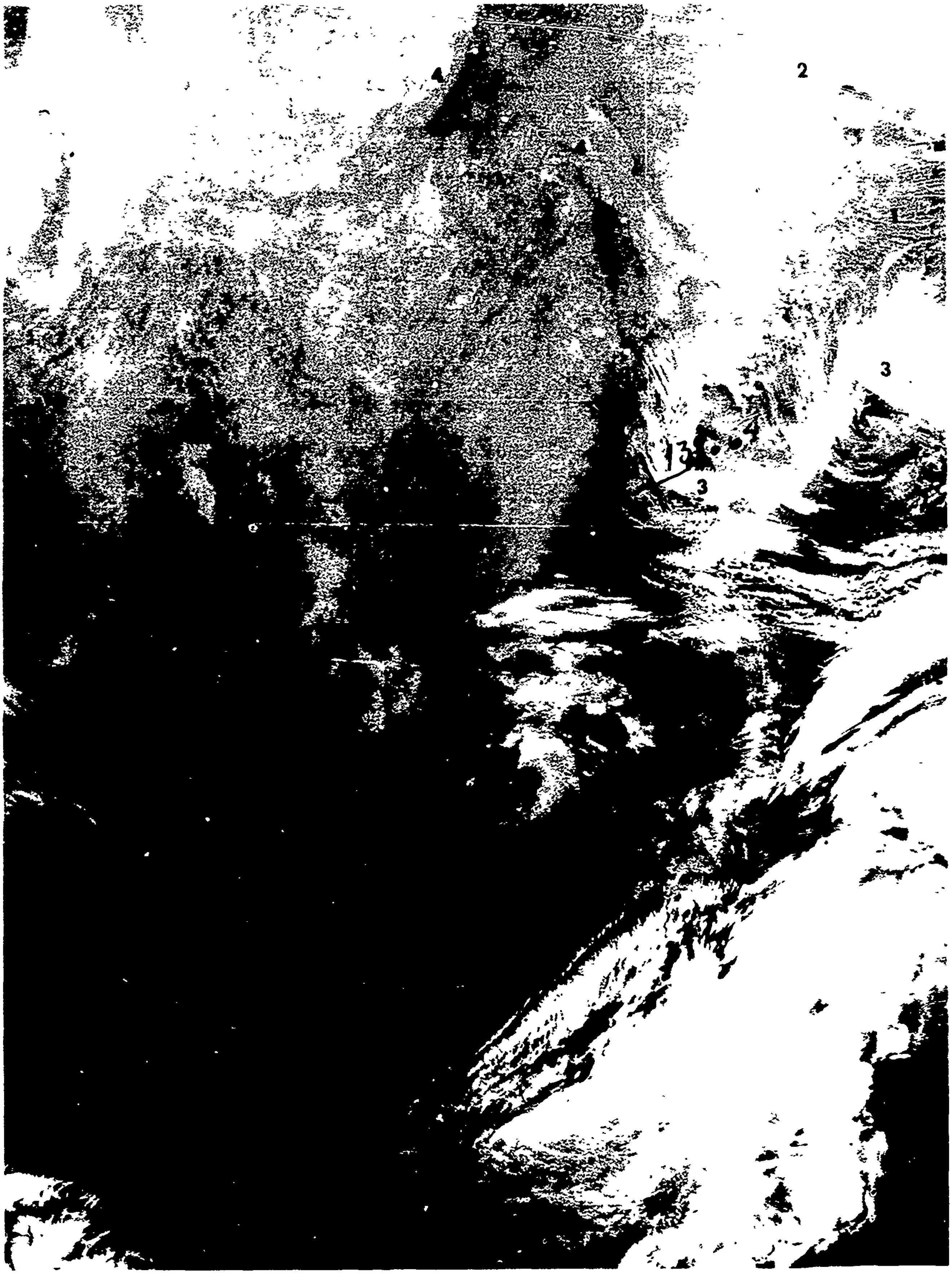

Figure S-6-3. Winter, Sea of Okhotsk. Infrared 24 February 1980.

FIGURE S-6-3. WINTER, SEA OF OKHOTSK. 24 FEB 80
Simultaneous Visual and Infrared Images (Visual: S-6-1)
OSAN AB Infrared DMSP: TN: 24/205 GMT

Synoptic Pattern: Northerly flow dominates the Sea of Okhotsk area. Convective cloud lines are forming right at the ice edge in the off ice flow areas. This indicates strong low level flow and large thermal contrasts between the ice and open water areas. An area of high cloudiness is located over the central Sea of Okhotsk. Areas of enhanced development associated with small vortices (polar lows) are located on either side of northern Hokkaido.

Satellite Image Features:

1. Convective cloud lines are forming over the northern Sea of Japan and over the full length of the Kuril Islands.

2. High cloudiness over the central Sea of Okhotsk is indicated by the light gray shades.

3. Enhanced convective activity is indicated by the lighter gray shades around the small vortices (polar lows) on either side of northern Hokkaido.

4. The land fast ice is lighter (colder) than the general pack ice. The areas of offshore flow where open leads or new ice exists are darker (warmer) than the general pack.

Forecast Aids:

1. Infrared imagery provides an aid in differentiating between, ice, water, and clouds.

2. Infrared imagery can be used to identify land fast, general pack, and new ice areas.

3. Relatively snow free thin first year ice (up to 1-2 ft) and open leads both appear as darker gray shades and can not be clearly separated in either infrared or visual imagery.

4. The areas of vertical development associated with small vortices (polar lows) show clearly in infrared imagery and can be used to designate the areas of most intense weather.

6.3.1.12 Electro-Optical Conditions (See section 2.3.)

The Sea of Okhotsk region is dominated by the circulation of the Siberian high during winter. The prevailing winds are northerly over the northern sea and northwesterly over the southern part. The cold dry continental air flowing over the area results in excellent E/O conditions in the free atmosphere. Due to the extreme cooling of the surface by radiational loses, the condition of terrestrial refraction (mirage) is a common surface phenomena in the high latitudes. Superior mirage or looming, the type most often observed at sea, results in the apparent raising of an object above the horizon. The object may appear to be increased in elevation or enlarged and brought nearer to the point of observation.

This superior type of mirage requires for its formation a layer of relatively warm air over a layer of cooler air. Sea fog is likely to form under these same conditions, and therefore superior mirages are frequently observed following the lifting of fog. These conditions can result in extended surface E/O ranges when fog is not a limiting factor.

Precipitation total amounts are at a minimum in the high latitudes during winter and are comprised basically of snow showers. At sea mixed rain and snow showers are likely. Intensities are always light compared to warmer regions. The frequency of light snow showers can be high, especially in sea regions where cold off-shore flow result in the formation of convective cloud lines (see Figure S-6-3, page 6-21).

The area is generally under the eastern side of the Siberian high and will generally have conditions favorable (subsidence aloft) for low level inversions. Therefore low level ducting is common and will be surface based at times. Under light wind conditions strong surface based ducts are likely. With increasing wind speeds the inversion will rise due to mechanical mixing. The character of cloud formations over water in the offshore flow regions will provide evidence of inversion strength and heights.

Elevated ducts or superrefraction layers occur infrequently (less than 10% of the time). The average heights are near 5900 ft (1800 m) over most of the area decreasing northeastward to a minimum of about 2600 ft (800 m).

The following table presents statistical information on duct heights for the regional area and season of interest:

CENTER OF AREA: 55°N 150°E SEASON: WINTER

EVAPORATION DUCT HISTOGRAM IN PERCENT OCCURRENCE

Height	December			January			February		
(m)	day	nite	both	day	nite	both	day	nite	both
0 to 4	57	60	59	86	90	88	66	78	72
4 to 8	21	17	19	9	6	7	27	18	23
8 to 12	9	10	9	0	0	0	3	2	2
12 to 16	2	0	1	0	1	0	1	0	0
16 to 20	2	2	2	0	0	0	0	1	0
20 to 24	2	2	2	3	0	2	0	0	0
24 to 28	2	2	2	0	0	0	0	0	0
28 to 32	0	0	0	0	1	0	1	0	0
32 to 36	0	0	0	0	0	0	0	0	0
36 to 40	0	0	0	0	0	0	0	0	0
above 40	4	8	6	2	3	2	2	1	1
Ave. Ht.	7	9	8	4	4	4	5	4	4

6.4 Spring (April to mid-June) (See section 2.2.1.6.)

Just as spring brings major changes to the rest of eastern Asia, it also brings change to the Sea of Okhotsk. The major influence of winter weather, the Siberian high, begins to lose strength, allowing a variation in weather patterns over the area. Figure 2-22 (page 2-42) depicts a generalized springtime synoptic pattern.

6.4.1 Climatology

The spring season is accompanied by a weakening of the Siberian high pressure cell and a gradual shift in position from its wintertime location near Lake Baikal southwestward to a location near 45°N 95°E. As the high weakens and moves, the low pressure center that is resident over the Sea of Okhotsk during winter also moves southwestward to a position over eastern Asia west of Sakhalin Island (Figure 2-22, page 2-42). The intense cold of winter over the Sea of Okhotsk starts to moderate as the northerly flow of arctic air is interrupted by periodic influxes of warmer marine air from the south.

The following sections address average conditions which prevail over the Sea of Okhotsk during the spring season.

6.4.1.1 Synoptic Patterns

Figure 2-6 (page 2-23) depicts the tracks of typical migratory extratropical cyclones. Of those depicted, three would typically impact the weather over some portion of the Sea of Okhotsk during the spring season: the Manchurian Low (track A), the Lake Baikal Low (track B), and the South Mongolia Low (track C).

Of the three types of cold fronts discussed, only the eastern (type Z) would be expected to affect the Sea of Okhotsk. Eastern fronts occur primarily during spring and summer. Figure S-6-4 provides a spring view of the Sea of Okhotsk region.

6.4.1.2 Surface Wind

Average wind speeds decrease gradually during spring. Figure 2-23 (page 2-45), which depicts wind statistics during May, shows that wind velocities ≤10 kt have a frequency of occurrence range of less than 40 percent in the south-central portion of the Sea of Okhotsk, to over 60 percent in some coastal areas. April's figures vary from less than 30 percent to over 60 percent, while June's figures range from less than 50 percent to over 70 percent.

6.4.1.3 Upper Level Winds

Figures 2-24 through 2-29 (pages 2-46 to 2-48) depict mean upper level flow patterns for May. While still relatively light, the winds are more zonal than during winter, with the jet stream core still located well south of the Sea of Okhotsk.

6.4.1.4 Visibility

Figure 2-30 (page 2-49) depicts frequency of occurrence of visibility limits during May. The occurrence frequency of visibility ≥5 n mi diminishes each month during the spring season, and the incidence of visibility <2 n mi rises, a result of the stable

Figure S-6-4. Spring regional view, Sea of Okhotsk. 18 May 1980.

FIGURE S-6-4. SPRING REGIONAL VIEW, SEA OF OKHOTSK. 18 MAY 80
OSAN AB Visual DMSP: TN: 18/0135 GMT

Synoptic Features: The Polar Front is well south of the area. A large 988 mb low is centered about 750 n mi west of the central Sea of Okhotsk. Southerly flow dominates the region.

Satellite Image Features:

NOTE: See Figure S-8-3 (page 8-27) for additional comments relative to labels 5-7, which relate to western North Pacific features.

1. Areas of low stratus/fog are seen over the eastern Sea of Okhotsk. A condition that will become more dominate with the approaching summer and prevailing warm southerly flow over the cold water.

2. Some loose pack ice remains east of Sakhalin Island, conditions over the western and northern part of the Sea are obscured by clouds.

3. Land fast ice, seen as bright white areas without breaks, still exists around northern Sakhalin and blocks the Tartar Strait.

4. Snow covers all but the southern most Kuril Islands as a reminder that summer has not yet truly arrived at these latitudes.

Forecast Aids:

1. The limited ice coverage reflects the rapid retreat of ice in the Sea of Okhotsk from its mid-March maximum.

2. The snow covered terrain and land fast ice conditions of northern Sakhalin plus remaining pack ice provide evidence of low temperatures (near zero) that exist over this area.

3. The stratus/fog patches imply a shallow marine layer and capping inversion. Note that there is an indication of a ridgeline over Kamchatka (anticyclonically curved clouds) and that the stratus/fog patches are concentrated near this ridgeline, rather than to the west and south where there is less likelihood of subsidence occurring.

conditions produced by warmer air from more southerly latitudes being transported northward over the cool waters of the Sea of Okhotsk.

6.4.1.5 Cloud Heights/Ceilings

Figure 2-31 (page 2-50) depicts low cloud statistics combined with visibility limits for May. The frequency of occurrence of low cloud ceilings (≥5/8 cloud amount) increases throughout the season, from about 50 to 70 percent in April, to 70 to 85 percent in June. The maximum occurrence in each month is near the Kuril Islands. The occurrence of low cloud ceiling <600 ft and/or visibility <2 n mi shows a similar trend during the season.

6.4.1.6 Precipitation

A significant change in the precipitation pattern occurs between March and April, and continues to change throughout the spring season. During April, there is a less than 5 percent frequency of occurrence of precipitation in the western Sea of Okhotsk, increasing to about 20 percent near the Kuril Islands. Snow probability (as a percentage of observations reporting precipitation) ranges from 30 percent near Hokkaido to 90 percent in Shelikov Gulf. By June, the precipitation probability is 10-15 percent over most of the sea, except for a 20 percent maximum centered near 56°N 146°E and less than 10 percent along the west and northern coastlines. Snow frequency has diminished to less than 10 percent, with the approximate snow limit line bisecting the sea from the southern tip of the Kamchatka Peninsula west-northwestward to about 56°N 138°E.

6.4.1.7 Sea State

As surface winds diminish gradually during spring (see section 6.4.1.2 above), wave heights also decrease. Figure 2-32 (page 2-51) depicts wave height statistics for May.

6.4.1.8 Surface Air Temperature

Spring brings a gradual moderation of the extremely cold temperatures of winter. Between March and April, there is an approximate 7°F (4°C) warming in mean temperatures over the entire Sea of Okhotsk. By June, air temperatures have warmed to about 50°F (10°C) in the southern areas and 41°F (5°C) in the central portion of the northern sea. Figure 2-33 (page 2-52) depicts mean surface air temperatures for May.

The extreme maximum temperature during May for the Sea of Okhotsk is about 55°F (13°C) over the southern sea and western and northern coastal waters. The extreme minimum temperature for the same month is about 16°F (-9°C) over the northern portion of the sea.

6.4.1.9 Freezing Level

As shown in Figure 2-35 (page 2-54), the mean altitude of the freezing level rises considerably during the spring season. An increase of about 5,000 ft is observed in the southern part of the Sea of Okhotsk between February and May.

6.4.1.10 Aircraft Carrier Operating Conditions

Optimum aircraft carrier operating conditions, defined as having a low cloud ceiling ≥5000 ft (or no low cloud ceiling), visibility ≥5 n mi, and wind 11-21 kt show a deteriorating frequency of occurrence during spring, occurring only about 10 percent or less of the time over most of the Sea of Okhotsk by June.

Poor conditions, defined as having a low cloud ceiling <300 ft, or visibility <1 n mi, or wind <6 kt or ≥34 kt show a commensurate increase, occurring from 45 to over 50 percent of the time over the entire sea by the end of the season, with the highest percentages occurring near the Kuril Islands and in the northern coastal areas.

6.4.1.11 Seasonal Oceanographic Features

The mean temperature of the sea surface shows gradual warming throughout the spring season. Whereas in April the temperature range is from about 28°F (-2°C) to 36°F (2°C), the June temperatures span 37°F (3°C) to 48°F (9°C). Figure 2-34 (page 2-53) depicts sea surface temperatures for May.

The extent of sea ice reduces considerably during spring, with the greater portion of the open sea in the Sea of Okhotsk being ice free by May (See Figure 2-34). Figures S-6-5 and S-6-6 (page 6-34) show the ice conditions on two consecutive early spring days.

Figure S-6-5. Ice conditions, Sea of Okhotsk. 16 April 1980.

FIGURE S-6-5. ICE CONDITIONS, SEA OF OKHOTSK. 16 APR 80
OSAN AB Visual DMSP: TN: 16/0159 GMT

Synoptic Features: The large scale ice pattern shows that more than 2/3's of the sea is ice covered. The ice free area along the eastern side of the sea relates to the inflow of the warmer, more saline north Pacific water. The extent of the ice cover is anomalously large for this time of year.

Satellite Image Features:

1. The general ice pattern, open on the eastern and southern sides, multiple leads and fractures over the central area, and consolidated pack over the northern and western areas reflect the combined effects of bathymetry and water circulation.

   A. Open eastern and southern parts where the warm and high saline north Pacific water enters the sea and starts its counterclockwise circulation.

   B. Consolidated pack over the northern and western sectors where depths are less than 100 m and air and water temperatures are lowest.

   C. Multiple leads and fractures over the deeper central portion.

2. Local minimum ice cover, plus late freeze up and early opening occur over the three deep basins.

   A. Tiuro Basin, depth greater than 400 m.
   B. Derugin Basin, depth greater than 800 m.
   C. Kuril Basin, depth greater than 1800 m.

3. Lines of stratocumulus form over the open water when relatively cold air flows off the ice pack, such as the area west of Kamchatka.

Forecast Aids:

1. Coastal ice begins to form in November and the maximum coverage occurs in mid-March, with coastal ice remaining into June.

2. Ice development, growth, and duration are related to currents and bathymetry. The currents flow counterclockwise with the warmest and more saline water entering through the northern Kuril Islands and flow northward off western Kamchatka, in some years portions of the eastern 1/3 of the sea never freeze over. The extensive shelf areas (inside the 100 m contour) of the northern and western sectors freeze over early, are the last to open, and exhibit few leads, fractures, or polynyas.

3. The southeast-central portion of the sea is typically the last to freeze over and first to open.

4. Large polynyas are known to develop over some of the deeper basins after the area is initially frozen over.

5. The ice coverage develops slowly during the growth season (November to March) and is punctuated by temporary reversals. The ice retreat is rapid (April to June) and proceeds smoothly. The retreat is particularly fast in the first week or two.

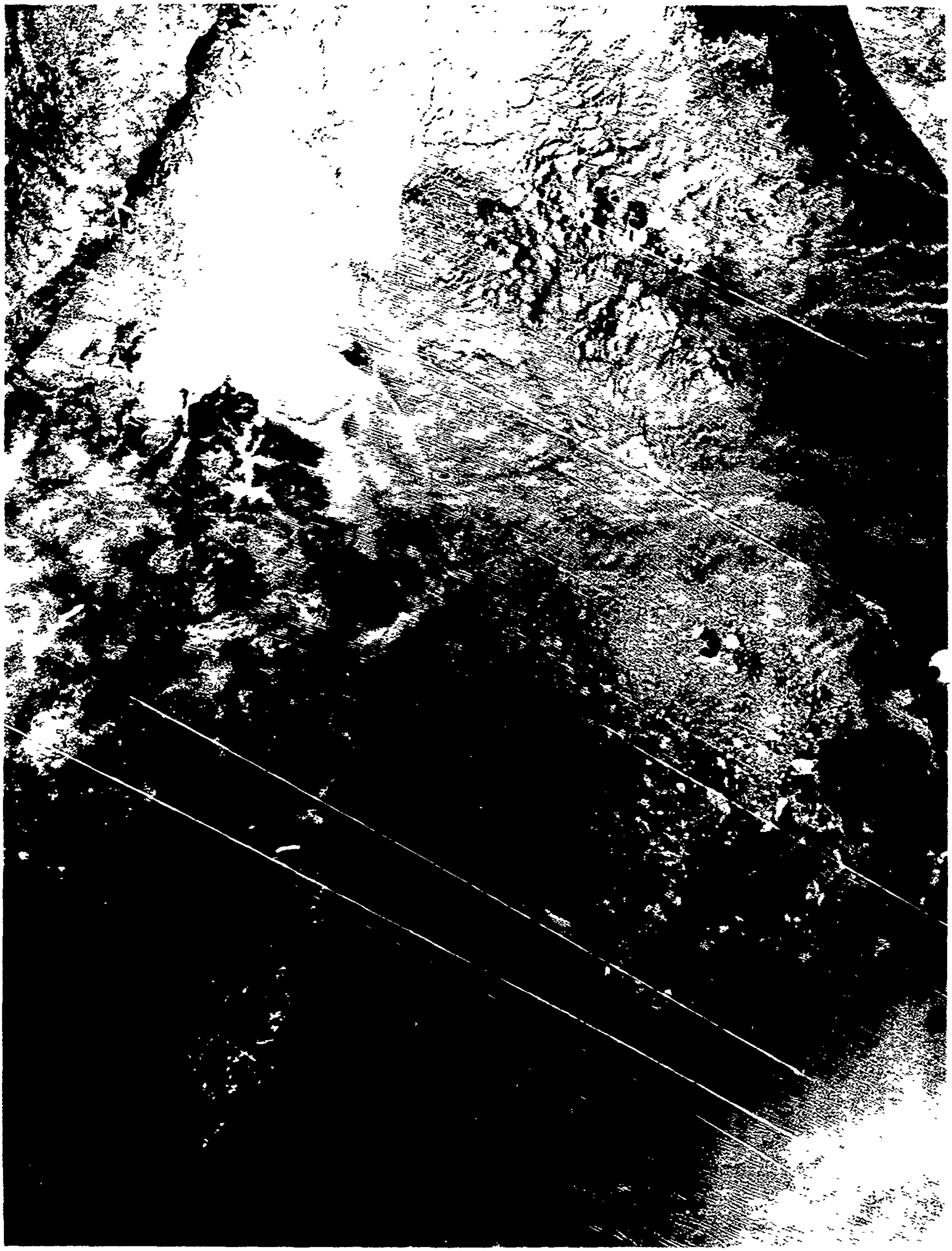

Figure S-6-6. Ice conditions, Sea of Okhotsk. 17 April 1980.

FIGURE S-6-6. ICE CONDITIONS, SEA OF OKHOTSK. 17 APR 80
OSAN AB Visual DMSP: TN: 17/0139 GMT

<u>Synoptic Features</u>: The satellite picture shows that more than 2/3's of the sea is ice covered. The ice free area along the eastern side of the sea relates to the inflow of the warmer, more saline north Pacific water. The extent of the ice cover is anomalously large for this time of year.

<u>Satellite Image Features</u>:

1. The vortices seen along the southern edge of the ice can be definitely related to ice features, rather than cloud, by their persistence from the previous day 16 April 80 (Figure S-6-5).

2. Coastal leads along southeastern Sakhalin Island have developed or increased in size on the order of 10 n mi during the 24 hour period between Figures S-6-5 and S-6-6. During this period the surface winds were southwesterly 15 to 20 kt.

3. The open water to the lee of large ice floes provides additional evidence of low level winds. The open areas are to the northeast in the southern part of the ice changing to the east and then southeast side in the central pack ice reflecting the wind shift from southwest to northwest.

<u>Forecast Aids</u>

1. Ice features are much more persistent than cloud features. Consecutive day views will help clarify features that may be in question.

2. Coastal leads will open within a fraction of a day if offshore winds develop and the offshore ice is not solid coverage and not under compression.

3. Local wind conditions can be deduced from day to day coastal lead changes and open water patterns around large ice floes. Be aware of the likelihood of moderately strong offshore drainage breezes.

6.4.1.12 Electro-Optical Conditions (See section 2.3.)

Spring arrives late over the Sea of Okhotsk, so winter conditions prevail longer than in lower latitudes or at similar latitudes over the open ocean. The shift from the prevailing winter northerly flow to southerly flow does not occur until June. The shift to southerly winds brings warmer moist air into the area with widespread advection fog. Precipitation in the form of drizzle or light rain is also a frequent event. Near surface E/O conditions are frequently degraded by the extensive fog, low stratus, and light precipitation.

The frequency of occurrence of elevated ducts or superrefraction layers continues at less than 10%. Average heights range from about 1640 ft (500 m) in the north to near 3936 ft (1200 m) in the south.

The following table presents statistical information on duct heights for the regional area and season of interest:

CENTER OF AREA: 55°N 150°E SEASON: SPRING

EVAPORATION DUCT HISTOGRAM IN PERCENT OCCURRENCE

Height (m)	March day	March nite	March both	April day	April nite	April both	May day	May nite	May both
0 to 4	63	75	69	60	77	69	72	82	77
4 to 8	25	19	22	17	14	16	13	10	11
8 to 12	4	3	3	6	2	4	3	2	2
12 to 16	1	0	1	4	1	3	2	1	2
16 to 20	2	1	1	1	2	2	2	2	2
20 to 24	1	1	1	2	0	1	1	1	1
24 to 28	1	0	0	2	1	1	1	1	1
28 to 32	1	0	0	1	0	1	1	0	0
32 to 36	0	0	0	1	0	0	1	0	1
36 to 40	0	0	0	1	0	0	1	0	1
above 40	3	1	2	4	2	3	3	1	2
Ave. Ht.	6	4	5	8	4	6	6	3	5

6.5 Summer (mid-June to mid-September) (See section 2.?.1.7.)

The summer season in the Sea of Okhotsk is marked by stable conditions as warmer air is transported northward over the cool waters of the sea. Some instability occurs during August along the Polar Front as it is located between the Kamchatka Peninsula and Sakhalin Island. Figure 2-36 (page 2-56) depicts a generalized summertime synoptic pattern.

6.5.1 Climatology

Summer is a period of light winds, mostly cloudy skies and relatively warm temperatures over the Sea of Okhotsk as the Siberian high is at its weakest strength. The mid-Pacific high is at its strongest, bringing warm, subtropical flow to the southern half of the sea. As shown in Figure 2-5 (page 2-18), the mean position of the Polar Front lies across the central Sea of Okhotsk during August. It is clear of the area during other months of summer. Figure S-6-2 (page 6-7) provides a late summer view of the Sea of Okhotsk region. The following sections address average conditions which prevail over the Sea of Okhotsk during the summer season.

6.5.1.1 Synoptic Patterns

Figure 2-6 (page 2-23) depicts the tracks of typical migratory extratropical cyclones. Of those depicted, two would be expected to impact the weather over the Sea of Okhotsk during the summer season: the Lake Baikal Low (type B), and the South Mongolia Low (type C).

During June, July, and September the Polar Front is south of the Sea of Okhotsk (Figure 2-5, page 2-18). But during August the mean position of the front is about 700 n mi north of its July position, bisecting the sea between the Kamchatka Peninsula and Sakhalin Island. Other frontal activity is limited to the eastern (type Z) fronts.

6.5.1.2 Surface Wind

As shown in Figure 2-37 (page 2-58), surface winds are generally light over the Sea of Okhotsk during August. Gale (≥34 kt) frequency is less than 5 percent during the entire season. Winds are lightest during July, gradually increasing until September, when winds ≤10 kt have a frequency of occurrence of less than 40 percent over most of the central sea.

6.5.1.3 Upper Level Winds

Figures 2-38 through 2-43 (pages 2-59 to 2-61) depict upper level flow patterns for the month of August. It can be seen that the weakened jet stream has moved to the northern Japan-Sakhalin Island area, bringing the strongest upper level winds of the year to the southern Sea of Okhotsk.

6.5.1.4 Visibility

After June, visibilities over the Sea of Okhotsk show gradual improvement through September. Figure 2-44 (page 2-62) depicts visibility limit occurrences during August.

6.5.1.5 Cloud Heights/Ceilings

From a maximum occurrence in June, low cloud ceiling (≥5/8 cloud amount) occurrence frequency decreases through the summer. The frequency of occurrence of the combined statistics of low cloud ceiling <600 ft and/or visibility <2 n mi reaches a maximum in July and then decreases through September. Figure 2-45 (page 2-63) depicts average low cloudiness statistics for August.

6.5.1.6 Precipitation

Except for the 20 percent maximum near 56°N 146°E in June discussed in section 6.4.1.6 above, precipitation over the Sea of Okhotsk has a maximum frequency of occurrence in August. The location of the Polar Front in Figure 2-5 (page 2-18) closely coincides with a 15-20 percent occurrence frequency for the month, while the remainder of the sea has about a 10-15 percent frequency.

6.5.1.7 Sea State

Frequencies of occurrence of wave heights during August for the Sea of Okhotsk are depicted in Figure 2-46 (page 2-64). Waves ≥5 ft (1.5 m) have a gradual increasing frequency of occurrence throughout the summer. Waves ≥8 ft (2.5 m) occur less than 10 percent of the time from June through August, but increase to 10 to 20 percent in September, with the highest percentage occurring along the Kuril Islands.

6.5.1.8 Surface Air Temperature

Surface air temperatures during August (Figure 2-47, page 2-65) are the warmest of the year for the Sea of Okhotsk, ranging from about 52°F (11°C) over the central northern area of the sea to near 63°F (17°C) near Hokkaido. By September the temperatures lower to a 48°F (9°C) to 61°F (16°C) range.

The extreme maximum temperature for August is about 81°F (27°C) near Hokkaido. The extreme minimum temperature for the same month is near 39°F (4°C) in Shelikov Gulf.

6.5.1.9 Freezing Level

Freezing levels reach the highest altitudes of the year over the Sea of Okhotsk in August. As shown in Figure 2-49 (page 2-67), the altitudes range from about 13,500 ft near Hokkaido to near 11,000 ft in Shelikov Gulf.

6.5.1.10 Aircraft Carrier Operating Conditions

Optimum aircraft carrier operating conditions, defined as having a low cloud ceiling ≥5,000 ft (or no low cloud ceiling), visibility ≥5 n mi, and wind 11-21 kt, occur between 5 and 15 percent of the time over the Sea of Okhotsk during August, with the lowest percentage along a north-south band between 150°E and 155°E.

Poor conditions, defined as having a low cloud ceiling <300 ft, or visibility <1 n mi, or wind <6 kt or ≥34 kt have a frequency of occurrence of about 40 to 50 percent over most of the sea, except less than 40 percent west of 142°E and greater than 50 percent near the Kuril Islands and along the north coast between 147°E and 160°E.

6.5.1.11 Seasonal Oceanographic Features

As shown in Figure 2-48 (page 2-66), the sea surface temperature range over most of the Sea of Okhotsk in August is between 50°F (10°C) and 55°F (13°C), except for Shelikov Gulf where the temperature is below 50°F (10°C).

Sea ice is largely gone from most of the sea in August and September (see Figure S-6-2, page 6-7) but, as shown in Figure 2-48, the maximum extent of 0.1 or greater ice coverage encircles the Shantar Islands in the extreme western part of the sea, with 0.1 to 0.4 ice coverage existing between the Shantar Islands and the Asian mainland southeast of the islands.

6.5.1.12 Electro-Optical Conditions (See section 2.3.)

During summer the prevailing winds are southerly and fog and low stratus are widespread. When winds are from the southwest clockwise through north generally clear weather occurs. The Polar Front lies over the southern Sea of Okhotsk and cyclone activity is at a maximum, but weak in intensity. The passage of these weak systems with intervening weak ridges of higher pressure result in shifting wind patterns and variations in cloud cover, type, and amounts. E/O conditions vary with these changing synoptic patterns.

The frequency of elevated ducts increases during periods of warm, moist southerly flow. The frequency of occurrence of elevated ducts or superrefraction layers reaches an annual maximum of about 15%. The average height values reverse their cold season slope, averaging about 5576 ft (1700 m) in the north to near 3280 ft (1000 m) over the southern portion. Low level or surface based ducts occur when high pressure prevails over the area. Due to the relatively cold sea surface cooling from below coupled with the subsidence associated with high pressure cells, widespread, strong surface based or low level ducting will occur when a high cell becomes stationary over the area for a few days.

The following table presents statistical information on duct heights for the regional area and season of interest:

CENTER OF AREA: 55°N 150°E   SEASON: SUMMER

EVAPORATION DUCT HISTOGRAM IN PERCENT OCCURRENCE

Height (m)	June day	June nite	June both	July day	July nite	July both	August day	August nite	August both
0 to 4	65	75	70	67	75	71	60	66	63
4 to 8	15	15	15	17	16	17	18	20	19
8 to 12	4	2	3	3	2	3	6	3	4
12 to 16	4	3	3	2	1	2	3	2	3
16 to 20	2	1	2	2	1	1	2	1	1
20 to 24	2	1	1	1	1	1	2	1	1
24 to 28	1	1	1	1	0	0	1	1	1
28 to 32	1	1	1	1	1	1	1	0	1
32 to 36	1	1	1	1	0	1	1	1	1
36 to 40	1	0	1	1	0	0	1	0	0
above 40	4	1	2	3	2	3	7	5	6
Ave. Ht.	7	4	5	6	4	5	8	7	7

6.6 Autumn (mid-September to mid-November) (See section 2.2.1.8.)

The onset of the autumn season is abrupt over the Sea of Okhotsk. The strengthening Siberian high pressure cell starts to influence the weather as early as September, and the Polar Front has already moved well south of the sea as autumn begins. Figure 2-50 (page 2-69) depicts a generalized synoptic pattern for autumn along eastern Asia but, due to the northern location of the Sea of Okhotsk, actually represents the end of autumn and the start of winter for the area.

6.6.1 Climatology

The following sections address average conditions which prevail over the Sea of Okhotsk during the brief autumn season.

6.6.1.1 Synoptic Patterns

Figure 2-6 (page 2-23) depicts the tracks of migratory extratropical cyclones that normally occur during the year. Of the six tracks depicted, three may affect the weather over the Sea of Okhotsk during autumn: the Manchurian Low (type A), Lake Baikal Low (type B), and the South Mongolia Low (track C).

Once the Polar Front has moved southward out of the Sea of Okhotsk (by early September -- see Figures 2-5, S-6-2, and S-6-7 (pages 2-18, 6-7, and 6-44), frontal activity is usually limited to eastern fronts (type Z). Eastern fronts are primarily a spring and summer phenomena but have a secondary frequency maximum in November.

6.6.1.2 Surface Wind

Surface wind speeds gradually increase over the Sea of Okhotsk during autumn. During September, winds ≤10 kt have an occurrence frequency of 35 to 40 percent over most of the central portion of the sea, increasing to about 60 percent near the coastlines. In November, frequencies drop to 20 to 30 percent over the southwestern two-thirds of the sea, increasing northeastward to over 40 percent in Shelikov Gulf. By November (Figure 2-51, page 2-71), gale frequency has increased to 5 to 10 percent in the southern half of the sea but remains less than 5 percent over the northern half.

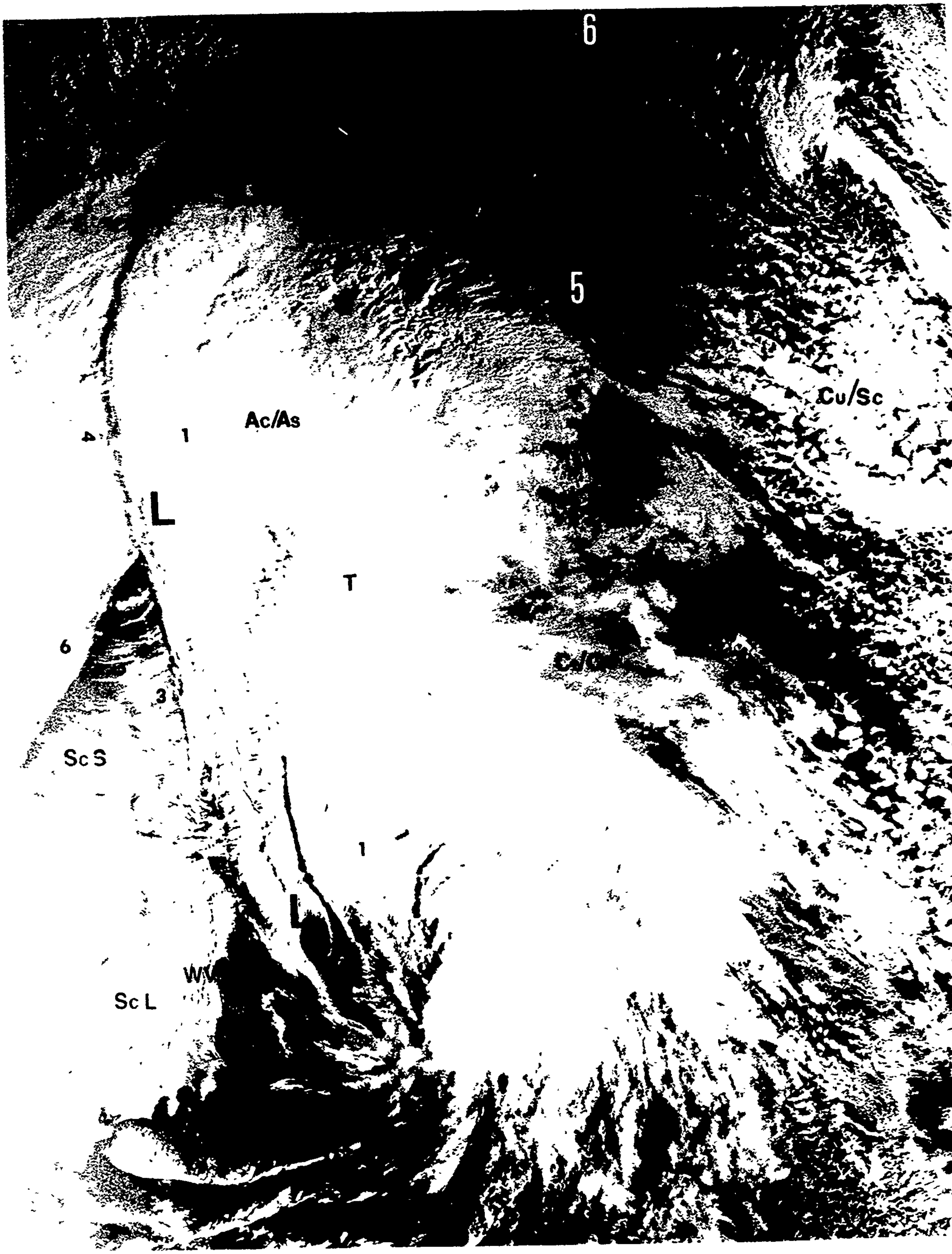

Figure 3 6 7. Autum [illegible]

FIGURE S-6-7. AUTUMN LOW, SEA OF OKHOTSK. 22 OCT 81
Scripps NOAA 6 Visual: TN: 22/2217 GMT

Synoptic Features: A deep low (972 mb) is centered near the Tartar Strait with an elongated trough extending south-southeast to a secondary center off northern Honshu.

Satellite Image Features:

1. The double low configuration is reflected in the cloud mass by two comma shaped clouds each with its own jet stream and cirrus outflow pattern.

2. A variety of cloud types and features are seen in this image and labeled as follows:

Ac/As	Altocumulus/Altostratus shields
Ci/Cs	Cirrus and cirrostratus outflow
T	Transverse banding of cirrus indicating horizontal shear near jet core
Sc L	Upslope stratocumulus over land
Sc S	Stratocumulus cloud line over sea
Cu/Sc	Cumulus/Stratocumulus fields (closed cell type)
WV	Wave clouds downstream from terrain
sV	Small vortex in stratocumulus field

3. The multi-layered nature of this cloud complex is shown by the various shadow patterns of progressively higher cloud layers. Note that over northern Japan (area indicated by number 3) the lowest cloud layer is the Sc cloud lines from off the Sea of Japan. The Sc cloud lines are oriented west to east with the low level flow. Overlaying the Sc is a deck of As extending from south to north and casting a shadow on the Sc. Slightly farther east, an area of convective build-ups aligned north-south cast shadows on the As deck, and finally to the east and north, the cirrus shields cast even wider shadows. An additional cloud layer of stratus is reported under the cloud canopy at this time.

4. This morning pass extends northwestward beyond the terminator (line of sun light). This low angle sun condition amplifies the shadows of higher cloud decks and is helpful in developing interpretation skills relative to the vertical distribution of cloud patterns/types. The perspective of cloud decks may be improved if the viewer rotates the image so the shadows are on the bottom. Our eye/mind communications have evolved under the assumption that shadows always are below the object that creates them.

5. A sharp ridgeline is indicated by the rapid cut off of downstream cirrus and the start of the low level cumulus/stratocumulus field. The ridge extends just about due south

from Kamchatka with the start of the closed cellular Cu/Sc marking the surface ridge line and the end of the Ac/As and Ci/Cs the 500 mb ridge line.

6. The strength of offshore flow is indicated by the length of the clear path offshore. Two regions of offshore flow reflect this in this image. First along the USSR coast of the northern Sea of Japan, the gradient weakens near the low center and the reduced winds are reflected by longer offshore clear paths from north to south. The second area is along eastern Kamchatka where the cloud form changes from near shore forming cloud lines off the northern coast to longer clear paths and cellular type clouds to the south. The light wind area corresponds with a col area over central Kamchatka and a ridge line extending to the south.

7. Small scale polar vortices, indicated by sV's, are seen in the northwesterly flow regions of a low centered to the east.

Forecast Aids:

1. The overall shape of the cloud pattern can provide evidence of complex or multi-centered systems. In areas of secondary cyclogenesis, satellite images may provide the initial indications of new development.

2. The small scale vortices are below the resolution of current operational numerical models and can only be detected and tracked by satellite image and/or observations. Conditions within these vortices are marked by enhanced convective development, heavier showers, and stronger wind shear. While they form first at mid-tropospheric levels they may be reflected at the surface by wind shifts and eventually cyclonic circulation.

3. The multi-layered arrangements of cloud decks in cyclonic systems can often be better detected in low sun angle images.

4. Strong offshore flow is marked by short cloud free paths and gradually enlarging and vertically developing cloud lines. Weak offshore flow is reflected by longer cloud free paths, in areas where winds are less than about 15 kt cellular type clouds will form rather than cloud lines.

6.6.1.3 Upper Level Winds

Figures 2-52 through 2-57 (pages 2-72 to 2-74) depict upper level flow patterns for the month of November. Although the core of the jet stream has moved southward from its summer position to southern Japan, the winds over the Sea of Okhotsk are the strongest of the year.

6.6.1.4 Visibility

As shown in Figure 2-58 (page 2-75), visibilities during November over the Sea of Okhotsk are improved when compared to those of August (Figure 2-44). October visibilities are the best of the season with an 80 to 90 percent occurrence frequency of visibility ≥5 n mi. There is a less than 5 percent occurrence frequency of visibility <2 n mi in the southwest and western portions of the sea, with 5 to 10 percent elsewhere.

6.6.1.5 Cloud Heights/Ceilings

The trend of decreasing cloudiness observed during the summer months over the Sea of Okhotsk is reversed during autumn. As shown in Figure 2-59 (page 2-76), low cloud ceilings (cloud amount ≥5/8) exceed 80 percent frequency of occurrence over most of the central portion of the sea during November decreasing to lesser values over the coastal waters of the western and eastern sea.

Statistics for low cloud ceiling <600 ft and/or visibility <2 n mi show that during October the occurrence frequency ranges from 5 to over 10 percent. The figures increase to 10 to over 20 percent in November.

6.6.1.6 Precipitation

The occurrence of precipitation over the Sea of Okhotsk increases significantly between September and November. September has a frequency of occurrence range of about 14 to 18 percent, with the snow limit line extending roughly east-west near 54°N. By November, the occurrence frequency increases from 20 percent in the extreme southern part of the sea to over 35 percent over much of the central area of the sea. The frequency of snow observation increases to 50 percent near Hokkaido to over 90 percent in the northern one-third of the sea.

6.6.1.7 Sea State

As shown in Figure 2-60 (page 2-77), the increase in wind velocities discussed in section 6.6.1.2 result in higher seas over the Sea of Okhotsk. The 10 percentile isoline for waves ≥12 ft (3.5 m) is approximately the same for October and November, but is absent in September statistics.

6.6.1.8 Surface Air Temperature

Air temperatures decrease rapidly during autumn over the Sea of Okhotsk as Arctic air invades the region. As shown in Figure 2-61 (page 2-78), the mean November air temperature is well below freezing over the northern two-thirds of the sea.

The extreme minimum temperature during November over the sea is about -8°F (-22°C) in the extreme western coastal regions. The extreme maximum temperature is about 25°F (-4°C) near the Kuril Islands.

6.6.1.9 Freezing Level

As shown in Figure 2-63 (page 2-80), by November the altitude of the freezing level is above the surface only in the extreme south end of the Sea of Okhotsk, a lowering of over 10,000 ft since August.

6.6.1.10 Aircraft Carrier Operating Conditions

Optimum aircraft carrier operating conditions, defined as having a low cloud ceiling ≥5,000 ft (or no low cloud ceiling), visibility ≥5 n mi, and wind 11-21 kt, occur less than 10 percent of the time in the central Sea of Okhotsk during November, increasing to about 20 percent along the western coastlines. Poor conditions, defined as having a low cloud ceiling <300 ft, or visibility <1 n mi, or wind <6 kt or ≥34 kt, have an occurrence frequency of 20-30 percent except over 30 percent in the northeast portion of the sea. The statistics for September and October are slightly improved over those for November.

6.6.1.11 Seasonal Oceanographic Features

By November (Figure 2-62, page 2-79) temperatures of the sea surface of the Sea of Okhotsk have decreased significantly from those of August (Figure 2-48, page 2-66). Sea ice extent is at a minimum in September (see section 6.5.1.9) and starts its yearly buildup in October (see Figure S-6-2, page 6-7).

6.6.1.12 Electro-Optical Conditions (See section 2.3.)

Early autumn brings the periods of fairest weather to the higher latitudes. The southerly flow weakens, shifting to other directions, and is lighter in general. The frequency of occurrence of elevated ducts or superrefraction layers is less than 10%. Heights are relatively uniform averaging between 2624 ft (800 m) and 3280 ft (1000 m) throughout the area. The SST has reached its warmest values and the amount of fog and low stratus decreases significantly. E/O conditions at the surface and low levels will be at their best. The end of autumn and beginning of winter tends to occur abruptly and brings rapid changes to weather and E/O conditions.

The change to winter-like flow patterns will result in a reversal in island barrier patterns and areas of on/offshore flow. These reversals must be considered in forecasting low level E/O conditions.

The following table presents statistical information on duct heights for the regional area and season of interest:

CENTER OF AREA: 55°N 150°E SEASON: AUTUMN

EVAPORATION DUCT HISTOGRAM IN PERCENT OCCURRENCE

Height	September			October			November		
(m)	day	nite	both	day	nite	both	day	nite	both
0 to 4	42	49	45	40	49	45	52	64	58
4 to 8	27	31	29	29	34	32	27	27	27
8 to 12	11	11	11	15	10	12	10	6	8
12 to 16	6	3	4	4	3	4	2	1	2
16 to 20	2	1	1	1	0	1	2	0	1
20 to 24	1	1	1	1	0	0	0	0	0
24 to 28	1	1	1	1	1	1	0	0	0
28 to 32	1	0	0	1	0	1	2	0	1
32 to 36	1	0	1	1	0	0	0	0	0
36 to 40	1	0	0	0	1	0	0	0	0
above 40	8	3	5	8	2	5	5	2	4
Ave. Ht.	10	7	8	10	6	8	8	4	6

7.0 PHILIPPINE SEA

7.1 Regional Features and Their Influence on Weather Phenomena

The Philippine Sea (Figure 7-1) is a portion of the North Pacific Ocean located east and north of the Philippine Islands. According to the Encyclopedia Britanica, it lies in "a basin formed by a series of geologic folds and faults that protrude above the surface." The limits of the basin are defined by the Philippine islands of Luzon, Samar, and Mindanao on the southwest, the islands of Belau (formerly Palau), Yap and Ulithi on the southeast, the Mariana Islands on the east, the Bonin and Volcano Islands (which include Iwo Jima) on the northeast, the Japanese islands of Honshu, Shikoku and Kyushu on the north, the Ryukyu Islands on the northwest, and Taiwan on the west. The sea has approximate dimensions of 1,800 n mi north-south and 1,500 n mi east-west with a general depth of about 19,700 ft (6,000 m). Adjacent waters include the Pacific Ocean to the east, East China Sea to the northwest, and the South China Sea to the west through the Luzon Strait.

The Japanese islands of Shikoku, Kyushu and Honshu, with mountain ranges commonly reaching elevations above 4,921 ft (1,500 m), exert a significant influence on the weather over the northern Philippine Sea. Extratropical weather systems, frequently moving northeastward out of the East China Sea during winter, seldom cross the mountain barriers. Instead, they either cross into the Sea of Japan through the Korea Strait or remain south of Japan moving east over the Philippine Sea before proceeding northeastward east of

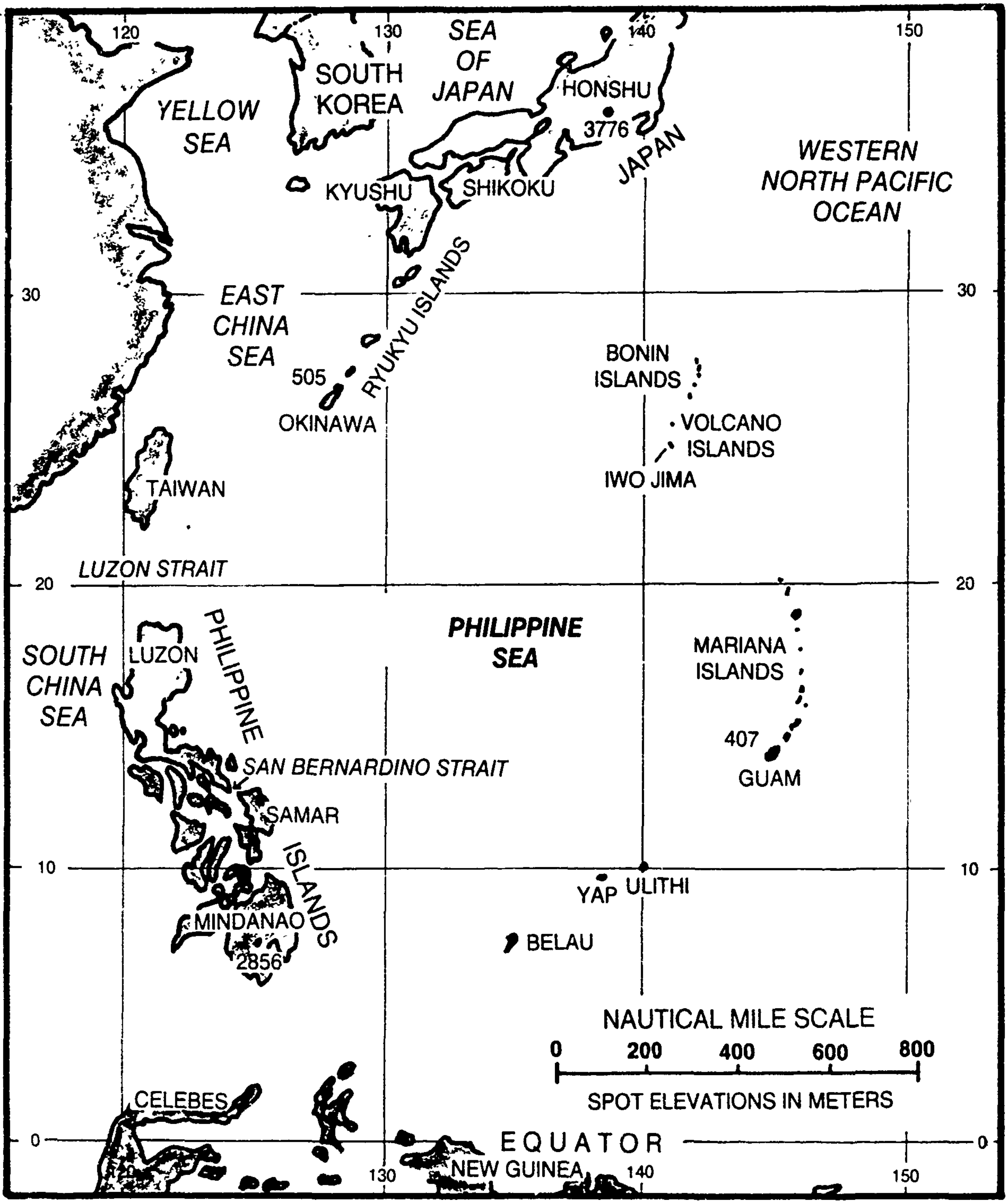

Figure 7-1. Philippine Sea.

Japan. The islands also inhibit and mask the movement of frontal systems crossing the Japanese islands.

Other than the Japanese islands, land areas adjacent to the Philippine Sea exert comparatively little influence on its weather. Except for local effects, the islands around the eastern border of the sea have minimal impact. The same is true of the Ryukyu Islands. The southerly latitude of the Philippine Islands places them in the northeast tradewind belt and on the leeward side of the sea: therefore, they have little effect on the weather over the Philippine Sea. They do, however, act as barriers to westward moving tropical cyclones, frequently blocking their direct transit across the major islands.

The mountainous island of Taiwan, with peaks of 12,743 ft (3,884 m) and 13,114 ft (3,997 m), also has minimal impact on the weather over the Philippine Sea. Like the effect of the Philippine Islands, tropical cyclones often skirt, rather than pass over, the island.

One of the most significant features of the region with respect to its influence of weather is not in the topography of the adjacent landmass, but lies in the sea itself. The bathymetry of the Philippine Sea as it influences various oceanographic parameters will be addressed in the next section, but since the sea exerts such a profound influence on the meteorology of the region, it will be briefly addressed here.

The North Equatorial Current flows westward at tropical latitudes in the western North Pacific Ocean until it reaches the Philippine Sea. It then veers northward as the Kuroshio Current (see Figure 2-4, page 2-11) and flows to southwestern Japan, where it splits into subcurrents (Figure S-7-1). As it moves northward across the Philippine Sea its path takes it east of Taiwan and along the Ryukyu Islands, with the western edge of the current approximately following the Okinawa trough (Figure 2-3, page 2-7). The eastern edge of the current lies east of the Ryukyus along the western side of the Philippine Sea. The Kuroshio is a warm current which exerts a strong influence on passing weather systems. Seemingly innocuous weather systems moving offshore from the Chinese mainland or forming offshore may develop into major storms after encountering the warm waters of the Kuroshio Current. The disturbances, known as Shanghai and Taiwan lows (Figure 2-6, page 2-23) are particularly evident during spring and autumn and the fleet meteorologist must be aware of their potential development and impact on Philippine Sea operations.

7.2 Philippine Sea Oceanographic Features

The Philippine Sea is an abyssal zone (depths generally greater than 2,000 m). The bottom topography is complicated by deep trenches (greatest depth over 6,000 m), belts of seamounts, deep basins, and number of island arcs. The Sea is separated on the east from the Pacific Basin proper by a number of oceanic island arcs and on the west from the marginal seas by the continental arcs of Japan, the Ryukyu Islands, and the Philippines (See Figure 2-3, page 2-7). The abyssal deep basin is separated into east and west basins by the Kyushu-Palau Ridge. The bottom sediments are pelagic red clays and oozes with volcanic material along the island arcs.

Figure S-7-1. Kuroshio Split. Infrared 18 May 1980.

FIGURE S-7-1. KUROSHIO SPLIT, SIMULTANEOUS VISUAL AND INFRARED IMAGES. 18 MAY 80
(Visual Image: S-3-7, page 3-36)
OSAN AB Infrared DMSP: TN: 18/0136 GMT

Synoptic Features: The large scale oceanic surface thermal features include: the Kuroshio split, the Tsushima Current flowing northward from the split and then northeast through the Tsushima/Korea Strait, the warmer waters of the Tsushima continue northward along the eastern Sea of Japan with outflow occurring through first the Tsugaru and farther north the Soya Straits. The warm outflow through these two straits turns sharply southward along the northeast coasts of Honshu and Hokkaido, respectively, in what is referred to as coastal modes. East of Tsugaru Strait a small portion of the perturbed area created by the converging cold Oyashio and warm Kuroshio Currents can be seen.

Satellite Image Features:

1. The Kuroshio split just south of the southern most part of Japan (warm areas of ocean are dark gray, cold areas light gray).

2. The northward flow from the split area of the Tsushima Current.

3. The thermal contrast across the Tsushima/Korea Strait, cold on the Korean side, warm on the Japan side.

4. The relatively warm waters on the east and south sides of the Sea of Japan and cold on the north and west sides. The minimum contrast of gray shades across the south central Sea of Japan in this image is likely caused by masking of the surface temperatures by the high level return from a cirrus band.

5. The outflow through the Tsugaru and Soya Straits. Note that the thermal pattern from north to south across these two straits is similar to that across the Tsushima, cold on the north, warm on the south.

6. The warm water turns southward after exiting the Tsugaru and Soya Straits and is confined to a narrow band along the coastline.

7. The western end of the perturbed areas resulting from the confluence of the cold Oyashio and warm Kuroshio Currents east of Japan is seen east of the Tsugaru Strait. This pattern extends eastward beyond 160°E.

Forecast Aids:

1. The major features of the Kuroshio and Tsushima Currents will persist over extended periods of time. The latest available

positioning view should be retained until direct evidence of a change becomes known or a new satellite view is available. Neither the large scale numerical analyses and forecasts, nor products derived from them will reflect the strong thermal boundaries that are evident in the imagery.

2. The infrared temperature sensed by the satellite sensor is an integrated value from the entire atmospheric column. The best SST readings are obtained through cold and dry atmospheric conditions. The normal strong gray shade contrast across the southern Sea of Japan caused by the cold water of the Limon Current along the north and west sides and warm Tsushima Current along the south and east side, are largely masked in this image due to the added high level moisture associated with the cirrus shield approaching from the west. The effects of increased atmospheric moisture include both attenuation which lowers all temperature values sensed and suppression of temperature differences because of increasing attenuation with increasing surface temperatures which reduce the real temperature differences or gradients.

3. The surface water of the northern parts of the Tsushima, Tsugaru, and Soya Straits will be colder than the southern side where the warm outflow is located. There are known variations to this, including:

A. The cold water flowing south and east around southern Korea sinks under the warm Tsushima water during winter. In spring and into summer when heavy run-off reduces the cold water salinity, it overrides the Tsushima waters and produces a frontal zone near a line between the islands of Cheju-do and Tsushima.

B. During the summer when surface heating results in uniform sea surface temperature values and a mixed layer (full-channel conditions), even though it is quite thin over the northern waters, the obvious thermal contrast is not there.

C. The inflow (Tsushima) and outflow (Tsugaru and Soya) are strongest during summer and therefore increasing portions of the Straits will be covered by warm water as the summer season approaches and also following it. During winter the cold water portion is largest.

4. The coastal mode outflow is a year round feature of the Soya Strait. The outflow of the Tsugaru changes to a warm gyre mode that extends eastward to near 143°E during the summer strong outflow period.

5. The perturbed area east of the Tsugaru Strait and the main Japan island of Honshu is a year round feature. A series of gyres are typically aligned east-west along it and its north-south extent is on the order of 300 n mi. Little evidence of this general feature is reflected in numerical products and the gyres are not likely to be reflected at all.

Special Regional Features

The following hydrographic phenomena are considered to have significant potential for impact on naval operations:

(1) Kuroshio Current,
(2) cold cyclonic meander,
(3) collocation of oceanic fronts and large bottom slopes, and
(4) opposing ocean currents and wind.

Kuroshio Current: The Kuroshio Current begins in the Philippine Sea east of northern Luzon, then flows out of the Sea into the East China Sea northeast of Taiwan. After flowing northward on the west side of the Ryukyu Islands the current reenters the Philippine Sea south of Kyushu and flows northeastward along southern Japan. During this northeastward set the current accelerates to 2-5 kt with the maximum speed occurring between 132°E and 137°E. The 15°C isotherm at 200 m is typically used as an indicator of the current axis. While flowing northeastward the current parallels the depth contours of 1,000-3,000 m. Near 134°E the path of the Kuroshio becomes more variable and in the region of 134°-139°E a cold cyclonic meander is frequently present (see Figure S-3-4, page 3-22). This meander is the most conspicuous feature of the Kuroshio in this area and once formed may last for several years. Some traits of the meander are:

(1) The north-south diameter is as much as 200 n mi.
(2) It develops in a short time, i.e., in a few months.
(3) It decays slowly, i.e, in several years and drifts eastward.
(4) The life of a meander is 3 to 10 years.

Collocation of Oceanic Fronts and Large Bottom Slopes: These conditions present special problems to ASW operations. Such collocations occur in several regions of the Philippine Sea. One area where this condition has been noted as a problem is located southeast of Okinawa (SHAREM Report 35 of March 1980 addresses this specific site problem). In general the numerical guidance provided by grid point or single point ASW data does not account for the loss of bottom bounce or redirection of bottom bounce in areas of steeply sloped bottoms.

Opposing Ocean Currents and Winds: Areas of warm SST's are known to decrease the stability of the lower atmosphere and allow for more efficient transfer of energy from the wind to the sea surface. Additionally it has been shown that when ocean current flow direction and wind direction are opposite or opposing each other the wind waves are higher, and steeper, and wavelengths are shorter. When northwesterly winds have occurred off southeastern Japan anomalously high waves have been reported. The elements brought to focus under this condition typically develop when a migratory high moves off Asia or a low passes south and east of Japan, resulting in cold northeasterly winds of 20 kt or greater flowing over the warm opposing northeasterly setting Kuroshio Current. The results are heavy seas and cold showery weather with winds significantly higher than those reported over coastal areas or to the south of the Kuroshio Current area. The surface winds and seas will be significantly higher than indicated by the numerical guidance with the area influenced by the Kuroshio. The Kuroshio width ranges from 30 to 100 n mi in this region outside the areas influenced by the large cold cyclonic meander. The meander has been known to have a north-south dimension of about 200 n mi and extend southward to around 29°N.

Tides: Tides are not a problem in the open ocean or seas.
Bathymetry: The bathymetry features are addressed in the opening paragraphs of this section.

Currents: In addition to the Kuroshio Current addressed in the Special Regional Features above, other major currents of the Philippine Sea are:

(1) North Equatorial Current which flows east to west between 10° and 20°N at speeds of 0.5-2.0 kt,
(2) Equatorial Countercurrent in latitudes 3°-10°N sets from west to east with a speed of 1-2 kt,
(3) Kuroshio Counter Current located south of the Kuroshio and sets to the SW-WSW across the Philippine Sea at speeds of 0.6-0.7 kt. This current is strongest in the winter under the Northeast Monsoon winds, and
(4) Subtropical Countercurrent setting eastward at 0.2-1.3 kt between 20°-24°N. The 22°-23°C isotherm at 100 m is used to identify the axis of this approximately 300 m thick and 100 n mi wide current.

Temperature and Salinity: The Philippine Sea has a stable thermal pattern with only the large scale seasonal changes affecting the majority of the area. Along the northern boundary where the Kuroshio flows strong thermal gradients are found. During the warm season, a fairly uniform SST of about 28°C covers all but the extreme northern and northeastern areas where the maximum is about 26°C. During winter the 25°C surface isotherm closely parallels 20°N, with decreasing temperatures northward to about 15°C near 35°N. To the south the increase is only about 3°C to the 28°C maximum near the equator. The dominate water mass is the North Pacific Central Water Mass (subtropic water mass) which rotates clockwise in a great gyre and exhibits highly saline surface water of 34.8°/oo - 35.2°/oo. At 200 m the temperature ranges from 23°C to 15°C and at 400 m, 10°C to 5°C. The maximum values are located between 15°-20°N at 200 m and shift northward to 20°-25°N at 400 m.

Sound Velocity Channel: The channel axis is quite deep throughout the Sea. An area of maximum depth of over 1500 m is found year round centered near 30°N, 135°E. The depths decrease to about 700-800 m near the western and northern boundaries of the Sea except during winter when those boundary values are about 900-1000

m. Water depths are a limiting factor not only in coastal areas but over the lesser depths along the Ryukyu and Mariana/Bonin Island Chains. Winter mixed layer or sonic layer depths range from less than 75 m in the southern sectors of the sea to a maximum of about 200 m between 32°-34°N and east of 140°E. Depths of near 100 m are common over the western portions of the Sea.

7.3 Winter (mid-December to mid-March) (See section 2.2.1.5.)

The northwestern portion of the Philippine Sea is under the influence of the Northeast Monsoon during the winter (S-7-2). The Polar Front lies approximately east-west about 18°N, separating the modified polar air north of the front from the maritime tropical air to the south. Figure 2-8 (page 2-29) depicts a generalized wintertime synoptic pattern.

7.3.1 Climatology

Due to its considerable north-south and east-west extent, the wintertime weather situation over the Philippine Sea actually encompasses three weather regimes: 1) the Northeast Monsoon over the western portion of the northern part of the sea, 2) a modified monsoonal influence over the eastern portion of the northern part of the sea, and 3) tropical weather over the southern part of the sea.

Eastern Asia is under the influence of the Siberian high during the winter. The high, which is at its greatest strength during January and February, forces continental polar air southward over the water areas adjacent to coastal Asia, creating the Northeast (winter) Monsoon. Originating over central and eastern USSR, the air is very cold at its source, with temperatures ranging

Figure S-7-2. Northeast Monsoon, Philippine Sea. 28 December 1977.

FIGURE S-7-2. NORTHEAST MONSOON, PHILIPPINE SEA. 28 DEC 77
USS KITTYHAWK (CVN 63) Visual DMSP: TN: 28/0145 GMT

Synoptic Features: High pressure extends eastward off the Asian coast with northerly low level flow dominating the Philippine Sea and oceanic areas surrounding Japan.

Satellite Image Features:

1. Low level clouds are seen along the windward side of: Eastern Luzon and northern Japan.

2. East-west shear lines extend eastward from off the southern part of the Philippine Islands (near 12°N, Mindanao) and off the northern part (near 18°N, Luzon).

3. Wave clouds over Japan reflect the northerly low level flow.

4. The cloud shield of a developing low is seen over the East China Sea/China coast.

5. The variation of cloud free path length south of Japan indicates areas of terrain sheltering (clear areas) or funneling (short cloud free areas).

6. The change from longitudinal to transverse banding indicates decreasing wind shear through the cloud layer.

7. The fine featured convective cloud lines over the central Philippine Sea are basically aligned with the low level winds. This alignment is typical for this type cloud pattern in the lower latitudes.

8. Lee side drying is indicated by the darker gray shade areas and cloud free areas south of Japan and west of the Philippines.

Forecast Aids:

1. The low level wind direction can be determined from the upslope cloud formations formed on the windward side of mountainous islands.

2. When high pressure cells move off of Asia the trailing edge of the cold fronts persist as generally east-west shear lines over the subtropical region of the Philippine Sea. Surface winds are generally increased and gusty in the vicinity of the shear lines and enhanced convective activity and light showers are typical.

3. Low level moisture and aerosol content are typically reduced in areas that are cloud free, such as the darker gray areas in the lee of islands. Visibility and E/O ranges are increased in these regions.

4. Over the open ocean, the small fine featured cloud lines are generally aligned with the surface winds, or more precisely, with the directional shear through the cloud layer.

5. The combined visual indicators of windward upslope clouds, drying and cloudline patterns downwind from islands, thin cloudline patterns over the open ocean, and shear line cloud patterns provide evidence of low level wind direction and wind speeds. On this date, reports in the area from over the Sea of Japan to the shear lines of the Philippine Sea indicate winds of 20 to 30 kt. The directions are, northerly over Japan, shifting to northeast over the Philippine Sea, and easterly over the Philippine Islands and coastal areas of China. With experience, the wind speeds and directions can be gleaned from the imagery alone.

from 15°F (-9°C) to -40°F (-40°C). The air is modified somewhat by adiabatic warming as it travels to the coast, and is further warmed and modified as it travels over the water areas. The western portion of the northern Philippine Sea is subject to the worst of the cold air outbreaks as it is closer to the source of the air. Consequently, the air has had a shorter time to warm over the water areas. The outbreaks of strong northeasterly flow can persist more-or-less uninterrupted for periods of 10 days to 2 weeks during the middle and latter parts of the winter. The extremely long fetch causes fully developed seas to form. Consequently, according to the Forecasters Handbook of the Gulf of Tonkin and the South China Sea, published by Fleet Weather Facility, Yokosuka, Japan in 1966 as FLEWEAFAC Yokosuka Instruction P3140.37, ships which would normally transit through the Luzon Strait during one of the outbreaks "may be well advised to use the San Bernardino Strait" (see Figure 7-1, page 7-2) "thence north through the central Philippine Sea to avoid the damaging seas that prevail in the normal shipping lanes." (The San Bernardino Strait is located between the Philippine Islands of Luzon and Samar.)

The eastern part of the northern Philippine Sea is also affected by outbreaks of cold air but its impact as a monsoonal force is less than that experienced to the west.

Because the mean position of the Polar Front is near 18°N in the Philippine Sea, the Northeast Monsoon's effect is essentially limited to the sea north of that latitude. Weather south of the Polar Front is dominated by typical warm, tropical conditions with east-northeasterly trade winds. Precipitation is at a minimum as winter is the driest season of the year for the tropics.

The following sections address average conditions which prevail over the Philippine Sea during the winter months.

7.3.1.1 Synoptic Patterns

Figure 2-6 (page 2-23) depicts the mean tracks of extratropical cyclones that normally occur during the year. Of those depicted, only one -- the Taiwan low (track F) -- will commonly affect the weather over the Philippine Sea during winter. As shown by its track, the major impact of a Taiwan low will be over the northern Philippine Sea. Shanghai lows (track D) are more common during spring and autumn, but may occur during winter.

Cold fronts of the eastern and central types (Figure 2-7, page 2-26) may affect the weather over the northern Philippine Sea during winter. As the fronts move southward into the tropical latitudes, they lose many of their cold frontal characteristics and become "shear lines" (see S-7-2, page 7-12). With a strong polar outbreak they will frequently intrude well into the tropics south of 15°N, commonly passing south of Guam (13.5°N 144.8°E), and intruding well into the Philippine Island of Luzon.

7.3.1.2 Surface Wind

As shown in Figure 2-9 (page 2-31), winter winds are lightest in a broad band across the central portion of the Philippine Sea. Prevailing directions are northwest near Japan, becoming northerly between 25°N and 30°N, and northeasterly over the remainder of the sea. The highest average velocity, about 20 kt, occurs over the waters of the western sea near the Luzon Strait.

7.3.1.3 Upper Level Winds

Figures 2-10 through 2-15 (pages 2-32 to 2-34) depict upper level flow patterns for the month of February. Maximum velocities at the specified pressure surfaces over the Philippine Sea occur along the south coast of Japan. In fact, the strongest and most persistent jet stream speeds in the world are observed there, with velocities exceeding 200 kt not uncommon.

7.3.1.4 Visibility

Visibility over the Philippine Sea is good during the winter. As shown in Figure 2-16 (page 2-35), during February the occurrence of visibility limits <2 n mi is less than 5 percent. Visibility limits of ≥5 n mi have a minimum frequency of occurrence of 80 percent near Taiwan (where the effects of the Northeast Monsoon would be strongest) to over 95 percent in the southeast portion of the sea.

7.3.1.5 Cloud Heights/Ceilings

The months of January and February have the highest percentage of occurrence of low cloud ceilings (cloud amount ≥5/8) over the Philippine Sea during winter. As shown in Figure 2-17 (page 2-36), the greatest incidence of cloud amount ≥5/8 during February occurs just south of Japan. Low cloud ceiling <600 ft and/or visibility <2 n mi have a maximum occurrence frequency in February.

7.3.1.6 Precipitation

Precipitation patterns remain essentially the same over the Philippine Sea during winter. A maximum precipitation frequency of occurrence of 10-15 percent is located south of and parallel to the Japanese coast decreasing to 5-10 percent over the central portion of the sea and increasing again to over 10 percent over the southern sea.

Snow occurs only infrequently in the northern Philippine Sea with the approximate snow limit line extending east-west across the sea about 150 n mi south of the Japanese coast.

7.3.1.7 Sea State

As shown in Figure 2-18 (page 2-37), wave heights on the Philippine Sea equal or exceed 5 ft (1.5 m) from less than 50 percent to over 70 percent of the time during February. The highest percentages occur in the southern latitudes where persistent tradewinds raise a constant sea, and in the north, where migratory extratropical cyclones bring increased winds to the Japanese coastal waters.

7.3.1.8 Surface Air Temperature

Because of its considerable north-south extent, the Philippine Sea experiences a wide range of mean temperatures during winter. As can be seen in Figure 2-19 (page 2-38), mean surface air temperatures during February range from 45°F (7°C) over Japanese coastal waters to 80°F (27°C) over the southern sea.

The extreme minimum temperature over the northern sea is about 39°F (4°C) while the extreme maximum temperature over the southern sea is near 90°F (32°C).

7.3.1.9 Freezing Level

Wintertime freezing level altitudes over the Philippine Sea vary greatly with latitude. Figure 2-21 (page 2-40), which depicts mean freezing level altitudes during February, shows an altitude range of 3,000 to 4,000 ft near Japan, increasing to 14,000 ft over the southern part of the sea.

7.3.1.10 Aircraft Carrier Operating Conditions

The frequency of occurrence of various aircraft carrier operating conditions varies only slightly during the months of winter. Optimum conditions, defined as having a low cloud ceiling ≥5,000 ft (or no low cloud ceiling), visibility ≥5 n mi, and wind 11-21 kt, occur about 10 to 20 percent of the time over the northern sea, increasing to over 40 percent over the southern sea.

Poor conditions, defined as having a low cloud ceiling <300 ft, or visibility <1 n mi, or wind <6 or ≥34 kt, occur generally 10 to 20 percent of the time except less than 10 percent in the extreme southeastern part of the sea.

7.3.1.11 Seasonal Oceanographic Features

As depicted in Figure 2-20 (page 2-39), water temperatures of the Philippine Sea during February vary from a low of 55°F (13°C) near Japan to about 80°F (27°C) near the southern Philippine Islands.

7.3.1.12 Electro-Optical Conditions (See section 2.3.)

During winter the Philippine Sea area will have large variations in E/O conditions. The western and northern sectors will be dominated by the Northeast Monsoon and exhibit a well mixed atmosphere of relatively cold dry air, while the southern and eastern will reflect tropical conditions. The Polar Front will be found between these two contrasting air masses and provide a third region of E/O conditions.

Surface evaporation ducts will form when cold air moves over warm SST areas and winds are light. While the appropriate air/sea temperatures contrasts will typically be found under the Northeast Monsoon flow, the winds are generally strong enough to generate a layer of well mixed air and cloud development. In these cases elevated inversions and potential ducts are likely to be found near the cloud top. The frequency of occurrence of elevated ducts or superrefraction layers varies widely in response to synoptic scale weather patterns. The average frequency ranges from about 30% in the northwest sector to 70% over the eastern sector. Average heights range from about 3936 ft (1200 m) in the northwest to 5904 ft (1800 m) in the eastern sector.

Local conditions associated with offshore flow, island barriers, and oceanic thermal fronts influence E/O conditions during winter.

The following table presents statistical information on duct heights for the regional area and season of interest:

CENTER OF AREA: 20°N 135°E SEASON: WINTER

EVAPORATION DUCT HISTOGRAM IN PERCENT OCCURRENCE

Height	December			January			February		
(m)	day	nite	both	day	nite	both	day	nite	both
0 to 4	2	2	2	2	2	2	4	4	4
4 to 8	3	4	3	4	5	5	5	8	7
8 to 12	7	10	9	11	15	13	12	17	15
12 to 16	15	20	18	18	25	22	16	23	20
16 to 20	23	31	27	23	27	25	21	25	23
20 to 24	21	21	21	17	16	17	15	14	14
24 to 28	11	8	9	8	5	7	7	5	6
28 to 32	5	2	3	3	2	3	3	1	2
32 to 36	2	1	1	2	0	1	2	0	1
36 to 40	1	0	1	1	0	1	1	0	1
above 40	11	2	6	10	2	6	14	2	8
Ave. Ht.	23	18	21	22	17	19	23	16	19

7.4 Spring (mid-March to mid-June) (See section 2.2.1.6.)

As is the case with most of the waters adjacent to eastern Asia, spring brings significant changes to the weather of the Philippine Sea. Most of the changes are evident over the waters of the northern sea rather than in the tropical latitudes. The major climatological cloud band feature is associated with the Mei-Yu/Bai-U front (see section 2.2.1.2, page 2-20).

7.4.1 Climatology

Spring (mid-March to mid-June) is a transition season for the Philippine Sea. The Siberian high begins to weaken, allowing the Polar Front to begin its migration northward from its wintertime position (Figures 2-5, page 2-18 and S-7-3). As the Polar Front moves northward, extratropical waves develop along the frontal zone, typically near Taiwan and in eastern China. Upper atmospheric disturbances (short wave troughs) transit the northern part of the sea. "Bubble highs" break off from the weakened Siberian high and move eastward, invariably producing cyclogenesis in the induced trough between the bubble high and the Siberian high.

Changes in the southerly latitudes are more subtle (S-7-4, page 7-26). The mid-Pacific ridge gradually strengthens and moves slowly northward, allowing a similar change in the position of the equatorial trough. The result is a northward shift of the east-northeasterly tradewind belt and increased likelihood of tropical cyclone formation north of the equator.

Figure [illegible]. Spring transition, Philippine Sea. 22 March 1980.

FIGURE S-7-3. SPRING TRANSITION, PHILIPPINE SEA. 22 MAR 80
OSAN AB Visual DMSP: DN: 22/0143 GMT

Synoptic Features: A 1008 mb low is located just off southwestern Japan. The surface observations at this time indicate a second low center near the southern tip of Korea. An area of enhanced convective activity is located east-southeast of Luzon. A weak ridge of high pressure extends from the subtropical Pacific high into the eastern Philippine Sea while strong high pressure remains over Asia.

Satellite Image Features:

1. The frontal cloud band associated with the warm front and extending eastward from the low off southwestern Japan appears better developed and more intense than the cold front which extends south-southwestward to near Taiwan. Surface observations support this appearance: winds of 25 to 30 kt and a temperature range change, from 4-8°C to 17-18°C, are noted within 150 n mi of either side of the warm front, while winds of 15 to 25 kt and a temperature range change, from 17-19°C to 20-22°C, are reported within 150 n mi either side of the cold front. Much colder temperatures (0 to 5°C) are noted about 300-400 n mi west of the cold front over coastal areas.

2. An anticyclonic cirrus plume is seen over the northern Korea area, further evidence of a double low formation.

3. A weak break, visible in the original image, (darker gray shades pinching into the broader sunglint pattern) in the sunglint pattern near 27°N and 135°E is evidence of the surface ridge line over the eastern Philippine Sea.

4. An organized convective cluster is seen southeast of Luzon.

Forecast Aids:

1. The intensity of frontal activity is reflected in the cloud patterns seen in satellite imagery.

2. The development of an anticyclonic curved cirrus plume over the northwestern portion of a cloud mass associated with an upper level trough (500 mb and above) is indicative of cyclogenesis. This cloud pattern occurs with a split in the mid to upper level flow, where there are typically 2 troughs in near north-south alignment that are slightly out of phase. The cirrus plume forms in the deformation zone and on the east side of the out-of-phase troughline (Weber and Walderotter, 1981). In this case the

development of a low north of Japan, coupled with the low off southwest Japan is likely to result in the well documented double low pattern. (See forecast rules from various area air stations.)

3. During the transition seasons, the weather north of the subtropical ridge will be winter-like, while south of it tropical conditions will prevail. Across the southwest to northeast oriented fronts, mid-latitude conditions exist to the south and sub-polar conditions to the north. In this case traveling from the mid Philippine Sea where temperatures are 22-26°C to near Tokyo, about 750 n mi will find temperatures in the 4-8°C range. West of Japan in the Yellow Sea and western Sea of Japan, surface temperatures are generally at or below freezing. Snow showers and structural icing in areas of strong wind/high seas can become problems.

4. E/O as well as all other environmental parameters, including human comfort factors, will change dramatically over the western Pacific region in relatively short time and space scales during the transition seasons. Forecasters beware.

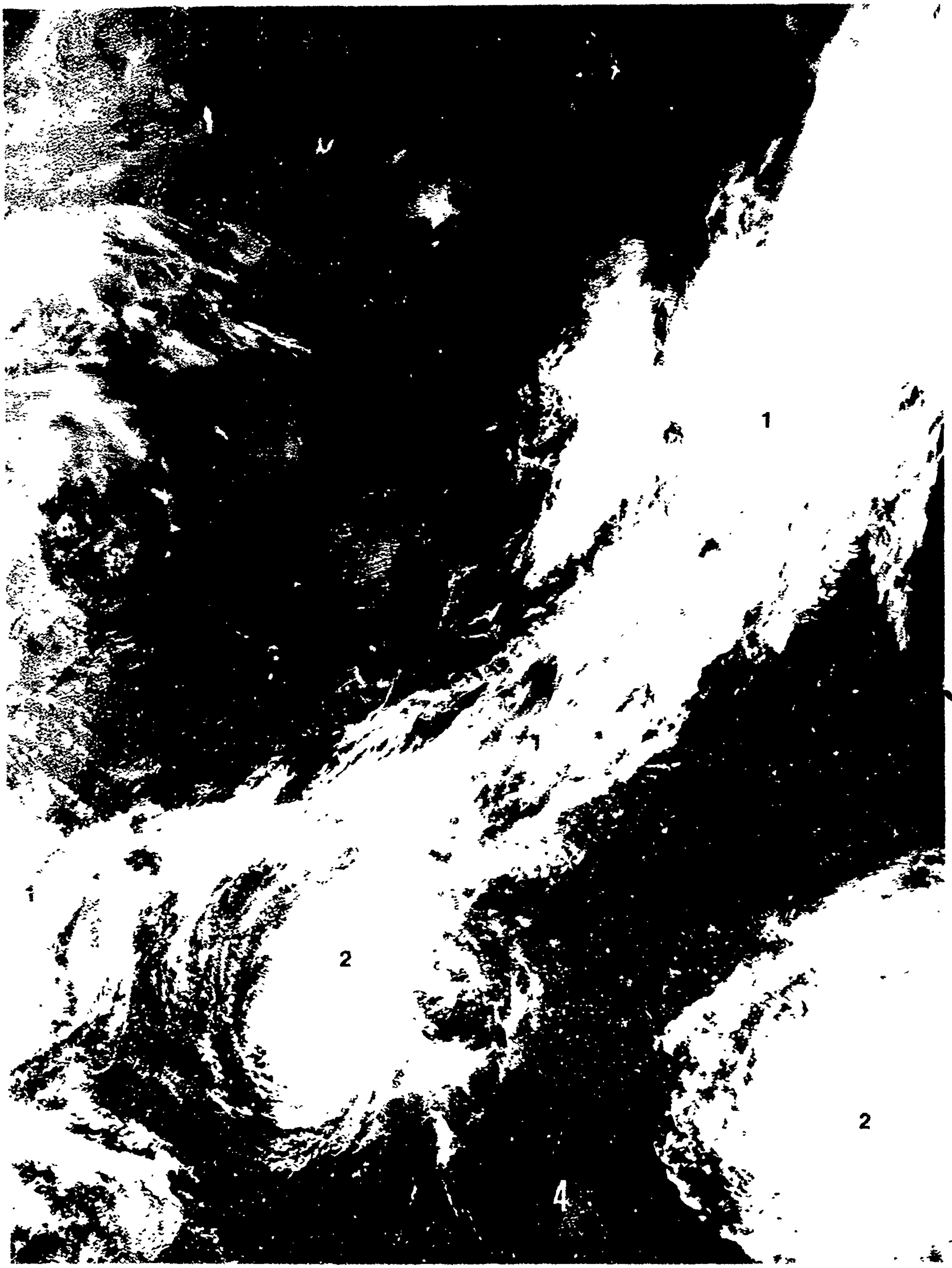

Figure B-7.4 Spring [illegible] view, Philippine Sea. [illegible] May 1980.

FIGURE S-7-4. SPRING REGIONAL VIEW, PHILIPPINE SEA. 18 MAY 80
OSAN AB Visual DMSP: TN: 18/0136 GMT

Synoptic Features: Twin tropical cyclones dominate the southern part of the Sea and the northward migrating Polar Front (Mei-Yu/Bai-U front) extends over the northwestern part of the Sea. Conditions vary from those of tropical cyclone threat, to typical Mei-Yu/Bai-U frontal weather, and from general tropical south of the front to northeasterly monsoon north of the front.

Satellite Image Features:

NOTE: See Figure S-4-6 (page 4-32) for additional comments relative to labels 1-4.

1. The retreating Polar Front Mei-Yu/Bai-U front is quite weak over the Philippine Sea area.

2. The twin tropical cyclones, while of the weaker category, are the dominate features.

3. A small scale convective cloud pattern forms south of Japan where the northerly surface winds flow over the warm Kuroshio Current.

4. The sunglint pattern splits the two TC's. Evidence of a small region of light winds is indicated by the dark gray shade and juxtaposition bright sunglint to the south of a line between the centers of the TC's.

Forecast Aids:

1. The value of polar orbiting satellite imagery is limited by the limited coverage each day. They are of use for making twice daily estimates of position and strength which is of importance when viewing the TC's from some distance. There are also useful indicators of local conditions for local small scale considerations. The distribution of convective cloud lines around the systems gives some evidence of the area of stronger winds. The distribution of strong winds along a line drawn from the bright sunglint area, northwestward across the western TC center and beyond, is indicated by the convective cloud lines to the northwest at a distance about equal to the bright sunglint areas. The development of convective cloud lines typically implies greater than 20 kt (20 to 30 kt are reported in this case) while the bright return implies near calm conditions. This only serves to support the well known dangerous semicircle concept of wind distribution.

7.4.1.1 Synoptic Patterns

Figure 2-6 (page 2-23) depicts the tracks of extratropical cyclones that normally occur throughout the year. Of the six tracks shown, two have tracks which would impact the weather over the northern Philippine Sea during spring: the Shanghai Low (track D), and the Taiwan Low (track F).

The northward migration of the Polar Front is shown in Figure 2-5 (page 2-18). Although it moves northward a considerable distance between March and June, it remains over the Philippine Sea during the entire season. The spring season also sees the formation of the Mei-Yu/Bai-U front over southern China, the southern East China Sea, and the western Philippine Sea. The Mei-Yu/Bai-U front is accompanied by extensive cloudiness and precipitation, making spring the rainy season of the region (Figure S-7-5).

Of the cold frontal types discussed (tracks depicted in Figure 2-7, page 2-26), the western and eastern types are most likely to affect the weather over the Philippine Sea during spring. The likelihood of significant cold frontal impact on the weather over the sea diminishes as the season progresses.

7.4.1.2 Surface Wind

Surface wind speeds over the Philippine Sea gradually diminish as spring progresses, with the overall symmetry of higher wind vs. lower wind areas changing only slightly during the season. During May the frequency of occurrence of winds ≤10 kt is lowest in

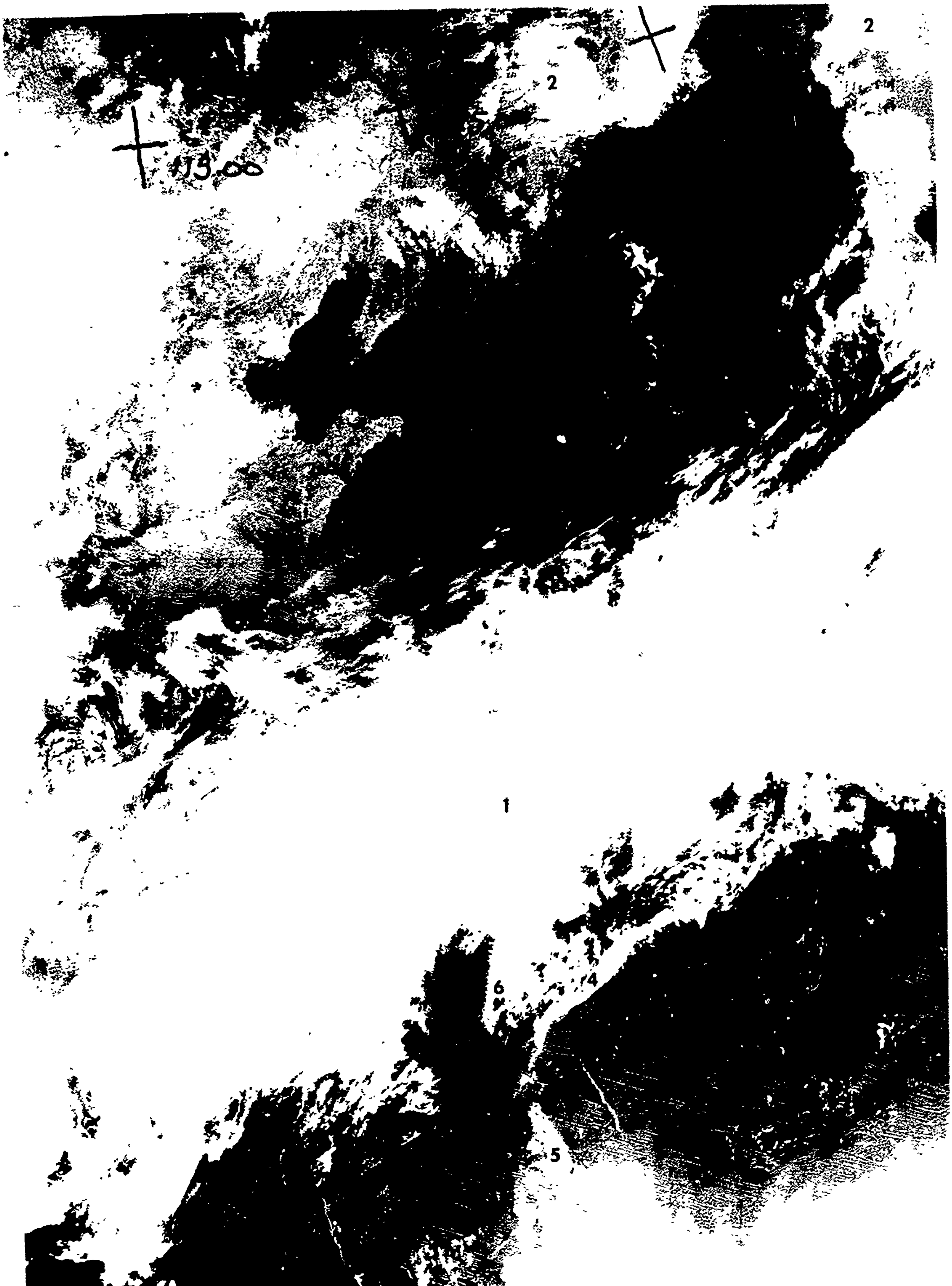

Figure S-7-5. Spring. Mei-Yu/Bai-u Front. [illegible] April [illegible]

FIGURE S-7-5. SPRING, MEI-YU/BAI-U FRONT. 25 APR 80
OSAN AB Visual DMSP: TN: 25/0224 GMT

<u>Synoptic Features</u>: The Mei-Yu/Bai-U front extends from south central China east-northeastward to just south of Japan. A 1024 mb high is centered southwest of the Shandong Peninsula.

<u>Satellite Image Features</u>:

1. The Mei-Yu/Bai-U frontal band dominates the picture (see section 2.2.1.2, page 2-20).

2. Convective cumulus is widespread over the USSR and northern Japan land areas in this late morning/mid day local time image. The cumulus buildups are just starting to show cirrus plumes. Surface observations at 0300 GMT indicate widespread low type 2 clouds with scattered reports of low 3 and 9 and occasional rain showers.

3. Clear skies prevail over the water areas clear of the Mei-Yu/Bai-U front, except for the remains of a land breeze front off eastern Korea.

4. The rope cloud along the leading edge of the cloud band east of Taiwan indicates the area of surface wind shifts. South of it surface winds are southwesterly, to the north they are east-northeasterly.

5. Brilliant sunglint around Luzon and on the Cagayan River of eastern Luzon implies light surface winds at this late morning pass time.

6. Low clouds along eastern Taiwan are filling the coastal valleys and provide evidence of the northeasterly low level flow and cloud levels of that area.

7. Thin cloud lines, as seen over the South China Sea, have been found to be aligned within 20 to 30° of the surface winds in the tropics. In this case indicating the southerly flow of the tropical circulation.

<u>Forecast Aids</u>:

1. The Mei-Yu/Bai-U front is the major weather producer over the waters off eastern Asia during the spring season. While it is an annual event, there are variations from year to year relative to time of passage and intensity. At any given time the front will have areas of enhanced convection and more intense weather migrating along it. These so called pulses generally have cyclic periods of about 18 hours.

2. When rows of small cumulus are seen over land in morning satellite passes, afternoon thunderstorms are likely.

3. Clear of the Mei-Yu/Bai-U front, the over water areas of the marginal seas generally experience mostly clear skies, light winds, and fair weather during the spring period.

4. The shift of surface winds associated with the Mei-Yu/Bai-U front typically occurs near the leading edge of the cloud band. If a rope cloud is present it is a strong indicator of the location of the surface wind shift.

5. A number of image features provides evidence of the surface wind pattern including: Sunglint patterns, rope clouds, thin cloud lines over tropical oceans, and land/sea breeze fronts.

an elongated band south of Japan and in the tropical latitudes east of the Philippines (Figure 2-23, page 2-45). The higher percentages are seen in the central sea in the location of the subtropical ridge between 25°N and 30°N.

Prevailing directions north of 20°N are northerly in March and April, becoming south to southwesterly in June, with May as a transition month. Wind speeds average about 15 kt early in the season, decreasing to 10 kt in June. Over the sea south of 20°N, the northeasterly directions in March veer to easterly in April and remain so through June, except for southeasterlies just east of the Philippine Islands in June. Wind speeds average about 15 kt in March and April, decreasing to 10 kt in May and June.

7.4.1.3 Upper Level Winds

Figures 2-24 through 2-29 (pages 2-46 to 2-48) depict upper level flow patterns for the month of May. The position of the jet stream has shifted slightly northward since February and weakened, although jet stream winds of over 100 kt would not be uncommon along the northern limit of the Philippine Sea.

7.4.1.4 Visibility

Philippine Sea visibility statistics during each month of spring vary only slightly. There is about a 5 percent occurrence frequency of visibility <2 n mi near Japan and less than 5 percent elsewhere. Visibility ≥5 n mi has a frequency of occurrence of about 80-90 percent near Japan, increasing to over 95 percent over the southeastern sea.

7.4.1.5 Cloud Heights/Ceilings

The beginning of the spring season brings a small decrease in overall occurrence of low cloud ceilings (low cloud amounts $\geq$5/8) but average occurrence frequencies vary little during the period April to June. Figure 2-31 (page 2-50), which depicts cloud statistics for May, is representative of the period.

The occurrence of low cloud ceiling <600 ft and/or visibility <2 n mi is about 5 to 10 percent over the northern sea during March and April, but increases to 10 to 20 percent in May (Figure 2-31) and June, due to the Mei-Yu/Bai-U front activity.

7.4.1.6 Precipitation

Precipitation patterns over the Philippine Sea change significantly during spring. In March, precipitation occurrence frequency is about 10 to 15 percent over the northern portion of the sea and 5 to 10 percent in the south, with the approximate snow limit line running east-west about 100 to 150 n mi south of Japan. By April the snow limit line has moved northward out of the area and the frequency of occurrence of precipitation has increased to over 15 percent near Japan. Little change occurs over the southern sea. During May and June, precipitation percentages south of Japan increase to over 20 percent in concert with the northward migration of the Polar Front and the formation of the Mei-Yu/Bai-U front. Precipitation frequency over the southern sea remains at 5 to 10 percent through June.

7.4.1.7 Sea State

Wave heights decrease somewhat during the spring season in agreement with decreasing wind speeds. Wave height statistics for May are depicted in Figure 2-32 (page 2-51).

7.4.1.8 Surface Air Temperature

Spring brings significant warming to air temperatures over the northern Philippine Sea. By May (Figure 2-33, page 2-52), the mean air temperature over Japanese coastal waters has risen to 65°F (18°C), a change of 20°F (11°C) since February. Temperature changes over the warmer southern sea are less, with a 5°F (3°C) rise seen along 20°N, raising the temperature from the 75°F (24°C) of February to 80°F (27°C) in May.

7.4.1.9 Freezing Level

Freezing level altitudes increase considerably during spring, rising to about 11,000 to 12,000 ft over Japanese coastal waters in May (Figure 2-35, page 2-54), a change of over 8,000 ft since February. Changes over the tropical waters south of 20°N are less significant, rising about 2,000 ft to 16,000 ft.

7.4.1.10 Aircraft Carrier Operating Conditions

During early spring, optimum aircraft carrier operating conditions, defined as having a low cloud ceiling ≥5,000 ft (or no low cloud ceiling), visibility ≥5 n mi, and wind 11-21 kt, occur about 20 to 30 percent of the time over all but the extreme southeast portion of the Philippine Sea, where the figure increases to over 40 percent. By May, a large portion of the sea between 25°N and 32°N has less than a 20 percent frequency of occurrence but the remainder of the sea is essentially unchanged.

Poor conditions, defined as having a low cloud ceiling <300 ft, or visibility <1 n mi, or wind <6 or ≥34 kt, have an occurrence frequency of 10 to 20 percent during the entire season, except in the most southerly latitudes during May and June where the percentage increases to 20 to 50 percent, likely due to lack of wind.

7.4.1.11 Seasonal Oceanographic Features

As the air temperatures rise, so do the temperatures of the sea surface, albeit to a lesser degree. The 55°F (13°C) water of coastal Japan during February warms to about 65°F (18°C) by May (Figure 2-34, page 2-53). The southern sea warms about 5°F (3°C), increasing from 80°F to 85°F (27°C to 29°C) in the extreme southern region (Figure S-7-6).

7.4.1.12 Electro-Optical Conditions (See section 2.3.)

The northward migration of the Polar Front during spring results in tropical conditions over the majority of the Philippine Sea. Only in the northwest sector will the conditions be influenced by the Polar Front.

The humid, well mixed tropical air tends to degrade most E/O ranges. Local effects are dominated by air mass convective cloud development. Areas of convergence will result in cloud development and shower activity with subsidence in the intervening clear areas. Some elevated inversions will be found in the clear zones, but they will generally be weak and limited in horizontal extent by the cloud patterns. The frequency of occurrence of elevated ducts or

Figure S-7-6. Kuroshio Current, Taiwan to Japan. 17 April 1980.

FIGURE S-7-6. KUROSHIO CURRENT, TAIWAN TO JAPAN. 17 APR 80
OSAN AB Infrared DMSP: TN: 17/0139 GMT

Synoptic Features: The major oceanic feature is the northward flowing warm Kuroshio Current between eastern Taiwan and south-western Japan where it splits. The warm Tsushima Current flows west and northward through the Tsushima/Korea Strait and the main portions of the Kuroshio flows eastward through the Tokara Strait and then northeastward along southern Japan.

Satellite Image Features:

1. The warm Kuroshio Current (dark shade) extends northeastward from Taiwan to near southwestern Japan.

2. Cooler water is located to the right in the area of the counter current.

3. From the core of the Kuroshio westward, progressively colder (lighter gray shades) surface water is seen.

4. The coldest coastal waters extend southward through the Taiwan Strait.

5. The Kuroshio split, which occurs near 30°N, 130°E, results in warmer water (darker) extending northward towards the southern Sea of Japan and northeastward along southern Japan. Note that the lines of convective clouds tend to start or become enhanced over the warmer water.

Forecast Aids:

1. Under certain atmospheric conditions (cold/dry air) and appropriate enhancement, infrared imagery can display the details of SST features well into the subtropical region.

2. The boundaries of the major currents remain within relatively fixed zones, but small scale eddies and filaments will cause a great deal of variations along the boundaries of these zones.

3. The SST contours of the cold shelf waters of the East China Sea tend to reflect the bathymetry contours. The more extensive the shallows, the larger the area of coldest water.

4. Due to the heating from below the atmospheric convective activity increases when air flows from areas of cold to warm water. The results include, enhanced convective cloud development, a deeper and better mixed marine layer, lifting and general weakening of the inversion near the cloud tops, initial improved visibility and E/O ranges, and increased surface winds and sea heights.

5. In the regions of the cold coastal waters half-channel conditions typically occur. Full-channel conditions persist year round in the Kuroshio Current flow. The boundaries of the main Kuroshio will extend 100's of meters below the surface and have little slope.

6. It is important to recall the impact of atmospheric moisture on SST values and gradients as depicted by gray shades. The colder and drier the air, the more accurate the gray shade depiction. Therefore, the SST patterns are best observed under cold outbreaks. In the warm, humid, tropical regions the patterns can be totally obscured.

superrefraction layers is quite high in the area dominated by the building subtropical high. Average frequencies over the eastern sector are about 70-80%, while over the northwestern sector they are only about 10%. Maximum heights are near 6232 ft (1900 m) over the eastern sector and average about 5248 ft (1600 m) elsewhere. Island barrier effects will result in enhanced E/O conditions downstream from the barriers where relatively dry air is found. These effects and enhanced E/O areas are evident in satellite images.

Local variations in E/O conditions will be forced by SST gradients in the region of the Kuroshio Current. The areas of cold water north of the Kuroshio, and in some years in the large cyclonic cold meander, will stabilize the lower layers of the atmosphere and increase the potential for low level inversion formation.

The following table presents statistical information on duct heights for the regional area and season of interest:

CENTER OF AREA: 20°N 135°E SEASON: SPRING

EVAPORATION DUCT HISTOGRAM IN PERCENT OCCURRENCE

Height (m)	March day	March nite	March both	April day	April nite	April both	May day	May nite	May both
0 to 4	8	7	7	16	12	14	15	12	13
4 to 8	7	10	8	8	13	11	8	14	11
8 to 12	11	19	15	11	19	15	12	21	16
12 to 16	15	25	20	13	23	18	13	22	17
16 to 20	17	22	19	12	17	14	11	15	13
20 to 24	12	10	11	8	6	7	7	7	7
24 to 28	6	4	5	5	3	4	5	3	4
28 to 32	3	1	2	2	1	2	3	2	2
32 to 36	2	1	1	2	1	1	2	1	1
36 to 40	1	0	1	2	0	1	2	0	1
above 40	18	3	10	22	5	13	23	6	15
Ave. Ht.	23	15	19	23	15	19	24	15	19

7.5 Summer (mid-June to mid-September) (See section 2.2.1.7)

The Philippine Sea is free of Polar Front activity from mid-June, when the front migrates northward across Japan, to early September, when the front shifts abruptly southward from its summer position over eastern Manchuria (see Figure 2-5, page 2-18). During the summer the weather over the sea is dominated by the flow of warm, moist, tropical air flowing around the western periphery of the mid-Pacific subtropical ridge, and similar air forced northward across the South China Sea/ Philippine Island area. The summer (southwest) monsoon becomes the dominant factor in determining the weather over the coastal waters of southeastern Asia. Figure 2-36 (page 2-56) depicts a generalized summertime synoptic situation.

7.5.1 Climatology

As summer begins in the Philippine Sea, two weather regimes are evident: the clouds and rainy weather associated with the Mei-Yu/Bai-U front and the northward migration of the Polar Front, and the extensive area south of the fronts dominated by the northward movement of warm, moist, maritime tropical (mT) air.

The Polar Front returns to the Philippine Sea in early September as it moves swiftly southward in response to a strengthening Siberian high pressure cell (Figure 2-5, page 2-18).

The following sections address the average conditions which prevail over the Philippine Sea during the summer months.

7.5.1.1 Synoptic Patterns

Because of the influence of the Southwest Monsoon and the southerly latitudes of much of the sea, extratropical cyclone activity is not commonly observed over the Philippine Sea during summer (Figure S-7-7, page 7-42). Frontal activity is essentially non-existent over the Philippine Sea during July and August while the Polar Front is north of the area.

The monsoon trough/intertropical convergence zone is frequently active with large areas of instability producing extensive cloudiness and precipitation.

Tropical cyclone activity increases during the summer months and continues into autumn. Appendix B includes figures, by calendar period, showing climatologically preferred storm tracks.

7.5.1.2 Surface Wind

The frequency of occurrence percentages depicted in Figure 2-37 (page 2-58) for August are also representative of June and July. September's statistics change slightly, with a 40 percent occurrence of wind ≤10 kt existing over the northeastern Philippine Sea.

Prevailing wind directions during July and August are generally southerly, and have mean wind speeds varying from 5 to 15 kt. By September, wind directions are primarily east to northeast north of the monsoon trough/inter-tropical convergence zone (12°N-15°N) and southwesterly south of the trough. Mean wind speeds are about 10 to 15 kt, with the higher velocities occurring in the vicinity of the Luzon Strait and near 22°N 137°E.

Figure S-7-7. Summer local effects. 18 July 1981.

FIGURE S-7-7. SUMMER LOCAL EFFECTS. 18 JUL 81
Scripps NOAA 6 Visual: DN: 18/2349 GMT

Synoptic Features: A period of weak surface winds during the summer monsoon is occurring. The subtropical ridge of high pressure extends westward across Kyushu, the southern island of the Japanese chain. The circulation around a tropical cyclone is reflected in the southern extremes of this image.

Satellite Image Features:

1. The marked variations from dark areas to brilliant reflection within the sunglint band (right 1/3 of image) indicate the predominance of local, small scale wind features. This lack of large scale forcing is a typical condition during mid latitude summer periods.

2. The subtropical ridge line is clearly indicated by the dark east-west stripes intruding into the north-south sunglint band near the southern end of Kyushu.

Forecast Aids:

1. When the sunglint pattern shows widespread marked variations with juxtaposition dark and brilliant areas, weak large scale forcing is implied and local conditions are dominate. These include land/sea breezes, strong diurnal variations, and afternoon convective activity over land areas.

2. Land/sea breeze fronts will cause local variations in E/O performances in coastal areas, nearly uniform conditions will occur over sea free of areas of scattered showers.

3. Sea surface temperature gradients are minimized during the summer monsoon season. Afternoon effects (1 to 3°C rises in skin temperatures) are likely under near calm conditions.

7.5.1.3 Upper Level Winds

Figures 2-38 through 2-43 (pages 2-59 to 2-61), which depict upper level flow patterns for August, show that the jet stream has moved well north of the Philippine Sea. A ridge lies east-west over the northern sea at about 30°N, bringing the lightest winds of the year to the region. Weak easterly flow exists over the southern sea.

7.5.1.4 Visibility

After June, summer visibility statistics over the Philippine Sea approximate those of August (Figure 2-44, page 2-62). Visibilities ≥5 n mi are observed about 90 percent of the time. As depicted in Figure 2-44, a small area of 5 percent frequency of occurrence of visibility <2 n mi occurs during August near 20°N 130°E, but is absent during other summer months.

7.5.1.5 Cloud Heights/Ceilings

The frequency of occurrence of low cloud ceilings (low cloud amount ≥5/8) decreases markedly after June, averaging approximately 20 to 30 percent across the central portion of the Philippine Sea. The figures increase to about 30 to 40 percent over the northern and southern portions of the sea. Low cloud ceiling <600 ft and/or visibility <2 n mi occur about 5 to 10 percent of the time over most of the sea. Figure 2-45 (page 2-63) depicts cloud statistics for August.

7.5.1.6 Precipitation

After June, when the Mei-Yu/Bai-U and Polar Fronts bring considerable precipitation to the Philippine Sea immediately south of Japan, the frequency of occurrence of precipitation decreases dramatically. Percentages average 10 to 15 percent south of about 25°N and near Japan, and 5 to 10 percent across the central portion of the sea.

7.5.1.7 Sea State

Wave height statistics for the Philippine Sea during summer largely reflect the effect of the persistent 10 to 15 kt wind speeds, with waves ≥8ft (2.5 m) having an occurrence frequency of only about 10 to 25 percent. As shown in Figure 2-46 (page 2-60) however, August statistics include a 10 percentile isoline enclosing a broad area of waves ≥12 ft (3.5 m). Since the mean wind speeds over the area could not produce waves of that size, they are likely due to seas generated by passing tropical cyclones.

7.5.1.8 Surface Air Temperature

As shown in Figure 2-47 (page 2-65), mean surface air temperatures over the Philippine Sea vary by less than 5°F (3°C) from north to south during August. The extreme minimum temperature for the northern sea during August is about 70°F (21°C). The extreme maximum temperature for the southern sea is about 90°F (32°C).

7.5.1.9 Freezing Level

Figure 2-49 (page 2-67), which depicts mean freezing level altitudes during August, shows that freezing levels are 15,000 to 16,000 ft north of 30°N over the Philippine Sea and exceed 16,000 ft south of that latitude.

7.5.1.10 Aircraft Carrier Operating Conditions

Optimum aircraft carrier operating conditions, defined as having a low cloud ceiling ≥5,000 ft (or no low cloud ceiling), visibility ≥5 n mi, and wind 11-21 kt have an occurrence frequency of about 20-30 percent in the Philippine Sea during the summer. Poor conditions, defined as having a low cloud ceiling <300 ft, or visibility <1 n mi, or wind <6 kt or ≥34 kt occur with about the same frequency.

Optimum conditions occur most often in the northwest and northeast sections of the sea while the greatest incidence of poor conditions is seen in the extreme southern portion of the sea, likely due to light winds.

7.5.1.11 Seasonal Oceanographic Features

By August (Figure 2-48, page 2-66), the surface temperature of the Philippine Sea has warmed to 80°F to 85°F (27°C to 29°C) over most of its extent.

7.5.1.12 Electro-Optical Conditions (See section 2.3.)

The Southwest Monsoon dominates the entire Philippine Sea during summer. Tropical conditions, hot and humid, create reduced

E/O ranges. The local variations due to convective cloud development and precipitation will be generally disorganized. The ocean thermal gradients are masked by the heating of surface waters. Night and early morning land breeze fronts will result in diurnal variations of E/O ranges in coastal areas. The occurrence of elevated inversions/ducts is at an annual minimum in the late summer. Heights are also at a minimum as inversions are typically related to night time cooling over land and therefore largely coastal and low in nature. The average frequency of occurrence of elevated ducts or superrefraction layers ranges from about 50% over the eastern central sector (under subtropical high subsidence) to about 25% elsewhere. Heights range from near 3280 ft (1000 m) in most areas to near 5248 ft (1600 m) under the subtropical high flow. Frequency values decrease to the south, west, and north of the subtropical high subsidence pattern.

The following table presents statistical information on duct heights for the regional area and season of interest:

CENTER OF AREA: 20°N 135°E   SEASON: SUMMER

EVAPORATION DUCT HISTOGRAM IN PERCENT OCCURRENCE

Height (m)	June day	June nite	June both	July day	July nite	July both	August day	August nite	August both
0 to 4	17	14	16	8	6	7	5	4	4
4 to 8	10	17	13	7	11	9	4	7	6
8 to 12	12	21	17	11	18	14	8	15	11
12 to 16	13	20	16	14	23	18	15	26	20
16 to 20	10	14	12	15	21	18	18	27	23
20 to 24	7	5	6	9	9	9	11	11	11
24 to 28	4	2	3	6	4	5	7	4	6
28 to 32	2	1	2	3	1	2	3	1	2
32 to 36	2	1	1	2	1	1	3	1	2
36 to 40	1	0	1	1	1	1	2	0	1
above 40	22	6	14	26	5	15	24	4	14
Ave. Ht.	23	14	18	27	16	21	27	17	22

7.6 Autumn (mid-September to mid-December) (See section 2.2.1.8.)

Autumn comes quickly to the northern portion of the Philippine Sea as the Polar Front makes its rapid transit southward. The Northeast Monsoon quickly becomes established as the Siberian high pressure cell strengthens.

7.6.1 Climatology

Rapid and significant changes occur in the weather over the Philippine Sea during autumn. The Polar Front, which in August is located in eastern Manchuria, shifts rapidly southward in early September to a position south of Japan. The strengthening Siberian high continues to force the front southward until it reaches its southernmost position near 18°N in December (Figure 2-5, page 2-18). The Northeast Monsoon becomes the dominant weather feature over eastern Asia, periodically interrupted by migratory extratropical cyclones transiting the area. The autumn season also brings strengthened easterly flow to the tropical area of the sea south of the Polar Front.

The following sections address the average conditions which prevail over the Philippine Sea during the autumn months.

7.6.1.1 Synoptic Patterns

The southward shift of the Polar Front during autumn makes the northern portion of the Philippine Sea more vulnerable to the likelihood of extratropical cyclone activity. Figure 2-6 (page

2-23) depicts the tracks of migratory extratropical cyclones that normally occur throughout the year in the Far East. Of the six tracks depicted, only one, the Taiwan Low (track F), would be expected to affect the weather over the Philippine Sea during the autumn season.

Cold frontal activity over the northern Philippine Sea increases with the progression of the autumn season (Figure S-7-8). Once the Polar Front has moved southward, frontal activity affecting the northern sea is of the western and eastern types.

Autumn brings a decrease in tropical cyclone activity, but a high probability of occurrence extends well into the season. Appendix B includes figures, by calendar period, showing climatologically preferred storm tracks.

7.6.1.2 Surface Wind

Surface winds increase during the autumn season. As shown in Figure 2-51 (page 2-71), winds ≤10 kt occur about 30 to 40 percent of the time over the central Philippine Sea during November, decreasing to less than 20 percent near the Luzon Strait. Gale (≥34 kt) frequency is less than 5 percent during each of the autumn months except December, when the 5 percentile isoline intrudes into the northeastern part of the Philippine Sea south of Japan.

Prevailing directions during November are northwesterly near Japan, veering with decreasing latitude, becoming easterly south of 20°N. Mean wind speeds average about 15 kt, except 20 kt near the Luzon Strait where the effect of the Northeast Monsoon is strongest.

Figure 3-7-8. Autumn, return of the Polar Front. [illegible] October 1979.

FIGURE S-7-8. AUTUMN, RETURN OF THE POLAR FRONT. 20 OCT 79
OSAN AB Visual DMSP: DN: 20/0053 GMT

Synoptic Features: A 960 mb low is centered just off northeast Hokkaido, the associated frontal band extends southward to below 20°N around 140°E. Surface winds in excess of 50 kt are reported off the northeast coast of Honshu, some 600 n mi south of the low center. Reports of 30 kt winds extend over 1000 n mi from the low center along the frontal band.

Satellite Image Features:

1. The vortex cloud pattern dominates this image.

2. The frontal band extends southward from near 45°N, 155°E over the northwest Pacific Ocean area along 150-155°E to about 15°N near 140°E in the Philippine Sea.

3. The westerly flow west of the front reflects the return of the winter circulation pattern while east of the front easterly flow reflecting the summer pattern continues.

4. The frontal band is not well organized, but is composed of a series of cloud lines along which showers and strong gusty type winds are indicated by ship observation.

Forecast Aids:

1. Autumn frontal systems will bring strong northwesterly surface winds (over 50 kt in this case), and showery turbulent weather to the northwest Pacific and northern Philippine Sea areas. Passage of these systems will result in abrupt changes from summer, warm, stable air masses to winter, cold, unstable air masses over the northwest Pacific.

2. Extension of the frontal bands, in the form of shear lines will penetrate southward into the Philippine Sea to below 15°N.

3. The Autumn frontal passages are frequently preceded and followed by migratory highs moving off Asia. These alternating conditions between frontal passages and migratory highs result in basic changes in the E/O environment. Forecasters must be alert to changes from frontal unstable conditions to high cell subsidence stable conditions over relatively short time scales (1 to 3 day cycles) and space scales (500-1000 n mi).

4. Within the circulation of each synoptic pattern (low, front, high) a wide array of preferred meso and local scale conditions will result in additional variations in wind, weather, and stability factors.

5. The extreme ranges of both large scale and small scale atmospheric events during transition seasons in areas of dynamic weather production, such as the northwest Pacific, create a major challenge to marine environmental forecasters. This can be particularly challenging to units that are transiting into the region from operations of relatively stable climates such as the tropics. Transiting forecasters beware.

7.6.1.3 Upper Level Winds

Significant changes occur in upper level wind flow between August (Figures 2-38 to 2-43, pages 2-59 to 2-61) and November (Figures 2-52 to 2-57, pages 2-72 to 2-74). The mean position of the jet stream moves southward to its wintertime position along southern Japan, and the jet stream wind speeds increase to near wintertime levels. Wind speeds slowly decrease south of the jet stream core.

7.6.1.4 Visibility

Autumn visibility over the Philippine Sea is generally good, with a 90 to 95 percent frequency of occurrence of visibility ≥5 n mi over a major portion of the sea for the entire season. The west-central portion of the sea has an occurrence frequency of 80 to 90 percent in November and December. A small area of 5 percent frequency of occurrence of visibility <2 n mi exists in waters adjacent to eastern Luzon in October, and near Taiwan in November and December. Figure 2-58 (page 2-75) depicts visibility statistics for November.

7.6.1.5 Cloud Heights/Ceilings

The occurrence frequency of low cloud ceilings (low cloud amount ≥5/8) increases slowly during autumn, from 20 to 40 percent frequency in September to 30-55 percent frequency in December. Figure 2-59 (page 2-76) depicts cloud amounts for November. Low cloud ceiling <600 ft and/or visibility <2 n mi frequencies of occurrence are essentially constant throughout the season at about 2 to 7 percent.

7.6.1.6 Precipitation

Precipitation frequencies over the Philippine Sea during autumn remain largely constant at 8 to 15 percent over most of the sea, with the higher percentages occurring in a broad band extending east-northeast to west-southwest south of and near to Japan. During November and December a small area exceeding 20 percent exists near Taiwan.

7.6.1.7 Sea State

Wave heights have increased since summer (Figure 2-60, page 2-77). The higher frequencies of occurrence of waves ≥5 ft (1.5 m), ≥8 ft (2.5 m) and ≥12 ft (3.5 m) are seen in the western portion of the Philippine Sea adjacent to the Luzon Strait where the effects of the Northeast Monsoon are the greatest.

7.6.1.8 Surface Air Temperature

Significant cooling of air temperatures occurs by November over the northern waters of the Philippine Sea, with about 61°F (16°C) evident along Japanese coastal waters as shown in Figure 2-61 (page 2-78). During November the extreme minimum temperature over the northern sea is about 46°F (8°C). The extreme maximum temperature for the same month over the southern sea is about 90°F (32°C), essentially the same as during August.

7.6.1.9 Freezing Level

Between August (Figure 2-49, page 2-67) and November (Figure 2-63, page 2-80), the mean altitude of the freezing level decreases by about 7,000 ft to near 9,000 ft over the northern Philippine Sea, about 4,000 ft to near 13,000 ft over the central sea, and about 2,000 ft to near 14,000 ft south of 24°N.

7.6.1.10 Aircraft Carrier Operating Conditions

Optimum aircraft carrier operating conditions, defined as having a low cloud ceiling ≥5,000 ft (or no low cloud ceiling), visibility ≥5 n mi, and wind 11-21 kt, occur about 20 to 40 percent of the time over the Philippine Sea during November, the lowest percentages occurring near Taiwan and in the tropics south of about 10°N. The highest percentages are seen over the eastern sea between 12°N and 20°N. Poor conditions, defined as having a low cloud ceiling <300 ft or visibility <1 n mi or wind <6 kt or ≥34 kt have a frequency of occurrence of about 10 to 15 percent, except less than 10 percent near the Ryukyu Islands and in a broad east-west band between 14°N and 19°N. Percentages greater than 15 occur south of 12°N.

7.6.1.11 Seasonal Oceanographic Features

By November (Figure 2-62, page 2-79) the temperature of the sea surface near Japan has decreased to about 66°F (19°C), a drop of some 14°F (8°C) since August.

7.6.1.12 Electro-Optical Conditions (See section 2.3.)

Autumn will bring the return of the Polar Front to the northwestern sector of the Philippine Sea. Major changes in E/O conditions will occur in the region of the front as well as to the north of the front. The frontal zone and associated cyclone/migratory high patterns will result in day to day variations in the E/O conditions reflecting the changing synoptic pattern. North of the frontal band the relatively cool dry air of the Northeast Monsoon will enhance E/O ranges. Tropical conditions will prevail over the area south of the Polar Front. The average frequency of occurrence reaches an annual minimum with values ranging from 20-40%, generally increasing to the east central area under the subtropical high influence. Heights average near 5248 ft (1600 m) throughout the area.

The following table presents statistical information on duct heights for the regional area and season of interest:

CENTER OF AREA: 20°N 135°E SEASON: AUTUMN

EVAPORATION DUCT HISTOGRAM IN PERCENT OCCURRENCE

Height	September			October			November		
(m)	day	nite	both	day	nite	both	day	nite	both
0 to 4	2	2	2	3	1	2	3	2	3
4 to 8	4	7	5	3	5	4	4	5	4
8 to 12	8	14	11	8	12	10	7	11	9
12 to 16	12	26	19	12	20	16	13	19	16
16 to 20	17	27	22	16	24	20	18	25	22
20 to 24	12	12	12	14	16	15	18	19	19
24 to 28	8	5	6	10	10	10	11	10	11
28 to 32	4	1	3	6	4	5	7	3	5
32 to 36	3	1	2	3	2	3	3	1	2
36 to 40	1	1	1	2	0	1	2	1	1
above 40	30	5	18	23	5	14	13	3	8
Ave. Ht.	30	18	24	28	20	24	24	19	22

8.Ø WESTERN NORTH PACIFIC OCEAN

8.1 Regional Features and Their Influence on Weather Phenomena

By definition, the western North Pacific Ocean is that portion of the Pacific Ocean located north of the equator and west of 18Ø°. Because this handbook is written for use in waters adjacent to Japan and not intended as a broad scale oceanic reference, it is necessary to limit the size of the area to be addressed. Consequently, for the purpose of this handbook the eastern boundary of the western North Pacific Ocean is placed at 16Ø°E and the southern boundary at 2Ø°N. The other boundaries include the southern end of the Kamchatka Peninsula and the Kuril Islands to the north, and Japan and the Bonin Islands to the west. See Figure 8-1.

The topography of Japan is rugged and exerts a significant influence on the weather over the western North Pacific Ocean. The principal mountain chain of Japan, the Japan Alps, is located in the central section of Honshu. See Figure 3-1 (page 3-2). The Alps average 4,921 to 11,483 ft (1,5ØØ to 3,5ØØ m) in elevation, with Mt. Fugi, the highest peak in Japan, reaching 12,388 ft (3,776 m). An extension of the Alps is located in northern Honshu and average 4,921 ft (1,5ØØ m) with the highest peak reaching 6,693 ft (2,Ø4Ø m). A second mountain chain, located on Hokkaido, has elevations commonly exceeding 1,64Ø ft (5ØØ m). Several peaks exceed 3,281 ft (1,ØØØ m) and one peak reaches 7,513 ft (2,29Ø m). A third Japanese mountain chain is on the Japanese island of Kyushu.

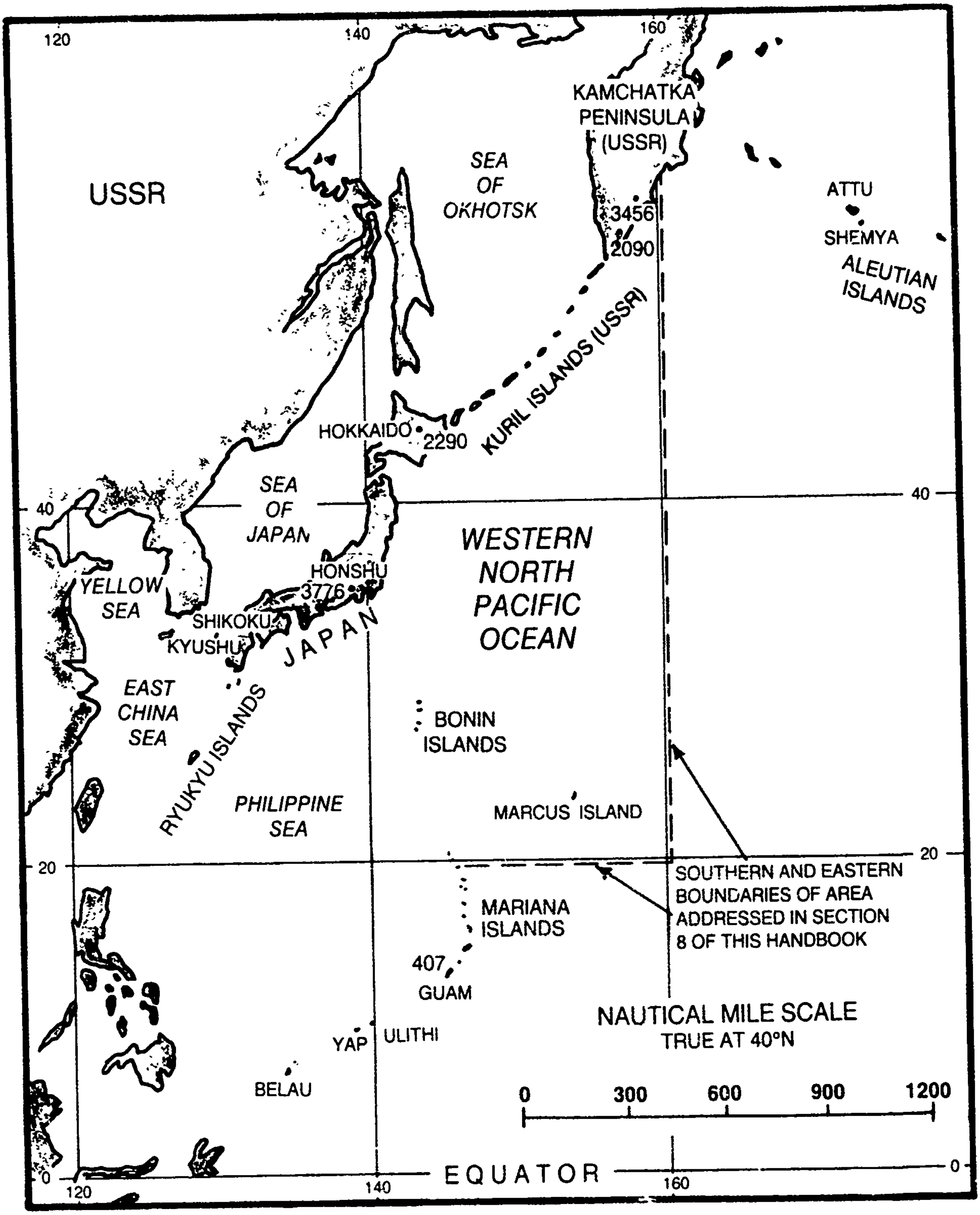

Figure 8-1. Western North Pacific Ocean.

Extratropical cyclones rarely cross Japan. Instead, they move northward along the northwest coast of Honshu on the Sea of Japan or skirt south of Japan along the coasts of Kyushu, Shikoku, and southern Honshu before moving northeast. Frontal systems associated with passing extratropical cyclones usually follow specific patterns. Warm front movement will be retarded by the mountains, causing an occlusion as the faster moving cold front overtakes it. Cold and occluded fronts are slowed on the windward (upward) slopes of the mountains and accelerated on the lee (downward) slopes, where they often lose typical weather and cloud characteristics as the cold air is warmed by adiabatic compression.

Once the "dry" fronts reach the Kuroshio Current (Figure 2-4, page 2-11) they regain moisture and reintensify (FWC/JTWC, 1978). Another effect of the topography of Japan is the formation of strong dynamic troughs which are formed in the lee of the mountain ranges under conditions of strong zonal flow aloft.

As is the case with much of eastern Asia, the veering of low level winds during frontal passage is frequently masked or delayed when a reporting station is situated in a valley having the same orientation as the front. Consequently, frontal velocity can be misinterpreted by an inexperienced meteorologist. The tracking and forecasting of any pressure system moving through eastern Asia (including Japan) is made difficult by the terrain. Wind directions can be unreliable when the speed is less than 15 kt. Temperatures and dew points can be misleading due to the complex topography. As documented by FWC/JTWC (1978) regarding analysis and forecasting of weather systems moving across eastern Asia, "Successful and accurate surface frontal analysis can only be achieved by careful analysis of the 850 mb level. At this level the elements of wind direction, temperature, dew point, etc., are relatively more accurate..." and discontinuities between air masses are more easily seen.

Except for the southern tip of the Kamchatka Peninsula, the remainder of the land areas adjacent to the western North Pacific Ocean exert minimal and mostly localized effects on the weather of the region. The mountains of the Kamchatka Peninsula, the Koryak Range, are oriented north-south. See Figure 6-1 (page 6-2). With elevations commonly exceeding 8,202 ft (2,500 m), the mountains pose a significant barrier to passing weather systems. A common result is a "Skaggerak depression", or splitting of a low pressure system. The primary low center remains over the Sea of Okhotsk west of the Kamchatka Peninsula while the "Skaggerak depression" or secondary low pressure center forms at the north end of the portion of the frontal system that continues its unimpeded eastward progress south of the peninsula.

In addition to the effect of the land areas adjacent to the western North Pacific Ocean, the ocean surface itself exerts a significant influence on the weather of the region. The warm Kuroshio Current, discussed in section 2.1.3.2, leaves the Philippine Sea and enters the western North Pacific Ocean near the Japan coast at about 36°N, flowing generally east but with a meandering path. It remains a relatively narrow concentrated current until it reaches approximately 160°E, where it transforms into the weak, broad North Pacific Current. The Kuroshio Current acts as a relatively warm moisture source for extratropical cyclones and/or fronts crossing or passing south of Japan, and can cause rapid intensification of the systems.

8.2 Western North Pacific Oceanographic Features

For this study the western North Pacific is limited to the ocean area west of 160°E and north of 20°N with the other boundaries consisting of the Bonin, Japanese, and Kuril Islands and Kamchatka Peninsula. The north-south extension along the eastern boundary is over 1800 n mi and the east-west maximum distance is about 800 n mi off northern Honshu.

The eastern, southern and southwestern boundaries are open sea, the Japanese Islands of Honshu and Hokkaido form the western boundary and the Kuril Island Archipelago and southern tip of Kamchatka the northern boundary. There are no islands within this area other than boundary and coastal islands.

Special Regional Features

The following hydrographic phenomena are considered to have significant potential for impact on naval operations:

(1) Kuroshio Extension and Oyashio Currents,
(2) the Perturbed Area,
(3) the extreme north-south oceanic thermal variations, and
(4) the deep trenches and basins.

Kuroshio Extension and Oyashio Currents: The Kuroshio Extension is the continuation of the Kuroshio Current eastward from near 140°E and the east coast of Honshu. It has a meandering course between latitudes 35°-38°N. In the region of the main current it has a thickness of about 400 m. The surface layer is always warmer than 15°C and is commonly 20°C or more to depths of 100 m. The meandering path of the Kuroshio Extension forms a transition zone between the cold water mass to the north and the warm subtropical water mass to the south. The amplitudes of the meanders are from 80 to 240 n mi with wavelengths of 300 to 500 n mi.

The Oyashio Current first flows southward along eastern Hokkaido and then turns eastward between 40-43°N. A segment of cold current flowing southward along the Kuril Islands is sometimes considered part of the Oyashio, but is also known as the Kuril Current.

Perturbed Area: The Perturbed Area is the boundary between the warm Kuroshio Extension Current and the cold Oyashio Current to the north. The area is on the order of 200-300 n mi wide, with its greatest width generally such off eastern Honshu. The axis of the Perturbed Area extends eastnortheastward to beyond 160°E. This boundary areas is typically composed of a series of eddies and meanders. The warm eddies (typically anticyclonic) that are larger than 80 n mi in diameter tend to be nearly stationary while those smaller than about 80 n mi, are apt to move northeastward and become weaker or diffused. The larger warm eddies, on the order of 150 n mi diameter will have lifetimes of a year or more. The velocity of the surface currents around these large eddies is about 3 kt while around the smaller eddies it is about 1 kt. The larger warm eddies significantly modify the water column to depths of 500-600 m and to lesser degrees below that.

The largest and most stable large warm eddies periodically form near 38°N, 143°E just off the eastern coast of Honshu. These large eddies with diameters of about 150 n mi are formed when large northward meanders of the Kuroshio Current break off from the main current. It has been noted that this pattern is likely to develop in association with frequent and/or strong atmospheric cyclonic disturbances tracking just south and east of Japan. The eddies are most apt to form during the spring and summer when the Kuroshio Current transport is at its maximum.

In general the Perturbed Area will exhibit marked hydrographic variations in relatively small horizontal distances (10-100 n mi) and in short time frames (days). The large eddies are an exception to this general rule, but still in fact reflect anomalous conditions compared to their immediate surroundings.

Extreme North-South Oceanic Thermal Variations: The change of hydrographic properties, thermal in particular, across the Kuroshio Extension and Oyashio Currents are some of the largest found in the open oceans. The thermal variations are most pronounced below the level of the seasonal surface layer warming (about 100 m) and above the deeper stable waters (1000-1500 m). A sample of the depth of the 10°C isotherm and the temperature at 300 m near 155°E from 31°N to 39°N reflects the marked thermal changes across the Kuroshio/Oyashio boundary:

Lat.	10°C depth	Temp. at 300 m
31°N	610 m	17°C
33°N	550 m	16°C
35°N	110 m	6°C
37°N	100 m	5°C
39°N	70 m	5°C

The gross structure of thermal features across this boundary zone can be detected in satellite infrared imagery during the seasons when the surface has not been heated sufficiently to mask the surface thermal contrasts (winter and spring). It should be noted that even in late summer and early autumn when the surface waters are quite uniformly heated, below the relatively thin seasonal mixed layer the strong thermal contrasts of the large scale water masses still exist.

The oceanic thermal structures in this zone create a number of challenges to environmental forecasters including:

(1) variations in low level atmospheric stability, cloud cover, visibility, and wind speeds,
(2) variations in surface wave conditions because of wind speed changes, energy transfer, and current direction changes around eddies and meanders, and
(3) significant variations in ASW related conditions over relatively small time and space frames.

Deep Trenches and Basins: The majority of the western North Pacific lies over deep basin areas. Several trenches ring the western boundary. The Kuril Trench (8,500 m) parallels the Kuril Island Chain on the Pacific side. The maximum depths are found off Hokkaido northward to the central Kuril Islands. The Japan Trench (10,500 m) is located just east of northern Honshu and continues southward to near 30°N. Continuing southward, the Bonin Trench (8,660 m) is found along the eastern edge of the Bonin Island Chain. All three of these trenches are to some degree a continuation along the western edge of the deep Pacific Basin which averages 5,000-6,000 m in depth.

West of these deep trenches the bottom slopes tend to be quite extreme as the ocean bottom rises rapidly to the relatively shallow continental shelf off Japan and the coastal areas of the Kuril and Bonin Island Archipelagos. Areas of steep bottom slopes create special problems in ASW operations. These bottom conditions when coupled with the areas of significant thermal variations are most difficult regions for ASW operations and forecasts.

Bathymetry: The majority of the ocean area addressed in this section is comprised of open ocean deep basins. The trenches and paralleling shallow areas along the western boundary are addressed above in special features.

Currents: Addressed as a special feature.

Sea Ice: The only sea ice that occurs in this region will be that which is advected out of the Sea of Okhotsk and flows southward along the Kuril Islands to the vicinity of the northeastern coast of Hokkaido. This will be found only in near coastal areas during spring and is of little concern to deep water vessels.

Temperature and Salinity: The temperature and salinity patterns reflect those of the open ocean major water masses. North of the Perturbed Area (near about 40°N) the Subarctic Water mass is found and is characterized by an average temperature between 2°C and 4°C and a salinity which near the surface may be as low as 32.00 ‰ but increases to approximately 34.00 ‰ at a depth of a few hundred meters and below that depth increases slowly to about 34.65 ‰ at the bottom. South of the Perturbed Area the water mass configuration becomes too complex to describe in detail. The general configuration is for the Kuroshio Waters with temperatures near 17°C and salinity near 34.8 ‰ to be found in the upper levels over Intermediate Waters which are characterized by a salinity minimum between 34.0 ‰ and 34.1 ‰.

The warm season heating creates a seasonal mixed layer which masks the water mass thermal properties at the surface and in infrared thermal images.

Sound Velocity Channel: The depth of the sound channel axis rises rapidly northward across the Perturbed Area. It is very near the surface north of about 42°N during the warmer months as a result of the surface warming and the near-surface sound speed maximum and resultant shallow minimum. During the colder months, the minimum reaches the surface and the channel disappears north of 42°N. Sound energy is then transmitted by half-channel mode with the entire water column functioning as a duct.

Throughout the year, the deep sound channel axis south of the Kuroshio Extension Current is found near 1300-1450 m in the western part of the area decreasing to about 1150-1200 m near 160°E. The most rapid rise of the deep sound channel axis is found between 140°-150°E where it changes from about 1400 m near 35°N to 200 m near 38°N. East of 150°E the change in depth fans out over about 6-8° latitude, but is still an area of rapid change. As noted earlier, the deep sound channel generally reaches the surface near and north of 42°N. This condition is modified by the warm season thin mixed layer which reaches a thickness of approximately 100 m in late summer and autumn.

The ranges to first convergence with a 50% probability of convergence have been computed for regions with depth excess of at least 400 m. In general the pattern is similar to the pattern of the deep sound channel axis depth. South of 35°N the range is about 64-66 kiloyards. During winter the range decreases northward to about 25-30 kiloyards near 40°N. In summer the ranges near 40°N are only reduced to 58-60 kiloyards and are 40-42 kiloyards around 45°N. In general the range shortens northward and disappears altogether where the sound speed minima are at the surface (i.e., north of about 43°N during the colder months).

8.3 Winter (mid-December to mid-March) (See section 2.2.1.5.)

Because of the considerable extent of the western North Pacific Ocean, it is subject to a wide variation of winter weather. The northern latitudes are dominated by the Siberian high pressure cell, which brings cold, Arctic air to the region (Figure S-8-1). The middle latitudes experience a mixture of influences as the area is frequently traversed by migratory extratropical cyclones, while the southern latitudes experience strengthened, warm trade winds. Figure 2-8 (page 2-29) depicts a generalized wintertime synoptic pattern.

8.3.1 Climatology

Winter arrives early to the northern part of the western North Pacific Ocean. The strengthening Siberian high pressure cell begins to influence the region as early as September and, with a shortened autumn season, winter begins by mid-November. The Siberian high is resident near Lake Baikal during the winter, and is at its greatest strength during January and February. The Aleutian low is well established east of the Kamchatka Peninsula near 53°N 170°E and is also at its strongest during January and February. A semi-permanent area of low pressure, sometimes evident only as a trough, becomes established over the eastern Sea of Okhotsk. It forms an anchor for a semi-permanent thermally induced trough which normally extends southwestward into the Sea of Japan.

Figure 8-8-1. [illegible]

FIGURE S-8-1. WINTER COLD OUTBREAK. 6 FEB 80
Visual DMSP: DN: 06/0006 GMT

Synoptic Features: A large 985 mb low near 39°N, 155°E and an intense 1064 mb Asian high are causing a strong northerly flow and an outbreak of cold air over the Sea of Japan and adjacent seas.

Satellite Image Features:

1. The widespread numerous cloud lines vividly depict the intensity of this cold air outbreak. Air temperatures at or below freezing covered the entire Yellow Sea, Sea of Japan, Sea of Okhotsk, and portions of the open Pacific north of about 40°N on this day in February 1980. Sustained surface winds were in the 20 to 40 kt range.

2. The local funneling patterns of valleys and breaks in the terrain are clearly indicated by the length of cloud free paths seaward and downwind from the terrain features. Cloud free paths are shorter downwind from valleys or low elevation terrain where minimum drying of the air during flow down the terrain slope to sea level has occurred.

3. Small scale vortices, likely terrain induced, are evident in the northern Sea of Japan.

4. The buildup of clouds on the windward side, and pronounced drying on the lee side is frequently seen over Japan and off the Asian continent.

5. A change in the cloud south and east of Japan indicates the change in low level flow from cyclonic to anticyclonic curvature.

6. Continuing downwind in the area of anticyclonic flow, the clouds take on a flat topped, closed cellular pattern, becoming continuous smooth topped, layered, stratiform type.

7. Variations in the mean vertical wind shear through the cloud layer result in three convective cloud regimes: (7a) Cellular under light shear, (7b) transverse bands with moderate shear, and (7c) longitudinal bands with strong shear.

8. The cloud lines change from lines parallel (longitudinal bands) to the wind shear through the cloud layer to rows of clouds perpendicular (transverse bands) to the wind shear in several areas of the image indicating weakening shear through the cloud layer (not labeled).

9. The length of the cloud free path increases with an increase in the upwind terrain height and decreases with the strength of the winter monsoon. These relationships are a result of increased drying of air during extended downslope flow and enhanced

thermodynamic effects (moisture flux and heating from below) during extreme cold and high wind conditions of strong outbreaks (not labeled).

Forecast Aids:

1. The intensity of cold air outbreaks is reflected in satellite imagery by the convective cloud regimes. Areas of strong outflow are marked by longitudinal bands, the stronger the outbreak the longer and wider the longitudinal bands.

2. Over the western Sea of Japan, the length of the cloud free path downwind from the western coastline will vary from less than 30 n mi under strong outbreaks to 180-240 n mi under weak outbreaks.

3. Opposite valleys and low terrain, the cloud free distances will be relatively small compared to areas opposite high terrain.

4. During winter outbreaks the dew points over USSR will be below -20°C, increase to about -10 to 0°C over Japan, and reach 10°C about 300 n mi south and east of Japan. Air temperatures will closely reflect the SST except near the coastlines and over terrain where lower air temperatures will reflect the source region and elevation factors.

5. The change from longitudinal to transverse to cellular convective cloud patterns reflect decreasing wind shear through the cloud layer. Typical values are: Shear greater than 4-5 kt/1000 ft results in longitudinal bands, for 3-4 kt/1000 ft transverse bands, and for less than 3 kt/1000 ft cellular clouds.

6. Under moderate or stronger outbreaks, light snow showers will occur over the eastern Sea of Japan, increasing in intensity to heavy showers along western Japan. Two regions of frequent enhanced convective clouds and shower activity have been noted near 40°N, 135°E and off the northwest corner of Sado Island. These are likely associated with SST pattern boundary regions.

7. Generally the length of the cloud free path will increase from the northern to southern portion of the western Sea of Japan.

8. Heavy snow will fall over western Japan under cold outbreak regimes, with deposits measured in feet over the western slopes of mountainous areas.

9. For E/O forecasts the best ranges will be in the regimes of cloud free and shower free areas. Conditions will vary between the alternating longitudinal/transverse bands. These bands have width dimensions of 10 to 60 n mi with 20 to 30 n mi widths being typical.

10. Improved E/O ranges in coastal regions will be found downwind from high terrain, in the lee of island barrier effects, and in the clear slots between cold bands.

11. A lee side pressure trough will typically be found off the Asian coast during cold outbreaks, with drops of 3-4 mb's typical.

12. During winter outbreaks the length of cloud free distances to the lee of the Japan Islands is near zero where the coastal $T_a = 0$. As the T_a decreases the cloud free path increases appreciably, reaching lengths of near 200 n mi where coastal T_a's are -15°C or less.

13. The wind profiles through the three convective cloud patterns all tend to show maximum speed shear in the layers below and immediately above the cloud layer. The profiles differ in that through longitudinal regimes the <u>shear is nearly constant</u> from the surface to approximately 3000 ft, while winds increase from surface speeds to as much as 60 to 70 kt at 3000 ft. Through transverse banding the <u>speeds are nearly constant</u> through the cloud layer, while in cellular regimes the <u>speed may actually decrease</u> through the cloud layer. In the latter two cases (transverse and cellular) the resulting wind shears (just above and just below with little or no shear through the cloud) may be of greater threat to aircraft than the case of the continuous shear through the longitudinal cloud layers.

14. The changes in convective cloud regimes shown in satellite imagery provide insights on forecasting low level turbulence due to wind shear.

Farther south, the influence of the Siberian high is moderated as migratory extratropical cyclones transit the area, commonly moving eastward along the south coast of Japan before entering the western North Pacific Ocean. Cold outbreaks frequently follow the passage of major winter cyclones.

The mean position of the Polar Front is near 20°N in the southern latitudes of the western North Pacific Ocean (Figure 2-5, page 2-18). Weather south of the front is dominated by typical tropical conditions -- warm, east-northeasterly trade winds. Precipitation is at a minimum as winter is the driest season for the tropics.

The following sections address the average conditions which prevail over the western North Pacific Ocean during the winter months.

8.3.1.1 Synoptic Patterns

Figure 2-6 (page 2-23) depicts the mean tracks of extratropical cyclones that normally occur during the year. Of those depicted, three typically affect the weather over the western North Pacific Ocean during winter: the Lake Baikal Low (track B), South Mongolia Low (track C), and Taiwan Low (track F).

Cold frontal activity continues throughout the winter in the northern and middle latitudes of the western North Pacific Ocean as cold outbreaks follow migratory extratropical cyclones transiting the area. As the fronts move southward into the tropical latitudes, they lose many of their cold frontal characteristics and become "shear lines". With a strong polar outbreak they will progress well into the tropics, occasionally passing south of Guam, which is located about 13.5°N 144.8°E.

8.3.1.2 Surface Wind

January is the month of highest wind velocities over the western North Pacific Ocean. Mean speeds of 25 kt occur from 35°N to 40°N between 150°E and 155°E, with 20 kt common elsewhere north of 30°N. The lightest winds -- mean speed about 15 kt -- occur south of 30°N. The other months of winter, including February (Figure 2-9, page 2-31), have slightly lower mean windspeeds. Gale (winds ≥34 kt) frequency is approximately the same for all months after December, with 10 percent or greater existing over most of the area north of 30°N. North to northwesterly winds prevail north of 35°N. Prevailing directions south of 35°N veer with decreasing latitude, becoming northeasterly south of 25°N. One exception to the above occurs during December, when an east-west band of westerly winds exists between 30°N and 35°N, sharply veering to northeasterly south of 30°N.

8.3.1.3 Upper Level Winds

The area near southern Japan is known to have the strongest and most persistent wintertime jet stream velocities in the world. The strong winds extend eastward from southern Japan over the western North Pacific Ocean. Figures 2-10 through 2-15 (pages 2-32 to 2-34) depict upper level flow patterns for the month of February.

It can be seen that although the strongest winds in the upper levels are near 35°N, relatively high velocities occur across a broad area, from about 25°N to 40°N.

8.3.1.4 Visibility

Figure 2-16 (page 2-35) depicts visibility statistics during February. Winter is a season of relatively good visibilities over the western North Pacific Ocean. Poorest visibility occurs in the northern latitudes, with ≥5 n mi having a frequency of occurrence of about 60 percent near the Kuril Islands, improving to over 95 percent in the southern latitudes. Visibility statistics vary only slightly between each of the winter months.

8.3.1.5 Cloud Heights/Ceilings

Wintertime cloudiness, which is depicted in Figure 2-17 (February) (page 2-36), does not vary much between the individual winter months. Maximum occurrence of low cloud ceiling (low cloud amount ≥5/8) is observed in the northern latitudes near the Kuril Islands, while the minimum occurrence is observed in the tropical latitudes. Similar distribution occurs for percent frequency of occurrence of low cloud ceiling <600 ft and/or visibility <2 n mi.

8.3.1.6 Precipitation

Little variation exists in precipitation patterns over the southern portion of the western North Pacific Ocean during winter, with occurrence frequencies generally in the 5 to 15 percent range south of about 30°N. North of 30°N, maximum precipitation percentages are seen in January and February, increasing from about 15 percent at 30°N to over 40 percent near and east of the Kuril Islands.

The approximate southward limit of snowfall is about 30°N. Snowfall percentages of precipitation occurrence increase sharply north of 30°N, reaching over 90 percent along the Kuril Islands.

8.3.1.7 Sea State

Figure 2-18 (page 2-37) depicts wave height statistics for the month of February. The greatest incidence of higher seas occurs in the eastern portion of the western North Pacific Ocean in the area where developing extratropical cyclones moving eastward south of Japan would be expected to intensify and generate high winds/seas.

8.3.1.8 Surface Air Temperature

Because of its considerable north-south extent, winter air temperatures over the western North Pacific Ocean vary greatly. During February (Figure 2-19, page 2-38) mean surface air temperatures range from about 23°F (-5°C) near the Kamchatka Peninsula to 77°F (25°C) along 20°N.

The extreme minimum temperature during February near the Kamchatka Peninsula is about 1°F (-17°C). The extreme maximum temperature during February along 20°N is about 84°F (29°C).

8.3.1.9 Freezing Level

As can be seen in Figure 2-21 (page 2-40), the altitude of the freezing level during February over the western North Pacific Ocean varies from the surface (north of 40°N to 45°N) to over 12,000 ft near 20°N.

8.3.1.10 Aircraft Carrier Operating Conditions

Optimum aircraft carrier operating conditions, defined as having a low cloud ceiling ≥5,000 ft (or no low cloud ceiling), visibility ≥5 n mi, and wind 11-21 kt, occur between 5 and 30 percent of the time during February. The lowest frequency, 5 to 10 percent, occurs over the central portion of the western North Pacific Ocean between 37°N and 45°N from 150°E to 160°E. The higher frequencies, over 20 percent, occur near the tip of the Kamchatka Peninsula, along Japan, and south of about 32°N.

Poor conditions, defined as having a low cloud ceiling <300 ft, or visibility <1 n mi, or wind <6 or ≥34 kt, occur 10 to 30 percent of the time. The lowest frequency occurs near 20°N, with 30 percent occurring near the Kamchatka Peninsula.

8.3.1.11 Seasonal Oceanographic Features

As shown in Figure 2-20 (page 2-39), wintertime sea surface temperatures over the western North Pacific Ocean range from near 30°F (-1°C) near the Kamchatka Peninsula to about 77°F (25°C) at 20°N.

The approximate maximum extent of 0.1 or greater sea ice lies seaward of, and roughly parallel to, Hokkaido and the Kuril Islands. The only consistent area of ice coverage greater than 0.1 lies along the eastern coast of the Kamchatka Peninsula.

8.3.1.12 Electro-Optical Conditions (See section 2.3.)

The E/O conditions of the western North Pacific during winter will exhibit extreme variations in day to day ranges. Several environmental features combine to produce this condition of large short term variability:

(1) a region of maximum jetstream activity and strength,
(2) strong low level baroclinic zones, and
(3) steep SST gradients.

These result in a region of maximum cyclogenesis, fast moving storms, and the large day to day variations.

The variability will extend from the near surface conditions to the upper troposphere. Generally the atmosphere will be in a well mixed condition and E/O conditions will be near normal. However, those systems sensitive to precipitation will have frequent periods of reduced ranges during passage of frontal systems and following shower activity. When bubble highs break and move off Asia, low level inversions will occur in regions of subsidence and potential ducting (see Figure S-8-1, feature #6, page 8-12). When major outbreaks of cold air occur the cold flow will extend eastward beyond Japan and patterns of convective cloud lines will result in significant small scale low level variations in E/O conditions. In addition to the atmospheric variability, the ever present contrasting warm Kuroshio Current and cold Oyashio Current in concert with the intervening Perturbed Area contribute to the low level variability in E/O (see Figure S-8-2).

Areas of elevated ducting will typically be found in the trailing edges of frontal bands and will be evident in satellite images by the presence of smooth topped low and middle cloud decks. The frequency of occurrence of elevated ducts or superrefraction layers varies widely from less than 10% over the northern sector to greater than 70% in the extreme southern latitude of this area (near 20°N). The change in frequency correlates closely with the SST/ocean current patterns, changing from 30% south of the Perturbed Area to less than 10% north of it. Heights are quite uniform averaging near 5900 ft (1800 m) over most of the area with a minimum near 4264 ft (1300 m) off eastern Honshu.

6 APR - AM

4 ID CVN-65; FTV 7540; AM; ASCEND REV 1502; PB; DATE 83-095; TR 19:30:30; DATA TYPE TF 6 BIT; SCALE X2; MIDPN

MOD: T-EXPD, T1-255/T2-277 ; TN 19:20:01; LN 196.50; ROLL +.000; ALT 442.5; SYS POS: LAT +00/LONG 000; +

RIL 1983 A.D. AG2 JONES

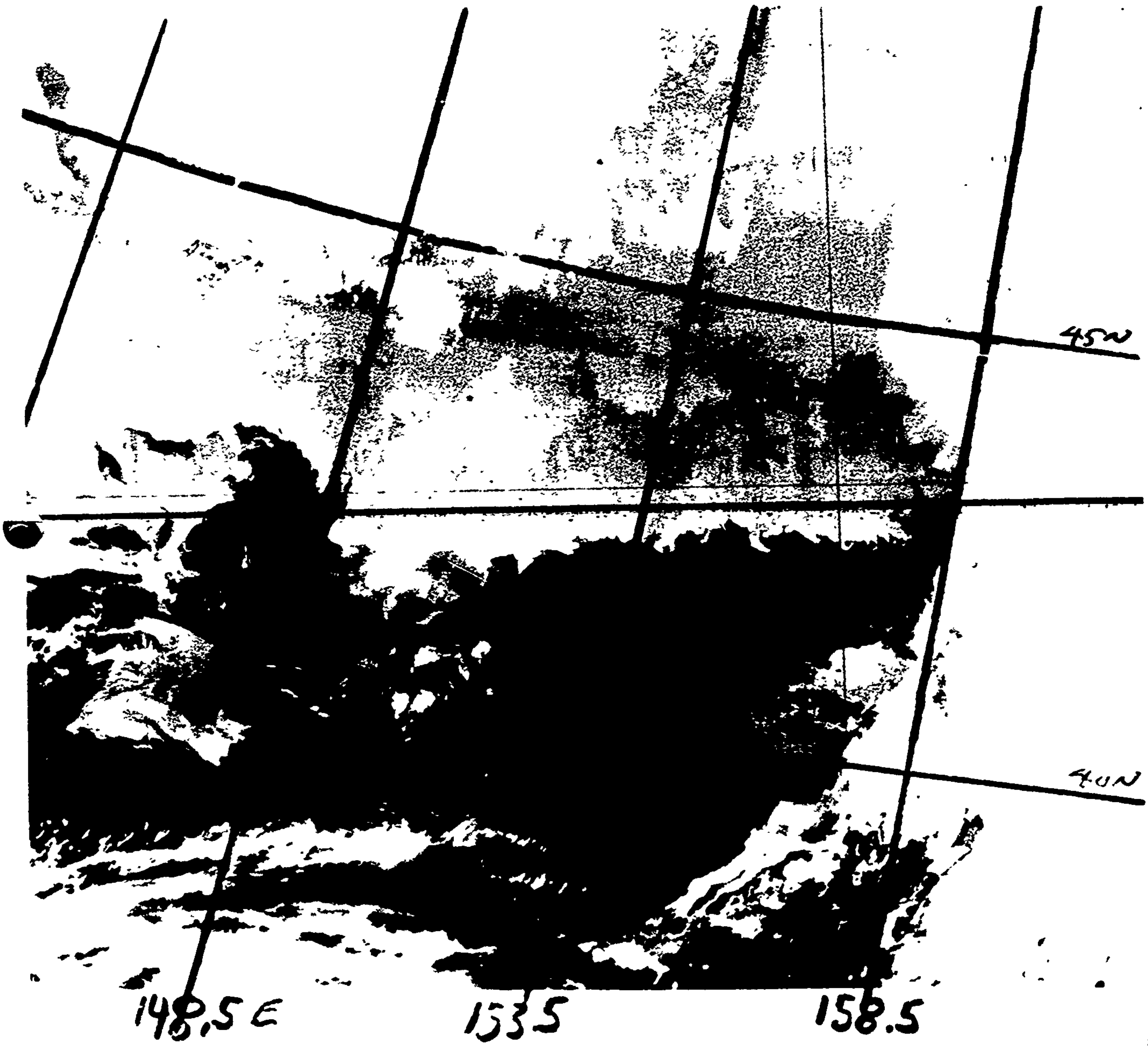

Figure 8-8-2. SST Perturbed Area, Northwest Pacific. 6 April 1983.

FIGURE S-8-2. SST PERTURBED AREA, NORTHWEST PACIFIC.
6 APR 83
USS ENTERPRISE (CVN 65) Infrared DMSP: TN: 05/1930 GMT

Synoptic Features: The feature of interest in this picture is the ocean SST gradient east of Japan between 40-45°N. This gradient reflects the boundary zone between the eastward extension of the Kuroshio warm current and the cold waters to the north.

Satellite Image Features:

About 7 shades of gray, representing approximately 11°C, are seen across about 300 n mi in the cloud free area of this image. Cloud features extend along the southern (bottom) edge, up the right side and across the top. The center portion is nearly cloud free.

Forecast Aids:

1. The SST perturbed area, which reflects the boundary between the warm Kuroshio and cold waters north of 40-45°N, extends eastward from Japan beyond 160°E.

2. Radiation temperatures from the sea that are sensed by infrared sensors are lowered due to atmospheric attenuation. The reduction is not linear due to wavelength variations of radiative transfer through the atmosphere. The warmer temperatures are attenuated more than the lower ones. The result is to suppress SST gradients.

3. It has been calculated that an 8°C SST difference, when viewed vertically through the 30°N July standard atmosphere, would be recorded as less than 3°C difference.

4. The best atmospheric conditions for viewing SST gradients are dry and cold, such as behind cold fronts. The worst are moist and hot, such as tropical air masses. Better SST definition is found during the cold season and at higher latitudes.

5. In regions where the SST contours run north-south, like along the Kuroshio between Taiwan and Japan, the north-south change in air mass properties will tend to suppress the SST gradients at the lower latitudes. In the imagery it may appear as though the SST becomes horizontally uniform, but this is not likely in areas where known boundaries of currents exist. This is less of a problem in areas like the perturbed area, seen in this figure, because the SST gradients are aligned east-west. In this area the SST gradients will be more evident behind cold fronts than in advance of them.

Sea surface temperature gradients are at a maximum during winter. Variations in low level atmospheric stability related to warm or cold surface waters will result in significant changes in near surface E/O conditions (well mixed atmosphere, but with enhanced cloud cover and possible showers over warm water and low level inversions and potential ducting over cold water).

The following table presents statistical information on duct heights for the regional area and season of interest:

CENTER OF AREA: 35°N 150°E SEASON: WINTER

EVAPORATION DUCT HISTOGRAM IN PERCENT OCCURRENCE

Height	December			January			February		
(m)	day	nite	both	day	nite	both	day	nite	both
0 to 4	3	3	3	3	3	3	5	4	4
4 to 8	5	6	5	5	6	6	9	10	9
8 to 12	14	15	14	16	19	17	19	22	20
12 to 16	22	25	24	28	31	29	28	32	30
16 to 20	28	29	28	27	27	27	24	21	22
20 to 24	16	15	16	14	10	12	10	7	8
24 to 28	6	5	5	4	3	4	3	2	2
28 to 32	2	1	2	1	0	1	1	1	1
32 to 36	1	0	1	0	0	0	0	0	0
36 to 40	1	0	0	0	0	0	0	0	0
above 40	3	1	2	1	1	1	2	1	2
Ave. Ht.	18	16	17	16	15	16	15	14	15

8.4 Spring (mid-March to mid-June) (See section 2.2.1.6.)

As is the case elsewhere in the Far East, spring over the waters of the western North Pacific Ocean is a season of major changes. The Siberian high pressure cell begins to weaken and retreat southwestward, the mid-Pacific ridge begins to strengthen, and the Polar Front starts to move northward. Refer to Figure 2-22 (page 2-42) which depicts a generalized springtime synoptic pattern. Figure S-8-3 provides a view of the spring cloud pattern on 18 May 1980.

8.4.1 Climatology

The spring season (mid-March to mid-June) brings significant changes to the weather of the western North Pacific Ocean. Migratory upper atmospheric disturbances transit the region of the weakening Siberian high pressure cell, allowing "bubble" highs to separate from the parent cell and move eastward across the Sea of Japan and Japan. Cyclogenesis typically occurs in the trough between the two high centers, producing clouds, precipitation, and gusty winds. The Polar Front starts its annual northward migration in response to a strengthening mid-Pacific high and weakening Siberian high. See Figure 2-5 (page 2-18). The Aleutian low weakens and the semi-permanent wintertime low moves southwestward to a position over northern Mongolia. Thermal lows may be expected to form over northeastern Manchuria and China as the season progresses.

The following sections address the average conditions which prevail over the western North Pacific Ocean during spring.

Figure 8-8-3. Spring regional view, Northwest Pacific. 18 May 1980.

FIGURE S-8-3. SPRING REGIONAL VIEW, NORTHWEST PACIFIC. 18 MAY 80
OSAN AB Visual DMSP: TN: 18/0136 GMT

Synoptic Features: The Polar Front is located just east of Japan and is the dominate feature in this image. A cloud pattern associated with a leeside trough is seen over the eastern coast of northern Honshu.

Satellite Image Features:

NOTE: See Figure S-6-4 (page 6-26) for comments relative to labels 1-4 which relate to Sea of Okhotsk features.

5. The frontal cloud band includes a classic anti-cyclonically curved cirrus shield. See Figure S-3-6 (page 3-30) for the simultaneous infrared image view.

6. There is no comma cloud visible and there was not a closed low on the surface analysis in this area. In the region of the break in the clouds (between numbers 6 and 7) a ship was reporting a northerly wind, indicating separate circulation patterns for the cloud patterns labeled 6 and 7.

7. The slightly comma shaped cloud pattern immediately east of Japan is associated with a leeside trough. The feature is separated from the main cloud mass by a break in the clouds with a ship reporting a southerly 10 kt wind in the break area instead of the prevailing northerly wind that would be expected in this area if only the the frontal circulation was involved.

Forecast Aids:

1. The northerly surface winds behind this cloud band will result in higher than normal waves for a given wind speed in the region where they flow opposite to the Kuroshio Current off eastern and southern Japan. Under conditions of surface winds opposing the surface ocean current the waves are shorter, steeper, and higher than normal. The numerical guidance will under forecast wave heights in these conditions (it does not sense the opposing currents).

2. During the transition seasons, such as this spring period, the north-south variations across the northwest Pacific are extreme. Tropical conditions and threats in the south, to freezing temperatures and icing hazards in the north. If north-south transiting of these areas occurs, forecasters should be aware of rapid changes in atmospheric and oceanic conditions.

8.4.1.1 Synoptic Patterns

Figure 2-6 (page 2-23) depicts the tracks of typical migratory extratropical cyclones. Of the six depicted, five would be expected to impact the weather over the western North Pacific Ocean during spring: the Manchurian Low (track A), the Lake Baikal Low (track B), the South Mongolia Low (track C), the Shanghai Low (track D), and the Taiwan Low (track F).

Of the three primary types of cold fronts discussed, two -- western and eastern -- can be expected to occur during the spring season. The third type -- central -- is primarily a mid-winter phenomenon, but may occur well into spring in association with an outbreak of Arctic air.

8.4.1.2 Surface Wind

Average wind speeds gradually diminish over the western North Pacific Ocean during spring. By May (Figure 2-23, page 2-45) winds ≤10 kt have a frequency of occurrence of about 35 to 65 percent, and gale (≥34 kt) frequency is less than 5 percent over the entire region. The prevailing northerly directions of winter persist through March, but are primarily southerly south of 45°N by May.

8.4.1.3 Upper Level Winds

Figures 2-24 through 2-29 (pages 2-46 to 2-48) depict upper level flow patterns for May. Strong westerlies still prevail over the western North Pacific Ocean, but the wind speeds of winter, the strongest of the year, have weakened somewhat and moved slightly northward.

8.4.1.4 Visibility

Visibility statistics over the western North Pacific Ocean reveal the changing weather patterns of spring. During March and April, visibilities ≥5 n mi are seen about 65 to 95 percent of the time, with the lower percentages occurring over the more northern waters. By May however (Figure 2-30, page 2-49), when warm, southerly flow starts to move over the cool, northern waters and fog forms, the occurrence of visibility ≥5 n mi decreases to less than 50 percent near the Kuril Islands, and further decreases to less than 40 percent by June. There is a commensurate increase in the incidence of visibility <2 n mi during the same period, with a 50 percent frequency of occurrence seen near the Kuril Islands in June.

8.4.1.5 Cloud Heights/Ceilings

The western North Pacific Ocean has a relatively high incidence of low cloud ceiling during all months of spring, but there is nevertheless a tendency toward increased cloudiness over the northern areas as the season progresses. At the start of the season (March) the percent frequencies of occurrence of low cloud ceiling (low cloud amount ≥5/8) range from about 30 percent near 20°N to about 80 percent near the Kamchatka Peninsula. By June, the occurrence frequency in the northern sector increases to over 90 percent north of 40°N. There is a similar increase in the occurrence of low cloud ceiling <600 ft and/or visibility <2 n mi. Figure 2-31 (page 2-50) depicts cloud height statistics for May.

8.4.1.6 Precipitation

Precipitation patterns over the western North Pacific Ocean change appreciably during spring, with the only consistency occurring south of about 28°N where the precipitation frequency remains 10 percent or less. North of 28°N, March precipitation frequencies increase from a low of about 15 percent near 33°N 140°E northeastward to over 30 percent near 48°N 160°E. By April, the range is reduced to 15 to 20 percent. May, however, has a significantly changed precipitation pattern as the Mei-Yu/Bai-U front and Polar Front become evident south of Japan. An elongated 15 to 20 percentile pattern exists from about 32°N 140°E to 38°N 160°E, with precipitation frequencies both north and south of the area being below 15 percent. June's pattern is similar to May's.

The approximate snow limit line parallels about 33°N in March, gradually retreating northward as the season progresses, until it reaches the southern tip of the Kamchatka Peninsula in June. The 90 percentile snow line (90% of precipitation observations report snow) is at roughly 48°N in March, moving northward to the Kamchatka Peninsula by April, and well north of the western North Pacific Ocean by May. The maximum snow occurrence percentage during May is about 35 percent along the Kamchatka Peninsula.

8.4.1.7 Sea State

Wave heights gradually diminish as the spring season progresses. By May (Figure 2-32, page 2-51) waves ≥5 ft (1.5 m) occur from 40 to 60 percent of the time over the western North Pacific Ocean. Waves ≥12 ft (3.5 m) have an occurrence frequency of less than 10 percent except 10 percent or more between 40°N and 50°N.

8.4.1.8 Surface Air Temperature

As indicated in Figure 2-33 (May) (page 2-52), surface air temperatures show gradual warming during spring. As is to be expected, the most significant warming is seen over the more northern waters where a 15°F (8°C) increase occurs between February (Figure 2-19, page 2-38) and May. The increase diminishes to only 10°F (6°C) at 30°N, and reduces further to only 5°F (3°C) at 20°N.

During May, the extreme minimum temperature near the Kamchatka Peninsula is about 27°F (-3°C), while the extreme maximum temperature near 20°N is about 90°F (32°C).

8.4.1.9 Freezing Level

The altitude of the freezing level rises significantly during spring, with the greatest changes seen over the waters east of Japan. Figure 2-35 (page 2-54) depicts the mean altitude of the freezing level during May.

8.4.1.10 Aircraft Carrier Operating Conditions

Optimum aircraft carrier operating conditions, defined as having a low cloud ceiling ≥5,000 ft (or no low cloud ceiling), visibility ≥5 n mi, and wind 11-21 kt, occur from 10 to 30 percent of the time over a major portion of the western North Pacific Ocean. A less than 10 percent frequency of occurrence occurs north of about 45°N, while a 30 to 50 percent occurrence frequency exists near 20°N in the southeast portion of the area.

Poor conditions, defined as having a low cloud ceiling <300 ft, or visibility <1 n mi, or wind <6 kt or ≥34 kt, occur with a 10 to 20 percent frequency south of 38°N, increasing to 20 to 40 percent north of 38°N. The higher percentages are seen near the Kamchatka Peninsula.

8.4.1.11 Seasonal Oceanographic Features

Sea surface temperatures warm slowly during spring, with increases of about 7°F (4°C) occurring in the northern waters near the Kamchatka Peninsula and 4°F (2°C) occurring near 20°N. Figure 2-34 (page 2-53) depicts mean sea surface temperatures during May.

Sea ice extent diminishes during spring. By May (Figure 2-34) the maximum extent of ice concentration 0.1 or greater is limited to coastal waters north of 50°N and along some of the southern Kuril Islands (Figure S-8-4).

Figure S-8-4 Ice conditions, [illegible]

FIGURE S-8-4 ICE CONDITIONS, SEA OF OKHOTSK. 16 APR 80
OSAN AB Visual DMSP: TN: 16/0159 GMT

Synoptic Features: The large scale ice pattern shows that more than 2/3's of the sea is ice covered. The ice free area along the eastern side of the sea relates to the inflow of the warmer, more saline north Pacific water. The extent of the ice cover is anomalously large for this time of year.

Satellite Image Features:

1. The general ice pattern, open on the eastern and southern sides, multiple leads and fractures over the central area, and consolidated pack over the northern and western areas reflect the combined effects of bathymetry and water circulation.

A. Open eastern and southern parts where the warm and high saline north Pacific water enters the sea and starts its counterclockwise circulation.

B. Consolidated pack over the northern and western sectors where depths are less than 100 m and air and water temperatures are lowest.

C. Multiple leads and fractures over the deeper central portion.

2. Local minimum ice cover, plus late freeze up and early opening occur over the three deep basins.

A. Tiuro Basin, depth greater than 400 m.
B. Derugin Basin, depth greater than 800 m.
C. Kuril Basin, depth greater than 1800 m.

3. Lines of stratocumulus form over the open water when the flow is off the ice pack, such as the area west of Kamchatka.

Forecast Aids:

1. Coastal ice begins to form in November and the maximum coverage occurs in mid-March, with coastal ice remaining into June.

2. Ice development, growth, and duration are related to currents and bathymetry. The currents flow counterclockwise with the warmest and more saline water entering through the northern Kuril Islands and flow northward off western Kamchatka, in some years portions of the eastern 1/3 of the sea never freeze over. The extensive shelf areas (inside the 100 m contour) of the northern and western sectors freeze over early, are the last to open, and exhibit few leads, fractures, or polynyas.

3. The southeast-central portion of the sea is typically the last to freeze over and first to open.

4. Large polynyas are known to develop over some of the deeper basins after the area is initially frozen over.

5. The ice coverage develops slowly during the growth season (November to March) and is punctuated by temporary reversals. The ice retreat is rapid (April to June) and proceeds smoothly. The retreat is particularly fast in the first week or two.

8.4.1.12 Electro-Optical Conditions (See section 2.3.)

The slow northward migration of the Polar Front during spring is followed by major changes in the E/O environment over the western North Pacific. In the vicinity of the front and to the north of it the winter patterns continue, while south of the front summer tropical type conditions will exist. Within the frontal zone the atmosphere is generally well mixed and near normal ranges are found, except for those systems that are degraded by precipitation and clouds. Elevated ducts will prevail in the northern sector of the frontal band and to the rear of the cloud band where large scale subsidence prevails. The area wide frequency of occurrence of elevated ducts or superrefraction layers show a decrease from winter. Values range from less than 10% north of the Perturbed Area to near 60% in the extreme southern latitudes. The change in occurrence across the Perturbed Area is similar to the winter pattern, 30% south of it to less than 10% to the north. Heights are generally near 4920 ft (1500 m) with lower values near 3936 ft (1200 m) off Honshu and northward along the Kuril Islands. Migratory highs moving through the area will result in areas of strong low level or surface based inversions and potential ducting.

The local conditions associated with the ocean currents and areas of strong surface temperature gradients are a problem through mid-spring or until surface heating develops a uniform surface temperature.

The following table presents statistical information on duct heights for the regional area and season of interest:

CENTER OF AREA: 35°N 150°E   SEASON: SPRING

EVAPORATION DUCT HISTOGRAM IN PERCENT OCCURRENCE

Height (m)	March day	March nite	March both	April day	April nite	April both	May day	May nite	May both
0 to 4	6	6	6	17	16	17	21	19	20
4 to 8	10	11	10	12	14	13	12	17	14
8 to 12	20	22	21	16	24	20	14	23	18
12 to 16	26	32	29	19	23	21	15	18	16
16 to 20	21	20	21	14	13	13	11	11	11
20 to 24	8	6	7	7	4	6	6	3	4
24 to 28	3	1	2	3	2	2	3	2	2
28 to 32	1	0	1	1	1	1	2	1	1
32 to 36	1	0	0	1	0	1	1	1	1
36 to 40	0	0	0	1	0	1	1	0	1
above 40	4	1	3	9	3	6	14	6	10
Ave. Ht.	16	14	15	16	12	14	18	13	16

8.5 Summer (mid-June to mid-September) (See section 2.2.1.7.)

The western North Pacific Ocean is dominated by the mid-Pacific high pressure cell during most of the summer. The Polar Front moves north of the area in mid-July to its summertime position across the Sea of Okhotsk where it remains until early September. Figure 2-36 (page 2-56) depicts a generalized summertime synoptic pattern. Figure S-8-5 provides a view of summer cloud patterns over the northwest Pacific on 9 August 1981.

Figure S-8-5. Northwest Pacific Summer. 9 August 1981.

FIGURE S-8-5. NORTHWEST PACIFIC SUMMER. 9 AUG 81
Scripps NOAA 6 Visual: DN: 09/2207 GMT

Synoptic Features: A high center is located just east of southern Kamchatka with a weak disturbance over the northern Kuril Islands. A tropical cyclone is located near 30°N, 163°E.

Satellite Image Features:

1. For reference purposes, the following geographical locations are marked: Central Honshu, extreme northern Sakhalin Island, and east central Kamchatka. Also the "H" is near 46°N, 170°E, the "L" is near 49°N, 155°E, and the "TC" is near 32°N, 163°E.

2. The numerous cloud patterns are rather diffuse and poorly organized reflecting the light wind and non-baroclinic nature of the season (not labeled).

3. Local light shower activity is indicated along 155°E north of about 38°N to near Kamchatka associated with the convergence area between the high over the Pacific and the weak disturbance south of Kamchatka.

4. The tropical cyclone is not well developed and at its present subtropical latitude would be expected to weaken further.

Forecast Aids:

1. Winds are generally light, free of areas influenced by tropical cyclones, during this season.

2. High pressure dominates the northwest Pacific area. The warm, moist, southerly flow results in widespread areas of stratus and fog over the areas of colder water, generally north of the Kuroshio extension.

3. Recurving tropical cyclones are the major heavy weather threat for this area during summer.

8.5.1 Climatology

Summer brings two weather regimes to the western North Pacific Ocean -- the clouds and weather associated with the Mei-Yu/Bai-U and Polar Fronts as summer begins, and the extensive area south of the fronts which is dominated by the northward transport of warm, moist maritime tropical (mT) air. As shown in Figure 2-5 (page 2-18), the Polar Front again influences the weather over the western North Pacific Ocean in early September as it shifts abruptly southward in response to a strengthening Siberian high pressure cell.

The following sections address the average conditions which prevail during the summer months.

8.5.1.1 Synoptic Patterns

Figure 2-6 (page 2-23) depicts the tracks of typical migratory extratropical cyclones that normally occur throughout the year. Of the six tracks shown, three would normally be expected to occur during summer and impact the weather over the western North Pacific Ocean: the Lake Baikal Low (track B), the South Mongolia Low (track C), and the Yellow Sea Low (track E).

At the start of summer, the Mei-Yu/Bai-U and Polar Fronts lie roughly parallel to the south coast of Japan, with the Polar Front extending eastward into the western North Pacific Ocean. Warm, moist air south of the front is forced aloft over the cooler air north of the front. The overrunning and resultant cloudiness and rain is similar to conditions one would expect north of a classic warm front. The slope of the front results in the effects of the overrunning being felt as much as 200 n mi north of the surface front (NOCD, Atsugi, 1980). This effect would be more pronounced over Japan and the Sea of Japan, but would also be observed to a lesser degree east of Japan. A typical Mei-Yu/Bai-U synoptic pattern is characterized by a series of weak low pressure centers on the front extending from China along the south coast of Japan into the western North Pacific Ocean.

Cold frontal activity is at a minimum during the summer. Western and eastern fronts may impact the weather over the northern part of the western North Pacific Ocean, but should occur only infrequently during the period when the Polar Front is north of the area.

Tropical cyclone activity increases during the summer months and continues into autumn. Appendix B includes figures, by calendar period, showing climatologically preferred tropical cyclone tracks.

8.5.1.2 Surface Wind

Wind speeds are the lightest of the year during the period June through August, with winds ≤10 kt observed 50 to 60 percent of the time over most of the sea. Wind speeds begin to increase in September, when the frequency of occurrence of winds ≤10 kt reduces to 35 to 50 percent over a major portion of the sea. Figure 2-37 (page 2-58) depicts surface wind statistics for August.

Southerly directions predominate over the area south of 45°N during most of the summer, except that easterlies are observed between 20°N and 30°N during August and September. Also, winds north of the Polar Front (after it moves abruptly southward) shift to northeasterly in September.

8.5.1.3 Upper Level Winds

Figures 2-38 through 2-43 (pages 2-59 to 2-61) depict upper level flow patterns for August. An examination of the figures shows wind velocities that are the lightest of the year. The band of maximum wind speeds has moved northward and now crosses the western North Pacific Ocean near 45°N, about 600 n mi north of its wintertime latitude.

8.5.1.4 Visibility

Visibility statistics over the western North Pacific Ocean remain largely constant during the months of June, July and August. Visibilities ≥5 n mi have an occurrence frequency of about 50 to 95 percent, with the lower percentages occurring near the Kuril Islands. Similarly, visibilities <2 n mi occur about 5 to 50 percent of the time, with the highest percentages seen near the Kuril Islands. In both cases, the reduced visibility near the Kurils is due to the transport of warm, moist air over the relatively cool waters of the northern latitudes. Figure 2-44 (page 2-62) depicts visibility statistics for August.

September brings an improvement to visibilities. Visibilities ≥5 n mi increase to about 60 to 95 percent of the time (lower percentages seen near the Kuril Islands), and visibilities <2 n mi decrease to about 5 to 30 percent of the time.

8.5.1.5 Cloud Heights/Ceilings

Cloud distribution patterns remain largely constant during the summer. Low cloud ceilings (low cloud amount ≥5/8) occur about 20 to 30 percent of the time over the lower latitudes, increasing to 90 percent over the higher latitudes during July and August. June differs slightly in the lower latitudes where low cloud ceiling occurrence frequency drops below 20 percent. September differs from July and August in the higher latitudes where low cloud ceiling percentages have a maximum value of about 75 percent. Figure 2-45 (page 2-63) depicts cloud height statistics during August.

8.5.1.6 Precipitation

After June, when the Mei-Yu/Bai-U and Polar Fronts increase precipitation along southern Japan and east-northeastward across the western North Pacific Ocean, precipitation percentages average 10 to 15 percent over the entire region. Snow observations do not commonly occur during summer.

8.5.1.7 Sea State

Wave heights are at their yearly minimum during the summer. As shown in Figure 2-46 (page 2-64), which depicts frequency of occurrence of wave heights during August, waves ≥5 ft (1.5 m) occur from 40 to over 60 percent of the time in the western North Pacific

Ocean. Higher waves, ≥8 ft (2.5 m), occur from 10 to about 25 percent of the time. Waves ≥12 ft (3.5 m) have an occurrence frequency of less than 10 percent.

8.5.1.8 Surface Air Temperature

As one would expect, summer air temperatures are the warmest of the year over the western North Pacific Ocean. During August (Figure 2-47, page 2-65), the mean temperature north of about 47°N is less than 55°F (13°C), but is over 80°F (27°C) south of 33°N.

The extreme minimum temperature during August is about 43°F (6°C) near the Kamchatka Peninsula. The extreme maximum temperature is about 90°F (32°C) south of 30°N.

8.5.1.9 Freezing Level

Summer brings high freezing levels to the western North Pacific Ocean. As shown in Figure 2-49 (August) (page 2-67), the freezing level is up to 12,000 ft in the extreme northern portion of the region, and increases to over 16,000 ft in the south.

8.5.1.10 Aircraft Carrier Operating Conditions

During August, optimum aircraft carrier operating conditions, defined as having a low cloud ceiling ≥5,000 ft (or no low cloud ceiling), visibility ≥5 n mi, and wind 11-21 kt, occur generally about 20 to 35 percent of the time south of about 40°N, and 5 to 20 percent north of 40°N.

Poor conditions, defined as having a low cloud ceiling <300 ft, or visibility <1 n mi, or wind <6 or ≥34 kt, have an occurrence frequency of about 20 percent south of 37°N. North of 37°N the percentages increase to over 50 percent near to and east of the Kuril Islands (Figure S-8-6).

Figure 5-8-6. Summer high, Northwest Pacific. 14 July 1981.

FIGURE S-8-6. SUMMER HIGH, NORTHWEST PACIFIC. 14 JUL 81
Scripps NOAA 6 Visual: DN: 14/2159 GMT

Synoptic Features: A 1022 mb high is centered near 45°N, 160°E about 400 n mi south-southeast of Kamchatka.

Satellite Image Features:

1. For geographical reference, the southern part of Kamchatka Peninsula and the eastern side of Sakhalin Island are labeled.

2. The anomalous cloud lines near the high position are the significant feature of this image. Such cloud lines result from ship stack exhaust in regions of subsidence under high pressure cells where strong low level inversions exist.

3. The clear areas northwest of the Kuril Islands are examples of barrier effects and provide evidence of the southerly flow on the west side of the high.

4. Enhanced cumulus exists in the weak frontal band associated with a low pressure area in advance of the migratory high. The most active cumulus (labeled) is near 30°N, 160°E.

5. The dark areas pinching into the sunglint area mark the ridge line in advance of the frontal band and a region of wind shifts from easterly to westerly.

Forecast Aids:

1. The occurrence of anomalous cloud lines infer conditions of:

A. A low level inversion below about 3000 ft.
B. The marine layer has a high moisture content, the surface winds are light, and general hazy conditions with patches of fog will reduce visibility. Fog/stratus may cover large (100's of n mi) areas.

2. E/O and surface to air radar ranges will be adversely affected by these conditions. Low level ducting will occur if the inversion is of sufficient strength.

3. These conditions will persist as long as the high cell remains undisturbed.

4. Surface wind conditions can be inferred through identification of imagery features such as barrier effects, sunglint patterns, fronts, and highs and lows.

8.5.1.11 Seasonal Oceanographic Features

As shown in Figure 2-48 (page 2-66), sea surface temperatures are at their warmest of the year during August, with temperatures ranging from 50°F (10°C) near the Kuril Islands to 85°F (29°C) in the southern latitudes.

8.5.1.12 Electro-Optical Conditions (See section 2.3.)

The Southwest Monsoon related flow dominates the western North Pacific during summer. Extensive areas of stratus and fog with associated low level temperature inversions and potential ducting are fcund north of the Perturbed Area or boundary between the warm Kuroshio Extension Current and the cold subarctic waters to the north (see Figure S-8-2, page 8-23). As the summer progresses and the seasonal warm sea surface temperatures develop the area of stratus and fog moves slowly northward. Under the influence of the southwesterly monsoon flow the atmosphere is well mixed, but tropical in nature relative to humidity content. E/O ranges will reflect tropical zone values under the southwest flow pattern. The frequency of occurrence of elevated ducts or superrefraction layers steadily decreases during summer over the area south of the Perturbed Area, but actually increases to the north in response to the advection of tropical air and development of a warm ocean surface layer. Values range from a maximum of near 50% over the southeast sector to about 15% in the extreme north with frequencies generally lower near coastal areas. Heights average about 3936 ft

(1200 m) with minimum near 2624 ft (800 m) near the southern Kuril Islands and maximum near 4592 ft (1400 m) over the southeast sector.

Local variations will be air mass related (lines of and scattered convective activity, clouds, and showers with intervening clear areas and subsiding air) in the southerly flow regimes. Water mass temperature differences will be masked by the warm seasonal surface layer.

The following table presents statistical information on duct heights for the regional area and season of interest:

CENTER OF AREA: 35°N 150°E SEASON: SUMMER

EVAPORATION DUCT HISTOGRAM IN PERCENT OCCURRENCE

Height	June			July			August		
(m)	day	nite	both	day	nite	both	day	nite	both
0 to 4	29	28	28	26	23	25	16	15	16
4 to 8	14	19	17	11	17	14	8	13	10
8 to 12	14	22	18	12	20	16	11	18	14
12 to 16	13	16	15	10	17	14	13	21	17
16 to 20	8	7	7	8	10	9	12	16	14
20 to 24	4	2	3	5	5	5	7	6	7
24 to 28	2	1	1	3	2	2	5	3	4
28 to 32	1	1	1	2	1	1	3	1	2
32 to 36	1	0	1	2	0	1	2	1	1
36 to 40	1	0	1	1	0	1	1	0	1
above 40	12	4	8	20	4	12	21	6	13
Ave. Ht.	15	10	13	20	12	16	23	15	19

8.6 Autumn (mid-September to mid-December) (See section 2.2.1.8.)

The autumn season has an early and abrupt onset over the northern half of the western North Pacific Ocean. The strengthening Siberian high pressure cell forces the Polar Front rapidly southward to a position south of Japan by mid-September, allowing cold air to invade the region north of the front. Figure 2-50 (page 2-69) depicts a generalized autumn synoptic pattern.

8.6.1 Climatology

The start of the autumn season brings rapid and significant changes to the weather of the western North Pacific Ocean. A combination of related events -- the strengthening Siberian high cell, the weakening of the mid-Pacific high, and the rapid southward movement of the Polar Front -- causes northerly flow to invade the northern half of the region by the end of September. The Polar Front continues to move southward during the season, reaching its southward limit of about 20°N (at 140°E) by mid-December.

The Aleutian low begins to become established southeast of the Kamchatka Peninsula by the end of the season. A quasi-stationary upper level low center, which is resident over the Sea of Okhotsk during winter, forms at about the same time, spawning short wave troughs which move across the northern portion of the western North Pacific Ocean.

Upper level westerly flow begins to strengthen early in the season as the jet stream moves southward from its weak summertime position across northern Japan and establishes itself across southern Japan.

As Autumn progresses, the Siberian high becomes the dominant weather feature over eastern Asia and adjacent waters. High pressure cells routinely break off from the Siberian high and move eastward across the Sea of Japan and western North Pacific Ocean (Figure S-8-7). Cyclogenesis frequently occurs in the induced trough west of the transient cell.

The following sections address the average conditions which prevail over the western North Pacific Ocean during autumn.

8.6.1.1 Synoptic Patterns

Figure 2-6 (page 2-23) depicts the tracks of extratropical cyclones that normally occur throughout the year. Of the six tracks depicted, five would typically be expected to affect the weather over the western North Pacific Ocean during autumn: the Manchurian Low (track A), the Lake Baikal Low (track B), the South Mongolia Low (track C), the Yellow Sea Low (track E), and the Taiwan Low (track F).

Other than the Polar Front, which moves southward through the region during the season, frontal activity is usually of the western and eastern types (with tracks depicted in Figure 2-7, page 2-26). As is the case with the Sea of Japan, the first series of cold fronts occurs between the latter part of October and early November, with a second and more severe series occurring in late December (Figure S-8-8).

Autumn brings a decrease in tropical cyclone activity. See Appendix B.

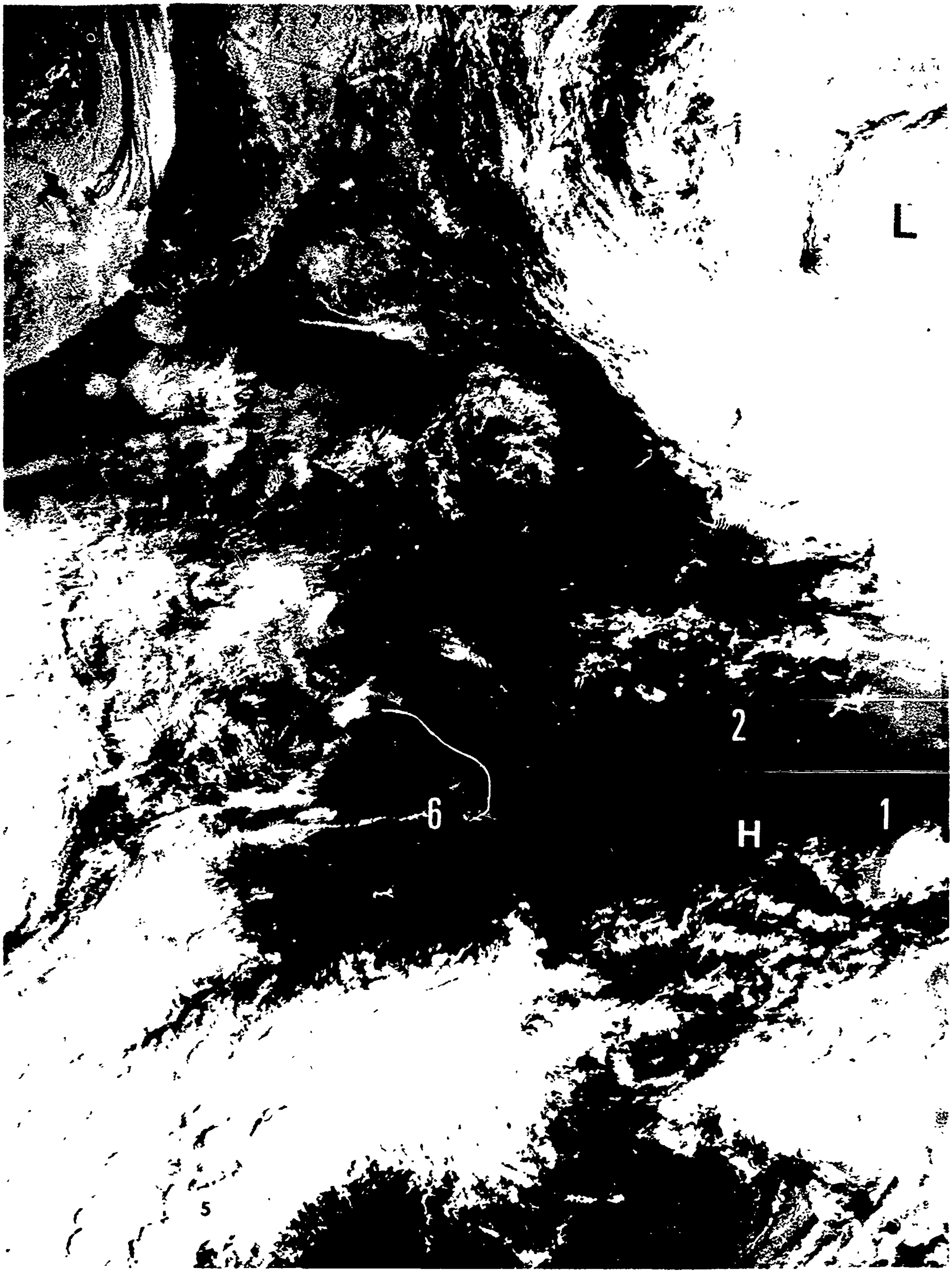

Figure 8-6 . Migr

FIGURE S-8-7. MIGRATORY ANTICYCLONE 7 OCT 81
Scripps NOAA 6 Visual: DN: 07/0250 GMT

Synoptic Features: A migratory 1021 mb anticyclone (high) is centered about 500 n mi east of northern Honshu. This high is following a frontal system associated with a mature 986 mb low centered off southeast Kamchatka and precedes a new developing low now over the the southern Sea of Japan. In the area dominated by the high circulation (approximately 30-50°N and 130-155°E) generally clear skies are seen north of the ridge line with cloudy conditions to the south.

Satellite Image Features:

1. The dark intrusion into the sunglint strip along the eastern third of this image clearly defines a zone of light surface winds associated with a surface ridge line.

2. North of the ridge line, and away from the cloudy areas associated with cyclones, the skies are nearly cloud free.

3. South of the ridge line cloudy conditions prevail, with enhanced convective activity and scattered showers likely.

4. Wave clouds over Sakhalin Island and the Kuril Islands provide evidence of the flow pattern and of the presence of an elevated inversion.

5. Heavy convective cells are seen in the forward half of the frontal band extending from southern Japan west-southwestward over the East China Sea.

6. A band of cirrus extends from the west over the Tsugaru Strait area, identifiable by the cloud shape. A second cirrus band near the western central portion of the image is identified by its shadow cast on the lower cloud deck.

7. The smooth topped clouds over and north of the western Sea of Okhotsk indicate a subsidence inversion in the ridging area between a low over the USSR and the mature low off Kamchatka.

Forecast Aids:

1. In the area of ridge lines, winds are very light, stable atmospheric conditions exist, inversions are likely, and E/O ranges under the inversion are degraded.

2. Terrain induced wave clouds indicate that the flow at and a few thousand feet above the terrain are nearly perpendicular to the ridge lines/mountains and the resulting wave cloud patterns.

Further, the formation of wave clouds implies a level of ducting and potentially enhanced E/O ranges.

3. Large expanses of flat, smooth topped clouds indicates a stable layer, typically an inversion tops the cloud deck.

4. Nocturnal radiational losses from cloud tops tend to strengthen elevated inversions, daytime radiational heating weakens the inversion.

5. The heavy convective activity embedded within the frontal systems moving off China tend to be concentrated in the leading half of the frontal bands. While light rain may be falling throughout the frontal band area, moderate to heavy rain will be associated with the convective cells.

6. E/O conditions will be quite persistent (slightly reduced) throughout the northern portion of migratory highs. They will vary widely (excellent to poor) under the southern half in response to precipitation activity. Under frontal bands they will closely correlate with the visibility ranges.

7. The general E/O conditions will change from tropical to mid-latitude when crossing the frontal band from south to north, and vice versa.


1
15721
147
2
2
4
5
4
4
3

FIGURE S-8-8. AUTUMN, RETURN OF THE POLAR FRONT. 20 OCT 79
OSAN AB Visual DMSP: DN: 20/0053 GMT

Synoptic Features: A 960 mb low is centered just off northeast Hokkaido, the associated frontal band extends southward to below 20°N around 140°E. Surface winds in excess of 50 kt are reported off the northeast coast of Honshu, some 600 n mi south of the low center. Reports of 30 kt winds extend over 1000 n mi from the low center along the frontal band.

Satellite Image Features: (Two photographic exposures were used in this image, the top part to best show cloud tops and the lower part to show fine low level cloud features.)

1. The vortex cloud pattern dominates this image.

2. The frontal band extends southward from near 45°N, 155°E over the northwest Pacific Ocean area along 150-155°E to about 15°N near 140°E in the Philippine Sea.

3. The westerly flow west of the front reflects the return of the winter circulation pattern while east of the front easterly flow reflecting the summer pattern continues.

4. The frontal band is not well organized, but is composed of a series of cloud lines along which showers and strong gusty winds typically occur.

Forecast Aids:

1. Autumn frontal systems will bring strong northwesterly surface winds (over 50 kt in this case), and showery turbulent weather to the northwest Pacific and northern Philippine Sea areas. Passage of these systems will result in abrupt changes from summer, warm, stable air masses to winter, cold, unstable air masses over the northwest Pacific.

2. Extension of the frontal bands, in the form of shear lines will penetrate southward into the Philippine Sea to below 15°N.

3. The Autumn frontal passages are frequently preceded and followed by migratory highs moving off Asia. These alternating conditions between frontal passages and migratory highs result in basic changes in the E/O environment. Forecasters must be alert to changes from frontal unstable conditions to high cell subsidence stable conditions over relatively short time scales (1 to 3 day cycles) and space scales (500-1000 n mi).

4. Within the circulation of each synoptic pattern (low, front, high) a wide array of preferred meso and local scale conditions will result in additional variations in wind, weather, and stability factors.

5. The extreme ranges of both large scale and small scale atmospheric events during transitions seasons in areas of dynamic weather production such as the northwest Pacific create a major challenge to marine environmental forecasters. This can be particularly challenging to units that are transiting into the region from operations of relatively stable climates such as the tropics. Transiting forecasters beware.

8.6.1.2 Surface Wind

Wind speeds gradually increase over the western North Pacific Ocean during autumn. The frequency of occurrence of winds ≤10 kt during September ranges from 45 to 55 percent with the lower figures occurring north 35°N. By December, the frequencies are reduced to 15 to 35 percent, with the largest area of lower percentages occurring east of 145°E and north of 33°N. The prevailing southerly directions of summer give way to northerly (northwest to northeast) as the Polar Front moves southward during autumn. Wind directions south of about 25°N remain easterly during each of the autumn months.

8.6.1.3 Upper Level Winds

Figures 2-52 through 2-57 (pages 2-72 to 2-74) depict upper level flow patterns for November. A comparison of the November figures with those for August (Figures 2-38 through 2-43, pages 2-59 to 2-61) shows that the jet stream has strengthened considerably since summer, and has moved southward to its wintertime position along southern Japan.

8.6.1.4 Visibility

September visibility statistics are similar to those of summer -- reduced visibilities over the more northern waters, especially near the Kuril Islands. During the period October through December, however, overall visibility statistics show improvement over September, likely the result of the interruption of southerly winds due to the southward movement of the Polar Front. Figure 2-58 (page 2-75) depicts the frequency of occurrence of visibility limits during November.

8.6.1.5 Cloud Heights/Ceilings

The incidence of low cloud ceiling (low cloud amount ≥5/8) remains relatively constant during autumn, with frequency of occurrence percentages ranging from about 20 percent over the southern waters near 20°N to over 70 percent east of the Kuril Islands. Figure 2-59 (page 2-76) depicts cloud height statistics for November.

8.6.1.6 Precipitation

The frequency of occurrence of precipitation south of about 30°N remains largely constant at 10 percent or less throughout the autumn season. North of 30°N, however, precipitation frequency increases as the season progresses. By December, the occurrence frequency of precipitation ranges from about 10 percent at 30°N to over 35 percent east of the central Kuril Islands.

Snow frequency (as a percentage of observations reporting precipitation) increases during the season from 15 percent near the Kamchatka Peninsula in October to over 90 percent in December over the same area. The snow limit progresses southward to a line between 31°N 140°E and 36°N 160°E by December.

8.6.1.7 Sea State

Since wave heights are directly related to wind speeds, the increase in wind speeds observed during autumn and discussed in section 8.6.1.2 result in a commensurate increase in wave heights. Figure 2-60 (page 2-77) depicts wave height distribution during November.

8.6.1.8 Surface Air Temperature

Air temperatures start to decrease after August. Decreasing each month throughout the autumn season, the changes in temperature are especially evident north of about 30°N. Figure 2-61 (page 2-78) depicts mean surface air temperature distribution during November.

The extreme minimum temperature over the northern part of the region during November is about 18°F (-8°C). The extreme maximum temperature is about 90°F (32°C) over the southern areas near 20°N.

8.6.1.9 Freezing Level

The altitude of the freezing level decreases throughout the autumn season. By November (Figure 2-63, page 2-80) the mean altitude of the freezing level ranges from the surface near the Kamchatka Peninsula to over 14,000 ft near 20°N.

8.6.1.10 Aircraft Carrier Operating Conditions

Optimum aircraft carrier operating conditions, defined as having a low cloud ceiling ≥5,000 ft (or no low cloud ceiling), visibility ≥5 n mi, and wind 11-21 kt, have a frequency of occurrence of about 10 to 40 percent during autumn, with the highest percentage seen over the southern waters near 20°N. The lowest percentages occur north of about 40°N.

Poor conditions, defined as having a low cloud ceiling <300 ft, or visibility <1 n mi, or wind <6 or ≥34 kt, have an occurrence frequency of about 10 to 25 percent, with the lowest percentages occurring over more southern waters while the highest incidence is seen north of about 40°N (Figure S-8-9).

8.6.1.11 Seasonal Oceanographic Features

Sea surface temperatures gradually decrease throughout the autumn season, reaching a minimum of about 36°F (2°C) near the Kamchatka Peninsula by December. The maximum extent of 0.1 or greater sea ice concentration starts to become evident along northeastern Hokkaido and the southern tip of the Kamchatka Peninsula in November. Figure 2-62 (page 2-79) depicts sea surface temperatures and sea ice distribution for the month of November.


L
4
3
3
4

FIGURE S-8-9. POST FRONTAL, NORTHWEST PACIFIC. 24 OCT 81
Scripps NOAA 6 Visual: TN: 24/2311 GMT

Synoptic Features: A mature decaying low is centered in the Sea of Okhotsk. The related frontal system has swept across the inland seas and northwest Pacific and post-frontal weather prevails.

Satellite Image Features:

1. The decaying mature center is located just west of Kamchatka. The spiraling open celled cumulus near the center indicates cold air has completely encircled the center at low levels (labeled with an L).

2. Cloud types are generally Sc with some scattered slightly enhanced cumulus. Enhanced cloud development and light showers are generally limited to regions of orographic lifting on the windward sides of Japan and Kamchatka.

3. Grassland areas with fresh snow cover are seen as light gray areas over USSR. The larger rivers are not yet frozen over and show as dark lines through the snow covered areas.

4. Wave clouds and plumes indicate the northerly flow over northern USSR while the cloud line forming over the Sea of Japan implies westerly flow there. The curvature of cloud lines from near Sakhalin to Kamchatka complete the picture of low level cyclonic flow around the mature low center.

Forecast Aids:

1. Lows, from which the frontal band has separated and cold air convective type clouds are encircling the center, are in a stage of filling.

2. Post frontal weather is marked by scattered Sc/Cu with widely scattered light showers and moderate to strong gusty surface winds. Overcast conditions with light precipitation is likely where orographic lifting occurs.

3. Over the northwest Pacific surface winds north of 35°N are 20 to 30 kt from the southwest, south of 35°N they are 15 to 20 kt and variable in direction.

4. Well mixed low level conditions will provide normal E/O conditions. An elevated stable layer is likely near cloud top levels, increasing in strength with increasing distance southwestward from the low, in the general direction of the following ridge.

8.6.1.12 Electro-Optical Conditions (See section 2.3.)

The southerly advance of the Polar Front occurs rapidly over the western portion of the western North Pacific. Over the central and northern portions of this area the increased frontal and cyclone action quickly changes the atmosphere from light wind, low level stratus and fog pattern to a pattern of variable conditions. The passage of fronts and cyclones with following ridges or highs result in the variations to E/O conditions occurring on and reflecting typical synoptic scale and pattern changes. As a front approaches, the atmosphere is generally well mixed (E/O conditions normal) with elevated inversions associated with moist/cloud layers. Within the frontal zone, clouds and precipitation patterns are the dominant factor on E/O conditions. The trailing edge of the frontal band and clear area behind it are likely locations of elevated inversions. The cloud conditions, smooth flat topped and or closed cell, provide evidence of inversion capped layers. Open celled or layer tops showing marked relief indicate well mixed conditions.

South of the frontal band summer/tropical E/O conditions will prevail, while in the northern sector of the area winter E/O conditions will be developing. During the transition seasons the change in E/O conditions, along a north/south transit of the western North Pacific will likely vary from near subarctic to tropical values. These are difficult conditions for operators and forecasters because of the large day to day changes as well as large changes in relatively small horizontal scales. The frequency of occurrence of elevated ducts or superrefraction layers reaches an annual minimum during autumn. Due to the marked changes in synoptic weather patterns over the area during this season, the large variations in values from which their averages are combined must be kept in mind. The average frequencies throughout the area range from 25-30%. Maximum average heights over the southern sector are near 4920 ft (1500 m) and range from 2624 ft (800 m) to 3936 ft (1200 m) over the northern sectors.

The following table presents statistical information on duct heights for the regional area and season of interest:

CENTER OF AREA: 35°N 150°E SEASON: AUTUMN

EVAPORATION DUCT HISTOGRAM IN PERCENT OCCURRENCE

Height	September			October			November		
(m)	day	nite	both	day	nite	both	day	nite	both
0 to 4	9	7	8	6	5	5	4	3	4
4 to 8	6	9	7	5	7	6	5	6	5
8 to 12	10	16	13	11	13	12	12	14	13
12 to 16	13	21	17	17	23	20	19	21	20
16 to 20	14	22	18	19	22	20	24	27	25
20 to 24	11	12	11	16	16	16	18	18	18
24 to 28	8	6	7	10	7	8	9	7	8
28 to 32	5	2	3	5	2	4	4	2	3
32 to 36	2	1	2	2	1	2	1	1	1
36 to 40	2	1	1	1	0	1	1	0	0
above 40	19	4	12	9	2	6	5	2	3
Ave. Ht.	24	17	21	21	17	19	19	17	18

9.0 Forecasting Aids and Thumb Rules

This section contains various forecasting aids for the use of the fleet environmentalist when preparing forecasts for the western North Pacific and marginal seas. Some of the aids have been extracted from forecaster's handbooks prepared by Navy, Marine Corps, and Air Force units assigned to military stations in the area, while others have been extracted from technical reports, scientific studies, or other published research documents.

Also listed in this section are guidelines, sometimes called thumb rules, that have been compiled over many years and found to have validity when applied to a particular forecasting situation at or by a particular station. Verification accuracy is listed where known, and credit is assigned to the activity from which the guideline originated.

The forecasting aids and guidelines are grouped for applicability to either year-round or seasonal conditions, as appropriate.

9.1 Synoptic Patterns

The following general guidelines are applicable to all seasons:

a. Pressure patterns associated with good weather are (NOCF Yokosuka, 1981):

(1) High to west - low to east

(2) High to southwest - low to northeast

(3) High to south - low to north

b. The following pressure patterns are associated with bad or deteriorating weather (NOCF, Yokosuka, 1981):

(1) High to east -low to west

(2) High to northeast - low to southwest

(3) High to north - low to south

c. A shift in the direction of the gradient wind to southwesterly from 3000 ft through 6000 ft signals the approach of bad weather. A shift from southwesterly to west or northwesterly signals rapidly improving weather (NOCF, Yokosuka, 1981).

9.2 Movement and Effect of Low Pressure Systems

9.2.1 General

a. Addressing the formation and movement of extratropical cyclones (NOCD, Atsugi, 1980): The northern lows -- Manchurian, Lake Baikal, and South Mongolia -- are all formed by movement of upper atmospheric short wave troughs through the low pressure source region.

The southern lows -- Shanghai, Taiwan, and Yellow Sea -- generally form over central and southern China, then track over the Yellow Sea, Sea of Japan, and Honshu or track over the East China Sea south of Japan between Kyushu and Okinawa. The southern lows are the major weather producers for the southern and eastern regions of Japan. They occur year-round and produce widespread precipitation, low ceilings, poor visibility and occasional thunderstorms or high winds. The movement of each system after leaving its source region determines its identification as a Shanghai Low, Yellow Sea Low, or Taiwan Low.

The formation of all of the lows of the Shanghai source region is a result of or a response to the deepening of the China thermal low. If the thermal low is deepened by a short-wave trough moving north of the Himalaya Mountains, a central pressure of less than 1012 mb will generate a Shanghai Low. If the low is deepened by a short-wave trough moving from the south of the Himalayas, a central pressure of less than 1000 mb will generate a Shanghai Low.

An empirical rule states that when a low is generated over China and passes 120°E south of 30°N, it will be a Shanghai Low and should pass south of Honshu. If the low passes north of 30°N, the low will be a Yellow Sea Low and will track into the Sea of Japan. Consideration must also be made of the position of the Polar Front and the Asian high, coupled with the steering winds aloft.

Taiwan Lows can form as a result of several different circumstances, but the most common instance is the formation of a migratory high over mainland China with an eastward track which projects it over Japan. As the front stagnates south of the high, a wave will form behind the receding high center and move over southern Honshu.

The southern lows present a complex problem for the forecaster in the southern Sea of Japan due to the rapid spread of poor weather northeast of the waves. A constant watch for early signs of low generation and wave formation over southeastern China and adjacent water areas is necessary for effective forecasting of these weather producing systems.

b. Thumb rules for the six types of cyclones (Lake Baikal - Type I, South Mongolia - Type II, Shanghai (Hwang Ho) - Type III, Yellow Sea (Central Basin) - Type IV, Taiwan (Yangtze) - Type V, and Manchurian - Type VI) (FWC/JTWC, 1969):

(1) Siberian lows such as Lake Baikal and South Mongolia are often weak due to the dry continental air in their source region; hence very little precipitation and variable amounts of clouds are associated with them. A typical situation may have cloudy skies on both sides of the occlusion or cold front with little change in temperature at the surface. If considerable precipitation and cloudiness are present in the cyclone area, the low and its frontal system may be associated with an unstable air mass and rapid eastward movement is a possibility.

(2) If a low pressure center appears in Manchuria and a wave is formed in China near Shanghai with a warm front extending easterly towards Kyushu, a weak trough aloft oriented north-south usually connects the low center with the frontal wave. The trough line will usually move slowly eastward.

Associated with this trough will be marginal weather to the east of the system, improving to the west. If the southerly cyclone indicates no rapid development or movement, surface winds on the west and east coast of Korea will veer from southeasterly to southwest and west giving an indication of a moderate secondary front approaching. The cyclone over the Yellow or East China Sea will remain weak and move eastward at about ten knots. As the secondary front crosses Korea considerable weather and wind from the northwest to west 20 to 35 knots may ensue for approximately six hours.

If, however, the southerly wave deepens, a secondary trough to the west may not appear or, if it does, it will be very weak. The weak north-south trough connecting the centers of the two lows will intensify and move easterly at the same rate of speed as the center of the southerly low. Six to twelve hours after the passage of the trough, weather conditions will improve and surface winds will return to west to northwest 20 to 30 knots. After 24 hours, excellent conditions should prevail over the Sea of Japan.

(3) If no low has formed in the Ryukyus or along the south coast of Japan and a low moves southeast from Siberia or Manchuria into the Sea of Japan, its development and movement will be governed by the intensity and position of any low over or near Kamchatka and the 700 mb flow over southern Japan. If the Kamchatka low is closer than 1000 n mi to the low in the Sea of Japan, the low will not develop but move slowly eastward across northern Japan. If the Kamchatka low is farther than 1000 n mi, the low in the Sea of Japan will develop rapidly and move northeastward across northern Japan. If, at the same time the 700 mb flow over Japan is strong southwesterly, there will be a rapid spreading of bad weather to the northeastward while two or three days of cold, dry weather will prevail over Korea in winter as a migrating ridge or high pressure center follows the low.

(4) A wind flow from the south through east from the surface to 700 mb, from Japan to Korea, will produce widespread bad weather in the area, and it may continue for 72 hours. With this type of wind flow a low pressure area or a series of low pressure waves usually exists over the East China Sea and along the southern coast of Japan. The East China Sea low may move either into the Sea of Japan or along the southern coast of Japan. The development of these systems is dependent on the proximity of neighboring low centers.

(5) If a northeasterly moving surface low south of Japan reaches a position 1,000 n mi or greater east or northeast of a low in the Sea of Japan, the low in the Sea of Japan will deepen and move northeastward. As long as the low south of Japan and the low in the Sea of Japan are within 800 n mi of each other, the low south of Japan will be the major system and the low in the Sea of Japan will move eastward behind the major system or be integrated with the intense low as it moves into the Pacific.

(6) When isobars on a surface pressure analysis have a northeast-southwest orientation approximately in line with the Islands of Japan, weak cyclones frequently form off southern Kysuhu. This type of pressure distribution often occurs when cyclones have passed southern Japan. The trailing cold fronts associated with these lows are often slow moving and tend to stagnate off the coast of Japan.

c. Deep lows aloft over northern Mongolia, with troughs or fronts extending to the southwest, tend to deepen as they move east-southeastward, with the trough/front traveling southeast at 20 to 25 kt. As the trough approaches the Gulf of Pohai, it tends to slow up slightly as a warm ridge builds ahead of it. There is then a good possibility that a low may develop over the Gulf of Pohai along the trailing edge of the front/trough. This low w' l then tend to track eastward, giving moderate/heavy precipitation to the northwest corner of South Korea. If the front/trough becomes oriented west-southwest/east-northeast, precipitation will tend to be light (Nestor, 1977).

d. Indications that a low is forming in the Yellow Sea are observed by overrunning at Kimpo, Korea with higher pressure east of a line from Kimpo to Cheju-do (U. S. Air Force 1964).

e. Low pressure systems with attending cold fronts oriented northeast-southwest that are located in the Lake Baikal region of the USSR move southeast with an average speed of 20-25 kt. They can be extrapolated across the "no-data" region with reasonable accuracy (U. S. Air Force, 1964).

9.2.2 <u>Winter</u>

a. Given a change in wind direction to the south or southeast at Ishigaki Shima (47918) and Miyako Jima (47927), the probability of cyclogenesis within 72 hours in the East China Sea area is 90%. Within 18 hours, the probability is 50% (NOCF, Yokosuka, 1981).

b. Lows generated in the Taiwan area follow a trajectory along the southern coast of Japan (NOCD, Atsugi, 1980 and (NOCF, Yokosuka, Japan, 1981).

c. A favorable situation for the formation of a Taiwan Low occurs during the winter as a ridge of high pressure extends from the Siberian High southeastward over Japan. A break will sometimes form near Taiwan with a "Taiwan Low" forming within this break and then tracking northeastward over Japan. This situation does not occur along the Polar Front and therefore does not result in frontal low formation or wave generation. Instead, the Siberian High pressure ridge re-establishes itself thereby terminating the low generation process (NOCD, Atsugi, 1980).

d. During winter, cyclogenesis occurs in the Manchurian basin on the majority of the cold fronts which pass over the Korea-Japan area. Within 24 hours these lows deepen and move eastward over the Sea of Japan and form well defined fronts (FWC/JTWC, 1969).

e. Generally, the cyclones of winter will move eastward along the southern Japanese coast and deepen rapidly. But in the spring, cyclones often cross into and deepen in the Sea of Japan (FWC/JTWC, 1969).

f. The appearance of a bubble high breaking off from the continental anticyclone is a reliable predictor for cyclogenesis and bad weather to follow. Shorter interval times between the occurrence of the high and the cyclogenesis are observed in winter than during April and September (George and Wolff, 1953). The above described synoptic pattern has been found so reliable in the past that a verification of nearly 100% will result with a forecast of cyclogenesis after a bubble high has moved off the Asian coast. Generally, highs with centers north of 35°N that move off-shore will generate lows that move into the Sea of Japan while highs with centers south of 30°N that move off-shore will generate lows that move south of Japan. Lows that are produced by highs moving off-shore with centers between 30°N and 35°N will move in relation to their position to the jet stream. Lows developing north of the jet stream tend to move southeast toward the jet and then along the jet's southern boundary, deepening rapidly as they pass under the jet core. The location of a favorable 850 mb advective pattern also gives a good indication of the location of cyclogenesis (NOCD, Atsugi, 1980).

g. Excluding typhoons, the most hazardous weather in the Japan area is caused by deep lows that form in the vicinity of Okinawa and Taiwan and move northward. These lows almost invariably show rapid, intense deepening, especially during autumn, winter and spring (FWC/JTWC, 1969).

h. In January, the major region of cyclogenesis lies beneath the southern jet stream at about 30°N in the East China Sea. First indications of formation are the sudden appearance of high and middle clouds near Okinawa. Cloudiness increases when winds over Taiwan back to 210°-240° and increase in speed. Rain begins as the low center arrives in the vicinity of 125°E-126°E. Forecast rain to stop and ceilings to lift when the wave crest moves east of 127°E (NOCD, Kadena, 1983).

i. The average period between polar outbreaks in fall and winter in Korea is approximately five days (U. S. Air Force, 1964).

j. In winter, if Paengnyong-Do's or Osan's pressures begin to drop rapidly, the rapid approach of a system or the development of a new system in the Yellow Sea area is indicated. It is advisable to maintain a close watch on the 24 and 48 hour pressure changes as indications of possible developments (U. S. Air Force, 1964).

k. Good weather usually persists over Korea as long as a 500 mb low is positioned in the vicinity of Sakhalin Island (U. S. Air Force, 1964.)

9.2.3 Spring

a. From late spring through early autumn, a cyclone family will often form along the Polar Front if it is associated with a Taiwan Low (NOCD, Atsugi, 1980).

b. The following guidelines address the formation and movement of Taiwan Lows during the spring season (NOCD, Kadena, 1983).

(1) Taiwan lows usually deepen 1 mb/3 hours after they form. They intensify 1 mb/hr after reaching the southern coast of Kyushu.

(2) A Taiwan low will move eastward across the Ryukyus about 24 hours after east-southeast winds are observed at Miyako Jima (47927) and Ishigaki Shima (47918).

(3) When a Taiwan low moves northeast, Miyako Jima and Ishigaki Shima will be in the warm sector and experience good weather.

(4) As a Taiwan low moves toward Okinawa and Kadena experiences pre-warm frontal weather, expect the cold front to pass within 5-6 hours after Miyako Jima indicates cold frontal passage.

(5) In some cases, Taiwan lows develop, deepen, and move through the Okinawa area in less than 24 hours.

(6) Look for a Taiwan low to develop in 24 to 36 hours when:

(a) The Polar Front is located south of Okinawa.

(b) There is a flat pressure gradient through Miyako Jima, Ishigaki Shima, and Taiwan.

(c) Miyako Jima and Ishigaki Shima surface winds are from the southeast.

(d) Kadena AB reports sea level pressure less than 1015 mb.

(e) The 700 mb wind is from the SW over Taiwan.

(f) The sea level pressure at Minami Daito Jima is greater than that at Taipei.

c. In the spring, Shanghai lows move at speeds of 20 to 40 kt, roughly paralleling and adjacent to the Kuroshio Current (NOCD, Kadena, 1983).

d. Waves forming east of Shanghai in the spring will cause low ceilings and visibilities throughout south and central Japan. The associated cold front will pass through Okinawa 6-8 hours after it passes Ishigaki Shima and Miyako Jima (NOCD, Kadena, 1983).

e. Most waves forming southwest of Okinawa during spring move northeast at 12-15 kt, but in isolated cases, move as fast as 25 kt. (NOCD, Kadena, 1983)

f. In the spring, given a change in wind direction at Ishigaki Shima (47918) and Miyako Jima (47927) to the south or southeast, the probability of cyclogenesis within 72 hours in the East China Sea area is 90%. Within 18 hours, the probability is 50%. (NOCF, Yokosuka, 1981.)

g. In the spring, Shanghai lows move at speeds of 20 to 40 kt, roughly paralleling and adjacent to the Kuroshio Current (NOCD, Kadena, 1983).

9.2.4 <u>Summer</u> (See applicable aids in Spring, page 9-8)

9.2.5 <u>Autumn</u> (See applicable aids in Spring, page 9-8)

a. In cases where Lake Baikal lows move eastward during autumn and follow a trajectory north of 48°N, waves often develop in Manchuria along the trailing edge of the cold front. This decelerates but intensifies the system with increased activity resulting as it passes. Simultaneous with the deceleration is the generation of a north-south oriented trough over the Yellow Sea which will move into Korea before the front (U. S. Air Force, 1964).

9.3 Movement and Effect of High Pressure Systems

9.3.1 General

a. The local area weather cycle associated with a migrating high will be better when the cell passes eastward south of the area rather than north of the area. (NOCD, Yokosuka, 1981).

b. When the Pacific High is well developed with a strong ridge extending to the west of Japan with the ridge-line north of 27°N, favorable weather will occur over the southern Sea of Japan (U. S. Marine Corps, 1967).

c. If a migratory, cold, polar high is ridging southward over Japan, any wave development will be south of 30°N and become dampened due to the influence of the high pressure cell and the associated lack of necessary atmospheric support (NOCD, Atsugi, 1980). (50-80%)

d. A "warm" (deep) migrating high will produce light winds, large diurnal temperature range, no ceilings and few clouds. Normally a warm season event. A "cold" (shallow) high will produce rapidly deteriorating weather after the center has passed east of the area. Normally a cold season event. (NOCD, Atsugi, 1980) (50-80%)

e. Early morning showers sometimes occur near the center of a cold, shallow migrating high (NOCD, Atsugi, 1980). (0-50%)

f. A ridge will maintain itself or build if analysis of present and past 12 hour upper air maps shows warm air entering the high center from south to west, assuming the high is warm-cored. A warm-cored high will show up at the 500 mb level. (Nestor, 1977)

g. Five days of good weather over Korea usually occurs from the time a Siberian high becomes oriented northwest-southeast with a ridge line south of Korea. This rule is not applicable in summer (U. S. Air Force, 1964).

9.3.2 Winter

a. In the winter, when a migrating high reaches the vicinity of 30°N 150°E, the subsequent cold front will pass over the Ryukyus (NOCD, Kadena, 1983).

9.3.3 Spring and Summer

a. During the Mei-Yu/Bai-U season, fair weather can be expected over central Japan when a Sea of Okhotsk High is ridging north-south over Japan into the East China Sea (NOCD, Atsugi, 1980). (50-80%)

9.3.4 Autumn

a. During autumn, when a Siberian high moves toward central China, crosses 110°E, and reaches the mouths of the Yangtze (Changjiang) and Yellow Rivers, the trough ahead of the high will cross the Ryukyus (NOCD, Kadena, 1983).

9.4 Fronts, Shear Lines and Easterly Waves

9.4.1 General

a. If a front is north of or in the central Japan area, examine the 700 mb chart for a ridge oriented north-south through the Sea of Japan and located over Honshu between Iwakuni (47764) and Komaki (47635). Winds to the left of the ridge should be from 230-250 degrees; winds to the right of the ridge should be from 290-300 degrees. Under this situation with northwest winds over the Tokyo area at 10,000 ft and above, the Polar Front will move south of the Tokyo area. The Sea of Okhotsk High will ridge into Central Japan with resulting northeasterly flow below 10,000 ft. (This is one synoptic exception to the basic rule that "Flow north of west aloft means good weather in central Japan; flow south of west aloft means bad or deteriorating weather.") (NOCD, Atsugi, 1980). (80-100%)

b. North-south fronts move relatively fast, followed by good weather. Cold fronts with a north-south orientation will cause widespread inclement weather over central Japan during passage (NOCD, Atsugi, 1980). (80-100%)

c. Approximately 36 hours after the initial outbreak of cold flow, a lee side trough usually forms along the east China coast. It should not be forecast to move until an upper air trough approaches it (Nestor, 1977).

d. When a migratory high cell moves across the East China Sea or a Pacific High develops south of Okinawa so that the East China Sea area is under the influence of strong warm southeasterly flow, it indicates that the main Polar Front will move northward to the Cheju-do area and that a wave will probably develop west of Taiwan (U. S. Air Force, 1964).

e. A good average speed for relatively shallow troughs moving from west to east is 15 kt (3^{o} of latitude every 12 hours) over land and 20-25 kt over water (Nestor, 1977).

f. The forecasting of the movement of shear lines has been a difficult experience for many meteorologists due to their unique nature and the paucity of reference material. The following guidelines have been taken from the 1969 edition of NWSED, Agana, Guam's Local Area Forecaster's Handbook and pertain to forecasting shear line passage on Guam once the shear line has passed south of Iwo Jima (24.8N 141.3E).

(1) If either Iwo Jima or Chi Chi Jima (27.1N 142.2E) has a sea level pressure of 1020 mb and there are no major waves on a frontal system south of 35N, chances are good that the shear line will pass the southern Marianas.

(2) A weak frontal inversion will be associated with the shear line.

(3) As the shear line approaches within 200 n mi of Guam, the trade inversion will strengthen.

(4) As the shear line passes Guam, winds will back from easterly and increase in speed. There will be a marked decrease in convective type clouds. An increase in the temperature-dew point spread will occur following passage of the shear line.

g. The following guidelines have been taken from the 1984 edition of the Forecaster's Handbook, NAS Cubi Point, R. P., published by the NOCF, Cubi Point, R. P.

(1) Easterly waves move at an average speed of 10 to 15 kt and reach their maximum intensity in the layer from 700 to 500 mb, sloping eastward with height.

(2) When the wave moves slower than the basic current in the low levels and faster than the basic current in the upper levels, the area west of the wave is characterized by subsidence and fair weather while areas of convergence and disturbed weather occur east of the trough.

(3) The best aid in looking for easterly waves is by use of consecutive satellite pictures. By looking for the inverted "V" cloud pattern, which is often diffused, and by keeping a daily track on these cloud patterns, the forecaster can determine its movement.

(4) Easterly waves generally stagnate over the Philippines or intensify the "lee side" trough to the west.

(5) Any time a station in the tropics is observed reporting haze, with the exception of industrialized Manila, it should be immediately suspected as being below the subsidence inversion in advance of an easterly wave (Figure S-9-1).

9.4.2 Winter

a. Approximately 36 hours after an initial outbreak of cold flow, a lee side trough usually forms along the east China coast. It should not be forecast to move until an upper level trough approaches it (Nestor, 1977).

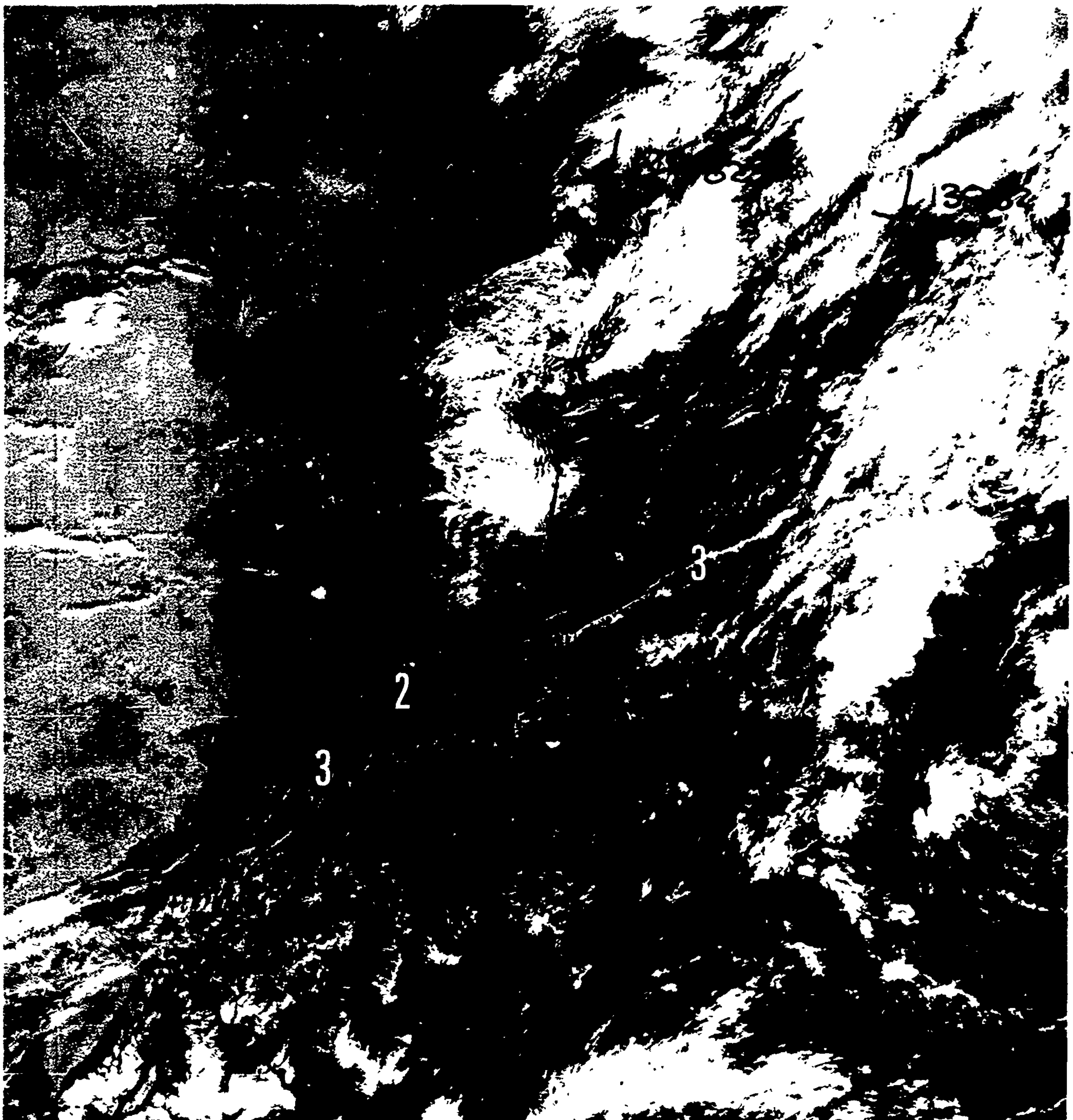
3
2
3
1

FIGURE S-9-1. EASTERLY WAVE, PHILIPPINE SEA. 23 OCT 79
OSAN AB Visual DMSP: TN: 23/2359 GMT

Synoptic Features: A ridge of high pressure extends westward from the Pacific High across southern Japan and the East China Sea to the Yangtze (Changjiang) River area. An easterly wave type disturbance is centered over the central Philippine Sea.

Satellite Image Features:

1. The area of enhanced convective activity and Cb's in the central Philippine Sea is located in an inverted trough, easterly wave type pattern.

2. The low level flow past Cheju-do Island results in a clear area on the leeward side (northern) and upslope clouds on the windward side (southern).

3. The change of cloud line structure from the fine features over the East China Sea to the more pronounced features of the Sea of Japan reflect a general increase in wind speed from less than 10 kt to 15 to 20 kt.

4. The hazy appearing area over China and the Yellow and East China Seas corresponds with an area where surface observations are reporting light fog (synoptic code 10). Note that the bathymetric features off China, are nearly totally obscured.

5. Three bar fog (code 45) is seen in valleys of southern China.

Forecast Aids:

1. Without terrain features to provide barrier clearing or upslope cloud patterns, the direction of surface winds associated with thin cloud lines over seas could be mis-interpreted 180° out of phase.

2. Light fog appears as a hazy area in DMSP satellite visual imagery while the heavy fog appears light gray and has sharp edges where it encounters terrain.

3. In the sub-tropics, areas of inverted troughs and easterly waves will contain general increased convective activity and surface wind speeds as well as clusters of Cb's and shower activity.

4. E/O ranges will be reduced in light fog areas. In tropical regions, the E/O ranges will vary widely from areas of precipitation to areas clear of clouds.

b. The appearance of a bubble high breaking off from the continental anticyclone is a reliable predictor for cyclogenesis and bad weather to follow (George and Wolff, 1953). See section 9.2.2.f for a discussion of the bubble high phenomenon.

c. The following guidelines are taken from NOCD, Kadena, (1983) and apply to conditions occurring during the late autumn and winter seasons.

(1) Mid-November through mid-February is the period of the "arctic fronts", as the Polar Front lies across the Philippines.

(2) In forecasting weather associated with outbreaks of the Siberian high:

(a) Prior to frontal passage, surface winds will become southwest to west 35+ kt and, in isolated cases, contain gusts to 65 kt.

(b) The cold front will be moving at speeds in excess of 20 kt.

(c) Rain will occur prior to passage of the front, with rainshowers for at least six hours subsequent to passage.

(d) With frontal passage, winds vary from west to north, ceilings may be reduced as low as 500 ft, and visibility may be one mile in brief heavy rain.

(e) Behind the front are persistent, strong, gusty surface winds, often 25 kt or higher, and 1-3 days of overcast stratocumulus with bases between 2,000 and 6,000 ft. Occasional light rainshowers or drizzle will accompany the overcast skies. This precipitation will usually end when winds decrease and shift to northeast to east.

(3) Frequently, scattered convective showers occur over water during the post-frontal northerly flow as a result of strong surface heating over the relatively warm water surrounding Okinawa.

(4) An arctic frontal passage at Kadena can be expected to occur within 16 hours after it passes Cheju-do if the 700 mb wind speed at Kadena (at the time of the frontal passage over Cheju-do) was 25 kt or greater.

(5) The cold front of a single low in the Sea of Japan will cross Okinawa as the low center passes over the Noto Peninsula (37°N 137°E).

(6) Eighty percent of the cold fronts approaching Okinawa from the northwest are inactive and fast-moving (25 kt). Some have been observed to move at speeds close to 50 kt.

d. After a strong cold frontal passage, one or more minor troughs or minor secondary fronts will pass through Korea (U. S. Air Force, 1964).

e. During the period September to May a front can be forecast to pass Seoul 48 hours after a secondary low becomes a closed cell at 700 mb in the area of Lake Baikal (U. S. Air Force, 1964).

f. Fronts passing the Kimpo area move 15 to 20 kt in spring and fall and 20 to 25 kt in winter (U. S. Air Force, 1964).

9.4.3 Spring

a. As a Taiwan low moves toward Okinawa and Kadena experiences pre-warm frontal weather, expect the cold front to pass within 5-6 hours after Miyako Jima indicates cold frontal passage.

9.4.4 Spring and Summer

a. Lows traveling from east China to the Sea of Japan during the rainy season indicate that the Mei-Yu/Bai-U front is moving northward (U. S. Air Force, 1970).

9.5 Tropical Cyclones

9.5.1 General

The following guidelines are applicable to all seasons in the Far East since tropical cyclone activity has been observed in all months of the year.

a. No storm will recurve until it reaches a region where south or southwest winds prevail aloft. The steering level may range from 500 mb to 200 mb depending on the strength of the storm. The steering level may be found by streamline analysis of various levels (NOCD, Atsugi, 1980). (50-80%)

b. Tropical cyclones approaching Japan on a northerly heading will form a secondary low in the Sea of Japan (U. S Marine Corps, 1967).

c. In situations where a tropical cyclone moves west from its breeding ground south of Guam, a high cell over the Bonin Islands is not likely to weaken. As a result, fair weather persists within the area of influence of the Bonin high (NOCD, Atsugi, 1980). (50-80%)

d. Typhoons are more prevalent during June through October, as the subtropical ridge builds up to 23°N-27°N. The area near Guam is a natural breeding ground for these storms (NOCD, Kadena, 1983).

e. As the typhoon approaches, light to moderate showers are the rule. Towering cumulus and isolated cumulonimbus clouds with their associated cirrostratus shields are common. Nearer the center, the weather changes to moderate to heavy intermittent rain and showers. Ceilings of 200 ft and visibilities of 1/2 to 5 mi are common. Near the eye, rain and blowing spray are mixed by winds so that complete obscuration is common. Visibility is usually around 5 mi when 30 kt of wind are experienced, 1 mi or less in heavy showers, and obscured when winds exceed 65 kt (NOCD, Kadena, 1983).

9.5.2 Spring

a. Tropical storms may develop and move into the area, but dissipate rapidly upon reaching the cool water and colder air temperatures north of 20°N (NOCD, Kadena, 1983).

9.6 Wind

9.6.1 General

a. Do not forecast gusty surface winds after the 24-hour isallobaric high center has passed east of the area (NOCD, Atsugi, 1980). (50-80%)

b. Do not forecast strong surface winds when a surface inversion is present or forecast to occur (NOCD, Atsugi, 1980). (50-80%)

c. Findlater (1966) documents a technique for forecasting winds based on the relationship between 900 mb winds and surface winds as follows:

The first step in the technique is to estimate either the forecast geostrophic winds or if the indicated air trajectory is strongly curved, the forecast gradient wind. See the following section for information on determining representative winds from winds calculated from surface pressure analysis. Short-term forecasts for 900 mb winds could be made from near current time surface wind reports. The next step is to forecast the temperature lapse rate in the lowest layers. Table 9-1 lists the established lapse classes.

TABLE 9-1. Lapse classes

Lapse class	Range of temperature lapse rate in degrees F/1000 ft
1	$\geq$5.5
2	4.0 to 5.4
3	2.5 to 3.9
4	1.0 to 2.4
5	$\leq$ 0.9

Diurnal changes of temperature lapse rate are small at sea and, in comparison with the problem over land, it is relatively easy to forecast the temperature lapse rate from a representative temperature sounding. Satellite imagery cloud features can be used to estimate special changes in the lower level lapse rate. The technique is applied by using the values in Table 9-2 which are the ration (per cent) of the 900 mb wind to the surface wind.

Example: Given a surface wind of 22 kt with a lapse class of 3, the 900 mb wind is calculated as 22 x 1.3 = 29 kt.

TABLE 9-2. Smoothed values of V_{900}/V_0 for classes of surface wind speed and lapse rate.

surface wind speed class (kt)	8-18	19-26	27-33	34-40	$\geq$41
Lapse class	V_{900}/V_0	V_{900}/V_0	V_{900}/V_0	V_{900}/V_0	V_{900}/V_0
1	1.03	1.10	1.18	1.23	1.28
2	1.11	1.19	1.27	1.32	1.35
3	1.18	1.30	1.41	1.49	1.56
4	1.25	1.39	1.52	1.64	1.69
5	1.33	1.47	1.59	1.72	1.85

d. The mean value of the V_{900}/V_0 ratio at sea is: V_{900}/V_0 = 1.25.

e. The change in direction at 900 mb is affected most by temperature lapse rate: near zero in very unstable air and near 25° in very stable air.

f. V_{900}/V_0 depends on both temperature lapse rate and wind speeds: ranges from 1.0 in unstable air and light winds to 2.0 in stable air and strong winds.

9.6.2 <u>Winter</u>

a. Hsueh and Romea (1983) established a relationship between calculated winds and observed winds over the east China Sea. The established result should have similar validity over the Sea of Japan. A summary of their findings follows. Wintertime geostrophic winds, calculated over the East China Sea from surface pressure maps, were compared to observed winds from the region. For mean winds, the average counterclockwise angle from calculated winds (geostrophic) to observed winds was 37°, and the average reduction in speed was 39%. For fluctuating winds the average direction and speed changes are 25° and 55%. The greatest reduction occurs for land stations, while the lowest (33%) occurs at an offshore buoy station.

b. When a Siberian high cold outbreak is evident, forecast surface winds of at least 20G35 kt at the time of frontal passage.

There may also be a second surge of gusty winds which reach 40+ kt occurring 1-2 hours after frontal passage (NOCD, Kadena, 1983).

c. Gusty surface winds from the northwest will persist for 24 to 36 hours after a strong cold frontal passage in the autumn, winter, or spring (U. S. Marine Corps, 1967).

d. High winds are caused by passage of a north-south or northwest-southeast oriented cold front in the autumn through spring. However, do not forecast strong winds if a trough persists behind the front over the Sea of Japan (NOCD, Atsugi, 1980). (50-80%).

e. Surface wind intensity varies with the width of weather bands. Narrow, rapid-moving bands are accompanied by gusts to 45 kt, while wide, slow-moving weather bands may be accompanied by gusts which seldom exceed 35 kt (NOCD, Kadena, 1983).

f. The most significant weather phenomena during winter are the post-frontal gusty surface winds (NOCD, Kadena, 1983).

g. During a surge of the Northeast Monsoon, surface winds reported by ships in the Taiwan Strait are appreciably higher than the pressure gradient indicates. This is because of a Venturi effect within the strait between China and Taiwan. To make a good estimate of the wind in the channel if no ships are reporting, add 10 to 15 kt to reported coastal land station wind speeds.

h. During the Northeast Monsoon, a Siberian high cell commencing to move southeasterly will cause the gradient to strengthen across southern China and the northern South China Sea. Usually a surface wind maximum will move south from the Yellow and East China Seas. The wind maximum may not be gale force, but when it reaches the Taiwan Strait it will increase by 10 to 15 kt. If a wind maximum with speeds of 20 kt or greater is approaching Taiwan, the forecaster should expect gale force winds in the channel. If the wind maximum was already gale force, then a storm warning should be considered. Similar conditions occur with an approaching tropical cyclone (FWC/JTWC, 1978).

i. When the 1017 mb isobar reaches the south coast of China and the pressure at Hong Kong (45005) is higher than the pressure at the southern tip of Taiwan, gale force winds will occur in the Taiwan Strait with speeds up to 40 kt (NOCF, Cubi Point, 1984).

j. Within 6 to 12 hours after a cold frontal passage at station 46734, gale force winds will prevail in the Taiwan Strait and spread into the South China Sea (NOCF Cubi Point, 1984).

9.7 Visibility

9.7.1 General

Most of the forecasting aids and guidelines contained in various forecaster's handbooks address visibility reductions resulting from the advection of industrial pollution over an individual land station; few address large-scale impairments to visibility, such as advection fog. Consequently, the fleet environmentalist must use general meteorological principles, rather than thumb rules, when issuing a visibility forecast.

At sea, visibility is usually reduced due to one or more of three phenomena -- haze, precipitation, and fog -- with an occasional occurrence of dust or sand reported whenever a strong wind situation transports the particles over the ocean. Haze can be caused by many factors, but away from the influence of industrial contamination, it usually takes the form of "salt haze". Salt haze is the result of the suspension of salt particles in the atmosphere near the sea surface, and can be caused by high winds or a stable lower layer of the atmosphere. When occurring, haze will usually not decrease visibility below 3-5 mi, although a severe occurrence could reduce visibility to the 1-3 mi range.

Visibility reduction due to precipitation is dependent on the intensity and type of precipitation. In general, heavier precipitation will reduce visibility to a greater extent than will light precipitation and snow will impact visibility more severely than will rain.

The prediction of fog at sea can be a difficult task, but can be made easier if some basic concepts are understood and followed. Fog at sea is usually of the advection type, and is usually caused by warm air moving over cool water, with both "warm" and "cool" being relative terms.

Steam fog, occurring when relatively colder air overlies warmer water, is caused by the air becoming almost immediately supersaturated due to evaporating water. The evaporated water recondenses and rises with the air that is heated from below. Steam fog is usually very shallow and appears as wisps of smoke rising from the water surface. When very cold air moves from a land mass over adjacent water that is relatively much warmer, the steam fog can become so intense that it condenses into fog, a phenomena that is called "arctic sea smoke" (Kotsch, W. J., 1983).

9.7.2 Winter

a. Dust (yellow sand) can restrict visibility for 2-3 days after intense cold frontal passages in the winter. This dust is first observed over the Gobi Desert and, with continued strong northwest flow in the upper levels, can move over the open ocean and extend as far east as Okinawa and beyond. Visibility may be reduced as low as 2-3 mi in dust and haze (NOCD, Kadena, 1983).

b. The occurrence of "sea smoke" and "frost smoke" is relatively common over the colder waters of the northern Sea of Japan, north of the Kuroshio Extension, and throughout the Sea of Okhotsk.

9.7.3 Spring

a. In spring, strong winds up to 20,000 ft (6,100 m) and above, assuming there is no precipitation, will often lower visibilities to a mile or less at the surface and 3-5 mi (5-8 km) above 500 ft (152 m) AGL as a result of blowing dust.

b. Two or three times each spring extensive dust and sand from the Gobi Desert will lower visibilities over South Korea to 2-4 mi (3-6 km) from the surface to approximately 25,000 ft (7,625 m) (Nestor, 1977).

9.8 Clouds

9.8.1 General

a. Slow clearing should be forecast after a wave cyclone passes if the winds aloft remain southwest (U. S. Marine Corps, 1967).

b. Cloudiness associated with the jet stream will level off within 2,000 ft (610 m) of the tropopause, usually at or somewhat above it in eastern Asia. Widespread cirrus and cirrostratus in advance of major systems, usually Shanghai lows, top out at 35,000 to 38,000 ft (10,675 to 11,590 m) except in late spring and early fall when they often reach to 40,000 to 45,000 ft (12,200 to 13,725 m). These tops will drop steadily as the overrunning warm ridge in advance of the storm moves eastward and tops fall into the middle cloud range (Nestor, 1977).

9.8.2 Winter

a. Low ceilings (900-1500 ft) extend far behind intense cold fronts (NOCD, Kadena, 1983).

9.9 Precipitation

9.9.1 General

a. The pattern of precipitation associated with cyclogenesis in the Shanghai area will reach western Kyushu area about 6 hours after it is first reported at Cheju-Do (NOCD, Atsugi, 1980). (50-80%)

b. The occurrence of hail, as distinguished from sleet, snow pellets or soft hail, is relatively rare over the coastal waters of the Far East. Reports of aircraft encountering hail at altitude have been recorded, however, so while documentation on hail is meager, some data have been included below for use by the environmentalist. The data come largely from two documents, Browning (1977) and Flora (1953), both of which deal with hailstorms that are commonly seen over the Great Plains of the United States. The mechanics of hail formation, wherever occurring, are likely similar so the information should be applicable in the Far East.

(1) Severe hailstorms tend to be associated with a temperature excess at 500 mb of 4°C or more (difference between lifted and surrounding air temperature) and are favored by: 1) strong convective instability, 2) abundant moisture at low levels, 3) strong wind shear, usually veering with height, and 4) a dynamic mechanism that can release the instability.

(2) The most favorable height of the wet bulb freezing level for production of large hailstones is near 8,000 ft.

(3) The fall of large hailstones to the earth's surface will be less probable when the wet bulb freezing level lies above 11,000 ft or below 5,000 ft.

The most likely occurrence of hail near the Sea of Japan would be near the mountains or islands where orographic lifting of an air mass with the proper characteristics could trigger the instability mechanisms required for hail formation.

9.9.2 Winter

a. When minor troughs aloft are located well behind the surface trough, most of the rain and low ceilings experienced will be post-frontal (NOCD, Kadena, 1983).

b. Although quite rare, thunderstorms with low tops (in the 18,000 to 25,000 ft range) may accompany a rapidly moving intense cold front (NOCD, Kadena, 1983).

c. When the trough aloft is located almost vertically over the surface front, most of the rain and low ceilings experienced will be pre-frontal, with rapid improvement occurring a few hours after frontal passage (NOCD, Kadena, 1983).

9.9.3 Spring

a. When the normal westerlies aloft back to southwest or south-southwest over Taiwan and areas farther west along the China coast, precipitation can be expected over Okinawa in 24 to 36 hours, as a result of a Taiwan low (NOCD, Kadena, 1983).

9.10 Temperature/Wind Chill

No specific guidelines are offered for determining the daily temperature range at sea because too many variables must be considered, including: season, air mass type and trajectory, lapse rate, sea surface temperature, moisture distribution, cloud cover, weather, and persistence.

Once a forecast temperature is determined, a related factor must be considered -- wind chill. It can be a critical factor to personnel working on exposed weather decks, especially during late autumn, winter, and early spring months. A chart to assist in determining wind chill is included as Figure C-1 in Appendix C.

9.11 Sea Surface Temperature

The temperature of the sea is perhaps the most conservative factor that a meteorologist must consider in forecasting. The temperatures change little from day to day, so once ship movement, ocean fronts, and currents are taken into account, accurate forecasting of sea surface temperature is based primarily on persistence.

Sea surface temperature is a critical factor when considering life expectancy for a person who accidentally falls overboard. Table 9-3 is provided to assist in determining life expectancy when length of time in the water and water temperature are considered.

Table 9-3. SURVIVAL TIMES VERSUS WATER TEMPERATURE (after Brower, et al., 1977)

Water Temperature °F	°C	Exhaustion or unconsciousness	Expected time of survival
32°F	0°C	15 mins	15-45 mins
32°F-41°F	0°C- 5°C	15-30 mins	30-90 mins
41°F-50°F	5°C-10°C	30-60 mins	1- 3 hrs
50°F-59°F	10°C-15°C	1- 2 hrs	1- 6 hrs
59°F-68°F	15°C-20°C	2- 7 hrs	2-40 hrs
68°F-77°F	20°C-25°C	3-12 hrs	3 hrs- indefinite
>77°F	25°C	Indefinite	Indefinite

9.12 Electro/Optical (E/O) Forecast Aids

A general overview of E/O conditions, systems, and forecast aids are provided in the Overview Section, paragraph 2.3. The following forecast aids relate to specific conditions in the northwest Pacific and marginal seas.

9.12.1 General

a. The seasonal influence on E/O conditions will vary from winter (good conditions) with cool dry air to summer (degraded conditions) with warm moist air. Winter conditions will be polar in nature and summer conditions will approach tropical values.

b. The persistent ocean currents and frontal zones will be reflected in E/O conditions.

c. Offshore flow from the areas of mountainous terrain will result in local variations of E/O conditions in response to the funneling of winds and down slope drying patterns. Gray shades and cloud patterns depicted in satellite imagery will provide information on these small scale variations.

d. Small scale effects, land/sea breeze fronts, coastal region radiational cooling, and evaporation ducts will dominate during light wind conditions when the seasonal monsoons are weak. Large variations in E/O conditions will be found over small distances.

e. The regions around the tips of the Shandong and Liaoning Peninsulas in the Yellow Sea are known upwelling areas with lower SST's and increased occurrence of fog and low stratus. E/O conditions will be degraded in these areas.

f. The pattern of E/O conditions over the Sea of Okhotsk will be stable and near normal in the free atmosphere, but with large variations in the near surface layer (planetary boundary layer). Little day to day change will occur during the period dominated by the Siberian high. Warm season conditions will vary with the changing synoptic patterns.

g. The relatively cold dry free atmosphere conditions north of the Polar Front will enhance E/O ranges over the mid latitude/tropical ranges.

h. Over the northern areas addressed in this handbook, strong surface based inversions, throughout the year, and extensive areas of fog and stratus during the warm season will cause large variations in near surface E/O conditions.

i. Elevated ducts or superrefraction layers occur infrequently over the Sea of Okhotsk. The maximum occurrence is about 15% during summer. The heights slope from south to north during the cold seasons ranging from about 4920-5900 ft (1500-1800 m) in the south to near 1640-2624 ft (500-800 m) in the north. The slope is reversed in summer with heights of about 5576 ft (1700 m) in the north to near 3280 ft (1000 m) in the south.

j. The E/O conditions over the Philippine Sea will exhibit large winter to summer variations in response to the changing monsoonal flows and air mass types over the area. The low level E/O conditions will exhibit large variations in the vicinity of the Kuroshio Current, especially during the colder seasons when the SST gradients are most pronounced.

k. The frequency of occurrence of elevated ducts or superrefraction layers over the Philippine Sea is at a maximum during winter (30-70%) and in general increases in frequency and height under the portion of the subtropical flow where subsidence/trade wind capped inversions is developed. Frequencies of occurrence decrease to the south due to surface heating and to the west due to atmospheric mixing and synoptic scale circulation.

l. The synoptic patterns are extremely variable and dynamic over the western North Pacific in winter. This region has one of the highest frequencies of cyclogenesis of any place in the world. The E/O conditions will reflect this large variability, but in general will be near normal due to the extremely well mixed atmosphere. Rapid moving synoptic scale features will dominate the day to day variations in E/O conditions.

m. The extremely variable atmosphere is superimposed over a region of strong oceanic temperatures gradients associated with the Kuroshio Extension, Perturbed Area, and Oyashio Current. The variation in SST and air temperature relationship will result in low level modifications to the well mixed atmosphere, stabilizing it over cold water and enhancing the mixing over warm water.

n. Over the western North Pacific area, the frequency of occurrence of elevated ducts or superrefraction layers is at a minimum during late summer and into fall. Heights are generally at a maximum in the warmer areas and decrease to the north and west. During the warm part of the year heights and frequency are fairly uniform throughout the area while during the cold part they decrease sharply north of the Perturbed Area and near coastal areas. During the colder seasons synoptic variations result in major day to day changes in occurrence and heights of ducting.

9.12.2 Winter

a. The cold dry continental air flowing off Asia under the Northeast Monsoon pattern dominates the oceanic areas bounded by the Asian landmass during winter. This large scale pattern is quite stable with the storm track generally south and east of the East China Sea and Sea of Japan areas.

b. The local effects will create relatively large variations in E/O conditions due to:

(1) The increase in atmospheric moisture and marine layer depth from northwest to southeast along the path of the low level flow.

(2) The small scale variation in atmospheric conditions when moving across the cloud line patterns which typically form under the winter flow patterns. The cloudy areas are caused by low level convergence and upward motion resulting in increased relative humidity and elevated weaker inversions. The cloud free areas are caused by local subsidence and divergence resulting in decreased relative humidity and lower stronger inversions.

c. The cross cloud line/cellular distance general ranges are:

cloud streets	15 to 30 n mi
open cellular	30 to 45 n mi
closed cellular	45 to 60 n mi

d. The mountainous terrain features along western shorelines will cause winds to be funneled through valleys resulting in increased sea states, aerosol content, and earlier cloud line formation seaward of the valleys. Down slope drying and blocking of the wind will reverse the process seaward of the higher terrain.

e. The colder and stronger the flow from land to open water regions, the faster moisture is picked up and the sooner clouds will form. Because the flow over the northern part of the Sea of Japan is much colder than to the south, the cloud lines tend to be shorter off the northern coasts. This results in a reversal of the general large scale improvement of E/O ranges from low to high latitude.

f. Local variability will have organized patterns reflecting the terrain features, oceanic fronts, and convective cloud patterns.

g. Surface based ducts are likely in areas of weak offshore flow. Once cloud lines start to form the lower atmosphere has become well mixed and the duct, if still existing, will be elevated.

h. Cold coastal water flows southward along the coastline of China during winter. The cold water extends seaward to near the 100 fathom depth contour. Surface inversion heights will slope upward from the near-shore coldest water to the warmer waters beyond the 100 fathom contour.

i. The cold dry continental air flowing off Asia under the Northeast Monsoon pattern dominates the Sea of Okhotsk during winter. The large scale pattern is quite stable with the synoptic scale storm track well south and east of the area. E/O conditions at altitudes above the surface boundary layer will be near normal and show little day to day change.

j. Over the Sea of Okhotsk, the E/O conditions within the surface layer will be dominated by local effects and exhibit rapid and frequent changes. Some local forcing and related conditions are:

1. Under offshore or off ice flow, low level cloud lines will form. Passage across these cloud line fields will result in alternating areas of enhanced wind, cloud, and shower conditions through the cloud line regions with areas of decreased wind and weather between the cloud lines. E/O conditions will vary with the weather. The cross cloud line distances will vary from 15 to 45 n mi depending on the windspeed and air/sea temperature difference. The larger the values the larger the cloud lines in both horizontal and vertical dimensions.

2. The low level wind flow will be markedly altered by terrain barriers. Barrier and cornering effects will reflect sharp boundaries and rapid and marked changes in near surface weather and E/O conditions.

k. Three different synoptic scale features will typically be found over parts of the Philippine Sea during winter: the cold dry air mass of the Northeast Monsoon over the western and northern sectors, the Polar Frontal zone along the leading edge of the Northeast Monsoon, and warm moist air mass of the the retreating subtropical high.

1. The E/O conditions will vary throughout the atmosphere within the three synoptic scale features.

2. E/O conditions will be near normal under Northeast Monsoon flow, vary widely within the frontal zone, and be degraded by high atmospheric humidity under the subtropical flow pattern.

l. The subtropical high flow area of the Philippine Sea will typically exhibit elevated inversions near the top of the trade wind regime. The character of convective clouds will reflect the height and strength of the trade wind inversion. In the southerly flow, near the western end of the subtropical high in advance of the

Polar Front, high level (10,000-20,000 ft) moist layers will result in ducting layers.

m. Marked leeward drying will occur downwind from mountainous islands in the trade wind belt. Enhanced E/O conditions can be expected in these leeward dry areas.

n. Under frontal bands, optical E/O ranges will vary with the visibility changes. When dealing with the Mei-Yu/Bai-U Front the leading portion of the cloud band normally contains the most severe convective activity. The trailing portion and clear area behind are likely to exhibit elevated inversions. The larger the clear areas and flatter the cloud tops the stronger the subsidence and related inversion/ducting potential.

o. In the region of the Northeast Monsoon flow the atmosphere is well mixed and E/O conditions are near normal.

p. Cyclogenic activity is at a maximum and a well mixed atmosphere with normal ranges outside of cloud and precipitation areas. However, these restrictions will be widespread, extensive in vertical and horizontal extent, and rapidly moving. Large variability of E/O conditions on the synoptic scale will be the norm.

q. Bubble highs moving off Asia will result in short term (1 to 2 days) interruptions in the prevailing well mixed type atmosphere. The typical subsidence patterns associated with highs will be evident, although smaller, weaker,and more transient than those related to large semi-permanent highs.

r. The SST gradients will be at maximum strength. Low level conditions will be strongly influenced by the warm to cold or reverse atmospheric flow patterns.

9.12.3 Spring

a. The northward migration of the Polar Front results in large changes in E/O conditions, tropical conditions to the south, near polar to the north, and synoptic type variations under the frontal cloud mass.

b. The spring transition is slow and discontinuous. The frontal area will vary in its north/south location from day to day.

c. Spring arrives late over the Sea of Okhotsk area.

d. The break up of the pack ice includes surface melting and a rapidly available low level moisture. Large areas of fog and low stratus will form and persist for days reducing near surface visual type E/O ranges.

e. Spring brings lighter winds and therefore local barrier and cornering effects will be largely reduced.

f. The retreat of the Polar Front with an increase in frontal activity related to the Mei-Yu/Bai-U season are the major changes from winter. Tropical like E/O conditions will prevail south of the front, and synoptic type variations will prevail over the rest of the area.

g. The spring transition is slow, and the northward shift of the Polar Front tends to be discontinuous.

h. Restricted E/O ranges due to precipitation will be at a maximum over the southwestern portion of the western North Pacific due to the Mei-Yu/Bai-U front activity.

9.12.4 Summer

a. The majority of the region is south of the Polar Front, under the influence of the Southwest Monsoon and will have tropical type E/O conditions.

b. The northern portion of the region will remain under the influence of the Polar Front and an occasional migratory high. E/O conditions will vary with synoptic changes.

c. Local variability will reflect the random nature of tropical air mass instability and showers.

d. Surface and low level ducting will be infrequent. Elevated ducts may occur at upper levels where the wind direction becomes westerly and drier air is over running the moist tropical Southwest Monsoon flow.

e. The ocean surface horizontal temperature gradients that are prominent during winter and spring are eliminated due to the intense solar heating. Therefore, local variations in E/O conditions will be related to atmospheric conditions, sucn as land/sea breeze regimes.

f. The formation of a mid troposphere trough over the SOO area, generally well defined at 500 mb, will result in variations in free atmosphere E/O conditions in response to this synoptic scale feature.

g. Weak migratory cyclones will pass through the area along the Polar Front and result in additional day to day variations in E/O conditions.

h. Under the influence of high pressure systems and associated subsidence in areas of the SOO and WP, strong low level inversions will cap the marine layer and fog and very low visibility conditions will last for days. Visual related E/O conditions will be of little use. A strong low level or surface based duct is likely.

9.12.5 Autumn

a. The rapid southward migration of the Polar Front and change from southwest to Northeast Monsoon conditions is of major concern during the autumn period.

b. The local air mass will change from warm moist tropical to cool dry modified continental. Local variability will take on the winter organized patterns associated with cloud line development and terrain forcing.

c. E/O ranges will improve in the drier air behind the Polar Front.

d. Surface ducts will be likely in the areas of weak offshore flow.

e. Local conditions will reflect the influence of small scale features such as land/sea breezes, surface ducts, and evaporation ducts during clear sky light wind conditions.

f. Early autumn will exhibit the fairest weather of the year and E/O conditions will improve.

g. The return of winter conditions will occur abruptly with increased northerly winds and lowered temperatures being the most obvious indicators. E/O visual conditions can be extremely good during this initial onset period.

h. Superior mirages are likely in coastal areas of the SOO where cold dry low level offshore flow underruns relatively warm/moist air. Surface based ducting is likely under these conditions.

i. The 500 mb trough line will move out of the Sea of Okhotsk region and the prevailing winter flow pattern and associated E/O conditions will return.

9.13 Atmospheric Turbulence

The occurrence of atmospheric turbulence is significant to the operation of aircraft. Other than extreme turbulence, when control of the aircraft is essentially lost, two turbulence classifications are of interest to aviation: moderate and severe.

The two generally accepted mechanisms responsible for the creation of clear air turbulence (CAT) are standing waves in the lee of a mountain barrier and strong vertical wind shear in a statically stable layer. Both mechanisms are at a maximum in the winter months when the wind speed and the horizontal temperature gradient are at a maximum.

Mountain induced standing waves extend from the ground into the lower stratosphere and are usually limited to an area between the ridge line and a point 200 km downstream (Figure S-9-2, page 9-48). Turbulence often exists within the entire volume occupied by the mountain waves, but it is usually at a maximum between 1,300 m above and below the tropopause in the vicinity of the high-level jet-stream core immediately downstream from the ridge line. The horizontal dimensions of this "most turbulent" volume may be 400 km

Figure 5-5-2. Wave cloud. [illegible]

FIGURE S-9-2. WAVE CLOUDS OVER JAPAN. 21 MAR 80
OSAN AB Visual DMSP: TN: 21/0203 GMT

Synoptic features: A cold front has passed over Japan and westerly flow is occurring over Japan.

Satellite Image Features:

1. A wave cloud pattern extends downwind from the mountains of Honshu.

2. The inner bay of Vladivostok is ice covered.

3. Snow covers the southern part of frozen lake Xingkathu located about 85 n mi north of Kamchatka.

4. The urban warm areas of towns in snow covered grassland areas show up as dark spots in the light gray snow fields.

Forecast Aids:

1. Wave clouds over Japan indicate the high probability of moderate or stronger turbulence over the Kanto Plains region of eastern Honshu.

2. Snow fields can be differentiated from clouds through knowledge and recognition of urban areas which show up as dark spots in the snow field.
long, depending on the length of the mountain range, and up to 200 km wide, centered on the jet stream core immediately downstream from the ridge line.

The following guidelines have been extracted from various forecaster's handbooks and are presented herein to alert the meteorologist to conditions which can exist at stations which aircraft may use.

9.13.1 <u>General</u>

a. Low-level turbulence will occur in the Kanto Plain (HONSHU ISLAND, east of Japan Alps) when moderate to strong southwesterly or westerly winds occur in the lower layers. Moderate turbulence below 5,000 ft should be forecast with low-level wind velocities of 35 kt or greater (NOCD, Atsugi, 1980). (50-80%)

b. Severe turbulence will be widespread over all South Korea with the winds at 1,000 to 3,000 ft (304 to 415 m) at or above 30 kt when directions are 060-130° or 240-310°. Moderate to severe turbulence will be experienced in hilly country, especially along the higher ridge lines, whenever the gradient level winds (1,000 to 2,000 ft/304 to 610 m) exceed 20 kt (Nestor, 1977).

c. During a strong surge in the southwesterly flow, the easterly jet stream is directly over Luzon and creates moderate turbulence between 10,000 and 25,000 feet (NOCF, Cubi Point, 1984).

9.13.2 Winter

a. When the surface wind at Kadena AB gusts above 25 kt, low-level turbulence at Ie Shima and over northern Okinawa becomes moderate to occasionally severe from the surface to 4000 ft (NOCD, Kadena, 1983).

b. Jet aircraft reports of moderate CAT from the north of Kadena to the ADIZ (Air Defense Identification Zone) boundary usually follow frontal passage at Kadena (NOCD, Kadena, 1983).

c. Reports of moderate to severe turbulence above 20,000 ft are common in the central and northern Kadena FIR (Flight Identification Region). Wind speeds aloft can double in 12 hours and increase to over 200 kt near the jet core, creating tremendous horizontal and vertical wind shear (NOCD, Kadena, 1983).

d. In crew briefings during November through February, the following should be emphasized: With strong winds over Japan flowing in a direction perpendicular to the mountains, severe to extreme turbulence is experienced over the Kanto Plain.

e. The following has been extracted from NOCF, Cubi Point, (1984):

(1) During the Northeast Monsoon, when strong winds are being funneled through the pass to the northeast of Cubi Point, moderate turbulence may be expected for all aircraft departing on runway 07 on climb through 5,000 feet.

(2) During the Northeast Monsoon, light to moderate turbulence up to 10,000 feet may be forecast on the lee side of the mountains in northern Luzon. Lenticular clouds are common with a mid-level inversion.

9.14 Ship Superstructure Icing

Superstructure icing can pose a serious threat to ships at sea. Three of the common types of ice accretion are freezing rain, freezing sea smoke (arctic frost smoke) and freezing spray.

Freezing rain is the least hazardous to ships of the three, but can pose a significant hazard to personnel working on the weather decks. Rates of accretion vary directly with the rates of rainfall accumulation, and are not usually great, especially in the colder climates.

According to Kotsch (1983), arctic frost smoke occurs when the air temperature is below 32°F (0°C) and the air is at least 16°F (8.9°C) colder than the sea. The arctic frost smoke "... is often confined to a layer only a few feet thick, and trawlermen in northern waters refer to it as white frost when the top of the layer is below the observer's eye level. It is referred to as black frost when it extends above the observer."

Rime ice is formed by arctic frost smoke, and is generally easier to remove than clear or glaze ice which forms in other circumstances. The rate of accumulation can be quite rapid, however. Kotsch (1983) relates one instance in which 4" of rime ice accumulated on deck in 12 hours, with a 12" thickness observed at the rail level on the ship's side. Air temperatures in the cited example were colder than 14°F (-10°C).

Freezing spray constitutes the largest number of icing cases and is the most dangerous form of icing for ships. According to La

Belle and Wise (1983) "Certain ranges of air temperature, water temperature, and wind speed must be met to cause significant accumulations of superstructure icing. These conditions are: (1) air temperature less than the freezing point of sea water (-1.7 to -1.9°C), depending on salinity of the water, down to about -30°C), (2) wind speed of 10 m per second or more, and (3) seawater temperature colder than 8°C."

Sea spray is formed in two ways - sea spray generated by the vessel as it meets waves, and spray created by the wind as it blows droplets of water off the wave crests. La Belle and Wise (1983) state that the former is the most important mechanism with regard to icing. Usually, sea spray icing is limited to heights of 15-20 m above the sea surface, but there have been reports of sea spray icing up to 60 m above the sea surface.

The most common circumstance for icing to occur is to have a wind flow from pack ice or cold land toward open water, and have a fetch sufficient to produce "sizable" waves and spray. As the distance from the shoreline or ice edge increases, the air is warmed by the influence of the water temperature, and the chance of icing is lessened. Because dry air has a greater capacity for absorbing latent heat of evaporation at the air-sea interface, it is more effective in cooling. Consequently, cold air with a low moisture content can produce more severe icing than air with a higher moisture content.

Appendix C contains two nomograms (Figures C-2 and C-3) which were taken from Pease and Comiskey, and relate the amount of superstructure ice accumulation to air temperature, water temperature, and wind speed. They were initially developed by Mertins (1968), adapted by Wise and Comiskey (1980) for forecasting ice intensity, modified by La Belle and Wise (1983), and updated by Pease and Comisky (1985). Two other nomograms were developed (updated in 1985) and are presented in Appendix C. One is for use under conditions with high relative humidity, while the other has been modified for use with lower relative humidity.

Protection from shipboard icing can be attained by avoiding areas of strong winds where air temperatures are below 28°F (-2.2°C). If strong winds cannot be avoided, the severity of icing can be reduced by heading for warmer air and water. Some relief can be obtained by seeking shelter in the lee of land due to reduction in wind speeds and less sea spray.

9.15 Aircraft Divert Field Guidelines

The following is a collection of various forecast guidelines that are applicable to the stations indicated.

9.15.1 Naval Air Station, Atsugi, Japan

9.15.1.1 General

a. The Kanto Plain is an area of some 50 mi in width from Tokyo westward to the mountains. A small scale low, the "Kanto Low", frequently forms in this area due to differential heating enhanced by a lee side effect. This low dominates the winds at Tokyo, Atsugi, and Yokosuka under weak gradient conditions and has its greatest affect during the day. It tends to drift southeastward at night and on infrequent occasions may move to seaward and develop (FWC/JTWC, 1969).

b. Copious precipitation occurs when a secondary low or front forms over the area south or southwest of Atsugi while a low exists in the Sea of Japan (a "double-eye" low system). (80-100%)

Both lows of a "double eye" system must pass to the east of a north-south line through the local area before precipitation will end. The passage of the low is followed by a sharp outbreak of polar air and strong gusty winds (NOCD, Atsugi, 1980). (50-80%)

c. Low-level turbulence will occur over the Kanto Plain when moderate to strong southwesterly or westerly winds occur in the lower layers. Moderate turbulence below 5,000 ft should be forecast with low-level wind velocities of 35 kt or greater (NOCD, Atsugi, 1980). (50-80%)

d. Mountain-wave turbulence over Atsugi will occur when strong westerly winds are evident from 5,000 to 15,000 ft. Winds of 50 kt produce moderate turbulence while 60 kt or more result in severe turbulence (NOCD, Atsugi, 1980). (50-80%)

e. If a front is situated along the southern coast of Japan with a tropical cyclone moving toward the Kyushu to Sea of Japan area, heavy showers and thunderstorms are observed in the Kanto Plain area (NOCD, Atsugi, 1980). (50-80%)

f. An east-west oriented front situated over Honshu often causes unfavorable weather in the Atsugi area. Such fronts move slowly, and when they shift southward, weather conditions improve slowly (NOCD, 1980). (80-100%)

g. When a low pressure system moves along the southern Japanese coastline, the most probable time for the onset of precipitation in the Atsugi area is 14 to 18 hours after it begins in Kyushu (NOCD, 1980). (80-100%)

9.15.1.2 Winter

a. Severe to extreme turbulence is experienced over the Kanto Plain when strong winds are present over central Honshu and have a direction perpendicular to the mountain chain (NOCD, Kadena, 1983).

9.15.1.3 Summer (The following adapted from NOCD, Atsugi, 1980)

a. In the summer, if the Showalter Stability Index lies between 0 and -2 on the morning sounding, forecast thunderstorms in the local area during the afternoon. If the index is less than -2, forecast thunderstorms over the field during the afternoon (0-50%).

b. Thunderstorms often occur over the Kanto Plain during the summer in a persistent three-day cycle (0-50%).

c. Thunderstorms usually develop with convective heating on sunny days by 1300 local and they often move over the Kanto Plain from the adjacent mountain fringe regions. One should not forecast thunderstorms when northeasterly flow prevails aloft; when there are strong prevailing winds over the area; or when a typhoon approaches within 25Ø mi or is centered north or northeast of the area (5Ø-8Ø%).

d. Southerly or westerly wind at Mt. Fuji (or if a generally weak southwest wind exists aloft over the Kanto Plain) at a speed below 3Ø kt, indicates that thunderstorms are likely to occur in the Kanto Plain during summer afternoon and evening hours (Ø-5Ø%).

e. Maximum time of occurrence of fog formation is Ø6ØØL-Ø8ØØL. Most favorable wind direction is N to NW and July is the most favored month. Forecast early morning fog if precipitation has ceased during the night and light winds are predicted (8Ø-1ØØ%).

f. If the 24 hour precip total of the present day exceeds Ø.2Ø inches, do not forecast stratus for the evening (8Ø-1ØØ%).

g. Northeast winds cause low visibilities with haze/smoke and the favored times are 2 hours after sunrise and 2 hours before sunset (8Ø-1ØØ%).

h. Haze/smoke will not usually restrict visibility if southerly winds greater than 12 kt are occurring (8Ø-1ØØ%).

9.15.2 Naval Air Facility, Misawa AFB, Japan

9.15.2.1 General (Unless otherwise noted, the following adapted from U.S. Air force, 1970)

a. If the winds at 850 mb are greater than 50 kt and the surface to 850 mb temperature difference is greater than 10°C, anticipate winds with gusts greater than 35 kt at Misawa.

b. When a static front separates a high cell in the area of the Bonin Islands from another in the Sea of Okhotsk, it causes unfavorable weather and large amounts of rain at stations on the east side of northern Honshu (NOCD, Atsugi, 1980 and U. S. Air Force, 1970). (50-80%)

c. When there is a strong high off the coast of extreme northeastern Honshu, it usually blocks any low approaching in the Sea of Japan and rain will not be observed at stations in northeastern Honshu. However, if the high shifts either to the east or to the north, rain will begin over most parts of the area.

d. Lows moving across central Honshu (north of Tokyo and south of Sendai), usually bring precipitation to the Misawa area. The precipitation will stop when the low moves off to the east.

e. Lows from Manchuria often cause precipitation at Misawa by the time they reach 136°E.

f. If vertical shear is greater than 4 kt/1000 ft below 850 mb and the horizontal shear at 850 mb is greater than 40 kt between Misawa and Sendai (47590), expect moderate to severe turbulence near Misawa.

g. Thunderstorms are often caused over north-eastern Honshu by fronts associated with a low in the northern part of the Sea of Japan and off the coast of northwest Hokkaido.

h. No fog is expected if cold air advection is occurring below 850 mb at Misawa.

i. If precipitation (any form) has occurred during the night at Misawa, existing fog and/or stratus may persist the following day unless a change of air mass is expected.

j. Radiation fog generally dissipates between 0700 and 0900 local time.

k. The most favorable situation for very low field conditions to persist all day is winds from ENE - ESE at Misawa.

l. Prolonged fog or stratus situations are most favorable when a high is northeast of Misawa such that a long over-water trajectory exists.

9.15.2.2 Winte.

a. At Misawa, the intensity of the northwest wind in the winter season reaches a maximum some six hours after a trough or low passage due to the build-up of the high cell behind the low and usually to the west of the mountains as though the cold air were "dammed up" behind the mountains before spilling over (U. S. Air Force, 1970).

9.15.2.3 Summer

a. In the summer months (June - August), field conditions less than 200 ft ceiling and/or visibility less than 1/2 mile occur about 5% of the time but are rare during mid-day (1000 - 1500 LT) (U.S. Air Force, 1970).

9.15.3 Kadena Air Base, Okinawa, Japan

9.15.3.1 General

a. Middle cloudiness appears then increases rapidly as Okinawa comes under the influence of the backside of high pressure areas. A typical warm frontal sequence is observed and it is often possible to draw a warm front between Taiwan and Okinawa on surface charts (U. S. Marine Corps, 1981).

b. Thunderstorms (not including frequently reported towering cumulus) are rare on Okinawa, occurring on an average of four days during the peak months of June and August and are normally not observed during the months of January, February, and November (U. S. Marine Corps, 1981).

c. Thunderstorms on Okinawa are comparatively mild (versus their North American counterparts), even when associated with squall lines (U. S. Marine Corps, 1981):

(1) Most of the associated lightning is cloud to cloud (versus cloud to ground).

(2) Little gustiness is associated with the storms. One exception occurs when the winds aloft are strong and the storms are fast moving, thus increasing the gusts by the speed of the storm.

(3) There is a noticeable absence of the up-draft/downdraft/first gust phenomena. When present, they are weak, and unless the storms are associated with frontal passages, there are usually no wind shifts as the storm passes.

(4) Stability indexes are of little value in forecasting thunderstorm occurrence on Okinawa, but when the stability index is -1 or -2, cumulonimbus clouds are usually observed around the island.

9.15.3.2 Winter

a. In January and February, forecast good weather in the Okinawa area when a migrating high center moves east along or south of 30°N (NOCD, Kadena, 1983).

b. Forecast overcast skies, a ceiling between 3,000 and 9,000 ft, and possible rain for the Okinawa area when a migrating high cell crosses the Sea of Japan during winter. Winds will be easterly, backing to the north when a trough comes through (NOCD, Kadena,1983).

c. The following guidelines are taken from NOCD, Kadena (1983) and apply to conditions occurring during the late autumn and winter seasons.

(1) Mid-November through mid-February is the period of the "arctic fronts", as the Polar Front lies across the Philippines.

(2) In forecasting weather associated with outbreaks of the Siberian high:

(a) Prior to frontal passage, surface winds will become southwest to west 35+ kt and, in isolated cases, contain gusts to 65 kt.

(b) The cold front will be moving at speeds in excess of 20 kt.

(c) Rain will occur prior to passage of the front, with rainshowers for at least six hours subsequent to passage.

(d) With frontal passage, winds vary from west to north, ceilings may be reduced as low as 500 ft, and visibility may be one mile in brief heavy rain.

(e) Behind the front are persistent, strong, gusty surface winds, often 25 kt or higher, and 1-3 days of overcast stratocumulus with bases between 2,000 and 6,000 ft. Occasional light rainshowers or drizzle will accompany the overcast skies. This precipitation will usually end when winds decrease and shift to northeast to east.

(3) Frequently, scattered convective showers occur over water during the post-frontal northerly flow as a result of strong surface heating over the relatively warm water surrounding Okinawa.

(4) An arctic frontal passage at Kadena can be expected to occur within 16 hours after it passes Cheju-Do if the 700 mb wind speed at Kadena (at the time of the frontal passage over Cheju-Do) was 25 kt or greater.

(5) The cold front of a single low in the Sea of Japan will cross Okinawa as the low center passes over the Noto Peninsula (37°N 137°E).

(6) Eighty percent of the cold fronts approaching Okinawa from the northwest are inactive and fast-moving (25 kt). Some have been observed to move at speeds close to 50 kt.

d. If cold fronts are well-defined (steep gradient behind front), there will be no clearing until the 700 mb trough passes the station. If the gradient is weak, partial clearing should occur within 6-8 hours. The worst weather occurs when the Polar Front stagnates just east and south of Okinawa (oriented northeast-southwest). Stable waves along the front bring bad weather and intense lows can form if the front is reinforced by a strong trough at 700 mb and 500 mb moving into the area from China. Indications of approaching bad weather can frequently be observed by monitoring reports from Taiwan, Ishigaki Shima and Miyako Jima (U. S. Marine Corps, 1981).

e. When a winter Siberian high outbreak is evident, forecast surface winds of at least 20G35 at the time of frontal passage. There may also be a second surge of gusty winds which reach 40+ kt occurring 1-2 hours after frontal passage (NOCD, Kadena, 1983).

f. Surface wind intensity varies with the width of weather bands. During the winter, narrow, rapid-moving bands are accompanied by gusts to 45 kt, while wide, slow-moving weather bands may be accompanied by gusts which seldom exceed 35 kt. (NOCD, Kadena, 1983).

g. Low ceilings (900-1,500 ft) extend far behind intense cold fronts (NOCD, Kadena, 1983).

h. Post-frontal (cold) cloudiness during the fall and winter months is characterized by stratiform conditions. Heavy showers, thunderstorms, etc., may be observed just prior to and with the frontal passage but, within a short time, nimbostratus and stratocumulus are observed (U. S. Marine Corps, 1981).

i. During the winter months, even though the sky cover is scattered to clear at sunset, forecast a broken to overcast layer of stratocumulus with bases between 3,000 and 4,000 ft and tops between 5,000 and 6,000 ft, forming under a very strong inversion by midnight. This deck will persist until one to two hours after sunrise, then become scattered (NOCD Kadena, 1983).

j. Although quite rare, thunderstorms with low tops (18,000 to 25,000 ft) may accompany a rapidly-moving, intense cold front during the winter season (NOCD, Kadena, 1983).

k. NOCD, Kadena, (1983) offers the following caution regarding winter flight forecasting and the aircraft icing problem: "Icing becomes a problem for propeller-type aircraft over routes extending northward to Korea, Japan, Midway, and Alaska."

l. Reports of moderate to severe turbulence above 20,000 ft is common in the central and northern FIR. Wind speeds aloft can double in 12 hours and increase to over 200 kt near the jet core, creating tremendous horizontal and vertical wind shear.

m. When the surface wind at Kadena AB gusts above 25 kt, low-level turbulence at Ie Shima and over northern Okinawa becomes moderate to occasionally severe from the surface to 4000 ft.

n. Jet aircraft reports of moderate clear air turbulence from the north of Kadena to the ADIZ boundary usually follow frontal passage at Kadena.

o. In January, the major region of cyclogenesis lies beneath the southern jet stream at about 30°N in the East China Sea. First indications of formation are the sudden appearance of high and middle clouds. Cloudiness increases when winds over Taiwan back to 210°-240° and increase in speed. Rain begins as the low center arrives in the vicinity of 125°E-126°E. Forecast rain to stop and ceilings to lift when the wave crest moves east of 127°E (NOCD, Kadena, 1983).

9.15.3.3 Spring (Unless otherwise noted, the following adapted from NOCD, Kadena, 1983)

a. When a Taiwan low moves northeast, cold frontal passage on Okinawa usually occurs within 24 hours after warm frontal passage. A squall line usually precedes the cold front, acting as a false frontal passage. Thunderstorms commonly accompany this squall line.

b. Waves forming east of Shanghai in the spring will cause low ceilings and visibilities throughout southern and central Japan. The associated cold front will pass through Okinawa 6-8 hours after it passes Ishigaki Shima and Miyako Jima.

c. During pre-warm frontal weather in the spring, a fog bank can form to the south-southwest, obscuring Naha. The bank lifts slightly over Kadena, and reduces visibilities to one mile or less.

d. In spring, stratus frequently prevails (around Kadena). The following rules apply:

(1) Stratus is apparently caused by the cooling of moist, southerly air flow over cooler, shallow water.

(2) Fog over water to the south-southwest lifts as it is advected over the island's edge and prevails as stratus until dissipation 2-3 hrs after sunrise. The situation is intensified when the southerly flow is 10-20 kt, causing rapid cooling and a lowering of the mixing condensation level (MCL).

(3) Stratus is generally less than 1,000 ft thick, with bases between 500 and 1,000 ft.

(4) Stratus will form with strong winds in the lower levels. It will be scattered to broken shortly after sunset. With south through southeast winds, it will be scattered over the island, broken on approach, and more prevalent to the east. Under these conditions, stratus is quite variable and burns off rapidly after sunrise, forming a scattered to broken deck of stratocumulus with bases at 1,500-2,000 ft by 1000L.

(5) With light lower-level winds, stratus generally remains as a scattered layer over the island until sunrise, becoming broken for two to four hours afterward, lifting from a base of 1,800 ft by 1100L. In this case, the cloud cover is generally independent of wind direction, making it difficult to forecast the amount of cloud cover and timing of ceiling periods.

(6) Forecast stratus when the surface to 2,000 ft winds are greater than 10 kt. By 12Z, the stratus ceiling will be below 1,000 ft and will be an intermittent condition, both in amount

of coverage and in height. It will remain until the surface temperature has risen 6°F above the minimum temperature.

e. When the normal westerlies aloft back to southwest or south-southwest over Taiwan and areas further west along the China coast, precipitation can be expected over Okinawa in 24 to 36 hours, as a result of a Taiwan low.

f. Southwesterly winds at 700 mb over station 46810 (southwest of Taiwan) during the autumn or spring indicate precipitation at Kadena within 24-36 hours.

g. Light rain will begin on Okinawa 3-6 hrs after a closed circulation east-northeast of Taiwan indicates deepening and definite movement.

h. As the wave from a Taiwan low passes to the south of Okinawa, expect showers and associated low ceilings.

i. If cold fronts are well-defined (steep gradient behind front), there will be no clearing until the 700 mb trough passes the station. If the gradient is weak, partial clearing should occur within 6-8 hours. The worst weather occurs when the Polar Front stagnates just east and south of Okinawa (oriented northeast-southwest). Stable waves along the front bring bad weather and intense lows can form if the front is reinforced by a strong trough at 700 mb and 500 mb moving into the area from China. Indications of approaching bad weather can frequently be observed by monitoring reports from Taiwan, Ishigaki Shima and Miyako Jima (U. S. Marine Corps, 1981).

9.15.3.4 Summer

a. Summer winds are prevailing southerly, and are light and variable during the period from sunset to sunrise. They increase during the early morning to 10-20 kt, and remain at that speed until approximately 1700L (NOCD, Kadena, 1983).

b. Thunderstorms are difficult to forecast during the summer. Most often, they are caused by the decrease of the surface to 500 mb wind speed to light and variable. In this case, the cumulus clouds build over the island, and, having no strong flow to advect them out, develop into thunderstorms. Waterspouts and funnel clouds are common during this period but cause little or no damage. Reports of water spouts over Buckner Bay, Okinawa from TCU, some with tops below 20,000 ft, are common. There have been a few occurrences of funnel clouds over the hills at Camp Hansen and points further up the island (NOCD, Kadena, 1983).

c. An interesting summer phenomenon on Okinawa is the relatively consistent formation of early morning fracto-cumulus/fractostratus that frequently creates a temporary IFR condition (usually between 0800-1000L). This cloudiness is quite thin, usually broken and at an altitude of 600-800 ft. Its formation is usually associated with a southeasterly/ southwesterly flow under 10 kt, as higher winds eliminate the clouds. The clouds are apparently caused by the ocean waters warming a shallow layer near the surface. The higher levels (1,000-1,500 ft) lose a greater amount of heat by radiation and create an unstable situation which in turn generates the shallow layer of clouds that is subsequently moved over land by the prevailing wind. Surface heating normally lifts these clouds above 1,000 ft by 1000L and changes their physical appearance to that of stratocumulus or cumulus humilis (U. S. Marine Corps, 1981).

9.15.3.5 Autumn

The following guidelines are taken from NOCD, Kadena (1983).

a. Autumn weather, which extends from the first cold frontal passage during September to the end of typhoon season, is variable. Early frontal passages usually contain imbedded thunderstorms, and become weak and disorganized to the south (near 25°N 125°E).

b. Excellent weather generally prevails for a two or three day period after frontal passage.

c. Typhoons occur frequently during this period, and will, if passing near Okinawa, change the Polar Frontal position and associated air mass over the island.

d. Frontal passages during early autumn have a 4-6 day cycle. Later in the season, this is reduced to a 2-4 day cycle.

e. Autumn frontal passages are usually brief; associated weather is 4-6 hours of light rain.

f. Showers will occur about 3-4 hours after cold frontal passage.

g. A cold front will pass Okinawa in 24 hours when:

(1) Temperature advection below 500 mb changes from cold to warm (veering winds with height); and

(2) Southerly winds appear in the layer between 4,000 and 7,000 ft.

h. During autumn, mid-clouds will generally constitute a ceiling, but are usually thin, around 2,000 ft thick. Bases may vary between 8,000 and 16,000 ft. These clouds usually burn off with daytime (diurnal) heating. The best indicator of their formation is a thin layer of moisture on the 1200Z sounding, capped by very dry air above.

9.15.4 Marine Corps Air Station, Iwakuni, Japan

a. During winter, late autumn, and early spring, expect snow or snowshowers rather than rain or rainshowers if the surface temperature is at or below 40°F during precipitation periods (U. S. Marine Corps, 1967).

b. Gusty surface winds from the northwest will persist for 24 to 36 hours after a cold frontal passage in the autumn, winter, or spring (U. S. Marine Corps, 1967).

9.15.5 Korean Airfields

9.15.5.1 General

a. The following general forecast guidelines are extracted from Nestor's 1977 document The Environment of South Korea and Adjacent Sea Areas, published by the Naval Environmental Prediction Research Facility. They are applicable to an area rather than a particular station.

(1) When the 500 mb chart shows a deep low aloft northwest of the Korean peninsula with a deep trough extending south to southwest through the Yellow Sea, frequent trough passages can be expected at about six hour intervals for approximately 24 hours.

(2) Any kind of trough or front in the Yellow Sea will tend to set off isolated rain showers along the west coast of the Korean peninsula (primarily from Kunsan to Osan) between 0500 and 1100 local time with broken low and medium level cloudiness during this period extending along the entire west coast. Cumulonimbus clouds and/or thunderstorms are very likely to develop in that area after 1200 local time and move northeast.

(3) Summer low cells which pass to the north do not cause much precipitation over South Korea. However, when they pass to the south, heavy continuous precipitation should be expected.

(4) Typhoons that move northeast south of Japan produce light, intermittent precipitation over areas of South Korea.

(5) South Korea receives heavy rain showers if a high is situated over the Sea of Japan and/or southern Siberia and a typhoon or tropical storm is positioned in the Taiwan area.

(6) Northeasterly wind flow over South Korea resulting from a Sea of Japan high usually brings low cloudiness with little precipitation.

(7) When 850 mb winds are less than 20 kt, the heaviest concentration of rain occurs in the Korean lowlands. When the winds are greater than 20 kt, the heaviest rain occurs in mountain areas.

(8) Low level air flow in winter from about 290° clockwise to 120° tends to give clear, cold weather to South Korea. Winds from any other direction tend to produce cumulus buildups and

scattered snow showers along the west coast, with ceilings and visibilities in the vicinity of showers lowering to about 2,000 ft (610 m) and 1 1/2 mi (2 1/2 km), respectively.

(9) In winter, strong northwesterly flow usually indicates the beginning of three to five days with fair skies, cold temperatures and no precipitation. After the third day, morning fog/smoke will often develop between 0800 and 1000 local time.

(10) Low cells passing south of Japan in winter cause considerable cloudiness but seldom bring rain to South Korea.

(11) At times during late winter and spring, dust from the Gobi Desert is carried south by active cold fronts moving from the northwest and spreads rapidly over Korea. Visibilities and ceilings are reduced below minimums for as long as 24 hours.

(12) During summer and winter, the central regions of South Korea will have the lowest minimum temperatures under clear skies/calm wind conditions. Maximum temperatures in summer will often occur near the DMZ rather than along the southern coast.

(13) Low cells moving eastward from the Yangtze (Changjiang) River area of China in spring cause South Korea to receive small amounts of rain if they move rapidly. Very heavy rain results if the low cells move slowly.

(14) During spring when there is strong northwest or west flow over Manchuria and China, yellow dust will sometimes be carried as high as 15,000 ft. This restricts in-flight visibility to 5-7 miles.

(15) In summer, if the winds at Cheju-do become southeast 8 kt or greater, rain will occur over Korea in 12 to 18 hours due to a wave on the Polar Front and will persist until a north-south line through the wave crest is east of Korea. However, if a trough is retarded over Korea from the closed circulation around the wave (with a general west-northwest/east-southeast orientation), continued cloudiness and rain should be forecast.

(16) When a Pacific high pressure ridge extends over Korea during the summer, thunderstorms and rain showers occur over western Korea.

9.15.5.2 <u>Specific Airfields</u>

The following guidelines, extracted from U. S. Air Force (1964), were written for use at individual stations as indicated. The location of each station can be found in Figure 9-1.

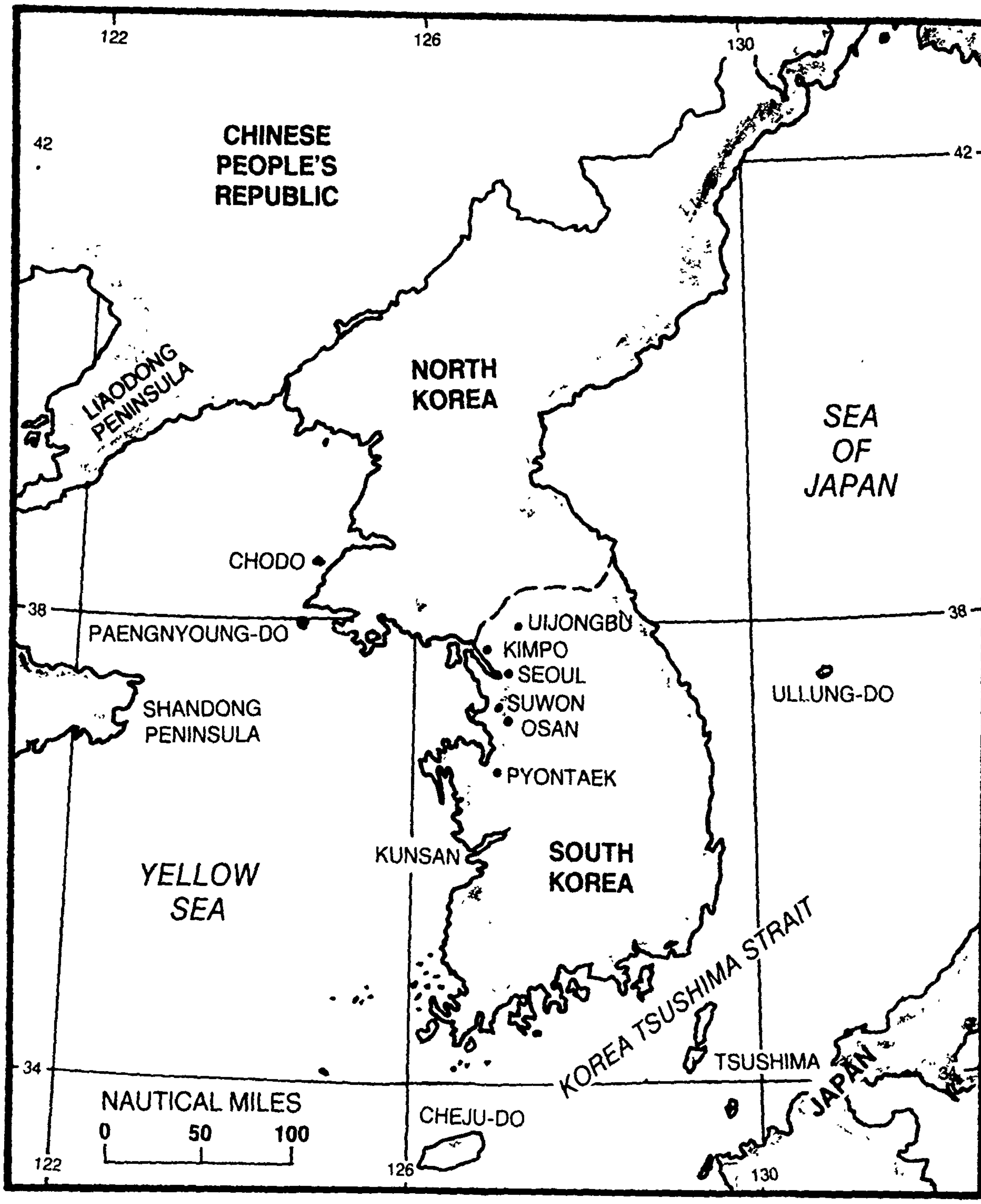

Figure 9-1. South Korea and adjacent areas.

a. <u>Suwon</u>

(1) Paengnyong-Do is a representative "upstream" station for the Suwon area.

(a) A cold front that moves southeast can be forecast to pass Suwon an average of 4 hours after it passes Paengnyong-Do.

(b) Precipitation occurs at Suwon 2 to 5 hours after it is reported on the island of Paengnyong-Do.

(2) When cyclogenesis occurs over east-central China the resulting low will move northeast causing a trough to be induced over the Yellow Sea with deteriorating weather in the Suwon area.

(3) When the 500 mb chart features a primary low centered between Lake Baikal and 130°E with a trough extending south through the Yellow Sea, it indicates that frequent frontal passages will occur at Suwon bringing extremely variable weather.

(4) When the 500 mb chart indicates a trough passage will occur at Suwon, a narrow band of unfavorable weather will occur if the trough axis is northeast-southwest or north-south. If, however, the axis is northwest-southeast a <u>wide</u> band of unfavorable weather should be forecast.

(5) Rainshowers can be expected to persist in the Suwon area after a cold frontal passage if the trough aloft remains over the Yellow Sea.

(6) A 0.9 correlation has been determined for fog to occur in the Suwon area 1 hour after it has been reported at Kimpo and/or Seoul.

(7) Favorable weather persists at Suwon in winter when an intense high is centered in the Lake Baikal area and its influence extends southeast to Japan.

(8) At times during winter a 4 to 8 kt west wind begins in the Suwon area which brings stratocumulus that has developed over the Yellow Sea during the day. This causes ceilings of 1500 to 2500 ft to occur at night, dissipating the following morning by 1000L. Light snow and rain occasionally results from this cloudiness during early morning hours.

(9) In winter when there is a small difference between maximum and minimum temperature on the same day with a steady decrease in temperature-dew point spread, fog should be forecast with minimum visibilities to occur between 0700L and 1030L.

b. <u>Osan</u>

(1) The island of Chodo (38°40'N 124°50'E) provides an excellent index for timing frontal approach and passage at Osan. Weather at Osan can be expected to parallel Chodo weather with a lag of some 6 to 8 hours.

(2) When the difference in sea-level pressure between Paengnyong-Do and Kimpo becomes or is forecast to become 5 mb,

surface winds with gust up to 30 kt should be forecast. For 6 or 7 mb differences, gusts of 35-40 kt should be forecast.

(3) Lows that deepen in the Sea of Japan cause the pressure gradient to steepen over the Korean peninsula and strong and gusty surface wind, usually of 8 to 10 hours duration, should be forecast for Osan.

(4) In winter a northwest wind usually indicates cP air over the area with the Siberian high in its usual winter position. This brings favorable weather to the Osan area.

(5) Polar outbreaks can be recognized in the Osan area in winter by analyzing the Kimpo upper air sounding. This is indicated when winds aloft veer to the northwest and increase to above normal intensity. When there is a jet stream associated with the outbreak, winds aloft can reach speeds of from 150 to 180 kt. Surface winds can increase to 50 kt with a strong surface gradient.

(6) If easterly surface flow is expected after a winter front or trough passage, forecast scattered low clouds and broken to overcast middle clouds to persist for at least 24 hours after passage.

(7) Very rapid clearing occurs at Osan after a frontal passage in winter.

(8) A thin cirrostratus overcast which forms over Osan and gradually thickens is often the first indication of a wave cyclone moving toward Osan. They usually reach the area 24 to 36 hours later. These passages are most frequent during spring.

(9) In June or July when the Polar Front is situated in the vicinity of Cheju-do and a ridge or cell of high pressure (highest pressure greater than 1010 mb) appears over the Sea of Japan on the surface chart, rain should be forecast to occur at Osan within 48 hours.

c. Kunsan

(1) Weather at Kunsan associated with secondary fronts from Siberia varies in accordance with the way they are oriented:

(a) East-west oriented fronts generally feature a narrow band of broken cumulus and scattered showers. Rapid clearing with frontal passage followed by continued fair weather can be expected as long as the upper air circulation is north to northeast.

(b) Northeast-southwest oriented systems are considerably more intense during passage with the intensity varying according to the strength and duration of the southwest circulation.

(2) Winter lows that develop in the Taiwan area and begin to deepen as they start to move have an associated deep trough line over the Yellow Sea which brings low ceilings of 1,000 to 2,000 feet in the Kunsan area. Other weather effects at Kunsan are:

(a) Precipitation which persists for periods of up to 18 hours and ends as the storm center passes 127°E.

(b) Low ceilings of 500 to 1,000 feet when the storm center reaches Kunsan.

(c) Cloud cover that persists from 24 to 36 hours.

(d) Ceilings and visibilities that drop to 600 feet and 3 miles or less a few hours after the beginning of precipitation which is usually in the form of rain or drizzle.

(3) Generally a deep (up to 10,000 ft) southwesterly flow with wind speeds in excess of 15 kt, persisting for a period of 12 hours, is necessary before extensive cloud cover is experienced at Kunsan. Ceilings range from 2,000 to 4,000 ft, occasionally as low as 1,000 ft.

(4) Sea stratus can move onshore over Kunsan at mid-day and should be forecast whenever the dew point temperature is equal to the sea surface temperature. Its greatest frequency of occurrence is just before sunset.

(5) Low (1,000 to 1,500 ft) scattered stratocumulus or flat cumulus observed just east of Kunsan and over the adjacent hills, usually indicates that dense fog will occur shortly after sunset.

(6) The areal extent of cloud cover inland in winter over western Korea can often be forecast by wind direction, for if winds flow from 330° at the 850 mb level, cloudiness will spread over the entire river valley.

(7) Low level airflow in winter from 330° clockwise to 060° causes clear, cold weather at Kunsan. The fine conditions also persist for easterly circulations with directions of from 060° clockwise to 140° provided the gradient wind velocities are light.

(8) If low level flow is from 060° clockwise to 140° and gradient winds speeds are 25 kt or more, heavy cumulus "build ups" may occur in mid-winter and cause frequent snow showers.

(9) The following empirical parameters apply chiefly during late winter, spring, and the first half of summer for the formation of fog or sea stratus in the Kunsan area.

(a) Winds in the layer from the surface to 2,000 ft persist from a direction between 270° clockwise to 330° with speeds greater than 5 kt. Winds most conducive for fog or stratus occurrence are from 300° at 10-12 kt.

(b) The dew point temperature is lower than and within a few degrees of the sea surface temperature at the time of maximum temperature.

(c) The station relative humidity is above 70% at the time of maximum temperature.

(10) When lows pass through the Tsushima strait in spring they produce ceilings of 500 to 1,000 feet in the Kunsan area and these persist for about 36 hours. Visibilities usually do not drop below 2 mi. Lows passing through central Korea bring ceilings of 500 to 1,000 ft for about 36 hours.

(11) Lows passing south of Kyushu in spring generally cause ceilings of 6,000 to 7,000 ft and light rain in the Kunsan area. The ceilings usually persist for 24 hours and the rain for 12. Visibilities rarely drop below 4 miles.

(12) Visibilities often drop to less than 3 miles 2 hours after precipitation begins when a warm front approaches in spring and drops to between 1/2 and 1 mile about 6 hours before a front passes.

(13) Advective sea fog occurs infrequently during summer months in the Kunsan area. It usually dissipates by mid-morning or is lifted by turbulence to form a deck of stratus.

d. Kimpo

(1) Cold fronts that move into the local area of Kimpo have usually gained enough moisture over the Yellow Sea to cause low ceilings and showers to persist for 1 to 3 hours. After tneir passage rapid clearing takes place.

(2) A wave system will often cause light rain and ground fog 8 to 12 hours before it passes Kimpo.

(3) When Kimpo experiences a warm or occluded frontal passage, rain and ground fog will restrict visibility from 1/2 to 1 mile and ceilings will drop to 200 to 400 ft.

(4) A scattered sky condition usually occurs 6 to 9 hours after a frontal passage in the Kimpo area.

(5) The amount of moisture revealed in the Lake Baikal sounding is some indication of the severity of weather to be anticipated with frontal passage at Kimpo.

(6) Even though a front may pass the Shandong Peninsula without rain, it often brings rain or snow to the Kimpo area because it gains moisture during its track over the Yellow Sea.

(7) It is normal for weather conditions at Kimpo to follow those at Paengnyong-Do by about 5 hours. For example, a cold front will normally pass Kimpo 5 hours after it passed Paengnyong-Do.

(8) Rain associated with Yellow Sea lows usually persists for two consecutive days. On the third and sometimes the fourth day strong convective activity and thunderstorms may occur.

(9) Visibility restrictions are usually lower and more intense at Kimpo than at Osan.

(10) Very few cases of strong southwesterly winds occur at Kimpo during winter. However, southwest winds of 15-25 kt ahead of a cold front occur frequently.

(11) Early morning smoke and haze are the major restriction to visibility in the Kimpo area. Kimpo city and

adjacent villages yield the largest amounts of smoke which reach the base with easterly surface flow. Consequently, visibilities below one mile should be forecast about one hour after sunrise in winter. When clear or scattered cloudiness occurs, visibilities can be expected to improve to 1 mile by 1000L to 1100L, and to 3 miles by 1400L to 1500L.

In most synoptic situations, only easterly surface winds will bring sufficient smoke to reduce the visibility below 1 mile in the Kimpo area.

(12) A well defined cold frontal passage causes very heavy rainshowers in the Kimpo area. Visibilities usually drop to less than 1/2 mile and the precipitation ceiling is less than 400 ft.

(13) A good rule to follow is to forecast no restriction to visibility to the Kimpo area during the first night following a frontal passage, after which the visibility should be reduced a little more each night until the axis of the high moves east of Kimpo.

(14) Strong northwest winds can be forecast for the Kimpo area when a rapidly intensifying or moving high pressure cell follows a cold frontal passage.

(15) Sea fog in the Kimpo area has a tendency to dissipate earlier each day with the progression of spring.

(16) In summer, stable, fast-moving waves travel eastward along the fronts that have become stationary after passing Kimpo. They cause spells of 3 or 4 days when low ceilings and rainshowers persist and the weather is extremely variable.

(17) In July, when winds over Kimpo at 850 mb are observed between 230° to 290° at 1800 local time, rain or thundershowers occur 75 percent of the time during the following 12 hours.

(a) In all occurrences ceiling and/or visibility dropped below 1,000 ft and 3 miles sometime during the period.

(b) In 60 percent of the cases, conditions below 400 ft and/or 1 mile were reported.

During July, if winds are observed between 230° and 290° at 850 mb over Kimpo, and the difference between the 850 and 500 mb level temperatures is 23-25°C, thunder-storms or rain should be forecast. (90% reliable)

(18) Reduced summer morning visibilities caused by a nocturnal land breeze from Yong Dong Po usually persist in the Kimpo area until 1100I when the land-sea gradient is reversed.

e. Pyongtaek

(1) Since lows generally follow an eastward progression across Siberia north of Korea, the Pyongtaek area experiences the passage of trailing sections of cold fronts. These are weak and slow moving, cause little or no precipitation, and are often difficult to detect. Frontal passage is often realized only by the cooling in the lower layers of the Kimpo sounding.

(2) Thick low stratus with drizzle frequently forms on spring mornings when the preceding day was warm (at least 70°F), had strong southwesterly winds which diminished at night, and was dusty and hazy. The night is usually clear.

(3) As the Yellow Sea warms during late spring the low, dense morning stratus is replaced by formations of thin decks at altitudes of 800 to 2,000 ft. Fog instead of stratus sometimes forms, especially if haze or dust are present at sunset the previous day.

f. Uijongbu

(1) The Showalter index alone is not a reliable guide in the Uijongbu area, most likely due to the effect of the terrain.

(2) Air mass type thunderstorms occur infrequently, most likely due to a lack of sufficient surface heating.

(3) With relatively thick fog and clear sky above, a 500 ft (base) stratus layer will form about 2 hours after sunrise, lifting to 1,000 ft and becoming scattered during the following 2 hours.

(4) After the first night of fog in the Uijongbu area, persistence can be used to make a good forecast for the time of formation and dissipation of the fog until there is a significant change in the local air mass.

(5) Landing areas located on plateaus or ridges will experience winds 5 to 8 kt stronger than those at the Uijongbu station.

(6) During winter, a sharp night time inversion causes visibilities of less than 1 mile by morning, normally improving to 1 mile by 0900L and 5 miles by mid-afternoon.

(7) Fog often occurs the second night after a frontal passage during fall and spring months.

(8) Precipitation during the summer rainy season is usually caused by waves that form on the Polar Front in the East China Sea and move eastward along the front. It is normal for rain to occur just in advance of the wave's warm sector while considerable cloudiness and scattered showers are observed behind the wave and its cold front. The leading edge of the precipitation is usually well defined so that locations which record moderate rain and those which observe a trace may be only five to ten miles apart.

(9) Air which overruns the Polar Front when it lies along the southern coast of Korea often causes light rain in the Uijongbu area. This is indicated on the Osan sounding 12 to 18 hours in advance by a warm layer of air from 3,000 to 5,000 ft thick between 10,000 and 20,000 feet.

g. Seoul AB

(1) The following rules are for forecasting duration and intensity of the visibility restriction at Seoul AB. They apply in winter and autumn with wind speeds less than 7 kt and if the wind is from the quadrant specified.

(a) Northeast quadrant. Early morning winds are vary rarely from the northeast. A visibility minimum of not less than 2 miles can be expected since Seoul Air Base is situated a considerable distance from smoke sources in this direction.

(b) Southeast quadrant. A visibility minimum of 1 to 3 miles will occur about 1 hour after sunrise and will persist for 4 to 5 hours. If an unusually strong or double inversion is present, visibilities below 5 miles will persist all day.

(c) Southwest quadrant. A minimum visibility of less than 1 mile in heavy smoke will normally occur 1 hour after sunrise. Heavy smoke will persist until the inversion breaks, or about one hour after the visibility minimum. However, since the southwest wind usually shifts to northwest within 1 hour after minimum visibility, the effect of the northwest quadrant then occurs.

(d) Northwest quadrant. No drop in visibility will occur if northwest flow has persisted throughout the night. If the wind shifted from southwest, rapid clearing occurs with well established northwest flow.

(e) Calm. The visibility minimum depends on the strength of the inversion, and can be expected to be about 1 mile in heavy smoke if skies are clear. The condition will persist until the wind starts, or until strong surface warming occurs, which usually takes about 3 to 4 hours.

(2) Early morning smoke restricts visibility for as much as two hours longer than normal when the temperature is below 5°F.

9.15.6 Naval Air Station, Agana, Guam

The following guidelines are taken from the 1983 edition of the Local Area Forecaster's Handbook, published by the Naval Weather Service Environmental Detachment, U. S. Naval Air Station, Agana Guam:

9.15.6.1 Easterly Waves

Troughs in the easterlies approaching Guam are sometimes difficult to locate. Frequently there are few, if any, reports between Wake and Guam. Often the best indication of a wave approaching the area will be from a pilot debrief. Sharp questioning by the forecaster concerning winds and weather enroute will often provide the clues needed to ascertain the location of a wave.

Try to determine the location and extent of any significant weather enroute. Probe any significant wind shifts, and determine the position of the shift in relation to the weather encountered. Once it has been determined the pilot did pass through a line of weather oriented north-south, and that he did experience a wind shift (from easterly to southeasterly, thence northeasterly (when proceeding westbound)) the probability that an easterly wave exists has been established.

Subsequent AIREPS and debriefs should be closely analyzed to determine the movement and intensity of the wave. If further debriefs and AIREPS are not available, history and continuity should be maintained. A good rule of thumb, when reports are not available, is to advance the wave at an average speed of 10 kt.

9.15.6.2 Typhoons/Tropical Storms

Passage of a storm near Guam presents local hazards and the forecaster must be aware of probable damage. Storms moving south of Guam will cause considerable rain and wind for about 24 hours. As the storm moves west of the area it is well to remember that feeder bands will cross the island causing additional heavy rains and gusts, a condition that can persist for an additional 12 to 24 hours.

When a storm passes north of the island, weather will not be as violent as with a "near miss" to the south but feeder bands crossing the island will often produce stronger winds and more weather than the actual passage of the eye. This is and example of the hazardous semicircle rule relative to T.C.'s

9.15.6.3 Intertropical Convergence Zone (ITCZ)

When the ITCZ lies south of Guam, a study of Micronesian reports will present the forecaster with a fair estimate of its position. When northerly migration begins and the ITCZ is north of a line between Yap (9.5N 138.1E) and Truk (7.5N 151.8E), pilot reports and satellite data must be used.

An increase in middle clouds and above normal convective activity can be expected as the ITCZ approaches Guam from the south. When the ITCZ moves to about 100 n mi south of the island a marked increase in shower activity can be expected. Weather at NAS Agana will improve rapidly when the ITCZ moves north of Guam and dissipates. The situation will be of short duration, however, as a new ITCZ will form within 12 to 24 hours near the mean seasonal position.

9.15.6.4 Air Mass Shower Activity (U. S. Navy, 1969B)

The following objective method of forecasting air mass shower activity is best employed during the summer months, but the applicability should not be limited to only one season.

PARAMETER (1200Z)	LIMITING VALUE	WEIGHING FACTOR
A. Avg g/kg 900-700 mb	>10 g/kg	25
B. LFC	$\leq 6,000$ ft	15
C. LCL	$<1,000$ ft	20
D. Temperature difference (CCL-500 mb) between free air and saturation adiabat through the CCL	$\geq 3.5^{\circ}C$	20
E. Dew point spread $6^{\circ}C$ or less (pressure at top)	≤ 800 mb	20
	TOTAL	

IF THE TOTAL IS	FORECAST
>85	RW/TRW
>70	RW
50-70	TCU
<50	NO RW

Reliability: Fifty-three soundings were evaluated prior to selection of the parameters involved. Stability indexes were found to have neither a positive nor a negative correlation with the occurrence of showers. Similarly, wet-bulb zero, height fall/rises, and vertical wind profile were found to be without concrete applicability.

Forecasting areal extent is largely subjective, and may be influenced by vorticity considerations, position of the mid-Pacific trough, etc.

Verification:	Total soundings evaluated	53
	Forecasts verified	40
	Percent accuracy	75

9.15.7 Naval Air Station, Cubi Pt., Republic of the Philippines

The following guidelines are taken from the Forecaster's Handbook, NAS Cubi Point, R. P. published by the NOCF, Cubi Point (1984).

9.15.7.1 Northeast Monsoon

a. Indications that a northeast surge is invading the Cubi Point area are: Gusty winds starting about 0200L, sea level pressure above normal between 0200L and 0400L, and temperatures slightly cooler than normal.

b. During the Northeast Monsoon, when the 3,000 to 5,000 ft winds are 10 to 15 kt and the inversion on the 1200 GMT Clark AB sounding is fairly deep, small craft conditions may be forecast for the following day.

9.15.7.2 Shear Lines

a. If the outbreak of polar air is weak, there will be increased mid-level cloudiness but no precipitation with the passage of a shear line at Cubi Point. If the shear line is particularly intense and well defined, rainfall will be heavier but will last for only a few hours and be followed by clearing weather.

b. With an isotach maximum of 30 kt or more over the South China Sea and moving westward, a shear line may form over Luzon.

c. When the sea level pressure difference between Cubi Point and Okinawa is 10 mb or more, light rain or drizzle will be experienced with passage of a shear line. If the pressure difference is less than 10 mb, only increased cloudiness will occur.

d. When the continental high pressure cell is moderate to strong and ridging east-southeastward behind a moderate cold front, the following guidelines apply.

(1) If the low associated with the front moves north of Japan, expect shear line passage at Cubi Point when the low moves east of 115°E.

(2) When the Shanghai low forms and moves along the southern coast of Japan, expect passage of the shear line at Cubi Point when the low passes 140°E.

9.15.7.3 Easterly Waves

Because of the lack of a good network of reporting stations east of the Philippines, it is difficult to forecast or detect passage of easterly waves at Cubi Point. At no time are they a typical occurrence and only in the spring when the easterly flow is best established is there much likelihood of their passage over the Cubi Point area.

a. Unless it is possible to analyze and follow the progress of an easterly wave from the time it passes Belau (91408), the first indication of entry into the Philippines may be its passage across eastern Mindanao.

b. Easterly wave passage at Cubi Point may be anticipated roughly 24 hours after the first indications of its approach are observed along the east coast of the Philippines.

c. Weather conditions during passage of an easterly wave consist of drizzle or showers, scattered to broken low clouds, broken middle clouds, and a high overcast.

d. If an easterly wave passes during the period of maximum heating of the day, it may set off a wide area of thunderstorm activity.

e. The most adverse weather conditions at Cubi Point during the winter months usually occur when an easterly wave passes over the Philippines at the same time that a shear line is approaching from the north.

9.15.7.4 Southwest Monsoon

a. A shift from southwesterly to easterly flow during the Southwest Monsoon will bring a period of fair weather to Cubi Point for the duration of the easterly flow.

b. With moderate southwesterly flow, weather over Cubi Point will be low overcast with reduced visibility and intermittent light to moderate rain and thunderstorms. This condition can be expected to last for at least a 24-hour period.

c. Tropical cyclones crossing the Philippines or moving through the Bashi Channel enhance the southwest flow once they reach the South China Sea.

d. During the Southwest Monsoon, expect the most frequent rainshower or thunderstorm activity between 0600L and 1000L with a break between 1100L and 1300L with rainshower activity commencing again at 1300L until 1700L. If the showers do not let up between 1100L and 1300L, but persist until about 1400L, there will be no further afternoon showers.

e. During the Southwest Monsoon, if the winds are southwesterly greater than 15 kt between the surface and 300 mb, continuous rain may be forecast.

9.15.7.5 Cloudiness

a. When surface winds are from the south-southwest through west-southwest (190°-240°), coming right up the mouth of the bay, conditions within the bay will be solid overcast. With surface winds from the west-southwest through west (240°-270°), coming over the mountains to the west of Cubi Point, broken conditions or breaks in the overcast may be forecast.

b. During the Northeast Monsoon, when the 1200Z Clark sounding shows a strong inversion and surface winds are forecast in the 6-10 kt range, broken stratocumulus may be forecast over the field from just before sunrise to two hours after sunrise. When the 1200Z sounding shows a mid-level inversion and the 850 mb winds are 10-20 kt, a middle cloud layer may be forecast over the field during the same time period.

9.15.7.6 Visibility

When showers are coming in from the east, visibility may be forecast as low as 3 to 5 miles; if approaching from the southwest through west, it is possible for visibility to go below minimums.

9.15.7.7 Thunderstorms

a. When the southwesterly flow is comparatively deep in the spring transition months or during the Southwest Monsoon, afternoon thunderstorms may be expected at Cubi Point.

b. During the Southwest Monsoon when a land breeze, however light, exists, expect a line of thunderstorms and associated rainshowers to form off the coast between 0500L and 0700L.

c. There is a good chance of thunderstorms if 850 mb winds are southwesterly 25 kt or greater.

9.15.7.8 Turbulence

a. During a strong surge in the southwesterly flow, the easterly jet stream is directly over Luzon and creates moderate turbulence between 10,000 and 25,000 feet.

b. During the Northeast Monsoon, when strong winds are being funneled through the pass to the northeast of Cubi Point, moderate turbulence may be expected for all aircraft departing on runway 07 on climb through 5,000 feet.

c. During the Northeast Monsoon, light to moderate turbulence up to 10,000 feet may be forecast on the lee side of the mountains in northern Luzon. Lenticular clouds are common with a mid-level inversion.

9.15.8 Naval Station, Adak, Alaska

The following guidelines are taken from the Local Area Forecasters Handbook, Naval Station, Adak, published by the NWSED, Adak (1978).

a. General.

(1) Due to terrain features, at least two or three tenths more of low cloudiness occurs at Adak than what normally would be expected, regardless of the flow pattern. Stratocumulus is the predominant low cloud type.

(2) Precipitation is predominantly showery. Showers are brief but frequent. Steady precipitation occurs only with cyclones moving along or south of the Aleutian chain or with advancing warm fronts and occluded fronts. Snow showers occur in winter and early spring months whenever any predominant flow is from the north quadrant and a lowering of the freezing level is anticipated. Mixed rain and snow generally accompanies any system moving around the southeast periphery of Adak in winter, with the showers being heavier than normal. The steady rain associated with a warm front usually extends out to about 300 mi ahead of the front. Warm frontal passages are often difficult to discern.

(3) True northwest winds seldom reach velocities over 15 kt regardless of gradient. Mount Moffett a 3,924 ft (1,196 m) mountain located about 6 mi west-northwest of the airfield) effectively blocks and deflects the wind to become west to west-northwesterly over the airfield. Winds from 120° to about 190° will generally be about one-third of the gradient wind due to the mountainous terrain south of the field unless the gradient exceeds 50 kt. Winds from 190° to 250° will normally be representative of the area gradient (although gusty) unless the pressure gradient shows signs of strengthening, at which time winds will be about one-

third more than the gradient flow due to lower mountainous terrain and more favorable orientation of passes that lead away from the airfield. Winds in any direction will be gusty when in excess of 15 kt, with gale force winds having gusts frequently as high as double the sustained velocity.

(4) The strongest winds are caused by isobar packing immediately in advance of frontal systems associated with low pressure systems transiting the area.

(5) The strongest diurnal winds occur near 1500L to 1600L with a minimum occurring from 2300L to 0600L.

(6) The following freezing levels are associated with the precipitation type specified:

(a) Above 2,500 ft - rain

(b) 800 to 2,500 ft - snow pellets

(c) Surface to 800 ft - snow

(7) Lows that remain south of 45°N will seldom have a cloud shield and never a rain shield that affects Adak

(8) In summer, with a high over the western Aleutians moving eastward, watch for a lowering of the subsidence inversion for forecasting either fog or very low stratus.

(9) Expect near zero-zero conditions in fog on Shemya (located approximately 52.7°N 174.1°E -a frequently used alternate

for Adak) if Shemya has southerly winds. This guideline is particularly applicable during the summer.

(10) The SKEW T, LOG P diagram is an excellent tool for estimating cloud bases and tops unless a completely new air mass has entered the Adak area since the upper air sounding was made or a frontal system is in the area.

(11) Turbulence can be expected above 3,000 ft whenever any strong flow (20 kt or more) exists that tends to cross the Aleutian chain from north to south or vice-versa.

(12) A blocking high centered near 40°N 160°W will cause all lows to move northeast to the Adak area.

b. Winter.

(1) If the surface temperature is above 25°F (-4°C) and snow is expected, it will most likely be wet and not drift badly. If the surface temperature is below 25°F the snow will be dry and may drift.

(2) Watch the line of warm and cold advection (trough line) at the 500 mb level to determine rain versus snow. During winter, frontal precipitation may begin as snow, changing to rain with the crossing of the line of warm advection at the 500 mb level. After frontal passage, rain showers will be followed by snow showers.

(3) During autumn and winter, cold maritime polar and continental arctic air masses flow over the relatively warmer waters of the North Pacific and Bering Sea, producing moderate to intense frontal systems. Cumuliform clouds and showery weather prevail over the local area most of the time except for brief periods when Adak is in the warm sector of a frontal system.

c. Spring.

In the spring and summer, fog is the prevalent situation through most of the North Pacific and Bering Sea due to the warm moist air flowing north over colder water. While conditions may be near zero-zero over the ocean, Adak is normally VFR. When the wind direction is from the southwest quadrant, stratus and fog will be lifted by orographic effects, the degree of which is determined by the wind speed. Calm winds or winds less than 5 kt from the north-northeast will result in ceilings and visibility at or near zero-zero. Normally worst around dawn, the conditions will improve with either an increase in wind speed or enough local heating.

d. Summer.

(1) For ceiling and visibility forecasts on Adak during the summer:

(a) Adak's ceiling will usually be between 300 and 600 ft and the visibility less than 1 mi with a wind of 10 to 20 kt from the southwest quadrant,

(b) When the wind speed decreases to less than 10 kt, the resultant ceiling may be as low as 100 to 200 ft and the visibility as little as 1/2 mi.

(c) A northwest to north wind of less than 10 kt will advect fog over the airfield from the water areas north of the station, resulting in ceilings of 200 to 500 ft. Visibility may reduce to near 1/2 mi.

(d) Calm winds or north-northeasterly winds of less than 5 kt will cause near zero-zero field conditions.

(e) Winds of less than 15 kt from the east-southeast clockwise to south-southeast will result in 200 to 600 ft ceilings and 1/2 to 2 mi visibility. Conditions will improve with higher winds.

9.16 Oceanographic Forecast Aids

9.16.1 General

a. The surface waters of the SOJ show large seasonal variations in response to local forcing, but the deep water, which is cut off from other deep water regions, exhibits extremely stable physical properties.

b. Full-channel ASW conditions exist throughout the SOJ during summer and autumn and year-round in the warm sector. Half-channel conditions develop about mid-autumn in the cold sector.

c. Tidal currents are quite strong through the various shallow silled straits of the SOJ: 3 kt in Tsushima/Korea Strait, 3 to 4 kt in Soya Strait, and 5 to 6 kt in Tsugaru Strait.

d. The ECS can be divided into three oceanic regimes: the continental shelf, the Kuroshio Current and extensions, and an intermediate area which is a mixture of water from the two other areas. These regimes dictate the use of shallow and deep water ASW procedures.

e. The seasonal variations of temperature, salinity, and density structures over the continental shelf of the ECS exhibit marked variations between summer and winter: highly stratified water with strong vertical gradients and thermoclines in summer which result in full-channel sound propagation, and destratified water but strong horizontal gradients and half-channel propagation in winter.

f. The strong horizontal temperature gradients which start to develop in fall and are strongest by late winter/early spring can be clearly seen in properly recorded or enhanced infrared imagery (the temperature values as depicted by gray shades must be enhanced in the range of the SST values). See satellite figures S-4-2 (page 4-7), S-4-3 (page 4-11), and S-4-4 (page 4-14) for examples of SST patterns in infrared imagery.

g. From the shelf break in the ECS to the floor of the Okinawa trough the bottom has a steep slope and is very rough. Bottom bounce characteristics change drastically over the shelf slope and generally render bottom bounce modes inoperative. ASW conditions change from shallow mode (shelf region) to deep mode (trough region) across the shelf slope.

h. The Yangtze (Changjiang) River discharge is a dominant feature of the western ECS. The discharge influences bottom type and depth, water turbidity, temperature, salinity, and local currents. The turbidity pattern is clearly depicted in visual satellite imagery. (See Figure S-4-1, page 4-3.)

i. Oceanic eddies frequent the region along the continental shelf break. The cold cyclonic eddies tend to be more stable than warm anticyclonic types. Cold eddies may persist for months, so once identified and located, by infrared imagery or otherwise, their persistence should be considered in forecasting procedures.

j. The continental shelf is widest (about 400 n mi) in the northern ECS and narrowest (about 15 n mi) near Taiwan. The oceanographic features affected by the shelf are similarly distributed, as are requirements on deep and shallow ASW procedures.

k. Near-surface salinity values of the YS and ECS vary widely with some summer values reduced to 20‰ by heavy runoff and rainfall and winter values generally in the 31‰ to 33‰.

l. Extreme tidal ranges of 13 to 26 ft (4 to 8 m) occur along the eastern side of the Yellow Sea (west coast of Korea). Elsewhere over the Yellow Sea the range is 3 to 10 ft (1 to 3 m) except in the innermost region of Pohai where the range is greater than 10 ft (3 m).

m. Large expanses of mudflats are exposed at low tide off the west coast of Korea.

n. Summer maximum SSTs range from 24-28°C over the YS. Bottom waters near and below 50 m depths remain near 5°C. Strong vertical temperature gradients and weak horizontal gradient patterns develop by mid to late spring and continue to develop throughout summer.

o. A relatively warm region typically remains south of the Shandong Peninsula through late autumn.

p. The South Korea Coastal front is formed during autumn by cold water flowing south along the west coast of Korea and then east into the Korea Strait where it converges with the warm Tsushima Current waters. The front typically extends from west of Cheju-do Island to the vicinity of Tsushima Island.

q. Cold dry air flowing over water removes heat from the water column, thereby inducing convective mixing and ultimately a well-mixed destratified water column resulting in half-channel sound propagation. This condition commences every autumn over coastal and continental shelf regions and reaches a maximum areal extent in late winter/early spring.

9.16.2 Winter

a. The sound channel axis lies below the seasonal zone in the warm sector of the SOJ. Its depth tends to be at a minimum during the winter when the inflow of warm water via the Tsushima Current is at a minimum.

b. Sea ice starts to form in the Tartar Strait by mid-November and extends southward beyond Vladivostok by mid-January. Vladivostok harbor tends to open around mid-April (see Figure S-3-5, page 3-26).

c. The ice duration lasts about 120 days along the Siberian coast, about 200 days in the Tartar Strait, and about 90 days along the west coast of Sakhalin.

d. The area of well-mixed, vertically homogeneous, and half-channel sound propagation of the ECS, YS, and SOJ expands to deeper and deeper water under the cumulative seasonal heat losses and convective mixing resulting from the cold dry winter northerly winds. By mid-winter the area extends to near the 50 m isobath and by late winter to near the 100 m isobath.

e. The usefulness of satellite infrared imagery in determining ocean currents and SST patterns is at its highest level due to the strong horizontal SST gradients and the minimum cloud cover.

9.16.3 Spring

a. Early spring oceanographic conditions resemble more closely the extreme conditions of winter and late spring than those of summer. The most rapid rise in SST occurs during May.

b. Satellite infrared imagery becomes progressively less useful through the spring period as:

(1) cloud coverage increases with the evolving southwest monsoon and Mei-Yu/Bai-U front,

(2) atmospheric moisture increases with the increasing air temperatures and expanding area of southerly winds, and

(3) the horizontal SST gradients weaken as the cold shelf waters warm.

c. The winter half-channel conditions will change rapidly to full-channel conditions as the seasonal atmospheric pattern changes from winter to summer monsoon circulations.

REFERENCES

Atlas, D., S-H. Chou, and W. P. Byerly, 1983: The Influence of Coastal Shape on Winter Mesoscale Air-Sea Interaction. Mon. Wea. Rev., Vol. 111, No. 2, 245-252.

Barkley, R. A., 1968: The Kuroshio front as a compound vortex street, J. Mar. Res. 26(2): pp. 83-104

Brower, W. A. J F. Diaz, A. S. Prechtel, H. W. Searby, and J. L. Wise: Cl Atlas of the Outer Continental Shelf Waters and Coastal Regi Alaska. Volume II, Bering Sea. Arctic Environmenta ormation and Data Center, University of Alaska, Anchorage, a. Published by the National Climatic Center-Environmental Data Service, Asheville, NC for the National Oceanic and Atmospheric Administration.

Browning, K. A., 1977: Hail: A Review of Hail Science and Hail Suppression. Part I: Hail Physics, The Structure and Mechanisms of Hailstorms. Meteorological Monographs, V. 16, No. 38, pp. 1-39.

COMAMPGRPONE, 1984: Commander Amphibious Group One ltr N36/Ser 407 of 21 Dec 1984.

Chen, G. T-J., 1980: Mesoscale Analyses for a Mei-Yu Case over Taiwan. Papers, Met. Rsch. Met. Soc. Republic China.

Chen, G. T-J. and C-Y, Tsay, 1978: A Synoptic Case Study of the Mei-Yu Near Taiwan. Papers in Meteorological Research., Vol. 1, 25-36.

Colon, D. M. 1982: On the Outflow Modes of the Tsugaru Warm Current La Mer 20, 60-64.

Cottrell, K. G., P. D. Try, D. B. Hodges, and R. F. Wachtmann, 1979: Electro-Optical Handbook, Volume 1, Weather Support for Precision Guided Munitions Air Weather Service AWS/TR-79/002, 97 pp.

Crutcher, H. L. and J. M. Meserve, 1970: Selected Level Heights, Temperatures and Dew Points for the Northern Hemisphere, NAVAIR 50-1C-52. Commander, Naval Weather Service Command, Washington, DC.

Crutcher, H. L., and R. G. Quayle, 1974: Mariners Worldwide Climatic Guide to Tropical Storms at Sea. Naval Weather Service Environmental Detachment, Asheville, NC, by direction of Commander, Naval Weather Service Command, Washington, DC.

Earle, M. D. and J. M. Bishop, 1984. A Practical Guide to Ocean Wave Measurements and Analysis. Endeco, Inc., Marion, MA.

The New Encyclopaedia Brittanica, 1982: Micropaedia, Volume VII, 15th edition, p. 946.

Fairbridge, R. W., 1966: The Encyclopedia of Oceanography. Reinhold Publishing Corporation, N. Y., 1021 pp.

Fett, R. W., 1977: Navy Tactical Applications Guide, Volume 1. NEPRF AP 77-03, pp. 2B-30 and 2B-31.

Findlater, J., et al., 1966: Surface and 900mb Wind Relationships. Meteorological Office Scientific Paper No. 23. Her Majesty's Stationery Office, London, England.

Fleet Weather Central/Joint Typhoon Warning Center (FWC/JTWC), Guam, 1969: Forecasters Handbook, Volume 1. U. S. Naval Weather Service Command, Washington, DC.

______________________, 1978: Area of Responsibility Forecaster's Handbook. U. S. Naval Weather Service Command, NSTL Station, Bay St. Louis, MS 39529

Fleet Weather Facility (FWF), Yokosuka, Japan, 1965: Korean Area Forecaster's Handbook.

Fleet Weather Facility (FWF), Yokosuka, Japan, 1966: Forecaster's Handbook for the Gulf of Tonkin and the South China Sea. FLEWEAFAC Yokosuka Instruction P3140.37. U. S. Naval Weather Service Command, Washington, DC.

Flora, S. D., 1956: Hailstorms of the United States. University of Oklahoma Press, Norman, Oklahoma.

George, J. J., and E. M. Wolff, 1953: Cyclogenesis Along East Coast of Asia. Technical Report on Task 13. Bureau of Aeronautics Project AROWA, Building R-48, U. S. Naval Air Station, Norfolk 11, VA.

Goroch, A. K. and T. Brown, 1980: Frequency of Adverse Weather Conditions Affecting High Energy Laser Systems Operations. NAVENVPREDRSCHFAC Technical Report TR 80-06.

__________. 1981: Climatology of Infrared Ranges in Pacific Ocean Regions of the Northern Hemisphere. NAVENVPREDRSCHFAC Technical Report TR 80-06

Guo, B. and Z. Xia, 1984. Ocean Hydrodynamics of the Japan and East China Seas. T. Ichiye (editor), Elsevier Oceanography Series, 39, pp 123-142.

Helvey, R. A. and J. S. Rosenthal, 1983: Guide for Inferring Refractive Conditions from Synoptic Parameters. Pacific Missile Test Center, Tech. Paper TP000005, 36 pp.

Hopkins, R. H., 1977: Forecasting Techniques of Clear Air Turbulence Including That Associated With Mountain Waves. Technical Note No. 3., WMO-No.482. Secretariat of the World Meteorological Organization, Geneva, Switzerland.

Hsueh, Y., and R. D. Romea, 1983: A Comparison of Observed and Geostrophically Calculated Wintertime Surface Winds Over the East China Sea. Journal of Geophysical Research, V. 88, No. C14, pp. 9588-9594.

Huffman, P. J., J. K. Luers, N. A. Engler, and J. E. Felt, 1983: Proceedings of Workshop to Standardize Atmospheric Measurements in Support of Electro-Optical Systems, November 2-4, 1982, Monterey, Ca., University of Dayton, UDR-TR-83-71, 53 pp.

Huh, O. K., 1982: Satellite Observations and the Annual Cycle of Surface Circulation in the Yellow Sea, East China Sea and Korea Strait, La Mer 20: 210-222, 1982, Societe franco-japonaise d'oceanographie, Tokyo.

Huh, O. K., L. J. Rouse, and P. F. Twitchell, 1982: Outbreaks of Polar Continental Air: Windows on the Mesoscale Structure of the Upper Ocean. Naval Research Reviews Special Issue on Remote Sensing, Vol. XXXIV, 27-38.

Ichiye, T. and K. Takano, eds., 1982: Japan and East China Sea Proceedings (JECSS), 94 pp.

Kotsch, W. J., 1983: Weather for the Mariner. Naval Institute Press, Annapolis, Maryland.

Kuo, Y.-H. and R. A. Anthes, 1982: Numerical Simulation of a Mei-Yu System over Southeast Asia. Papers. Met. Rsch. Met. Soc. Republic China., Vol. 5, No. 1, 15-35.

LaBelle, J. C. and J. L. Wise, 1983: Alaska Marine Ice Atlas. Arctic Environmental Information and Data Center, University of Alaska, 707 A Street, Anchorage, Alaska 99501

Matsumato, S. and Y. Tsuneoka, 1970: Time Lapse Composite Echo Pattern of Wave Disturbances Embedded in the Baiu Front. J. Met. Soc. Japan, Vol. 48, No. 3, 198-203.

Matsumato, S., S. Yoshizumi, and M. Takeuchi, 1970: On the Structure of the "Baiu Front" and the Associated Intermediate-scale Disturbances in the Lower Atmosphere. J. Met. Soc. Japan, Vol. 48, No. 6, 479-491.

Marr, J. C., 1970: The Kuroshio. A Symposium on the Japan Current. East-West Center Press, Honolulu, 614 pp.

Mertins, H. O. 1968: Icing on fishing vessels due to spray. Marine Observer. 38(221), pp. 128-136.

Murakami, T., 1981: Orographic Influence of the Tibetan Plateau on the Asiatic Winter Monsoon Circulation, Part I, Large Scale Aspects. Journal of the Meteorological Society of Japan, Ser. II, V. 59, No. 1, pp. 40-84.

Naval Oceanography Command Detachment (NOCD), Atsugi, Japan, 1980: Area of Responsibility Forecaster's Handbook. Commander, Naval Oceanography Command, NSTL Station, Bay St. Louis, MS 39529.

Naval Oceanography Command Detachment (NOCD), Kadena (Okinawa), Japan, 1983: Forecaster's Handbook, NAF Kadena, Okinawa, JA. Commander, Naval Oceanography Command, NSTL Station, Bay St. Louis, MS 39529.

Naval Oceanography Command Facility (NOCF), Cubi Point, R. P., 1984: Forecaster's Handbook, NAS Cubi Point, R. P. Commander, Naval Oceanography Command, NSTL Station, Bay St. Louis, MS 39529.

Naval Oceanography Command Facility (NOCF), Yokosuka, Japan, 1981: Forecaster's Handbook, Yokosuka Japan. Commander, Naval Oceanography Command, NSTL Station, Bay St. Louis, MS 39529.

Naval Weather Service Environmental Detachment (NWSED), Adak, Alaska, 1978: Local Area Forecaster's Handbook, Naval Station, Adak. Commander, Naval Weather Service Command, NSTL Station, Bay St. Louis, MS 39529.

Naval Weather Service Environmental Detachment (NWSED), U. S. Naval Air Station, Agana, Guam, 1983: Local Area Forecaster's Handbook. U. S. Naval Weather Service Command, Washington, DC.

Nestor, M. J. R., 1977: The Environment of South Korea and Adjacent Sea Areas. Naval Environmental Prediction Research Facility, Monterey, CA 93940.

Newspaper Enterprise Association, Inc., 1978: The World Almanac and Book of Facts, 1979. Published for the Seattle Times by the Newspaper Enterprise Association, Inc., New York.

Ninomiya, K., 1984: Characteristics of Baiu Front as a Predominant Subtropical Front in the Summer Northern Hemisphere. J. Met. Soc. Japan., Vol. 62, No. 6, 880-893.

Ownbey, J. W., 1973: Climatic Summaries for Major Seventh Fleet Ports and Waters. Naval Weather Service Environmental Detachment, Asheville, NC., by direction of the Commander, Naval Weather Service, Washington, DC, 103 pp.

Streten, N. A., 1975: Cloud Cell Size and Pattern Evolution in Arctic Air Advection Over the North Pacific. Arch. Met. Geoph. Biokl., Ser. A, Vol. 24, 213-228.

Strommel, H. and K. Yoshida, eds., 1972: Kuroshio Physical Aspects of the Japan Current. University of Washington Press, Seattle and London, 517 pp.

Sverdrup, H. U., et al, 1942: The Oceans: Their physics, chemistry, and general biology. Prentice Hall, New York, 1087 pp.

Sweet, W., 1980: Meteorological Factors Affecting Evaporation Duct Height Climatologies. NAVENVPREDRSCHFAC Technical Report TR 80-02, 3? pp.

Tsuchiya, K. and T. Fujita, 1967: A Satellite Meteorological Study of Evaporation and Cloud Formation over the Western Pacific under the Influence of the Winter Monsoon. J. Met. Soc. Japan. Vol. 45, No. 3, 232-249.

Uemura, H. 1981: Mesoscale disturbances causing heavy snowfall over the coastal areas of the Sea of Japan. Proceedings, Nowcasting: Mesoscale observations and short-range predictions, 25-28 August 1981, Hamburg, Germany.

U. S. Air Force, 1964: Terminal Forecast Manual. Detachment 18, 30th Weather Squadron, Seoul, Republic of Korea.

U. S. Air Force, 1965: Far East Climatic Atlas. 1st Weather Wing Special Study 105-7. Department of the Air Force, 20th Weather Squadron (MATS), APO San Francisco 96525.

U. S. Air Force, 1965: February Climate of Korea. 1st Weather Wing Special Study 105-2/2. 30 pp. Department of the Air Force, Headquarters 1st Weather Wing (MAC), APO San Francisco, 96553.

U. S. Air Force, 1965: May Climate of Korea. 1st Weather Wing Special Study 105-2/5. 26 pp. Department of the Air Force, Headquarters 1st Weather Wing (MAC), APO San Francisco, 96553.

U. S. Air Force, 1965: August Climate of Korea. 1st Weather Wing Special Study 105-2/8. 28 pp. Department of the Air Force, Headquarters 1st Weather Wing (MAC), APO San Francisco, 96553.

U. S. Air Force, 1965: November Climate of Korea. 1st Weather Wing Special Study 105-2/11. 29 pp. Department of the Air Force, Headquarters 1st Weather Wing (MAC), APO San Francisco, 96553.

U. S. Air Force, 1970: Climatology for the Western Pacific Area. Prepared by Environmental Services, Headquarters, 1st Weather Wing.

U. S. Air Force, 1970: Terminal Forecast Reference Manual, Misawa Air Base, Japan. Detachment 13, 20th Weather Squadron, Misawa Air Base, Japan.

U. S. Air Force, 1982: AWS Climatic Briefs, Asia. USAFETAC/ DS-81/058. USAF Environmental Technical Applications Center, Scott Air Force Base, Illinois 62225

Ushijima, T., 1968: Analytical Study of the Low-Level Jet Stream. J. Met. Soc. Japan., Vol. 47, No. 1, 13-22.

U. S. Marine Corps, 1967: Iwakuni Forecaster's Handbook. Weather Service, U. S. Marine Corps Air Station, FPO San Francisco, 96664

U. S. Marine Corps, 1981: Local Area Forecaster's Handbook for MCAS(H) Futenma, Okinawa. Weather Service, MCAS(H) Futenma, Okinawa, FPO Seattle, WA 98772

U. S. Navy, 1969: Monthly Charts of Mean, Minimum, and Maximum Sea Surface Temperature of the North Pacific Ocean. Naval Oceanographic Office, Washington, DC.

U. S. Navy, 1970: Naval Arctic Manual, ATP 17(A). Chief of Naval Operations, Washington, DC.

U. S. Navy, 1977: U. S. Navy Marine Climatic Atlas of the World, Volume II, North Pacific Ocean, NAVAIR 50-1C-529. Naval Weather Service Detachment, Asheville, NC, for the Director, Naval Oceanography and Meteorology, Bay St. Louis, MS. 388 pp.

U. S. Navy, undated: Contrails Forecasting Manual. NAVWEPS 50-1P-522. Chief of Naval Operations, Washington, DC.

Weber, E. M. and S. Walderotter, 1981: Satellite Interpretation. Department of the Air Force, 3WW/TN-81/001.

Wise, J. L., and A. L. Comiskey, 1980: Superstructure Icing in Alaska Waters. Pacific Marine Environmental Lab., U. S. National Oceanic and Atmospheric Administration, Seattle, Wa. 30 pp.

World Meteorological Organization, 1954: Meteorological Aspects of Aircraft Icing. Technical Note No. 3., WMO-No. 30. TP.9. Secretariat of the World Meteorological Organization, Geneva, Switzerland.

Yoshino, M. M., 1965: Four Stages of the Rainy Season in Early Summer over East Asia (Part I). Journal of the Meteorological Society of Japan, V. 43, No. 5, pp. 231-245.

APPENDIX A

GLOSSARY OF GEOGRAPHIC EQUIVALENTS FOR JAPAN AND ADJACENT SEAS HANDBOOK

The following terms are used by the USSR, China, Japan, Korea, and Southern Asia but may not be all-inclusive of terms used on charts and maps.

Ai	a saddle between hills	China
Am	mountain, peak,rock	Korea
An	embankment, shore, cliff, coast, riverbank	China
An-chiao	submerged rocks, reef	China
Ao	bay, cove, inlet, dock	China
Ap	cape, point	Korea
Arkhipelag	archipelago	USSR
Bana	cape	Japan
Bandao	peninsula	China
Barrage	dam	S. Asia
Bei	north	China
Bereg	coast, shore	USSR
Bolshoi, Bolshaya	big	USSR
Bol'sh-oy,-oye,-oya	great	USSR
Bong	hill, mountain peak	Korea
Bukhta	bay, gulf	USSR
Bukit	hill, mountain	S. Asia
Bum	hill, mountain	S. Asia
Caka	lake	China
Cha	lock, dam, flood barrier	China
Chae	pass, peak, hill, mountain	Korea
Chai	camp, house	China
Chan	railroad station	China
Chang	mountain	China
Chao	bog, marsh	China
Chau	island, islet(s)	China
Ch'e-chan	railroad station	China
Chen	town, market town	China
Ch'eng, Chin	town, city, walled town	China
Chi	obstruction, ledges in river	China
Ch'i	stream, point, river, head, cape, mountain, seven	China
Chia	cape, bluff, point	China
Ch'ia	custom's barrier	China
Chiang, Chiang-k'ou	bay, harbor, inlet, sound, lagoon, estuary, stream, anchorage, river, shoal, port, river mouth	China
Chiang-tao	channel, strait, sound, river mouth	China
Chiao	point, cape, promontory, headland, reef, rock, bank, island, islet, shoal	China
Ch'iao	bridge	China
Chien	mountain, peak, island	China
Ch'ien	shallow, shoal rock	China
Ch'ien-lai	bank, shoal	China
Ch'ien-t'an	sandbanks, bank, shoal	China
Ch'ien-tui	bank	China

Ch'ih	lake, pool, pond	China
Chih-chiang-tao	reach	China
Chih-k'ou	river mouth	China
Chih-liu	channel, tributary	China
Ching	capital city, isthmus, ford, ferry	China
Chink	escarpment	China
Chiu	nine	China
Ch'o	point, rock in water, reef	Korea
Ch'on	stream	Korea
Chou	island, bank, islet, shoal	China
Chow	town of the second rank	China
Chow-Chow	rippling and swirling water	China
Ch'uan	stream, river	China
Chuang	village	China
Chueh	cape, point	China
Chung	middle, center, mountain	China
Chung-yuan	mainland	China
Ch'un-tao	archipelago, group of islands	China
Ch'wi	point	Korea
Co	lake	China
Da	great, greater	USSR
Dae	hill, mountain, peak	Korea
Dake	mountain, peak	Japan
Dan	point, cape	Korea
Dao	island	China
Daryacheh	lake	S. Asia
Dasht	desert, plain	S. Asia
Deo	pass	S. Asia
Ding	mountain	China
Do	island, islands, rock, rocks	Korea
Doi	hill, mountain	S. Asia
Dong	east	China
Dong	populated place	Korea
Du	point, hill	Korea
Erh	two	China
Fang	hamlet, house, shore, street	China
Feng	mount, peak, hill	China
Fon	wind	China
Fou	port	China
Fow fu	buoy	China
Fu	province, capital, peak	China
Gak	point, cape	Korea
Gang	stream, inlet, harbor, bay	Korea
Gang	harbor	China
Gangri	mountain, peak	USSR
Gaoyuan	plateau	China
Gap	point	Korea
Gata	bay, inlet, lake	Japan
Gawa	river	Japan
Gi	point, peninsula, reef	Korea
Goe	pass	Japan
Golets	mountain, peak	USSR
Gor-a,-no,-y	mountain-ous,-s	USSR
Got	point, cape	Korea
Gowd	depression	S.Asia
Gu	entrance	Korea
Guan	pass	China

Guba	bay, gulf	USSR
Gunto	archipelago, island chain	Japan
Gunung	mountain	S. Asia
Ha	stream	Korea
Hada	mountain	China
Hae	gulf, bay, sound	Korea
Haehyop	strait	Korea
Haeman	bay	Korea
Hai	sea, gulf, ocean	China
Hai	lake	China
Hai-ching	strait, channel	China
Hai-hsia	do	China
Hai-kau	bight, creek	China
Hai-k'ou	channel entrance	China
Hai-pin	seashore, beach	China
Hai-tao	island	China
Hai-wan	bay, gulf	China
Haixia	strait, channel	China
Hamun	depression, lake	S.Asia
Hang	dry	China
Hang	harbor, inlet	Korea
Hang-lu	fairway	China
Hang-men	pass navigable to ships	China
Hanto	peninsula	Japan
Hao	ditch, crane	China
Hei, Heh	black	China
Hiang Tsun	village	China
Higashi, Higasi	east	Japan
Ho	river, waterway	China
Hoi	channel, bay, anchorage, inlet	China
Ho-k'ou	river mouth	China
Hoku	north	Japan
Ho Tun	lighthouse	China
Hsi	west, mountain, stream, swamp	China
Hsia	strait, gorge, lower	China
Hsiang	rural area, village	China
Hsiao	small	China
Hsien	district, district capital, steep hill	China
Hsin	new	China
Hsu	islet(s), island, village	China
Hsuan	eddies	China
Hu	lake, reservoir	China
Huang	yellow	China
Hung	red, desert	China
Hwang	yellow	China
Hyon	pass, hill	Korea
Iwa	island, islet, rock	Japan
Jae	pass, peak, hill, mountain	Korea
Jehil	lake	S. Asia
Jiang	river	China
Jiao	cape	China
Jima	island-s, rock-s	Japan
Ju	sandbar, shallow	Korea
Kai	sea	Japan
Kaikyo	channel, strait	Japan
Kan	dry, harbor, port	China

Kanal	canal, channel	USSR
Kang	mound, hill, bridge	China
Kang	stream, inlet, harbor, bay	Korea
Kangr-i	mountain, peak	S. Asia
Kao	high	China
Kao	mountain	S. Asia
Kao-chiao	promontory	China
Kao-yuan	plateau	China
Kavir	salt desert	S. Asia
Kawa	river	Japan
Kel', Kol, Kul'	lake	USSR
Khao	hill, mountain, peak	S. Asia
Khi,Ki	river	China
Khrebet	mountain range	USSR
Kiang	river	China
Kiao	point	China
King	capital, city	China
Kita	north	Japan
Kkut	point, cape	Korea
K'o	point	Korea
Ko	island, lake	Japan
Ko	island	S. Asia
Kogae	pass	Korea
Koh	island	S. Asia
Kok	point, corner, angle, horn peninsula	China
Kong	river	China
Kosa	spit	USSR
Kosui	lake	Japan
Kot	point, cape	Korea
Kou	stream, ravine, gully, ditch, estuary	China
K'ou	bay, cove, inlet, river mouth, mountain pass	China
Kowtal	pass	S. Asia
Kryazh	mountains, range	USSR
Ku	valley, gorge	China
Kuan	barrier, customs	China
Kuh	mountain	S. Asia
Ku-k'ou	ravine	China
Kum	sandy desert	USSR
Kun	rock	Korea
Kundo	islands	Korea
Kuo	country, kingdom, state	China
Kuro	black	Japan
Kwai	cliff	China
Kwan	customhouse	China
Kyun	island	S. Asia
La	pass	S. Asia
Lai	shoal, submerged rock	China
Lan	blue, marketplace	China
Lao	old, tower	China
Lednik	glacier	USSR
Leng	chain of hills, mountain pass	China
Li	inner, one-third of a mile, gravel, shingle	China
-li	village, settlement	Korea

Liao	distant	China
Liedao	archipelago, islands	China
Lieh-hsu	reef	China
Lieh-tao	group of islands, islands	China
Lieh-yen	group of rocks	China
Liman	bay, estuary	USSR
Lin	forest	China
Ling	mountain-s, range	China
Ling	chain of hills, mountain pass, mountain, mountain range	China
Liu	stream, current, six	China
Lu	road	China
Lyong	mountain, hill, peak, pass	Korea
Mal	point, cape, headland	Korea
Mae Nam	river	S. Asia
Mal-yy,-aya,-oye	little, small	USSR
Man	bay	Korea
Mao-ti	anchorage	China
Ma Tao	jetty, strait	China
Melkosopochnik	undulating plain	USSR
Men	gate, pass, entrance, channel	China
Miao	temple	China
Minami	southern	Japan
Mis	cape	USSR
Misaki	cape, peninsula, point	Japan
Miu	bay, cove	China
More	sea	USSR
Mu	a wood, trees, grave	China
Myoji	anchorage	Korea
Mys	cape	USSR
Nada	gulf, sea	Japan
Nagorno, Nagor'ye	highland, plateau, upland	USSR
Naka	middle	Japan
Nam	river	S. Asia
Namakzar	salt waste	S. Asia
Namco	lake	S. Asia
Nan	south	China
Nan, Nam	south, southern	China
Nashan	south mountain	China
Nei, Nui	inner	China
Nei-ao	basin	China
Ngam, Ngaam	point, cliff, rock	China
N'i	mud	China
-ni	village, settlement	Korea
Nishi, Nisi	west	Japan
Nizhn-ily,-yaya,-eye	lower	USSR
Nizmennost'	lowland	USSR
Nong	lake	S. Asia
Nos	cape	USSR
Novi, Novaya	new	USSR
Nur	lake, salt lake	China
Nusa	island	S. Asia
Nyong	mountain, hill, pass, peak	Korea
O	big	Japan
Ostrov,-a	island-s	USSR
Ozer-o,-a	lake-s	USSR
Pa	embankment, quay, eight	China

Pai, peh	rock, shoal, islet, white	China
Pakchi	anchorage	Korea
Pando	peninsula	Korea
Pan-tao	peninsula	China
Pao	lake	China
Pao	hill, town, village, rampart	China
P'ao-t'ai	fort	China
Pau	mountain, rock in water	Korea
Pawi	rock in water	Korea
Pei (Peh, Pak)	north, northern	China
Peng	stream, creek	China
Pereval	pass	USSR
Peski	desert, sand	USSR
Phou	hill, mountain, range	S. Asia
Pi	point, cape, nose	China
Piao	rock, islet	China
Pik	mountain, peak	USSR
Ping-chou	level shoals	China
Plato	plateau, upland	USSR
Ploskogor'ye	plateau, upland	USSR
P'o	arm of the sea, port, sound	China
P'o	inlet, harbor, sound, bay, cove	Korea
Poloustrov	peninsula	USSR
Pong	hill, mountain, peak	Korea
Po-ti	anchorage, roadstead	China
Proliv	strait	USSR
P'u	citadel, commercial village, inlet, creek, village, town, rampart	China
Pulou, Pulo	island	S. Asia
Pwang Shih	rocks	China
Qu	canal	China
Qundao	archipelago, islands	China
Rann	swamp	S. Asia
Ras	cape	S. Asia
Ravnina	lowland, plain	USSR
Reka	river	USSR
Retto	chain of islands	Japan
-ri	village, settlement	Korea
Sagar	lake, sea	S. Asia
Sai	west	Japan
Saki	cape, point	Japan
Sammyaku	mountain range	Japan
Sampan	boat	China
San	hill, mountain	Japan
San	mountain, hill, peak, ridge	Korea
San (see Shan)	three	China
San-chiao-chou	delta	China
Sanmaek	mountain range	Korea
Se	reef, rock, shoal-s	Japan
Se	river	S. Asia
Seto	strait	Japan
Sever-nyy,-o	north-ern	USSR
Sha	sand, sandbank, sand island, low sandy point, sand cay	China
Sha-chiao	sandspit	China
Sha-ch'iu	sand dune	China
Sha-kan	banks	China

Shamo....................desert................................China
Shan.....................mountain-s, range, island-s..........China
Shan.....................hill, mountain, island...............China
Shang....................upper.................................China
Shan-hu..................coral.................................China
Shan-hu-Chiao............coral reef............................China
Shankou..................mountain pass, range..................China
Shan-mo..................mountain range........................China
Shan-sha.................bar, sandbar..........................China
Shan-t'ien...............mountain summit.......................China
Shan-tau.................bluff, cliff, island..................China
Shan-tzu.................island................................China
Shao.....................upper, small, few.....................China
Sha-sien.................shoal.................................China
Sha-t'an.................sandy shoal, sandflats................China
Sha-tsui.................sandspit..............................China
Sha-tui..................sandbank..............................China
She Tan..................reef..................................China
Shen.....................deep..................................China
Sheng....................province..............................China
Shi......................municipality..........................China
Shih.....................stone, rock, hill, ten, city, market.China
Shih-t'ai................ridge of rocks........................China
Shih-ti..................swamp.................................China
Shima....................island-s, rock-s......................Japan
Shimo....................lower.................................Japan
Shin.....................land..................................Japan
Shiro....................white.................................Japan
Sho......................island, reef, rock....................Japan
Shoto....................archipelago...........................Japan
Shu......................tree..................................China
Shuiko...................reservoir.............................China
Shu-lin..................forest................................China
Shuan-chou...............bar...................................China
Shui.....................small river, water, stream...........China
Shui-kuan................customs...............................China
Shui-lu..................channel passage.......................China
Shu-tao..................reach, channel, strait, passage.......China
Si.......................west, western.........................China
Sia......................lower.................................China
Siao.....................small, little.........................China
Siao HO..................small river, rivulet..................China
Sin......................new...................................China
Sing.....................spring................................China
So.......................island, reef, rock, rocks............Korea
So.......................town, village.........................China
Sok......................rocks.................................Korea
Som......................island................................Korea
Sopka....................volcano...............................USSR
Sor......................salt lake, salt pan...................USSR
Sredni, Srednyaya........middle................................USSR
Ssu......................temple, monastery, four...............China
Stari, Staraya...........old...................................USSR
Strep....................treeless plain........................USSR
Stung....................river.................................S. Asia
Su.......................stream................................Korea
Su (also, see Hsu).......island, islet.........................China

Su	reef, river, rock, stream	Japan
Sudo	channel	Korea
Suido	channel, strait	Japan
Sungei	river	S. Asia
Ta	great, large	China
T'a	pagoda	China
Tae	hill, mountain	Korea
Tai (also, see Tui)	plateau	China
Take	peak, ridge	Japan
Tam	cove, pool, lake	China
Tan	point	Korea
Tan, T'an	rapids, shoal, bar, bank, flat	China
Tandjong, Tanjung	cape, point	S. Asia
Tang, T'ang	pond, embankment, canal, stream	China
Tang lao	lighthouse	China
Tao	island, island group, road, paddy field	China
T'ao	bay	China
Tao Tu	clay	China
Tao-tzu	islet	China
Teng Lao	lighthouse	China
Thale	sea, lake	S. Asia
Than	rapids	China
Ti	low, point, cape, head, embankment, dike, earth, ground, place, bottom	China
T'ien	arable land, field, swamp	China
Ting	peak, summit	China
To	island, islands, rocks	Korea
To	east	Japan
T'o	stone, rocky eminence	China
To	island-s, rock-s	Japan
T'oe	reef, shoal	Korea
To Mu	wooded	China
Toge	pass	Japan
Tong	cove, pool, lake, bay	China
To-tzu	stone, rocky knob, islet	China
Tou, T'ou	cape, headland, point	China
Tsi	ravine	China
Tso	lake	S. Asia
Tsui	cape, point, spit, mouth	China
Tsui Sha	gravel	China
Ts'un	village	China
Tu	ferry, ford	China
Tui	sandbank, bank	China
Tung	east, eastern, mountain	China
Tui-tsui (see Tui)	bank, spit	China
Udjung	point	S. Asia
Umi	bay	Japan
Ura	bay, inlet, lake	Japan
Uval-y	hill-s, slope	USSR
Verkhni	upper	USSR
Vishni, Vishnyaya	high	USSR
Vodokhranilishche	reservoir	USSR
Vostoch-no,-ny	east-ern	USSR
Vozvyshennost'	hill-s, upland, plateau	USSR
Wa	swamp	China
Wai	outer	China

Wan	bay, gulf, bend in river	China
Wan	bay, gulf	Japan
Wei	headland, walled town, bay, cove	China
Wen	rock	China
Xi	west	China
Xiao	lesser, little	China
Yai	cliff	China
Yama	mountain	Japan
Yanchi	salt lake	China
Yang	ocean	China
Yang	bay, inlet, wide water, ocean	China
Yang	sea, sound	Korea
Yeh	moorland	China
Yen	embankment, rock, reef, dike, cliff	China
Yen-t'an	salt pan	China
Yen tun	beacon, buoy	China
Yo	island, rocks	Korea
Yolto	islands	Korea
Yom	island	Korea
Yoma	mountain range	S. Asia
Yong	mountain, hill peak, pass	Korea
Yu	island, islet	China
Yugo, Yuzhnyy	south-ern	USSR
Yumco	lake	China
Yunhe	canal	China
Yun-ho	canal	China
Zaki	cape, point	Japan
Zaliv	bay, gulf	USSR
Zapad-no,-nyy	west-ern	USSR
Zaliv	bay, gulf	USSR
Zan	mountain	Japan
Zangbo	river	China
Zemlya	land	USSR

APPENDIX B

This appendix includes Section I from NAVENVPREDRSCHFAC Technical Paper TP 5-76 of June 1976, Typhoon Havens Handbook for the Western Pacific and Indian Oceans, by S. Brand and J.W. Blelloch. Note that 'Fleet Weather Central (FWC)' is now known as Naval Oceanography Command Center (NAVOCEANCOMCEN).

I TROPICAL CYCLONES— A GENERAL DISCUSSION

1. TROPICAL CYCLONE DEVELOPMENT

Tropical cyclones are warm-core, nonfrontal low-pressure centers that develop over tropical or subtropical waters. Although the tropical cyclone formation process is not fully understood, it is well known that they require tremendous amounts of energy to develop and sustain the high wind velocities present. Only the warm moisture-laden air of the tropics possesses this quantity of energy. For this reason, tropical cyclones usually develop within 20° of the equator and begin to dissipate as they move into midlatitudes.

2. WIND CIRCULATION AND INTENSITY

The wind circulation associated with tropical cyclones is counterclockwise about the eye in the Northern Hemisphere and clockwise in the Southern Hemisphere. Figure I-1 depicts the wind pattern around the eye of a typical large, intense 150-kt typhoon. Note that the more intense winds are located in the right semicircle of the circulation. For this reason the right side of a tropical cyclone is known as the "dangerous semicircle."

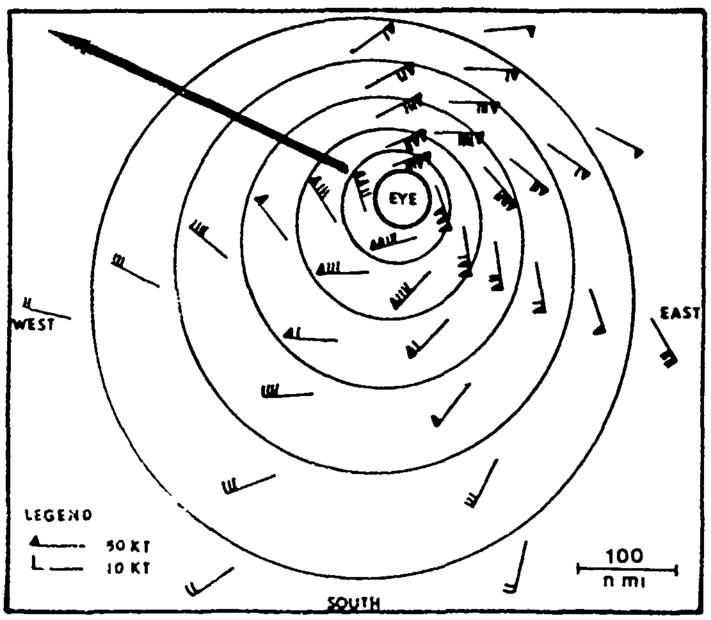

Figure I-1. Distribution of surface wind speeds (in knots) around a large, intense typhoon in the Northern Hemisphere over open water. The arrow indicates direction of movement (after Harding and Kotsch, 1965).

TROPICAL CYCLONES

The highest winds associated with tropical cyclones have never been accurately measured; however, based on data from past storms, tropical cyclone winds may attain speeds well in excess of 150 kt. The following classification system concerning the intensity of tropical cyclones has been established by international agreement:

Tropical Depression:	Maximum sustained winds no greater than 33 kt
Tropical Storm:	Maximum sustained winds in the range 34-63 kt
Typhoon:	Maximum sustained winds in excess of 63 kt

3. TROPICAL CYCLONE MOVEMENT

The subject of tropical cyclone movement is very complicated since precise speed and direction of movement is a function of wind and pressure patterns from the sea surface to the top of the atmosphere. In general, tropical cyclones in WESTPAC begin in the tropics and move west or west-northwest. In some cases the movement eventually becomes northward and finally northeastward. This shifting of direction is known as recurvature. Appendix I-A presents the mean tracks of tropical storms and typhoons in the western North Pacific by month and part-monthly periods (NAVAIR 50-1C-61, 1974).

Prior to recurvature, tropical cyclones generally move at speeds from 8 to 14 kt; however, after recurvature they may accelerate and within 48 hours reach speeds 2-3 times greater than that at the point of recurvature. (This acceleration varies with the time of year.) During the recurvature process the tropical cyclone is moving farther from the tropics; in doing so, it comes into contact with cooler surface waters and air from extra-tropical regions is drawn into its circulation. These factors result in the ultimate dissipation of the tropical cyclone. Approximately 40% of western North Pacific tropical cyclones recurve (Burroughs and Brand, 1972).

Appendixes I-B through I-D present the mean tracks of tropical cyclones for the North Indian Ocean, Southwest Indian Ocean and the Southwest Pacific Ocean/Australian areas respectively.

4. SEA STATES AROUND TROPICAL CYCLONES

It is important to realize that sea conditions affecting ship movement will extend well beyond the wind field associated with a tropical cyclone, and that a miscalculation concerning sea conditions could result in a destructive rendezvous with the storm. The extent of the sea state generated by a tropical storm is primarily a function of storm size, duration and intensity. Figure I-2

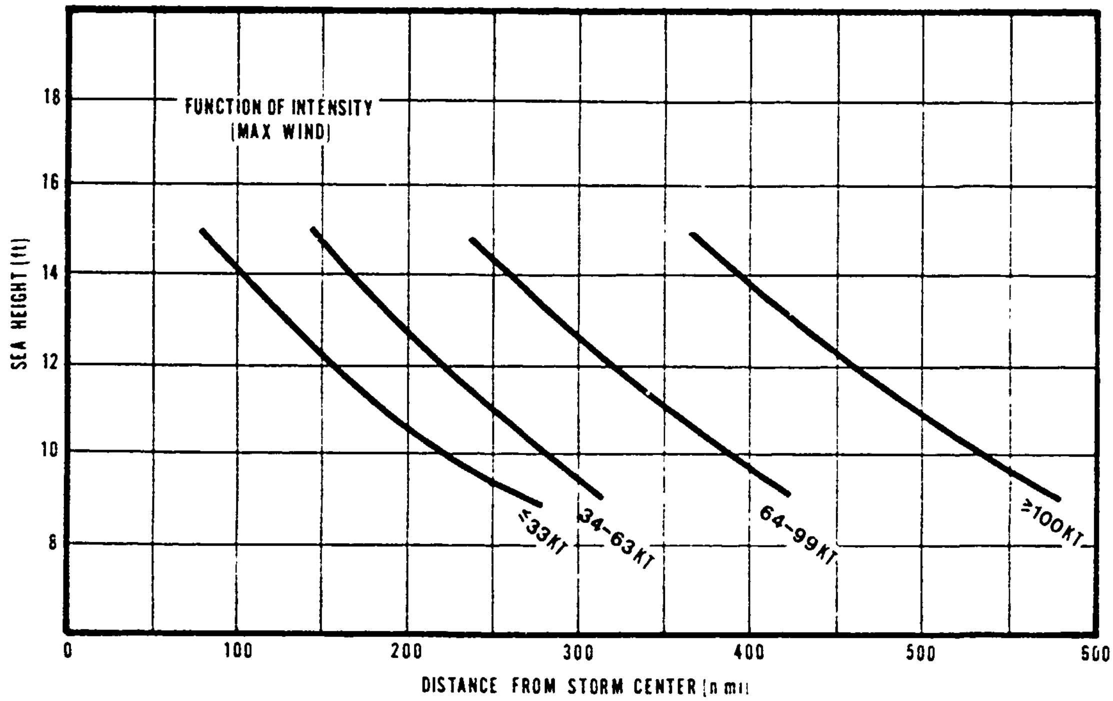

Figure I-2. The sea height (9 to 15 ft range) around 21 tropical storms and typhoons (based on 173 analyses for the year 1971) plotted against distance from storm center and given as a function of intensity.

shows the sea height associated with 21 tropical storms and typhoons to the east of the Philippines (based on 173 analyses for the year 1971) plotted as function of distance from the storm center and storm intensity (Brand, et al., 1973). There is a large variation in the sea state with storm intensity. A tropical storm (winds 34-63 kt) could produce 12-ft seas 217 n mi from the storm center; while an intense typhoon (winds ≥ 100 kt) could produce 12-ft seas 454 n mi from the center. The distances given are mean distances since the isopleths of sea height are not symmetric about the storm center.

Brand, et al. (1973) found that the actual wave heights are at least partially dependent on the direction in which the storm is moving. For example, Figure I-3 shows the average sea-height isopleth pattern for storms moving to the west, northwest, and northeast and is based on sea-state analyses for tropical storms and typhoons that occurred during 1971. Note that the greatest area of higher seas (9-15 ft range) tends to exist to the rear and toward the right semicircle of the storm.

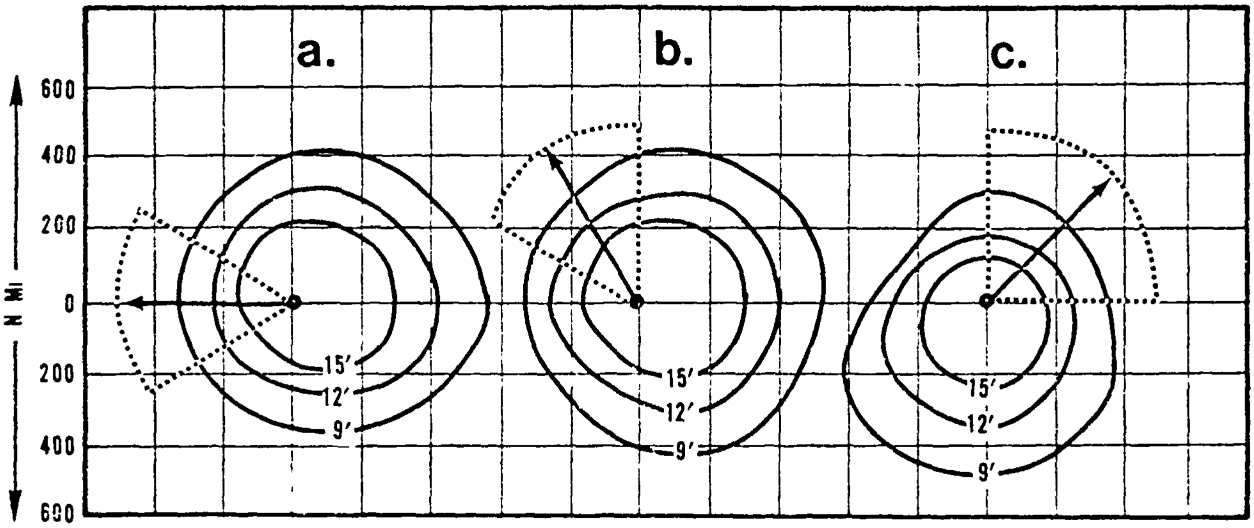

Figure I-3. The sea height isopleths (9-15 ft) about tropical storms and typhoons given as a function of direction of movement (a = 240°-300°; b = 301°-360°; c = 001°-090°).

5. SHIP SPEED OF ADVANCE VERSUS SEA STATE AND WIND

Figure I-4 represents the estimated resultant speed-of-advance of a ship in a given sea condition. The original relationships were based on data of speed versus sea state obtained from studies of many ships by James (1957). They should not be regarded as truly representative of any particular ship (Nagle, 1972).

For example, from Figure I-4, for a ship making 15 kt encountering waves of 16 ft approaching from 030° (relative to the ship's heading) one can expect the speed-of-advance to be slowed to about 9 kt. Twenty-foot seas, under the same condition, would result in a speed-of-advance of slightly less than 6 kt. However, it is emphasized that these figures are averages and the true values will vary from ship to ship.

Figure I-5 shows the engine speed required to offset selected wind velocities for various ship types (computed for normal loading conditions).

Figure I-4. Expected ship speed as a function of wave height and wave direction relative to ship's heading for (a) a ship speed of 15 kt and (b) a ship speed of 20 kt.

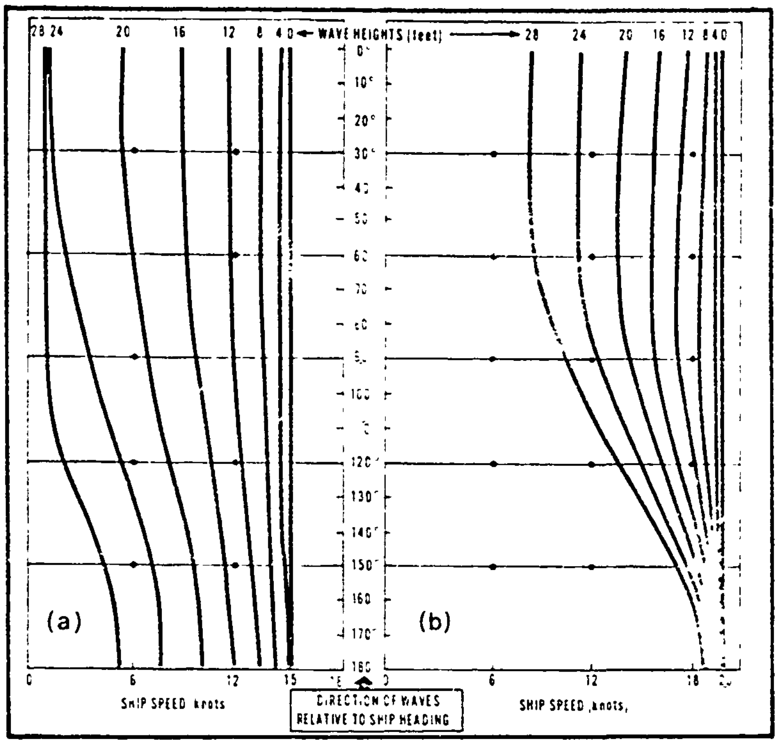

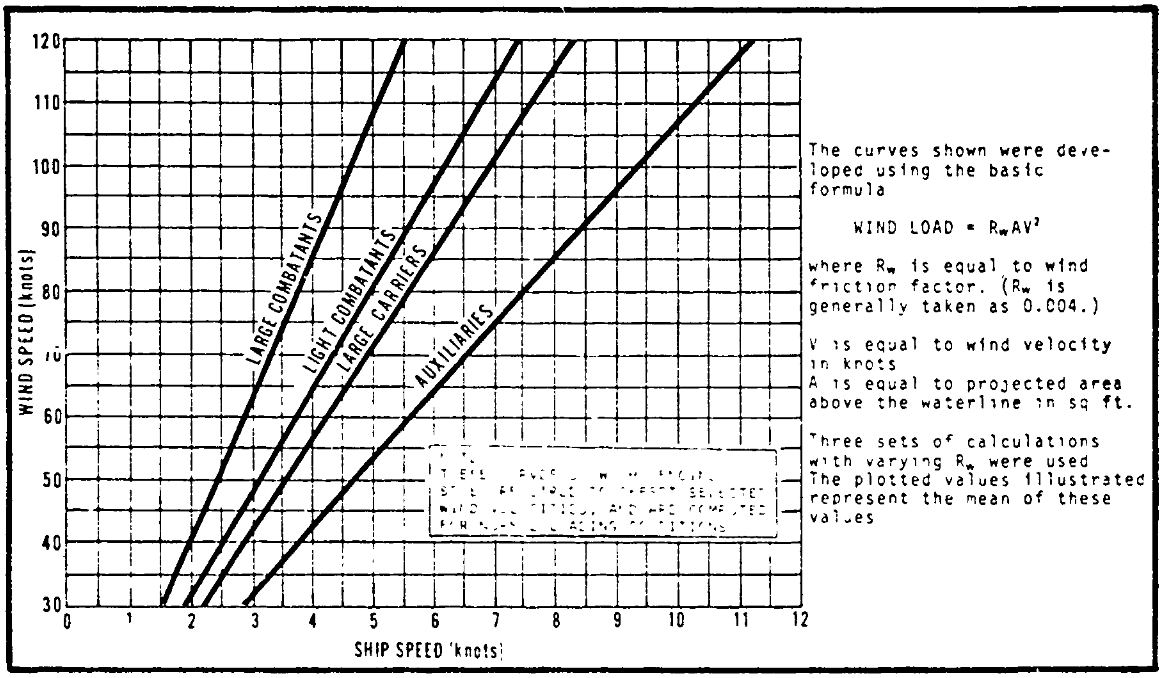

Figure I-5. Engine speed vs wind velocity for offsetting force of wind (from Crenshaw, 1965).

6. WARNING AND ADVISORY SERVICES

Fleet Weather Central/Joint Typhoon Warning Center, Guam (FWC/JTWC) offers a variety of warning and advisory services to WESTPAC and Indian Ocean units in accordance with COMNAVWEASERVINST 3140.1 (series). In the Northern Hemisphere west of the 180th meridian, the following tropical cyclone related bulletins are transmitted on Fleet broadcasts (see CINCPAC INST 3140.1 (series) for details):

SIGNIFICANT TROPICAL WEATHER ADVISORY - A narrative message which summarizes significant tropical atmospheric conditions (issued at 0600Z daily).

TROPICAL CYCLONE FORMATION ALERT MESSAGE - Issued when meteorological data indicates that formation of a tropical cyclone is likely.

TROPICAL CYCLONE WARNINGS -* Issued on all tropical cyclones four times a day in the Western Pacific. Warnings are issued within 2 hours of 000Z, 0600Z, 1200Z, and 1800Z, with the constraint that two consecutive warnings may not be more than 7 hours apart. In the Bay of Bengal and Arabian Sea, the warnings are issued twice a day within 2 hours of 0800Z and 2000Z.

PROGNOSTIC REASONING MESSAGE - Issued for the WESTPAC area only, this message (at 0000Z and 1200Z daily) provides technical reasoning for latest forecast.

In the Southern Hemisphere, only Tropical Cyclone Formation Alerts and Tropical Cyclone Warnings are issued. The warnings are transmitted at 0000Z and 1200Z daily.**

7. CALCULATING DANGER ZONES

Through aircraft reconnaissance and satellite observations, modern techniques for locating tropical cyclones and monitoring their progress have become quite sophisticated. Nevertheless, the present state of meteorological knowledge does not permit a perfect prediction of storm movements. Many variables exist which can alter the path of a typhoon; hence, every typhoon should be treated with the utmost respect.

COMSEVENTHFLT OPORD 201-(YR), Annex H (also CINCPACFLT OPORD 201-(YR), Annex H), describes the techniques to be used when plotting the Fleet Weather Central/Joint Typhoon Warning Center (FWC/JTWC) typhoon warning track positions. An average 24-hr forecast error of 135 n mi should always be incorporated when plotting the 24-hr forecast position in order to expand the radius of 30-kt winds, given in the warning, by the average forecast error. Figure I-6 demonstrates this procedure and utilizes the 135 n mi average 24-hr forecast position error in obtaining the "danger area." Note the radius of 30-kt winds is greater on the right side of the storm track -- the dangerous semicircle. In this example the radius to the 30-kt isotach is 200 n mi to the north and 150 n mi to the south of the storm at the current position. The radius to the 30-kt isotach

* Since this paper was originally published, some changes have been made. This paragraph should now read: "Issued on all tropical cyclones four times a day in the northwest Pacific and north Indian Oceans These warnings are issued within two and one-half hours of 0000Z, 0600Z, 1200Z and 1800Z."

** This should now read "The warnings are transmitted at 0000Z and 1200Z daily or 0600Z and 1800Z daily " is forecast to expand to 225 n mi to the north and 175 n mi to the south of the storm center at the 24-hr forecast position. At the 24-hr forecast time the danger area is then 360 n mi (225 plus 135) to the north and 310 n mi (175 plus 135) to the south of the storm.

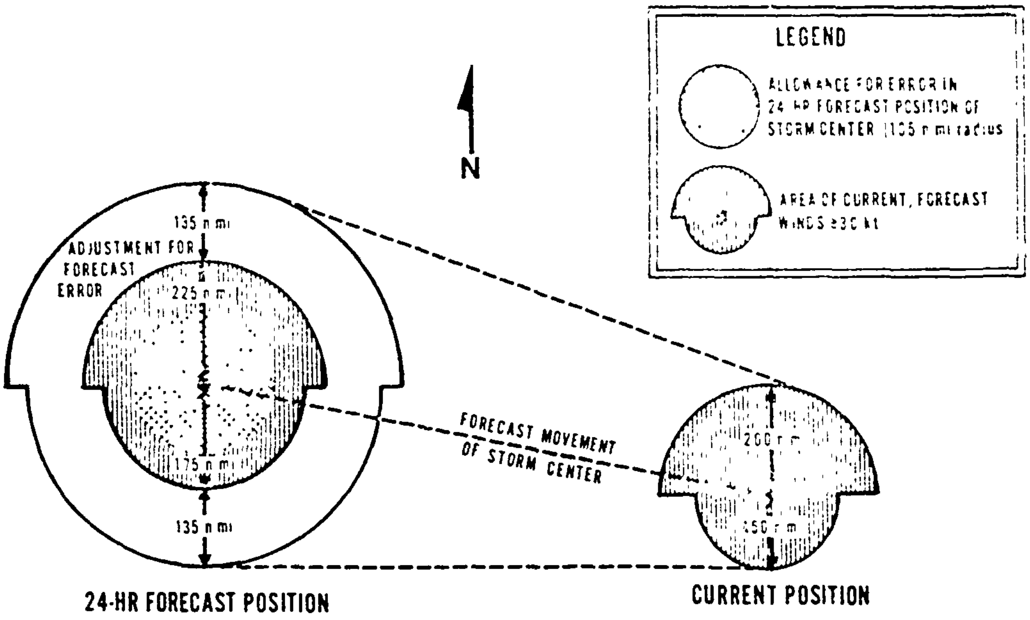

Figure I-6. Method of calculating the danger area for moving typhoons and tropical storms.

REFERENCES

Brand, S., J.W. Blelloch and D.C. Schertz, 1973. State of the sea around tropical cyclones in the western North Pacific Ocean. ENVPREDRSCHFAC Tech. Paper No. 5-73.

Burroughs, L.D., and S. Brand, 1973: Speed of tropical storms and typhoons after recurvature in the western North Pacific Ocean. J. Appl. Meteor., 12, 452-58.

Crenshaw, R.S., Jr., Capt., USN, 1965. Naval Shiphandling. Maryland: U.S. Naval Institute, 533 pp.

Crutcher, H.L. and R.G. Quayle, 1974. Mariners worldwide climatic guide to tropical storms at sea. NAVAIR 50-1C-60.

Harding, E.T. and W.J. Kotsch, 1965. Heavy Weather Guide. Maryland: U.S. Naval Institute, 209 pp.

Nagle, F.W., 1972. A numerical study in optimum track ship routing climatology. ENVPREDRSCHFAC Tech. Paper No. 10-72

The following summaries are excerpted from the Typhoon Havens Handbook. Each summary includes a section number to assist in referencing the Havens Handbook. For specific port information about typhoons and typhoon statistics, the reader should refer to the Typhoon Havens Handbook.

APRA HARBOR, GUAM - SECTION II,2

SUMMARY

There are no aspects of Apra Harbor that recommend it as a typhoon haven. Typhoon Karen (November, 1962) gave Apra Harbor sustained winds of 150 kt! The surrounding topography is low and does not provide an extensive wind break. The harbor entrance is open to the west and is in close proximity to the berths and moorings in the outer harbor. Consequently, westerly winds and seas associated with the typhoon passage have a devastating effect within the harbor.

In the past, all U. S. Navy ships capable have sortied from the harbor upon the approach of a typhoon. Additionally, the Port Operations Officer desires that ships not use Apra Harbor as a typhoon haven since the harbor's and NAVSHIPREPFAC Guam's yard and service craft occupy virtually all desirable berths in the harbor during typhoon conditions.

KAOHSIUNG, TAIWAN - SECTION III,2

SUMMARY

The conclusion reached by this study is in full agreement with the opinion held by Kaohsiung harbor authorities, both military and civil: "...Kaohsiung harbor is not to be considered a haven during typhoon conditions..." The key factor in reaching this conclusion was not weather conditions, but the threat posed by other ships in the confined harbor.

It is the recommendation of this study that all U.S. Navy ships capable take action to evade at sea when typhoon conditions threaten Kaohsiung, Taiwan.

CHILUNG (KEELUNG), TAIWAN - SECTION III,3

SUMMARY

The conclusion reached in this study is that Chilung harbor is a poor haven during typhoon conditions. The key factors in reaching this conclusion were:

1. Sea states in the outer harbor can exceed 20 ft during typhoon conditions.

2. The threat of other vessels adrift in the confined harbor.

3. The lack of sheltered berths.

It is the recommendation of this study that all U.S. Navy ships capable take action to evade at sea when typhoon conditions threaten Chilung, Taiwan.

HONG KONG - SECTION IV

SUMMARY

This study of Hong Kong Harbor as a possible typhoon haven must concur with previous conclusions that the harbor can not be designated a "safe" haven in time of severe winds and waves associated with the passage of tropical cyclones. Previous results, as stated in COMSEVENTHFLT INST 5000.1H, Annex W, dated 29 Feb 1972, readily indicate that "... it is considered that Hong Kong is not a suitable haven for Seventh Fleet units." This is also in agreement with the findings of the British, that "the Royal Navy does not consider Hong Kong a suitable haven under typhoon conditions."

The first step to making a safe evasion is in recognizing that a potential threat to the port of Kong Kong exists, based on current tropical cyclone warnings (from U.S. FWC/JTWC, Guam) and a knowledge of past tropical cyclone tracks that have affected Hong Kong. Smaller ships, such as minesweepers or patrol craft, unable to outrun and evade at sea, or those ships unable to put to sea should be thoroughly familiar with the potential problems of remaining in port. It is recommended that all other Fleet units should take early decisive action to clear Hong Kong Harbor and evade at sea.

YOKUSUKA, JAPAN - SECTION V,2

SUMMARY

The conclusion reached in this study is that the port of Yokosuka is a "safe" typhoon haven; a port in which to remain if already there or in which to seek shelter if at sea when threatened by a typhoon. The primary factors in reaching this conclusion are:

(1) The port provides shelter from wind and sea due to the surrounding land masses.

(2) Wave action induced by typhoons has been negligible in the port.

(3) Storm surge has negligible effect.

(4) The orientation of the berths and drydocks with respect to the local topography is good.

(5) The experience level and the high degree of competence of the Port Services personnel.

(6) The only situation in which the port would not be a safe haven is when a very intense typhoon ($\geq$120 kt) passed directly over Yokosuka.

(7) The history of the port. Conversations with Japanese employees at Fleet Activities, Yokosuka indicated that since 1945 there is no recollection of U.S. Navy, Japanese Maritime Self Defense Force or merchant ships sortieing from the port of Yokosuka due to a typhoon. It should be noted however that the port has never been truly tested as a haven by U.S. Navy aircraft carriers.

IWAKUNI AND KURE, JAPAN - SECTION V,4

SUMMARY

The conclusions reached by this study are first that Kure Harbor is a favorable typhoon "haven" for all ships; and second, Iwakuni Harbor, although not recommended as a "haven," has easily accessible anchorages close by which are considered safe during typhoon passage. These conclusions are based on the following:

1. The location and topography of the entire Iwakuni/Kure area significantly reduces the effects of winds attending tropical cyclones.

2. Anchor holding in the designated anchorage areas is rated as excellent.

3. Surge effect is almost negligible and wave heights are not severe in the designated anchorage areas.

4. Port services and repair facilities at Kure (also available to ships at Iwakuni) are among the best in all of Japan.

5. Conversations with local harbor and meteorology officials.

SUMMARY

The conclusion reached in this study is that Suruga Bay, including the Numazu Operating Area should not be considered a "safe" typhoon haven for ships operating in the area or transiting the south central coast of Honshu. The primary factors in reaching this conclusion are:

(1) The openness of the bay to the effects of the ocean -- especially in the southwestern quadrant.

(2) The lack of any suitable sheltered area for a ship to lie to or anchor in.

(3) Wind and swell wave action can be as devastating in the Suruga Bay area as on the open ocean if these effects are being felt from the south-southwest. (A southwesterly wind gust of 97 kt was recorded at Numazu on 25 September 1966 as Typhoon Ida passed 30 n mi to the west. Winds in excess of 34 kt existed for 5 hours.)

Some protection from northeasterly winds (associated with a tropical cyclone passing to the east) may be found by keeping close to the Izu Peninsula (eastern) side of the bay. This should reduce the effects of the wind and wind generated waves because of the shorter fetch the winds would blow over. In spite of the deep water in Suruga Bay, caution should be exercised when operating close to land as visibility may be reduced and radar reception hindered by the effects of a tropical cyclone passing close by. Also the confused sea state with accompanying wind may set up unpredictable local currents.

Additionally, it has been concluded that surf conditions in the Numazu Operating Area may be unsafe for small craft operation for a number of days after a tropical cyclone passes CPA because of the slow decay rate of swells associated with such a storm. This conclusion can also be applied to tropical cyclones, especially typhoons, that pass well to the south of the 180 n mi threat circle used in this study.

To avoid the effects of tropical cyclones that pose a threat to the Numazu Operating Area, evasion to the Yokosuka/Tokyo Bay area is highly recommended.

SASEBO, JAPAN - SECTION V,5

SUMMARY

The conclusion reached by this study is that Sasebo Harbor is a favorable typhoon haven for all ships except aircraft carriers. This conclusion is based on the following reasons:

1. The harbor topography provides excellent protection from winds out of the north or east and good protection from southerly winds. However, due to the large "sail area" of a carrier, winds may affect the ship severely.

2. The anchor holding capability in the typhoon anchorage is excellent.

3. There is sufficient maneuvering room at typhoon anchorages in the outer harbor. However, aircraft carriers may be too restricted if many ships are present.

4. The inner harbor provides little protection for aircraft carriers. Ships of the size of AR's, AOE's, and AF's can find good protection at India Basin, Berths 8 and 9. Small ships have excellent protection in wet drydocks.

5. Surge effect is, in most cases, minimal and wave action in the past has not been too severe during the passage of a typhoon.

6. Port services available are excellent.

NAHA, OKINAWA - SECTION V,8

SUMMARY

The conclusion reached in this study is that Naha Harbor is a poor haven during typhoon conditions. The key factors in reaching this conclusion were:

1. Lack of sheltered berths.

2. The threat of other vessels adrift in the confined harbor.

3. High sea states within the harbor area for winds of 25 kt and greater.

4. Poor anchor holding action of the harbor bottom.

It is recommended that all U.S. Navy ships capable take action to evade at sea when typhoon conditions threaten Naha, Okinawa.

KAGOSHIMA, JAPAN - SECTION V,6

SUMMARY

The conclusion reached in this study is that Kagoshima Harbor is not a safe harbor during the passage of an intense tropical cyclone. The key factors in reaching this conclusion are:

1. Due to the size and shape of Kagoshima Bay and surrounding land masses, the harbor provides little shelter from wind and seas. (During the period 1947-74, the highest recorded wind gust in Kagoshima was 100 kt due to Typhoon Louise (29 September 1955). This typhoon passed 30 n mi to the west of Kagoshima and contributed 5 hours of gale force winds.)

2. Wave action induced by gale force winds can be quite dangerous.

3. The holding action of the bottom in the harbor area is considered very poor under adverse weather conditions.

4. The restricted nature of the anchorage itself would give a commanding officer little reaction time in the event the anchor began to drag.

This conclusion is in full agreement with the Kagoshima Harbor authorities and the Japanese Maritime Safety Agency concerning ships that are anchored.

It is recommended that commanding officers and masters of vessels take early evasion action commensurate with operational constraints. For U. S. Navy or contracted DOD vessels, it is recommended that Sasebo or Hiroshima Bay be given priority consideration as typhoon havens. If evasion at sea is more desirable, it is recommended that the ship be placed in the Yellow Sea or Sea of Japan where effects from the typhoon will be considerably lessened.

BUCKNER BAY, OKINAWA - SECTION V,7

SUMMARY

The conclusion reached by this study is that Buckner Bay is not considered to be a haven during typhoon conditions. The lack of extensive protection from wind due to the relatively low topography of the surrounding land mass and the exposure of ships to wind and seas with any easterly component severely limits Buckner Bay as a storm refuge.

It is recommended that all Navy ships capable take action to evade at sea when typhoon conditions threaten Buckner Bay.

SUBIC BAY, PHILIPPINES - SECTION VI,3

SUMMARY

Previous texts classifying Subic Bay as a typhoon haven have done so with certain reservations or qualifications. It is true that many ships have successfully weathered the numerous typhoons which have affected Subic Bay. However, it is also a fact that Subic Bay has never really been tested by the passage of a truly severe tropical cyclone. Those storms whose eyes have crossed directly over Subic Bay have been relatively weak storms; in the case of severe tropical cyclones the eyes have only come close, with the strongest winds missing Subic Bay by 50-100 n mi, and the remaining winds being further reduced by the topography of the surrounding terrain. The highest sustained wind recorded during the period 1955-1973 was 56 kt.

In any event, it is felt that the potentially most dangerous situation is not presented by a cyclone passing directly over Subic, but rather by a close south-southwestward passage between 15-50 n mi. Consider a case where a cyclone has crossed the Philippines through the San Bernardino Strait, losing little of its intensity, and then moves northward (perhaps starting to recurve), so that the eastern and southern portions of the wall cloud and feeder band activity have unobstructed access to the bay.

After considering the above facts and after many discussions with experienced personnel at Subic Bay, it is the conclusion of this study that, although Subic Bay does provide some degree of shelter from typhoon passage, it should not be considered an "unqualified" typhoon haven. The sheltering effect provided by the surrounding terrain qualifies Subic Bay as a much safer port in heavy weather than Hong Kong, Kaohsiung, or Chilung (Keelung). However, large combatants (CVA, cruisers, etc.) would find the relatively small size of Subic Bay restrictive. The cost in terms of time and money of evasion would be small since the evasion routes are short and direct. Smaller craft, given ample warning time, should also be able to evade into the navigable semicircle. If ample warning time is not given, or the means to evade does not exist, relatively safe typhoon anchorages are present in the inner basin of Port Olongapo for a limited number of small vessels. Also certain anchorages close to the western shore of the bay provide some degree of shelter.

MANILA, PHILIPPINES - SECTION VI,4

SUMMARY

It is the conclusion of this study that Manila Harbor is not a safe harbor and Manila Bay is not a safe refuge during a passage of a typhoon. The policy of the Port Captain of the South Harbor, Manila, is to evacuate all vessels at least 24 hours prior to typhoon passage. The harbor is extremely busy and congested with primarily merchant and commercial shipping vessels. These vessels are, more often than not, equipped with inadequate or inferior mooring equipment and they may evacuate to any area in Manila Bay outside the confines of South Harbor. Because of the danger of ships breaking loose from anchor during the storm (poor holding) and the shallowness of the bay, it is recommended that all U.S. Navy or contracted DOD vessels sortie from Manila Bay as well as from Manila Harbor. Since the evasion route is generally southwesterly into the South China Sea, the sortie should be relatively short, low in operating costs, and free of peril.

CLIMATOLOGY OF NORTH PACIFIC TROPICAL CYCLONE TRACKS

In April 1988, the Naval Environmental Prediction Research Facility (NEPRF) updated the Pacific Tropical Cyclone Track climatology. The following information is exerpted from that publication:

Mean Path Chart: This chart displays those paths most often followed by tropical cyclones in the period. The numbers on the paths represent the percentage of tropical cyclones for the period which follow the indicated path. Tracks which contained less than 5% of the tropical cyclones for the period were not analyzed. This chart also contains statistics similar to those in Table 1 but only for the applicable period. For periods in which 10 tropical cyclones or less occurred, a blank Mean Paths chart ıs supplied containing only the statistics.

NOTE: When one path branches off into multiple paths, the sum of the percentages on the branches does not necessarily equal the percentage indicated on the parent path. This is due to the fact that not all tropical cyclones follow a mean path and some develop/dissipate along a path.

Speed of Movement Chart: Isopleths are drawn to show the mean scalar movement speed of the tropical cyclone in knots. Each tropical cyclone was interpolated to hourly positions using the method of Akima. Speeds were averaged for each 5^{o} square (5^{o} latitude x 5^{o} longitude). Those squares which contained 5% or less of the tropical cyclones in the period were not considered in the analysis. The figure also lists the average speed and sample size in each square.

Table 1 gives backgrouna information on tropical cyclones (> 33 kts). A subjective path classification of straight, recurver, or odd-moving was made. A recurver is defined as a tropical cyclone which turns from its initial westward or northwestward path to a path toward the north or northeast. A straight tropical cyclone is one whose general direction of movement remains constant throughout its life with a heading between 250° and 360°.

TABLE 1. TROPICAL CYCLONE DATA FOR WESTERN PACIFIC (1945-1987)

Average Number Of Tropical Cyclones (> 33 kts) 25.37/year

	Number	Percent	Avg. Life (Days)
Straight	397	36.4	5.77
Recurver	464	42.5	7.37
Odd-Moving	230	21.1	6.71
Total	1091	100.0	6.65
Tropical Storms	355	32.6	4.42
Typhoons	572	52.5	7.29
Super Typhoons	162	14.9	9.32

MEAN PATHS FOR DEC 24 - JAN 8

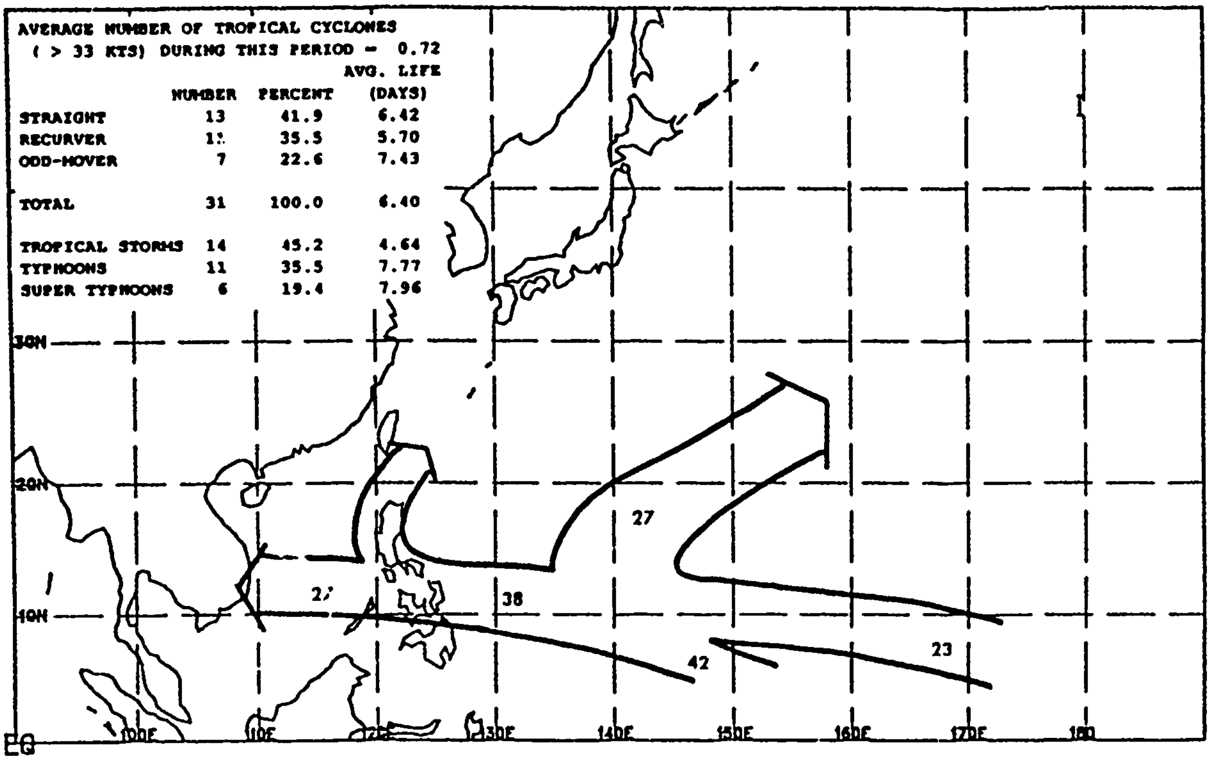

Mean tropical cyclone (> 33 kts) path. Numbers represent the percentage of tropical cyclones (> 33 kts) which followed the indicated path. These numbers may not add up to 100% since not all tropical cyclones (> 33 kts) follow a mean path and some develop/dissipate along a path. Tracks which contained less than 5% of the tropical cyclones (> 33 kts) are ignored. Dashed line represents mean recurvature position of tropical cyclones (> 33 kts) classified as recurvers.

SPEED OF MOVEMENT FOR DEC 24 - JAN 8

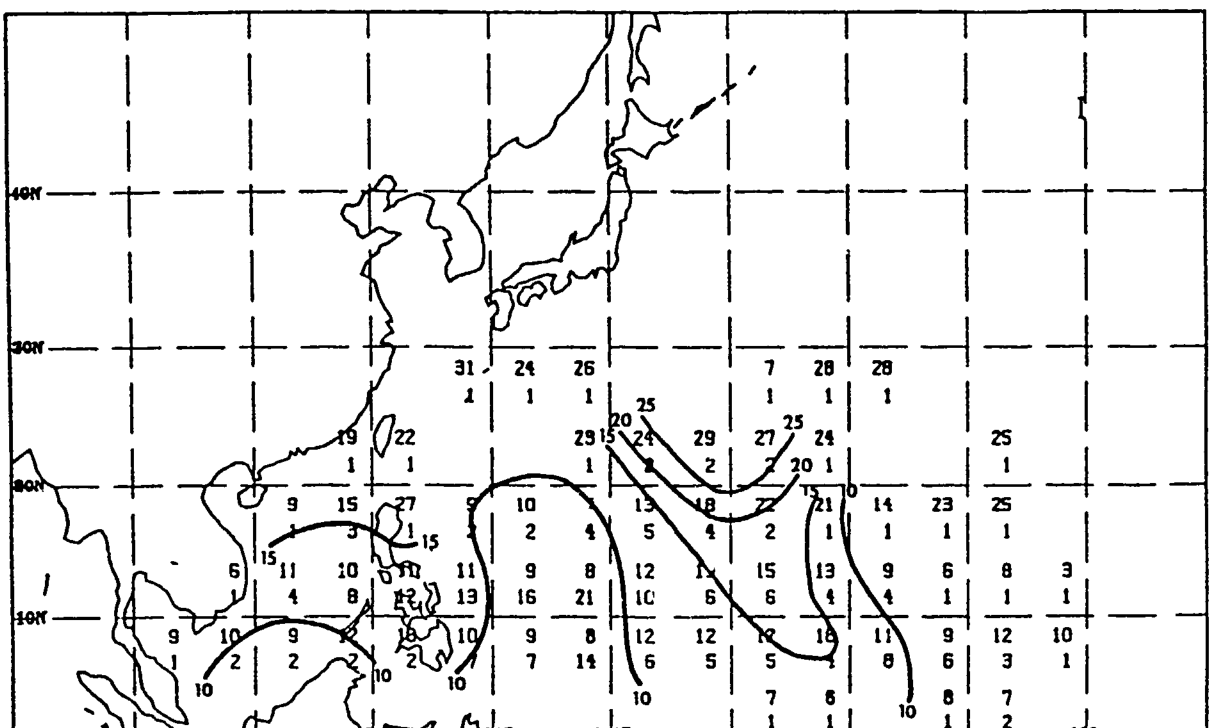

Average tropical cyclone (> 33 kts) Speed (top number) in knots and sample size (bottom number) for each 5° latitude by 5° longitude square. Contours are drawn only to those squares containing at least 5% of the sample.

MEAN PATHS FOR JAN 9 - JAN 23

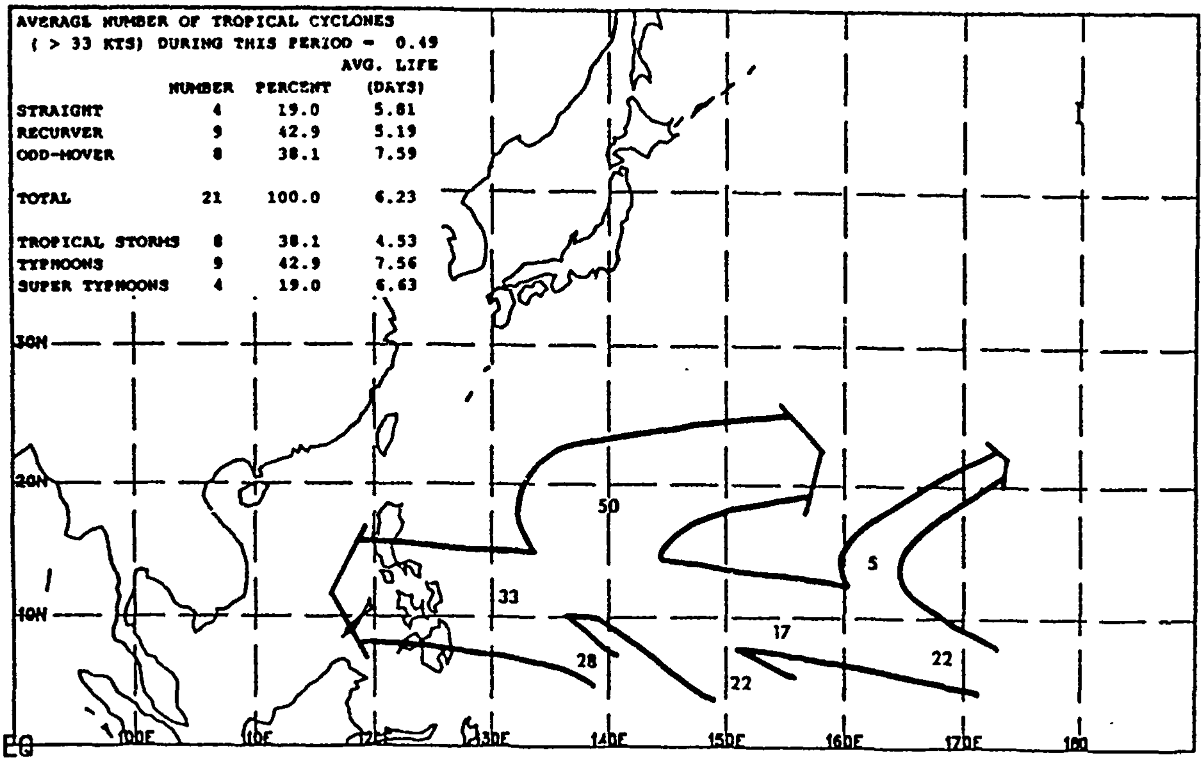

Mean tropical cyclone (> 33 kts) path. Numbers represent the percentage of tropical cyclones (> 33 kts) which followed the indicated path. These numbers may not add up to 100% since not all tropical cyclones (> 33 kts) follow a mean path and some develop/dissipate along a path. Tracks which contained less than 5% of the tropical cyclones (> 33 kts) are ignored. Dashed line represents mean recurvature position of tropical cyclones (> 33 kts) classified as recurvers.

SPEED OF MOVEMENT FOR JAN 9 - JAN 23

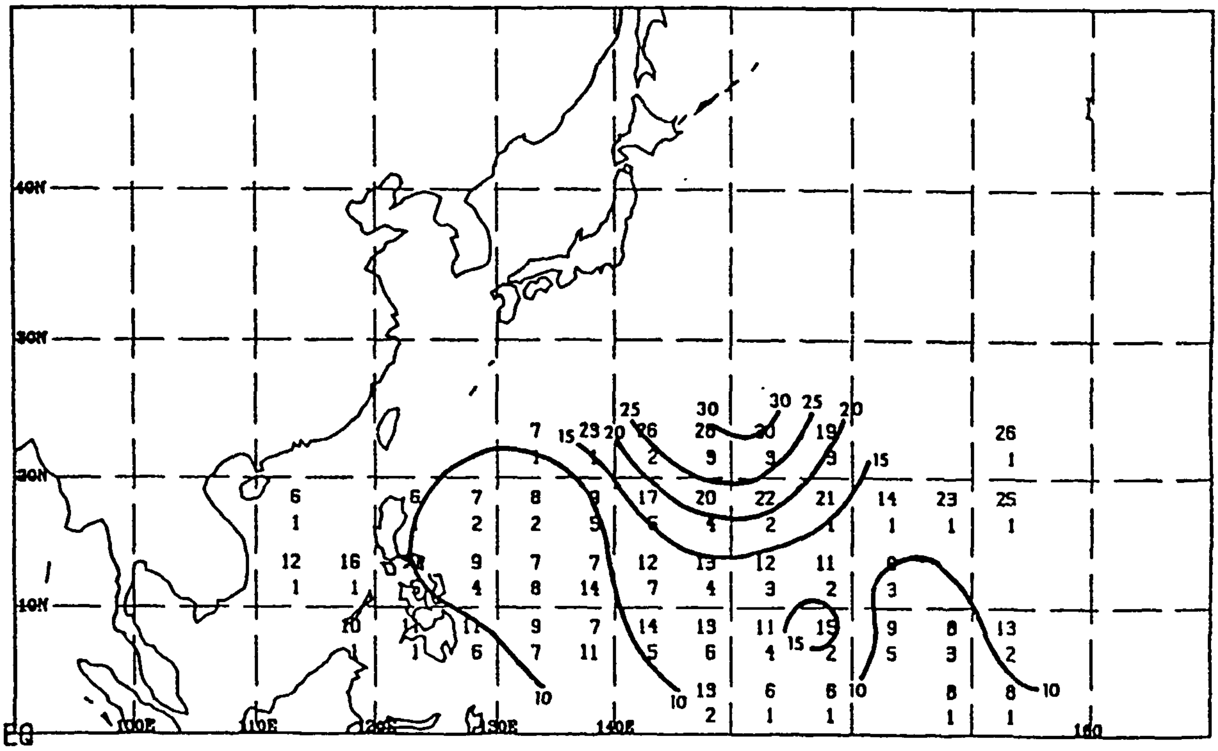

Average tropical cyclone (> 33 kts) Speed (top number) in knots and sample size (bottom number) for each 5° latitude by 5° longitude square. Contours are drawn only to those squares containing at least 5% of the sample.

MEAN PATHS FOR JAN 24 - FEB 8

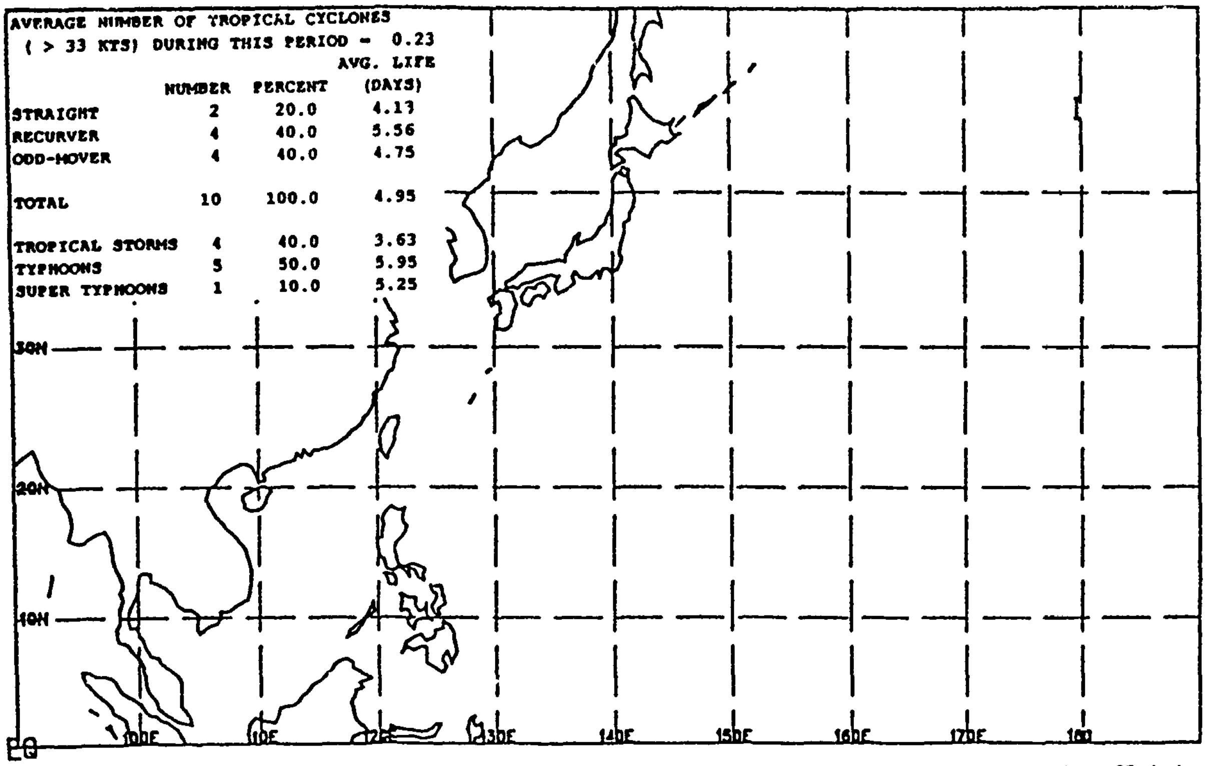

	NUMBER	PERCENT	AVG. LIFE (DAYS)
STRAIGHT	2	20.0	4.13
RECURVER	4	40.0	5.56
ODD-MOVER	4	40.0	4.75
TOTAL	10	100.0	4.95
TROPICAL STORMS	4	40.0	3.63
TYPHOONS	5	50.0	5.95
SUPER TYPHOONS	1	10.0	5.25

Mean tropical cyclone (> 33 kts) path. Numbers represent the percentage of tropical cyclones (> 33 kts) which followed the indicated path. These numbers may not add up to 100% since not all tropical cyclones (> 33 kts) follow a mean path and some develop/dissipate along a path. Tracks which contained less than 5% of the tropical cyclones (> 33 kts) are ignored. Dashed line represents mean recurvature position of tropical cyclones (> 33 kts) classified as recurvers.

SPEED OF MOVEMENT FOR JAN 24 - FEB 8

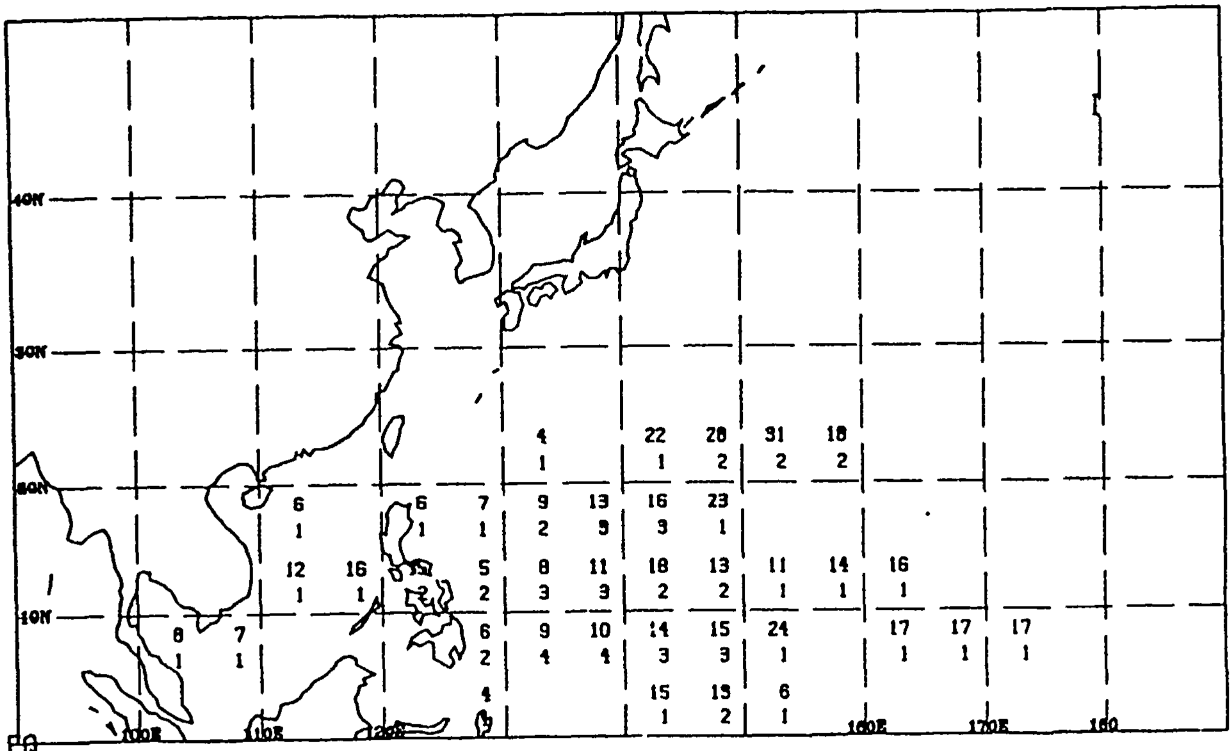

Average tropical cyclone (> 33 kts) Speed (top number) in knots and sample size (bottom number) for each 5° latitude by 5° longitude square. Contours are drawn only to those squares containing at least 5% of the sample.

MEAN PATHS FOR FEB 9 - FEB 23

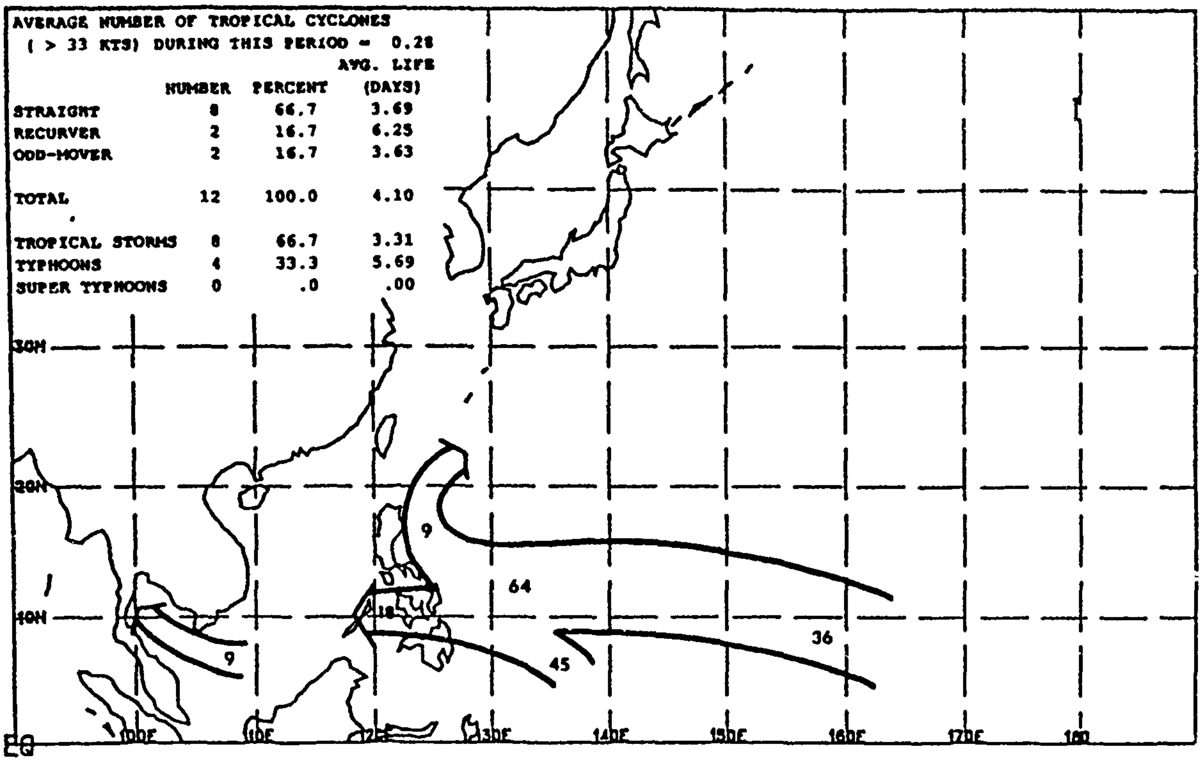

AVERAGE NUMBER OF TROPICAL CYCLONES (> 33 KTS) DURING THIS PERIOD = 0.28

	NUMBER	PERCENT	AVG. LIFE (DAYS)
STRAIGHT	8	66.7	3.69
RECURVER	2	16.7	6.25
ODD-MOVER	2	16.7	3.63
TOTAL	12	100.0	4.10
TROPICAL STORMS	8	66.7	3.31
TYPHOONS	4	33.3	5.69
SUPER TYPHOONS	0	.0	.00

Mean tropical cyclone (> 33 kts) path. Numbers represent the percentage of tropical cyclones (> 33 kts) which followed the indicated path. These numbers may not add up to 100% since not all tropical cyclones (> 33 kts) follow a mean path and some develop/dissipate along a path. Tracks which contained less than 5% of the tropical cyclones (> 33 kts) are ignored. Dashed line represents mean recurvature position of tropical cyclones (> 33 kts) classified as recurvers.

SPEED OF MOVEMENT FOR FEB 9 - FEB 23

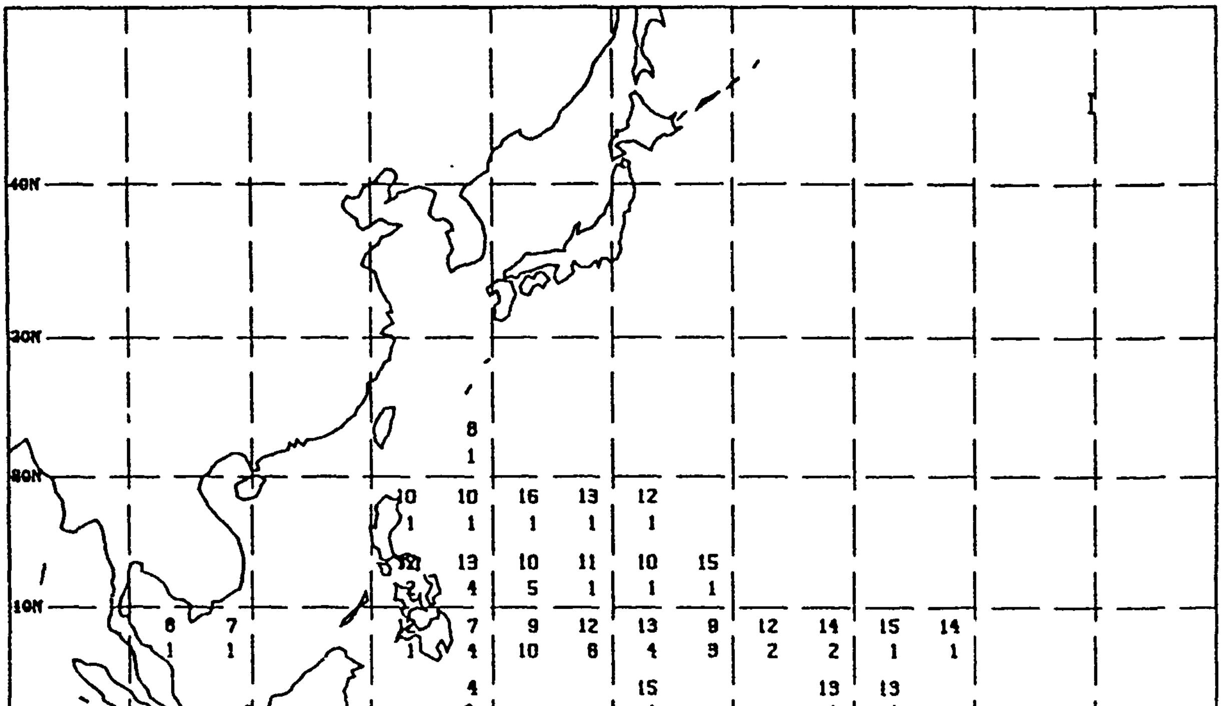

Average tropical cyclone (> 33 kts) Speed (top number) in knots and sample size (bottom number) for each 5° latitude by 5° longitude square. Contours are drawn only to those squares containing at least 5% of the sample.

MEAN PATHS FOR FEB 24 - MAR 8

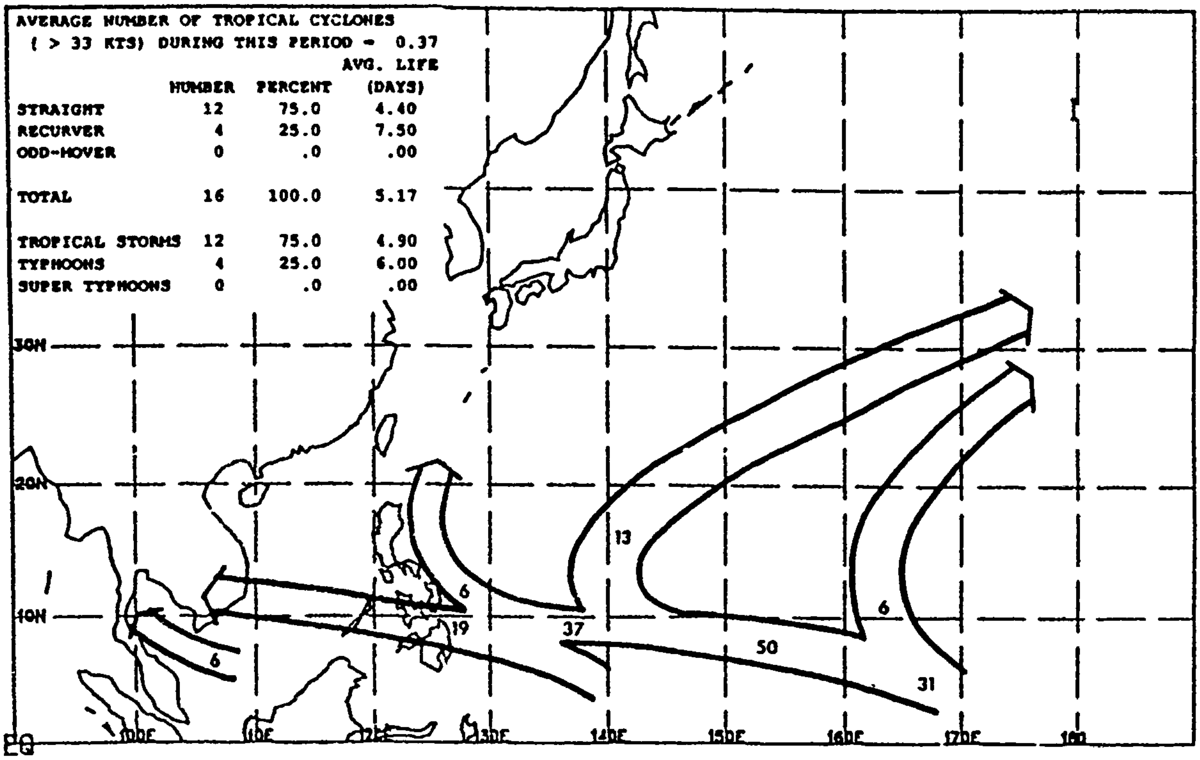

Mean tropical cyclone (> 33 kts) path. Numbers represent the percentage of tropical cyclones (> 33 kts) which followed the indicated path. These numbers may not add up to 100% since not all tropical cyclones (> 33 kts) follow a mean path and some develop/dissipate along a path. Tracks which contained less than 5% of the tropical cyclones (> 33 kts) are ignored. Dashed line represents mean recurvature position of tropical cyclones (> 33 kts) classified as recurvers.

SPEED OF MOVEMENT FOR FEB 24 - MAR 8

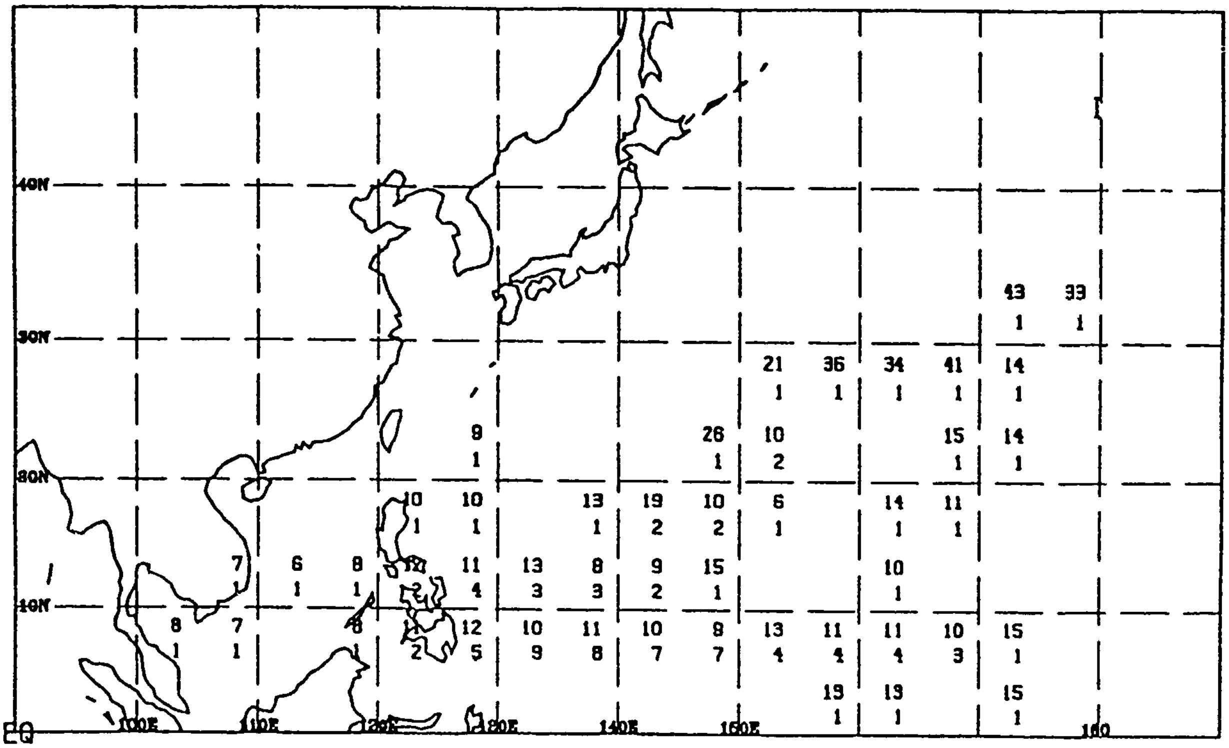

Average tropical cyclone (> 33 kts) Speed (top number) in knots and sample size (bottom number) for each 5° latitude by 5° longitude square. Contours are drawn only to those squares containing at least 5% of the sample.

MEAN PATHS FOR MAR 9 - MAR 23

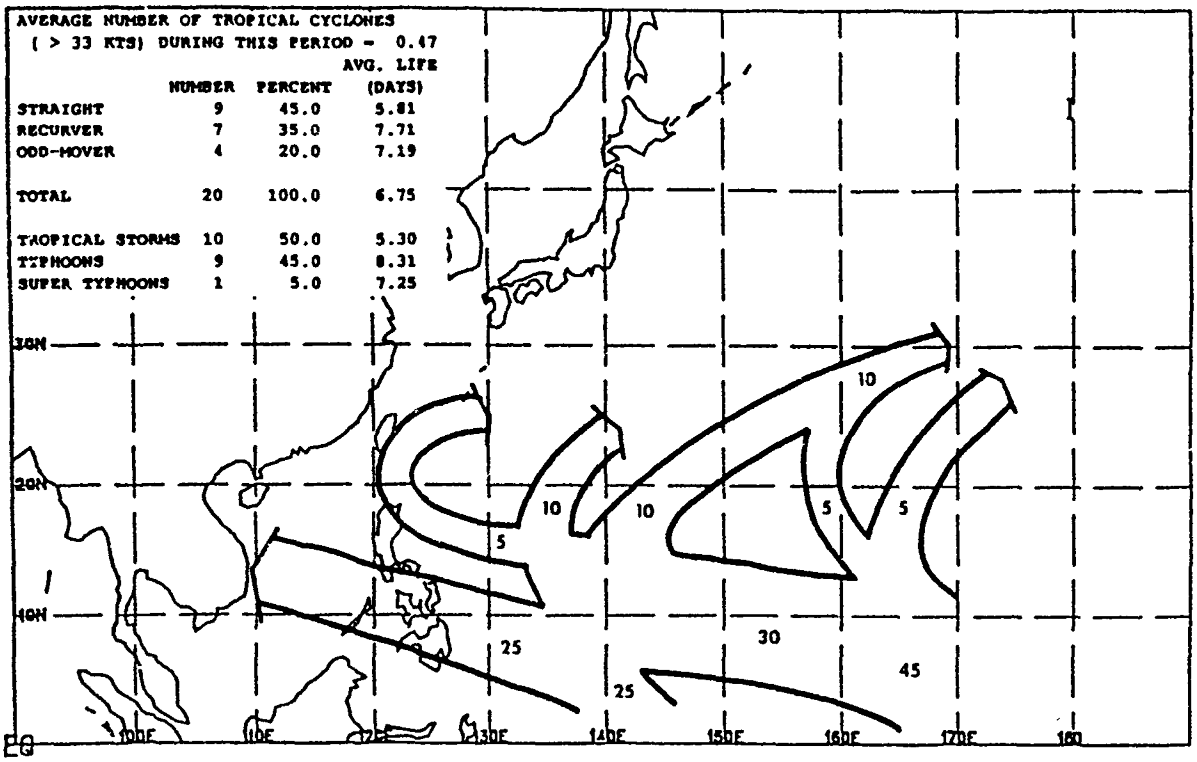

	NUMBER	PERCENT	AVG. LIFE (DAYS)
STRAIGHT	9	45.0	5.81
RECURVER	7	35.0	7.71
ODD-MOVER	4	20.0	7.19
TOTAL	20	100.0	6.75
TROPICAL STORMS	10	50.0	5.30
TYPHOONS	9	45.0	8.31
SUPER TYPHOONS	1	5.0	7.25

Mean tropical cyclone (> 33 kts) path. Numbers represent the percentage of tropical cyclones (> 33 kts) which followed the indicated path. These numbers may not add up to 100% since not all tropical cyclones (> 33 kts) follow a mean path and some develop/dissipate along a path. Tracks which contained less than 5% of the tropical cyclones (> 33 kts) are ignored. Dashed line represents mean recurvature position of tropical cyclones (> 33 kts) classified as recurvers.

SPEED OF MOVEMENT FOR MAR 9 - MAR 23

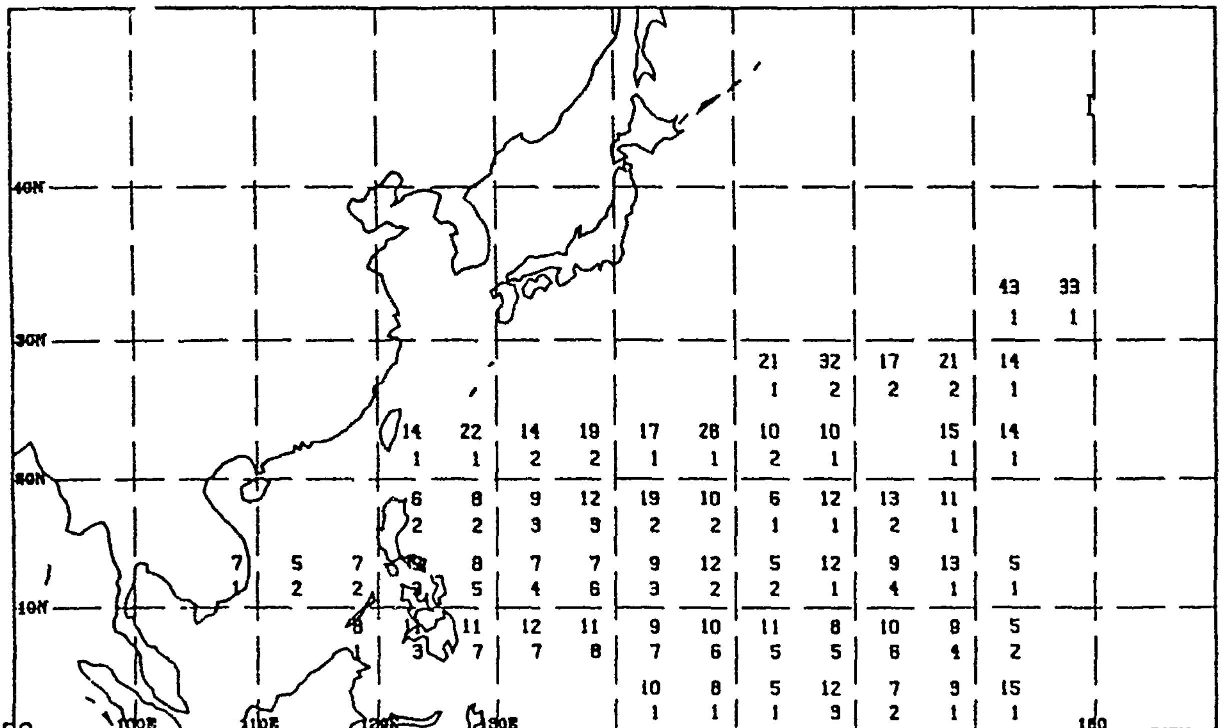

Average tropical cyclone (> 33 kts) Speed (top number) in knots and sample size (bottom number) for each 5° latitude by 5° longitude square. Contours are drawn only to those squares containing at least 5% of the sample.

MEAN PATHS FOR MAR 24 - APR 8

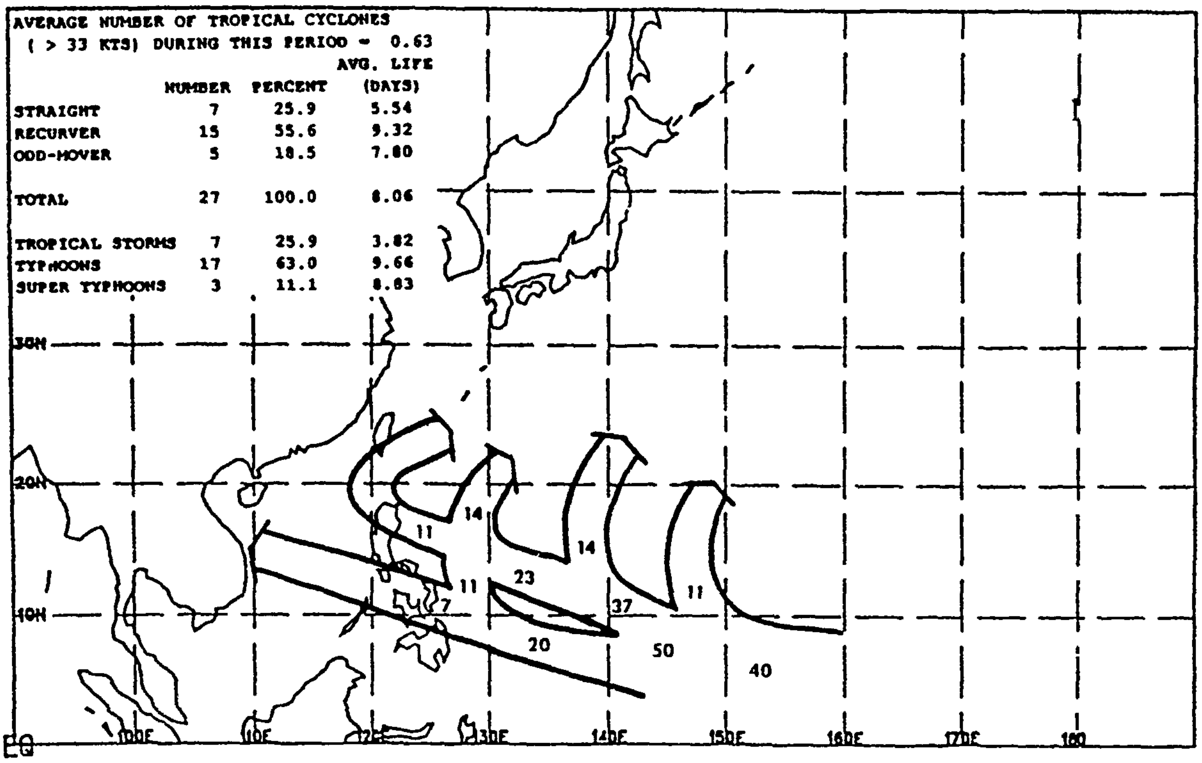

Mean tropical cyclone (> 33 kts) path. Numbers represent the percentage of tropical cyclones (> 33 kts) which followed the indicated path. These numbers may not add up to 100% since not all tropical cyclones (> 33 kts) follow a mean path and some develop/dissipate along a path. Tracks which contained less than 5% of the tropical cyclones (> 33 kts) are ignored. Dashed line represents mean recurvature position of tropical cyclones (> 33 kts) classified as recurvers.

SPEED OF MOVEMENT FOR MAR 24 - APR 8

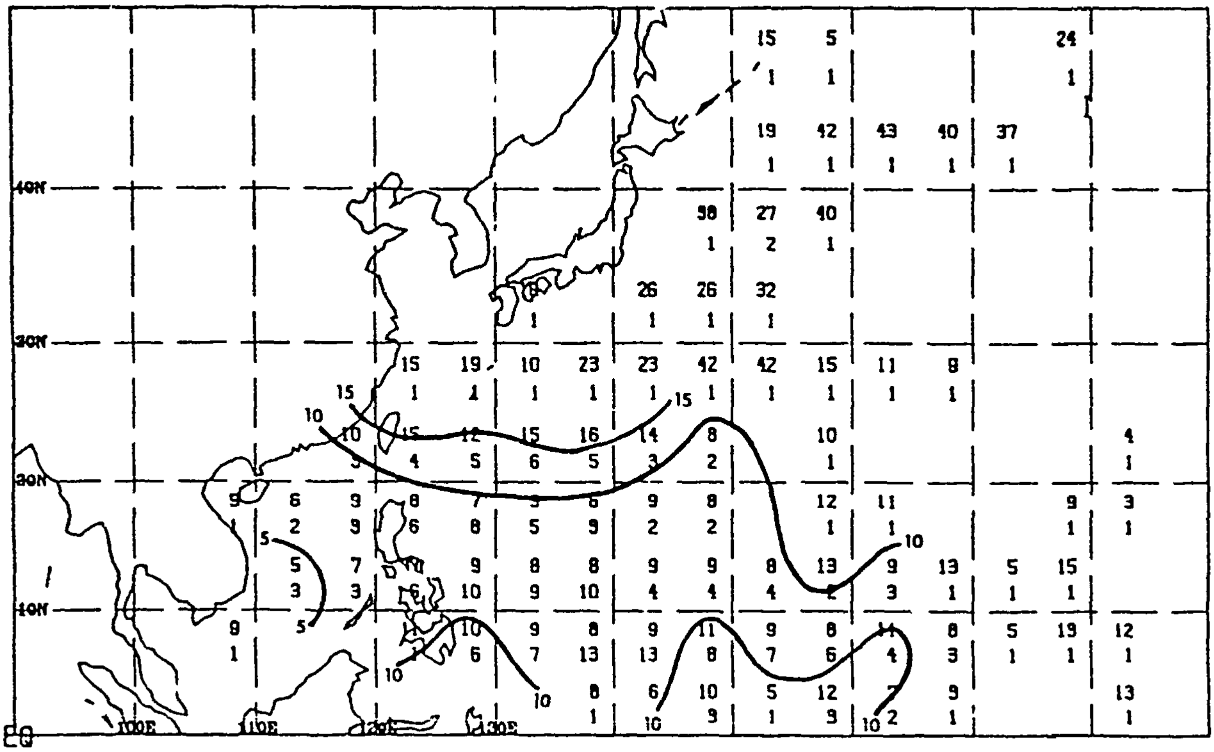

Average tropical cyclone (> 33 kts) Speed (top number) in knots and sample size (bottom number) for each 5° latitude by 5° longitude square. Contours are drawn only to those squares containing at least 5% of the sample.

MEAN PATHS FOR APR 9 - APR 23

AVERAGE NUMBER OF TROPICAL CYCLONES (> 33 KTS) DURING THIS PERIOD - 0.70

	NUMBER	PERCENT	AVG. LIFE (DAYS)
STRAIGHT	8	26.7	6.28
RECURVER	16	53.3	9.23
ODD-MOVER	6	20.0	8.58
TOTAL	30	100.0	8.32
TROPICAL STORMS	8	26.7	6.56
TYPHOONS	18	60.0	8.68
SUPER TYPHOONS	4	13.3	10.19

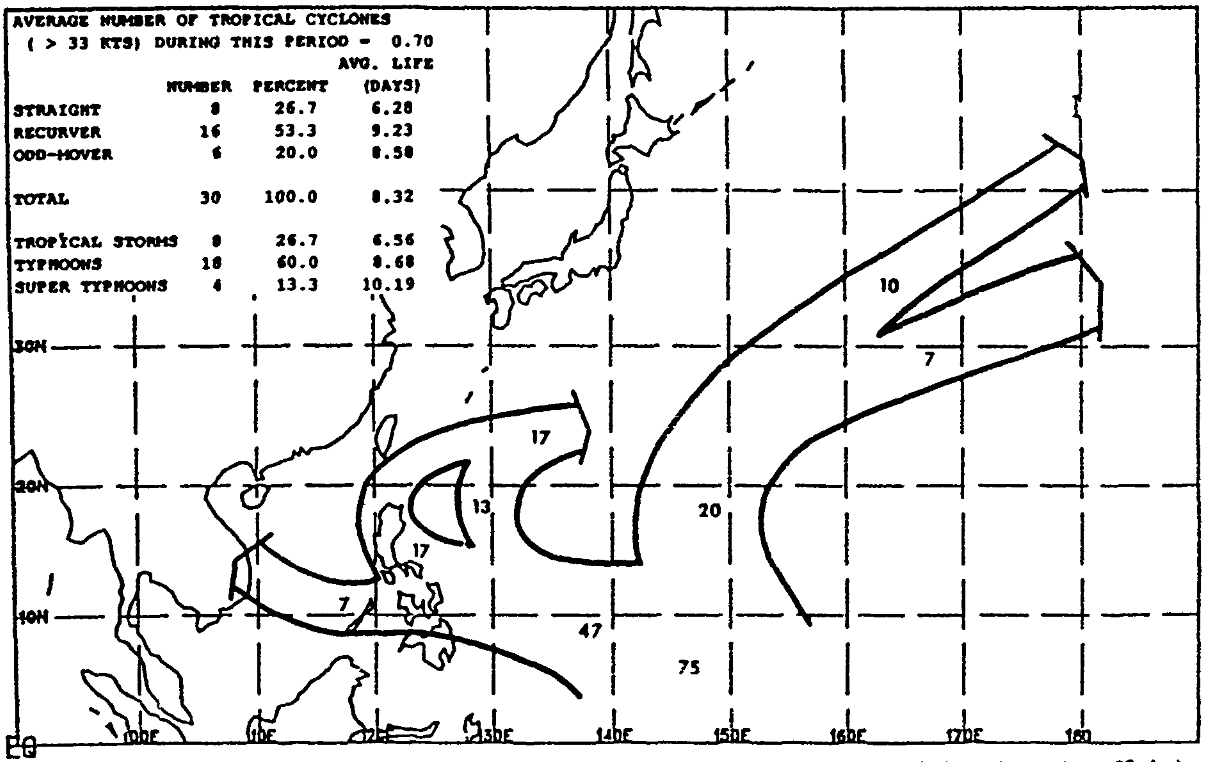

Mean tropical cyclone (> 33 kts) path. Numbers represent the percentage of tropical cyclones (> 33 kts) which followed the indicated path. These numbers may not add up to 100% since not all tropical cyclones (> 33 kts) follow a mean path and some develop/dissipate along a path. Tracks which contained less than 5% of the tropical cyclones (> 33 kts) are ignored. Dashed line represents mean recurvature position of tropical cyclones (> 33 kts) classified as recurvers.

SPEED OF MOVEMENT FOR APR 9 - APR 23

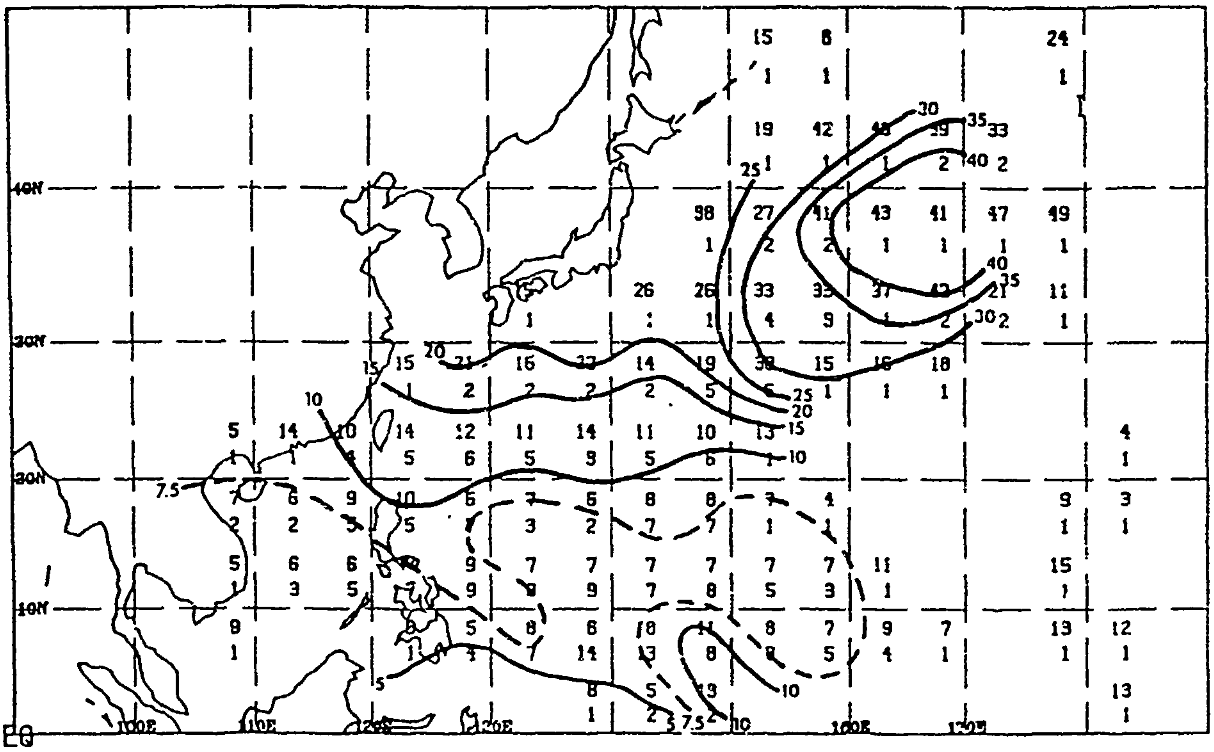

Average tropical cyclone (> 33 kts) Speed (top number) in knots and sample size (bottom number) for each 5° latitude by 5° longitude square. Contours are drawn only to those squares containing at least 5% of the sample.

MEAN PATHS FOR APR 24 - MAY 8

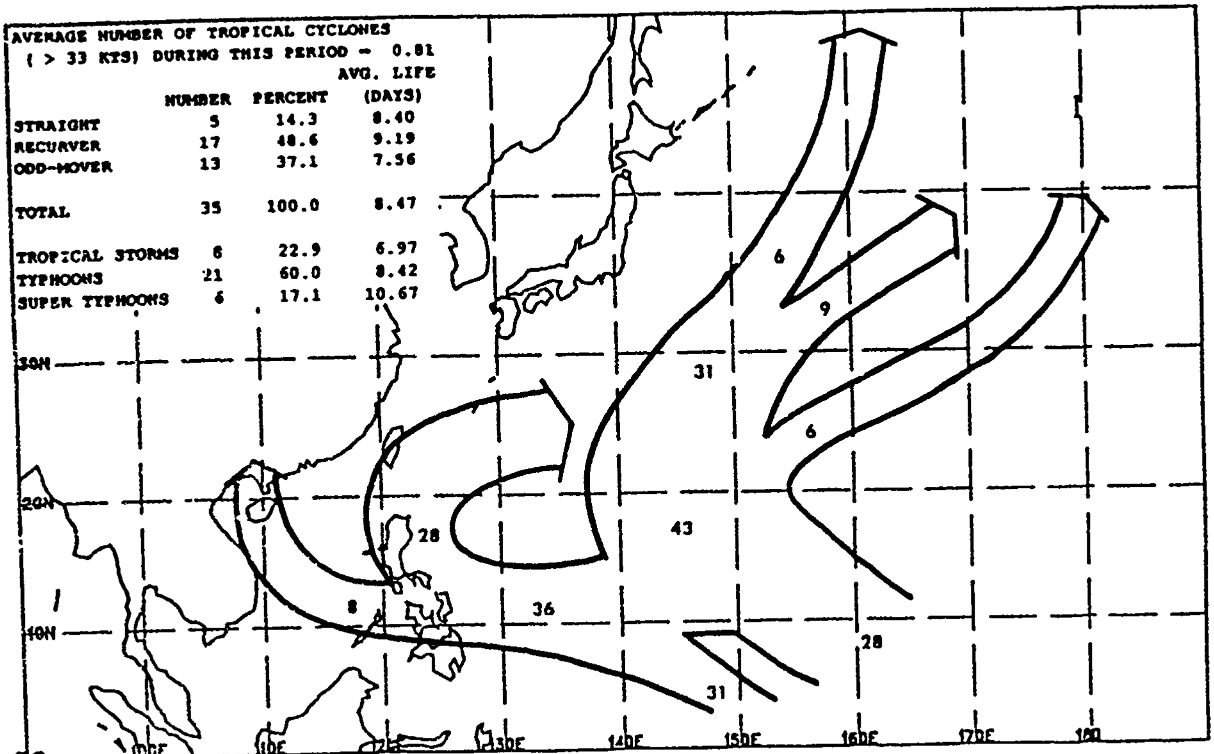

Mean tropical cyclone (> 33 kts) path. Numbers represent the percentage of tropical cyclones (> 33 kts) which followed the indicated path. These numbers may not add up to 100% since not all tropical cyclones (> 33 kts) follow a mean path and some develop/dissipate along a path. Tracks which contained less than 5% of the tropical cyclones (> 33 kts) are ignored. Dashed line represents mean recurvature position of tropical cyclones (> 33 kts) classified as recurvers.

SPEED OF MOVEMENT FOR APR 24 - MAY 8

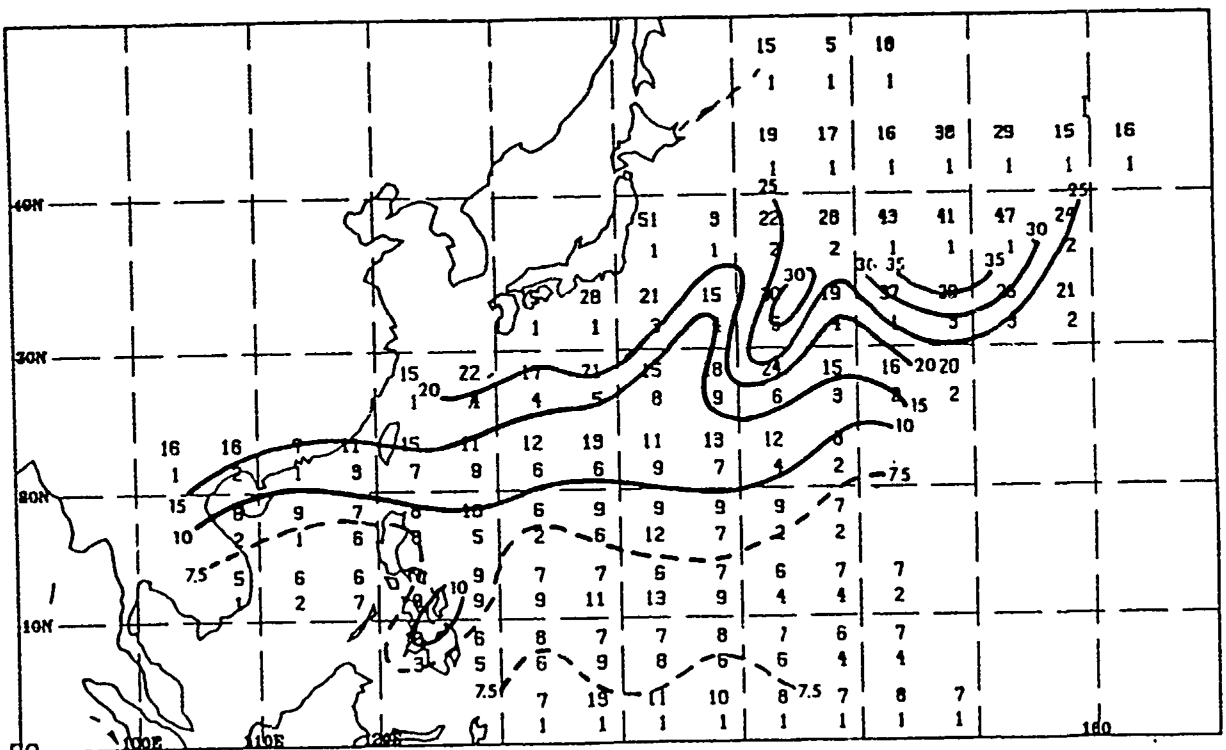

Average tropical cyclone (> 33 kts) Speed (top number) in knots and sample size (bottom number) for each 5° latitude by 5° longitude square. Contours are drawn only to those squares containing at least 5% of the sample.

MEAN PATHS FOR MAY 9 - MAY 23

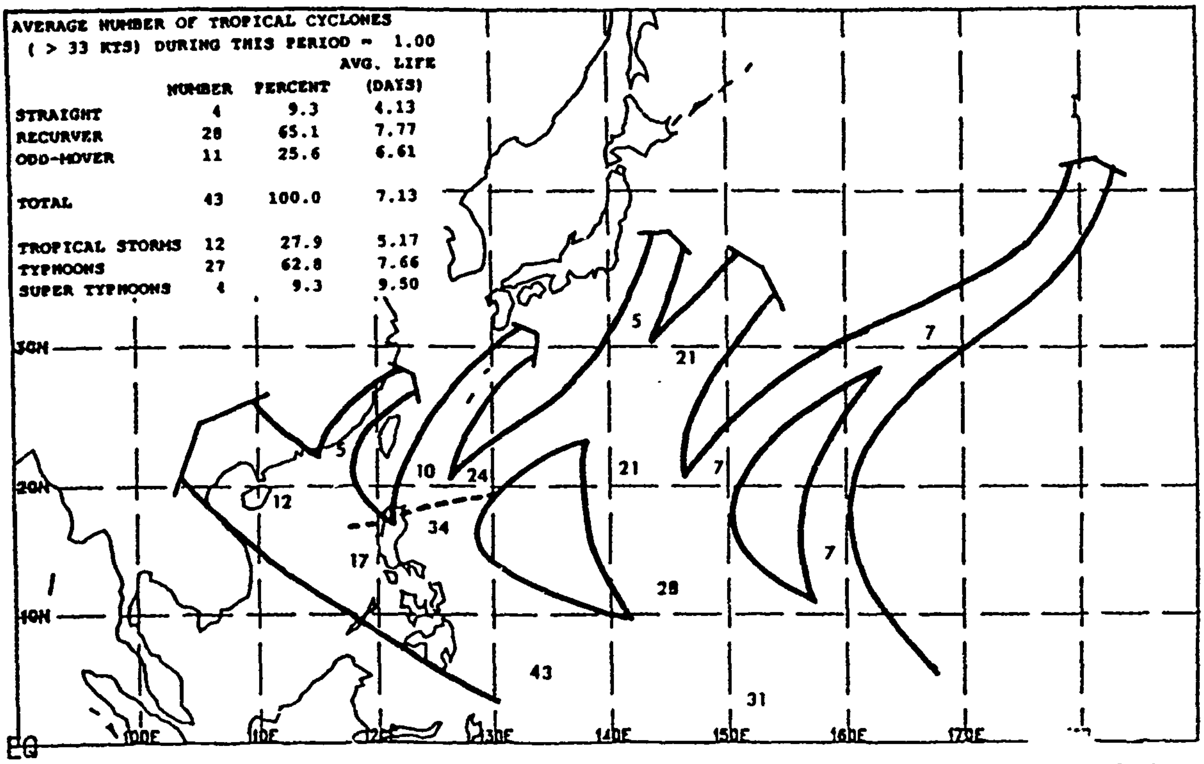

Mean tropical cyclone (> 33 kts) path. Numbers represent the percentage of tropical cyclo- 33 kts) which followed the indicated path. These numbers may not add up to 100% since not all ... cyclones (> 33 kts) follow a mean path and some develop/dissipate along a path. Tracks which contained less than 5% of the tropical cyclones (> 33 kts) are ignored. Dashed line represents mean recurvature position of tropical cyclones (> 33 kts) classified as recurvers.

SPEED OF MOVEMENT FOR MAY 9 - MAY 23

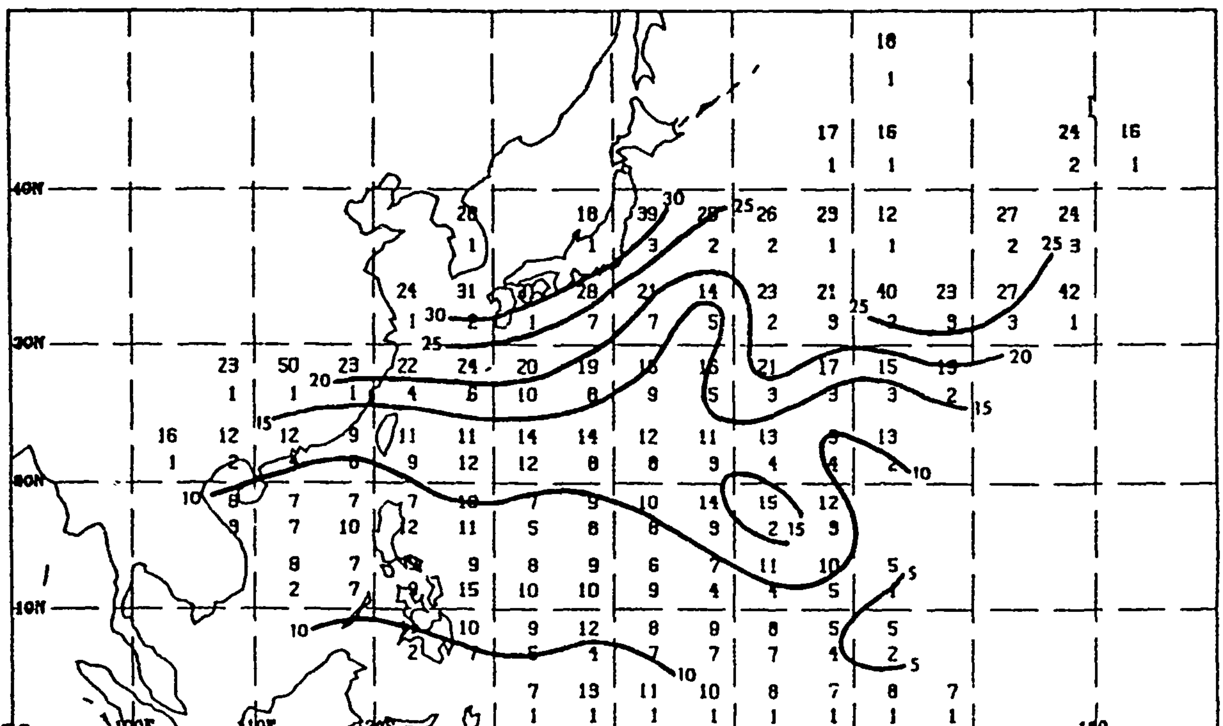

Average tropical cyclone (> 33 kts) Speed (top number) in knots and sample size (bottom number) for each 5° latitude by 5° longitude square. Contours are drawn only to those squares containing at least 5% of the sample.

MEAN PATHS FOR MAY 24 - JUN 8

AVERAGE NUMBER OF TROPICAL CYCLONES (> 33 KTS) DURING THIS PERIOD = 1.09

	NUMBER	PERCENT	AVG. LIFE (DAYS)
STRAIGHT	9	19.1	3.25
RECURVER	30	63.8	6.48
ODD-MOVER	8	17.0	5.50
TOTAL	47	100.0	5.69
TROPICAL STORMS	18	38.3	5.04
TYPHOONS	25	53.2	5.78
SUPER TYPHOONS	4	8.5	8.06

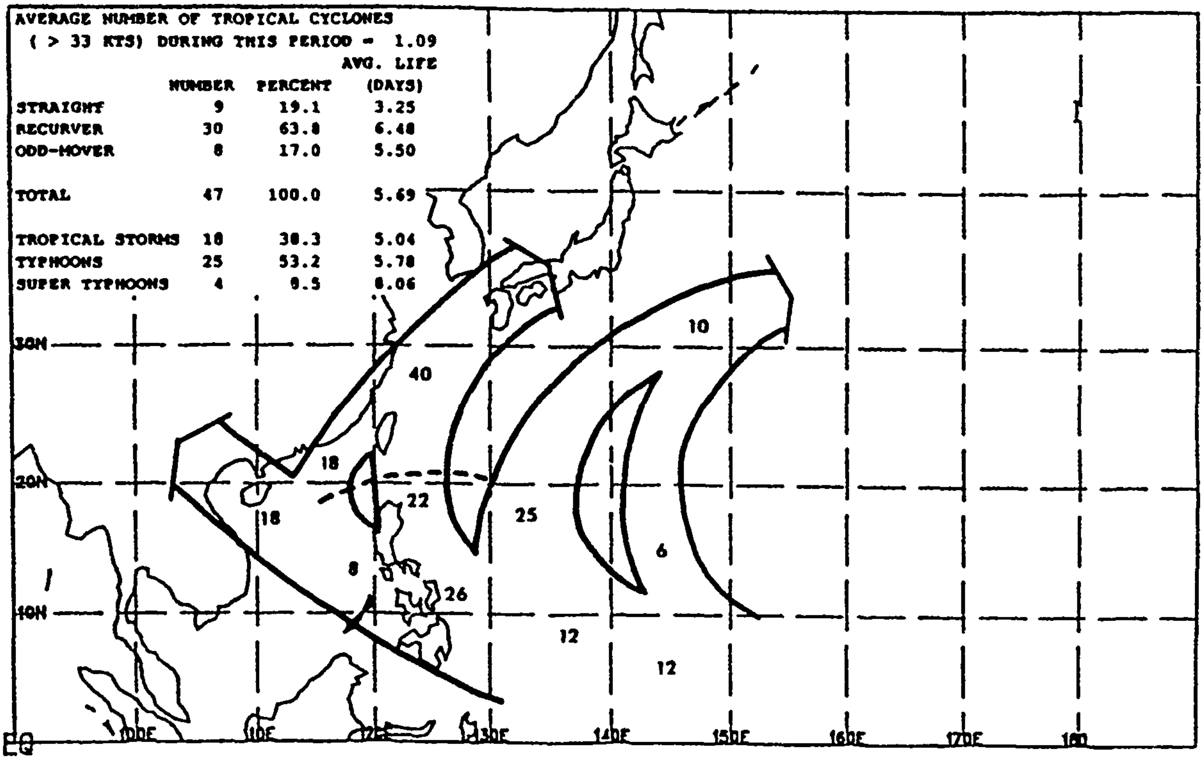

Mean tropical cyclone (> 33 kts) path. Numbers represent the percentage of tropical cyclones (> 33 kts) which followed the indicated path. These numbers may not add up to 100% since not all tropical cyclones (> 33 kts) follow a mean path and some develop/dissipate along a path. Tracks which contained less than 5% of the tropical cyclones (> 33 kts) are ignored. Dashed line represents mean recurvature position of tropical cyclones (> 33 kts) classified as recurvers.

SPEED OF MOVEMENT FOR MAY 24 - JUN 8

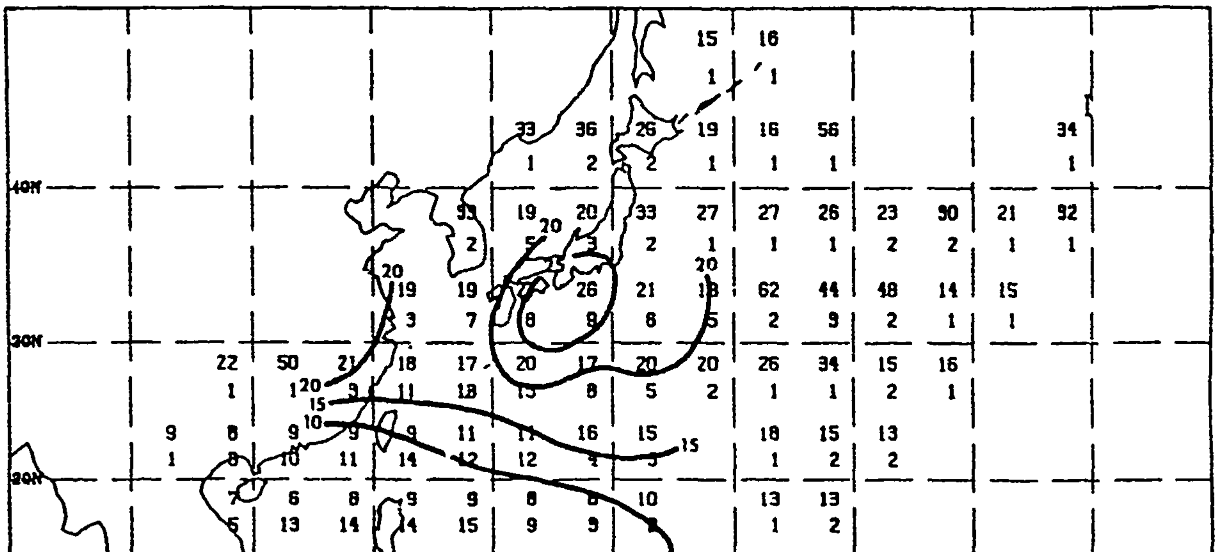

Average tropical cyclone (> 33 kts) Speed (top number) in knots and sample size (bottom number) for each 5° latitude by 5° longitude square. Contours are drawn only to those squares containing at least 5% of the sample.

MEAN PATHS FOR JUN 9 - JUN 23

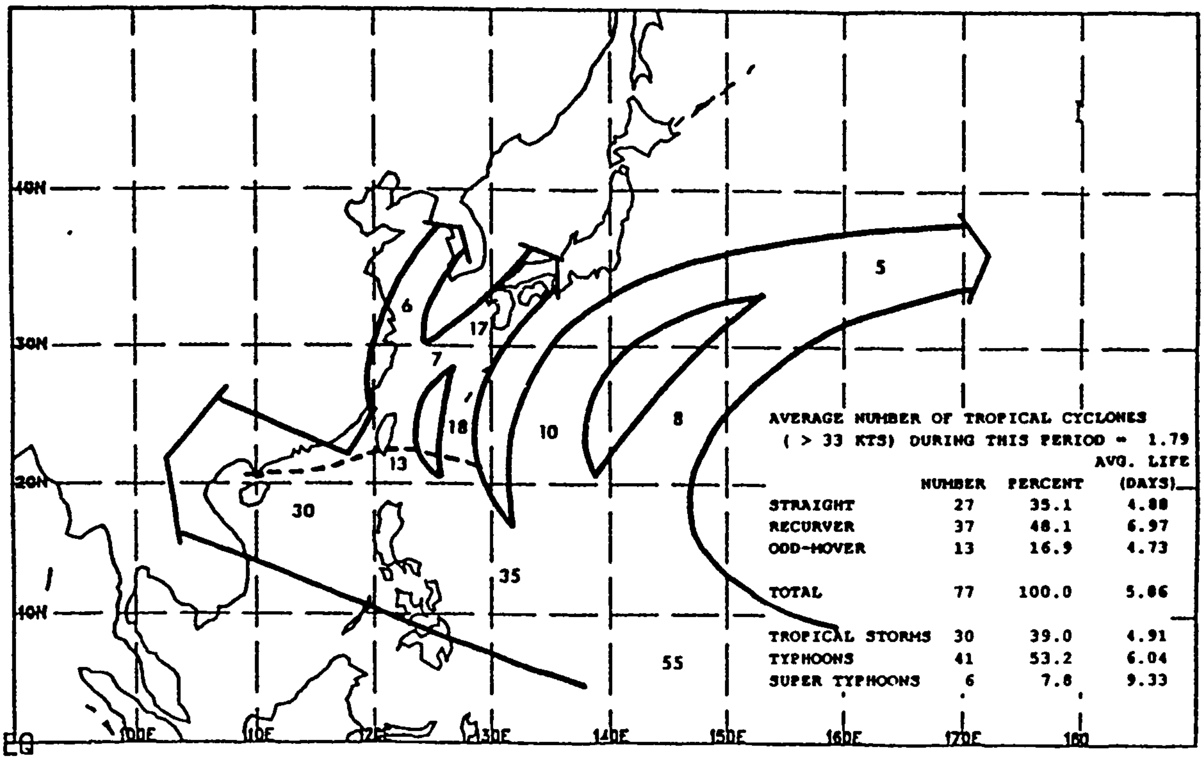

Mean tropical cyclone (> 33 kts) path. Numbers represent the percentage of tropical cyclones (> 33 kts) which followed the indicated path. These numbers may not add up to 100% since not all tropical cyclones (> 33 kts) follow a mean path and some develop/dissipate along a path. Tracks which contained less than 5% of the tropical cyclones (> 33 kts) are ignored. Dashed line represents mean recurvature position of tropical cyclones (> 33 kts) classified as recurvers.

SPEED OF MOVEMENT FOR JUN 9 - JUN 23

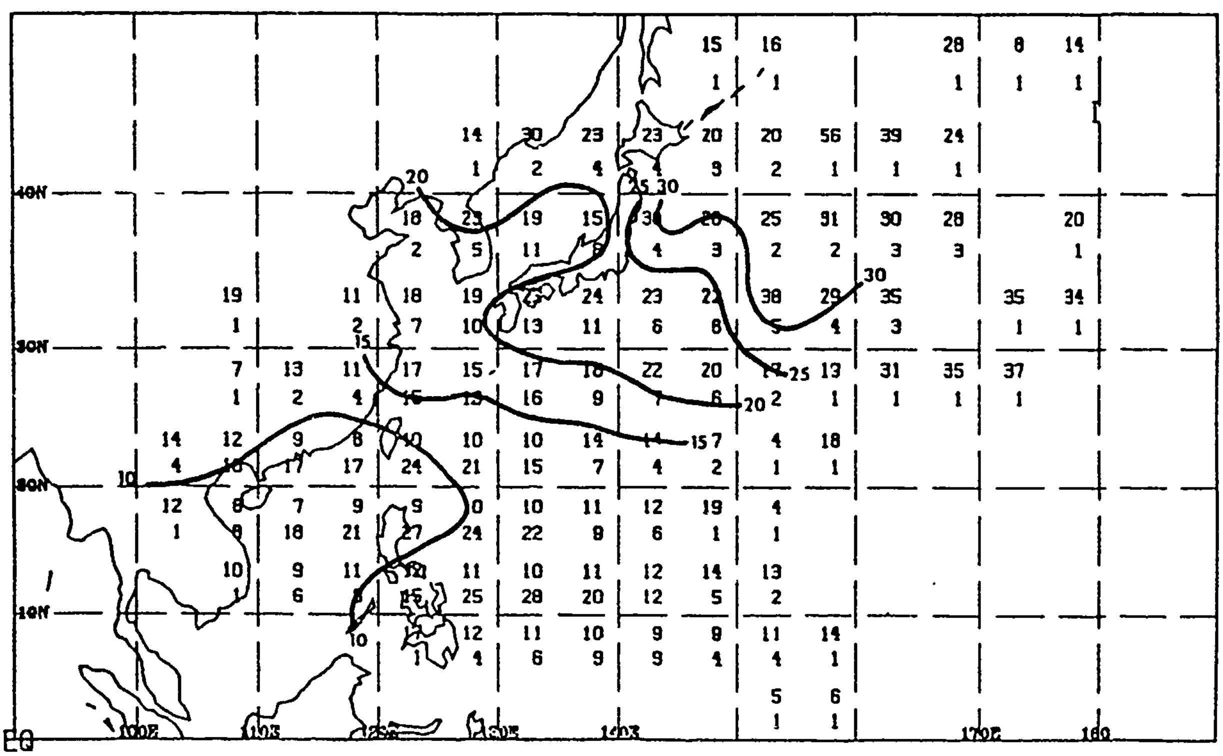

Average tropical cyclone (> 33 kts) Speed (top number) in knots and sample size (bottom number) for each 5° latitude by 5° longitude square. Contours are drawn only to those squares containing at least 5% of the sample.

MEAN PATHS FOR JUN 24 - JUL 8

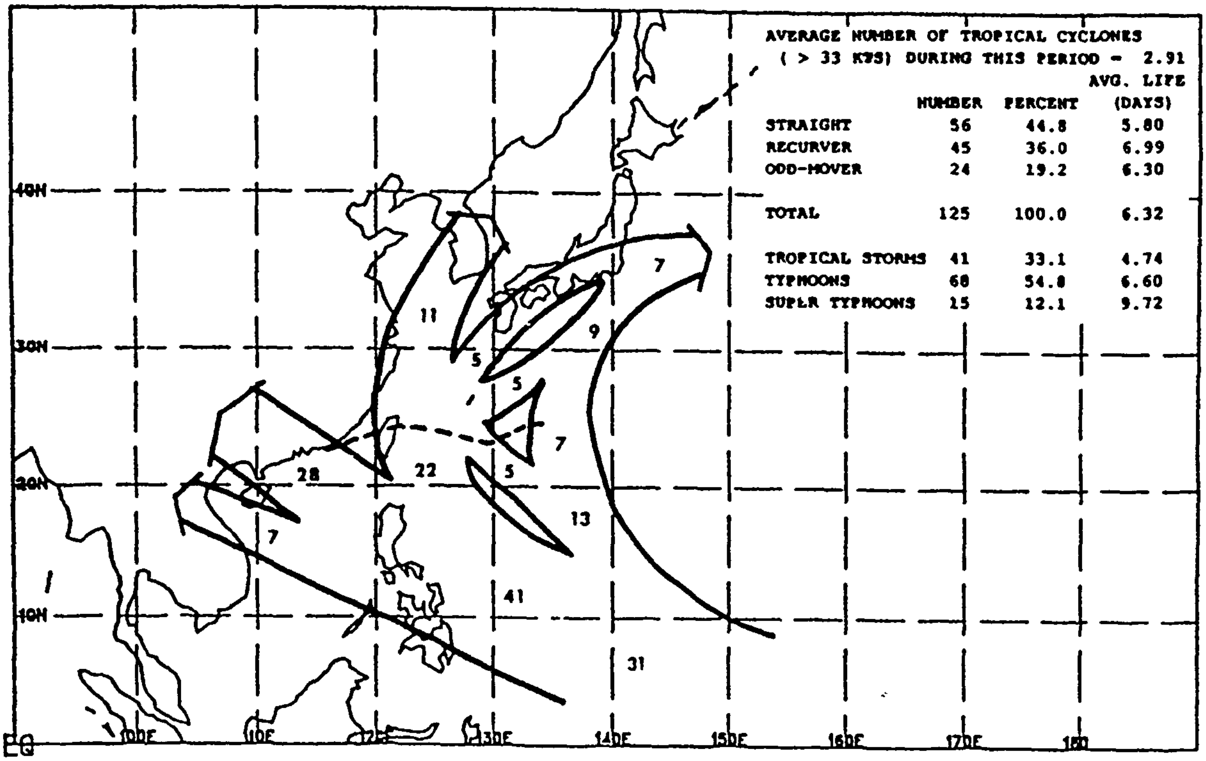

Mean tropical cyclone (> 33 kts) path. Numbers represent the percentage of tropical cyclones (> 33 kts) which followed the indicated path. These numbers may not add up to 100% since not all tropical cyclones (> 33 kts) follow a mean path and some develop/dissipate along a path. Tracks which contained less than 5% of the tropical cyclones (> 33 kts) are ignored. Dashed line represents mean recurvature position of tropical cyclones (> 33 kts) classified as recurvers.

SPEED OF MOVEMENT FOR JUN 24 - JUL 8

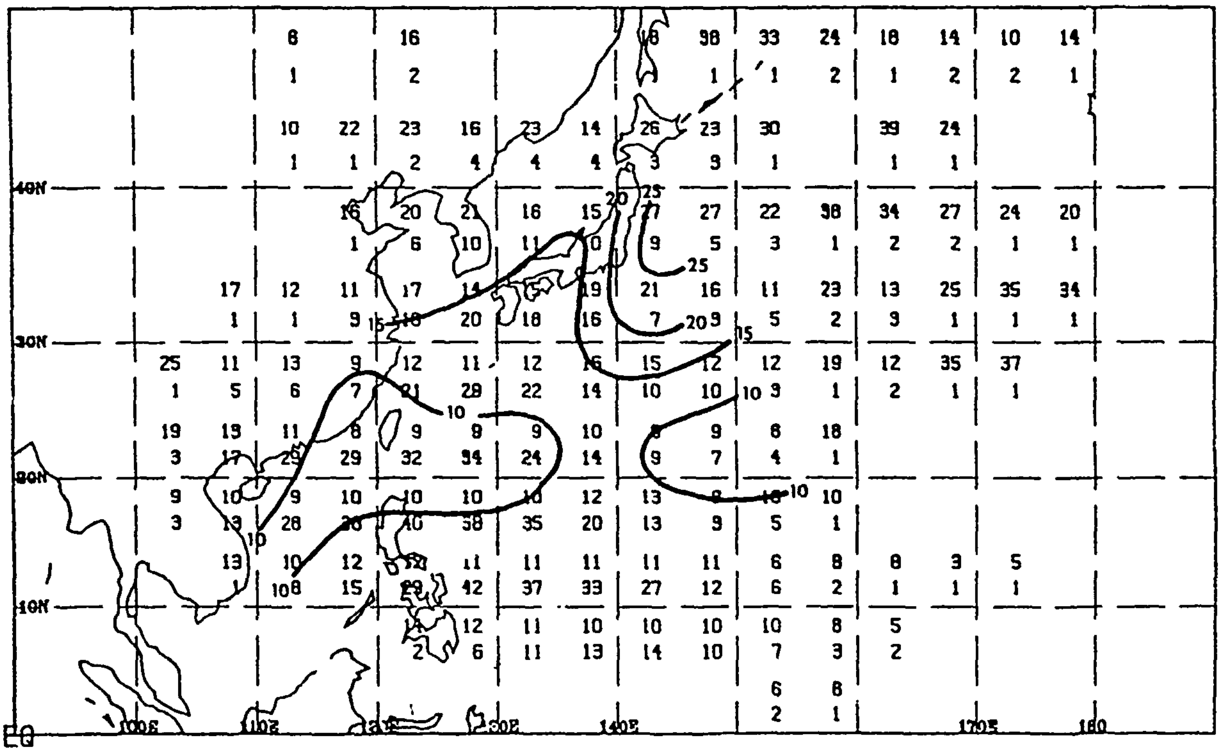

Average tropical cyclone (> 33 kts) Speed (top number) in knots and sample size (bottom number) for each 5° latitude by 5° longitude square. Contours are drawn only to those squares containing at least 5% of the sample.

MEAN PATHS FOR JUL 9 - JUL 23

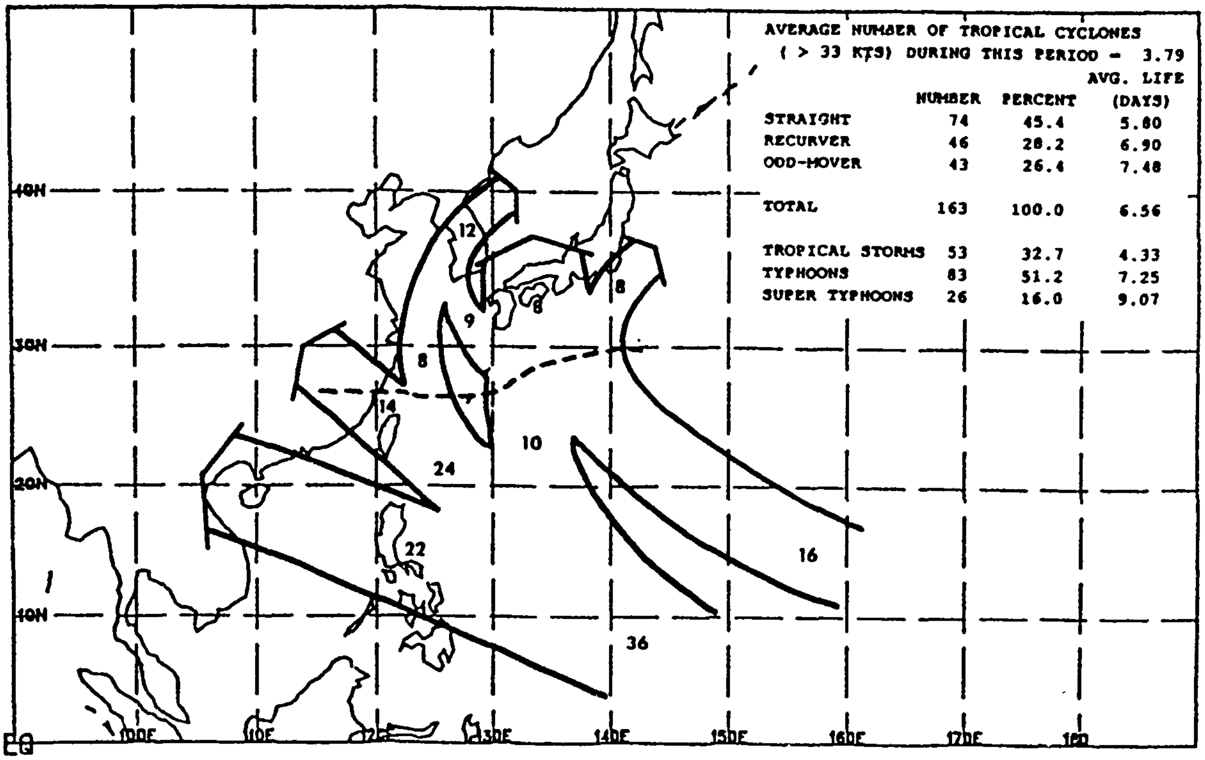

Mean tropical cyclone (> 33 kts) path. Numbers represent the percentage of tropical cyclones (> 33 kts) which followed the indicated path. These numbers may not add up to 100% since not all tropical cyclones (> 33 kts) follow a mean path and some develop/dissipate along a path. Tracks which contained less than 5% of the tropical cyclones (> 33 kts) are ignored. Dashed line represents mean recurvature position of tropical cyclones (> 33 kts) classified as recurvers.

SPEED OF MOVEMENT FOR JUL 9 - JUL 23

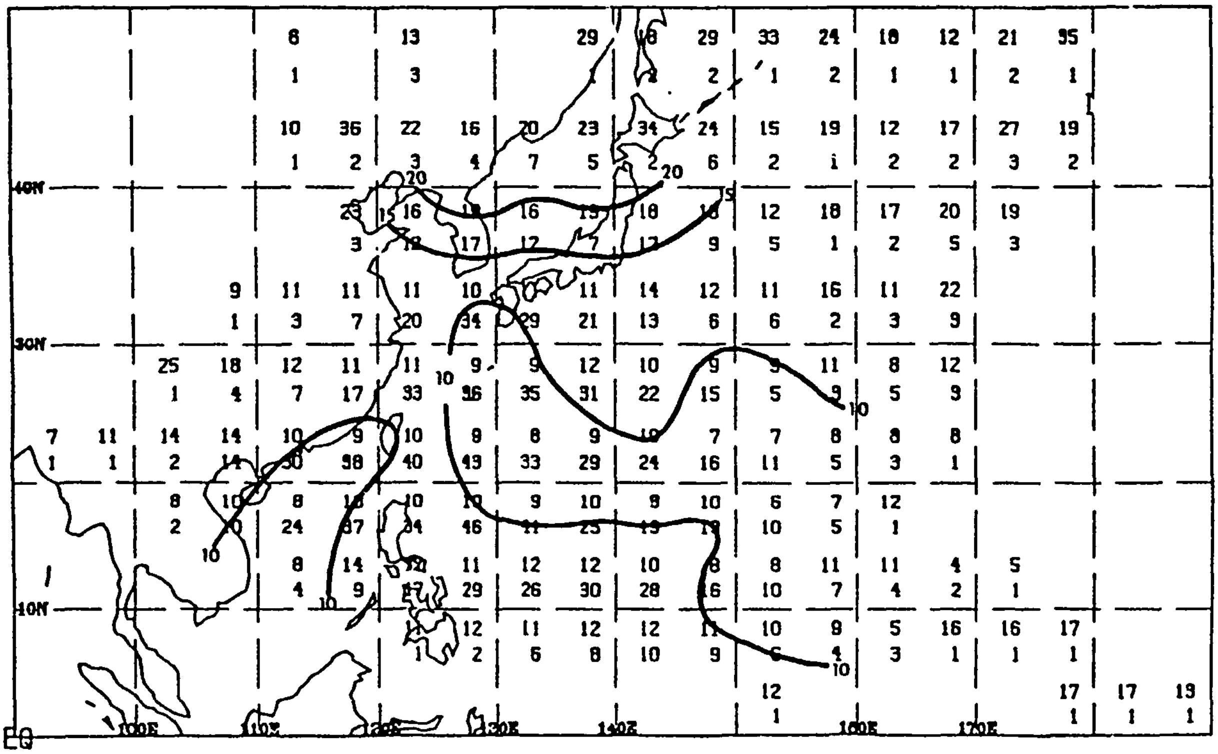

Average tropical cyclone (> 33 kts) Speed (top number) in knots and sample size (bottom number) for each 5° latitude by 5° longitude square. Contours are drawn only to those squares containing at least 5% of the sample.

MEAN PATHS FOR JUL 24 - AUG 8

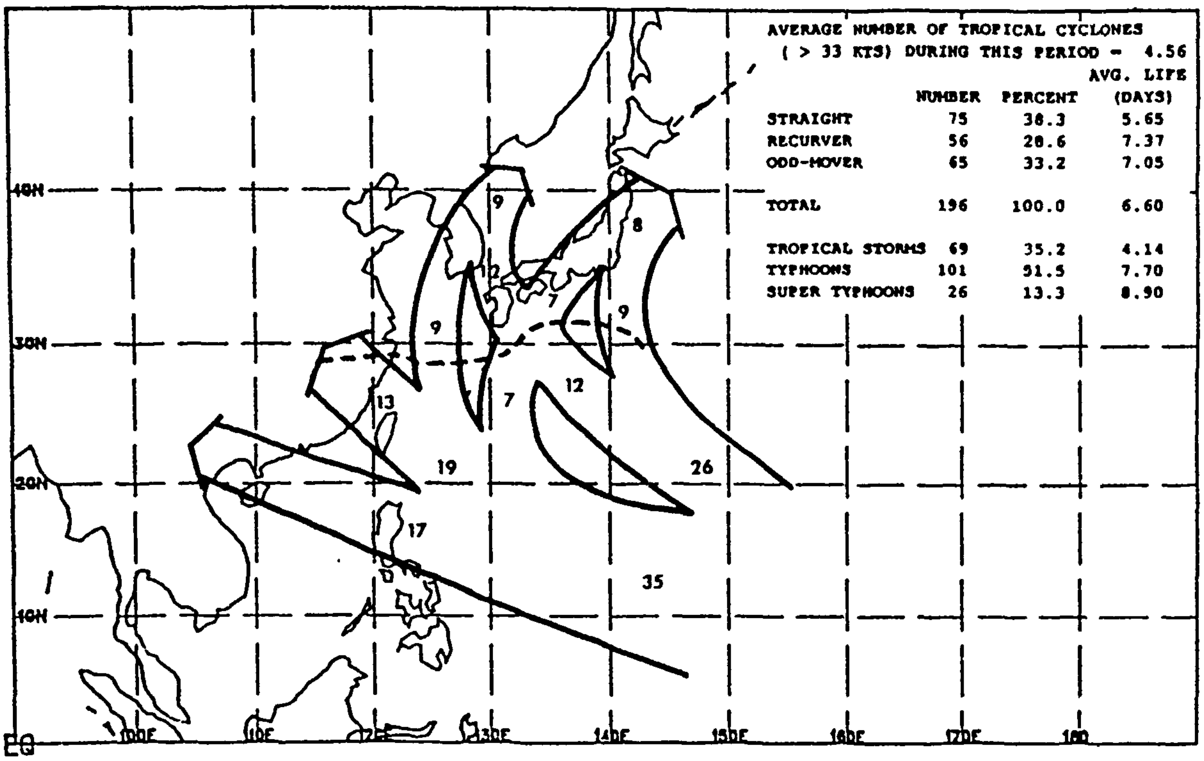

AVERAGE NUMBER OF TROPICAL CYCLONES (> 33 KTS) DURING THIS PERIOD - 4.56

	NUMBER	PERCENT	AVG. LIFE (DAYS)
STRAIGHT	75	38.3	5.65
RECURVER	56	28.6	7.37
ODD-MOVER	65	33.2	7.05
TOTAL	196	100.0	6.60
TROPICAL STORMS	69	35.2	4.14
TYPHOONS	101	51.5	7.70
SUPER TYPHOONS	26	13.3	8.90

Mean tropical cyclone (> 33 kts) path. Numbers represent the percentage of tropical cyclones (> 33 kts) which followed the indicated path. These numbers may not add up to 100% since not all tropical cyclones (> 33 kts) follow a mean path and some develop/dissipate along a path. Tracks which contained less than 5% of the tropical cyclones (> 33 kts) are ignored. Dashed line represents mean recurvature position of tropical cyclones (> 33 kts) classified as recurvers.

SPEED OF MOVEMENT FOR JUL 24 - AUG 8

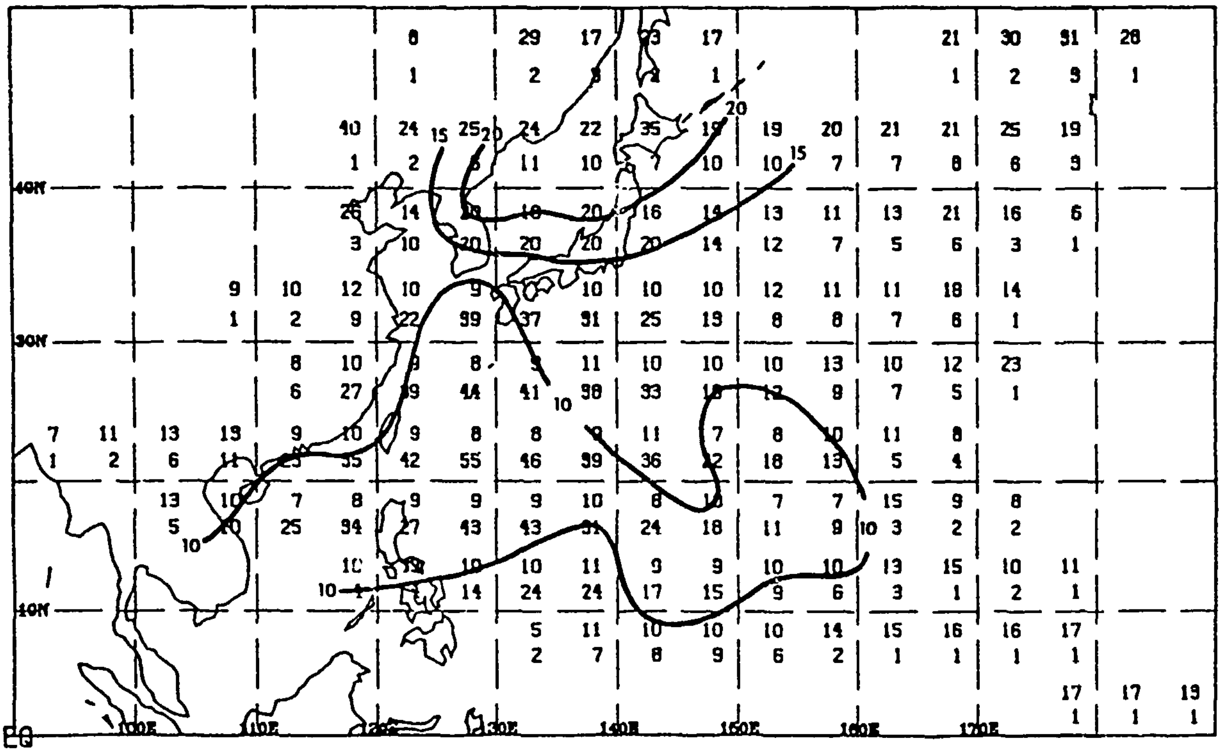

Average tropical cyclone (> 33 kts) Speed (top number) in knots and sample size (bottom number) for each 5° latitude by 5° longitude square. Contours are drawn only to those squares containing at least 5% of the sample.

MEAN PATHS FOR AUG 9 - AUG 23

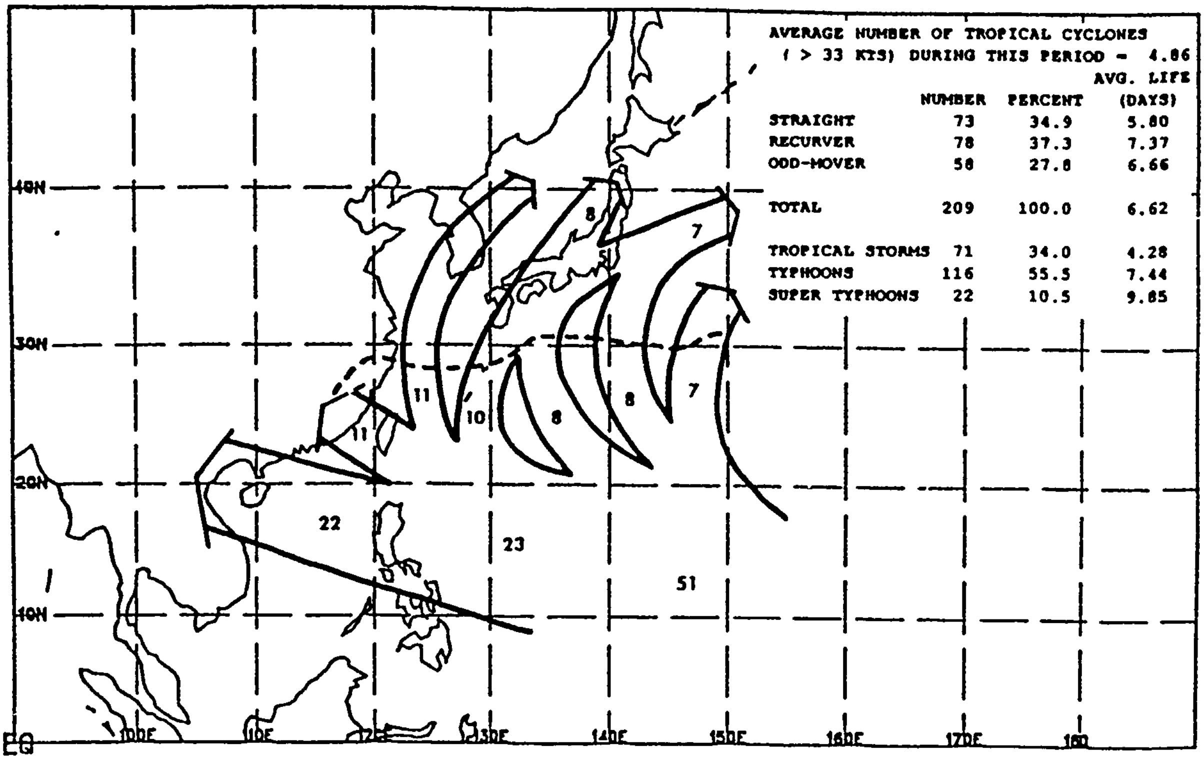

Mean tropical cyclone (> 33 kts) path. Numbers represent the percentage of tropical cyclones (> 33 kts) which followed the indicated path. These numbers may not add up to 100% since not all tropical cyclones (> 33 kts) follow a mean path and some develop/dissipate along a path. Tracks which contained less than 5% of the tropical cyclones (> 33 kts) are ignored. Dashed line represents mean recurvature position of tropical cyclones (> 33 kts) classified as recurvers.

SPEED OF MOVEMENT FOR AUG 9 - AUG 23

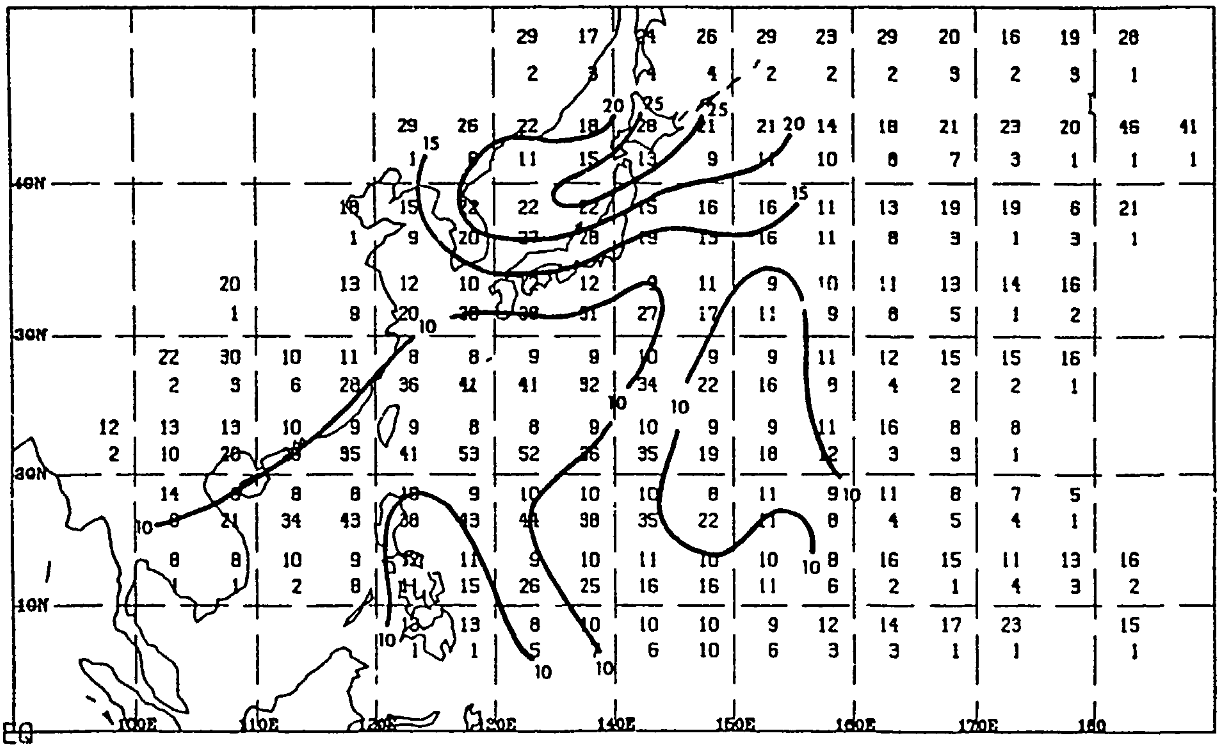

Average tropical cyclone (> 33 kts) Speed (top number) in knots and sample size (bottom number) for each 5° latitude by 5° longitude square. Contours are drawn only to those squares containing at least 5% of the sample.

MEAN PATHS FOR AUG 24 - SEP 8

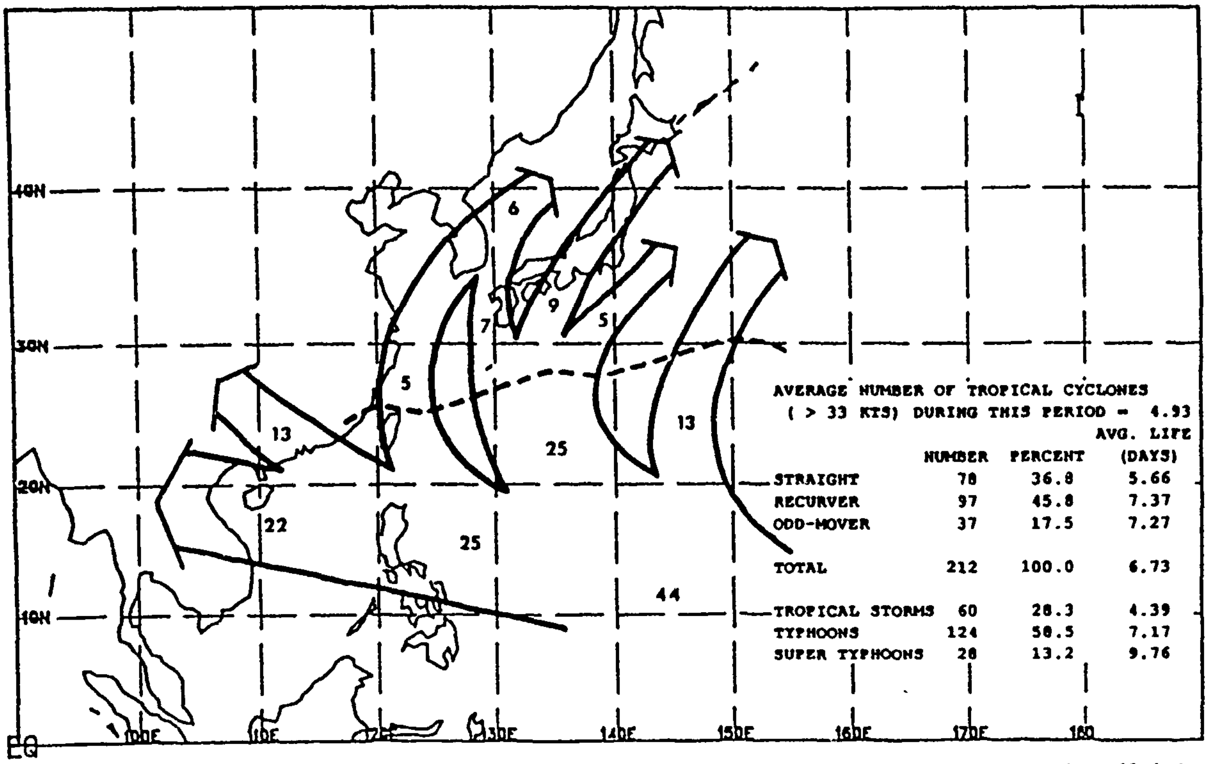

Mean tropical cyclone (> 33 kts) path. Numbers represent the percentage of tropical cyclones (> 33 kts) which followed the indicated path. These numbers may not add up to 100% since not all tropical cyclones (> 33 kts) follow a mean path and some develop/dissipate along a path. Tracks which contained less than 5% of the tropical cyclones (> 33 kts) are ignored. Dashed line represents mean recurvature position of tropical cyclones (> 33 kts) classified as recurvers.

SPEED OF MOVEMENT FOR AUG 24 - SEP 8

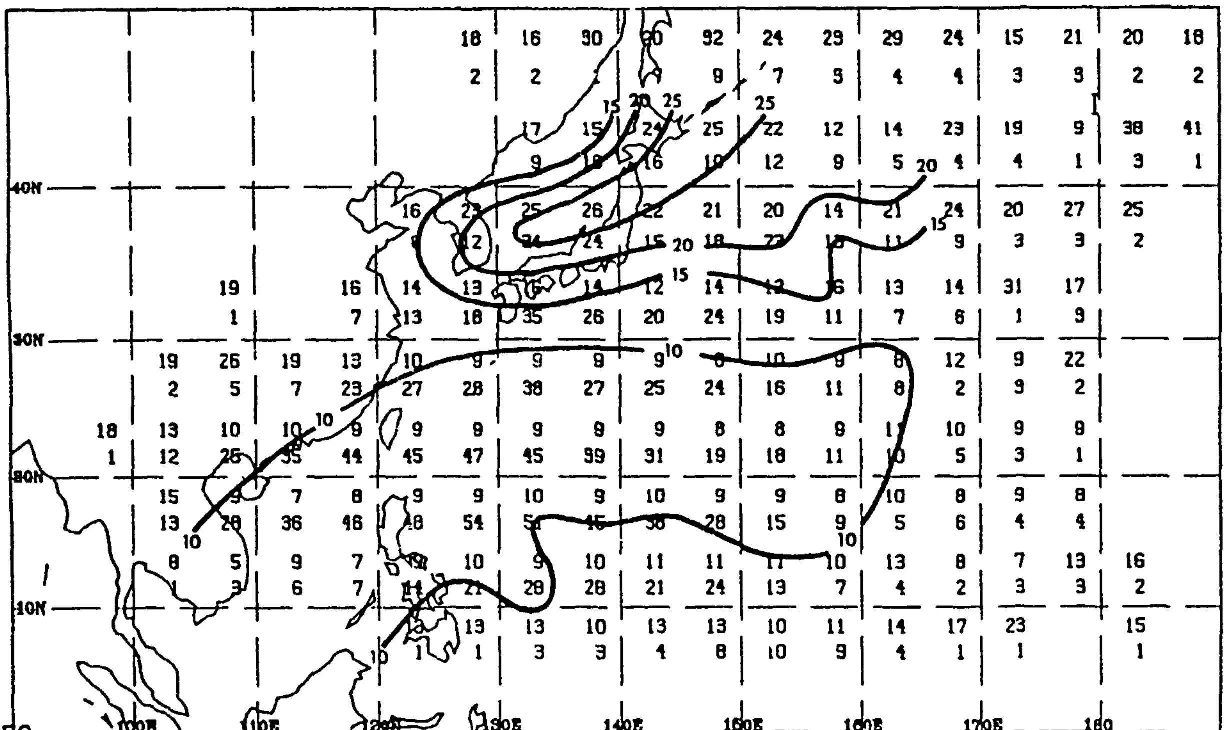

Average tropical cyclone (> 33 kts) Speed (top number) in knots and sample size (bottom number) for each 5° latitude by 5° longitude square. Contours are drawn only to those squares containing at least 5% of the sample.

MEAN PATHS FOR SEP 9 - SEP 23

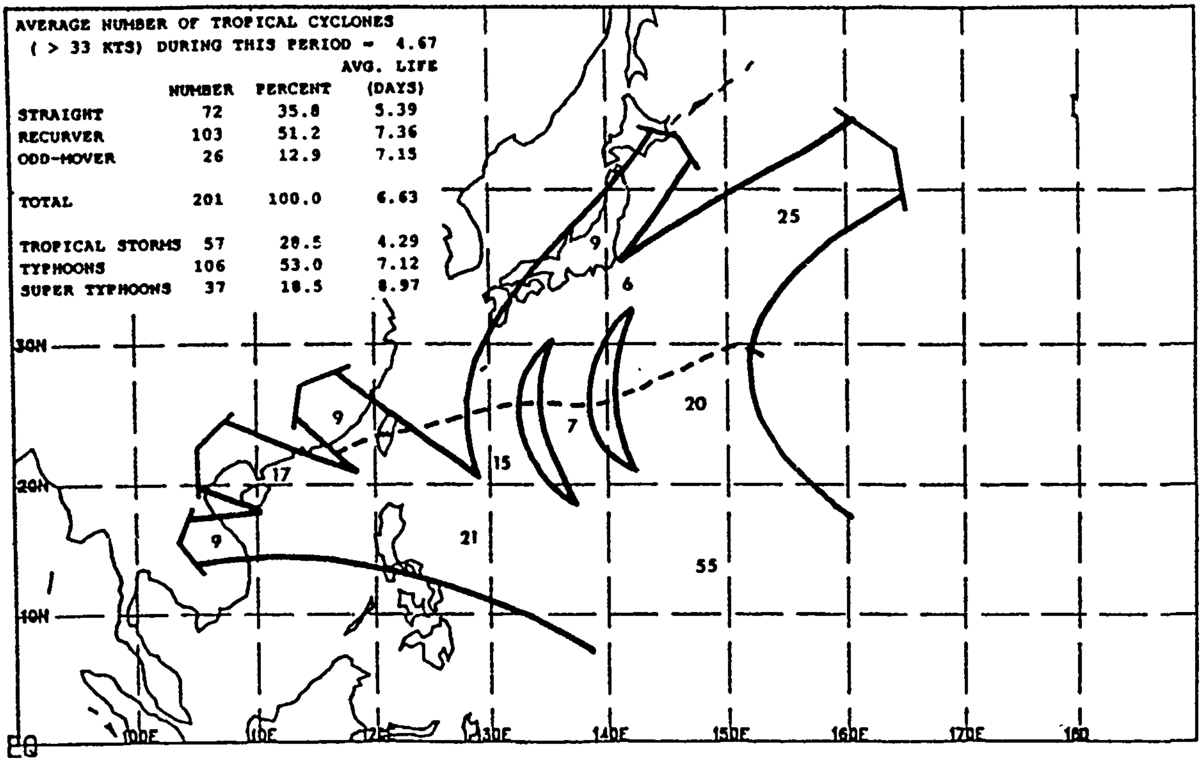

Mean tropical cyclone (> 33 kts) path. Numbers represent the percentage of tropical cyclones (> 33 kts) which followed the indicated path. These numbers may not add up to 100% since not all tropical cyclones (> 33 kts) follow a mean path and some develop/dissipate along a path. Tracks which contained less than 5% of the tropical cyclones (> 33 kts) are ignored. Dashed line represents mean recurvature position of tropical cyclones (> 33 kts) classified as recurvers.

SPEED OF MOVEMENT FOR SEP 9 - SEP 23

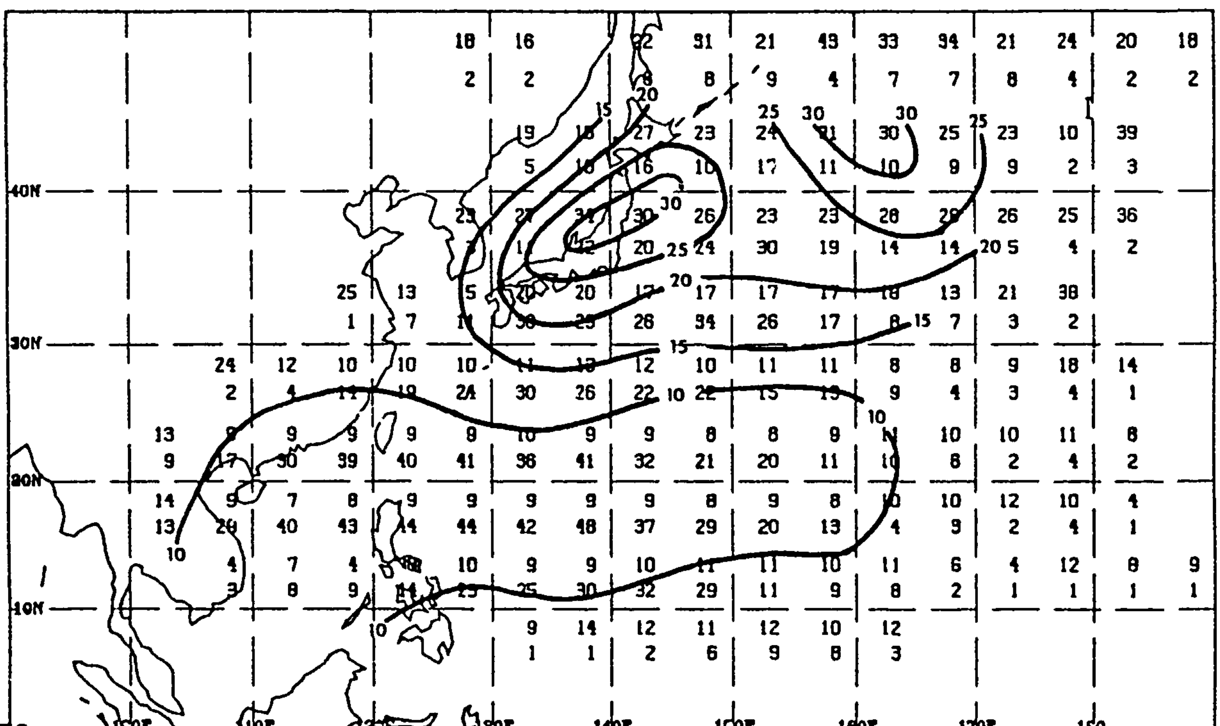

Average tropical cyclone (> 33 kts) Speed (top number) in knots and sample size (bottom number) for each 5° latitude by 5° longitude square. Contours are drawn only to those squares containing at least 5% of the sample.

MEAN PATHS FOR SEP 24 - OCT 8

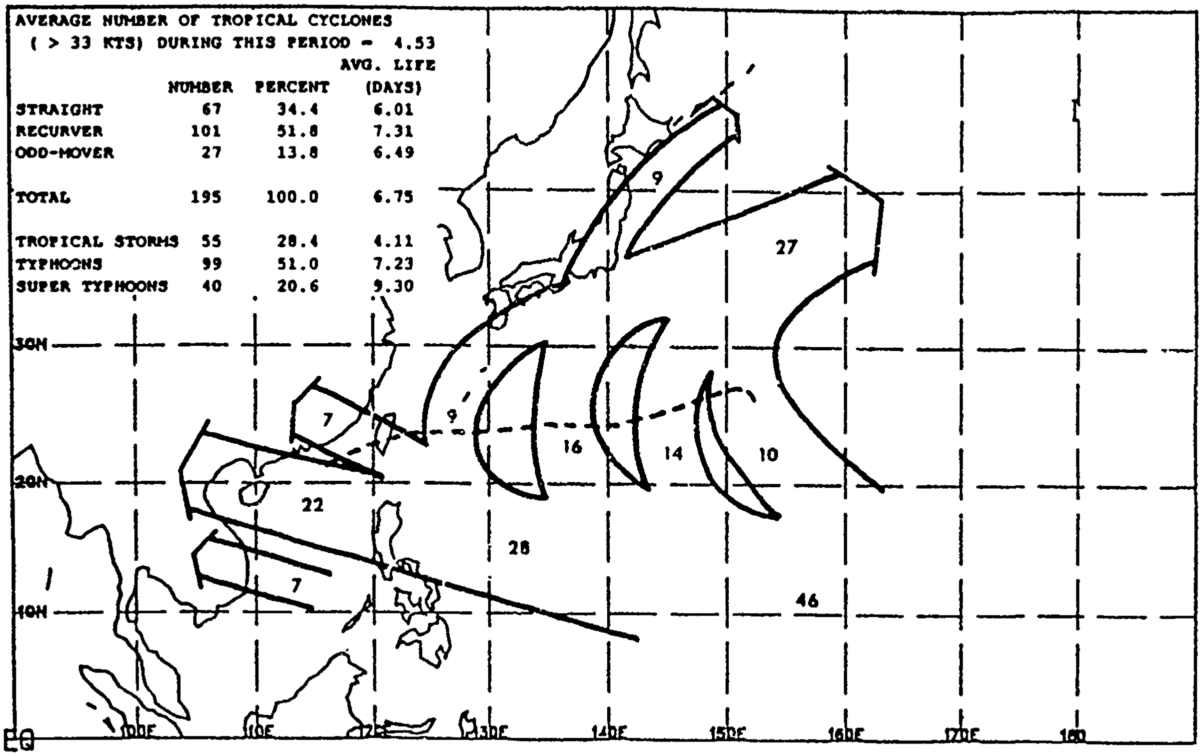

Mean tropical cyclone (> 33 kts) path. Numbers represent the percentage of tropical cyclones (> 33 kts) which followed the indicated path. These numbers may not add up to 100% since not all tropical cyclones (> 33 kts) follow a mean path and some develop/dissipate along a path. Tracks which contained less than 5% of the tropical cyclones (> 33 kts) are ignored. Dashed line represents mean recurvature position of tropical cyclones (> 33 kts) classified as recurvers.

SPEED OF MOVEMENT FOR SEP 24 - OCT 8

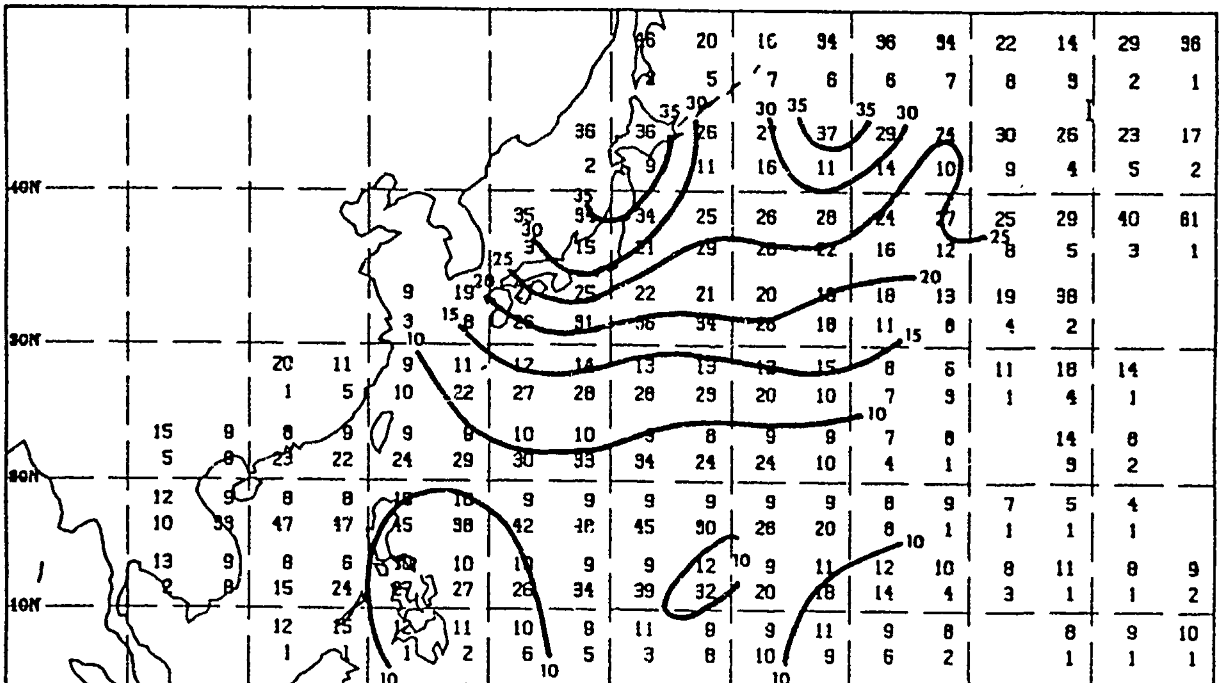

Average tropical cyclone (> 33 kts) Speed (top number) in knots and sample size (bottom number) for each 5° latitude by 5° longitude square. Contours are drawn only to those squares containing at least 5% of the sample.

MEAN PATHS FOR OCT 9 - OCT 23

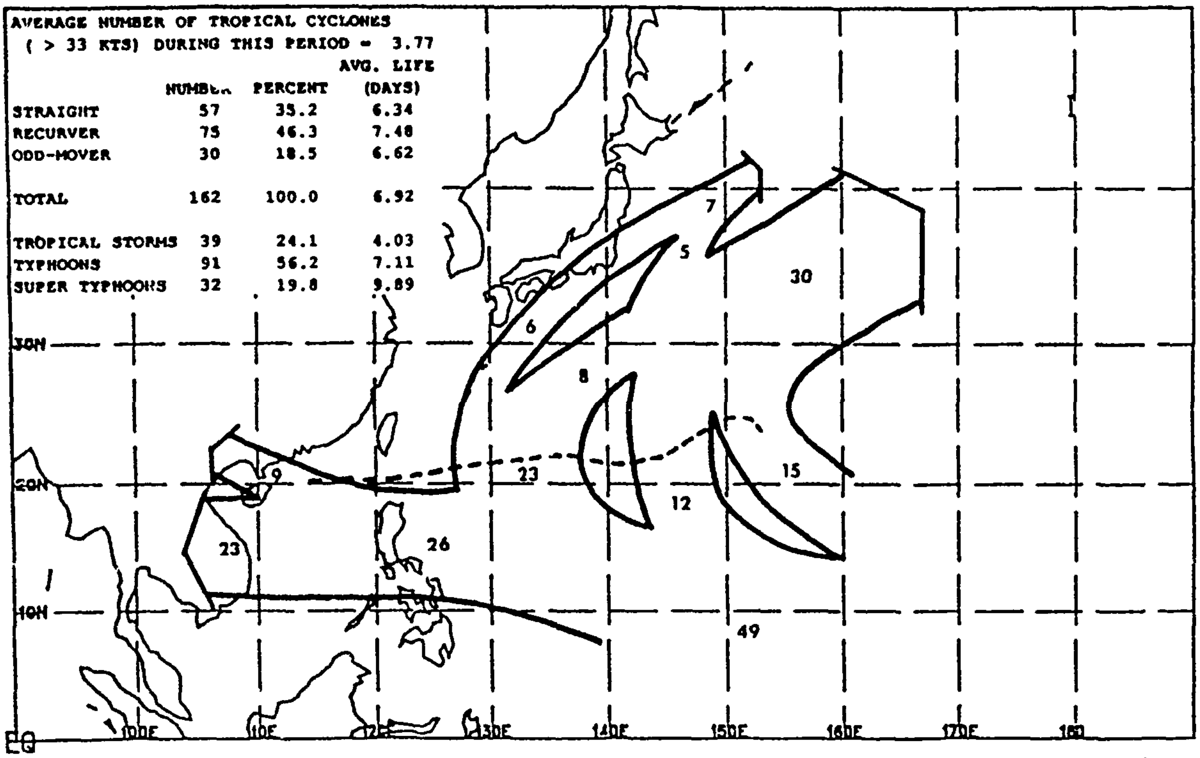

Mean tropical cyclone (> 33 kts) path. Numbers represent the percentage of tropical cyclones (> 33 kts) which followed the indicated path. These numbers may not add up to 100% since not all tropical cyclones (> 33 kts) follow a mean path and some develop/dissipate along a path. Tracks which contained less than 5% of the tropical cyclones (> 33 kts) are ignored. Dashed line represents mean recurvature position of tropical cyclones (> 33 kts) classified as recurvers.

SPEED OF MOVEMENT FOR OCT 9 - OCT 23

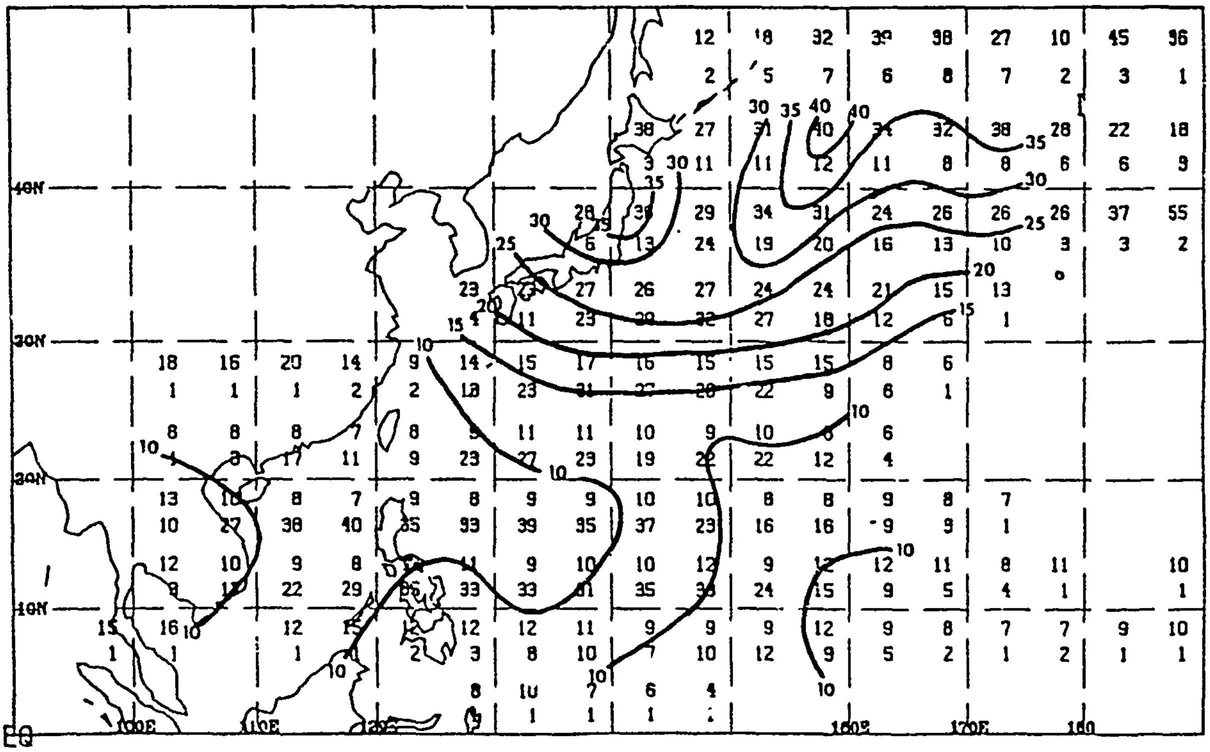

Average tropical cyclone (> 33 kts) Speed (top number) in knots and sample size (bottom number) for each 5° latitude by 5° longitude square. Contours are drawn only to those squares containing at least 5% of the sample.

MEAN PATHS FOR OCT 24 - NOV 8

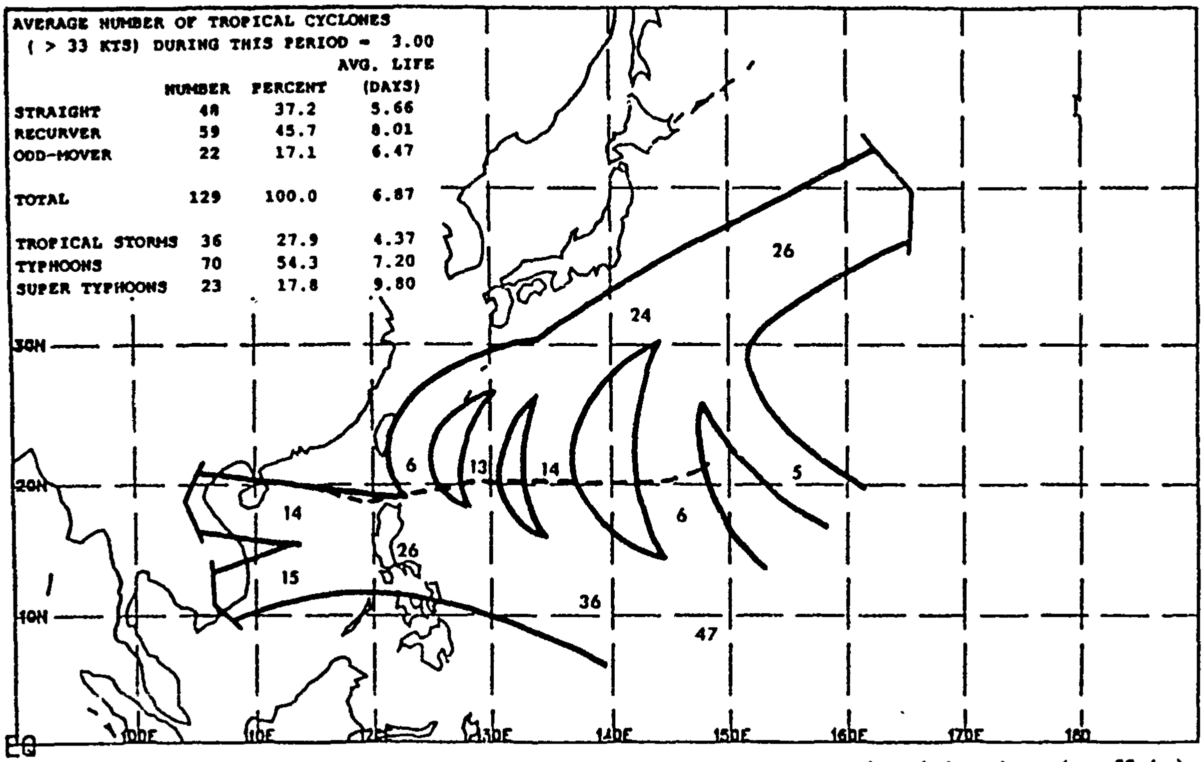

Mean tropical cyclone (> 33 kts) path. Numbers represent the percentage of tropical cyclones (> 33 kts) which followed the indicated path. These numbers may not add up to 100% since not all tropical cyclones (> 33 kts) follow a mean path and some develop/dissipate along a path. Tracks which contained less than 5% of the tropical cyclones (> 33 kts) are ignored. Dashed line represents mean recurvature position of tropical cyclones (> 33 kts) classified as recurvers.

SPEED OF MOVEMENT FOR OCT 24 - NOV 8

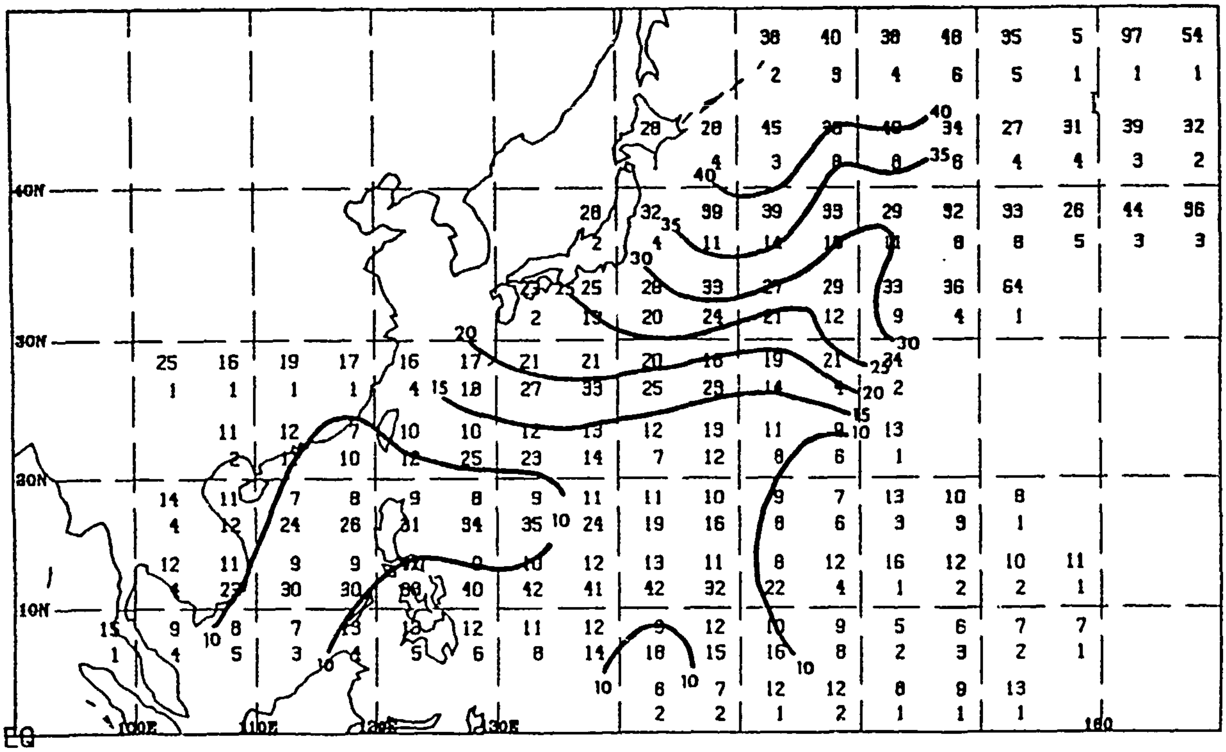

Average tropical cyclone (> 33 kts) Speed (top number) in knots and sample size (bottom number) for each 5° latitude by 5° longitude square. Contours are drawn only to those squares containing at least 5% of the sample.

MEAN PATHS FOR NOV 9 - NOV 23

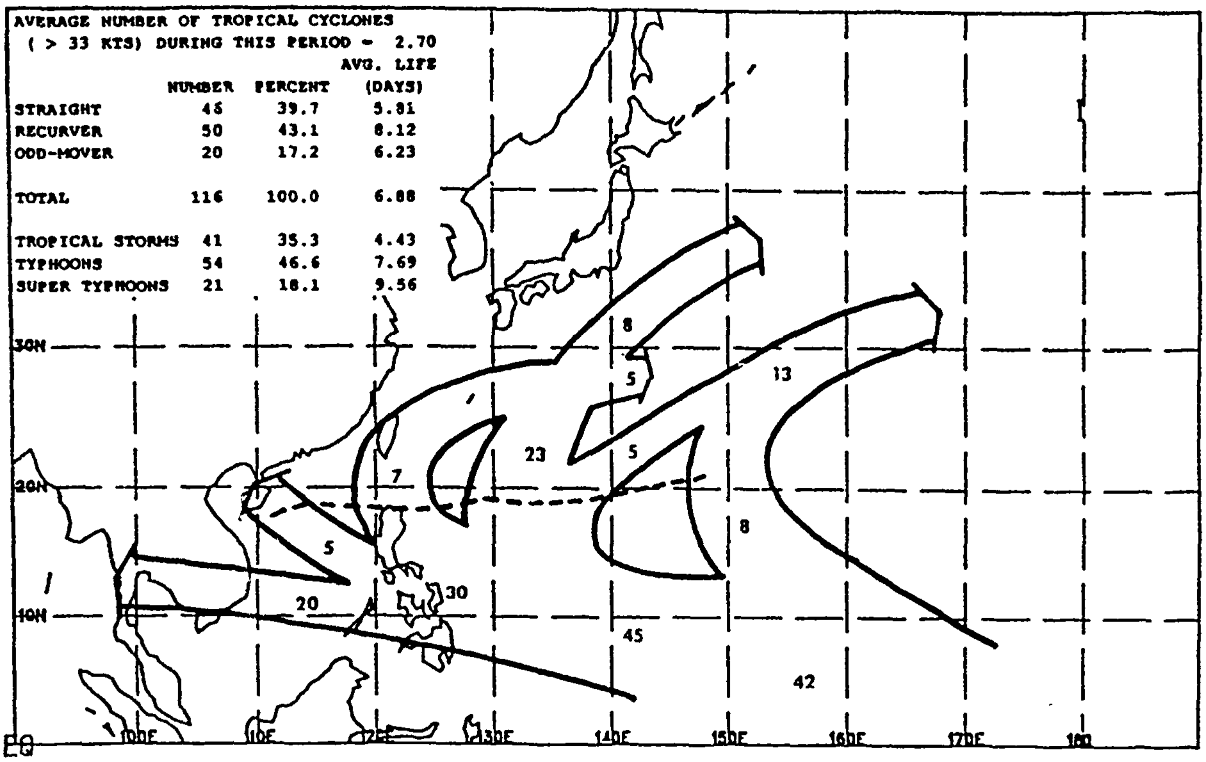

Mean tropical cyclone (> 33 kts) path. Numbers represent the percentage of tropical cyclones (> 33 kts) which followed the indicated path. These numbers may not add up to 100% since not all tropical cyclones (> 33 kts) follow a mean path and some develop/dissipate along a path. Tracks which contained less than 5% of the tropical cyclones (> 33 kts) are ignored. Dashed line represents mean recurvature position of tropical cyclones (> 33 kts) classified as recurvers.

SPEED OF MOVEMENT FOR NOV 9 - NOV 23

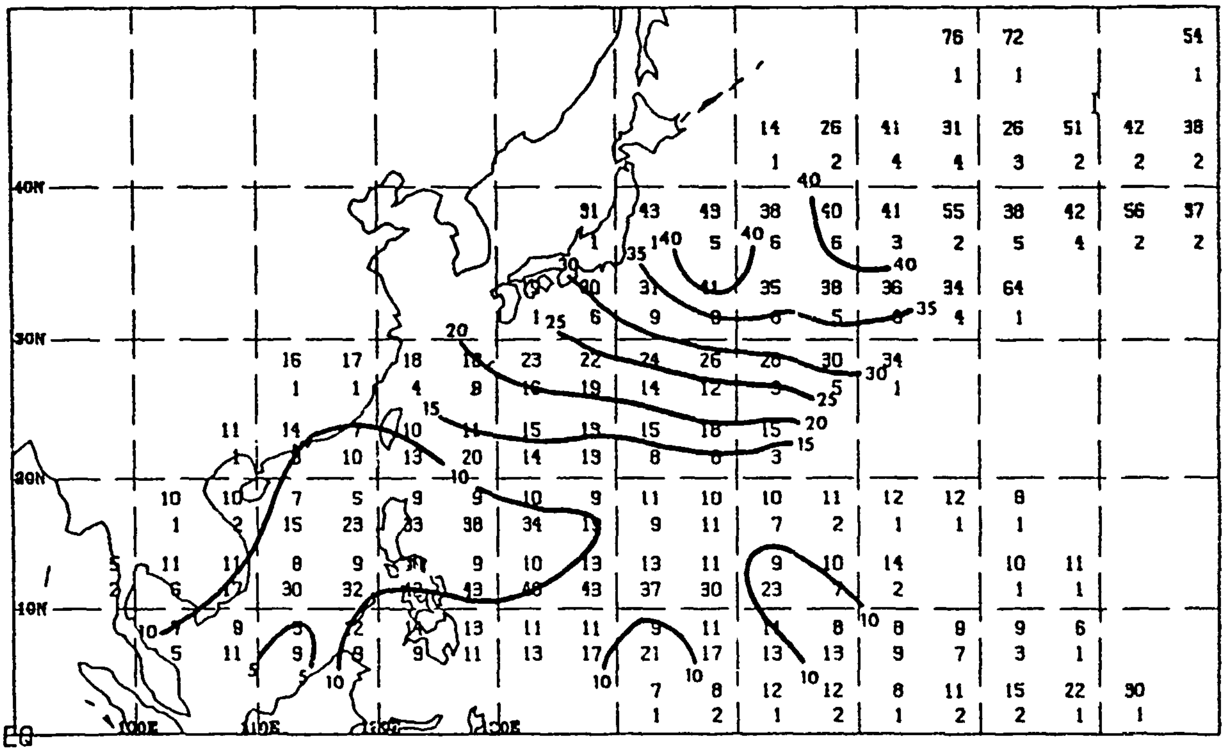

Average tropical cyclone (> 33 kts) Speed (top number) in knots and sample size (bottom number) for each 5° latitude by 5° longitude square. Contours are drawn only to those squares containing at least 5% of the sample.

MEAN PATHS FOR NOV 24 - DEC 8

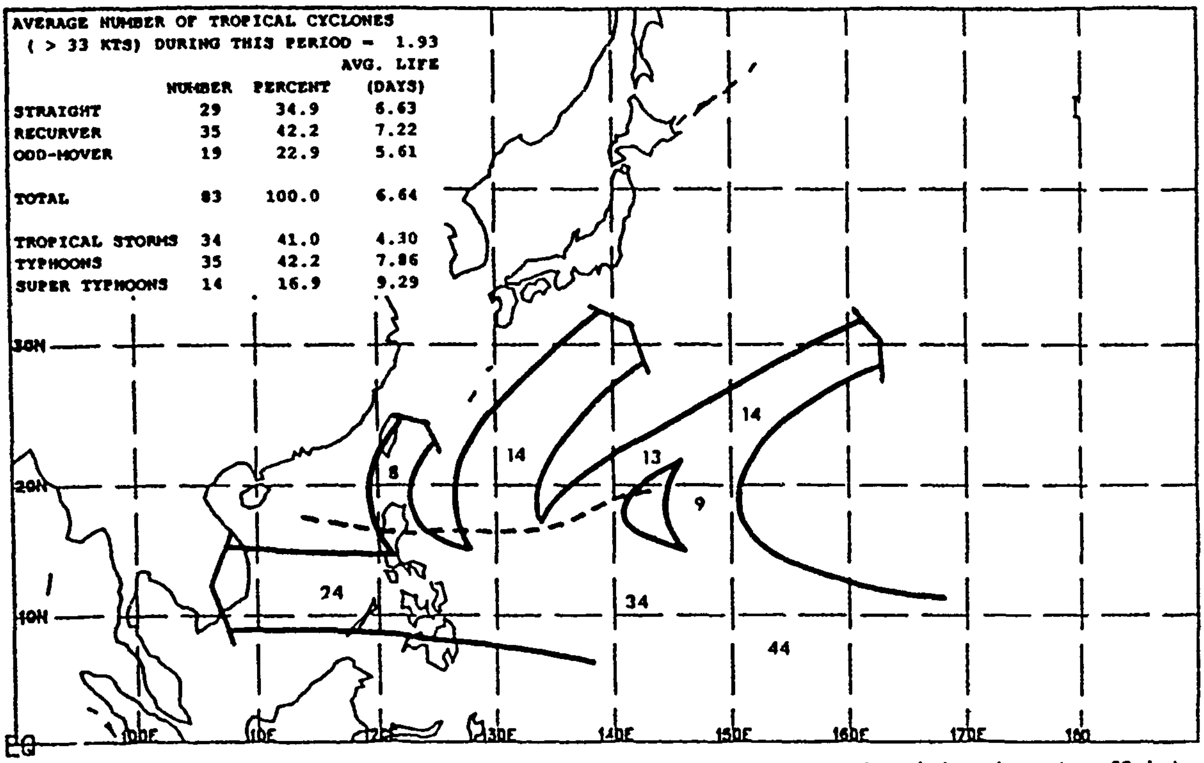

Mean tropical cyclone (> 33 kts) path. Numbers represent the percentage of tropical cyclones (> 33 kts) which followed the indicated path. These numbers may not add up to 100% since not all tropical cyclones (> 33 kts) follow a mean path and some develop/dissipate along a path. Tracks which contained less than 5% of the tropical cyclones (> 33 kts) are ignored. Dashed line represents mean recurvature position of tropical cyclones (> 33 kts) classified as recurvers.

SPEED OF MOVEMENT FOR NOV 24 - DEC 8

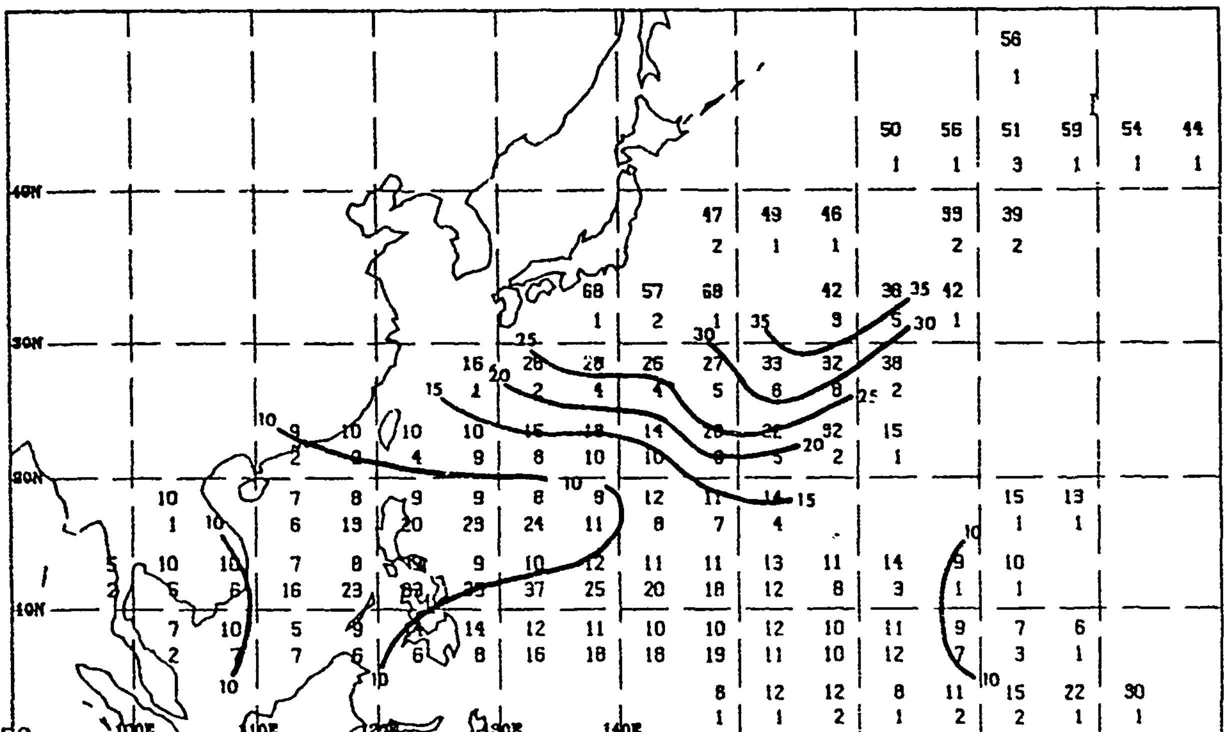

Average tropical cyclone (> 33 kts) Speed (top number) in knots and sample size (bottom number) for each 5° latitude by 5° longitude square. Contours are drawn only to those squares containing at least 5% of the sample.

MEAN PATHS FOR DEC 9 - DEC 23

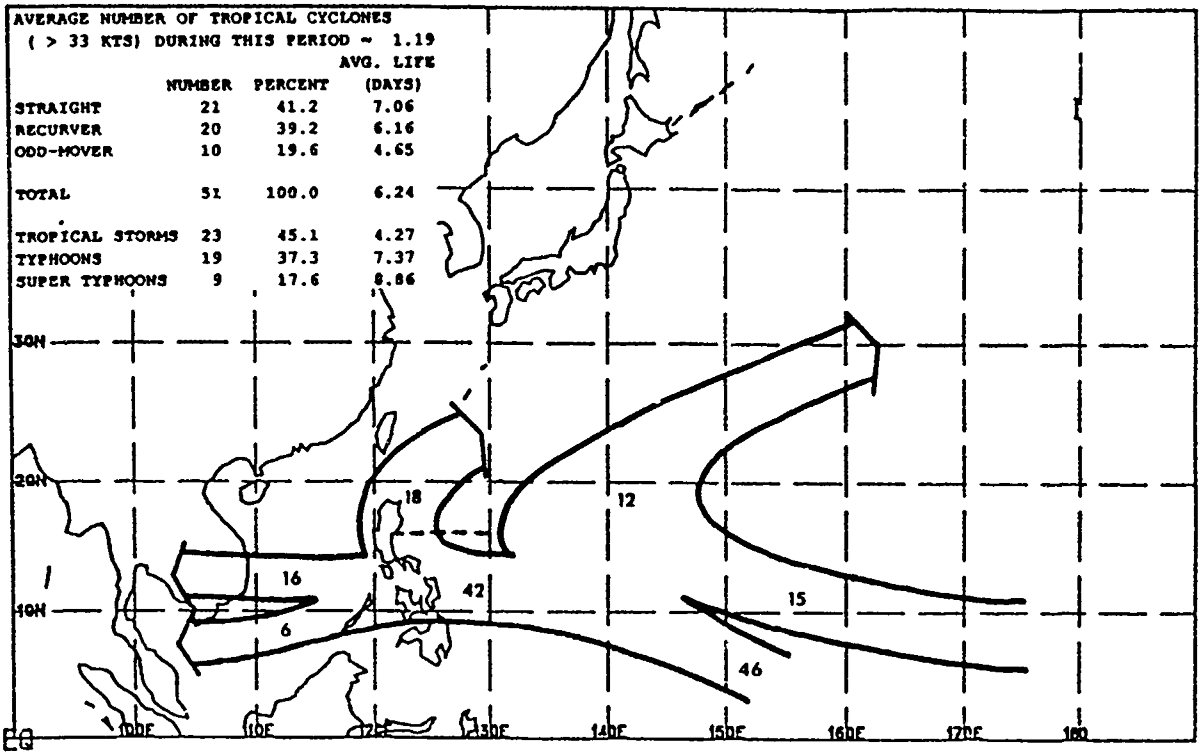

Mean tropical cyclone (> 33 kts) path. Numbers represent the percentage of tropical cyclones (> 33 kts) which followed the indicated path. These numbers may not add up to 100% since not all tropical cyclones (> 33 kts) follow a mean path and some develop/dissipate along a path. Tracks which contained less than 5% of the tropical cyclones (> 33 kts) are ignored. Dashed line represents mean recurvature position of tropical cyclones (> 33 kts) classified as recurvers.

SPEED OF MOVEMENT FOR DEC 9 - DEC 23

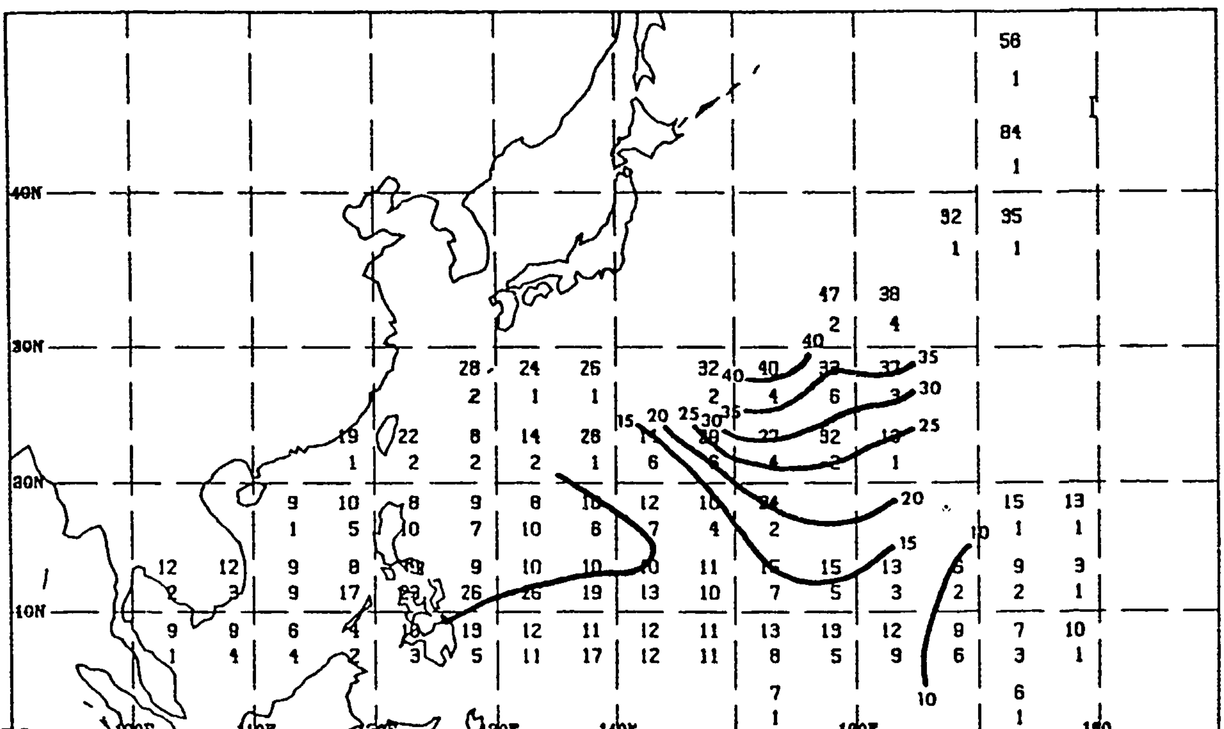

Average tropical cyclone (> 33 kts) Speed (top number) in knots and sample size (bottom number) for each 5° latitude by 5° longitude square. Contours are drawn only to those squares containing at least 5% of the sample.

MEAN MONTHLY AND COMBINED MONTHLY TROPICAL STORM AND CYCLONE TRACKS FOR THE NORTH INDIAN OCEAN (FROM NAVAIR 50-1C-61)

While it must be realized that tropical storms and cyclones deviate from the mean tracks presented in this appendix, the use of these tracks should be of particular benefit in long range planning. The application of the average tracks to specific short range situations should be avoided. Warnings issued by FWC/JTWC Guam are the immediate source of information on predicted movement.

Table I-B-1 presents the frequency of North Indian Ocean tropical storms and cyclones by month.

Table I-B-1. North Indian Ocean tropical storm and cyclone frequency (from NAVAIR 50-1C-61).

NORTH INDIAN OCEAN	JAN	FEB	MAR	APR	MAY	JUN	JUL	AUG	SEP	OCT	NOV	DEC	ANNUAL
TROPICAL STORMS	0.1			0.1	0.3	0.5	0.5	0.4	0.4	0.6	0.5	0.3	3.5
CYCLONES				0.1	0.5	0.2	0.1		0.1	0.4	0.6	0.2	2.2
TROPICAL STORMS AND CYCLONES	0.1		0.1	0.3	0.7	0.7	0.6	0.4	0.5	0.5	1.1	0.5	5.7

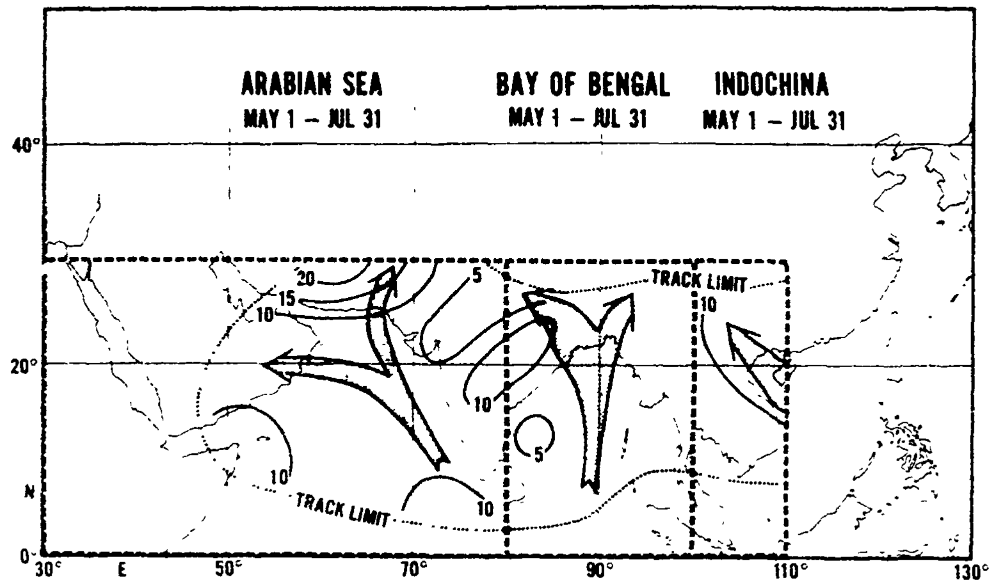

Figure I-B-1. Preferred North Indian Ocean tropical storm and cyclone tracks (May 1-Jul 31). Isolines show the average storm speed of movement in knots.

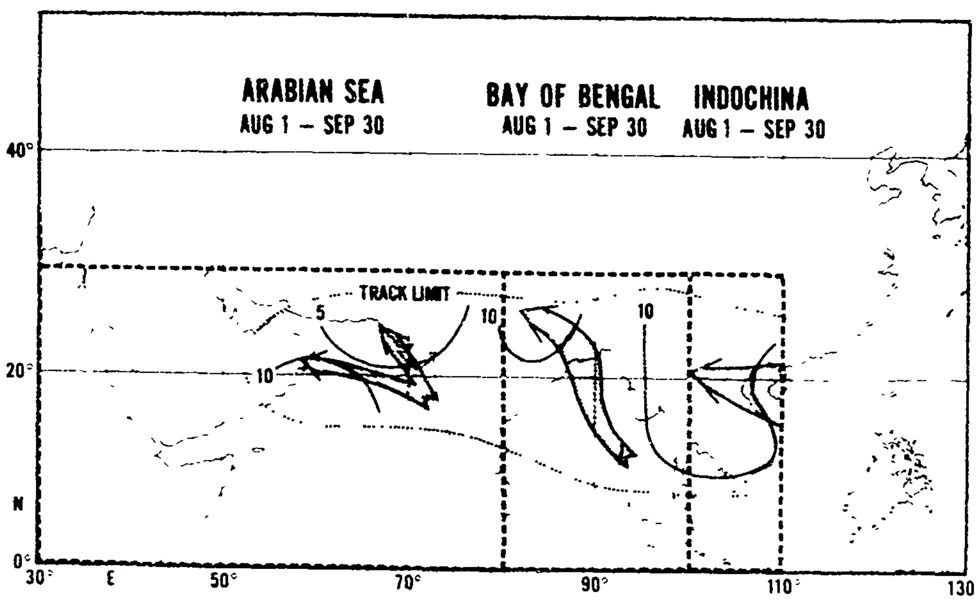

Figure I-B-2. Preferred North Indian Ocean tropical storm and cyclone tracks (Aug 1-Sep 30). Isolines show the average storm speed of movement in knots.

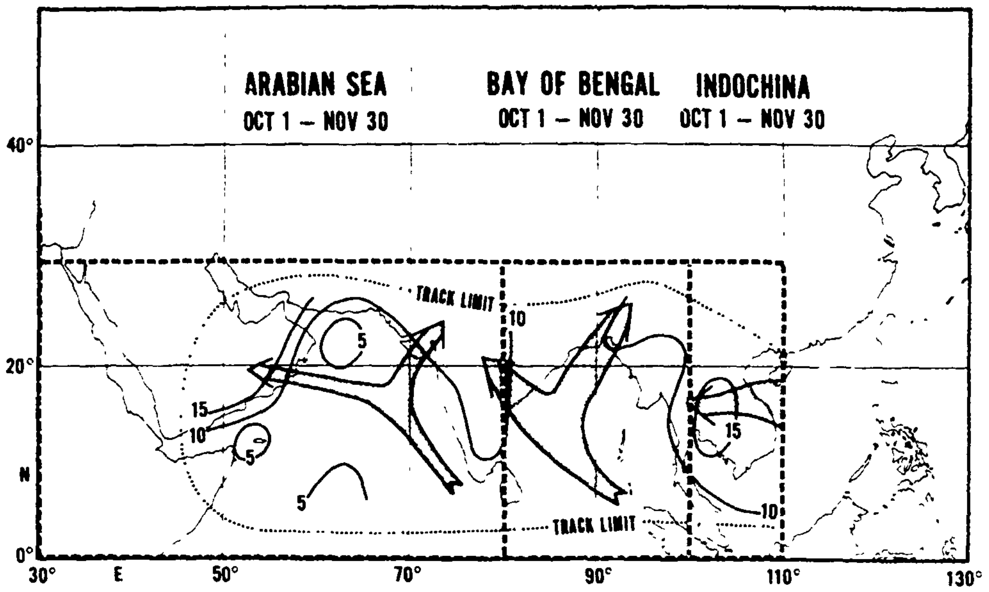

Figure I-B-3. Preferred North Indian Ocean tropical storm and cyclone tracks (Oct 1-Nov 30). Isolines show the average storm speed of movement in knots.

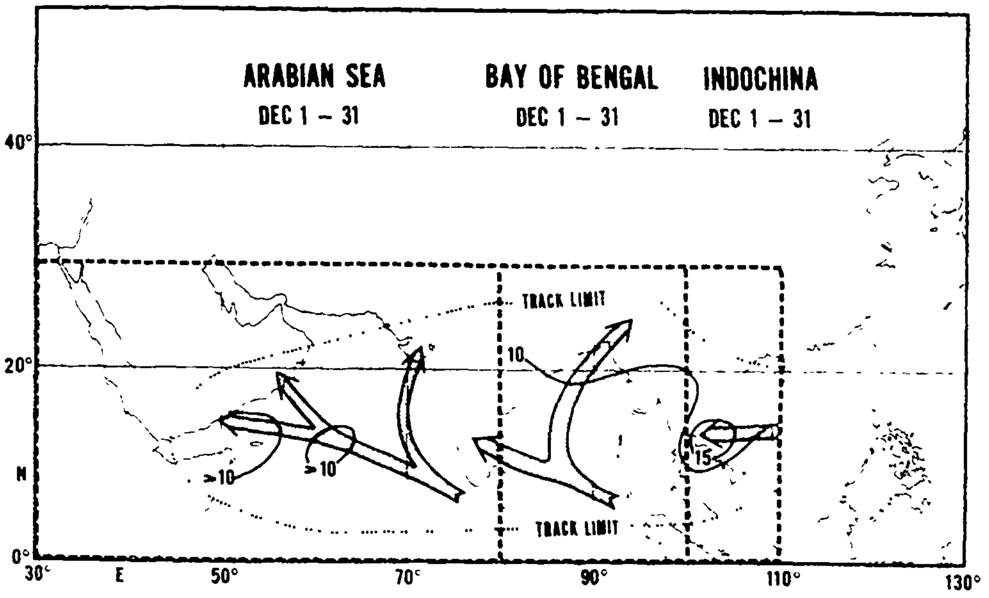

Figure I-B-4. Preferred North Indian Ocean tropical storm and cyclone tracks (Dec 1-31). Isolines show the average storm speed of movement in knots.

MEAN MONTHLY AND PART MONTHLY TROPICAL STORM AND HURRICANE TRACKS FOR THE SOUTHWEST INDIAN OCEAN (FROM NAVAIR 50–1C–61)

While it must be realized that tropical storms and hurricanes deviate from the mean tracks presented in this appendix, the use of these tracks should be of particular benefit in long range planning. The application of the average tracks to specific short range situations should be avoided. Warnings issued by FWC/JTWC Guam are the immediate source of information on predicted movement.

Table I-C-1 presents the frequency of Southwest Indian Ocean tropical storms and hurricanes by month.

Table I-C-1. Southwest Indian Ocean tropical storm and hurricane frequency (from NAVAIR 50-1C-61).

SOUTHWEST INDIAN OCEAN	JAN	FEB	MAR	APR	MAY	JUN	JUL	AUG	SEP	OCT	NOV	DEC	ANNUAL
TROPICAL STORMS	2.0	2.2	1.7	0.6	0.2					0.3	0.3	0.8	7.4
HURRICANES	1.3	1.1	0.8	0.4								0.5	3.8
TROPICAL STORMS AND HURRICANES	3.2	3.3	2.5	1.1	0.2					0.3	0.4	1.4	11.2

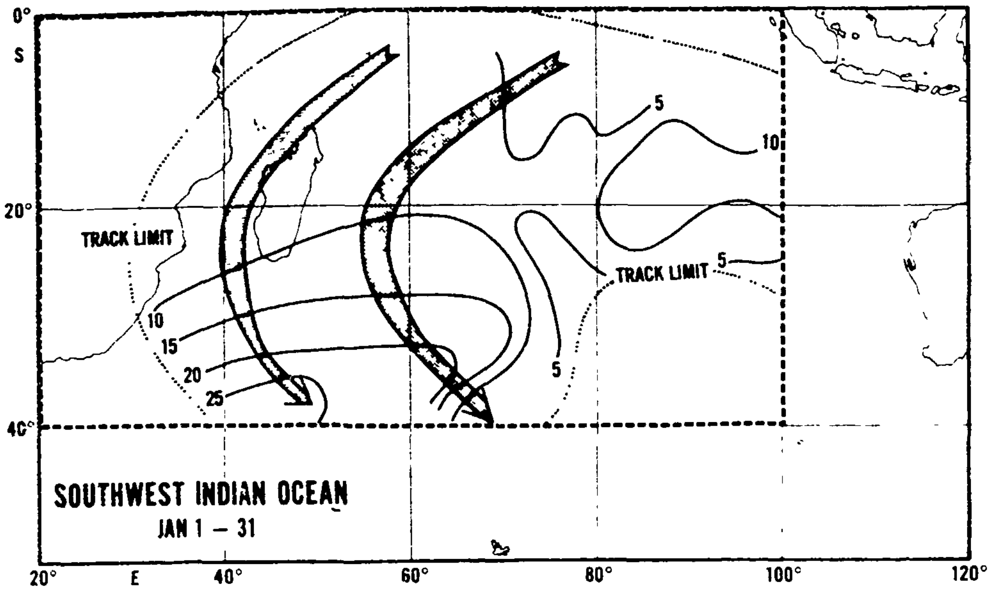

Figure I-C-1. Preferred Southwest Indian Ocean tropical storm and hurricane tracks (Jan 1-31). Isolines show the average storm speed of movement in knots.

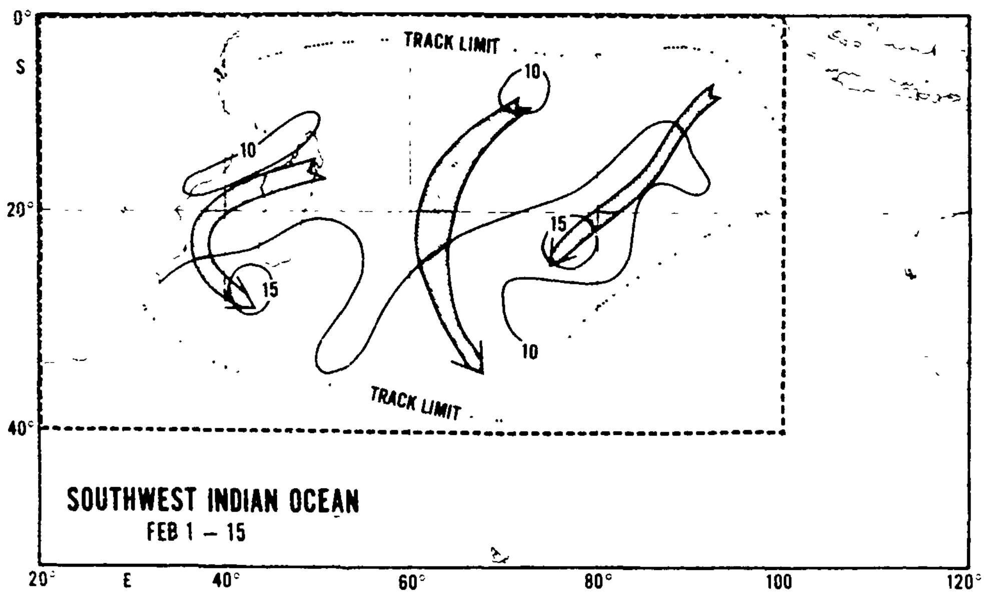

Figure I-C-2. Preferred Southwest Indian Ocean tropical storm and hurricane tracks (Feb 1-15). Isolines show the average storm speed of movement in knots.

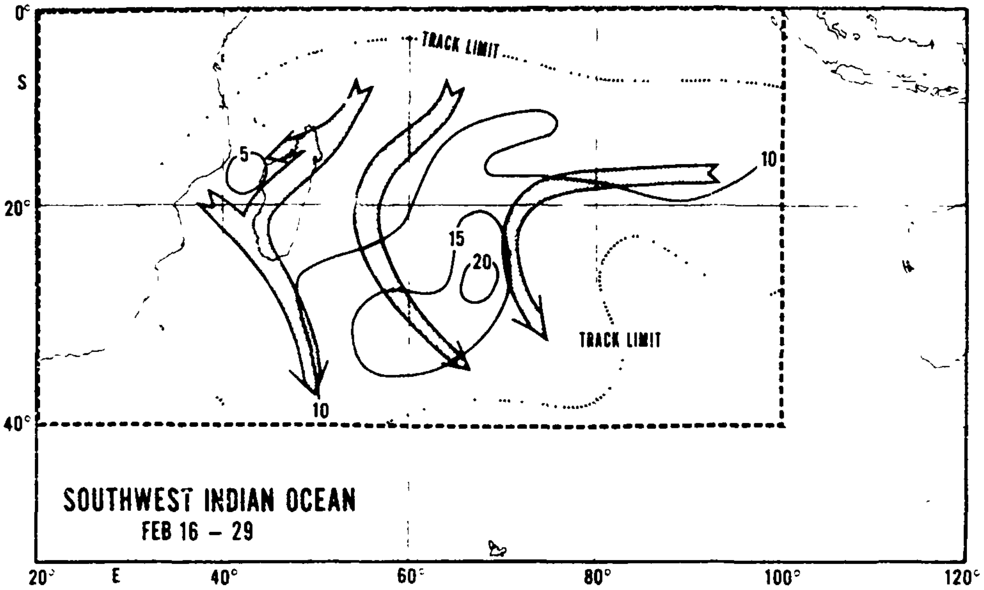

Figure I-C-3. Preferred Southwest Indian Ocean tropical storm and hurricane tracks (Feb 16-29). Isolines show the average storm speed of movement in knots.

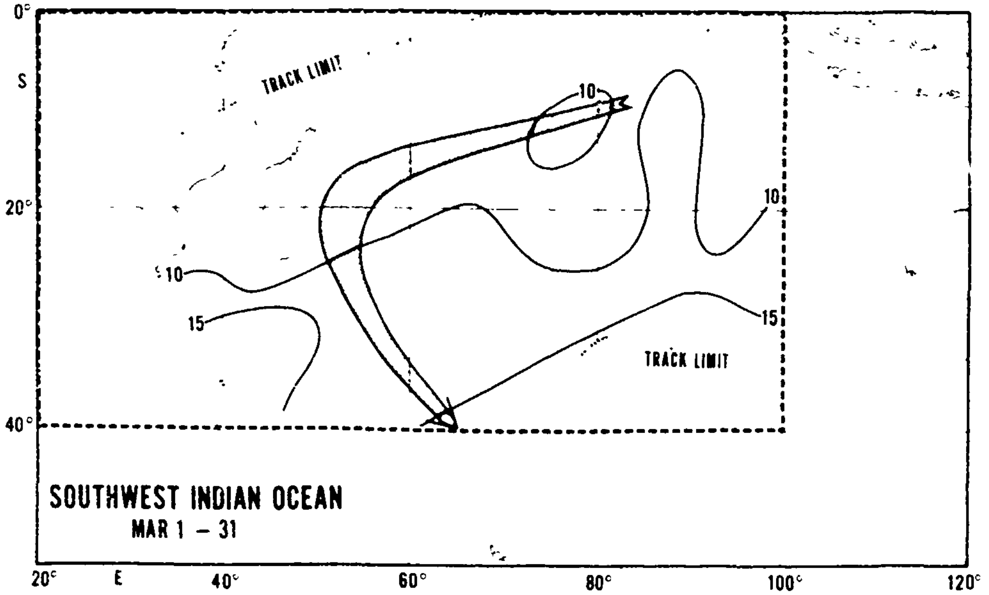

Figure I-C-4. Preferred Southwest Indian Ocean tropical storm and hurricane tracks (Mar 1-31). Isolines show the average storm speed of movement in knots.

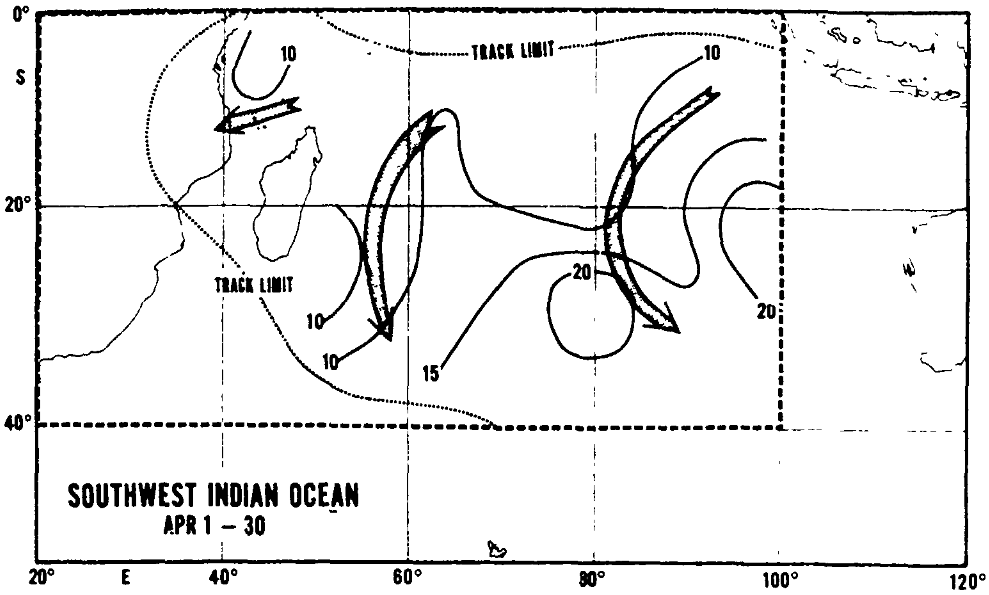

Figure I-C-5. Preferred Southwest Indian Ocean tropical storm and hurricane tracks (Apr 1-30). Isolines show the average storm speed of movement in knots.

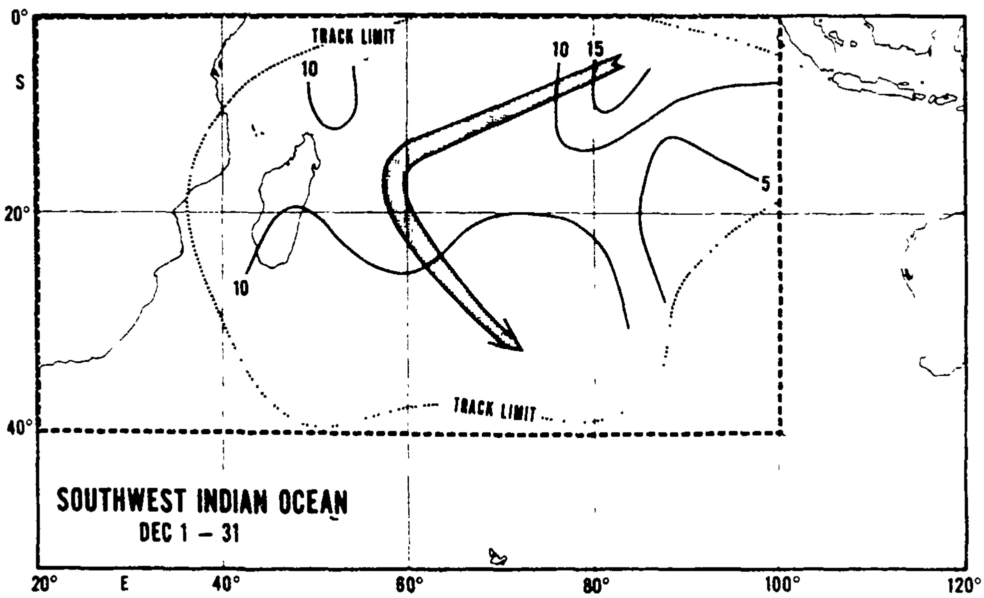

Figure I-C-6. Preferred Southwest Indian Ocean tropical storm and hurricane tracks (Dec 1-31). Isolines show the average storm speed of movement in knots.

MEAN MONTHLY AND PART MONTHLY TROPICAL STORM AND HURRICANE TRACKS FOR THE SOUTHWEST PACIFIC OCEAN AND AUSTRALIAN AREA (FROM NAVAIR 50–1C–61)

While it must be realized that tropical storms and hurricanes deviate from the mean tracks presented in this appendix, the use of these tracks should be of particular benefit in long range planning. The application of the average tracks to specific short range situations should be avoided. Warnings issued by FWC/JTWC Guam are the immediate source of information on predicted movement.

Table I-D-1 presents the frequency of Southwest Pacific and Australian area tropical storms and hurricanes by month.

Table I-D-1. Southwest Pacific and Australian area tropical storm and hurricane frequency (from NAVAIR 50-1C-61).

SOUTHWEST PACIFIC AND AUSTRALIAN AREA	JAN	FEB	MAR	APR	MAY	JUN	JUL	AUG	SEP	OCT	NOV	DEC	ANNUAL
TROPICAL STORMS	2.7	2.8	2.4	1.3	0.3	0.2				0.1	0.4	1.5	10.9
HURRICANES	0.7	1.1	1.3	0.3			0.1	0.1			0.3	0 5	3.8
TROPICAL STORMS AND HURRICANES	3.4	4.1	3.7	1.7	0.3	0.2	0.1	0.1		0 1	0.7	2.0	14.8

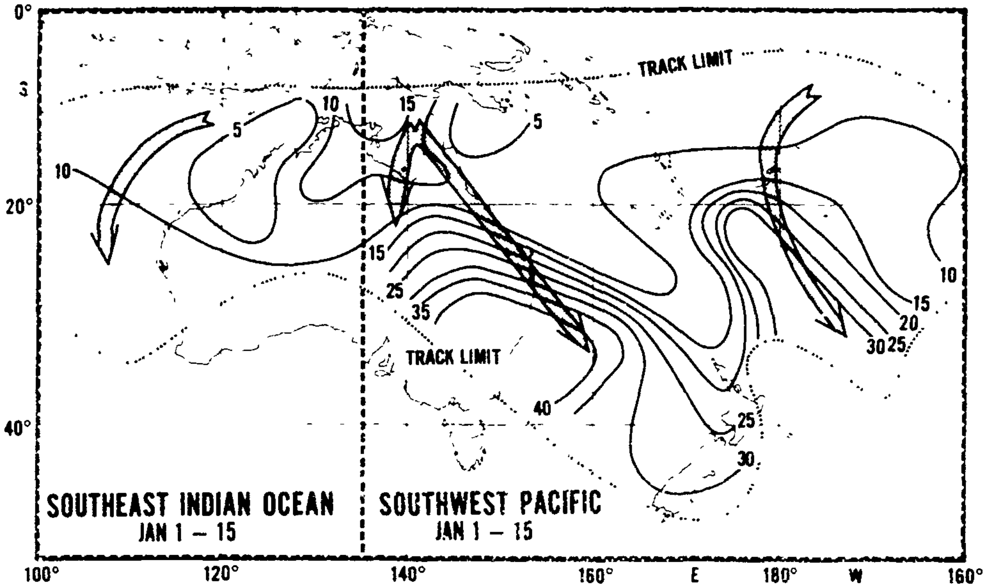

Figure I-D-1. Preferred Southwest Pacific and Australian area tropical storm and hurricane tracks (Jan. 1-15). Isolines show the average storm speed of movement in knots.

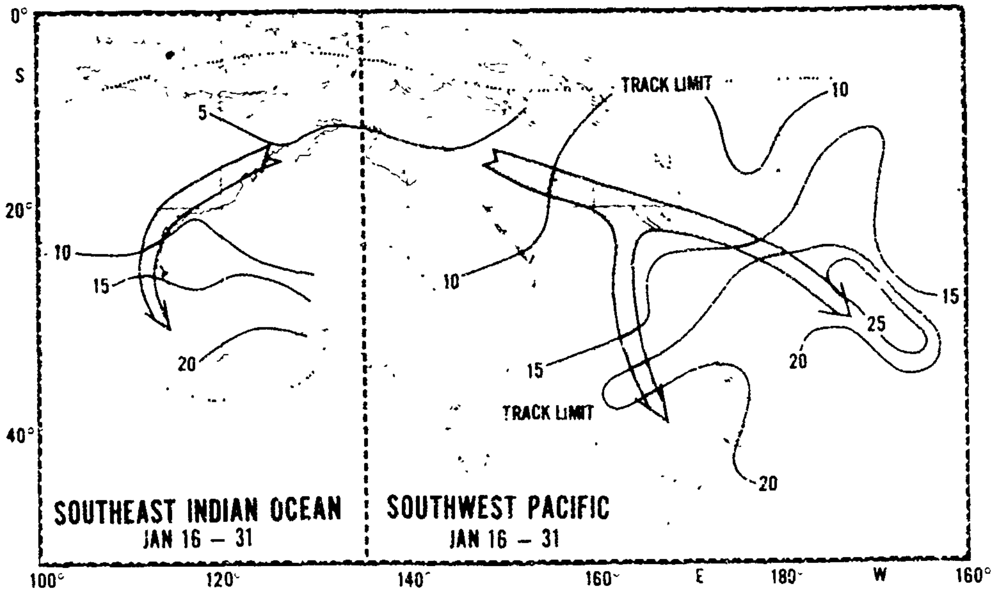

Figure I-D-2. Preferred Southwest Pacific and Australian area tropical storm and hurricane tracks (Jan 16-31). Isolines show the average storm speed of movement in knots.

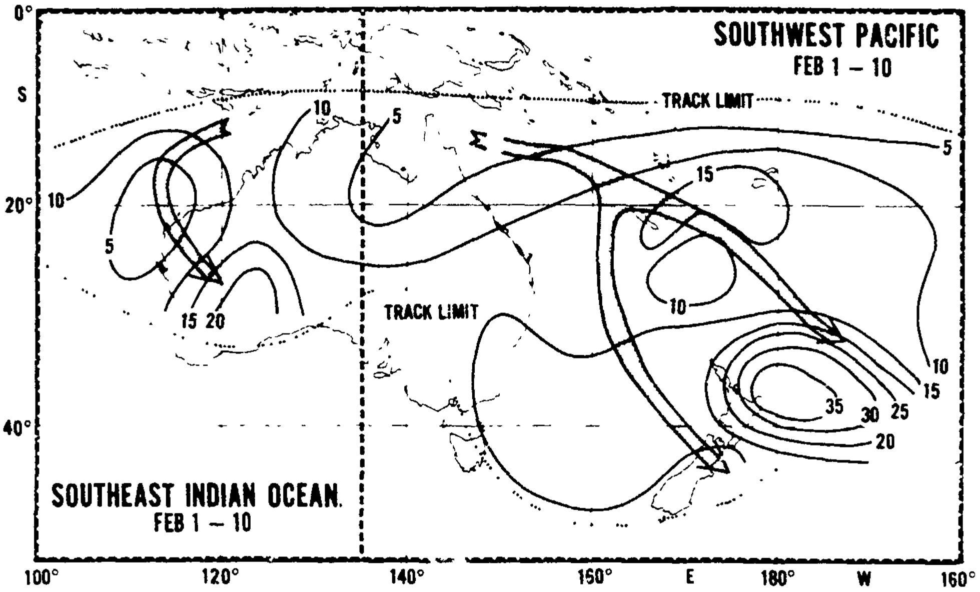

Figure I-D-3. Preferred Southwest Pacific and Australian area tropical storm and hurricane tracks (Feb 1-10). Isolines show the average storm speed of movement in knots.

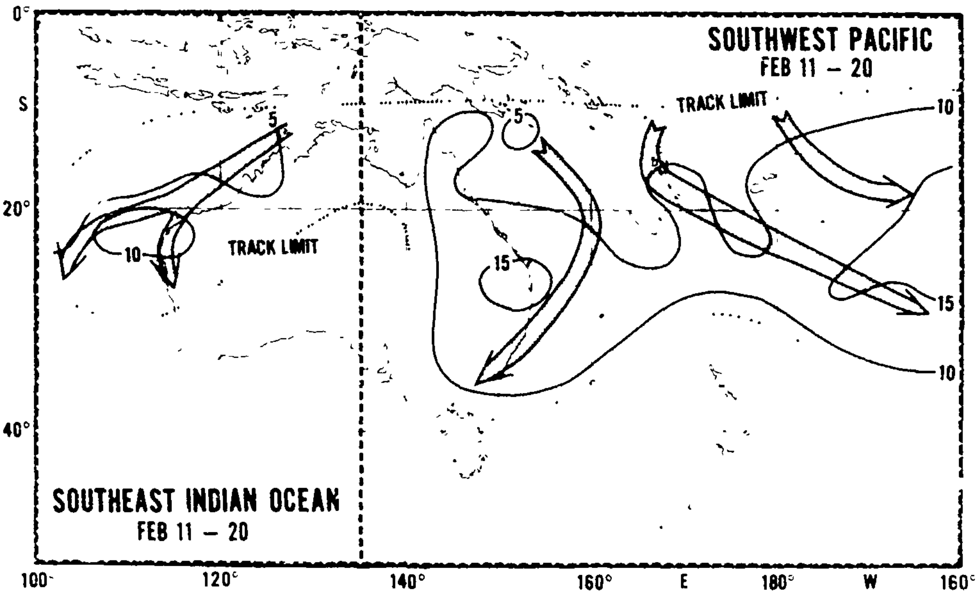

Figure I-D-4. Preferred Southwest Pacific and Australian area tropical storm and hurricane tracks (Feb 11-20). Isolines show the average storm speed of movement in knots.

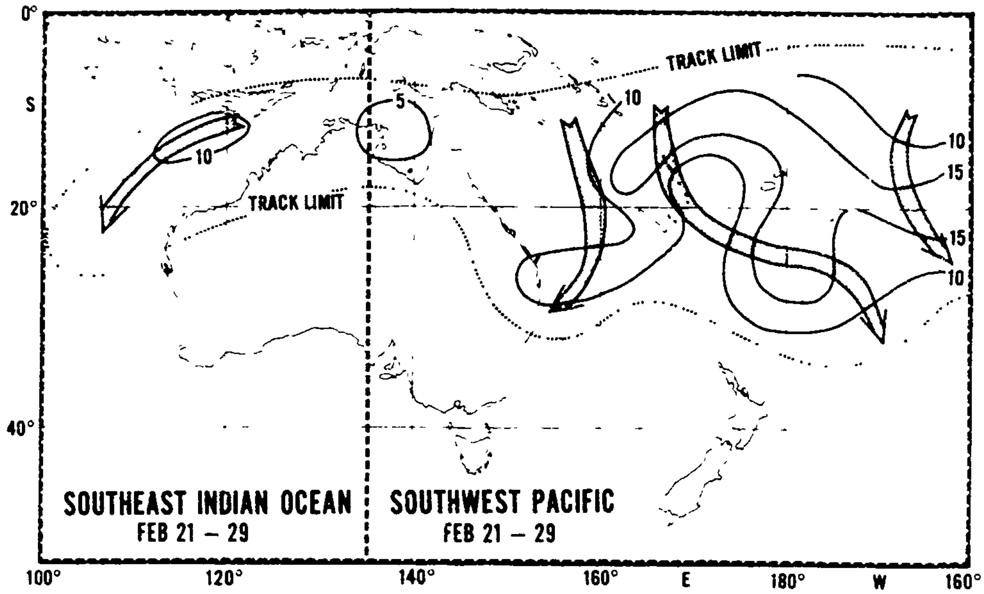

Figure I-D-5. Preferred Southwest Pacific and Australian area tropical storm and hurricane tracks (Feb 21-29). Isolines show the average storm speed of movement in knots.

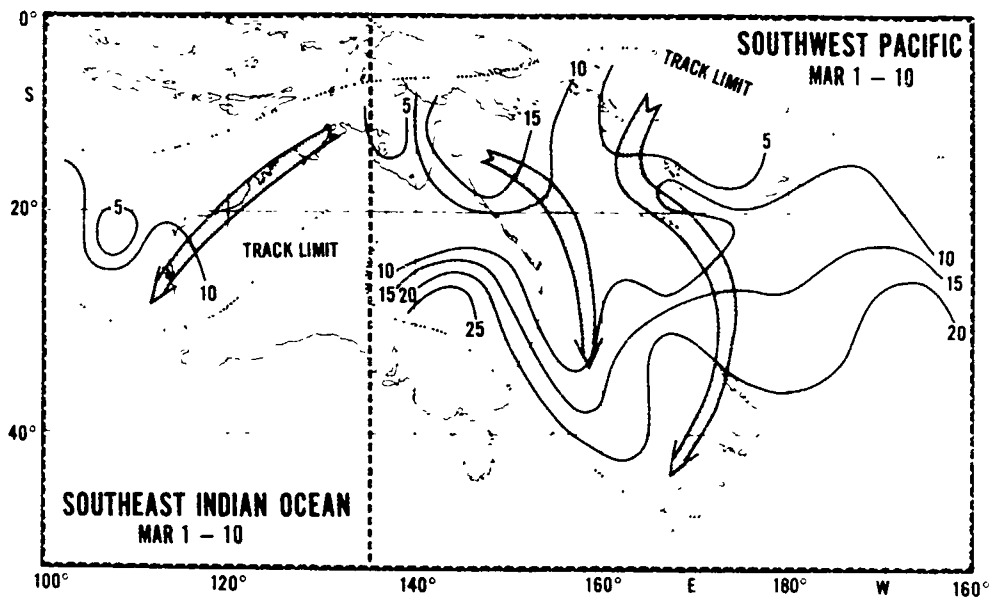

Figure I-D-6. Preferred Southwest Pacific and Australian area tropical storm and hurricane tracks (Mar 1-10). Isolines show the average storm speed of movement in knots.

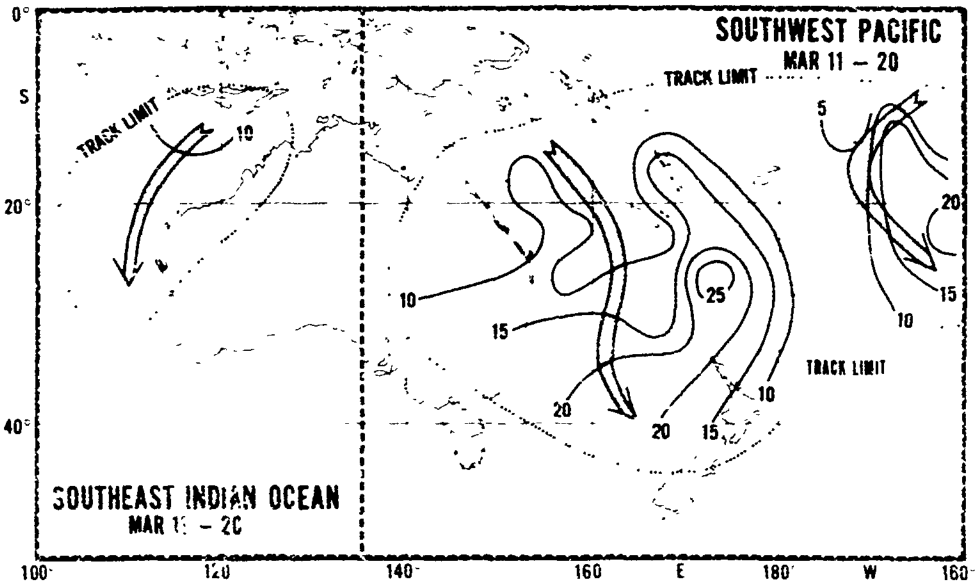

Figure I-D-7. Preferred Southwest Pacific and Australian area tropical storm and hurricane tracks (Mar 11-20). Isolines show the average storm speed of movement in knots.

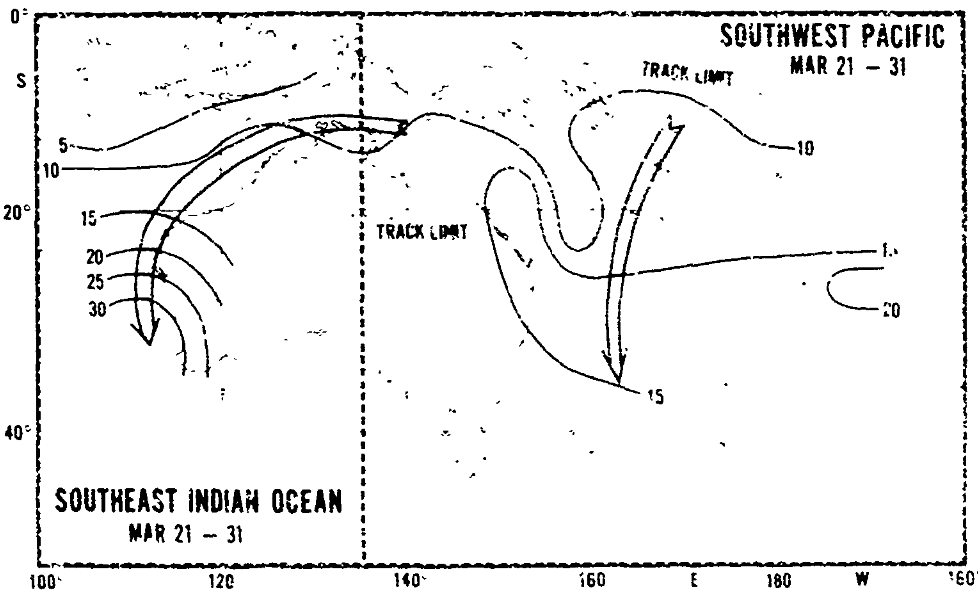

Figure I-D-8. Preferred Southwest Pacific and Australian area tropical storm and hurricane tracks (Mar 21-31). Isolines show the average storm speed of movement in knots.

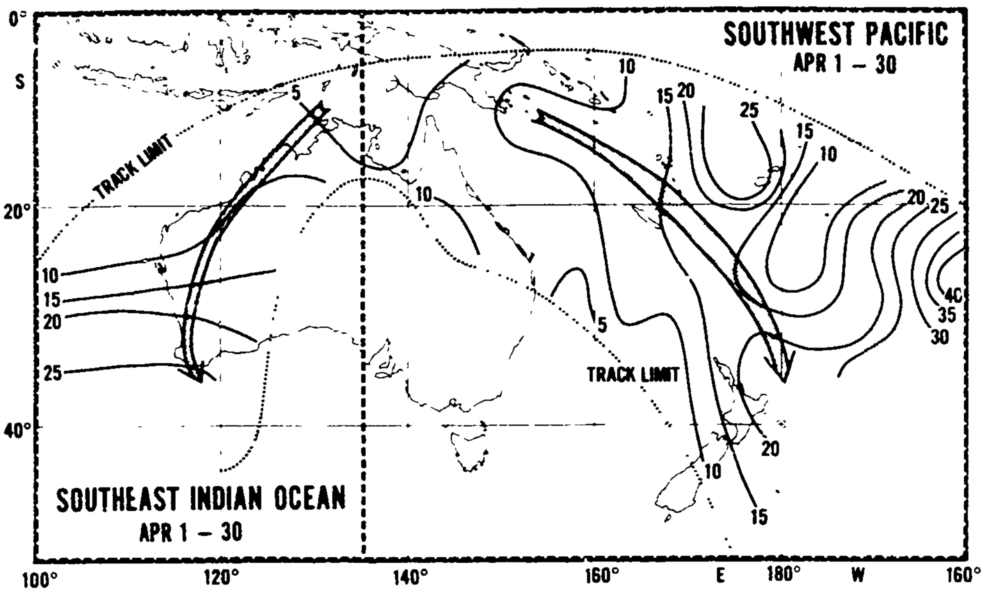

Figure I-D-9. Preferred Southwest Pacific and Australian area tropical storm and hurricane tracks (Apr 1-30). Isolines show the average storm speed of movement in knots.

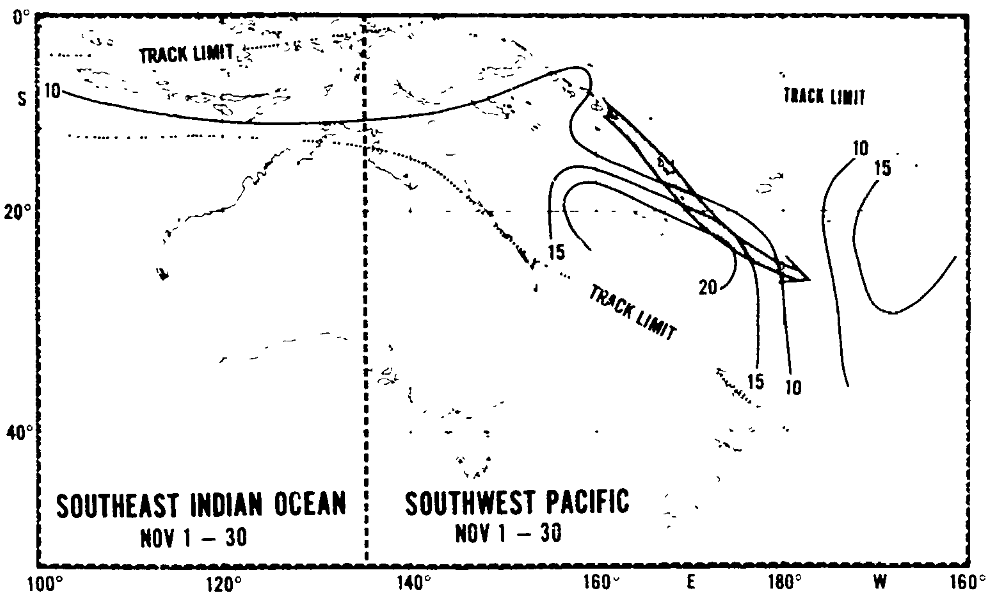

Figure I-D-10. Preferred Southwest Pacific and Australian area tropical storm and hurricane tracks (Nov 1-30). Isolines show the average storm speed of movement in knots.

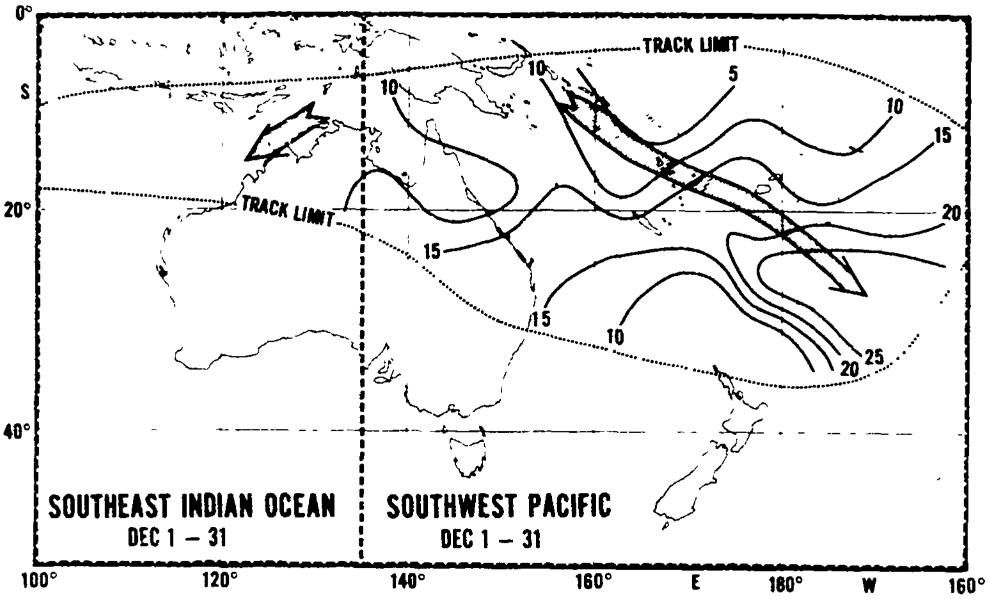

Figure I-D-11. Preferred Southwest Pacific and Australian area tropical storm and hurricane tracks (Dec 1-31). Isolines show the average storm speed of movement in knots.

APPENDIX C

Equivalent Wind Chill

and

Vessel Superstructure Icing

Equivalent Wind Chill

The movement of air (wind) about a heat source such as a human body increases the rate of loss of heat. This rate of loss can be determined for different combinations of wind and air temperatures and is referred to as the chill factor. Figure C-1 provides equivalent wind chill temperatures for various wind speed and air temperature combinations. The values in the figure represent the temperature that would produce the same loss of heat at about 3 kt, the normal speed of a person walking vigorously.

The figure is divided into three sections which represent increasing levels of danger of freezing exposed flesh for properly clothed individuals. The equivalent wind chill temperatures of -30°C (-22°F) represents the temperature at which exposed flesh can freeze within one minute. With winds of 27 kt or greater this can occur with air temperatures of -8°C (18°F), an air temperature that would be likely to occur when operating near the ice edge or high latitude coastlines with off ice/land winds during the cold seasons. The colder air temperatures over land/in port will also be a threat for personnel on vessels that have been operating at sea where the warming affect of the ocean modifies the cold season temperatures. Additional loss of body heat will result from handling or touching cold objects, such as top side rails, lines, metal tools, etc.

Equivalent Wind Chill Temperature													
Wind Speed	Cooling Power of Wind Expressed As "Equivalent Chill Temperature"												
knots	Temperature(°C)												
Calm	12	8	4	0	-4	-8	-12	-16	-20	-24	-28	-32	-36
	Equivalent Chill Temperature (°C)												
3	12	8	4	0	-4	-8	-12	-16	-20	-24	-28	-32	-36
5	9	5	0	-4	-8	-13	-17	-22	-26	-31	-35	-40	-44
11	5	0	-5	-10	-15	-21	-26	-31	-36	-42	-47	-52	-57
16	3	-3	-8	-14	-20	-25	-31	-37	-43	-48	-54	-60	-65
22	1	-5	-11	-17	-23	-29	-35	-41	-47	-53	-59	-65	-71
27	0	-6	-12	-18	-25	-31	-37	-43	-49	-56	-62	-68	-74
32	0	-7	-13	-19	-26	-32	-39	-45	-51	-58	-64	-70	-77
38	-1	-7	-14	-20	-27	-33	-40	-46	-52	-60	-65	-72	-78
43	-1	-8	-14	-21	-27	-34	-40	-47	-53	-60	-66	-73	-79
49	-1	-8	-14	-21	-27	-34	-40	-47	-53	-60	-66	-73	-79
54	-1	-8	-14	-21	-27	-34	-40	-47	-53	-60	-66	-73	-79
	Little Danger					Increasing Danger (Flesh May Freeze Within 1 Minute)				Great Danger (Flesh May Freeze Within 30 Seconds)			
	Danger Of Freezing Exposed Flesh For Properly Clothed Individuals												

Figure C-1. Equivalent wind chill temperature. Adapted from NWS/NOAA Technical Procedures Bulletin No. 165.

Vessel Superstructure Icing

Superstructure icing is a hazard of high latitude operations. Fleet experience with this hazard is generally minimal. The icing hazard is greatest to small vessels and in fact has caused the loss of many small and medium fishing vessels. For larger vessels it can adversely affect their seaworthiness and operational capabilities.

The rate of icing depends on environmental conditions such as air temperature, strong winds, precipitation, and cool sea temperatures. The actual icing potential is a characteristic of each vessel and the manner of operation.

The rate of icing reflects the amount of liquid water or spray flux that strikes an exposed surface. Three sources of water are important; wind generated spray, precipitation, and wave generated spray. Wind generated spray is of concern only to small boats or low objects such as buoys. Precipitation is of concern to all size vessels and can accumulate as either clear icing (liquid precipitation) or rime icing (condensation, mixed liquid/solid precipitation). Wave generated spray is the most serious hazard in that it provides the largest amount of airborne liquid water to impact on elevated vessel structures.

The amount of airborne liquid water depends on the wave characteristics, vessel motion, and the interaction of the vessel and the waves. In general the worst case is for vessels heading into the waves at high relative speeds, with vessel length/wave lengths such that vessel vertical motion is extreme.

The following comments are provided for general background information on vessel icing.

1. The spray flux diminishes with elevation, ship speed, and heading angle relative to the wave crest.

2. The spray flux is greatest for ships heading into the waves and diminishes with decreasing angles of impact.

3. For impact angles of 90°, the ship's speed does not affect the amount of spray generated.

4. For ships heading into the waves a doubling of spray flux results for a speed increase of 6 to 13 kt.

5. The ratio of spray increase for relative wind speed values of 20, 40, and 60 kt are 1, 8, and 22. In other words, the amount of spray at a relative wind (wind plus ship speed) of 40 kt is 8 times greater than at 20 kt.

6. The approximate ratios of spray flux for height above mean sea level versus relative wind speeds for selected height/wind speeds (Zabrzewski, 1986) are:

	Wind speed (kt)		
Height (ft)	20	40	60
8	35	181	375
15	12	163	128
25	2	12	25
40	0.2	0.8	1.7

Note: In heavy seas, even the deck level of carriers will at times be much closer to mean sea level than the freeboard height.

Figures C-2 through C-5 show nomograms for icing rates for vessels heading into or abeam of the wind for four different sea temperatures. These figures are based on data analyzed by Pease and Comiskey (1985) and are based on actual observations from fishing, tow, and Coast Guard vessels operating in the Alaskan waters. The vessels ranged from 20-75 m in length and therefore the absolute threat levels are not appropriate for larger vessels. However, the relative threat level should be appropriate to all ship sizes and operations. The freeboard heights of these smaller vessels are generally less than 15 feet. For large ships some indication of actual threat level can be obtained from comparing values provided in comment 6 above and the following nomograms. For example, the spray flux ratio for 8 ft and 20 kt (35) is about the same as for 25 ft and 60 kt (25). Therefore, the icing threat at a deck level of 25 ft with 60 kt is about what would be found in the following nomograms for a smaller vessel (8 ft height) at 20 kt.

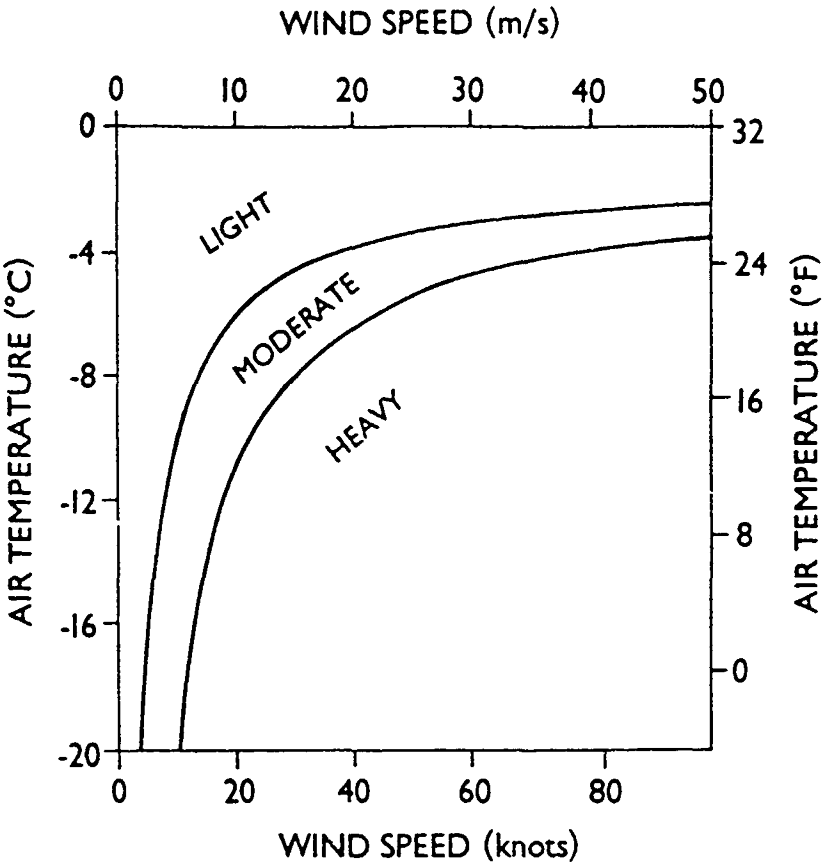

Icing conditions for vessels heading into or abeam of the wind for water temperatures of + 1°C (34°F)

Light Icing - Less than 0.7cm/hr (0.3in/hr)
Moderate Icing - 0.7cm/hr (0.3in/hr) to 2.0 cm/hr (o.8in/hr)
Heavy Icing - Greater than 2.0cm/hr (0.8in/hr)

Figure C-2. Nomogram of Superstructure icing conditions for vessels up to about 75 m (250 ft) in length due to spray for water about 1°C (34°F) (from Pease and Comiskey, 1985). Use in conjunction with information on spray flux ratios based on height above mean sea level versus wind speed for determining icing rates for larger ships.

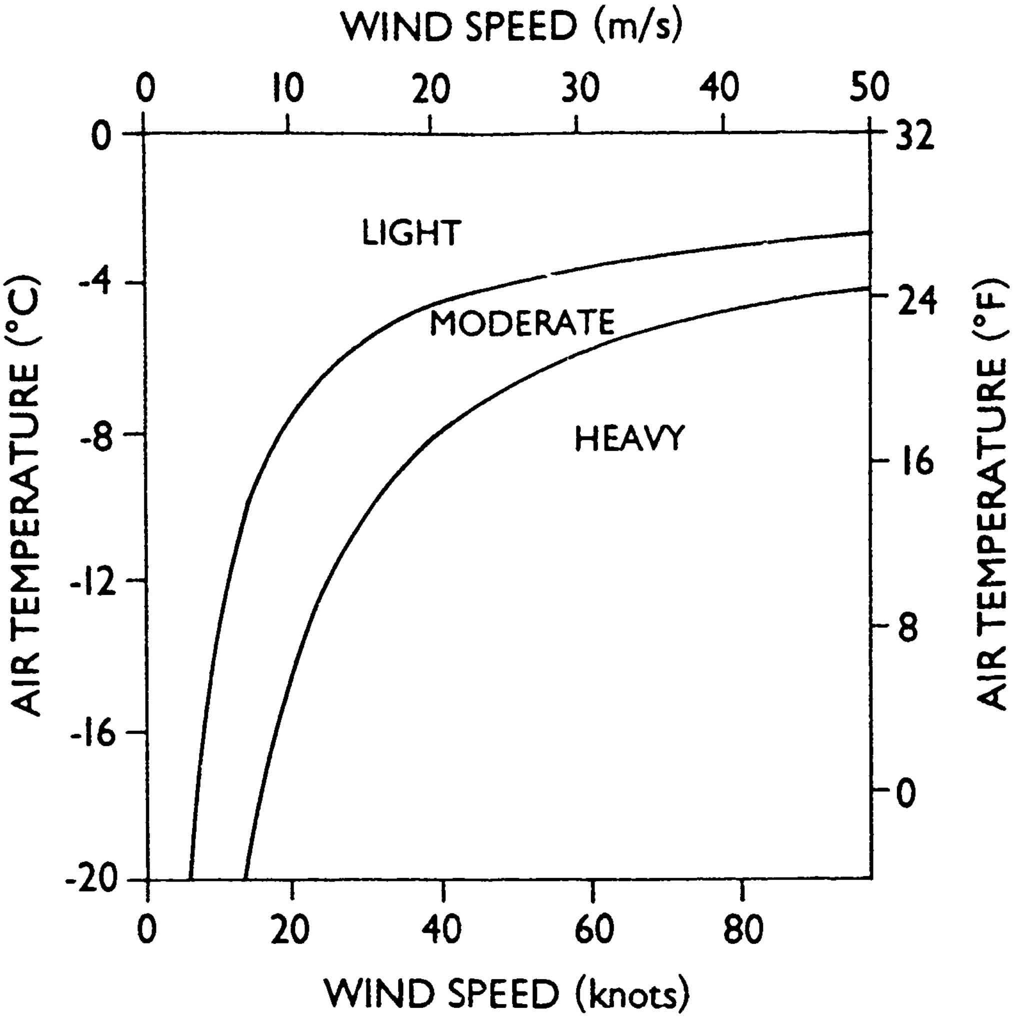

Icing conditions for vessels heading into or abeam of the wind for water temperatures of +3°C (37°F)

Light Icing - Less than 0.7cm/hr (0.3in/hr)
Moderate Icing - 0.7cm/hr (0.3in/hr) to 2.0 cm/hr (0.8in/hr)
Heavy Icing - Greater than 2.0cm/hr (0.8in/hr)

Figure C-3. Nomogram of Superstructure icing conditions for vessels up to about 75 m (250 ft) in length due to spray for water about 3°C (37°F) (from Pease and Comiskey, 1985). Use in conjunction with information on spray flux ratios based on height above mean sea level versus wind speed for determining icing rates for larger ships.

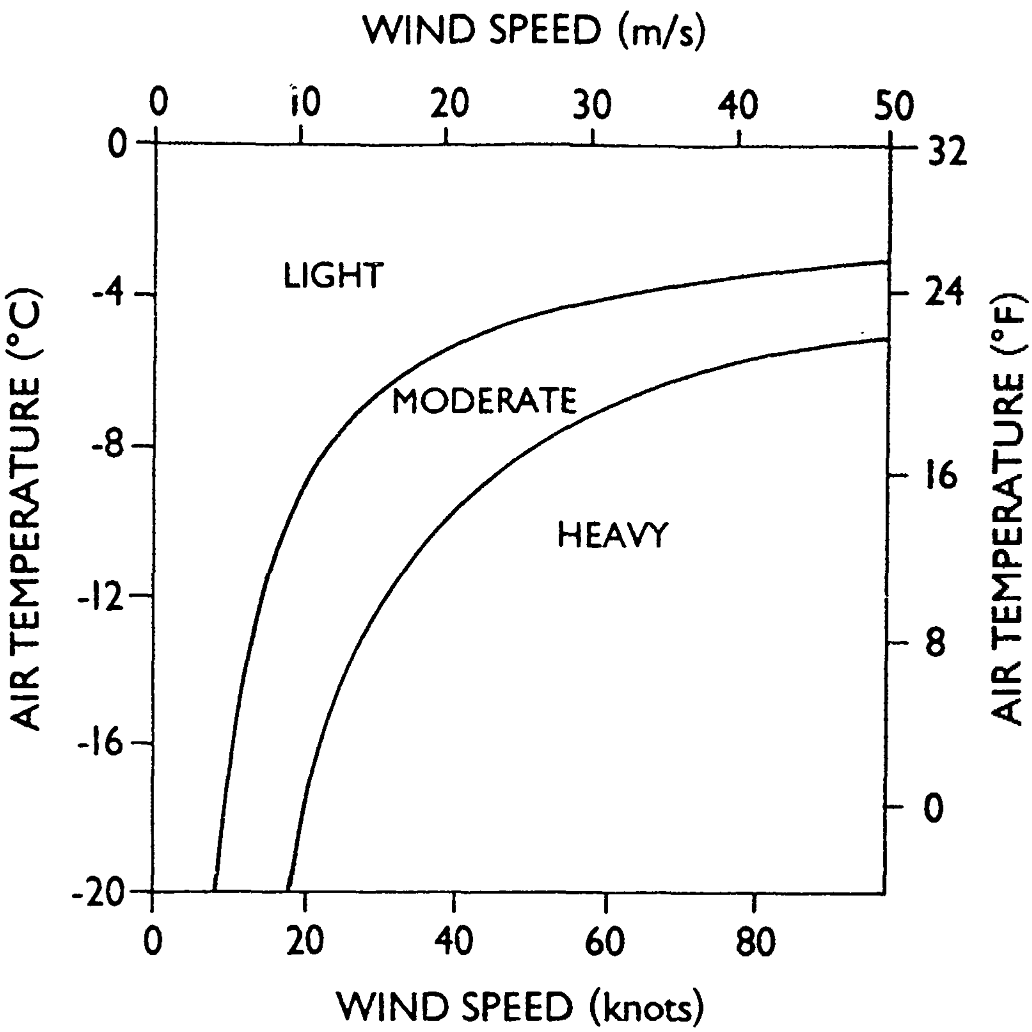

Icing conditions for vessels heading into or abeam of the wind for water temperatures of +5°C (41°F)

Light Icing - Less than 0.7cm/hr (0.3in/hr)
Moderate Icing - 0.7cm/hr (0.3in/hr) to 2.0 cm/hr (0.8in/hr)
Heavy Icing - Greater than 2.0cm/hr (0.8in/hr)

Figure C-4. Nomogram of Superstructure icing conditions for vessels up to about 75 m (250 ft) in length due to spray for water about 5°C (41°F) (from Pease and Comiskey, 1985). Use in conjunction with information on spray flux ratios based on height above mean sea level versus wind speed for determining icing rates for larger ships.

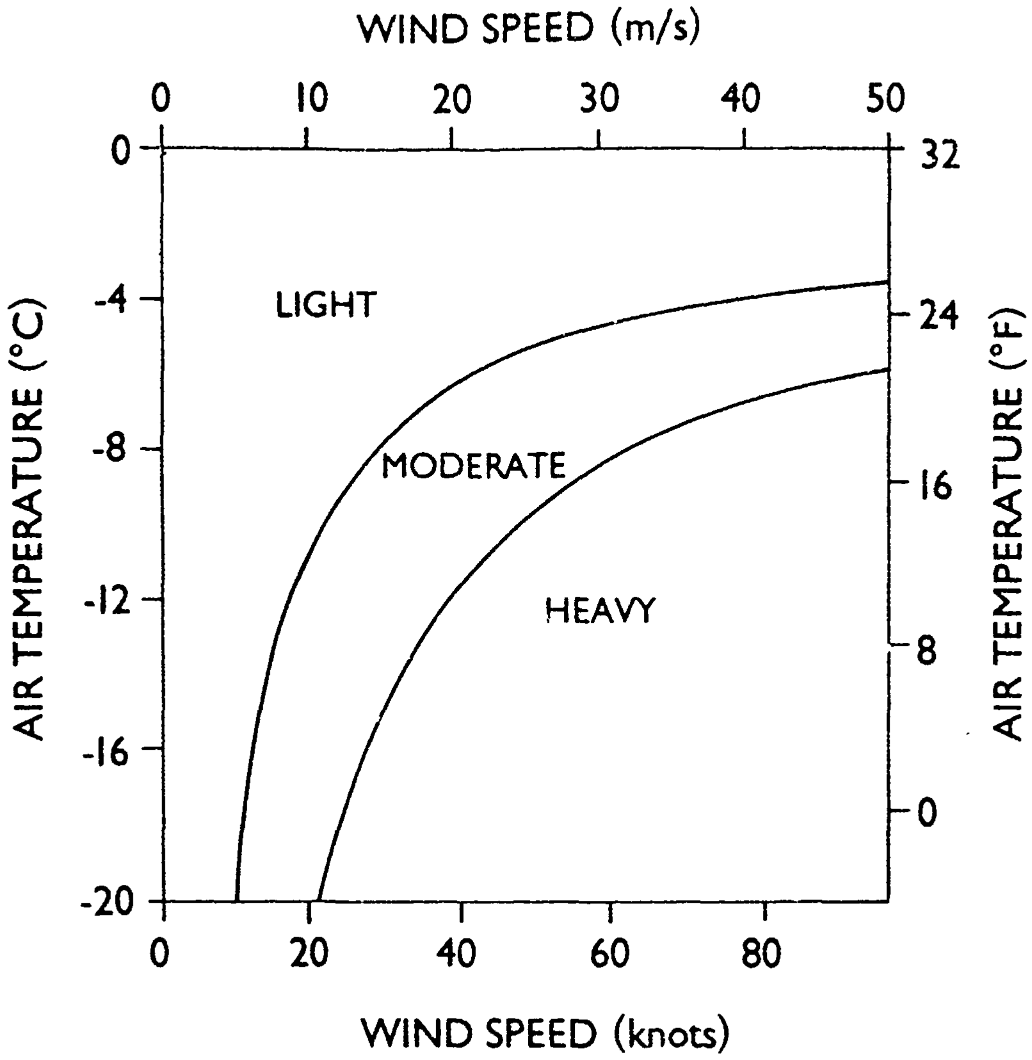

Icing conditions for vessels heading into or abeam of the wind for water temperatures of +7°C (45°F)

Light Icing - Less than 0.7cm/hr (0.3in/hr)
Moderate Icing - 0.7cm/hr (0.3in/hr) to 2.0 cm/hr (0.8in/hr)
Heavy Icing - Greater than 2.0cm/hr (0.8in/hr)

Figure C-5. Nomogram of Superstructure icing conditions for vessels up to about 75 m (250 ft) in length due to spray for water about 7°C (45°F) (from Pease and Comiskey, 1985). Use in conjunction with information on spray flux ratios based on height above mean sea level versus wind speed for determining icing rates for larger ships.

REFERENCES

Pease, C. H. and A. L. Comiskey, 1985: Vessel Icing in Alaskan Waters - 1979 to 1984 Data Set. NOAA Data Report ERL PMEL-14.

Zabrzewski, W. P., 1986: Icing on Ships. Part I. Splashing A Ship With Spray. NOAA Technical Memorandum ERL PMEL-66.

DISTRIBUTION

COMMANDER IN CHIEF
U.S. PACIFIC FLEET
ATTN: CODE 02M
PEARL HARBOR HI 96860-7000

COMTHIRDFLT
ATTN: FLT METEOROLOGIST
FPO SAN FRANCISCO 96601-6001

COMSEVENTHFLT
ATTN: FLT METEOROLOGIST
FPO SAN FRANCISCO 96601-6003

COMTHIRDFLT
ATTN: NSAP SCIENCE ADVISOR
PEARL HARBOR, HI 96860-7500

COMSEVENTHFLT
ATTN: NSAP SCIENCE ADVISOR
BOX 167
FPO SEATTLE 98762

COMMANDER
U.S. NAVAL FORCES, JAPAN
FPO SEATTLE 98762-0051

COMMANDER
U.S. NAVAL FORCES, MARIANAS
FPO SAN FRANCISCO 96630-0051

COMMANDER
U.S. NAVAL FORCES, KOREA
APO SAN FRANCISCO 96301-0023

COMMANDER
AMPHIBIOUS GROUP 2
ATTN: METEOROLOGICAL OFFICER
FPO NEW YORK 09501-6007

COMMANDER
AMPHIBIOUS GROUP 1
ATTN: METEOROLOGICAL OFFICER
FPO SAN FRANCISCO 96601-6006

COMMANDER
NAVAL SURFACE GROUP WEST PAC
FPO SAN FRANCISCO 96601-6011

COMMANDING OFFICER
USS NIMITZ (CVN-68)
ATTN: MET. OFFICER, OA DIV.
FPO NEW YORK 09542-2820

COMMANDING OFFICER
USS CONSTELLATION (CV-64)
ATTN: MET. OFFICER, OA DIV
FPO SAN FRANCISCO 96635-2780

COMMANDING OFFICER
USS ENTERPRISE (CVN-65)
ATTN: MET. OFFICER, OA DIV.
FPO SAN FRANCISCO 96636-2810

COMMANDING OFFICER
USS KITTY HAWK (CV-63)
ATTN: MET. OFFICER, OA DIV.
FPO SAN FRANCISCO 96634-2770

COMMANDING OFFICER
USS MIDWAY (CV-41)
ATTN: MET. OFFICER, OA DIV.
FPO SAN FRANCISCO 96631-2710

COMMANDING OFFICER
USS RANGER (CV-61)
ATTN: MET. OFFICER, OA DIV.
FPO SAN FRANCISCO 96633-2750

COMMANDING OFFICER
USS CARL VINSON (CVN-70)
ATTN: MET. OFFICER, OA DIV.
FPO SAN FRANCISCO 96629-2840

COMMANDING OFFICER
USS NEW JERSEY (BB-62)
ATTN: MET. OFFICER, OA DIV.
FPO SAN FRANCISCO 96688-1110

COMMANDING OFFICER
USS BLUERIDGE (LCC-19)
ATTN: MET. OFFICER
FPO SAN FRANCISCO 96628-3300

COMMANDING OFFICER
USS BELLEAU WOOD (LHA-3)
ATTN: METEOROLOGICAL OFFICER
FPO SAN FRANCISCO 96623-1610

COMMANDING OFFICER
USS NEW ORLEANS (LPH-11)
ATTN: MET. OFFICER
FPO SAN FRANCISCO 96627-1650

COMMANDING OFFICER
USS OKINAWA (LPH-3)
ATTN: MET. OFFICER
FPO SAN FRANCISCO 96625-1630

COMMANDING OFFICER
USS PELELIU (LHA-5)
ATTN: MET. OFFICER
FPO SAN FRANCISCO 96624-1620

COMMANDING OFFICER
USS TARAWA (LHA-1)
ATTN: MET. OFFICER
FPO SAN FRANCISCO 96622-1600

COMMANDING OFFICER
USS TRIPOLI (LPH-10)
ATTN: METEOROLOGICAL OFFICER
FPO SAN FRANCISCO 96626-1645

COMMANDING OFFICER
USS MISSOURI (BB-63)
ATTN: METEOROLOGICAL OFFICER
FPO SAN FRANCISCO 96689-1120

COMCARGRU 1
ATTN: OCEAN/MET OFFICER
FPO SAN FRANCISCO 96601-4301

COMCARGRU 5
ATTN: OCEAN/MET OFFICER
FPO SAN FRANCISCO 96601-4305

COMCARGRU 3
ATTN: OCEAN/MET OFFICER
FPO SAN FRANCISCO 96601-4303

COMCARGRU 7
ATTN: OCEAN/MET OFFICER
FPO SAN FRANCISCO 96601-4303

COMCRUDESGRU 1
ATTN: OCEAN/MET OFFICER
FPO SAN FRANCISCO 96601-4700

COMCRUDESGRU 5
ATTN: OCEAN/MET OFFICER
FPO SAN FRANCISCO 96601-4703

COMCRUDESGRU 3
ATTN: OCEAN/MET OFFICER
FPO SAN FRANCISCO 96601-4702

COMMANDING GENERAL
1ST MARINE AIRCRAFT WING
FPO SAN FRANCISCO 96603

COMMANDING OFFICER
3RD MARINE AIRCRAFT WING
MCAS, EL TORO
SANTA ANA, CA 92709

WEATHER SERVICE OFFICER
MWSS 173, MAG 24 FMF
1ST MAB, FMF
MARINE CORPS AIR STATION
KANEOHE, HI 96863-6012

USCINCPAC
BOX 13
STAFF CINCPAC J37
CAMP SMITH, HI 96861

COMMANDER
U.S. NAVAL FORCES, PHILIPPINES
BOX 30/N3
FPO SAN FRANCISCO 96651-0051

ASST. FOR ENV. SCIENCES
ASST. SEC. OF THE NAVY (R&D)
ROOM 5E731, THE PENTAGON
WASHINGTON, DC 20350

CHIEF OF NAVAL RESEARCH (2)
LIBRARY SERVICES, CODE 784
BALLSTON TOWER #1
800 QUINCY ST.
ARLINGTON, VA 22217-5000

OFFICE OF NAVAL RESEARCH
CODE 1122AT, ATMOS. SCIENCES
ARLINGTON, VA 22217-5000

OFFICE OF NAVAL TECHNOLOGY
ONR (CODE 22)
800 N. QUINCY ST.
ARLINGTON, VA 22217-5000

CHIEF OF NAVAL OPERATIONS
(OP-006)
U.S. NAVAL OBSERVATORY
WASHINGTON, DC 20390

CHIEF OF NAVAL OPERATIONS
NAVY DEPT., OP-622C
WASHINGTON, DC 20350

CHIEF OF NAVAL OPERATIONS
NAVY DEPT. OP-986G
WASHINGTON, DC 20350

CHIEF OF NAVAL OPERATIONS
OP-962
U.S. NAVAL OBSERVATORY
WASHINGTON, DC 20390

CHIEF OF NAVAL OPERATIONS
OP-953
NAVY DEPARTMENT
WASHINGTON, DC 20350

OJCS/J3/ESD
THE PENTAGON, ROOM 2B887
WASHINGTON, DC 20301-5000

OFFICER IN CHARGE
NAVOCEANCOMDET
NAVAL STATION
FPO SEATTLE 98791-2943

OFFICER IN CHARGE
NAVOCEANCOMDET
BOX 81, USNAS
FPO SAN FRANCISCO 96637-2900

OFFICER IN CHARGE
NAVOCEANCOMDET
FEDERAL BLDG.
ASHEVILLE, NC 28801-2696

OFFICER IN CHARGE
NAVOCEANCOMDET
U.S. NAVAL AIR FACILITY
FPO SEATTLE 98767-2933

OFFICER IN CHARGE
NAVOCEANCOMDET
NAVAL AIR STATION
BARBERS PT., HI 96862-5750

CENTER FOR NAVAL ANALYSES
4401 FORT AVENUE
P.O. BOX 16268
ALEXANDRIA, VA 22302-0268

OFFICER IN CHARGE
NAVOCEANCOMDET
MONTEREY, CA 93943-5004

OFFICER IN CHARGE
U.S. NAVOCEANCOMDET
APO SAN FRANCISCO 96519-5000

OFFICER IN CHARGE
NAVOCEANCOMDET
NAVAL AIR STATION
MOFFETT FIELD, CA 94035

OFFICER IN CHARGE
NAVOCEANCOMDET
NAS, WHIDBEY ISLAND
OAK HARBOR, WA 98278-5100

OFFICER IN CHARGE
NAVOCEANCOMDET
NAVAL AIR STATION
SAN DIEGO, CA 92145-5851

OFFICER IN CHARGE
U.S. NAVOCEANCOMDET
FPO SAN FRANCISCO 96685-2905

OFFICER IN CHARGE
U.S. NAVOCEANCOMDET
FLEET ACTIVITIES
FPO SEATTLE 98770-0051

OFFICER IN CHARGE
NAVOCEANCOMDET
NAVAL AIR STATION
ALAMEDA, CA 94501-5011

COMMANDING OFFICER
FLEET INTELLIGENCE CENTER
(PACIFIC)
PEARL HARBOR, HI 96860

COMMANDER
NAVAL OCEANOGRAPHY COMMAND
STENNIS SPACE CENTER
JCSSC, MS 39529-5000

COMMANDING OFFICER
NAVAL OCEANOGRAPHIC OFFICE
STENNIS SPACE CENTER
JCSSC, MS 39522-5001

COMMANDING OFFICER
FLENUMOCEANCEN
MONTEREY, CA 93943-5005

COMMANDING OFFICER
NAVWESTOCEANCEN
BOX 113
PEARL HAPBOR, HI 96860

COMMANDING OFFICER
NAVPOLAROCEANCEN, NAVY DEPT.
4301 SUITLAND RD
WASHINGTON, DC 20395-5180

COMMANDING OFFICER
U.S. NAVOCEANCOMCEN
BOX 12, COMNAVMARIANAS
FPO SAN FRANCISCO 96630-2926

COMMANDING OFFICER
U.S. NAVOCEANCOMFAC
FPO SEATTLE [illegible]62-3500

COMMANDING OFFICER
U.S. NAVOCEANCOMFAC
BOX 63, NAS (CUBI PT)
FPO SAN FRANCISCO 96654-2909

CHAIRMAN
OCEANOGRAPHY DEPT.
U.S. NAVAL ACADEMY
ANNAPOLIS, MD 21402

DIRECTOR OF RESEARCH
U.S. NAVAL ACADEMY
ANNAPOLIS, MD 21402

NAVAL POSTGRADUATE SCHOOL
METEOROLOGY DEPT.
MONTEREY, CA 93943-5000

PRESIDENT
NAVAL WAR COLLEGE
GEOPHYS. OFFICER, NAVOPS DEPT.
NEWPORT, RI 02841

COMSPAWARSYSCOM
ATTN: CAPT WOOLDRIDGE
CODE 3213, NAVY DEPT.
WASHINGTON, DC 20363-5100

COMSPAWARSYSCOM
ATTN: CODE PWM 141
NAVY DEPT, BLDG NC1, ROOM 2E18
WASHINGTON, DC 20363-5100

COMMANDING OFFICER
WEATHER SERVICE OFFICE
U.S. MCAS (HELICOPTER)
FPO SEATTLE 98772

COMMANDING OFFICER
WEATHER SERVICE OFFICE
U.S. MCAS (IWAKUNI)
FPO SEATTLE 98764

COMMANDING OFFICER
WEATHER SERVICE OFFICE
MCAS
KANEOHE BAY, HI 96863

HQ, U.S. MARINE CORPS
CODE ASL-44
WASHINGTON, DC 20380

COMMANDING OFFICER
MAG-11, SQDN-11
ATTN: WEATHER VANS
MCAS, EL TORO
SANTA ANA, CA 92709

COMMANDING OFFICER
MAG-13, SQDN-13
ATTN: WEATHER VANS
MCAS, EL TORO
SANTA ANA, CA 92709

COMMANDER
AWS/DNXS
SCOTT AFB, IL 62225

USAFETAC/TS
SCOTT AFB, IL 62225

3350TH TECH. TRNG GROUP
TTGU/2/STOP 623
CHANUTE AFB, IL 61868

OFFICER IN CHARGE
SERVICE SCHOOL COMMAND
DET. CHANUTE/STOP 62
CHANUTE AFB, IL 61868

HQ 1ST WEATHER WING/DN
HICKAM AFB, HI 96853

20 WS/DON
APO SAN FRANCISCO 96328-5000

DET 5, 20 WS
APO SAN FRANCISCO 96274

DET. 8, 20 WS
APO SAN FRANCISCO 96239

DET 17, 20 WS
APO SAN FRANCISCO 96328

DET 18, 30 WS
APO SAN FRANCISCO 96301

DIRECTOR (12)
DEFENSE TECH. INFORMATION
CENTER, CAMERON STATION
ALEXANDRIA, VA 22314

CENTRAL INTELLIGENCE AGENCY
ATTN: OCR STANDARD DIST.
WASHINGTON, DC 20505

SPACE FLIGHT METEORO. GROUP
ATTN: STEVE SOKOL, CODE Z8
JOHNSON SPACE CENTER
HOUSTON, TX 77058